National Library
of Canada

Bibliothèque nationale
du Canada

Canadian Theses Service

Service des thèses canadiennes

Ottawa, Canada
K1A 0N4

NOTICE

The quality of this microform is heavily dependent upon the quality of the original thesis submitted for microfilming. Every effort has been made to ensure the highest quality of reproduction possible.

If pages are missing, contact the university which granted the degree.

Some pages may have indistinct print especially if the original pages were typed with a poor typewriter ribbon or if the university sent us an inferior photocopy.

Previously copyrighted materials (journal articles, published tests, etc.) are not filmed.

Reproduction in full or in part of this microform is governed by the Canadian Copyright Act, R.S.C. 1970, c. C-30.

AVIS

La qualité de cette microforme dépend grandement de la qualité de la thèse soumise au microfilmage. Nous avons tout fait pour assurer une qualité supérieure de reproduction.

S'il manque des pages, veuillez communiquer avec l'université qui a conféré le grade.

La qualité d'impression de certaines pages peut laisser à désirer, surtout si les pages originales ont été dactylographiées à l'aide d'un ruban usé ou si l'université nous a fait parvenir une photocopie de qualité inférieure.

Les documents qui font déjà l'objet d'un droit d'auteur (articles de revue, tests publiés, etc.) ne sont pas microfilmés.

La reproduction, même partielle, de cette microforme est soumise à la Loi canadienne sur le droit d'auteur, SRC 1970, c. C-30.

NL-339 (r. 88/04)

Canada

THE UNIVERSITY OF ALBERTA

NEAR FACE BEHAVIOR OF DEEP TUNNELS IN ROCK

by

Ⓒ FABRIZIO PELLI

A THESIS

SUBMITTED TO THE FACULTY OF GRADUATE STUDIES AND RESEARCH

IN PARTIAL FULFILMENT OF THE REQUIREMENTS FOR THE DEGREE

OF DOCTOR OF PHILOSOPHY

DEPARTMENT OF CIVIL ENGINEERING

EDMONTON, ALBERTA

FALL 1987

Permission has been granted to the National Library of Canada to microfilm this thesis and to lend or sell copies of the film.

The author (copyright owner) has reserved other publication rights, and neither the thesis nor extensive extracts from it may be printed or otherwise reproduced without his/her written permission.

L'autorisation a été accordée à la Bibliothèque nationale du Canada de microfilmer cette thèse et de prêter ou de vendre des exemplaires du film.

L'auteur (titulaire du droit d'auteur) se réserve les autres droits de publication; ni la thèse ni de longs extraits de celle-ci ne doivent être imprimés ou autrement reproduits sans son autorisation écrite.

ISBN 0-315-41171-6

Energy, Mines and Resources Canada
Énergie, Mines et Ressources Canada

Research and Technology
Recherche et Technologie

Canada Centre for Mineral and Energy Technology
Centre canadien de la technologie des minéraux et de l'énergie

Coal Research Laboratories
Laboratoires de Recherches sur le Charbon

Cape Breton Coal
Research Laboratory
210 George Street
Sydney, N.S.
B1P 1J3

Your file Votre référence

Our file Notre référence
CA3520

September 9, 1987

Mr. F. Pelli
Dept. of Civil Engineering
220 Civil/Electrical
Engineering Building
University of Alberta
Edmonton, Alberta
T6G 2G7

Dear Mr. Pelli:

Subject: CANMET Donkin-Morien Contract Figures

With reference to your letter of September 3, 1987, I am writing to give you permission to use the figures (listed in your letter) from the CANMET Donkin-Morien Contract (DSS No. 26SQ.23440-2-9159) in your thesis. The only condition that I am attaching for their use, is that each must be appropriately referenced.

I wish you luck with your thesis.

Yours sincerely,

T.R.C. Aston

Dr. T.R.C. Aston
Research Scientist
Strata Mechanics

TRCA/bb

Canada

Dr. T. Aston
210 George Street
Sidney, Nova Scotia
BIP IJ3

Edmonton 9-3-1987

Dear Dr. Aston,

the research that I am conducting at the University of Alberta, on the interpretation of the monitoring data collected at the Donkin-Morien project, is almost concluded. My Ph.D. thesis is virtually ready and my defense will take place in October.

I would appreciate if you could give me written permission to include in my thesis some of the figures contained in the CANMET Contract Report No.26SQ.23440-2-9159 (list enclosed). This would allow a considerable time saving in the preparation of my thesis. In order to be able to use your permission I should receive it by the end of September, beginning of October.

I thank you in advance for your kind cooperation.

Sincerely yours

Fabrizio Pelli

LIST OF FIGURES.

. . . . I-4.4
. . . . I-4.7
. . . . I-4.10
. . . . I-4.11
. . . . I-5.1
. . . . I-5.4
. . . . II-2.1
. . . . II-3.5
. . . . II-3.6
. . . . II-3.7
. . . . II-3.8

THE UNIVERSITY OF ALBERTA

RELEASE FORM

NAME OF AUTHOR FABRIZIO PELLI

TITLE OF THESIS NEAR FACE BEHAVIOR OF DEEP TUNNELS IN ROCK

DEGREE FOR WHICH THESIS WAS PRESENTED DOCTOR OF PHILOSOPHY

YEAR THIS DEGREE GRANTED FALL 1987

Permission is hereby granted to THE UNIVERSITY OF ALBERTA LIBRARY to reproduce single copies of this thesis and to lend or sell such copies for private, scholarly or scientific research purposes only.

The author reserves other publication rights, and neither the thesis nor extensive extracts from it may be printed or otherwise reproduced without the author's written permission.

(SIGNED) Fabrizio Pelli

PERMANENT ADDRESS:

VIA PRINCIPE AMEDEO, 243
00185 ROMA
ITALY

DATED October - 19 1987

THE UNIVERSITY OF ALBERTA

FACULTY OF GRADUATE STUDIES AND RESEARCH

The undersigned certify that they have read, and recommend to the Faculty of Graduate Studies and Research, for acceptance, a thesis entitled NEAR FACE BEHAVIOR OF DEEP TUNNELS IN ROCK submitted by FABRIZIO PELLI in partial fulfilment of the requirements for the degree of DOCTOR OF PHILOSOPHY.

....

Supervisor

....

....

....

....

....

External Examiner

Date..October 14 - 1987..............

ABSTRACT

A three dimensional approach is needed in order to allow a proper interpretation of monitoring data collected during excavation and for the prediction of the loads on the support. Few parametric studies have been carried out so far on three dimensional models, and most of them were based on the assumption of axisymmetric initial stress field and isotropic, linear elastic material properties.

A series of truly three dimensional finite element analyses were conducted and the results are presented in this thesis. A non-axisymmetric initial stress field was selected and various constitutive relationships, both linear and non-linear, were assumed for the rock. The purpose of this study was to provide tools for monitoring data interpretation by analyzing stresses and displacements as they develop during tunnel construction. The load distribution on the support was also subject of the investigation. Field measurements collected at the Donkin-Morien project were analyzed in order to verify the findings of the numerical analyses. The limitations of the monitoring program laid out at this particular project were identified and guidelines for a monitoring program permitting optimal data interpretation are given.

This research led to a rationale for the effective use of monitoring data to back-analyze the strength and deformational properties of the rock mass. It is shown that by proper three dimensional modelling reliable information

can be extracted from field measurements. In particular, the data collected by multipoint radial extensometers can reveal both the elastic and non-elastic properties of the ground if the magnitude and shape of the radial displacement curves are considered. The monitoring program, however, must be laid out properly in order to get unique results, and a sufficient number of measurements must be taken for each instrumented section. The excavation round length was found to dominate the longitudinal distribution of loads on liners.

ACKNOWLEDGMENTS

I wish to express my gratitude to my supervisor Dr. N. R. Morgenstern for providing continuous and enthusiastic guidance, support and encouragement throughout the course of my thesis. Special thanks are also due to Dr. P. K. Kaiser, who co-supervised this research and whose contribution in terms of time and valuable ideas is gratefully appreciated.

I wish to thank Dr. E. Hoek for his comments on my thesis; thanks are also extended to Dr. Z. Eisenstein, Dr. K. Barron and Dr. A. Elwi. My appreciation is also due to Dr. D. H. Chan and Dr. T. M. Hrudey who assisted me in various occasions.

The financial support made available by Dr. N. R. Morgenstern and by the Department of Civil Engineering is gratefully acknowledged.

I wish to further thank my fellow graduate students, in particular T. T. Wong, R. Wan, D. Tannant, B. Indraratna and H. Heinz.

My gratitude also goes to Dr. M. Ottaviani of the University of Rome who first encouraged me to join the Ph.D. program.

A special thanks goes to Graziella and my family.

Table of Contents

Chapter Page

1. INTRODUCTION 1

1.1 Three Dimensional Characteristics of the Tunnelling Problem 1

1.2 Purpose of the research 4

2. NEAR FACE BEHAVIOR OF DEEP TUNNELS 7

2.1 Introduction 7

2.2 Unlined Tunnels 8

2.2.1 Unlined Tunnels in Linear Elastic Rock 8

2.2.2 Effects of Non-Isotropic Rock Behavior 16

2.2.3 Unlined Tunnels in Non-Linear and Non-Elastic Media 20

2.3 Rock-Support Interaction During the Excavation of Supported Tunnels 24

2.3.1 The Convergence Confinement Method (CCM) ..26

2.3.2 Modelling of Near Face Behavior by Simplified Two Dimensional Plane Strain Analyses 29

2.3.3 Review of Three Dimensional and Simplified Axisymmetric Numerical Analyses Found in Literature 31

2.4 The Role of Back-Analysis in Tunnel Design 36

2.5 Conclusions 38

3. UNLINED TUNNELS IN LINEAR ELASTIC ROCK 40

3.1 Introduction 40

3.2 Description of the Analysis 41

3.3 Stresses near Tunnel Face 47

3.4 Displacements 52

3.5 Some Implications for Monitoring Data Interpretation 62

3.5.1 Convergence Records 62

3.5.2 Multipoint Extensometer Records 70

3.5.3 Shape of Radial Displacement Profiles 75

3.6 Conclusions 76

4. UNLINED TUNNELS IN ANISOTROPIC ROCK 79

4.1 Introduction 79

4.2 Description of the Analysis 79

4.3 Stresses Near Tunnel Face 83

4.4 Displacements 96

4.5 Implications for Monitoring Data Interpretation 101

4.5.1 Convergence Records 101

4.5.2 Multipoint Extensometer Records 104

4.5.3 Shape of Radial Displacement Profiles 108

4.6 Conclusions 111

5. UNLINED TUNNELS IN NON-LINEAR ROCK 113

5.1 Introduction 113

5.2 Description of the analysis 114

5.2.1 Tunnel in Non-Linear Medium, Exhibiting Hyperbolic Stress-Strain Relationship 114

5.2.2 Tunnel in Linear Elastic, Ideal Plastic Medium 117

5.2.3 Remarks to the FEM Model 119

5.3 Stresses 120

5.4 Displacements 137

5.5 Implications for Monitoring Data Interpretation 144

5.5.1 Convergence Records 144

5.5.2 Multipoint Extensometer Records 145

5.5.3 Shape of Radial Displacement Profiles 149

5.6 Conclusions 152

6. SUPPORTED TUNNELS 155

6.1 Introduction 155

6.2 Description of the Analyses 156

6.2.1 General 156

6.2.2 Parameters for Tunnels in Isotropic Rock .157

6.2.3 Parameters for Tunnels in Anisotropic Rock 160

6.3 Displacements 163

6.3.1 Effect of the Relative Stiffness 163

6.3.2 Effect of Delay and Excavation Round Length 166

6.3.3 Radial Multipoint Extensometer Records ...170

6.4 Loads on the Support 184

6.4.1 Calculation of Thrust and Bending Moments 185

6.4.2 Effects of Relative Stiffness of Support .188

6.4.3 Effects of Delay 202

6.4.4 Effects of the Excavation Round Length ...205

6.4.5 Thrust and Bending Moments Along the Tunnel Axis 210

6.4.6 Effects on Rock Anisotropy on Thrust and Bending Moments 213

6.5 Conclusions 222

7. Back-Analysis of Field Data 225

7.1 Introduction 225

7.2 Description of the Project 226

7.2.1 Excavation and Support 229

7.2.2 Rock Properties and In Situ Stresses 229

7.2.3 Monitoring Program 234

7.2.4 Supplemental Remarks 235

7.3 Multipoint Extensometer Records in the Mixed Sediments 236

7.3.1 Back-analysis of Rock Mass Strength 237

7.3.1.1 Influence of Inhomogeneities 250

7.3.1.2 Effects of Low-Strength Rock at the Tunnel Crown 257

7.3.2 Back-Analysis of Rock Mass Modulus 263

7.4 Multipoint Extensometer Records in Portal Sandstone 273

7.4.1 Analysis of the Total Relative Displacements 273

7.4.1.1 Back-Analysis of the Sandstone Elastic Modulus 280

7.4.2 Shape of the Radial Displacement Curves Ahead of the Tunnel Face 283

7.4.3 Analysis of the Radial Displacement Curves Behind the Tunnel Face 285

7.4.4 Prediction of the Radial Displacements by Curve Fitting 295

7.5 Conclusions 303

8. Conclusions and Recommendations 307

8.1 Introduction 307

8.2 Unsupported Tunnels 307

8.2.1 Effects of Zero Reading Delays 308

8.2.2 Effects of Initial Stress Distribution ...309

8.2.3 Shape of the Relative Displacement Profiles (U_r vs r) 309

8.2.4 Shape of the Radial Displacement Curves (U_r vs X) 310

8.3 Supported Tunnels 312

8.3.1 Effects on Monitoring Data 312

8.3.2 Loads on the Support 313

8.4 Back-Analysis of Field Data 314

8.4.1 Multipoint Extensometer Records 314

8.4.2 Recommendations for Monitoring Programs ..316

8.5 Recommendations for Further Research 318

BIBLIOGRAPHY 319

APPENDIX A
Unlined Tunnels in Linear Elastic Isotropic Rock 328

APPENDIX B
Unlined Tunnels in Linear Elastic
Transverse-Isotropic Rock 342

APPENDIX C
Unlined Tunnels in Non-Linear Isotropic Rock 376

APPENDIX D
Lined Tunnels in Linear Elastic Isotropic Rock 398

List of Tables

Table Page

6.1 Parameters Selected for Cases 1 to 6 (Isotropic Rock) 159

6.2 Parameters Selected for Cases 1A to 3A (Transverse Isotropic Rock) 161

7.1 Results of Laboratory and Field Testing (Summarized from Yuen et al., 1985) 232

List of Figures

Figure Page

2.1 Radial Stresses, σ_r, in the Axial Plane for Axisymmetric and Non-Axisymmetric Loading Conditions (Modified after Galle and Wilhoit, 1962). 10

2.2 Shear Stresses, τ_{ar}, in the Axial Plane for Axisymmetric and Non-Axisymmetric Loading Conditions (Modified after Galle and Wilhoit, 1962). 11

2.3 Principal Stresses on the Axial Plane for Initial Stress Normal (a) and Parallel (b) to the Tunnel Axis (Modified after Niwa et al.,1978). 15

2.4 Effect of the Initial Axial Stress, P_a, on the Horizontal Movement at the Tunnel Face (Modified after Descoeudres, 1974) 17

2.5 Schematic Representation of Transverse Isotropic Medium 19

2.6 Schematic Representation of the Excavation-Support Sequence. RL=Round Length ; DEL=Delay. 25

2.7 Schematic Representation of the Convergence Confinement Method 27

2.8 Support Delay Correction Factor (Modified after Schwartz and Einstein, 1980, and Hutchinson, 1982) 33

3.1 Front View of the Three Dimensional Finite Element Mesh 42

3.2 Side View of the Three Dimensional Finite Element Mesh 43

3.3 Boundary Conditions 44

3.4 Radial Stresses, σ_r, at the Tunnel Springline (K_0=2) 49

3.5 Shear Stresses, τ_{ar}, at the Tunnel Springline (K_0=2) 51

3.6 Tangential Stresses, σ_t, at the Tunnel Crown (K_0=2) 53

3.7 Axial Stresses, σ_a, at the Tunnel Springline (K_0=2) 54

Figure Page

3.8 Radial Displacements, U_r, at the Tunnel Springline ($K_0=2$) 55

3.9 Effect of P_a on Convergence at the Tunnel Crown ($K_0=2$) 57

3.10 Schematic Representation of Principal Stress Trajectories near the Tunnel Face ($P_v=P_h=0$) 59

3.11 Effect of P_a on Convergence at the Tunnel Springline ($K_0=2$) 61

3.12 Effect of Zero-Reading Location, $(X/2R)_0$, on Convergence Measurements at the Tunnel Springline ($K_0=2$) 63

3.13 Effect of Zero-Reading Location, $(X/2R)_0$, on Convergence Measurements at the Tunnel Crown ($K_0=2$) 65

3.14 Effect of P_a on Convergence Measurements at the Tunnel Springline; $(X/2R)_0=0.0$, $K_0=2$ 67

3.15 Effect of P_a on Convergence Measurements at the Tunnel Crown; $(X/2R)_0=0.0$, $K_0=2$ 68

3.16 Effect of P_a on Convergence Measurements at the Tunnel Crown; $(X/2R)_0=0.25$, $K_0=2$ 69

3.17 Relative Displacement Measurements at the Tunnel Springline; Total Values ($K_0=2$) 71

3.18 Relative Displacement Measurements at the Tunnel Crown; Total Values ($K_0=2$) 73

3.19 Relative Displacement Measurements at the Tunnel Crown; Partial Values ($K_0=2$; $P_a=P_v$) 74

3.20 Fitting of the Relative Displacement Curves Calculated at the Tunnel Springline ($r/R=1$ and $r/R=1.85$) by the Ramberg-Osgood Analytical Function ($K_0=2$) 77

4.1 Orientation of the Elastic Properties for the Cases Investigated 82

4.2 Radial Stresses, σ_r, at the Tunnel Springline; Case 1 84

4.3 Radial Stresses, σ_r, at the Tunnel Springline; Case 2 85

Figure Page

4.4 Radial Stresses, σ_r, at the Tunnel Springline; Case 3 86

4.5 Radial Horizontal Stresses, σ_r, at the Tunnel Axis, Ahead of the Face; Cases 1 to 3 88

4.6 Horizontal Movement at the Tunnel Face; Cases 1 to 3 89

4.7 Shear Stresses, τ_{ar}, at the Tunnel Springline; Cases 1 to 3 90

4.8 Tangential Stresses, σ_t, at the Tunnel Crown; Cases 1 to 3 92

4.9 Axial Stresses, σ_a, at the Tunnel Springline; Cases 1 to 3 93

4.10 Effect of Anisotropy on the Axial Stress Distribution at the Tunnel Face 94

4.11 Convergence at the Tunnel Crown and Springline; Case 1 97

4.12 Convergence at the Tunnel Crown and Springline; Case 2 99

4.13 Convergence at the Tunnel Crown and Springline; Case 3 100

4.14 Normalized Convergence Curves, U_r/U_{rmax}, at the Tunnel Springline; Cases 1 to 3 and Isotropic 103

4.15 Relative Displacements at the Tunnel Crown (Partial Values); Cases 1 to 3 105

4.16 Relative Displacements at the Tunnel Crown (Partial and Total Values); Case 3 107

4.17 Normalized Convergence Curves, U_r/U_{rmax}, at the Tunnel Springline, Fitted by the Ramberg-Osgood Function; Cases 1 to 3 109

5.1 Schematic Representation of the Hyperbolic Stress-Strain Relationship 115

5.2 Schematic Representation of the Linear-Elastic, Ideal-Plastic Stress-Strain Relationship 118

Figure Page

5.3 Horizontal Radial Stresses, σ_r, Ahead of the Tunnel Face (r/R=0.0); Linear-Elastic, Hyperbolic and Elasto-Plastic 121

5.4 Horizontal Radial Stresses, σ_r, Ahead of the Tunnel Face (r/R=0.8); Linear-Elastic, Hyperbolic and Elasto-Plastic 123

5.5 Horizontal Radial Stresses, σ_r, Ahead of the Tunnel Face (r/R=1.1); Linear-Elastic, Hyperbolic and Elasto-Plastic 124

5.6 Plastic Zone at the Tunnel Face 126

5.7 Plastic Zone at the Springline (a) and Crown (b) 127

5.8 Shear Stresses, τ_{ar}, at the Tunnel Springline; Linear-Elastic and Elasto-Plastic 129

5.9 Tangential Stresses, σ_t, at the Tunnel Crown (r/R=1.1); Linear-Elastic, Hyperbolic and Elasto-Plastic 130

5.10 Tangential Stresses, σ_t, at the Tunnel Crown (r/R=1.3); Linear-Elastic, Hyperbolic and Elasto-Plastic 132

5.11 Tangential Stresses, σ_t, at the Tunnel Crown (r/R=2.65); Linear-Elastic, Hyperbolic and Elasto-Plastic 133

5.12 Axial Stresses, σ_a, at the Tunnel Crown; Linear-Elastic and Elasto-Plastic 135

5.13 Axial Stresses, σ_a, at the Tunnel Springline; Linear-Elastic, Hyperbolic and Elasto-Plastic 136

5.14 Convergence at the Tunnel Springline; Linear-Elastic, Hyperbolic and Elasto-Plastic 138

5.15 Convergence at the Tunnel Crown; Linear-Elastic, Hyperbolic and Elasto-Plastic 140

5.16 Radial Displacements at the Tunnel Crown; Hyperbolic 142

Figure Page

5.17 Radial Displacements at the Tunnel Crown; Elasto-Plastic 143

5.18 Relative Displacements at the Tunnel Springline (Partial Values); Linear-Elastic, Hyperbolic and Elasto-Plastic 146

5.19 Relative Displacements at the Tunnel Crown (Partial Values); Linear-Elastic, Hyperbolic and Elasto-Plastic 148

5.20 Radial Displacements at the Tunnel Springline (r/R=1.3); Linear-Elastic, Hyperbolic and Elasto-Plastic 150

5.21 Convergence at the Tunnel Sprigline Fitted by the Ramberg-Osgood Function; Linear-Elastic and Elasto-Plastic 151

5.22 Convergence at the Tunnel Crown Fitted by the Ramberg-Osgood Function; Linear-Elastic and Elasto-Plastic 153

6.1 Orientation of the Elastic Properties for Cases 1A to 3A (Transverse Isotropic Rock) 162

6.2 Convergence Curves for Cases 1 to 3; Variable Relative Stiffness 164

6.3 Convergence Curves for Cases 1,4 and 5; Variable Delay and Round Length 165

6.4 Excavation Support Sequence for Cases 4 (No Delay) and 5 (1R Delay) 167

6.5 Effects of the Delay on Radial Displacements and Pressure on the Support 168

6.6 Effect of the Round Length on the Stress Distribution in the Liner 171

6.7 Relative Displacements at the Tunnel Springline (Total Values); Unlined and Cases 4 and 5 172

6.8 Relative Displacements at the Tunnel Crown (Total Values); Unlined and Cases 4 and 5 174

Figure Page

6.9 Schematic Diagram for Explanation of the Compressive Zones Detected at the Back of the Liner 175

6.10 Radial (σ_r) and Tangential (σ_t) Stresses vs Distance from Tunnel Wall; Case 4 176

6.11 Relative Displacements at the Tunnel Springline (Partial Values); Case 4 178

6.12 Relative Displacements at the Tunnel Springline (Partial Values); Case 5 179

6.13 Relative Displacements at the Tunnel Crown (Partial Values); Case 4 180

6.14 Relative Displacements at the Tunnel Crown (Partial Values); Case 5 181

6.15 Array of Multipoint Radial Extensometers (Kaiser and Mckay, 1983) 182

6.16 Relative Displacements Measured in the Shaft (Modified After Mckay, 1982) 183

6.17 Displacements of the Liner Due to Face Advance 186

6.18 Support Ring Used for Computation of Loads in the Liner (a) and Interpolation Functions for Radial and Tangential Displacements (b) 187

6.19 Three dimensional Support Shell 189

6.20 Thrust Forces in the Liner for Case 1 190

6.21 Longitudinal Distribution of the Thrust Forces in the Liner 192

6.22 Thrust Forces in the Liner for Cases 2 (a) and 3 (b) 193

6.23 Bending Moments in the Liner for Case 1 195

6.24 Bending Moments in the Liner for Cases 2 (a) and 3 (b) 196

6.25 Effects of Relative Stiffness on Thrust Forces for FEM 3-D Analyses and 2-D Einstein and Schwartz (1979) Closed Form Solution 197

Figure Page

6.26 Effects of Relative Stiffness on Bending Moments for FEM 3-D Analyses and 2-D Einstein and Schwartz (1979) Closed Form Solution 198

6.27 Difference Between the 3-D Analyses and the E/S Relative Stiffness Solution 200

6.28 Reduction Factors λ_T (a) and λ_M (b) 201

6.29 Thrust Forces in the Liner for Cases 4 (a) and 5 (b) 203

6.30 Bending Moments in the Liner for Cases 4 (a) and 5 (b) 204

6.31 Reduction Factors λ_T (a) and λ_M (b) 206

6.32 Thrust Forces in the Liner for Cases 1 (a) and 6 (b) 207

6.33 Bending Moments in the Liner for Cases 1 (a) and 6 (b) 208

6.34 Reduction Factors λ_T (a) and λ_M (b) 209

6.35 Thrust in the Axial Direction (T_a) for Case 4 211

6.36 Development of Tensile Axial Thrust (T_a) in the Liner 212

6.37 Thrust Forces in the Liner for Case 1A 215

6.38 Thrust Forces in the Liner for Cases 2A (a) and 3A (b) 216

6.39 Effect of Rock Anisotropy on Thrust in the Liner 218

6.40 Bending Moments in the Liner for Case 1A 219

6.41 Bending Moments in the Liner for Cases 2A (a) and 3A (b) 220

6.42 Maximum Thrust and Bending Moments for Cases 1A, 2A and 3A 221

7.1 Map Showing Position of the Tunnels (Yuen et al., 1985) 227

7.2 Longitudinal Section Through Tunnel No.2 (Modified After Yuen et al., 1987) 228

Figure Page

7.3 Propulsion System of the LOVAT M-300 TBM 230

7.4 Longitudinal Section, Showing Geology near Tunnel No.2 at Chainage 2263 m (Yuen et al., 1985) 239

7.5 Longitudinal Section, Showing Geology near Tunnel No.2 at Chainage 3205 m (Yuen el al., 1985) 240

7.6 Radial Displacement Profile at Chainage 2263 m (Relative to Deepest Anchor) (Yuen et al., 1985) 242

7.7 Radial Displacement Curves at Chainage 2263 m (Relative to Deepest Anchor) 243

7.8 Radial Displacement Profile at Chainage 3205 m (Relative to Deepest Anchor) (Yuen et al., 1985) 244

7.9 Radial Displacement Curves at Chainage 3205 m (Relative to Deepest Anchor) 246

7.10 Tangential Stresses at the Tunnel Crown as Predicted by a Three Dimensional Finite Element Analysis (Linear Elastic, $K_0=2$) 247

7.11 Intersection of Hoek-Brown Surface with Octahedral Plane 251

7.12 Axial Stresses at the Tunnel Crown as Predicted by a Three Dimensional Finite Element Analysis (Linear Elastic, $K_0=2$) 252

7.13 Longitudinal Section, Showing Geology near Tunnel No.2 at Chainage 1428 m (Yuen et al., 1985) 253

7.14 Radial Displacement Profile at Chainage 1428 m (Relative to Deepest Anchor) (Yuen et al., 1985) 255

7.15 Radial Displacement Curves at Chainage 1428 m 256

7.16 Longitudinal Section, Showing Geology near Tunnel No.2 at Chainage 2996 m (Yuen et al., 1985) 258

Figure Page

7.17 Radial Displacement Profile at Chainage 2996 m (Relative to Deepest Anchor) (Yuen et al., 1985) 259

7.18 Radial Displacement Curves at Chainage 2996 m (Relative to Deepest Anchor) 260

7.19 Radial Stresses at the Tunnel Crown as Predicted by a Three Dimensional Finite Element Analysis (Linear Elastic, K_0=2) 262

7.20 Radial Displacement Profiles at the Tunnel Crown, Predicted by two Three Dimensional Finite Element Analyses (Elastic and Elasto-Plastic) 265

7.21 Schematic Representation of Tunnel Shape Change due to Yielding 266

7.22 Measured and Predicted Radial Displacement Curves at Chainage 2996 m; Fitted at 1.5m from the Wall (E=1.65 GPa) 268

7.23 Radial Displacements Curves at Chainage 3205 m (Relative to Deepest Anchor) 270

7.24 Radial Displacements Curves at Chainage 3205 m; Near Tunnel Face 271

7.25 Measured and Predicted Radial Displacement Curves at Chainage 1428 m; Fitted at 3m from the Wall (E=0.5 GPa) 272

7.26 Section Through Horizontal Extensometer Placed at Chainage 800 m (Modified After Yuen et al., 1985) 274

7.27 Results of In Situ Dilatometer Tests in the Sandstone at Chainage 800 m (Yuen et al., 1985) 275

7.28 Radial Displacements Profile at Chainage 800 m 276

7.29 Schematic Diagram for Explanation of Radial Compressive Zone 278

7.30 Relative Radial Displacement Profiles with and without Stiff Zone (Finite Element Analyses) 279

Figure Page

7.31 Comparison Between Relative Radial Displacements Measured in the Field (Total Values) and Calculated by the Finite Element Method 281

7.32 Radial Displacement Curves for Springline at Chainage 800 m 284

7.33 Convergence Curves for Tunnels in Linear Elastic, Hyperbolic and Elasto-Plastic Rock (FEM) 286

7.34 Radial Displacement Profile Measured at Three Meters from the Tunnel Wall Fitted by FEM (E=10 GPa); Chainage 800 m, Datum at 42 m from the Tunnel Wall) 288

7.35 Convergence Curves Calculated for Various Axial Stresses (FEM) at the Tunnel Springline (K_0=2, $(X/2R)_0$=0.0) 290

7.36 Radial Displacement Profiles Measured at 7m from the Tunnel Wall Fitted by FEM (E=7.5 GPa; Chainage 800 m; Datum at 42 m from the Tunnel Wall 291

7.37 Radial Displacement Profiles Measured at 3m from the Tunnel Wall Fitted by FEM (E=10 GPa; Chainage 800 m; Datum at 21 m from Tunnel Wall) 293

7.38 Radial Displacement Profiles Measured at 7m from the Tunnel Wall Fitted by FEM (E=5.75 GPa; Chainage 800 m; Datum at 21 m from Tunnel Wall) 294

7.39 Fitting of the Radial Displacement Curve by the Ramberg-Osgood Function with Various m Values 296

7.40 Definition of the Ramberg-Osgood Function by Initial Gradient and 2 Known Points 298

7.41 Prediction of the Radial Displacement Curve by Curve Fitting (Variable m) 299

7.42 Definition of the Ramberg-Osgood Function by Initial Gradient, Shape Factor and One Known Point 301

7.43 Prediction of the Radial Displacement Curve by Curve Fitting (Constant m) 302

Figure Page

A.1 Tangential Stresses, σ_t, at the Tunnel Springline (K_0=2) 329

A.2 Shear Stresses, τ_{ar}, at the Tunnel Crown (K_0=2) 330

A.3 Radial Displacements, U_r, at the Tunnel Springline (K_0=2; P_a=0.0) 331

A.4 Radial Displacements, U_r, at the Tunnel Springline (K_0=2; P_a=P_v) 332

A.5 Radial Displacements, U_r, at the Tunnel Springline (K_0=2; P_a=4P_v) 333

A.6 Radial Displacements, U_r, at the Tunnel Crown (K_0=2; P_a=0.0) 334

A.7 Radial Displacements, U_r, at the Tunnel Crown (K_0=2; P_a=2P_v) 335

A.8 Radial Displacements, U_r, at the Tunnel Crown (K_0=2; P_a=4P_v) 336

A.9 Radial Displacement Profiles at the Tunnel Springline (Partial Values; K_0=2) 337

A.10 Radial Displacement Profiles at the Tunnel Crown (Partial Values; K_0=2) 338

A.11 Radial Displacement Profiles at the Tunnel Springline (Total Values; K_0=2; P_a=P_v) 339

A.12 Radial Displacement Profiles at the Tunnel Springline (Partial Values; K_0=2; P_a=P_v) 340

A.13 Radial Displacement Profiles at the Tunnel Crown (Total Values; K_0=2; P_a=P_v) 341

B.1 Radial Stresses, σ_r, at the Tunnel Crown (Case 1) 343

B.2 Tangential Stresses, σ_t, at the Tunnel Springline (Case 1) 344

B.3 Tangential Stresses, σ_t, at the Tunnel Crown (Case 1) 345

B.4 Axial Stresses, σ_a, at the Tunnel Springline (Case 1) 346

Figure Page

B.5 Axial Stresses, σ_a, at the Tunnel Crown (Case 1) 347

B.6 Shear Stresses, τ_{ar}, at the Tunnel Springline (Case 1) 348

B.7 Shear Stresses, τ_{ar}, at the Tunnel Crown (Case 1) 349

B.8 Radial Displacements, U_r, at the Tunnel Springline (Case 1) 350

B.9 Radial Displacements, U_r, at the Tunnel Crown (Case 1) 351

B.10 Radial Displacement Profiles at the Tunnel Springline (Total Values; Case 1) 352

B.11 Radial Displacement Profiles at the Tunnel Crown (Total Values; Case 1) 353

B.12 Radial Stresses, σ_r, at the Tunnel Crown (Case 2) 354

B.13 Tangential Stresses, σ_t, at the Tunnel Springline (Case 2) 355

B.14 Tangential Stresses, σ_t, at the Tunnel Crown (Case 2) 356

B.15 Axial Stresses, σ_a, at the Tunnel Springline (Case 2) 357

B.16 Axial Stresses, σ_a, at the Tunnel Crown (Case 2) 358

B.17 Shear Stresses, τ_{ar}, at the Tunnel Springline (Case 2) 359

B.18 Shear Stresses, τ_{ar}, at the Tunnel Crown (Case 2) 360

B.19 Radial Displacements, U_r, at the Tunnel Springline (Case 2) 361

B.20 Radial Displacements, U_r, at the Tunnel Crown (Case 2) 362

B.21 Radial Displacement Profiles at the Tunnel Springline (Total Values; Case 2) 363

B.22 Radial Displacement Profiles at the Tunnel Crown (Total Values; Case 2) 364

Figure Page

B.23 Radial Stresses, σ_r, at the Tunnel Crown (Case 3) 365

B.24 Tangential Stresses, σ_t, at the Tunnel Springline (Case 3) 366

B.25 Tangential Stresses, σ_t, at the Tunnel Crown (Case 3) 367

B.26 Axial Stresses, σ_a, at the Tunnel Springline (Case 3) 368

B.27 Axial Stresses, σ_a, at the Tunnel Crown (Case 3) 369

B.28 Shear Stresses, τ_{ar}, at the Tunnel Springline (Case 3) 370

B.29 Shear Stresses, τ_{ar}, at the Tunnel Crown (Case 3) 371

B.30 Radial Displacements, U_r, at the Tunnel Springline (Case 3) 372

B.31 Radial Displacements, U_r, at the Tunnel Crown (Case 3) 373

B.32 Radial Displacement Profiles at the Tunnel Springline (Total Values; Case 3) 374

B.33 Radial Displacement Profiles at the Tunnel Crown (Total Values; Case 3) 375

C.1 Radial Stresses, σ_r, at the Tunnel Springline (Hyperbolic) 377

C.2 Radial Stresses, σ_r, at the Tunnel Crown (Hyperbolic) 378

C.3 Tangential Stresses, σ_t, at the Tunnel Springline (Hyperbolic) 379

C.4 Tangential Stresses, σ_t, at the Tunnel Crown (Hyperbolic) 380

C.5 Axial Stresses, σ_a, at the Tunnel Springline (Hyperbolic) 381

C.6 Axial Stresses, σ_a, at the Tunnel Crown (Hyperbolic) 382

C.7 Shear Stresses, τ_{ar}, at the Tunnel Springline (Hyperbolic) 383

Figure Page

C.8 Shear Stresses, τ_{ar}, at the Tunnel Crown (Hyperbolic) 384

C.9 Radial Displacements, U_r, at the Tunnel Springline (Hyperbolic) 385

C.10 Radial Displacement Profiles at the Tunnel Springline (Total Values; Hyperbolic) 386

C.11 Radial Displacement Profiles at the Tunnel Crown (Total Values; Hyperbolic) 387

C.12 Radial Stresses, σ_r, at the Tunnel Springline (Elasto-Plastic) 388

C.13 Radial Stresses, σ_r, at the Tunnel Crown (Elasto-Plastic) 389

C.14 Tangential Stresses, σ_t, at the Tunnel Springline (Elasto-Plastic) 390

C.15 Tangential Stresses, σ_t, at the Tunnel Crown (Elasto-Plastic) 391

C.16 Axial Stresses, σ_a, at the Tunnel Springline (Elasto-Plastic) 392

C.17 Shear Stresses, τ_{ar}, at the Tunnel Springline (Elasto-Plastic) 393

C.18 Shear Stresses, τ_{ar}, at the Tunnel Crown (Elasto-Plastic) 394

C.19 Radial Displacements, U_r, at the Tunnel Springline (Elasto-Plastic) 395

C.20 Radial Displacement Profiles at the Tunnel Springline (Total Values; Elasto-Plastic) 396

C.21 Radial Displacement Profiles at the Tunnel Crown (Total Values; Elasto-Plastic) 397

D.1 Radial Displacement Profiles at the Tunnel Springline (Total Values; DEL=0.0; RL=1R) 399

D.2 Radial Displacement Profiles at the Tunnel Crown (Total Values; DEL=0.0; RL=1R) 400

Figure Page

D.3 Radial Displacement Profiles at the Tunnel Springline (Total Values; DEL=1R; RL=1R) 401

D.4 Radial Displacement Profiles at the Tunnel Crown (Total Values; DEL=1R; RL=1R) 402

D.5 Radial Displacement Profiles at the Tunnel Springline (Total Values; DEL=0.0; RL=2R) 403

D.6 Radial Displacement Profiles at the Tunnel Crown (Total Values; DEL=0.0; RL=2R) 404

D.7 Radial Displacement Profiles at the Tunnel Springline (Partial Values; DEL=0.0; RL=2R) 405

D.8 Radial Displacement Profiles at the Tunnel Crown (Partial Values; DEL=0.0; RL=2R) 406

LIST OF SYMBOLS

A_s	Area of the support cross section
c	Cohesion of the ground
C	Compressibility ratio
DEL	Delay of support installation
DEL_{SE}	Delay of support installation as defined by Schwartz and Einstein (1980)
E	Young's modulus of ground
E_{av}	Average Young's modulus
E_i	Initial Young's modulus for the hyperbolic model
E_s	Young's modulus of support
E_1	Minimum Young's modulus for transverse isotropic ground
E_2	Maximum Young's modulus for transverse isotropic ground
F	Flexibility ratio
G	Shear modulus
G_1, G_2	Shear moduli for transverse isotropic rock
I_s	Moment of inertia of the support cross section
I_1, I_2, I_3	First, second and third invariants of the stress tensor
J_2, J_3	Second and third invariants of the stress deviation tensor
K	Modulus number for the hyperbolic model
K_{ur}	Unloading-reloading modulus number
K_0	Initial stress ratio P_h/P_v (P_a=P_h if not otherwise specified)

m	Shape factor of the Ramberg and Osgood's function
$\bar{m}$	Empirical parameter of the Hoek-Brown failure criterion
M	Bending moment
n	Exponent of the hyperbolic function
P_a	Initial axial stress (horizontal, parallel to tunnel axis)
P_{atm}	Atmospheric pressure
P_h	Initial horizontal stress (normal to tunnel axis)
P_v	Initial vertical stress
Q	Plastic potential function
r	Distance from tunnel axis
R	Tunnel radius
R_f	Failure ratio for the hyperbolic model
RL	Round length
$\bar{s}$	Empirical parameter of the Hoek-Brown failure criterion
S_i	Initial slope (at face) of convergence profile
S_p	Final slope (far from face) of convergence profile
th	Liner thickness
T	Thrust force in the arch
T_a	Axial thrust
U_a	Axial displacement
U_r	Radial displacement
U_{rf}	Radial displacement at tunnel face
U_{rmax}	Radial displacement far behind tunnel face
U_t	Tangential displacement

U_0	Asymptote parameter for the Ramberg-Osgood function
X	Distance from the tunnel face
Y	Yield function
γ_{xy}	Shear strain (x-y plane)
γ_{yz}	Shear strain (y-z plane)
γ_{zx}	Shear strain (z-x plane)
ϵ_a	Axial strain
ϵ_x	Strain (x-direction)
ϵ_y	Strain (y-direction)
ϵ_z	Strain (z-direction)
$\bar{\Theta}$	Lode angle
λ_M	Bending moment reduction factor
λ_T	Thrust reduction factor
$\lambda_{T(SE)}$	Thrust reduction factor as defined by Schwartz and Einstein (1980)
ν	Poisson's ratio of ground
ν_s	Poisson's ratio of support
ν_1, ν_2	Poisson's ratios for transverse isotropic ground
σ_a	Axial stress
σ_c	Uniaxial compressive strength of intact rock
σ_{cm}	Uniaxial compressive strength of rock mass
σ_r	Radial stress
σ_t	Tangential stress
σ_1	Major principal stress
σ_2	Intermediate principal stress
σ_3	Minor principal stress
τ_{ar}	Shear stress (plane a-r)

τ_{rt}	Shear stress (plane r-t)
τ_{ta}	Shear stress (plane t-a)
ϕ	Friction angle
ψ	Dilation angle

1. INTRODUCTION

1.1 Three Dimensional Characteristics of the Tunnelling Problem

A tunnel can be regarded as a highly constrained three dimensional structure wherein complex stress redistribution takes place during face advance.

The usual approach to tunnel design completely neglects the near face behavior and the opening is reduced to a hole in a plate deforming under plane strain conditions. Closed form solutions are available for simple plane strain problems in linear elastic materials, and for those cases where numerical analyses are needed a simple two dimensional model results in a substantial reduction of computational costs. Recently computers able to handle three dimensional finite element simulations economically have become available to engineers.

These simplifications can be more or less acceptable depending on the parameters governing the real problem and on what kind of information the analysis is expected to provide. In general, though, a three dimensional approach is more appropriate for most tunnelling problems.

The three dimensional near face behavior has to be considered if one or more of the following circumstances occur:

1) The stress state at the tunnel face has to be calculated in order to assess tunnel stability in that

region;

2) The tunnel is excavated in rock exhibiting stress path dependency. In this case modelling the complex stress paths occurring near the excavation front may be essential for a correct estimate of the stresses and deformations characterizing the opening far behind the tunnel face;

3) A support is installed relatively close to the tunnel face as the excavation proceeds. In this case a complex rock-structure load transfer process takes place that cannot be ignored during the support design stage;

4) In order to back-analyze the initial stress distribution in the rock mass and/or the rock deformation properties a monitoring program is established. Especially for those cases where only partial measurements can be taken (e.g., in deep tunnels deformation measurements are usually taken only behind the tunnel face) a sound knowledge of the near face behavior is needed for their interpretation.

On the other hand a plane strain two dimensional approach is sufficient if all the following conditions are met:

1) The stability of the tunnel face is taken for granted a priori (based, for instance, on previous experiences in the same or in similar ground conditions);

2) The rock is known to behave as a linear elastic material;

3) The liner, if any, is placed far from the tunnel face (at least two diameters) and the load on the support

depends almost exclusively on long term (i.e., time dependent) rock behavior.

Simplified approaches were developed in the past to account for the "face effect" in tunnel design, especially in order to predict the load on the support. The "Convergence Confinement Method" (CCM) proposed by Fenner (1939) and discussed by many other authors in the past few years has played a key role in understanding the ground-liner interaction in advancing tunnels. Techniques have also been proposed to simulate the three dimensional near face behavior by means of simple two dimensional plane strain models (these simplified approaches will be the object of further discussion in Chapter 2).

The use of these simplified means can be acceptable in certain cases, but knowledge of their limitations as well as a sound understanding of the complexities involved in real tunnelling problems are a basic requirement without which misleading approaches may lead to unrealistic conclusions.

Simplified three dimensional axisymmetric analyses have been carried out extensively to study stress distribution, deformations and ground support interaction near the tunnel face. The limitation of this approach is found in its lack of generality as it is acceptable only for very specific initial stress distributions, ground conditions and excavation-support procedures. For this reason extension of the results obtained by axisymmetric analyses to more general tunnelling conditions must be undertaken with great care.

Some studies on truly three dimensional numerical and physical models have been conducted in the past. However most of the efforts have been directed towards the investigation of particular case histories, and only the case of unlined tunnels in linear elastic media have been the object of relatively extensive parametric studies.

A critical review of general design concepts and of the literature dealing with near face effects in tunnels is presented in Chapter 2.

1.2 Purpose of the research

The purpose of this research is to analyze the tunnelling problem from a three dimensional perspective in order to study stresses and deformations as they develop near the face of an advancing tunnel. The investigation is based on FEM analyses and is restricted to deep tunnels with circular cross section and excavated by a full-face excavation technique.

The case of unlined tunnels was investigated first (Chapter 3 to Chapter 5) and linear elastic isotropic, linear elastic anisotropic, non-linear elastic and elasto-plastic constitutive relationships were selected to simulate different rock conditions.

The main objective is to provide a useful tool for the interpretation of monitoring data, in particular of convergence and relative displacement measurements (as given by radial extensometers) as they are often available for deep tunnels.

The stresses around the opening are also investigated and the factors generating stress concentrations at specific locations are discussed as they affect the stability of the tunnel.

The case of supported tunnels was analyzed (Chapter 6) in order to study the effect of rock-liner interaction near the tunnel face. Both support and rock masses were assumed to obey linear elasticity. The effect of relative stiffness rock-support, Delay (DEL) of liner installation, excavation Round Length (RL) and rock anisotropy were investigated (note: DEL and RL are defined in Chapter 2).

The main objectives were selected as follows:

1) investigate the effects of different support conditions on measurements taken during face advance;

2) study the rock-liner load transfer mechanism in order to identify the most important parameters to be considered in liner design.

Finally, data obtained from a tunnel in sedimentary rock (Donkin-Morien Project, Sidney, Nova Scotia) will be analyzed in Chapter 7. The main objectives of this part of the research can be summarized as follows:

1) verify the applicability of the theoretical findings (Chapter 3 to Chapter 6) to a real tunnelling problem;

2) propose improvements to the current monitoring practice in order to obtain data more useful for

back-analysis purposes;

3) investigate the possibility of predicting the ultimate deformed configuration of the tunnel, far behind the tunnel face, on the basis of partial near face measurements. This should permit to back-analyze tunnel behavior more rapidly.

The ultimate goal of this research as a whole is to provide information to improve the design process both in terms of prediction of tunnel performance and back-analysis of monitoring data. For this purpose the effort has been directed towards a better understanding of the physical phenomena characterizing advancing tunnels excavated in various conditions. A selective approach was chosen by which more complex constitutive relationships and support conditions were progressively introduced in the study.

2. NEAR FACE BEHAVIOR OF DEEP TUNNELS

2.1 Introduction

Up to now tunnelling problems have been studied mostly by means of two dimensional approaches. The availability of two dimensional closed form solutions and the difficulties involved with large three dimensional numerical analyses have influenced this trend. However for many cases a two dimensional approach is not adequate because it doesn't account for complexities that profoundly affect tunnel performances and that should be fully considered in design.

Simplified three dimensional axisymmetric analyses have been carried out by many authors in the past thirty years. The assumption of axial symmetry (with respect to the tunnel axis) for tunnel geometry, material properties and initial stress field greatly reduces the computational effort. This simplification is acceptable only if the following conditions are met:

1) The tunnel cross section is circular,

2) The tunnel is deep (i.e., far from any free surface, the effect of gravity can be neglected),

3) The deformation properties of the rock and the initial in situ stresses are constant in any direction normal to the tunnel axis, and

4) The excavation-support technique is consistent with the axisymmetric configuration.

Despite the restrictive axisymmetric assumption some valuable parametric studies have been conducted based on this simplified approach and they will be discussed in a later paragraph.

In the present chapter past efforts to account for the three dimensionality of the tunnelling problem will be summarized and critically reviewed. Some simplified design tools will also be discussed and their merits and limitations pointed out.

The case of unlined tunnels will be discussed first and various rock conditions will be considered. Then the effect of the liner will be introduced and elements of interest found in literature will be summarized. The popular "Convergence Confinement" concept and some other simplified techniques developed to analyze the ground-support interaction will also be discussed.

2.2 Unlined Tunnels

2.2.1 Unlined Tunnels in Linear Elastic Rock

The most extensive studies on both numerical and physical models have been conducted based on the assumption of linear elasticity. This is obviously the simplest problem to be solved because of the following reasons:

1) This is the simplest stress strain relationship available for deformable materials, requiring only two material constants (i.e., E and ν) to be defined,

2) Closed form solutions are provided by the elasticity theory that allows comparison at certain locations (i.e., far behind the tunnel face),

3) Availability of photoelastic techniques for the determination of stresses in elastic media,

4) Computational advantages for numerical modelling including the possibility of using the Boundary Element Method, and

5) The stress path independency of linear elastic materials allows, for unlined tunnels, simulation of excavation in a single step.

At a time when computers did not allow large truly three dimensional analyses to be carried out economically, extensive photoelastic studies were performed for this purpose.

Galle and Wilhoit (1962) studied the stresses around a wellbore based on a three dimensional approach. Various load combinations were applied to the epoxy resin model so that, by proper superposition of the obtained solutions, the state of stress due to any combinations of principal normal stresses and internal pressure in the wellbore could be obtained.

The results were presented by the authors in the form of contour curves for each stress component, for the axisymmetric and the non-axisymmetric loading cases (Figures 2.1 and 2.2). They show the complexity of the three dimensional stress distribution near the end of the cavity.

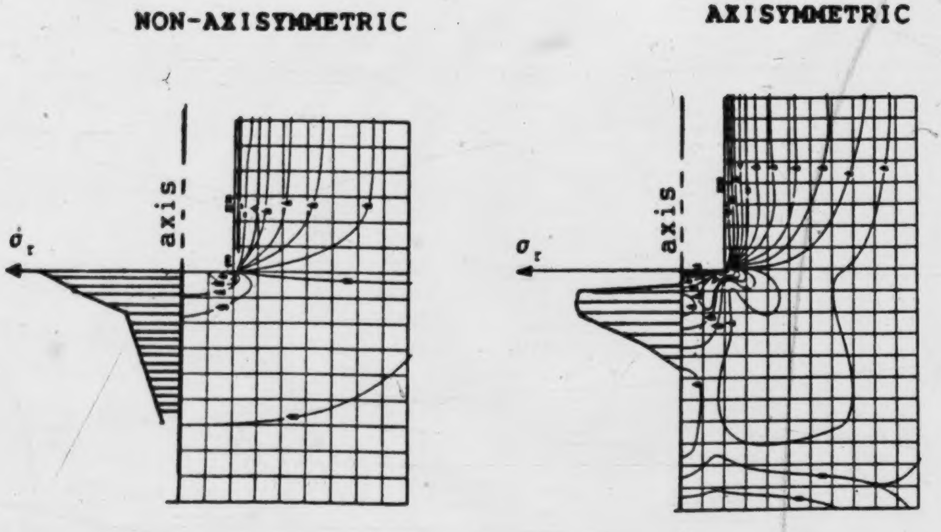
NON-AXISYMMETRIC
AXISYMMETRIC
σ_r
axis
σ_r
axis

Figure 2.1 Radial Stresses, σ_r, in the Axial Plane for Axisymmetric and Non-Axisymmetric Loading Conditions (Modified after Galle and Wilhoit, 1962).

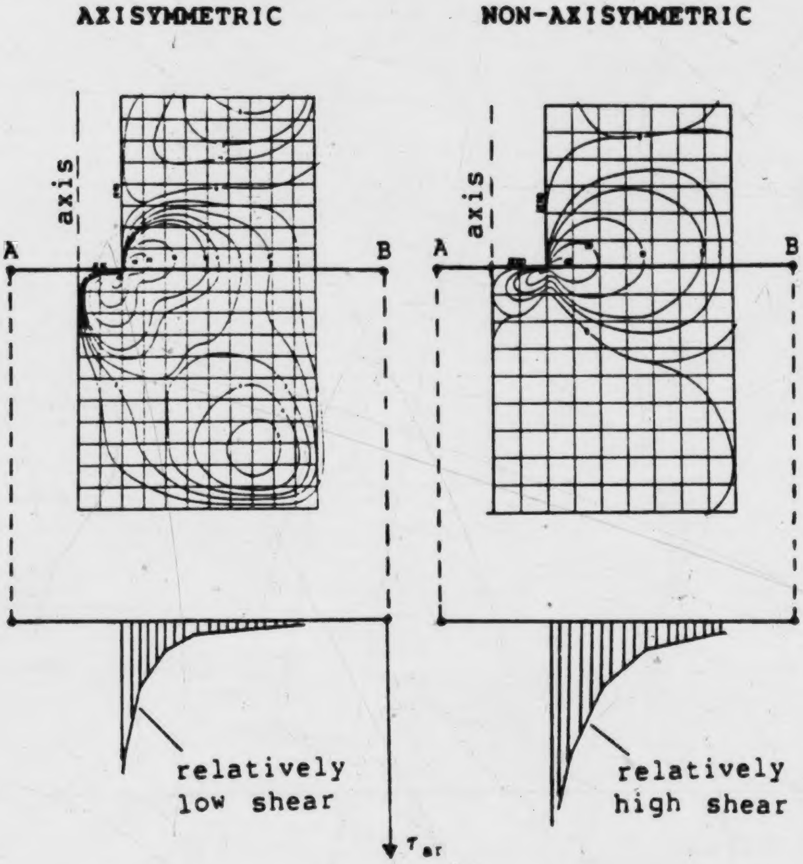
AXISYMMETRIC
NON-AXISYMMETRIC
axis
axis
A
B
A
B
relatively low shear
relatively high shear
τ_{ar}

Figure 2.2 Shear Stresses, τ_{ar}, in the Axial Plane for Axisymmetric and Non-Axisymmetric Loading Conditions (Modified after Galle and Wilhoit, 1962).

For the non-axisymmetric load (uniaxial load normal to the axis of the hole) a radial stress peak along the tunnel axis is found at the tunnel face (Figure 2.1). For the axisymmetric load conditions low radial stresses are found at the face and a stress peak is detected about one radius ahead of the excavation front. This is partly due to the initial stress in the axial direction, P_a, that tends to generate tensile radial stress at the tunnel face (see later in this chapter).

In Figure 2.2 the shear stresses (τ_{ar}) are shown for the axisymmetric and the non-axisymmetric cases and a stress peak is found, along AB, at the corner. It is interesting to notice that the magnitudes of the shear stresses along AB are very different for the two cases. As it will be discussed in Chapter 3, the shear stress near the tunnel face is associated with deformations that may affect measurements taken at that location considerably.

Some limitations of this photoelastic analysis must be pointed out. First, the epoxy resin used for the models had a Poisson's ratio of about 0.48 whereas the Poisson's ratio of most rocks ranges between 0.15 and 0.3. Moreover, the model used by Galle and Wilhoit (op.cit.) was criticized by Abel and Lee (1973) for being too small and thereby affected by the boundaries. However, Galle and Wilhoit's results emphasized some of the key features that characterize the three dimensional stress distribution mechanism near the face of an advancing tunnel.

In order to analyze the deformations occurring around the bottom of a borehole, de la Cruz and Goodman (1969) carried out a series of axisymmetric finite element analyses assuming a linear elastic constitutive relationship. Both axisymmetric and non-axisymmetric stress fields were considered. By means of non-linear regression and polynomial interpolation they derived expressions for radial displacements at several points along the axis of the borehole.

Applying the same axisymmetric model technique Coates and Yu (1970) studied the stress distribution around the bottom of a borehole and derived stress concentration factors.

Truly three dimensional numerical studies able to investigate stresses and deformations around tunnels in non-axisymmetric initial stress conditions were conducted by the use of the Boundary Integral Equation Method (BIEM). Using this technique Hocking (1976) calculated stress concentration factors around the end of a cylindrical cavity in an elastic medium. Several initial stress ratios, K_0, and Poisson's ratios, ν, were selected.

By the application of the same method Niwa et al. (1978) investigated stresses and displacements around the face of an advancing tunnel. The results were obtained for three fundamental cases. For the first case a unidirectional normal stress field, perpendicular to the tunnel axis, was considered. For the second the initial stresses were taken parallel to the axis of the tunnel where shear stresses in the axial planes (τ_{ar}) were applied to the model for the third case. By appropriate superposition of these results any initial stress condition can be simulated (the initial shear stress in the transverse plane, τ_{rt}, must be neglected). Niwa et al. (op.cit.) presented the first parametric study of this kind. Their results are applicable to non-axisymmetric stress conditions ($K_0 \neq 1$) and have been used for comparison with field data by Lo and Lucajic (1984) and Yuen et al. (1986). Niwa's work has several limitations that reduce its applicability to practical problems:

1) The displacement field around the excavation is only depicted at few locations. Radial displacements are only shown at the tunnel wall and along a line radiating from the tunnel face. A more detailed description of the deformations occurring in the rock at different distances from the tunnel wall is needed for practical purposes, e.g.,for the interpretation of monitoring data. This limitation is also found in most numerical analyses available in literature,

2) The effect on radial displacements of the initial axial stresses is not considered. It will be shown in this research that neglecting the initial axial stress is not acceptable if relatively high K_0 values characterize the initial stress field .

In Figure 2.3, the principal stresses on an axial plane for the two load conditions (uniaxial stress normal to the tunnel axis and uniaxial stress parallel to the tunnel axis)

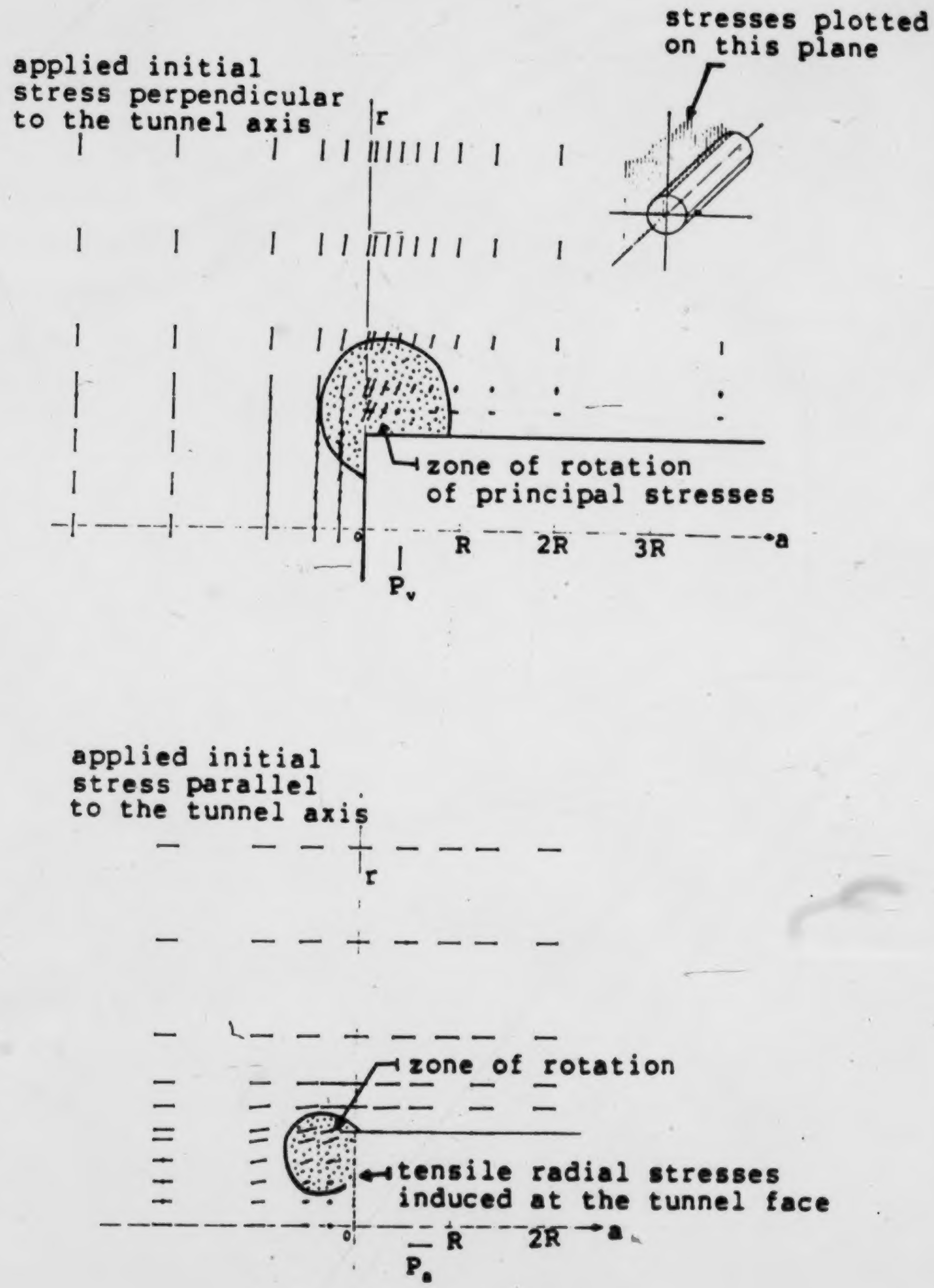
stresses plotted on this plane
applied initial stress perpendicular to the tunnel axis
r
zone of rotation of principal stresses
o
R
2R
3R
a
P_v
applied initial stress parallel to the tunnel axis
r
zone of rotation
tensile radial stresses induced at the tunnel face
o
R
2R
a
P_a

Figure 2.3 Principal Stresses on the Axial Plane for Initial Stress Normal (a) and Parallel (b) to the Tunnel Axis (Modified after Niwa et al.,1978).

are shown. The rotation of the principal stress trajectories near the face of the tunnel (arching) is visible. It can also be observed that the axial stress, P_a, generates tensile radial stresses at the tunnel face and it can be concluded that the action of P_a tends to reduce the radial stress concentration at the face. This observation is important because high radial stresses at the tunnel face may generate instabilities at that location.

The influence of the initial axial stresses on the horizontal deformations at the tunnel face was investigated by Descoeudres (1974) who carried out three dimensional finite element analyses for tunnels in linear elastic and elasto-plastic rock. As shown in Figure 2.4, high P_a values result in considerable bulging of the excavation front whose effect on the radial displacements, and hence on the measurements taken during tunnel advance, will be one of the objects of the present research.

2.2.2 Effects of Non-Isotropic Rock Behavior

Many rocks and rock masses behave as anisotropic materials.

The effects of texture and micro-structural features on rock anisotropy were summarized by Crea et al. (1980). The idea of modelling stratified or laminated rock masses as anisotropic, elastic media led Kawamoto (1963) to develop a closed form solution for the analysis of stresses and displacements around circular tunnels in non-isotropic rock.

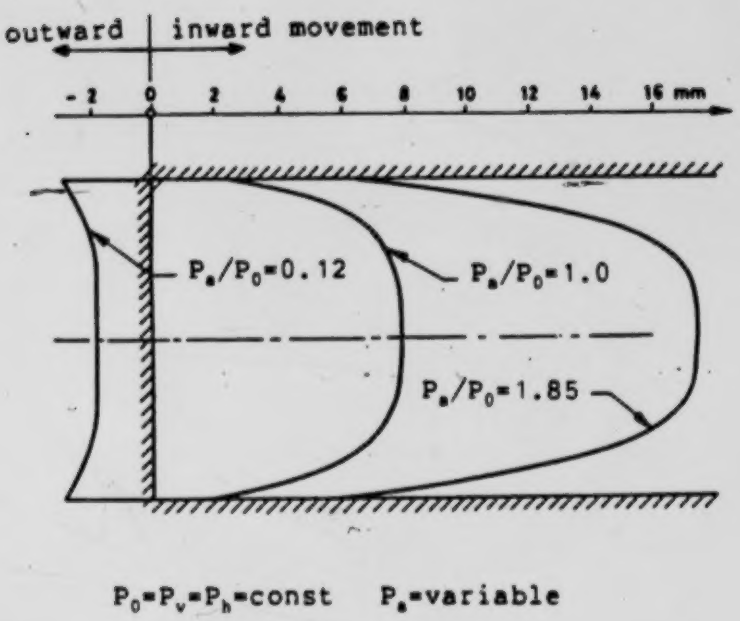

Figure 2.4 Effect of the Initial Axial Stress, P_a, on the Horizontal Movement at the Tunnel Face (Modified after Descoeudres, 1974)

Zienkiewicz et al. (1966) investigated the stresses around a circular tunnel in anisotropic rock by two dimensional finite element simulations, and a three dimensional approach for the modelling of tunnels in anisotropic jointed rock was proposed by Wittke(1970). Gerrard(1977) summarized a large number of experimental results, many of which were conducted on large samples, and showed that the ratio between the maximum and the minimum Young's moduli can reach very high values (in excess of twenty) for some metamorphic rocks.

For thinly layered or laminated rocks perfect symmetry of behavior about any axis perpendicular to the planes of stratification can be assumed (see Figure 2.5). In this case, the medium is said to obey transverse isotropy and the general theory for elastic anisotropic materials can be reduced to a simple form (discussed in Chapter 4).

The non-isotropic behavior of rock has considerable implications on tunnelling as it promotes high stress concentrations near the opening (Lekhnitskii, 1963; Savin, 1970; Kawamoto, op.cit.) and also affects the displacements measured during face advance by the field instrumentation. However, the problem of tunnelling in anisotropic rock masses has not been much studied in the past and few three dimensional analyses are found in the literature. The main reason is that simplified axisymmetric models cannot be used for non-isotropic rock conditions, except for the special case of tunnels with axis perpendicular to the planes of stratification.

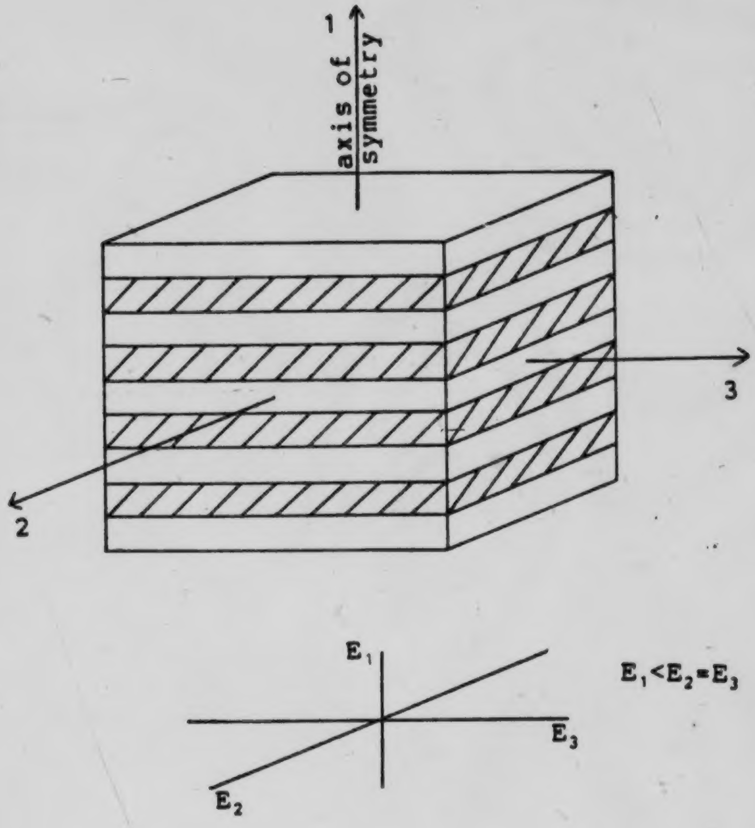
1
axis of symmetry
2
3
E_1
E_2
E_3
$E_1<E_2=E_3$

Figure 2.5 Schematic Representation of Transverse Isotropic Medium

The effects of anisotropy on stress changes and deformations due to tunnelling constitute one of the objects of investigation of the present research.

2.2.3 Unlined Tunnels in Non-Linear and Non-Elastic Media

Most geologic media exhibit non-linear stress-strain relationships, and energy dissipation occurs as the straining process takes place.

In the pre-failure range, the rock mass tends to soften (increase its deformability) as the applied deviatoric stress is increased and, during unloading, only a portion of the total strain is recovered. Large scale triaxial tests performed by Natau et al.(1983) on interbedded sedimentary rock and tests on large granite blocks conducted by Nose (1964) indicated non-linear stress-strain relationships for the rocks tested, and Natau et al.(op.cit.) also observed that the strain induced in the samples was partially unrecoverable.

If failure is reached a decrease in the strength of the material may occur and part of the energy stored is released.

Non-linear and non-elastic behavior leads to a stress redistribution process around the opening that affects the deformations in the rock mass and the load on the support.

Desai and Reese (1970) studied the propagation of the plastic zone in proximity of a borehole in elastic, ideal plastic ground. They made use of the finite element method and modelled the borehole as an axisymmetric problem.

Daemen and Fairhurst (1972) carried out a series of axisymmetric finite element analyses in order to study the behavior of deep tunnels excavated in failing rock (see also Daemen, 1975). The constitutive relationship was approximated by a strain dependent variation of a set of orthotropic elastic constants; in this manner a stiffness reduction as defined by a set of stress-strain curves as well as a volumetric increase associated with failure could be simulated.

Two sets of analyses were performed for different material types, with or without loss of strength in the post failure range. The mesh was loaded by applying an external boundary pressure that was gradually increased. For stress path dependent materials, as the ones considered for the rock by Daemen and Fairhurst, a more realistic simulation (i.e., incremental excavation in a pre-stressed mesh) would have been more appropriate. The results showed that the plastic zone tends to develop first at the tunnel wall behind the face where high deviatoric stresses tend to concentrate. If the tunnel is excavated in ground exhibiting weakening a substantially larger volume of material fails, due to the more pronounced stress redistribution process that takes place under these conditions. If a relatively high pressure is applied to the mesh boundaries the core immediately ahead of the excavation front fails also. These analyses showed that rock failure may increase tunnel closure considerably.

A truly three dimensional finite element analysis was conducted by Descoeudres (1974) in order to study the behavior of tunnels in elasto-plastic media under non-axisymmetric load conditions. The Drucker-Prager failure criterion was selected for the rock and an initial stress ratio $K_0=2$ was chosen. Due to the low strength of the rock with respect to the applied initial in situ stress an extensive plastic zone developed at the tunnel crown, at the springline and ahead of the excavation front. The convergence at the springline and at the crown for the plastic case was, respectively, two and six times larger than for the elastic case. The quarter mesh used by Descoeudres was very coarse and small (four diameters long and two diameters wide) and no incremental excavation was performed; all these factors make his results interesting but unreliable in terms of accuracy.

Ranken and Gaboussi (1975) carried out a series of linear and non-linear axisymmetric analyses by means of the finite element method. Both frictionless and frictional elastic, ideal plastic materials were considered. The study was mostly directed towards the investigation of tunnels in soils, and because of the low strength assumed for the ground, extensive plastic zones as well as large convergence resulted. The stresses in an axial plane (plane containing the axis of the tunnel) are shown in a contour map and the variations due to yielding are clearly visible in proximity of the excavation.

Panet and Guenot (1982) performed a series of axisymmetric finite element analyses to investigate the behavior of tunnels in elasto-plastic purely cohesive materials. The model was submitted to a uniform isotropic boundary pressure P_0 without simulating incremental excavation. The analyses were carried out for four different stability numbers, $N_s=2P_0/c_u$, and plastic zones around the excavation and convergence curves for the four cases were depicted. The chosen purely cohesive model restricts the applicability of these analyses to tunnels excavated in saturated soils and rocks exhibiting a very low permeability.

The literature review presented above leads to the following conclusions:

1) Among the authors mentioned, only Descoeudres (op.cit.) conducted a truly three dimensional analysis where the remainder based their research on the restrictive axisymmetric assumption.

2) Only Ranken and Gaboussi (op.cit.) conducted an incremental excavation as is appropriate for stress-path dependent materials. All the others authors mentioned above simply applied an external pressure to the pre-excavated initially unstressed mesh.

3) The displacements occurring far from the tunnel face are never presented even though they are often measured in the field by means of radial borehole extensometers. This is

in part understandable because a large size finite element mesh is needed to obtain reasonably accurate displacements relatively far from the excavation.

4) Descoeudres (op.cit.) and Ranken and Gaboussi (op.cit.) assumed the ground to behave as an elasto-plastic, frictional medium but they did not specify the chosen flow rule. Most likely associated flow plasticity was selected for their analyses. This constitute a major limitation because, generally, frictional geologic media do not exhibit as much dilation at failure as predicted by the associated flow rule.

2.3 Rock-Support Interaction During the Excavation of Supported Tunnels

In order to study the load transfer mechanism taking place during the advance of supported tunnels, a complex rock-structure interaction problem needs to be solved.

Mining is a progressive activity that causes changes in the tunnel geometry. When a portion of the rock is removed, displacements take place in the rock mass and the external and body forces produce some work that is expended in deforming the rock and the support. As a result of this energy transfer process the support attracts more or less load, depending on its stiffness (relative to the stiffness of the rock) and on the installation procedure adopted.

In Figure 2.6, the excavation-support sequence in an advancing tunnel is depicted schematically. The parameter

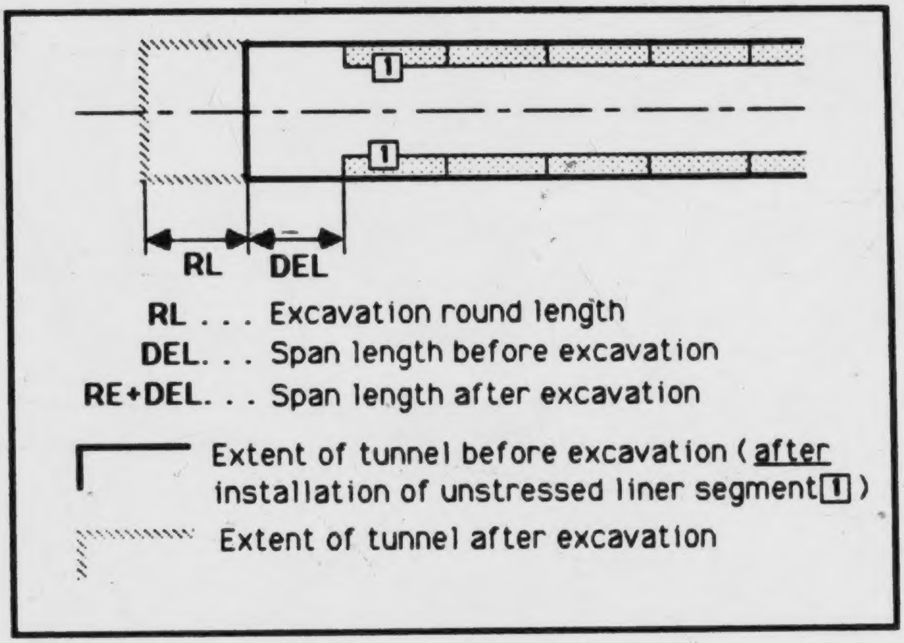
1
1
RL
DEL
RL . . . Excavation round length
DEL. . . Span length before excavation
RE+DEL. . . Span length after excavation
Extent of tunnel before excavation (after installation of unstressed liner segment 1)
Extent of tunnel after excavation

Figure 2.6 Schematic Representation of the Excavation-Support Sequence. RL=Round Length ; DEL=Delay.

"Delay" (DEL) is introduced which is the distance between the leading edge of the liner and the tunnel face immediately after installation of an unstressed liner segment and immediately before excavation (note that some authors give a different definition). The length of the tunnel section excavated at each step (equal to the length of one liner section) is called excavation "Round Length" (RL).

The importance of accounting for the relative stiffness of rock and support and for the delay has been recognized for a long time. However the influence of the excavation round length on the final load distribution on the liner has been neglected by most authors.

2.3.1 The Convergence Confinement Method (CCM)

The CCM was introduced by Fenner(1939) and discussed more recently by many authors (Gesta et al., 1980; Kerisel, 1980; Duddeck, 1980; Brown et al., 1983). In its simplest form it consists in drawing two characteristic curves, one for the ground and the other for the support, relating radial displacements U_r to radial pressure σ_r at the tunnel wall.

In Figure 2.7, Point A represents the initial undisturbed condition for which $\sigma_r/P_0=1$ (P_0 is the initial hydrostatic in situ stress). Point B, intersection of the two characteristic curves, represents the equilibrium conditions reached, far behind the excavation front, by the

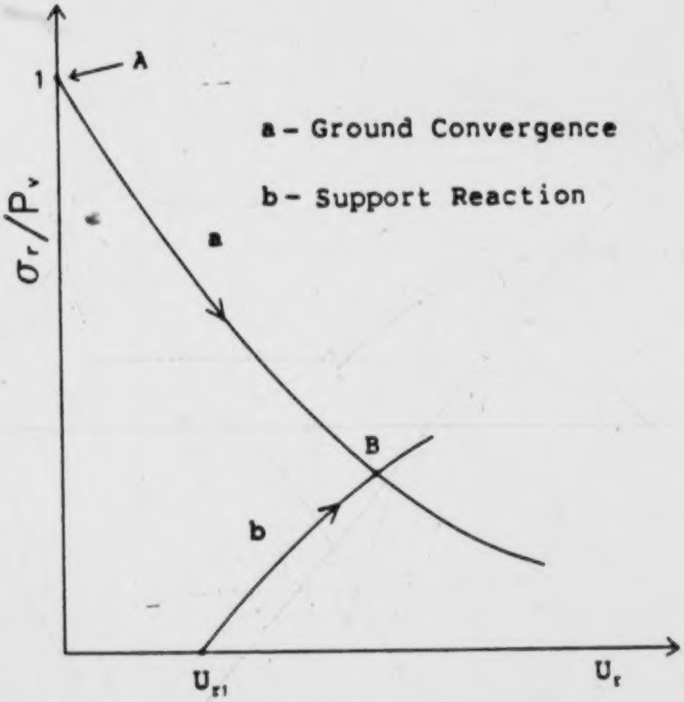
1
A
a - Ground Convergence
b - Support Reaction
σ_r/P_v
a
B
b
U_{r1}
U_r

Figure 2.7 Schematic Representation of the Convergence Confinement Method

ground-support system. The CCM accounts for the effects of the relative stiffness of ground and liner and for the delay. As a conceptual model, the method has been used successfully by several authors to explain aspects of the rock-structure interaction. Daemen(1975) showed how a pressure increase on the liner has to be expected in case of rock failure; Lombardi(1970) used the CCM to discuss the effect of a weak rock core on tunnel face stability; Yow and Goodman(1987) applied the concept of ground reaction to block stability problems. As a practical design tool, the method presents several limitations:

1) The Ground Convergence Curve (Curve a in Figure 2.7) is unknown a priori and difficult to determine,

2) The radial displacement occurring before support activation (U_{r1} in Figure 2.7) is also unknown and a three dimensional approach is needed for its prediction (Daemen and Fairhurst, 1972; Panet and Guenot, 1982),

3) The complex three dimensional load transfer mechanism taking place near the tunnel face is not well approximated by the method (see Eisenstein et al., 1984) and it completely neglects the stress concentration that may occur at the leading edge of the liner,

4) Far from the tunnel face a plane strain condition may not be reached in many real cases because of non-homogeneous stress distribution in the liner (along the axis of the tunnel), and

5) The convenience of the CCM is restricted to those cases where $K_0=1$ can be assumed (note: an extension for $K_0 \neq 1$ was presented by Pender, 1980, but only for a frictionless rock-liner interface).

The CCM is a simple tool that has the merit of emphasizing some of the important aspects governing the rock-liner interaction. However a comprehensive knowledge of the three dimensional near face conditions is essential to understand the value and the limitations of this method.

2.3.2 Modelling of Near Face Behavior by Simplified Two Dimensional Plane Strain Analyses

The importance of considering the three dimensionality of the tunnelling problem and the difficulties associated with three dimensional modelling led to the development of various simplified methods.

Panet(1976) suggested a two dimensional approach where the tunnel is modelled by a hole in a plate with a fictitious internal pressure equal to the initial in situ stresses. By decreasing the internal pressure a certain amount of radial displacement is allowed in order to account for the movement taking place ahead of the liner. The support is then installed and the remaining pressure is removed.

This method is based on the same principle as the CCM. The fictitious support pressure σ_r (see Figure 2.7) is applied to the wall of the tunnel and controls the convergence process up to the installation of the liner. Conceptually this model is far from reality because it completely neglects the shear stresses $\tau_{\theta r}$ associated with tunnel closure in proximity of the excavation front (see Lombardi, 1980). Moreover a set of practically relevant limitations affect this approach:

1) The amount of radial displacement to be allowed before liner installation is arbitrary;

2) The extension of the method to $K_0 \neq 1$ conditions is not straight forward because the amount of displacement to be allowed at each location around the axis of the tunnel is not known a priori (i.e., the deformed shape of the hole when the support is installed is unknown);

3) The delay in support installation is the only three dimensional feature considered. Other important aspects such as near face arching and excavation round length are neglected;

4) Simplified stress paths are modelled in the two dimensional simulations. This may lead to errors if stress dependent ground masses are considered.

Similar simplified methods were proposed by Laabmayr and Swoboda(1978) and Sakurai(1978). Laabmayr and Swoboda suggested a reduction of the elastic modulus of the core to simulate the radial displacement due to the delay; whereas Sakurai modelled the tunnel advance by changing the initial stresses in the finite element mesh according to a pre-defined function.

2.3.3 Review of Three Dimensional and Simplified Axisymmetric Numerical Analyses Found in Literature

Ranken and Gaboussi (1975) modelled the progressive excavation and support of tunnels in linear elastic and elasto-plastic media by a finite element axisymmetric model. The effects of the delay and of different soil conditions on stresses and deformations in the ground-support system were investigated. The action of the support resulted in both less convergence than for the unlined cases and in smaller plastic zones. These effects were more significant for the case of a liner installed immediately behind the tunnel face. The thrust forces calculated in the liner were higher for the case of zero delay and a peak load was detected at the leading edge of the support (about one radius behind the tunnel face). This load concentration is obviously associated with the three dimensional arching mechanism at the excavation front. The authors stressed the importance of a proper incremental simulation of the excavation support procedure.

Another extensive study by axisymmetric finite element analyses was carried out by Schwartz and Einstein (1980) in order to investigate the effect of delay and ground properties on the loads in the liner. Analyzing lined tunnels incrementally excavated in linear elastic media for different delays and relative stiffnesses ground-support they produced a delay factor $\lambda_{T(SE)}$ to be used in conjunction with the two dimensional relative stiffness solution

(Einstein and Schwartz, 1979).

In Figure 2.8, the approximately linear relationship between $\lambda_{T(SE)}$ and the delay DEL_{SE} is depicted. Note that DEL_{SE} is different from the delay defined earlier in this chapter and it measures the distance between the tunnel face and the mid-point of the leading support section. Based on a similar set of analyses Hutchinson(1982) suggested that the line in Figure 2.8 should be translated as shown.

Schwartz and Einstein (op. cit.) also carried out a set of analyses in elastic, ideal plastic material to investigate the effect of yielding on the loads on the support. The ground was characterized by a Drucker and Prager failure criterion and by an associated flow rule. A substantial increase in the load on the support was detected for yielding grounds especially if the support is installed with a relatively large delay. Liners installed very close to the face of the tunnel were found to be very effective in inhibiting the propagation of the plastic zone by providing a confinement to the surrounding medium.

Schwartz and Einstein's work certainly represents a valuable contribution to the study of rock-liner interaction, but it contains also some limitations that must be considered:

1) The axisymmetric model does not allow one to investigate the development of bending moments in the support;

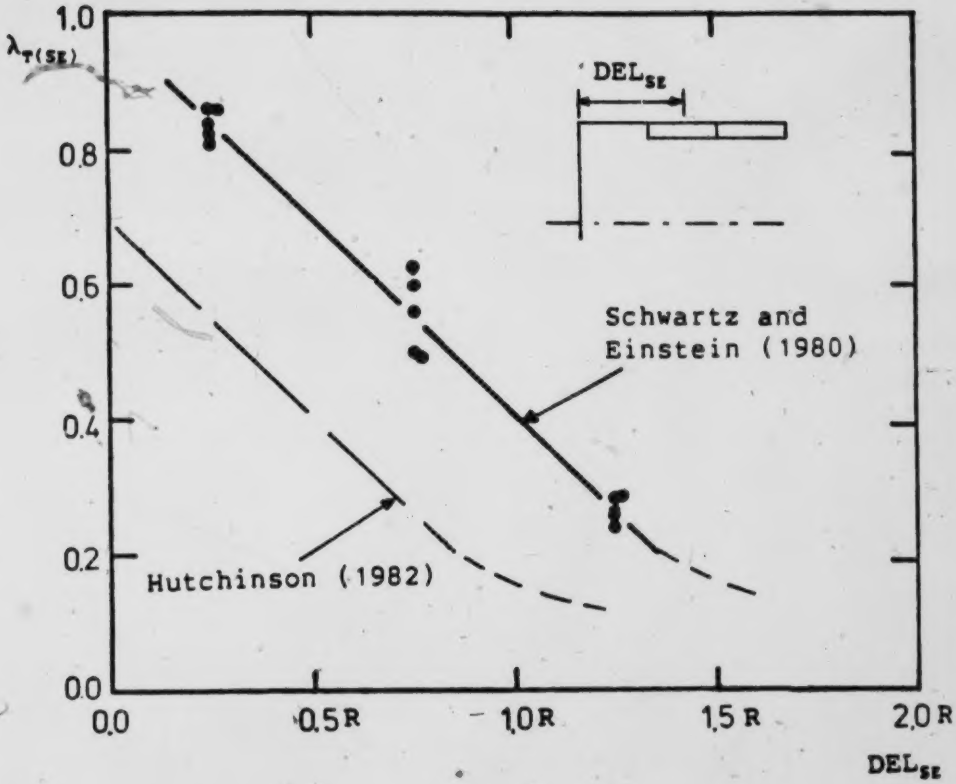

Figure 2.8 Support Delay Correction Factor (Modified after Schwartz and Einstein, 1980, and Hutchinson, 1982)

2) The excavation round length is not considered and the variability of the load in the liner is neglected;

3) The assumption of associated flow rule is not appropriate for frictional geologic media.

Other axisymmetric and truly three dimensional numerical analyses have been carried out, in the past years, in order to investigate the ground-support interaction and will be mentioned briefly for reference.

Gaboussi and Gioda (1977) investigated the effects of time dependent rock properties on advancing supported tunnels by means of axisymmetric finite element analyses. The Kelvin rheological model was adopted for the ground in series with a spring accounting for the instantaneous ground shear deformations. Both the cases of continuum excavation and stoppage for fully and partially lined tunnels were investigated.

Advancing unsupported and supported tunnels in creeping ground where studied by Hanafy and Emery (1980) and Hanafy and Emery(1982), by means of axisymmetric finite elements analyses. By expanding loads, displacements and strains into Fourier's series, initial stress ratios other than one were considered.

The effects of rock damage due to blasting on lined tunnels was discussed by Kaiser and Hutchinson (1982). A series of finite element axisymmetric analyses was performed and the damaged rock was assumed to behave as a linear elastic material.

Del Greco et al. (1986) performed truly three dimensional finite element analyses to investigate the behavior of a deep mine tunnel. The rock was assumed to behave as an elastic, ideal plastic material of the Drucker-Prager type with associated flow rule. The application of the rock bolts was simulated by nodal forces.

Some truly three dimensional finite element analyses were also carried out for the study of shallow tunnels.

By the use of a three dimensional finite element model, a subway tunnel in Nuremberg was analized by Gartung et al. (1979). An elasto-brittle plastic constitutive relationship was assumed for the ground and the heading bench excavation sequence was simulated. Shell elements were selected to model the thin shotcrete liner where confinement pressure was applied at the wall of the tunnel to account for the action of the tensioned rock bolts.

Wittke and Gell (1980) studied a shallow subway tunnel in Bachum by three dimensional finite element modelling. An elasto-plastic constitutive relationship was assumed for the ground and both heading-bench and full face excavation sequences were simulated.

Katzenbach and Breth (1981) investigated the surface settlements due to a tunnel excavated by NATM in Frankfurt clay. The soil behavior was approximated by a hyperbolic stress strain relationship and good agreement with field data was obtained.

The effects of the liner thickness and of the overburden on the ground surface settlements and on the stresses in the support were investigated by Pierau(1982) by means of three dimensional finite element analyses. The ground was assumed to be linear elastic and several E and ν values were considered.

A study of supported shield-excavated tunnels in linear elastic soil was conducted by Kasali and Clough (1983) by performing true three dimensional finite element simulations.

Heinz (1984) modelled tunnels in linear elastic soil driven by NATM. Both 'full face' and 'heading and bench' excavation techniques were investigated.

2.4 The Role of Back-Analysis in Tunnel Design

Since Rabcewicz(1964) introduced the New Austrian Tunnelling Method (NATM) monitoring of strains, displacements and stresses to assess the adequacy of the design and performance of tunnels during construction has become an integral part of the modern observational approach. In particular, displacement measurements are relatively easy to obtain and monitor continuously during excavation (Beniawski, 1984).

The data collected during tunnel advance are used principally as a mean of empirical stability assessment based on the observations of the following aspects:

1) Magnitude of the displacements measured compared with elastic theory or with other measurements taken previously in stable sections,

2) Closure rates compared with empirical values,

3) Observed movement compared with the displacements that would cause failure of the support or of the surrounding rock.

Recently Sakurai(1981) introduced a Direct Strain Evaluation Technique based on the concept of strain at failure or "critical strain", as an attempt to give a quantitative interpretation to the results of displacement measurements.

In the last few years many efforts have been directed towards developing methods to back-analyze ground properties and initial stress distribution from monitoring data and numerical computations. Gioda and Maier (1980) back-analyzed cohesion, friction angle and in situ stresses by numerical interpretation of measurements taken during a tunnel pressure test. The rock parameters were calculated by applying a "direct search method" for function minimization. Sakurai and Takeuchi (1983) developed a finite element program for back-analysis of elastic properties and insitu stresses based on the "inverse approach". It is not the purpose of this discussion to review in any detail the advantages and limitations of these methods as well as their theoretical backgrounds (see Gioda, 1985; Cividini et al., 1981).

Even though so much interest has been placed in the interpretation of monitoring data for back-analysis purposes, little effort has been spent in order to investigate how the near face behavior may affect such interpretations and to provide further insight in the back-analysis process. While it is well appreciated by the tunnelling community that in reality only a portion of the total stress, strain and displacement change is actually observed, little is known about the effects of the three dimensional conditions near the face on field measurements.

2.5 Conclusions

The discussion presented in this chapter introduces the object of this research that intends, by overcoming some limitations detected in previous studies, to contribute to the understanding of the three dimensional near face conditions for unsupported and supported tunnels.

On the basis of this literature review the following conclusions can be drawn:

1) A three dimensional approach to tunnelling problems is needed to assist the back-analysis of monitoring data and the design of the support.

2) Simplified design methods, as the CCM, are insufficient for design purposes unless a profound understanding of the three dimensional near face behavior is available.

3) Many studies conducted in the past were based on the assumption of axisymmetry. A more general approach is needed in order to consider initial stress ratios other than one and anisotropic rock behavior.

4) Most truly three dimensional analyses available from the literature were carried out to study specific case histories. Relatively extensive parametric studies were conducted only for the case unlined tunnels in linear elastic media.

5) Up to now, the effects of ground conditions, initial stress distribution and supporting procedure on measurements taken during tunnel advance have not been the object of detailed investigation.

6) Some important aspects regarding the development of stresses in the liner due to face advance, such as the effect of the Round Length, have been neglected in previous studies.

7) Elasto-plastic modelling of the ground has usually been conducted by assuming an associated flow rule. A non-associated flow rule should be used for frictional material to avoid unrealistic dilation at failure.

Hence, it is the purpose of the following to address these deficiences and to assist the practicing tunneller to gain more from near face measurements.

3. UNLINED TUNNELS IN LINEAR ELASTIC ROCK

3.1 Introduction

The study of unlined tunnels excavated in linear elastic rock represents the starting point of this research.

Even though the assumption of linear elasticity is not realistic for most geologic media, the outcome of this analysis includes findings of considerable practical interest.

Some studies on stresses and displacements near the face of tunnels in elastic material were carried out in the past and are available in the literature. In particular Niwa et al. (1979) performed a relatively extensive parametric study by the use of the integral equation method. Their results were found to compare well with the outcome of this research. It is not the intention of the present work to repeat or summarize what has already been shown by others. The discussion is focused on stresses and deformations developing at various distances from the tunnel wall. The main purpose is to provide information useful for monitoring data interpretation by selectively analyzing the effect of the initial stress distribution on the measurements taken during face advance.

The material contained in this chapter is also needed for comparison with subsequent analyses, where more complex conditions are assumed.

3.2 Description of the Analysis

In order to study the behavior of deep unlined tunnels in linear elastic rock a series of three dimensional finite element analyses were carried out, using the program ADINA.

The mesh chosen for the analysis, depicted in Figures 3.1 and 3.2, represents only one quarter tunnel. This simplification was possible because both tunnel geometry and initial stress field were assumed to be symmetric with respect to the horizontal and the vertical planes containing the tunnel axis. A circular cross section, common in modern tunnelling, was selected and the directions of the principal stresses were assumed to be parallel and perpendicular to the tunnel axis and, hence, parallel to the axes of the global coordinate system. The initial stress field was assumed to be constant throughout thereby neglecting gravity. This assumption is reasonable for deep tunnels where the stress variation with depth is usually not significant when compared with the average stress magnitude.

A preliminary study, conducted with both plane strain and three dimensional models, showed that, in order to obtain a reasonably accurate strain field around the tunnel, a large mesh, with boundaries located far from the excavation wall, was needed. The final mesh was eight diameters wide and ten diameters long.

The boundary conditions are shown schematically in Figure 3.3. At the "Front" and at the "Back" of the mesh the nodes were constrained to move on planes perpendicular to

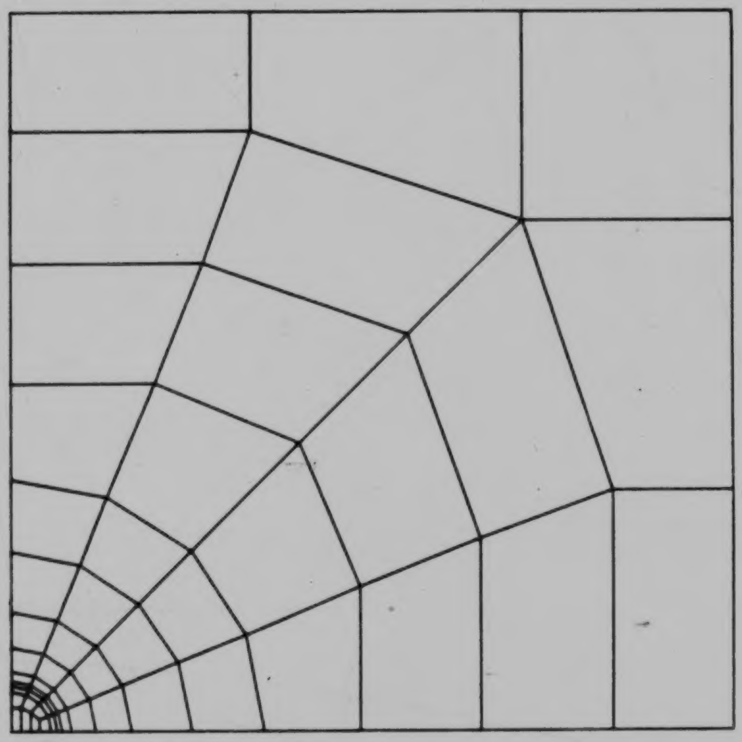

Figure 3.1 Front View of the Three Dimensional Finite Element Mesh

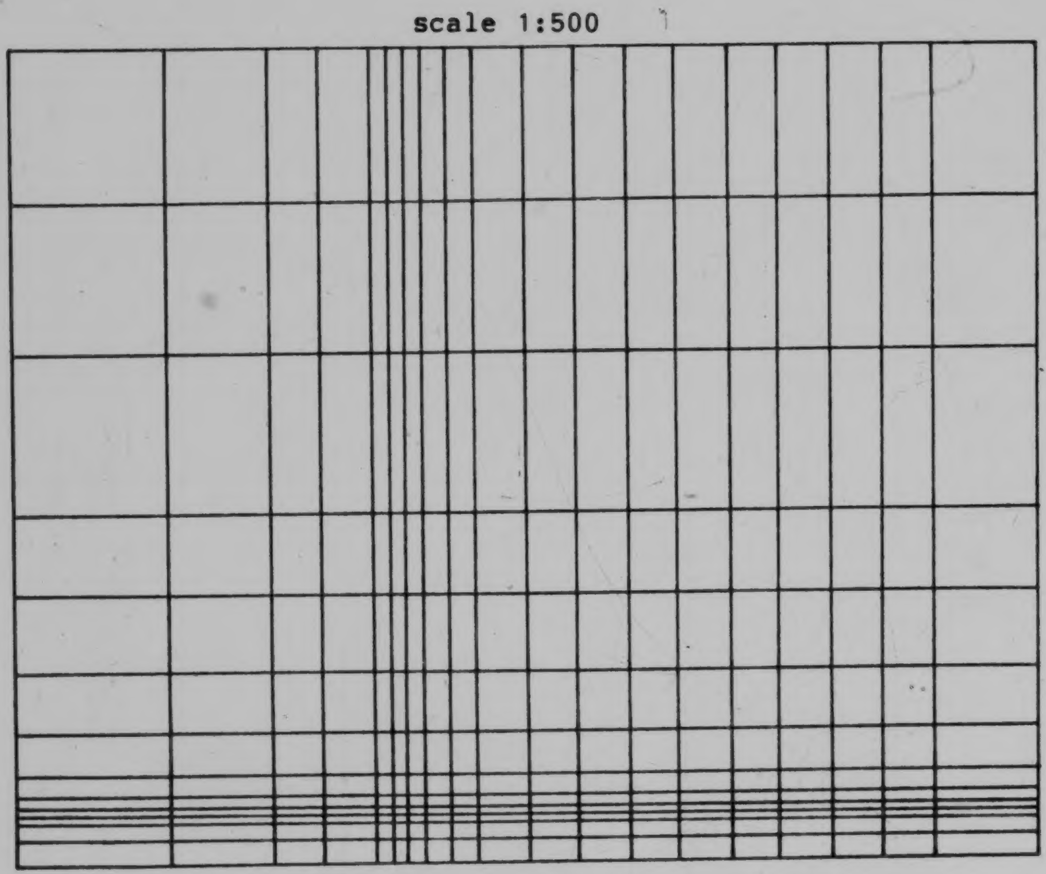

Figure 3.2 Side View of the Three Dimensional Finite Element Mesh

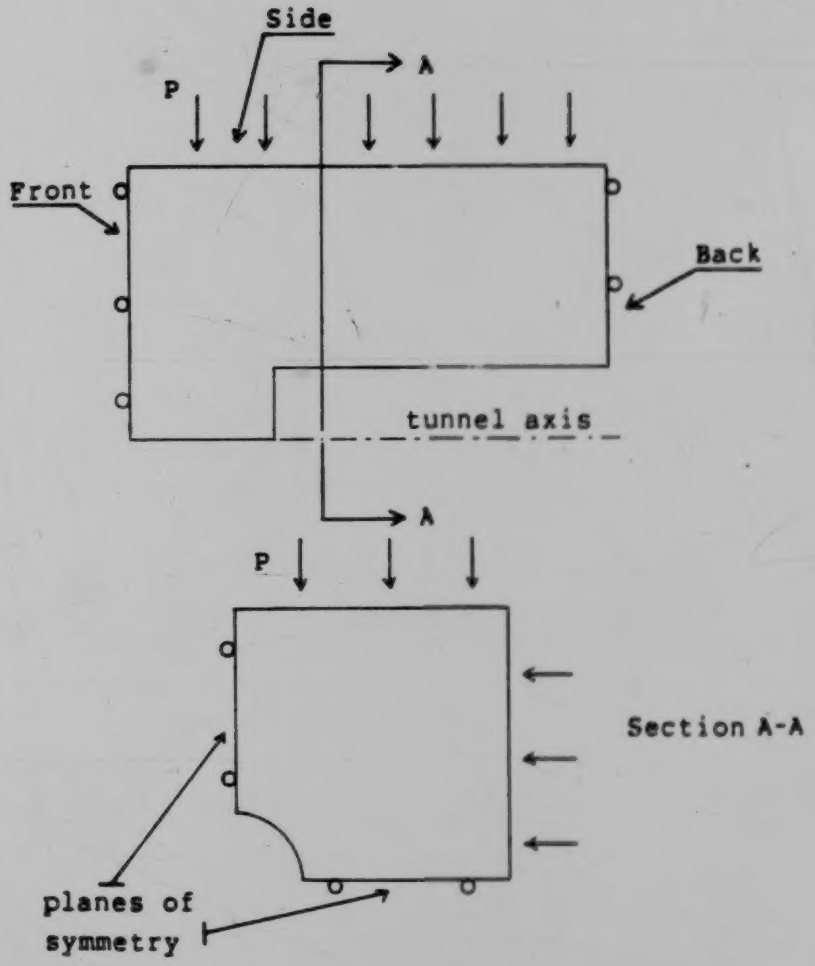
Side
A
P
Front
Back
tunnel axis
A
P
Section A-A
planes of
symmetry

Figure 3.3 Boundary Conditions

the tunnel axis. The "Side" boundaries of the mesh were assumed to be a constant pressure boundaries. A preliminary study was carried out with two dimensional models to compare stresses and strains obtained by adopting constant pressure boundaries or fixed node boundaries. No significant differences were found. The nodes lying on the two planes of symmetry were constrained to move on them.

Because of the computational effort involved in numerical analyses of this kind, the degree of refinement of the finite element mesh was by necessity a compromise between quality of the results and the cost (time) at which they could be obtained. The final mesh is finer than most three dimensional meshes found in the literature and is larger in order to achieve a more appropriate positioning of the boundary conditions.

The mesh was defined by 3145 nodal points and 988 3-D isoparametric solid elements. Twenty node elements were placed near the wall and in front of the tunnel face where high stress-strain gradients were expected to occur. Eight node elements were used to model the rock far from the tunnel and in the core.

In order to generate the initial stress field the "Side" boundary pressure, complemented by axial displacements applied to the "Back" of the mesh, was imposed to the unexcavated, initially unstressed, model.

Excavation was simulated by means of the "birth-death" option. In this fashion the terms corresponding to the "excavated" elements were eliminated from the stiffness matrix and the stress values in the "excavated" zone were reset to zero. This generates a non equilibrated condition at the boundary of the opening and influences the stresses in the surrounding medium. Excavation was performed in a single step because the tunnel was unlined and in a linear elastic medium.

The displacements associated with the application of the initial stress field were eventually subtracted from the final total values during the data post-processing stage.

Two cases were analyzed assuming two different initial stress conditions:

$P_v \neq 0$; $P_h = P_a = 0$

$P_a \neq 0$; $P_v = P_h = 0$

where P_v, P_h and P_a are the initial stresses in the rock mass (see list of symbols).

The results obtained by these analyses were superimposed and values for any initial stress condition could be found.

The results were normalized with respect to initial vertical stress P_v, elastic modulus E, and tunnel radius R. A Poisson's ratio of 0.25 was selected for all cases.

Benchmarking analyses showed that radial displacements at the tunnel wall differed from the analytical linear elastic solution by, on average, 10%, and this accuracy was considered acceptable for the purposes of the present work. This error was expected, as the numerical method gives only an approximate solution whose accuracy depends on the degree of refinement of the mesh and on the order of the shape functions of the elements. In the the following paragraphs the results of the finite element analysis are discussed. Emphasis is placed on presentation and interpretation of the three dimensional effects near the tunnel face as they affect monitoring data.

3.3 Stresses near Tunnel Face

A linear elastic finite element analysis was carried out using the program SAFE, assuming an initial stress ratio K_0=2, and the stresses obtained are presented in this section. The stresses calculated by SAFE were selected for convenience. First, the stresses obtained by ADINA did not have to be superimposed (as done for the displacements); second, the data presented in this paragraph are directly comparable with the results of the non-linear analyses presented in Chapter 5, that were obtained by using the same program. The stresses calculated by ADINA and SAFE were compared at some locations and were found to be virtually identical although slightly different boundary conditions were applied to the mesh depending on the program used (see Chapter 5 for further details).

All the data are shown in normalized form. The normalized stresses, σ/P_v, are plotted against the normalized position coordinate (X/2R) (X=distance to tunnel face). The sign convention is positive for tensile stresses and for positions behind the tunnel face, in the excavated section of the tunnel. The excavation front stands at X/2R=0.

An initial stress ratio K_0=2 was assumed, that represents a moderately high value, not uncommon for deep underground excavations.

The stresses are plotted on the horizontal and vertical planes containing the tunnel axis (i.e., symmetry planes shown in Figure 3.3) to emphasize the effect of near face conditions. In order to obtain stresses on such planes, values calculated at the integration points were interpolated by means of the local smoothing technique proposed by Hinton and Campbell(1974) and Hinton et al. (1975). Each curve represents stresses calculated either at the crown or at the springline at a normalized distance from the tunnel axis (r/R). In this manner a rather complete picture of the stress field surrounding the excavation can be given. At each location radial, tangential, axial and shear stresses σ_r, σ_t, σ_a and τ_{ar} were plotted. The two shear components, τ_{at} and τ_{rt}, vanish on the selected planes because of symmetry.

Only the results relevant to this discussion are presented here. The remainder are summarized in Appendix A.

In Figure 3.4, the normalized radial stresses at the springline are plotted against normalized distance to the tunnel face. Far ahead of the tunnel face the stress field is unaffected by the advancing excavation. Far behind the

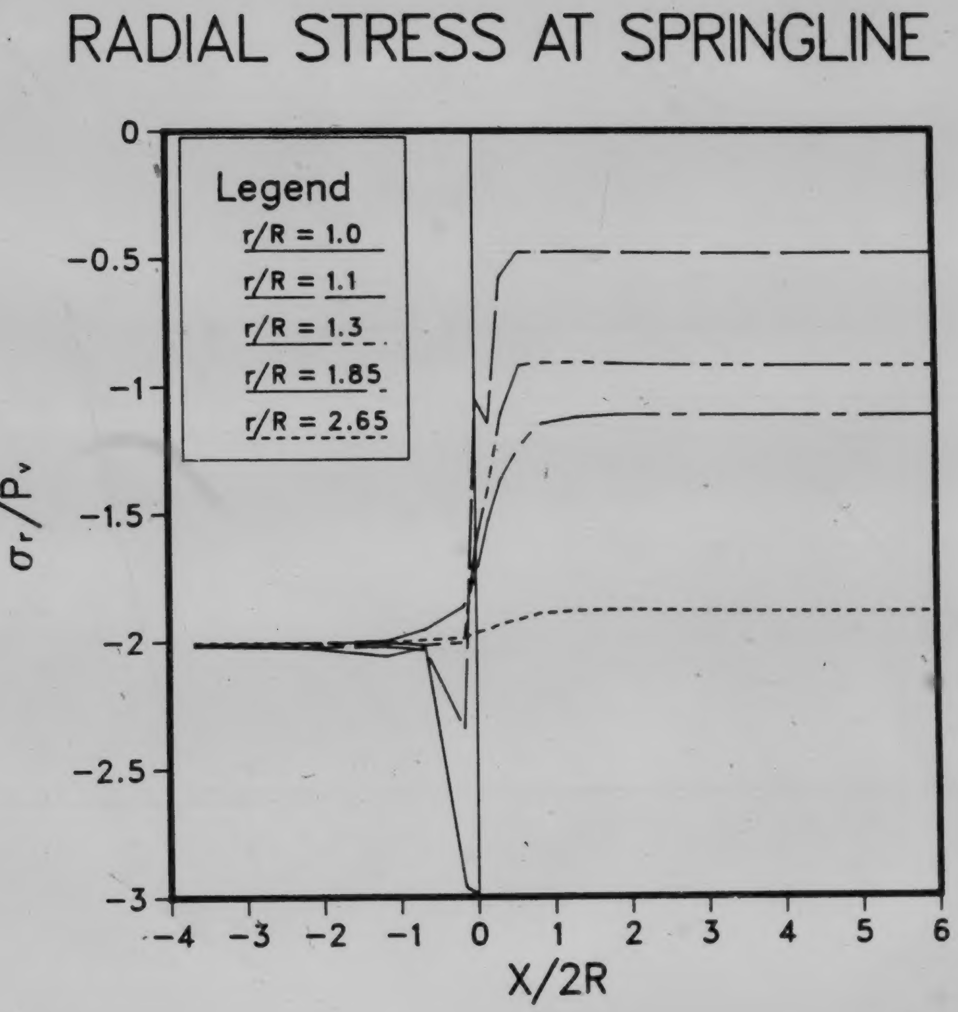

Figure 3.4 Radial Stresses, σ_r, at the Tunnel Springline (K_0=2)

tunnel face the final stress state, consistent with plane strain conditions, is reached. The radial stress change is largest at the tunnel wall where it drops to zero on the excavation free surface. It gradually decreases as the distance from the excavation wall increases. At about two to three radii from the tunnel axis the radial stress change is almost negligible. In Figure 3.4, the radial stress at the tunnel wall is plotted only ahead of the tunnel face.

Of particular interest is the transition zone near the tunnel face. It begins about one diameter ahead of the excavation and ends at about one diameter behind the face where the final equilibrium configuration is almost reached and the "Face Effect" is no longer evident. In the transition zone three dimensional stress redistribution mechanisms dominate. The tunnel face is subjected to a sharp increase in radial compressive stress. This stress peak is associated with arching caused by excavation. Arching involves shear stresses which enable load transmission ahead of the tunnel face.

In Figure 3.5, these shear stresses, τ_{ar}, at the springline are plotted against distance from the tunnel face. Since the initial normal stresses P_v, P_h and P_a are principal stresses, no shear is detected far ahead of the tunnel face, where the rock is still undisturbed, and far behind, where plane strain conditions dominate. As shown schematically by Lombardi(1980), shear stresses develop at the tunnel face and are related to the increase in radial

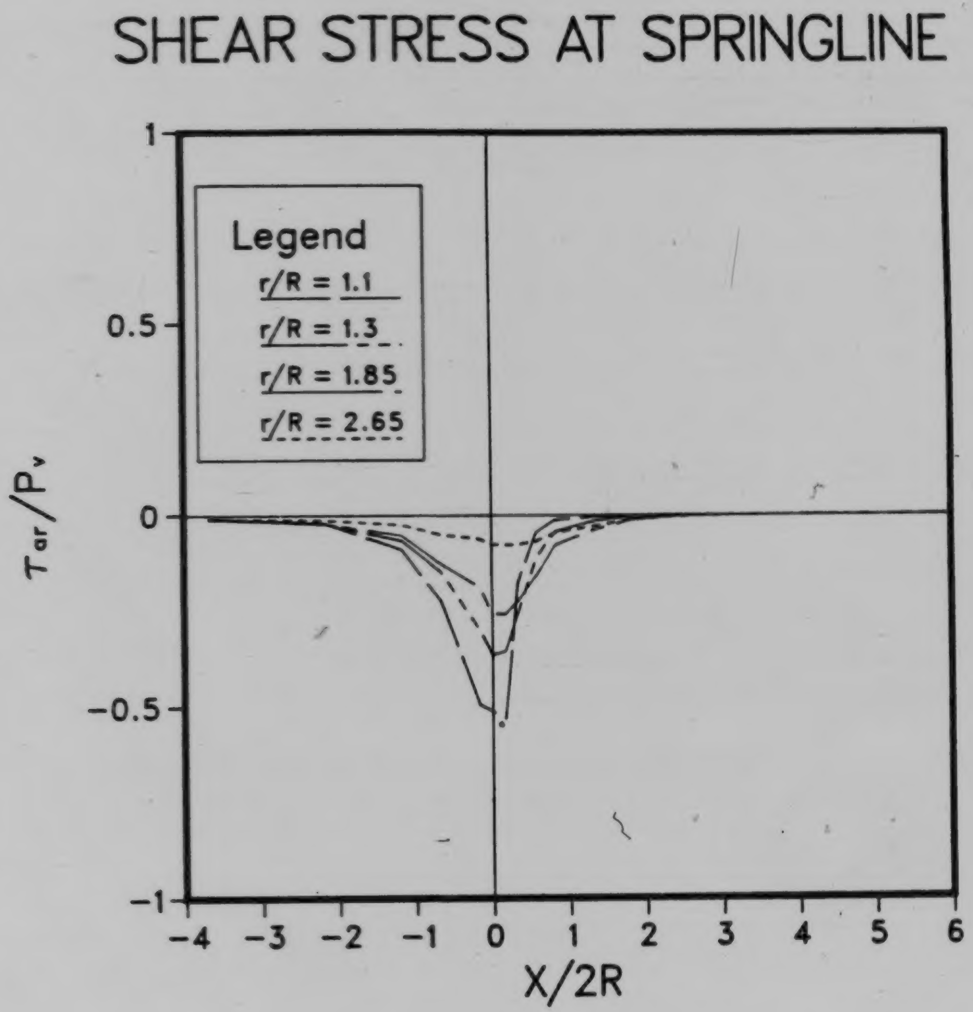

Figure 3.5 Shear Stresses, τ_{ar}, at the Tunnel Springline (K_0=2)

stress detected at that location.

In Figure 3.6, the normalized tangential stresses σ_t/P_v are plotted at the crown. It can be noted that transverse arching (arching in the r-t planes) develops fully within two diameters, where the shear stresses at the springline vanish.

Shear stresses play a key role in controlling near face convergence and in delaying the development of transverse arching.

An increase in axial stresses was also found at the tunnel face, as can be seen in Figure 3.7. This stress peak is due to arching generated by release of axial stresses at the face during excavation.

Similar features to those observed at the springline were found at the crown (Appendix A). They all reflect the gradual rotation of the principal stresses near the tunnel face during advance.

3.4 Displacements

In Figure 3.8, the normalized radial displacements calculated for the springline at various distances from the tunnel axis (r/R) and for $K_0=2$ ($P_a=P_h=2P_v$) are plotted against distance from tunnel face.

The displacements are normalized with respect to the elastic modulus of the rock, E, the tunnel radius, R and in situ vertical stress, P_v. The distance to the tunnel face, X, is normalized with respect of the tunnel diameter, 2R.

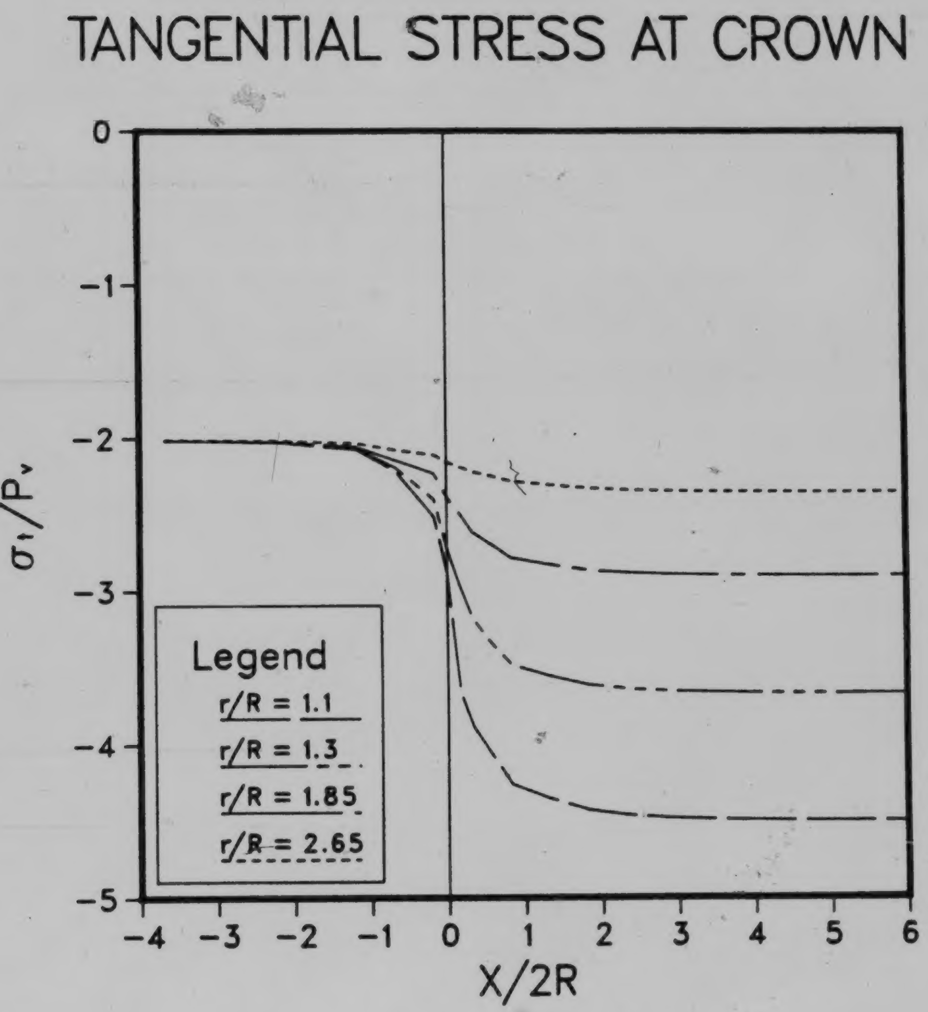

Figure 3.6 Tangential Stresses, σ_t, at the Tunnel Crown (K_0=2)

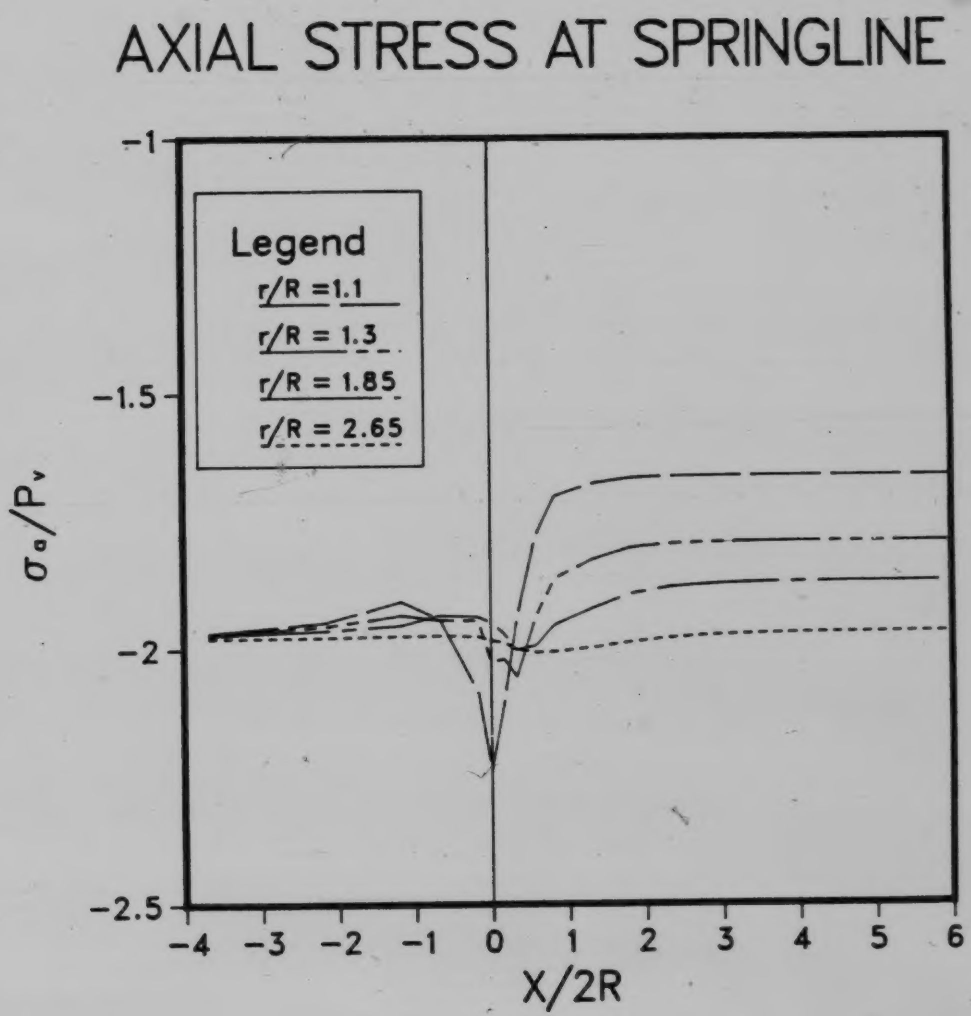

Figure 3.7 Axial Stresses, σ_a, at the Tunnel Springline (K_0=2)

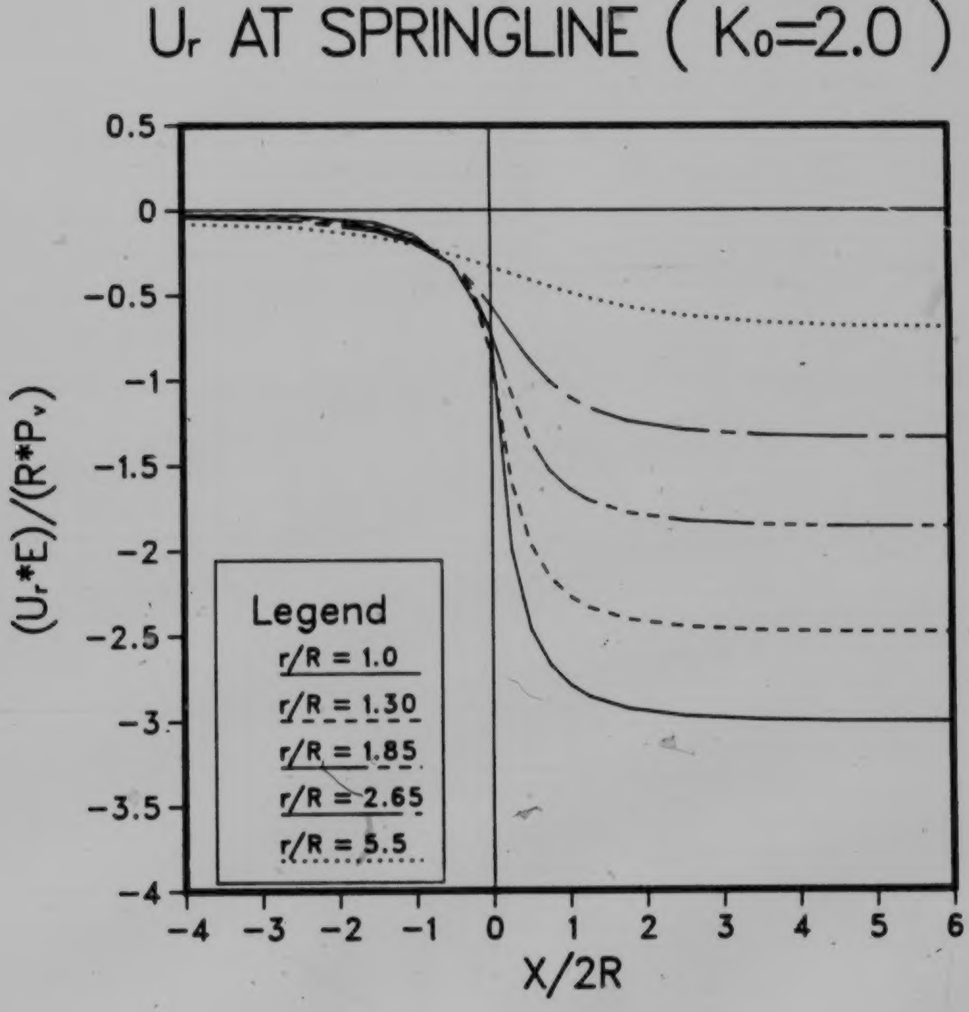

Figure 3.8 Radial Displacements, U_r, at the Tunnel Springline (K_0=2)

Values of r/R varying between 1 and 5.5 were selected.

Convergence begins about two diameters ahead of the tunnel face and increases monotonically until the final value, consistent with plane strain conditions, is reached. The maximum convergence gradient occurs at the tunnel face where an inflection point is located. It can be seen that for r/R=1 (tunnel wall), only 27% of the total convergence is found at tunnel face where, for r/R=5.5, the radial displacement at the face reaches 41% of the total movement. This indicates that the shape of the radial displacement profiles gets flatter far from the tunnel axis (i.e., movement begins earlier and ends later with respect to what happens near the tunnel wall). For instance, two diameters behind the tunnel face about 98% of the total convergence was found at the wall (r/R=1) but only 88% of the total radial displacement was detected for r/R=5.5. This aspect will be discussed further in the following paragraph, where its implications for the interpretation of monitoring data will be pointed out.

Radial displacements occurring at the tunnel face were found to be strongly affected by the magnitude of the initial axial stress, P_a. In Figure 3.9, convergence profiles at the tunnel crown are plotted for various P_a values. All curves represent displacements at the tunnel wall (r/R=1) for $K_0=2$ (i.e., $P_h/P_v=2$=constant, where P_a is varied independently). For high P_a values three major features were observed:

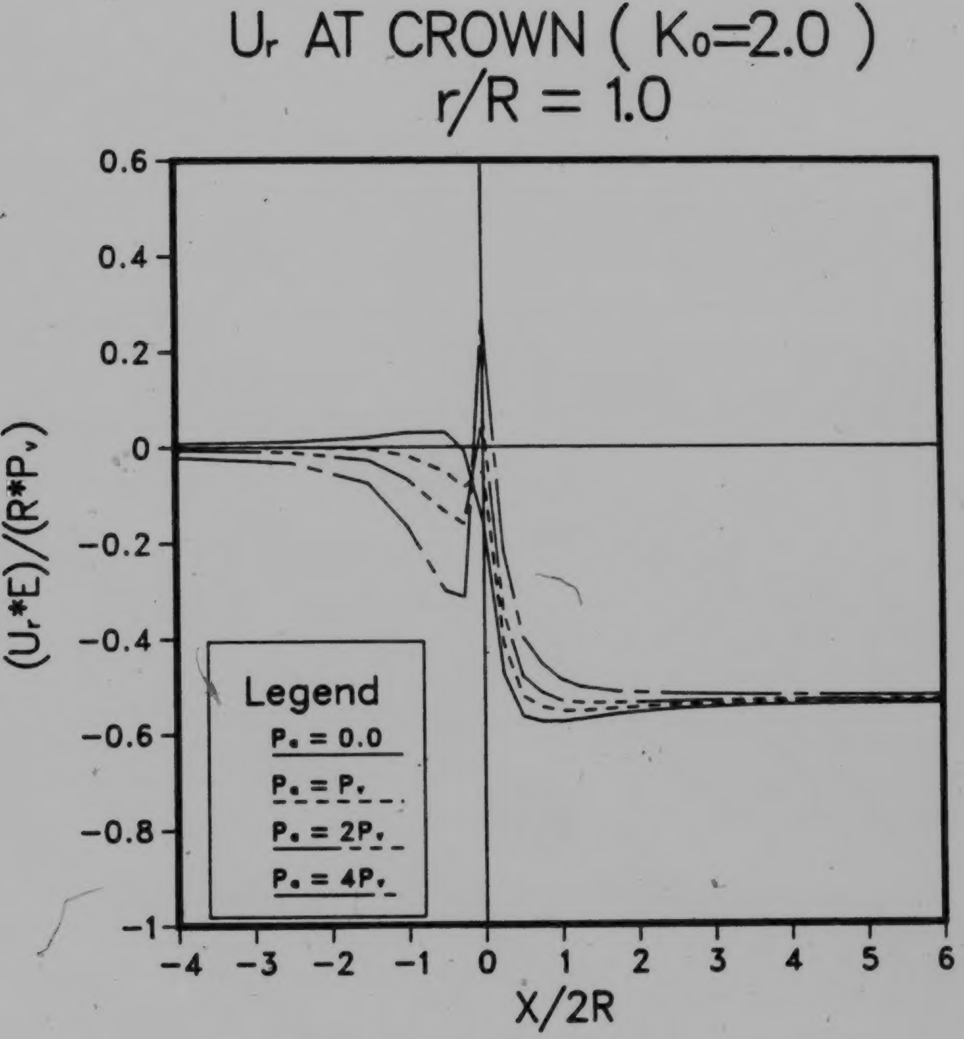

Figure 3.9 Effect of P_a on Convergence at the Tunnel Crown (K_0=2)

1) Ahead of the tunnel face high P_a causes relatively high inward radial displacement. This is due to the tendency of the tunnel face to move towards the opening when excavation is performed. The magnitude of such movement depends on P_a.

2) At the tunnel face higher P_a values involve lower inward radial displacement or even outward radial movement.

3) For high P_a values, convergence behind the tunnel face increases monotonically but for low P_a values the maximum convergence at the crown is reached near the face (at $0.5 \le (X/2R) \le 1$). Farther behind the face, outward movement occurs until transverse arching (in r-t planes) is fully developed. Near face arching is responsible for this phenomenon by drastically modifying the shape of the convergence profile at the face.

The effect of the initial axial stresses on the convergence near the tunnel face, is consistent with the stress redistribution mechanism around the excavation front. In Figure 3.10, this mechanism is schematically depicted by showing the trajectories of the major principal stresses, as they bend around the excavation. In order to emphasize the effect of the initial axial stress P_a, all the other initial stress components (P_v and P_h), are assumed to be zero. In the lower part of the figure, the radial displacements at the wall are also shown, schematically, along the tunnel axis

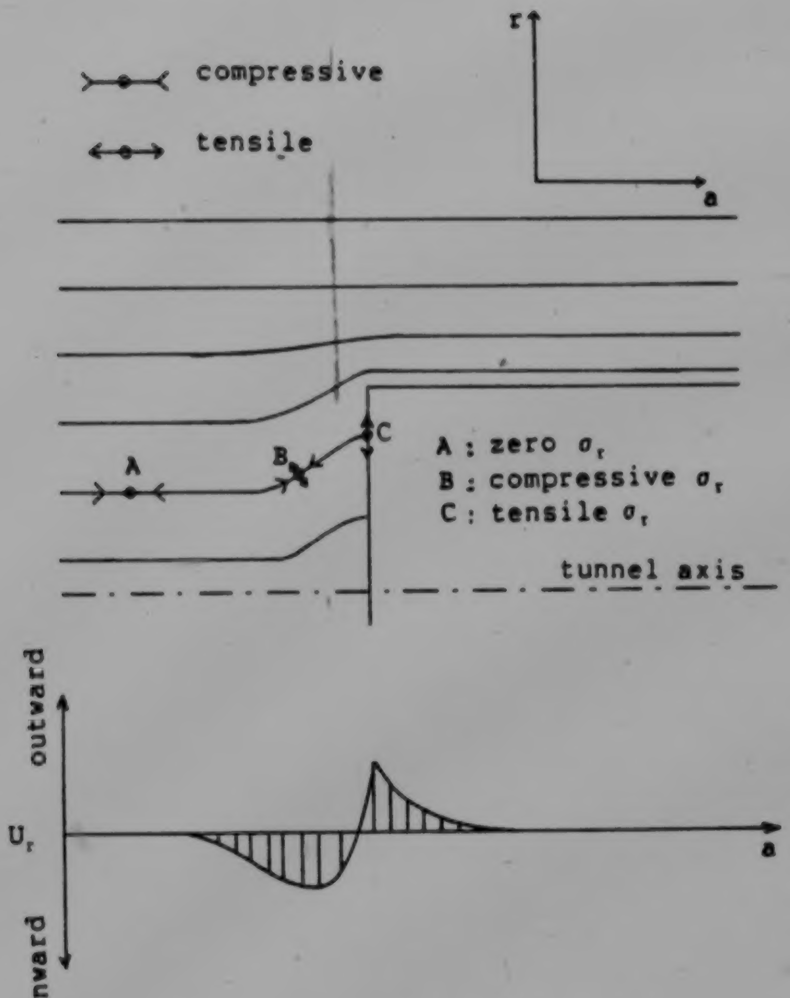
compressive
tensile
r
a
A
B
C
A : zero σ_r
B : compressive σ_r
C : tensile σ_r
tunnel axis
outward
U_r
inward
a

Figure 3.10 Schematic Representation of Principal Stress Trajectories near the Tunnel Face ($P_v = P_h = 0$)

Far ahead of the tunnel face (Location A in Figure 3.10) the rock is unaffected by the excavation and the initial stresses are unchanged (i.e., zero radial stress). Closer to the face (Location B) the major stresses begin to rotate and a small compressive radial stress develops. A tensile minor principal stress, associated with separation of the stress trajectories, also appears. At Location B the development of compressive radial stress, together with the decrease in axial stress, is consistent with the radial inward movement found for high P_a values.

At Location C, at the tunnel face, tensile stress in the radial direction is found where the axial stress drops to zero. This stress condition can be compared with what happens at the crown of a tunnel for an extreme stress ratio (for instance K_0=0). In that situation the rotated principal stresses are associated with tensile stresses at the crown and with outward movement at the springlines. Similarly, at the tunnel face, rotation of the principal axial stresses generates tensile stresses at the excavation front "pushing" outward the wall of the tunnel.

In Figure 3.11 convergence profiles are shown, at the springline, for various P_a values. The considerations regarding tunnel crown still apply but the effect of P_a appears to be less crucial for this case. The reason is that release of axial stresses, due to excavation, generates an axisymmetric deformation field, around the tunnel, that mostly affects measurements taken at those locations where

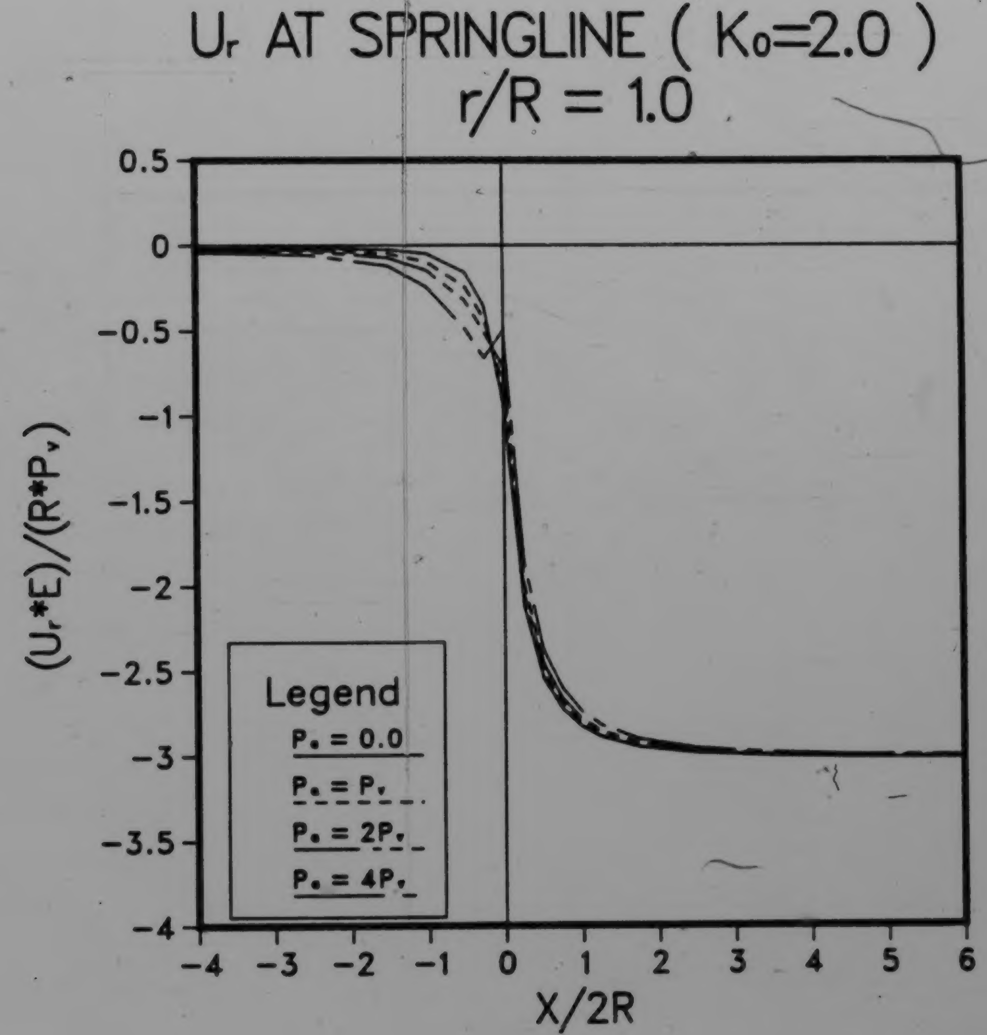

Figure 3.11 Effect of P_a on Convergence at the Tunnel Springline (K_0=2)

smaller radial movement occurs (i.e., in the direction of the minimum initial stress).

3.5 Some Implications for Monitoring Data Interpretation

3.5.1 Convergence Records

Convergence measurements, often carried out during tunnel advance, usually start as close as possible to the tunnel face.

In Figure 3.12, a set of curves is plotted at the springline for K_0=2. Each curve represents measurements relative to a different zero reading location. For instance, for the solid curve the zero reading was taken at the tunnel face, for the broken line the zero reading was taken half radius behind the tunnel face and so on. The subscript $_0$ (see figure legend) indicates distances from face at which the zero reading was assumed to be taken.

Near the tunnel face, where the displacement gradient is very high, small delays in convergence point installation result in drastic reductions of the measured radial displacements. In general, misinterpretation of monitoring data due to delayed zero readings may lead to an underestimate of in situ stresses and rock deformability.

For K_0=2 the convergence values measured at the springline, behind the tunnel face, are smaller than the total radial displacements (i.e., including the movement ahead of tunnel face). This is due to the fact that the

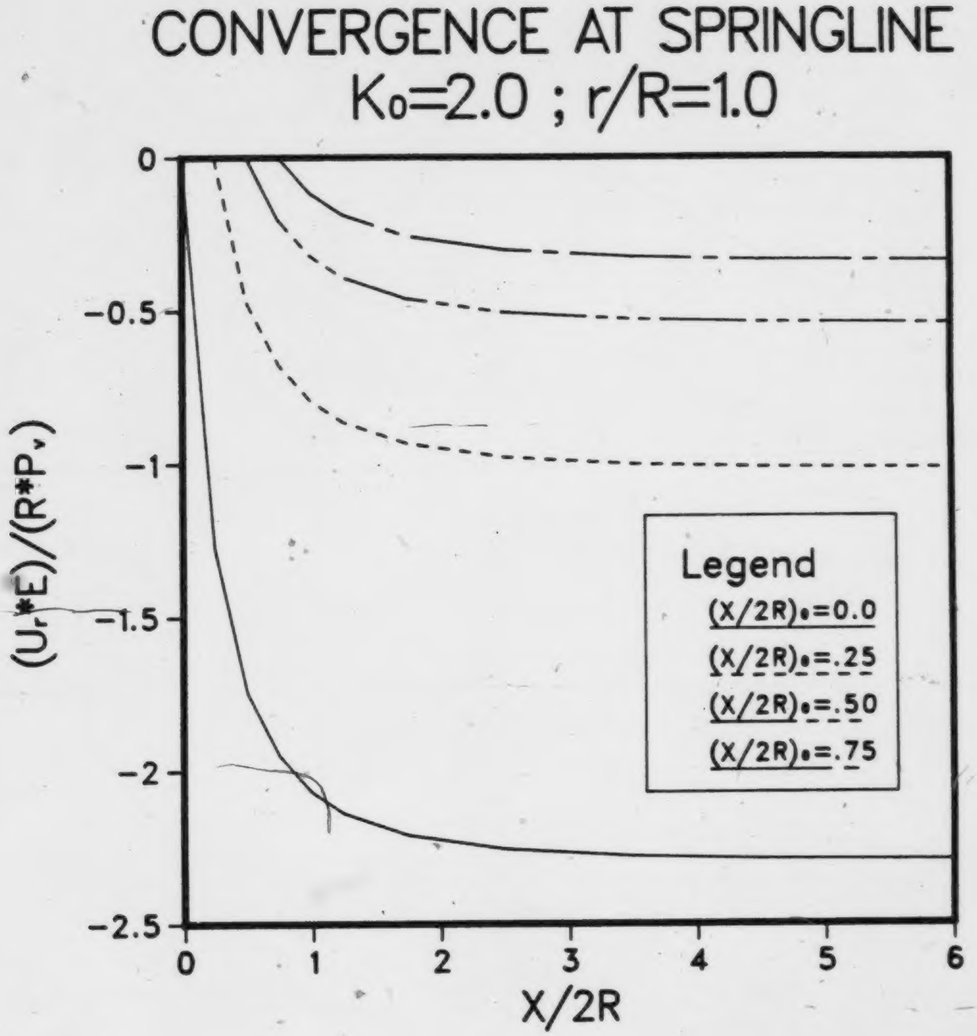

Figure 3.12 Effect of Zero-Reading Location, $(X/2R)_0$, on Convergence Measurements at the Tunnel Springline (K_0=2)

radial movements ahead and behind the tunnel face are inwards (i.e., they have the same sign, see Figure 3.8). On the contrary, at the tunnel crown, outward radial movements can be induced at the face by a high initial axial stress P_a (Figure 3.9). For this case, the convergence monitored starting immediately behind the tunnel face ($(X/2R)_0=0$) is larger than the total radial displacements. This phenomenon can be observed in Figure 3.13 where a set of convergence curves, for $K_0=2$ conditions, are plotted at the crown (or invert). Each curve is associated with a certain zero reading delay. For $(X/2R)_0=0$ (zero reading taken at tunnel face) the final, "measured" radial displacement is larger than the total movement. Extrapolation of the rule of increasing the measured displacement by a certain amount (say 27%) to account for deformation occurring ahead of tunnel face, as it applies to $K_0=1$ conditions (see Panet and Guenot,1982), would fail, for this case, to give a realistic picture. However, since displacements at the crown are very small as opposed to relatively large movements at the springline, K_0 values back-calculated using the "27% rule" and obtained by considering the ratio of radial displacements at crown and springline, would give an error not larger than about 15%. A more significant error would arise if, only knowing convergences at crown and invert, the rock mass deformability were to be found. Even if P_v, P_h, P_a and Poisson's ratio were known exactly, the "27% rule" alone would lead to an error in excess of 30%.

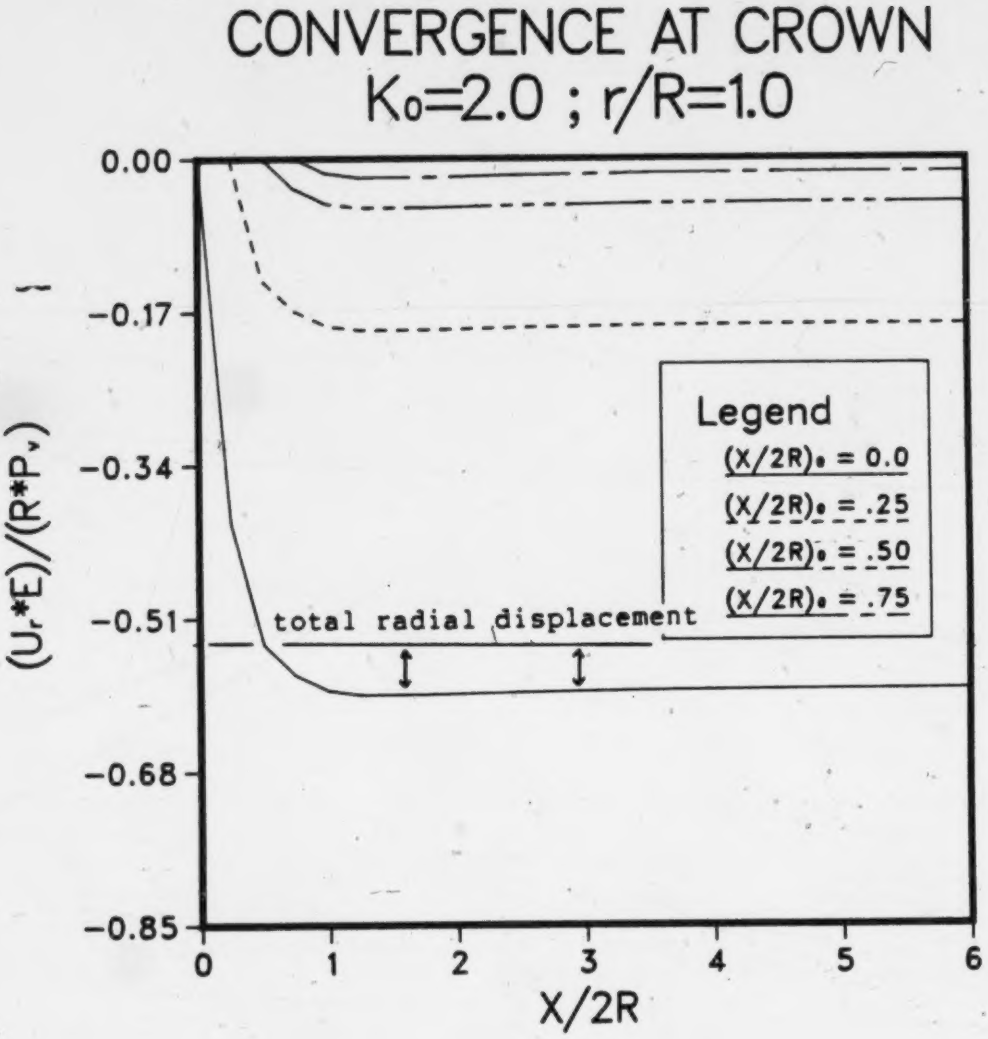

Figure 3.13 Effect of Zero-Reading Location, $(X/2R)_0$, on Convergence Measurements at the Tunnel Crown (K_0=2)

In Figure 3.14, convergence curves having zero readings taken at the tunnel face are plotted at the springline for different values of axial initial stress ($0 \le P_a \le 4P_v$). Figure 3.15 shows the corresponding curves for the crown. It is apparent that sensitivity of radial convergence measurements to the initial axial stress magnitude is much more pronounced at the crown and invert than at the springline (for $K_0=2$). At the springline the difference in measured displacements between the two extreme values is 20% (of the smaller value) whereas it is 120% at the crown. If a narrower range is examined, for instance $P_a=P_v$ and $P_a=2P_v$, a 5% difference is found at the springline and a 20% difference at the crown. If the zero reading is taken half radius behind the tunnel face, the effect of P_a becomes much more pronounced at the crown (Figure 3.16). For this case the radial displacement measured for $P_a=4P_v$ is 5.1 times larger than for $P_a=0.0$ (410% difference), and a 215% difference is detected between $P_a=P_v$ and $P_a=2P_v$. Almost no change is instead observed at the tunnel springline.

A few conclusions can be drawn from these observations:

1) The zero readings should be taken, if possible, right at the tunnel face. Even small delays may sensibly change the outcome of the back-analysis because of high deformation gradients present near the face. Alternatively, the location where the zero reading is taken must be determined accurately, and blast damage should be considered,

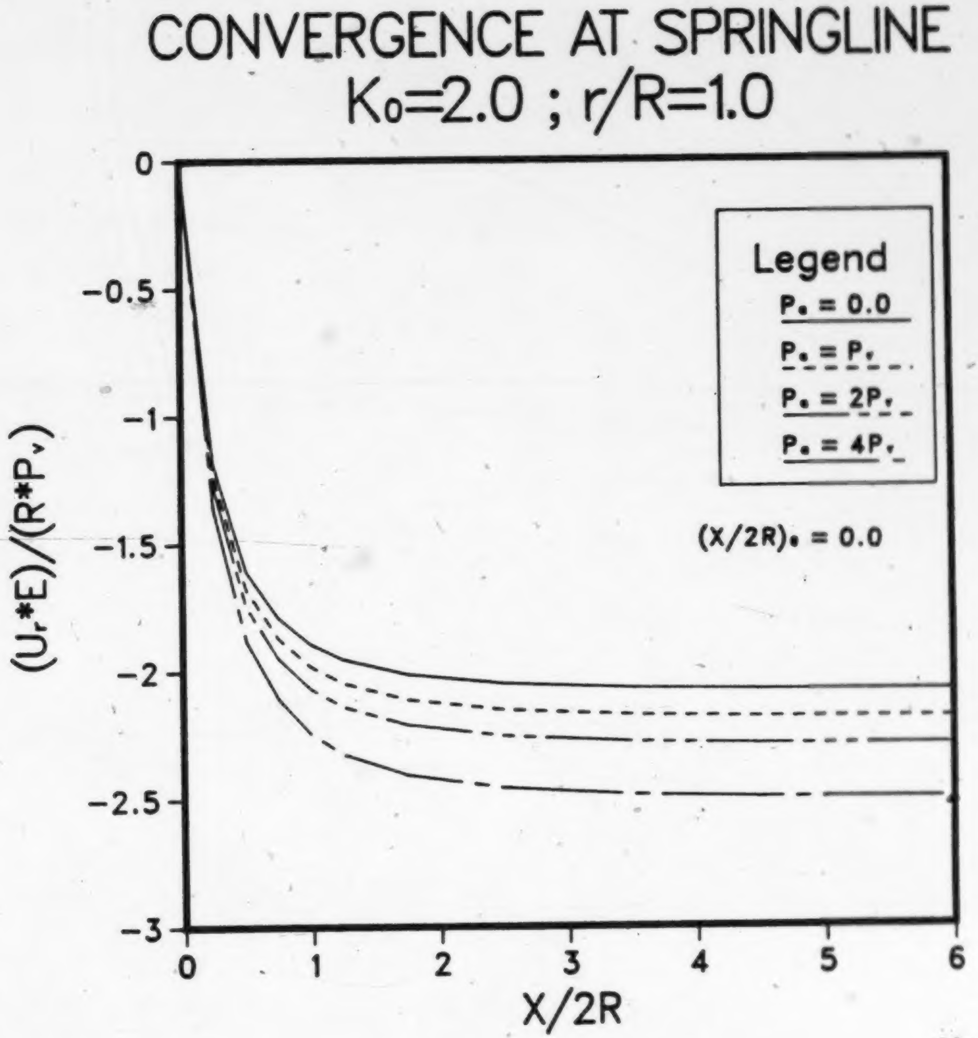

Figure 3.14 Effect of P_a on Convergence Measurements at the Tunnel Springline; $(X/2R)_0$=0.0, K_0=2

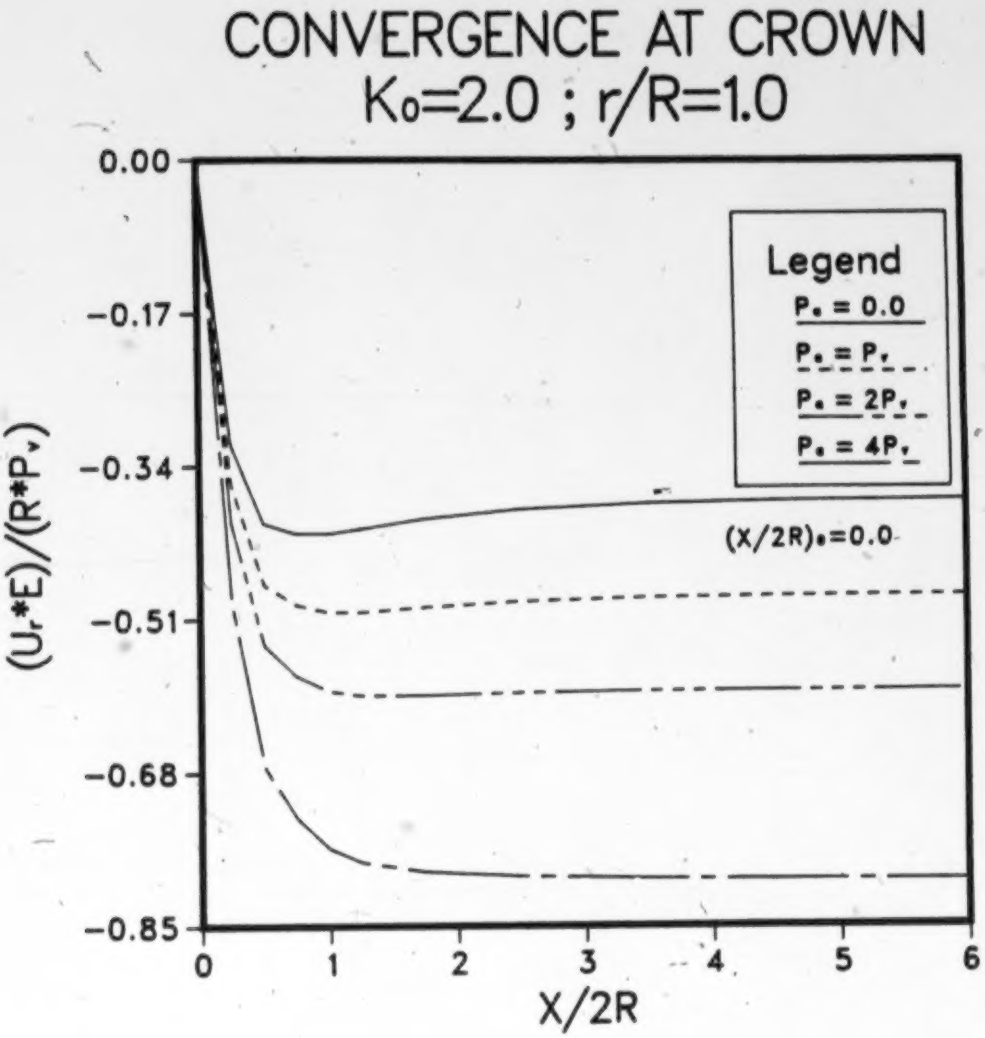

Figure 3.15 Effect of P_a on Convergence Measurements at the Tunnel Crown; $(X/2R)_0=0.0$, $K_0=2$

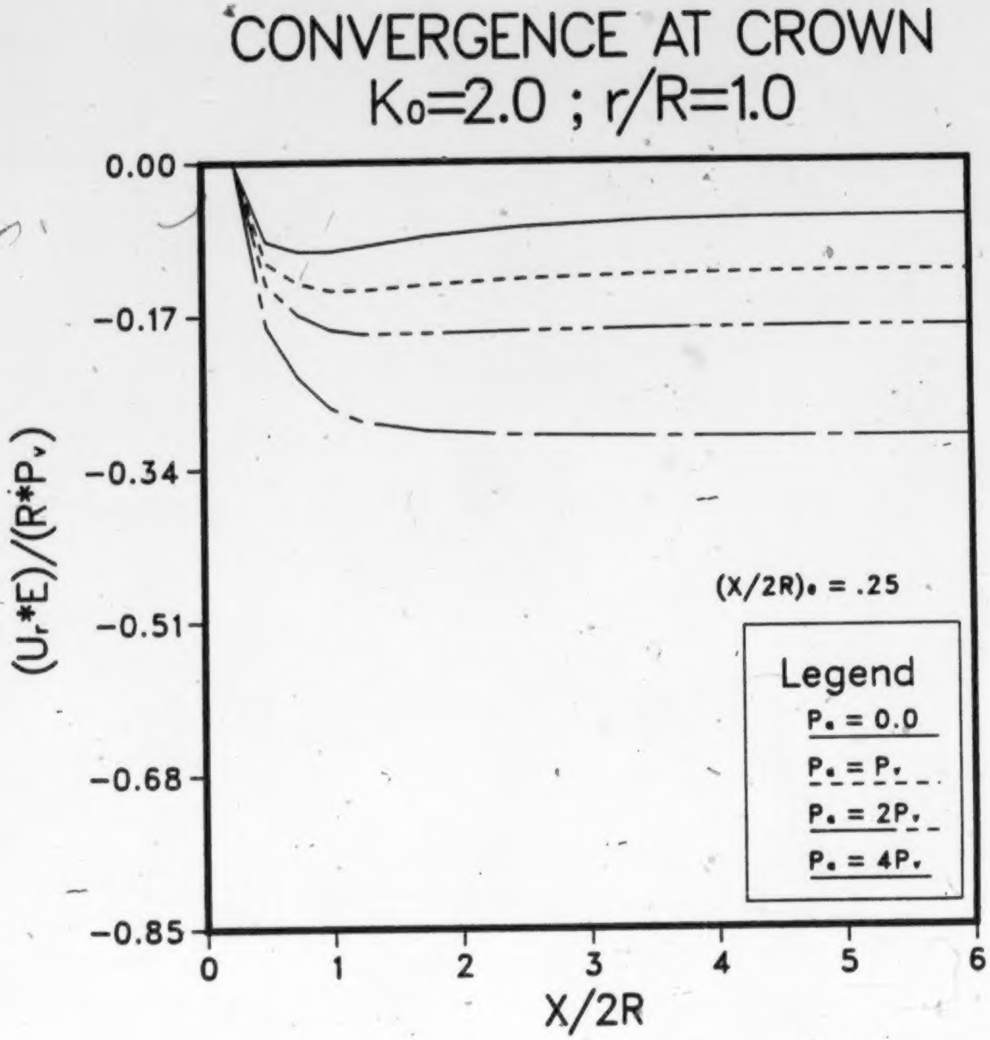

Figure 3.16 Effect of P_a on Convergence Measurements at the Tunnel Crown; $(X/2R)_0$=0.25, K_0=2

2) Back-analysis should be based on measurements taken at least at two different locations (crown and springline) to minimize the magnitude of errors, and

3) In the direction of the minor principal stress (crown and invert for K_0=2) sensitivity to axial stress magnitude is high. Especially if the zero readings are taken at a certain distance behind the face (e.g., X/2R=0.25), back-analysis based on data taken at these locations only may lead to considerable errors.

3.5.2 Multipoint Extensometer Records

Sometimes multiple anchor extensometers are placed around the opening for the purpose of measuring the distribution of radial deformations in the rock mass. If the instrument can be placed far ahead of the tunnel face, for instance by advancing a borehole from another deep excavation, total relative displacements are found.

In Figure 3.17 total relative displacements along a radial multiple extensometer, placed at the tunnel springline are shown for K_0=2. Displacements are plotted against distance to the tunnel axis (r/R) and each curve represents what would be recorded at a certain distance from the tunnel face $(X/2R)_{ms}$ (note: $_{ms}$ stands for measurement). The solid line, for instance, represents readings taken at the tunnel face where the dashed line (short dashes) represents readings taken far behind the tunnel face. The datum of the measurements was assumed at an infinite

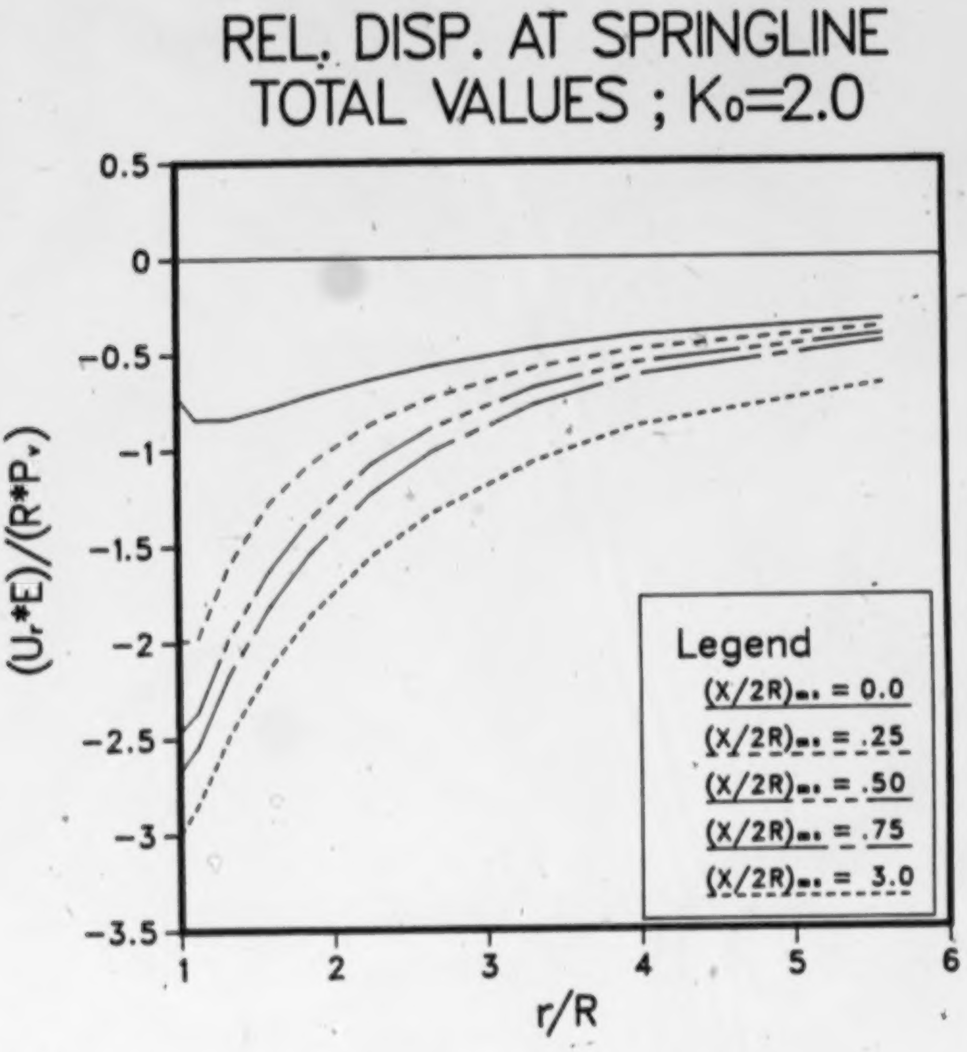

Figure 3.17 Relative Displacement Measurements at the Tunnel Springline; Total Values (K_0=2)

distance from the tunnel axis. Therefore a correction must be applied to the diagram if comparison with real data (datum at finite distance) has to be made.

At the tunnel face a zone of radial compression, about one half radius deep, occurs. The compression zone reduces gradually as the face advances until it completely vanishes. If an extensometer is placed at the face, only the difference between the solid and short dashed lines (partial values) is measured (see below).

In Figure 3.18 a similar set of curves is shown for the tunnel crown. At this location only a minor portion of rock near the tunnel wall is mobilized by the straining process. In practical terms this implies that, at this location, a relatively short multiple anchor extensometer (i.e., 4 radii long) would be sufficient to monitor the mobilized rock.

Usually radial extensometers can only be placed at some distance from the tunnel face, and partial measurements are obtained. As a result, depending on the distance from the tunnel face at which the instruments are placed, steeper or flatter profiles, than for the total displacement case, may be obtained. This is due to the fact that points located at different distances from the tunnel axis displace at different rates.

Small radial compression may sometimes be observed in measurements of this kind if relatively low P_a values are assumed. In Figure 3.19, for instance, readings for various zero reading locations, taken at the tunnel crown for K_0=2

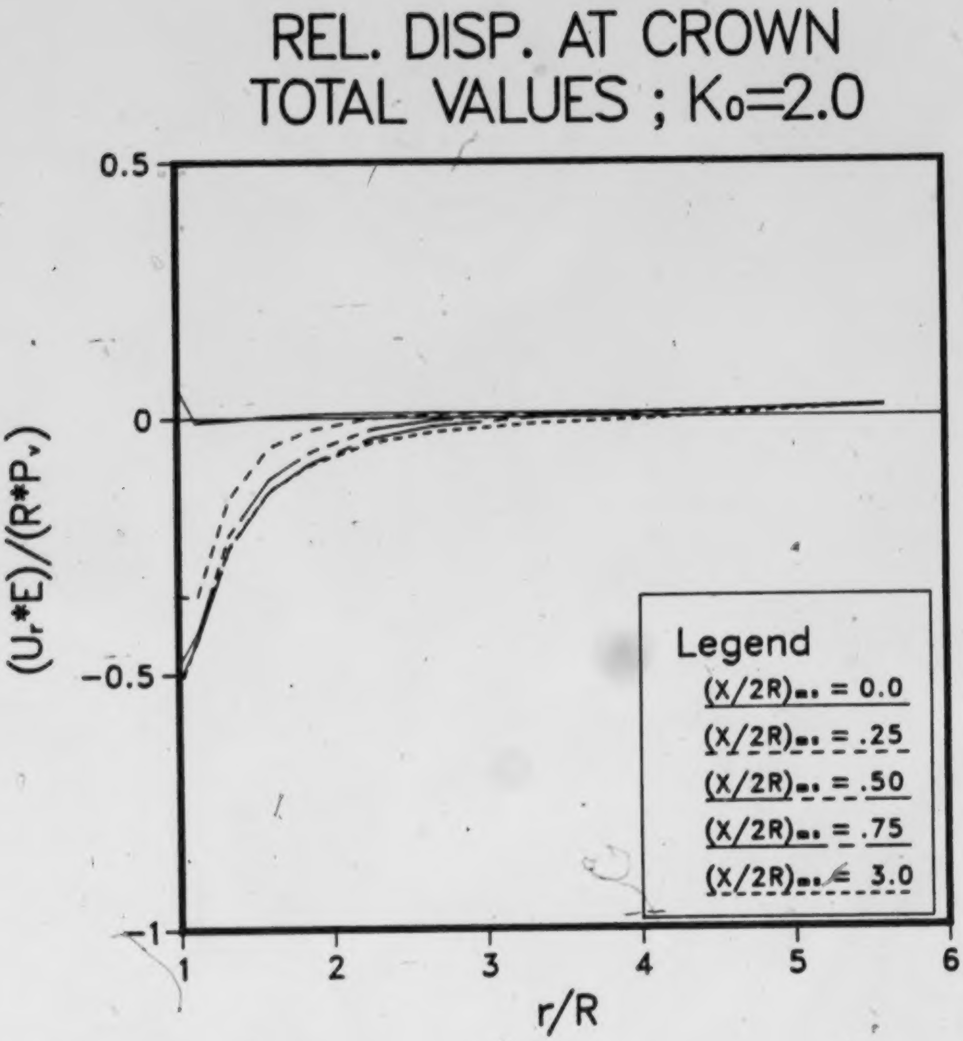

Figure 3.18 Relative Displacement Measurements at the Tunnel Crown; Total Values (K_0=2)

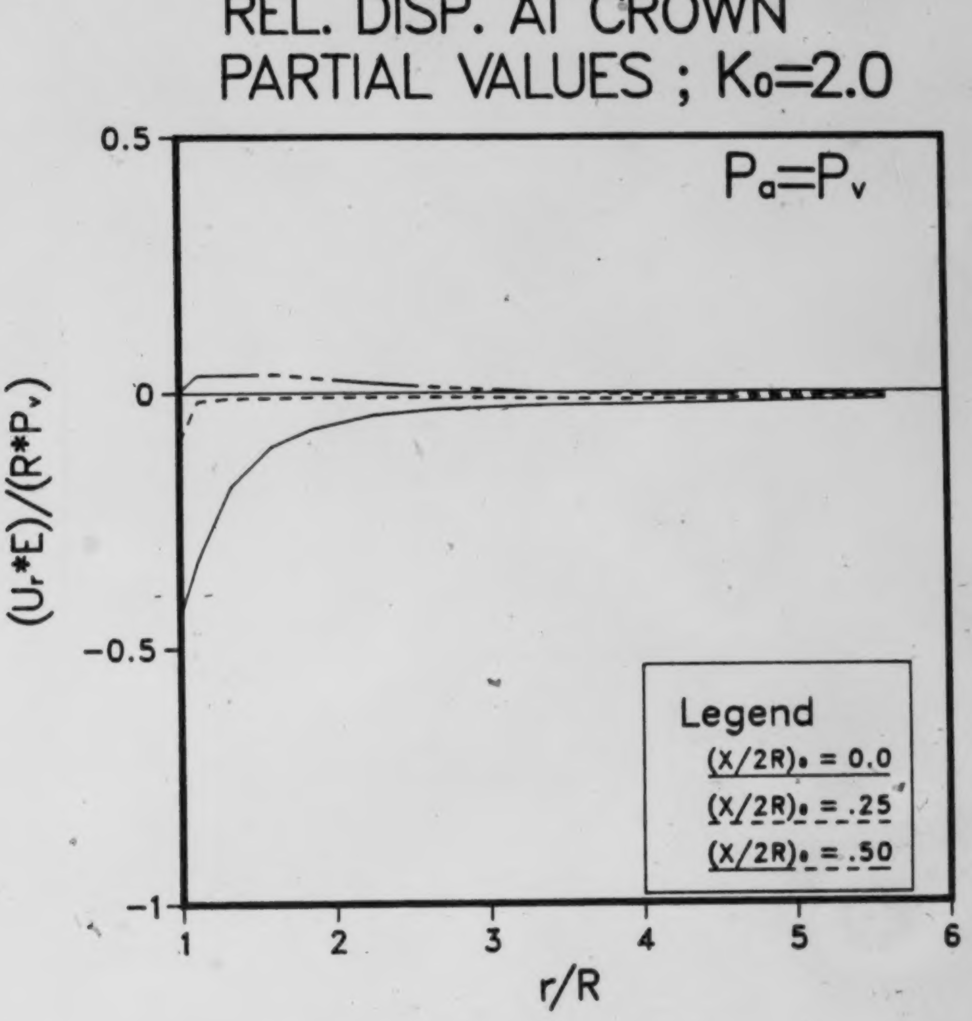

Figure 3.19 Relative Displacement Measurements at the Tunnel Crown; Partial Values (K_0=2; P_a=P_v)

and $P_a=P_v$ are shown. If the extensometers were installed one half diameter ($(X/2R)_0=0.5$) behind the tunnel face, relative radial compression would be recorded due to the development of transverse arching.

3.5.3 Shape of Radial Displacement Profiles

The analytical function developed by Ramberg and Osgood(1943) in the form given by Desai and Wu(1976), was found to match reasonably well the convergence curves given by convergence points and radial extensometers installed at the tunnel face. The function is defined by an initial gradient, S_i, a final gradient, S_f, the location of the asymptote at X=0, U_0, and a shape factor, m (see inset in Figure 3.20). It can be expressed as follows:

$$U_r=(S_i-S_f)X\left(1+\left|\frac{(S_i-S_f)X}{U_0}\right|^m\right)^{-1/m}+S_fX \qquad [3.1]$$

Low m values indicate slow convergence to the asymptote and large curvature radii. Rapid slope variations are associated with high m values. For m=1 the Ramberg Osgood function degenerates to an hyperbola. S_f can be assumed to be equal to zero (horizontal asymptote) for the time independent problems considered in this thesis; i.e., U_0 is directly related to the final convergence.

For more information on the meaning of these parameters the reader is referred to Richard and Abbott(1975).

The parameter m is important for defining the shape of curves having the same initial gradient. For such cases a lower m value corresponds to a flatter curve.

Radial displacements profiles may contain useful information which could be revealed by back-analysis. One of the factors affecting the shape of the convergence curves is the distance from the tunnel axis at which displacements are measured.

Two convergence curves, for r/R=1.0 and 1.85, are shown in Figure 3.20. Radial displacements are normalized with respect to the the final convergence and plotted against distance to tunnel face. The curves were calculated at the springline for the K_0=2 case and zero readings were assumed to be taken at the tunnel face. The function parameters (Eqn.3.1) used to fit visually the two curves are depicted in the figure legend. The shape factor m is 1.35 for r/R=1 (tunnel wall) and 2.15 for r/R=1.85 whereas S_i decreases from 2.0 to 0.69. This substantial variation of the normalized initial gradient shows that the radial displacement curves become flatter at greater distances from the tunnel axis. The distance from the wall at which the measurements have been taken must be considered carefully if the shape of the radial displacement profiles has to be used for back-analysis purposes.

3.6 Conclusions

In this chapter, stress distribution and displacements near the face of an advancing unsupported tunnel in linear elastic isotropic rock were studied. A few conclusions of practical interest can now be drawn:

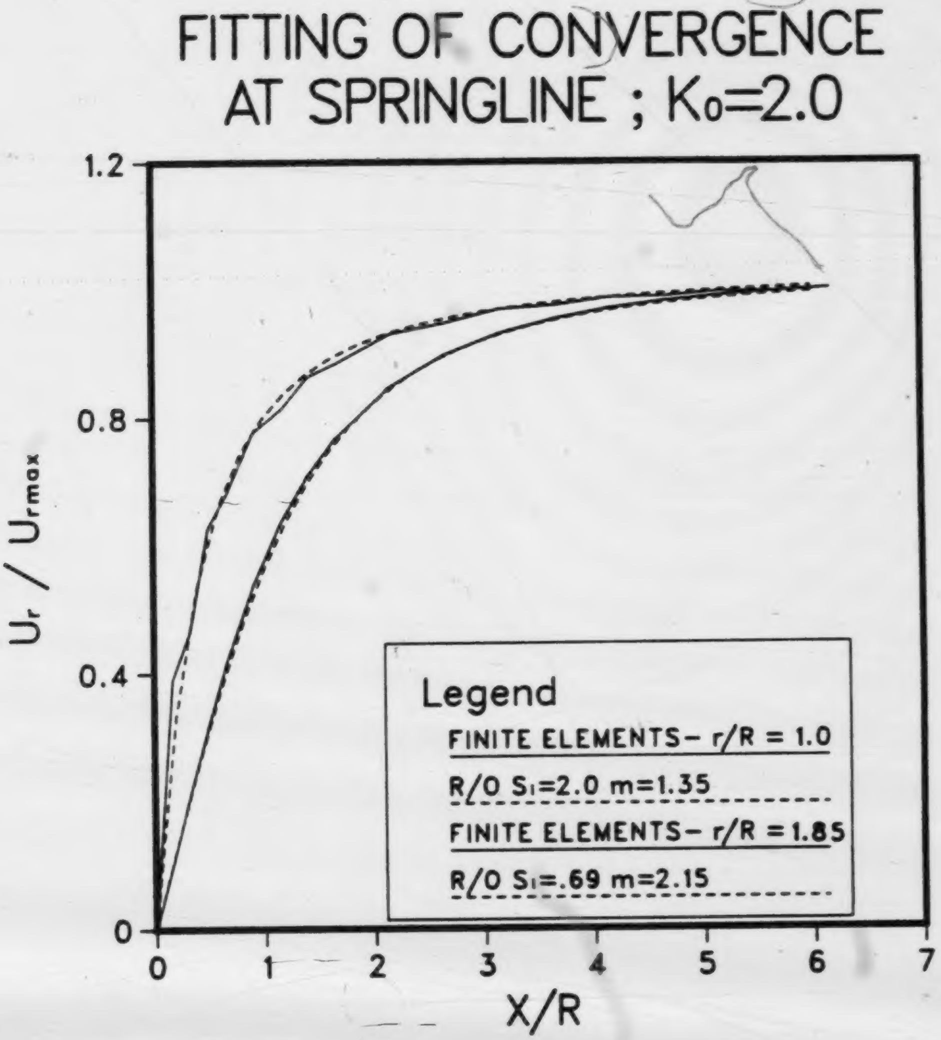

Figure 3.20 Fitting of the Relative Displacement Curves Calculated at the Tunnel Springline (r/R=1 and r/R=1.85) by the Ramberg-Osgood Analytical Function (K_0=2)

1) Convergence measurements should be started immediately behind the tunnel face. Even a small delay may have a substantial influence on the results, because of the high convergence gradient near the excavation front.

2) Displacement profiles given by radial multipoint extensometers are also affected by the distance from the tunnel face at which the instruments are placed. It was shown that for low initial axial stress ($K_0=2$; $P_a=P_v$) an "apparent" compression zone may be detected at the tunnel crown if the measurements are started one radius behind the tunnel face.

3) Measurements should be taken at least at two locations, at crown and springline or in both principal stress directions, to minimize errors. Monitoring at the tunnel crown only (direction of the minimum principal stress) may lead to serious back-analysis errors, as radial movements at that location are highly sensitive to the magnitude of the initial axial stress P_a.

4) The radial displacement profiles have different shapes depending on the distance from the tunnel axis at which the measurements are taken. In general, the profiles get flatter as the distance from the tunnel increases. The radial displacements profiles measured in field should be compared with curves calculated at the same distance from the tunnel wall.

4. UNLINED TUNNELS IN ANISOTROPIC ROCK

4.1 Introduction

In the previous chapter the distribution of stresses and deformations near the face of a tunnel in linear elastic isotropic rock was studied. The influence of the initial axial stresses on the near face behavior was emphasized, as it affects the measurements taken during excavation.

In the present chapter the effects of rock anisotropy on elastic stresses and deformations is discussed.

This work does not intend to be a comprehensive treatise on tunnels excavated in non isotropic rock. Only some aspects, related to the near face behavior of advancing tunnels, are discussed.

It is also shown that initial stress distribution and rock anisotropy may have similar effects in terms of deformations in the rock around the opening. Some of these similarities are pointed out as they should be considered during monitoring data interpretation.

4.2 Description of the Analysis

A series of three dimensional finite element analyses were carried out, using the program ADINA, in order to study the behavior of deep unlined tunnels in linear elastic anisotropic rock.

The selected finite element mesh, as well as the assumptions regarding boundary conditions and principal stress directions and distribution, are described in Chapter 3.

In its most general form, anisotropic elasticity involves twenty one mutually independent parameters. In layered or stratified materials perfect symmetry of behavior about any axis perpendicular to the planes of stratification can be assumed. In this case the medium is said to obey transverse isotropy and the following relationships can be written:

$$\epsilon_x=\frac{1}{E_1}\sigma_x-\frac{\nu_2}{E_2}\sigma_y-\frac{\nu_2}{E_2}\sigma_z \qquad [4.2]$$

$$\epsilon_y=-\frac{\nu_1}{E_1}\sigma_x+\frac{1}{E_2}\sigma_y-\frac{\nu_2}{E_2}\sigma_z \qquad [4.3]$$

$$\epsilon_z=-\frac{\nu_1}{E_1}\sigma_x-\frac{\nu_2}{E_2}\sigma_y+\frac{1}{E_2}\sigma_z \qquad [4.4]$$

$$\gamma_{xy}=\frac{1}{G_1}\tau_{xy} \qquad [4.5]$$

$$\gamma_{yz}=\frac{1}{G_2}\tau_{yz}=\frac{2(1+\nu_2)}{E_2}\tau_{yz} \qquad [4.6]$$

$$\gamma_{zx}=\frac{1}{G_1}\tau_{yz} \qquad [4.7]$$

By the principle of conservation of energy (e.g., Fung, 1965) the matrix of the coefficients of Eqns. 4.2 to 4.7 must be symmetrical and, therefore, the following relationship must be satisfied:

$$\frac{\nu_1}{E_1}=\frac{\nu_2}{E_2} \qquad [4.8]$$

The parameter G_1 is independent and empirical formulas are found in the literature for its determination. The following relationship (Zienkiewicz, 1968):

$$\frac{1}{G_1}=\frac{1}{E_1}+\frac{1}{E_2} \qquad [4.9]$$

was adopted in the present work.

Three tunnels, excavated in transverse isotropic rock, were modelled . A constant ratio $E_2/E_1=10$ was chosen where E_2 is the elastic modulus for any direction parallel to the strata. This rather high E_2/E_1 value is realistic for metamorphic foliated rocks (Gerrard, 1977), and was selected to emphasize the effects of rock anisotropy on stresses and deformations near the tunnel. The parameter ν_2 was given a value of 0.25; consequently (from eqn. 4.3) $\nu_1=0.025$ was assumed. A constant stress ratio $K_0=2$ was selected for the three cases whereas a different orientation in space of the rock's elastic properties was assumed for each case, as depicted in Figure 4.1.

Case 1 represents a tunnel driven in horizontally layered rock. For this case the minimum Young's modulus, E_1, is associated to the vertical direction. The maximum Young's modulus , E_2, characterizes the rock in any horizontal direction. The shear deformations in the cross sectional planes (r,t) and in the vertical axial plane are controlled by the shear modulus G_1, where the modulus G_2 is associated with the horizontal axial plane. For the anisotropy ratio chosen in this work, the value of G_1 (given by Eqn. 4.3) turns out to be about 4.5 times smaller than G_2.

For Case 2, the elastic properties of the rock are rotated by 90°, with respect to Case 1, around the tunnel

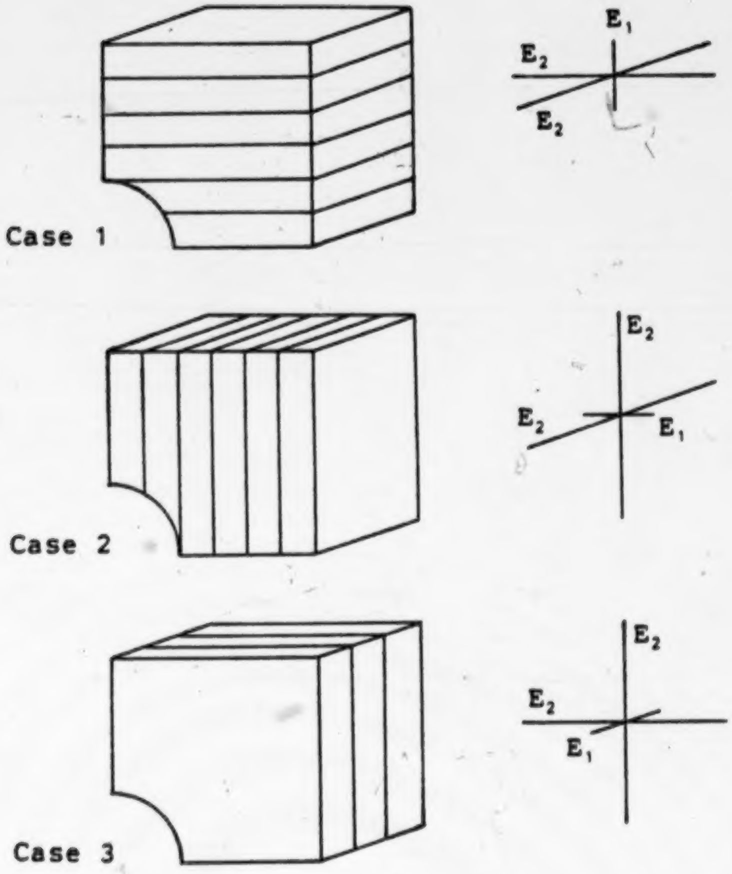
E₁
E₂
E₂
Case 1
E₂
E₂
E₁
Case 2
E₂
E₂
E₁
Case 3

Figure 4.1 Orientation of the Elastic Properties for the Cases Investigated

axis.

For Case 3, the orientation of the minimum elastic modulus, E_1, corresponds with the axial direction, where the maximum modulus, E_2, is associated with any direction perpendicular to the tunnel axis. A high shear modulus, G_2, controls, for this case, the shear deformations in the cross sectional planes (r,t). The axial planes (a,r) are characterized by the low shear modulus G_1.

In the following paragraphs the results of the finite element analyses are discussed. Emphasis is placed on how anisotropy affects the behavior of the tunnel near the face and monitoring data.

4.3 Stresses Near Tunnel Face

In Figures 4.2 to 4.4, normalized radial stresses at the tunnel springline are plotted for Cases 1 to 3. Each curve represents a different normalized distance from the tunnel axis r/R (see legend).

For Case 1 (Figure 4.2), a stress peak at the tunnel face is observed, at r/R=1.0, due to arching. For locations farther away from the opening, little stress change occurs ahead of the tunnel face.

For Case 2 (Figure 4.3), a much less significant stress peak is observed at the face. The reason is that, for this case, the tunnel face is highly deformable in the horizontal direction, relatively to Case 1, due to the orientation of the rock properties. It can then be stated that if the

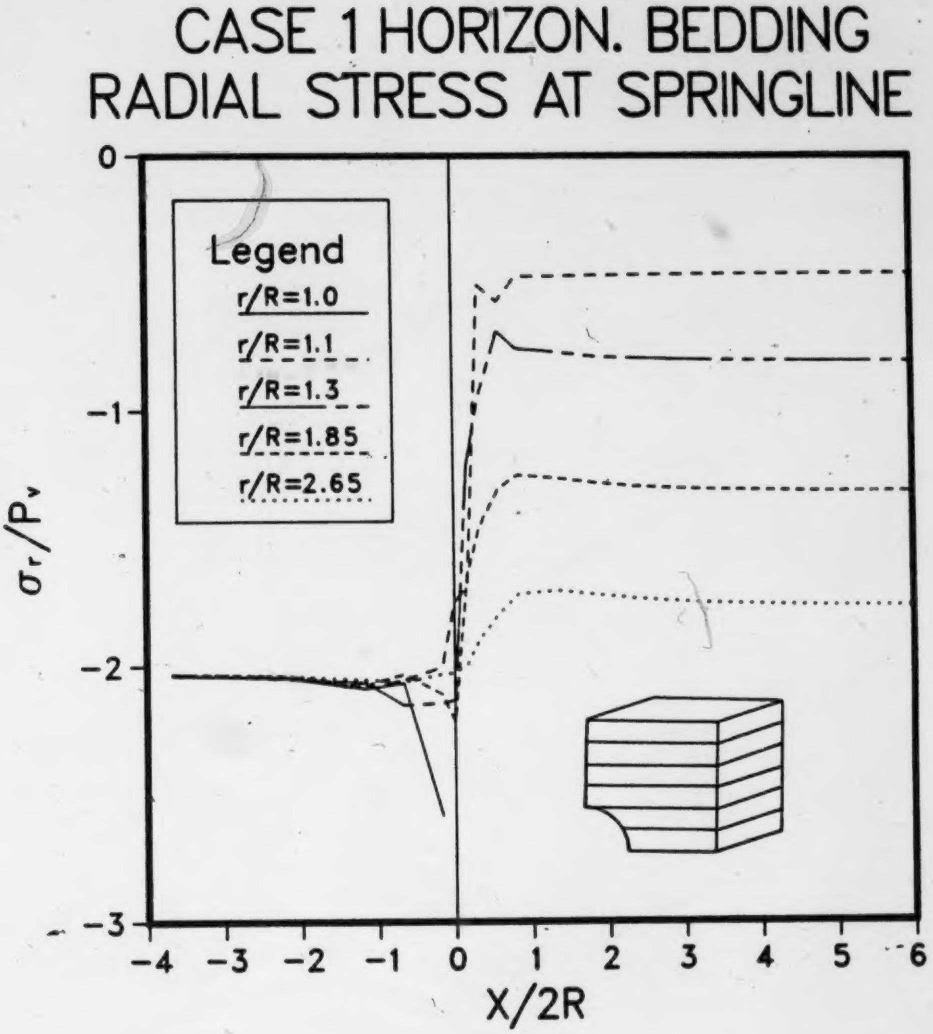

Figure 4.2 Radial Stresses, σ_r, at the Tunnel Springline; Case 1

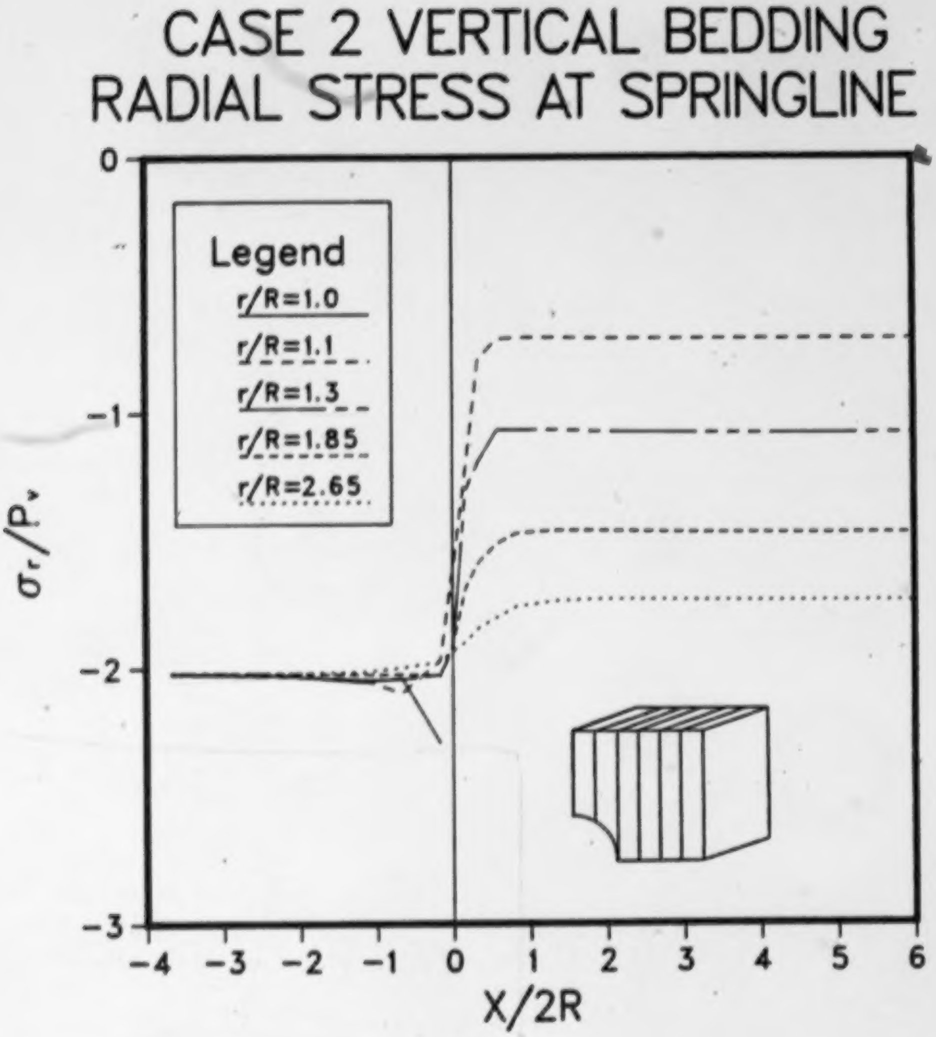

Figure 4.3 Radial Stresses, σ_r, at the Tunnel Springline; Case 2

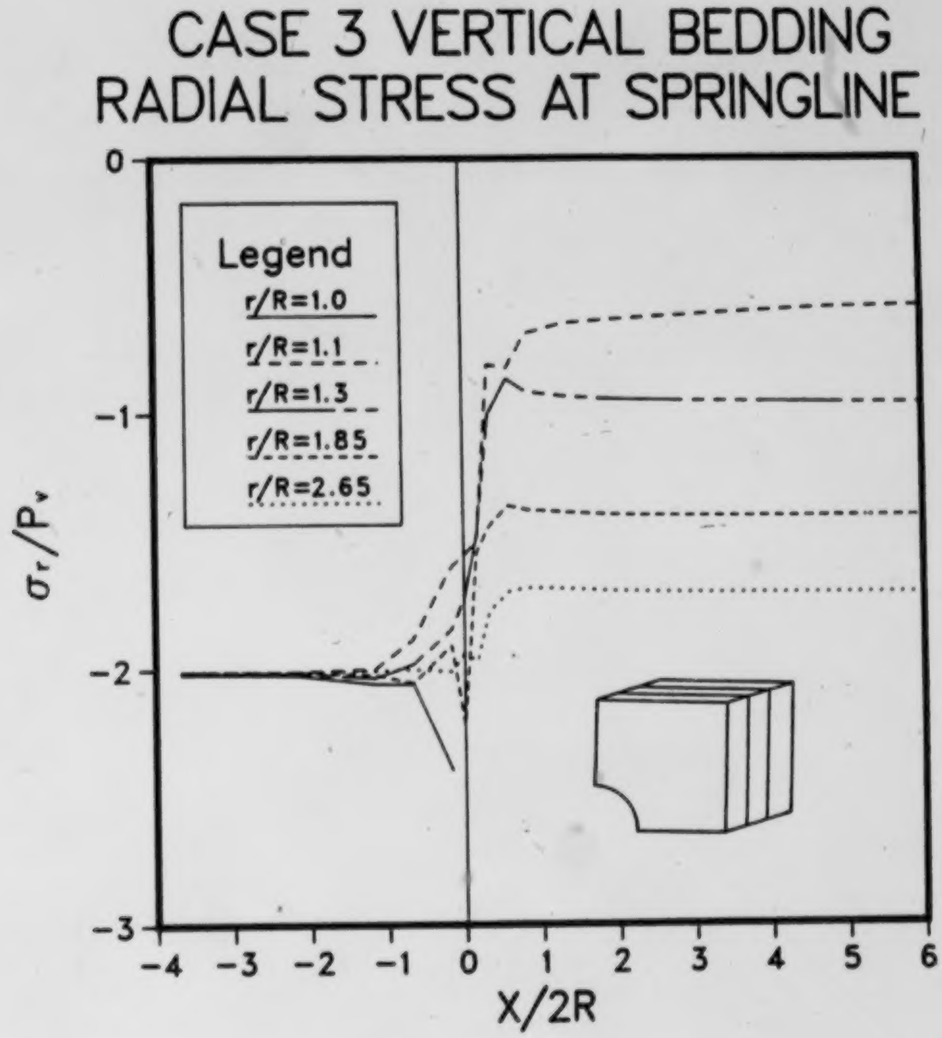

Figure 4.4 Radial Stresses, σ_r, at the Tunnel Springline; Case 3

maximum initial stress (normal to the tunnel axis) acts in the direction of the minimum elastic modulus (Case 2) lower stress concentrations are expected to occur at the excavation front. In Figure 4.5, the radial horizontal stresses ahead of the tunnel face calculated at the tunnel axis are compared for the three cases. The maximum stress value is found, at the face, for Case 3 whereas the minimum is detected for Case 2. This observation has important practical implications, because stress concentrations at the tunnel face may lead to instabilities.

For Case 3 (Figure 4.4), the portion of rock immediately ahead of the tunnel face, for r/R=1.1 and 1.3, presents radial stresses considerably lower than for Cases 1 and 2. This is due to the low elastic modulus in the axial direction that causes large inward movement of the tunnel face(see Figure 4.6). As will be shown later in this chapter, this movement encourages relatively large convergence ahead of the tunnel face that is consistent with the observed stress decrease.

The shear stresses at the tunnel springline are plotted, in Figure 4.7, at r/R=1.1. A stress peak can be observed, for each case, at the face. The lowest value is found for Case 3, due to the low elastic modulus along the axis of the tunnel that allows large inward movement of the face during excavation. In conjunction with this movement, relatively high shear stresses (τ_{ar}), having opposite sign with respect to the ones due to the wall convergence,

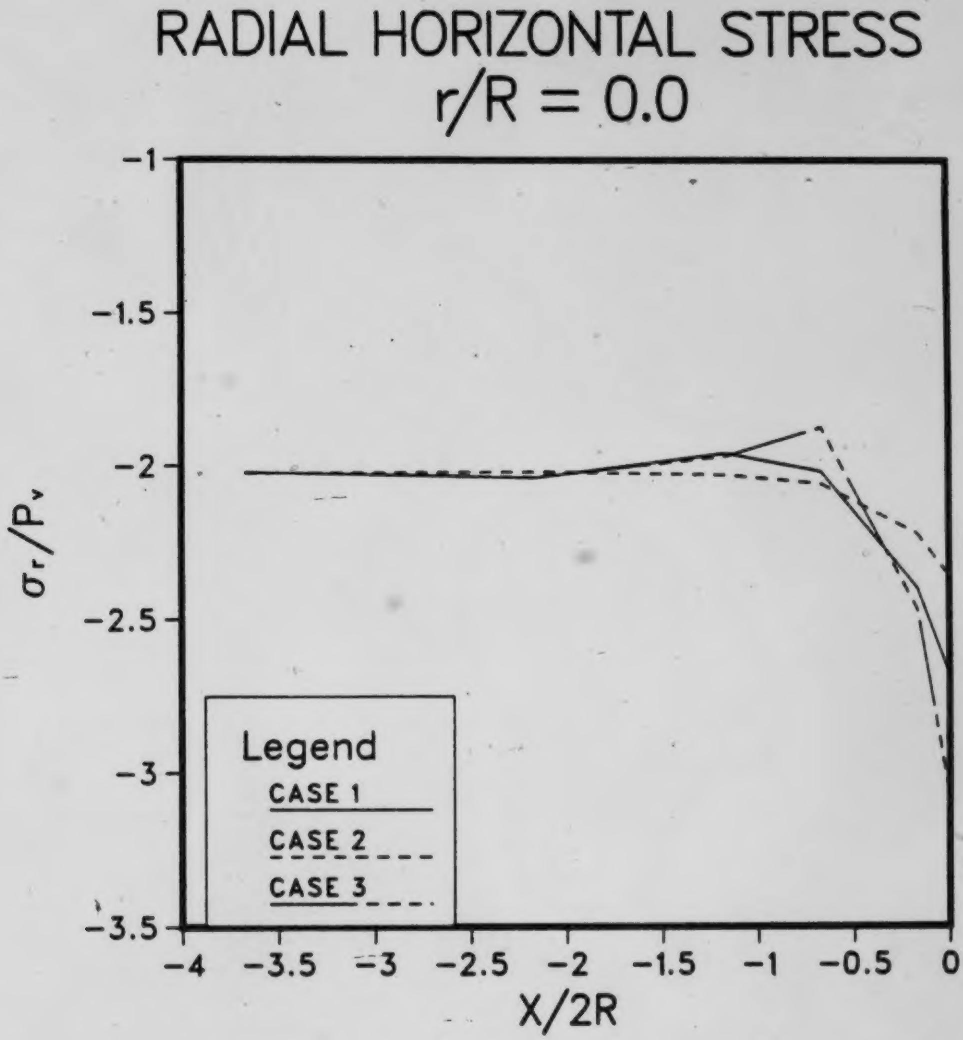

Figure 4.5 Radial Horizontal Stresses, σ_r, at the Tunnel Axis, Ahead of the Face; Cases 1 to 3

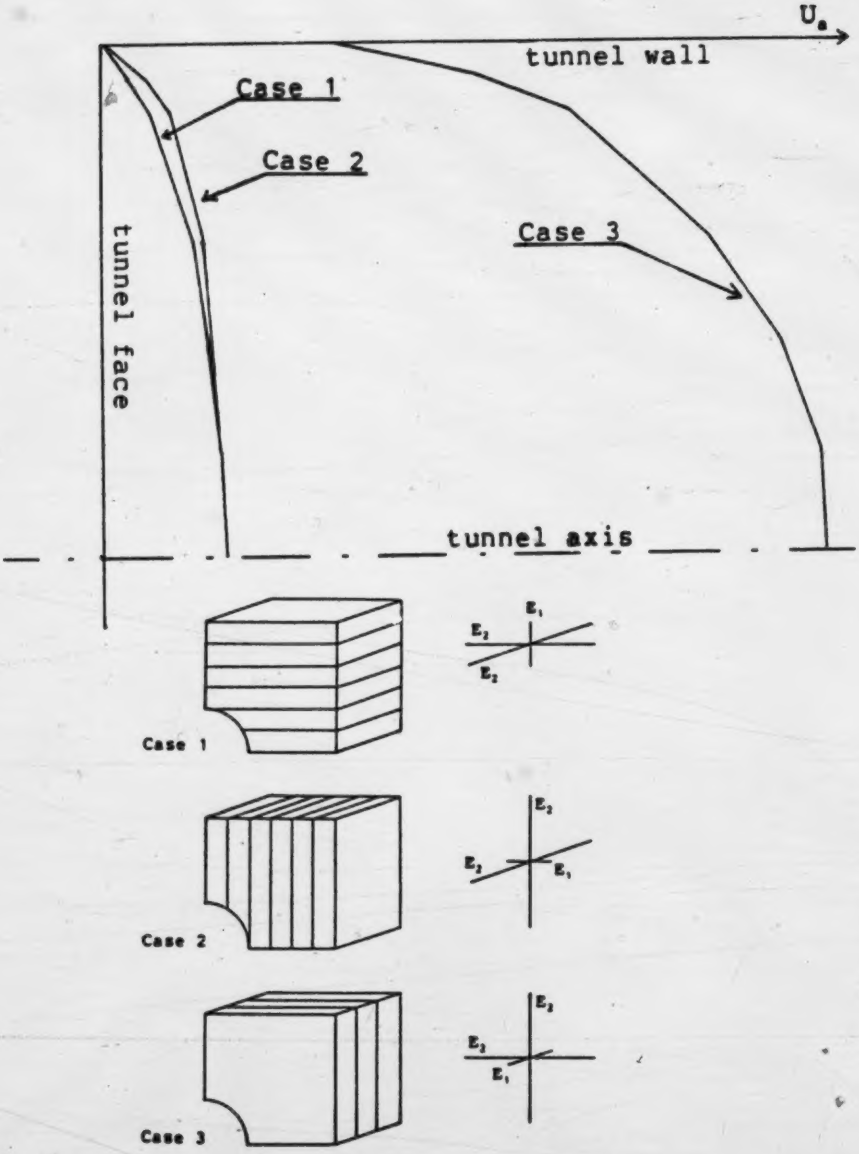

Figure 4.6 Horizontal Movement at the Tunnel Face; Cases 1 to 3

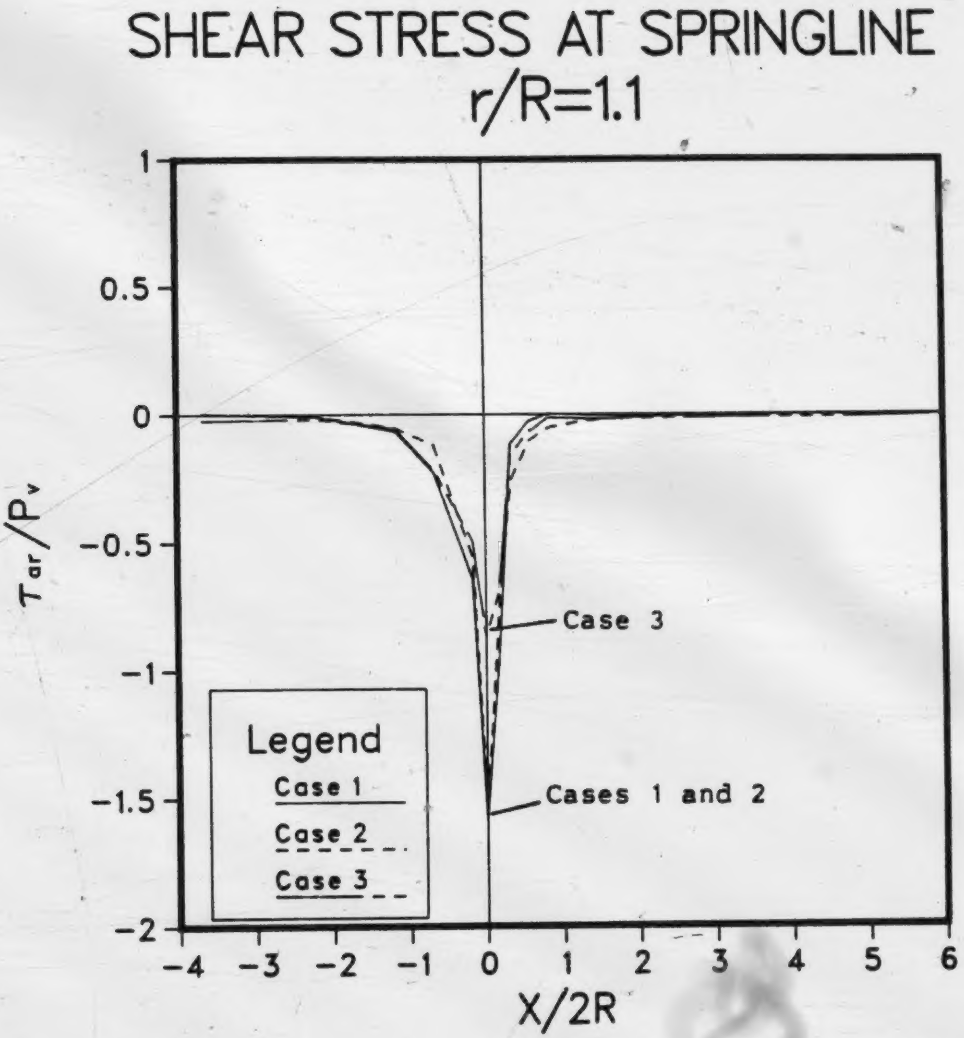

Figure 4.7 Shear Stresses, τ_{ar}, at the Tunnel Springline; Cases 1 to 3

develop and relatively low τ_{ar} values result at the tunnel face.

The tangential stresses calculated at the tunnel crown for r/R=1.3 are plotted in Figure 4.8. This figure shows the influence of the magnitude of the shear modulus in the axial planes (a-r) on the development of the transverse arching. For Case 3, the low shear modulus G_1 results in a high stress gradient near the tunnel face. The ultimate tangential stress is reached relatively close to the excavation front. As will be shown later in this chapter, this is a clear indication of high convergence rates.

It can also be seen that far behind the face the tangential stresses are highest for Case 1. This is due to the high stiffness of the medium in the horizontal direction. This phenomenon has been discussed further by Lekhnitskii (1963) and Savin (1970).

In Figure 4.9, the axial stresses at the tunnel springline are plotted for r/R=1.1. The axial stresses at the face are much lower in magnitude for Case 3. In Figure 4.10, a schematic diagram for the explanation of this phenomenon is given. The medium around the tunnel is assumed to be composed of a set of parallel horizontal beams, having a Young's modulus E. The beams are connected to each other by means of interface elements, able to transmit shear stress, having a shear stiffness G. If the beams are very stiff with respect to the interface elements (high E/G) most of the axial stress increase, due to excavation, occurs in

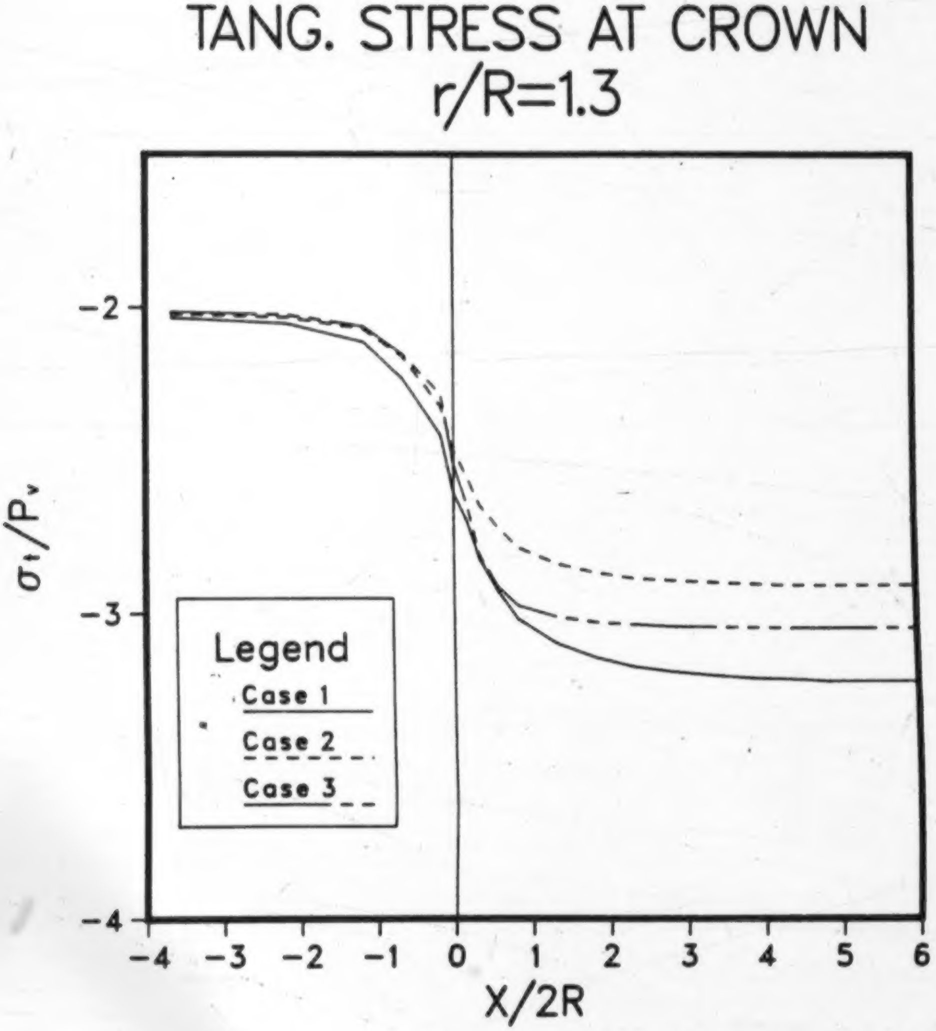

Figure 4.8 Tangential Stresses, σ_t, at the Tunnel Crown; Cases 1 to 3

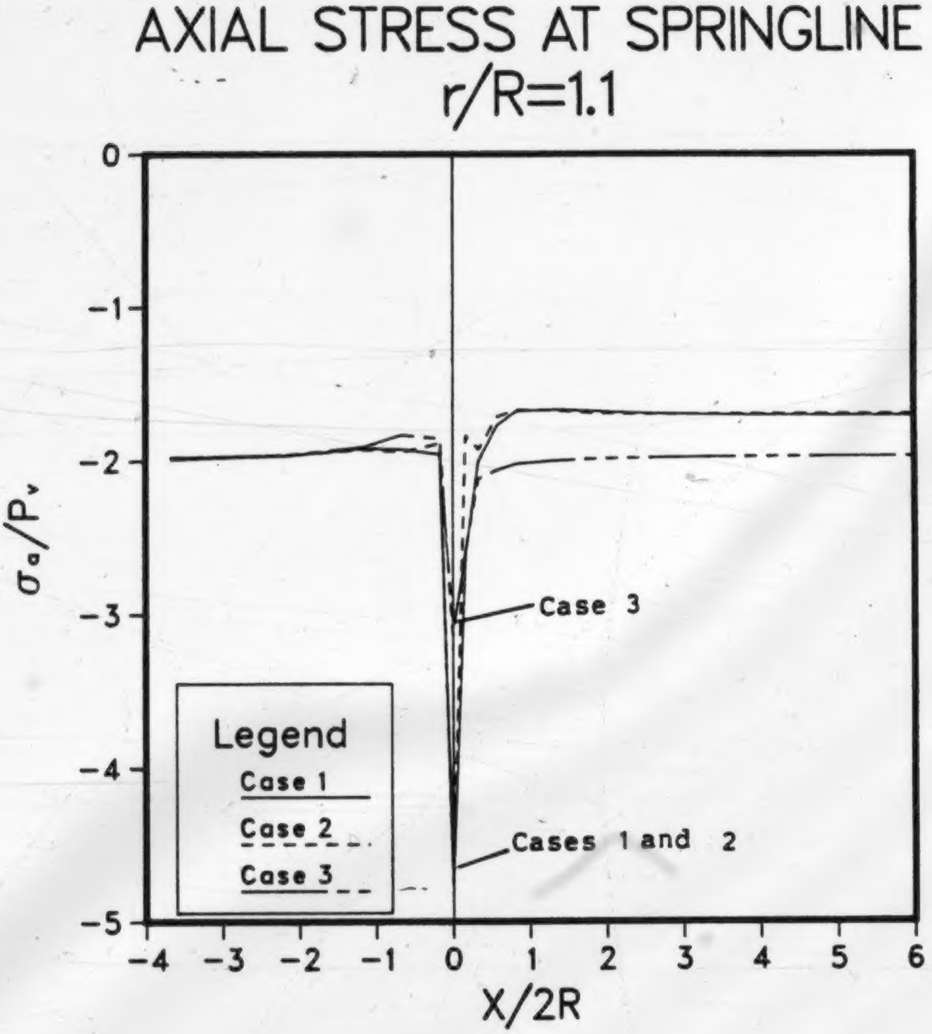

Figure 4.9 Axial Stresses, σ_a, at the Tunnel Springline; Cases 1 to 3

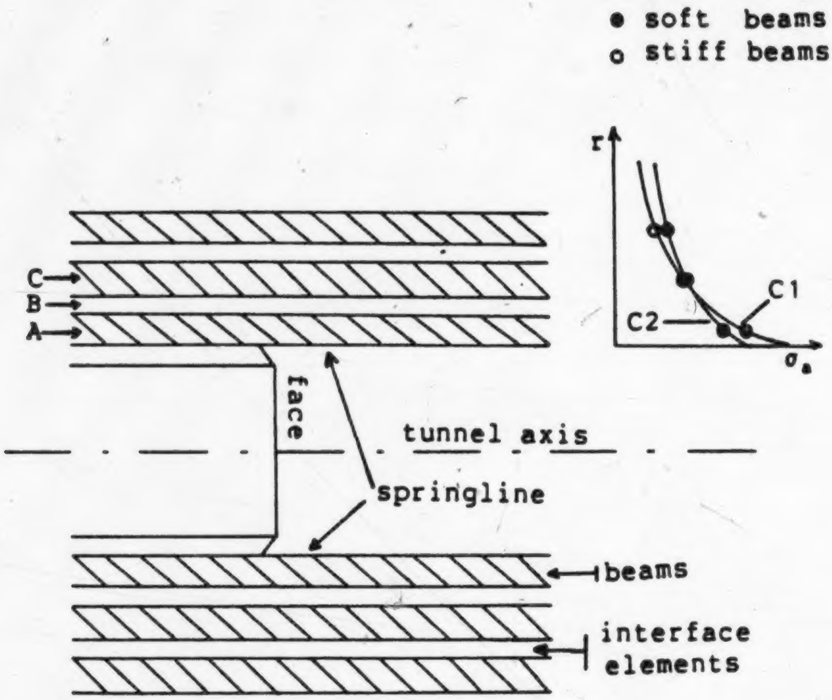
● soft beams
○ stiff beams
r
C1
C2
σ_a
C
B
A
face
tunnel axis
springline
beams
interface elements

Figure 4.10 Effect of Anisotropy on the Axial Stress Distribution at the Tunnel Face

Beam A. This is because the transmission of load to Beam C requires large relative displacements in Interface B. A high elastic modulus in the axial direction results in a stress distribution curve having a high gradient near the tunnel wall (Curve C1 in Figure 4.10).

On the other hand, if the beams are soft with respect to the interface elements (low E/G) the stress increase is easily transmitted to beams located farther away from the tunnel and a relatively flat axial stress distribution results (Curve C2 in Figure 4.10). This is what occurs in Case 3, where a low shear modulus characterizes the a-r planes, and explains why a low axial stress concentration is found at the face, near the tunnel wall. Behind the tunnel face the stress decrease detected at the excavation front for Case 1 and Case 2 (as well as for isotropic media), does not occur for Case 3 where virtually no change in axial stress is found (see Figure 4.9). This is also due to the low Young's modulus in the axial direction characterizing Case 3 which involves small axial stress changes for plane strain conditions.

In conclusion, it has been observed that the orientation of the rock's elastic parameters considerably influences the stress distribution near the tunnel face.

If the minimum elastic modulus is parallel to the axis of the tunnel, low shear stresses at the tunnel face are found. This has an impact on the radial displacements around the opening, as discussed in the next paragraph.

A low shear modulus in the axial planes, as in Case 3, causes a rapid development of transverse arching behind the tunnel face. From this observation a high convergence gradient can be anticipated.

Far behind the tunnel face high tangential stresses occur if the tunnel axis is parallel to the strata and if the major initial stress (normal to the tunnel axis) acts parallel to the direction of high stiffness. This could lead to unexpected rock failure if the degree of anisotropy were neglected in design.

4.4 Displacements

The displacements developing around the tunnel due to the excavation are shown in the usual form (see Chapter 3). The radial displacements are normalized with respect to the average Young's modulus E_{av} defined as:

$$E_{av} = \frac{E_1 + E_2}{2} \qquad [4.10]$$

In Figure 4.11, convergence at the tunnel crown and springline is plotted, for Case 1, against distance to the tunnel face. The maximum initial stress, normal to the axis of the tunnel, acts in the same direction as the maximum Young's modulus. The minimum Young's modulus (in the vertical direction) is parallel to the minimum initial stress.

The ultimate convergence is larger at the crown than at the springline, opposite to the isotropic case. If partial displacement measurements are taken, neglecting the movement

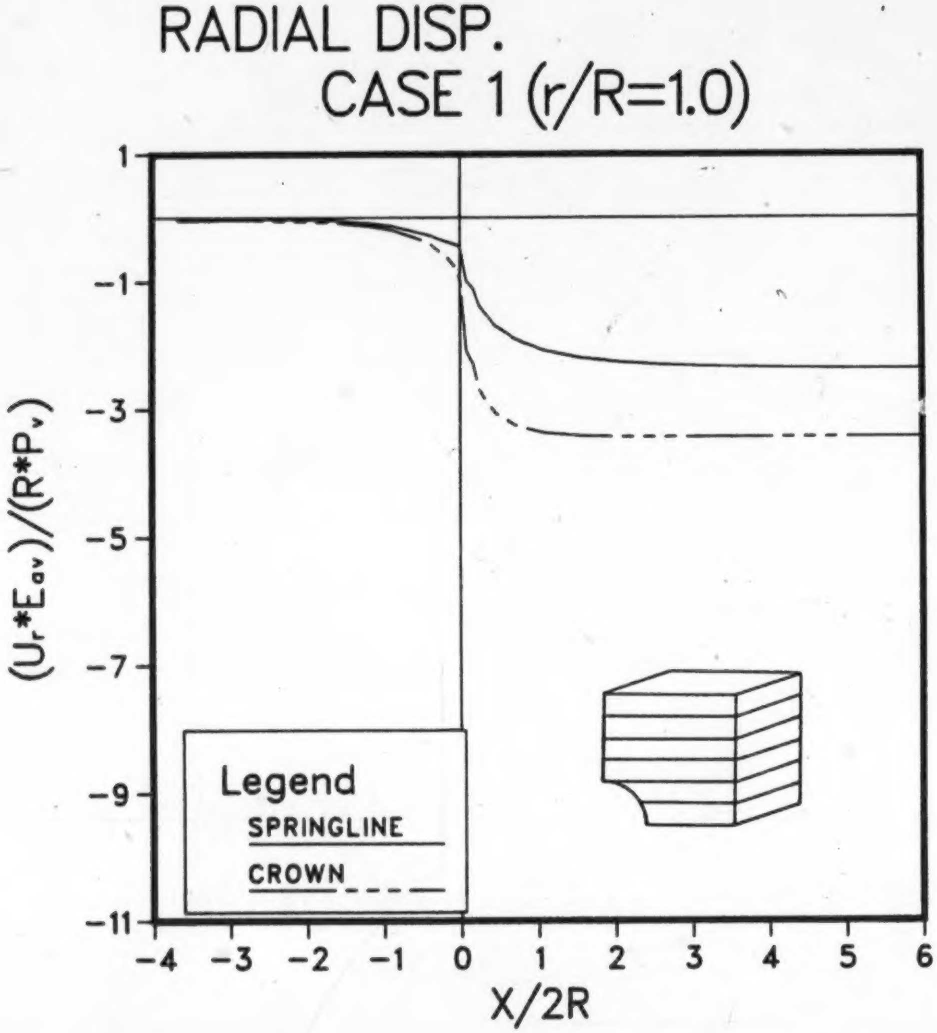

Figure 4.11 Convergence at the Tunnel Crown and Springline; Case 1

occurring ahead of the face, a ratio U_r(springline)/U_r(crown)=0.75 is found. This ratio would correspond to a ratio K_0=0.87 (instead of 2.0) for tunnels in isotropic rock (based on two dimensional close form solution).

For Case 2 (Figure 4.12), the maximum initial stress, normal to the tunnel axis, acts in the direction of minimum stiffness. A relatively large inward displacement takes place at the springline and the tunnel crown moves outward. A displacement ratio of 8.45 is found (if the convergence ahead of the face is neglected). Close form solutions for isotropic elastic media predict, on the basis of this ratio, a K_0=4.5. Note that if the total displacements are considered (including convergence ahead of the face) an even higher displacement ratio (and K_0) is found.

These observations lead to the conclusion that either the initial stresses or the degree of anisotropy of the rock should be known before the back-analysis is attempted. This is because stress distribution and orientation of the elastic parameters produce similar effects on displacements.

In Figure 4.13, the convergence profiles for Case 3 are shown. Note that a larger scale has been used for this diagram. The low stiffness direction is parallel to the axis of the tunnel. It can be seen that some outward movement occurs at the tunnel face, especially at the crown.

An analogy with tunnels in isotropic rock, excavated under high axial stresses, is apparent. Another feature to

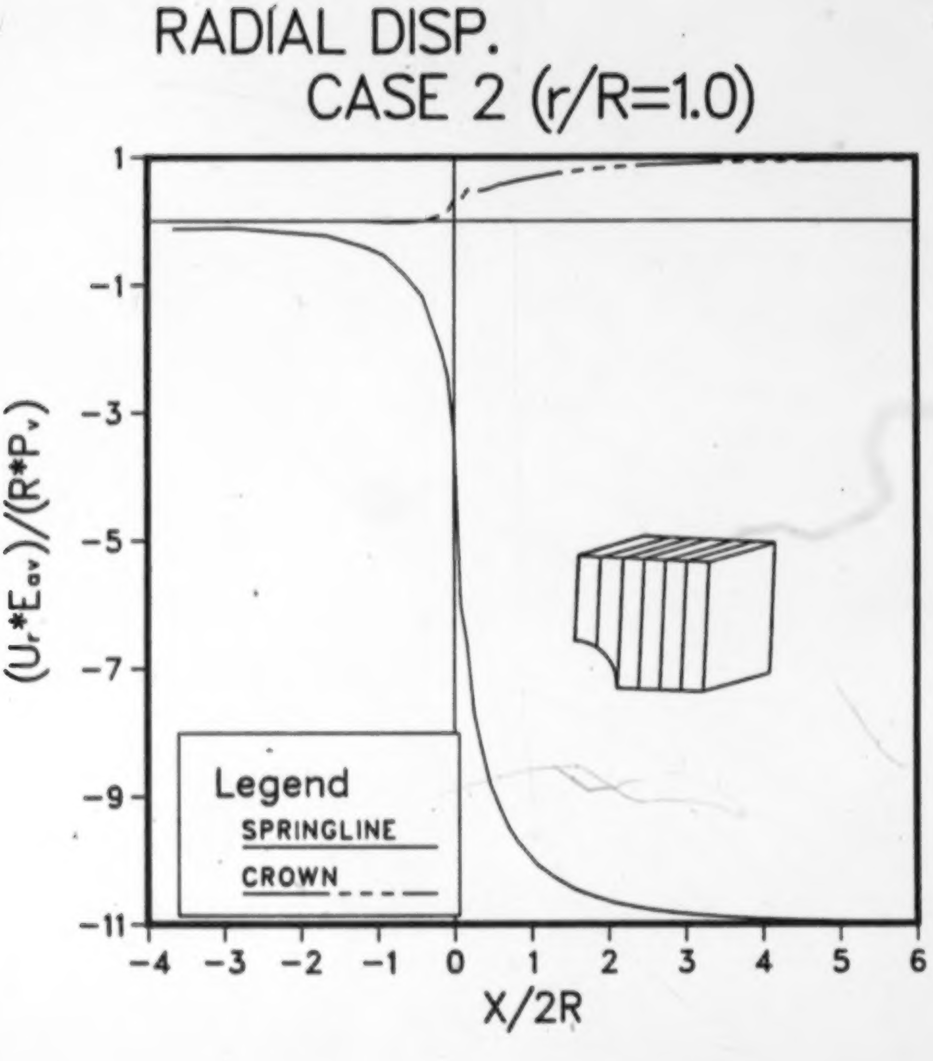

Figure 4.12 Convergence at the Tunnel Crown and Springline; Case 2

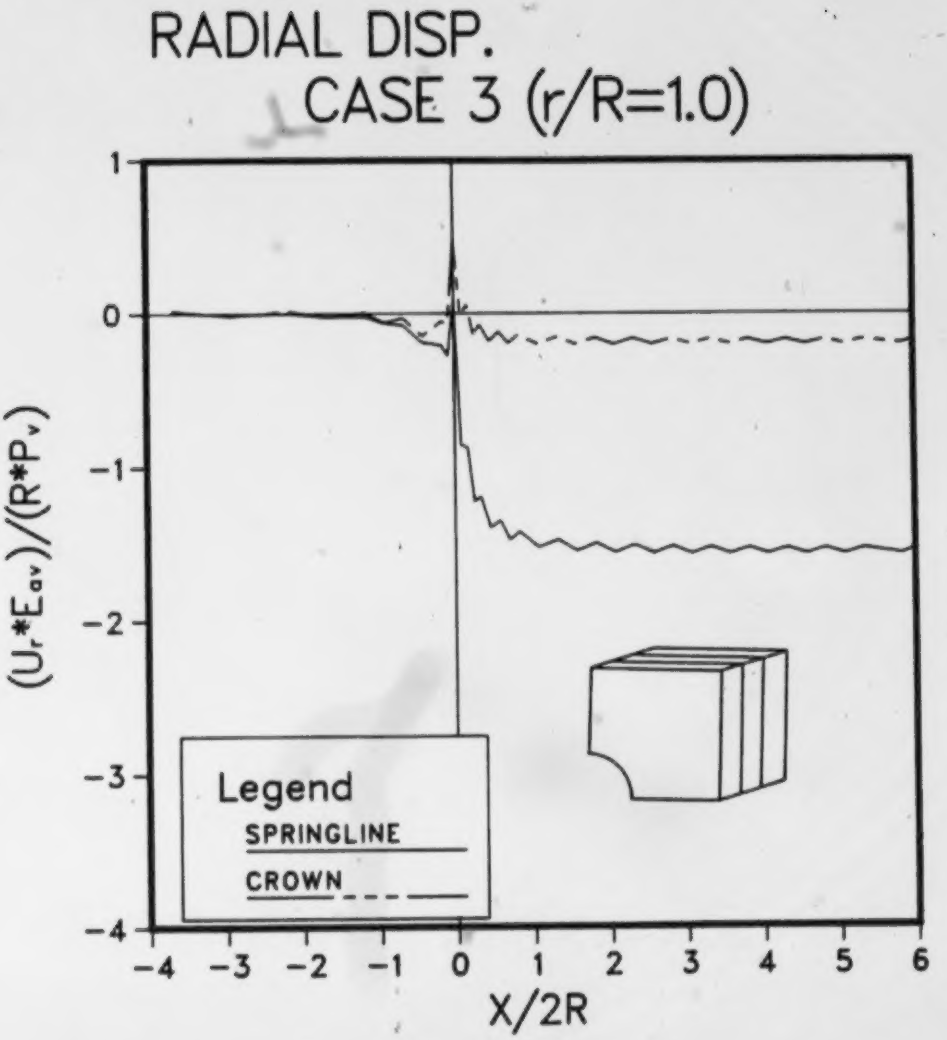

Figure 4.13 Convergence at the Tunnel Crown and Springline; Case 3

be observed is the high gradient characterizing the convergence curves for Case 3. This phenomenon, which will be discussed more extensively later in this chapter, is consistent with the stress distribution shown in the previous paragraph, that revealed a rapid development of transverse arching for this case.

In conclusion, some similarities were found between the effect of the stress distribution and the orientation of the principal directions of deformability. This makes it difficult to back-analyze the rock parameters and the stress distribution at the same time.

On the other hand, the shape of the convergence curves may be able to give, in some cases, additional information. It was found, for instance, that a low elastic modulus in the axial direction, associated with a low shear modulus on the axial planes, results in high convergence gradients near the tunnel face.

4.5 Implications for Monitoring Data Interpretation

4.5.1 Convergence Records

In the previous chapter it was pointed out that, when convergence measurements are carried out, the zero readings should be taken as close as possible to the tunnel face. It was in fact recognized that even a small delay may affect considerably the outcome of the measurements due to the high convergence gradient near the face.

In this context the shape of the convergence curve plays an important role. In Figure 4.14, four convergence curves at the tunnel springline are shown in normalized form. Radial displacements are normalized with respect to the maximum convergence (U_r/U_{rmax}) and are plotted against normalized distance to the face (r/R). The three anisotropic cases and the elastic isotropic case are compared.

If the zero reading is assumed to be taken one half radius behind the tunnel face (marked by a vertical line in Figure 4.14), only a portion of the displacements taking place behind the face is found. For the isotropic case 37% of the radial displacements is measured. For Cases 1 and 2 the convergence curves are flatter than for the tunnel in isotropic rock, and, respectively, 51 and 43% of the displacements is measured. For Case 3 only 21% of the dispacement is measured, due to the relatively low shear modulus in the axial planes (planes containing the tunnel axis).

The relationship between shape of the convergence curves and orientation of the elastic properties of the rock will be discussed further at the end of this chapter. For now it can be concluded that rock anisotropy may increase or decrease the sensitivity of the convergence measurements to delays, with respect to the tunnel face, at which the zero readings are taken. In particular, if the minimum elastic modulus is associated with the axial direction, high convergence gradients (i.e., high sensitivity to delays)

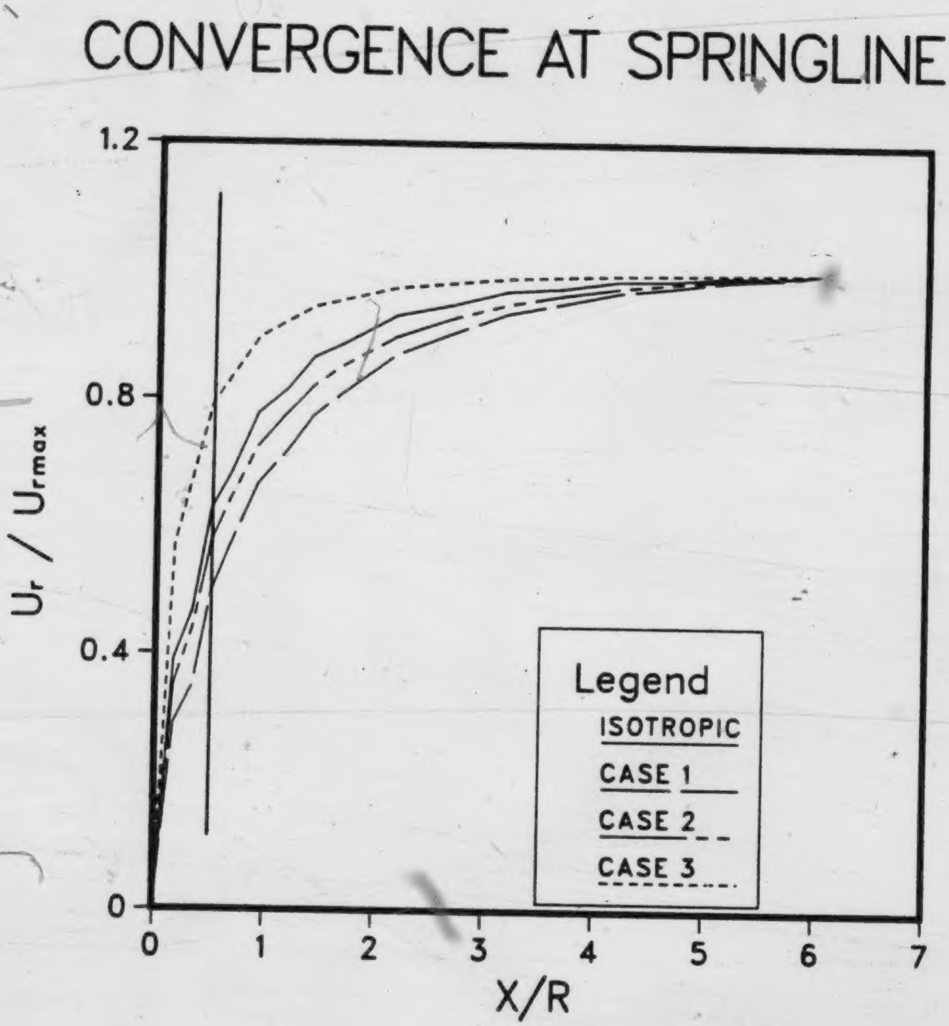

Figure 4.14 Normalized Convergence Curves, U_r/U_{rmax}, at the Tunnel Springline; Cases 1 to 3 and Isotropic

must be expected.

4.5.2 Multipoint Extensometer Records

The relative displacements calculated at the tunnel crown are plotted, in Figure 4.15, against the distance from the tunnel axis r/R. The displacements ahead of the tunnel face are not considered (these are partial values) so that these data can be compared with measurements taken by means of radial multiple anchor extensometers placed immediately at the tunnel face.

In terms of radial displacements at the tunnel wall, the value calculated for Case 1 is largest. This is due to the low Young's modulus in the vertical direction. For Case 2, outward movement is found due to the combination of high elastic modulus and low radial initial stress in the vertical direction.

In the previous chapter it was observed that, for $K_0=2$, relatively short radial extensometers, placed at the tunnel crown, are sufficient to depict the strain field near the tunnel. It is here found that, not only the initial stress distribution, but also the orientation of the elastic parameters affects the propagation of the straining process. It can, in fact, be observed that for Case 3 no displacements are detected for r/R larger than 4 while, for Case 1 and Case 2, significant movement occurs at $r/R \geq 6$ (i.e. flatter relative displacements curves are found for Cases 1 and 2).

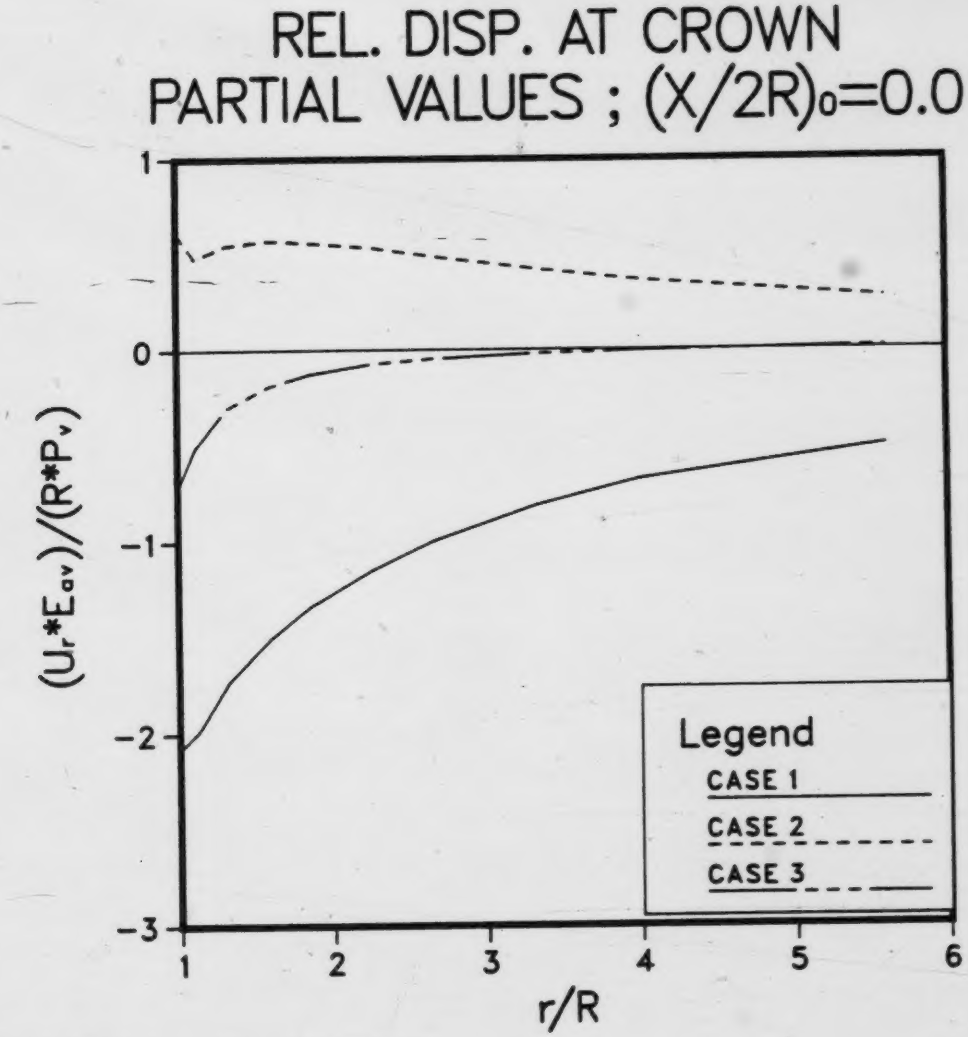

Figure 4.15 Relative Displacements at the Tunnel Crown (Partial Values); Cases 1 to 3

Consequentely, it can be stated that for those cases for which the tunnel axis is parallel to a direction of maximum stiffness (Cases 1 and 2), radial multiple anchor extensometers of considerable length may be necessary to describe the deformation field around the opening. This observation is very important, in practice, because it concerns tunnels excavated in thinly stratified or laminated rocks, with the axis parallel to the strata, if a significant degree of anisotropy characterizes the overall behavior of the rock mass. For these tunnels, if the initial stress field is known, the distance of propagation of the strain field can provide a useful indication to detect anisotropic rock behavior.

In the previous paragraph the outward movement, occurring at the tunnel face, for Case 3 was discussed. Such behavior is particularly pronounced at the crown and considerably affects the partial measurements, with zero readings taken at the excavation front. In Figure 4.16, partial and total relative displacements calculated at the tunnel crown for Case 3 are compared. The purpose is to show how different the displacements given by an extensometer placed at the face (partial values) are with respect to the displacements given by an extensometer placed far ahead of the tunnel face (total values). The partial readings, usually the only available data for deep tunnels, have larger magnitudes than the total measurements. This may cause misleading conclusions to be drawn, especially if the

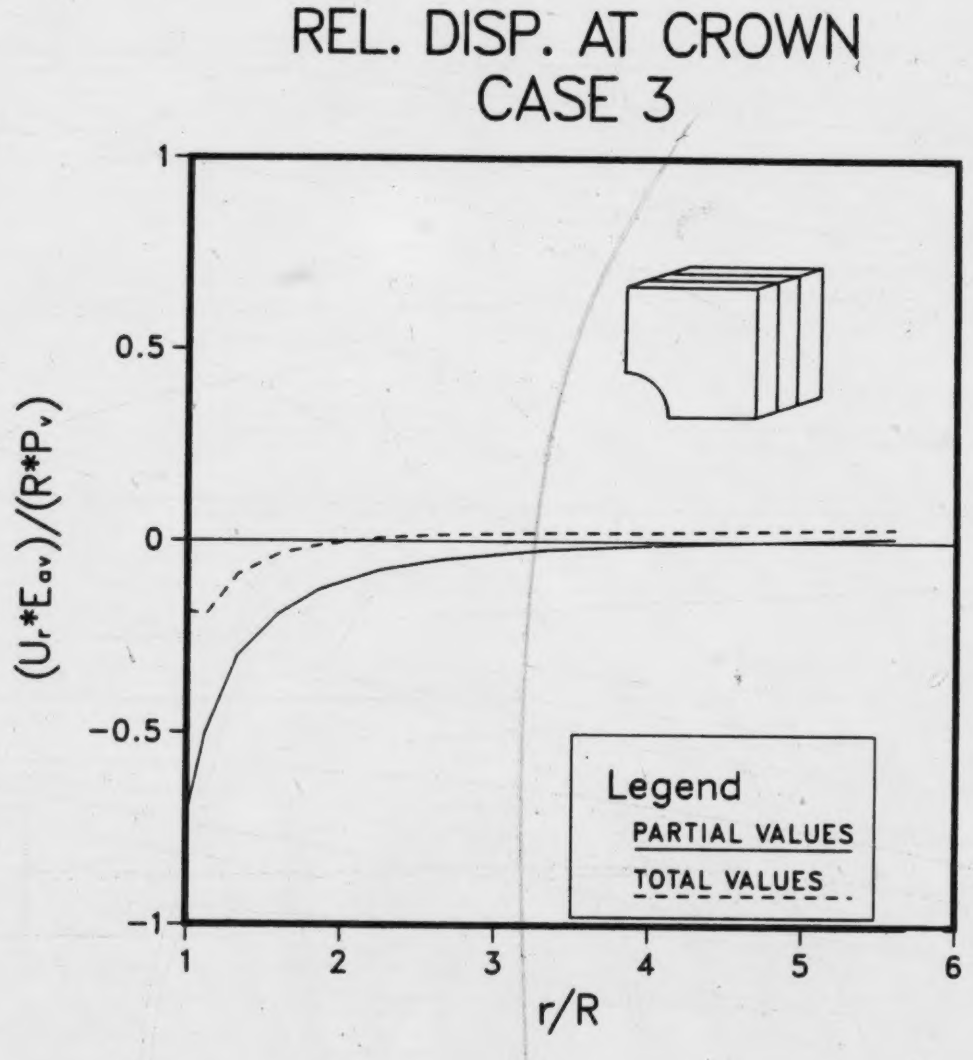

Figure 4.16 Relative Displacements at the Tunnel Crown (Partial and Total Values); Case 3

tunnel crown is the only monitored location.

It can be concluded that, especially at the tunnel crown (direction of the minimum initial stress), the shape of the relative displacement curves, as given by the radial extensometers placed at the tunnel face, are sensibly affected by the orientation of the rock elastic properties. Relatively flat curves,with large radial displacements far from the tunnel wall, are found if the axial direction is associated with the maximum elastic modulus. If the minimum elastic modulus controls deformations along the axis, the radial displacements are concentrated near the wall of the tunnel.

4.5.3 Shape of Radial Displacement Profiles

The shape of the convergence curve is sensitive to the orientation of the rock elastic properties. In Figure 4.17, the convergence curves at the tunnel springline are shown, for the three cases, in normalized form. The finite element results have again been fitted by the Ramberg-Osgood function. The initial gradients S_i and the shape factors m selected for the fitting are shown in the legend.

The initial gradient associated with Case 3 is two times as large as for the other two cases. The high normalized initial gradient found for Case 3 is due to the low modulus controlling shear deformation on the axial planes.

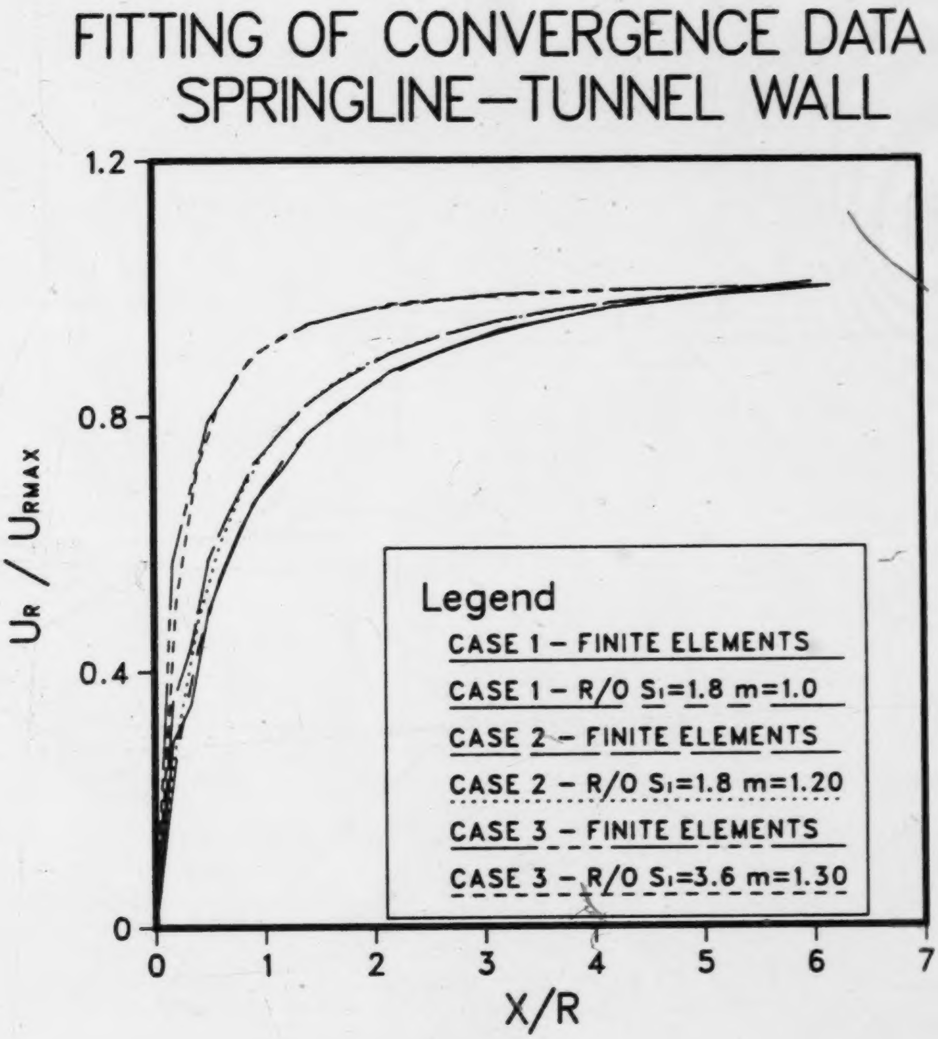

Figure 4.17 Normalized Convergence Curves, U_r/U_{rmax}, at the Tunnel Springline, Fitted by the Ramberg-Osgood Function; Cases 1 to 3

The shape of the convergence curves is related to the ratio between the shear modulus in the axial planes G, and the elastic modulus controlling convergence far behind the tunnel face E (the effect of the Poisson's ratio is neglected). For a tunnel in elastic isotropic rock, for $\nu=0.25$, a ratio $G/E=0.4$ is found. For Case 3 this ratio is 0.09 and a steeper convergence curve is observed. For Cases 1 and 2 the ratio G/E assumes different values, depending on the orientation of the axial planes. For Case 1, for instance, the ratio G/E in the horizontal plane is 0.4, as for the isotropic case, and 0.9 in the vertical plane. The same situation, rotated by 90°, is found for Case 2. On average, the ratio G/E for Cases 1 and 2 is the highest, and relatively flat convergence curves are in fact observed.

The m value varies between 1 and 1.3 for the three cases. Such parameter seems to be valuable in defining shape differences only for those cases where normalized convergence curves having equal initial gradients are compared.

In conclusion, the shape of the convergence curves are sensitive to the orientation of the elastic parameters. They can be regarded as a useful tool for back-analysis, especially for those cases where a low elastic modulus controls deformations in the axial direction.

4.6 Conclusions

The effects of rock anisotropy on tunnel behavior, as investigated in this chapter, can be summarized as follows:

1) Back-analysis of the initial stress field, based on displacement measurements taken in a tunnel in anisotropic rock, may lead to serious errors if the non-isotropic nature of the medium is not understood. Either initial stress field or orientation of the elastic properties of the rock mass should be known a priori.

2) The sensitivity of the convergence measurements to the distance from the tunnel face at which the zero readings are taken, discussed in the previous chapter, may be further increased if the minimum elastic modulus controls deformations in the axial direction.

3) The partial convergence measurements, taken at the tunnel crown, may have larger magnitudes than the total radial displacements if the minimum elastic modulus controls deformations in the axial direction. This may cause misleading conclusions to be drawn, especially if the tunnel crown is the only monitored location.

4) The shape of the displacement profiles, as given by multiple anchor extensometers at the tunnel crown (direction of the minimum initial stress), can indicate non-isotropic rock behavior. For the cases investigated, relatively flat curves, with large displacements measured far from the tunnel wall, were found when the maximum elastic modulus was assumed to control deformations along the axis of the

tunnel.

5) The shape of the convergence curves is related to the ratio between shear modulus in the axial planes and elastic modulus controlling convergence far behind the tunnel face. In general, low G/E ratios lead to steep convergence profiles where relatively flat curves are found for high G/E values. This feature can be useful, during the back-analysis process, because it can reveal the anisotropic nature of the rock mass.

5. UNLINED TUNNELS IN NON-LINEAR ROCK

5.1 Introduction

In the previous two chapters the stress-strain distribution around unlined tunnels in linear elastic rock was studied. It is very well known, however, that most geologic media exhibit non-linear and non-elastic behavior, allowing a certain amount of energy dissipation to occur as the straining process takes place.

A tunnel can be regarded as a highly constrained structure; if portions of the rock mass yield under high loads, a complex mechanism of stress redistribution intervenes to re-establish equilibrium. The purpose of this chapter is to study the effects of such mechanisms on stresses, deformations and stability near the tunnel face. For this reason, the results of linear and non-linear analyses are systematically compared and the differences are emphasized.

The main objective is to provide information useful in detecting non-linear and non-elastic rock behavior by means of monitoring data interpretation.

Two simple models have been selected for the analysis in order to simulate non-linearity in the pre-failure range and at failure.

Only the results of interest for the discussion are shown here. The remainder can be found in Appendix C.

5.2 Description of the analysis

In order to study the behavior of unlined tunnels excavated in rock exhibiting non-linear stress-strain relationship, two finite element analyses were carried out using the program SAFE. For both of them a stress ratio $K_0=2$ was selected.

5.2.1 Tunnel in Non-Linear Medium, Exhibiting Hyperbolic Stress-Strain Relationship

One of the analyses was performed to study the effects of non-linear behavior in the pre-failure range on the stresses and the displacements induced by the excavation in the rock mass. For this case the hyperbolic stress-strain relationship proposed by Konder (1963) was selected for the rock in the form given by Duncan and Chang (1970). Although it is not ideal to model relatively complex stress paths, this model has the advantage of being simple as it is defined by six parameters having direct physical meaning. The main characteristics of the hyperbolic relationship are shown schematically in Figure 5.1. The function relates axial strain ϵ_1 to stress difference $(\sigma_1-\sigma_3)$ as they can be measured at different stages of a triaxial test (σ_3=constant). It is defined by an initial modulus E_i, and an ultimate stress difference value $(\sigma_1-\sigma_3)_{ult}$ which both vary depending on the minor principal stress σ_3. The effect of the intermediate principal stress σ_2 is neglected. Experimental studies conducted by Janbu (1963) on soils lead

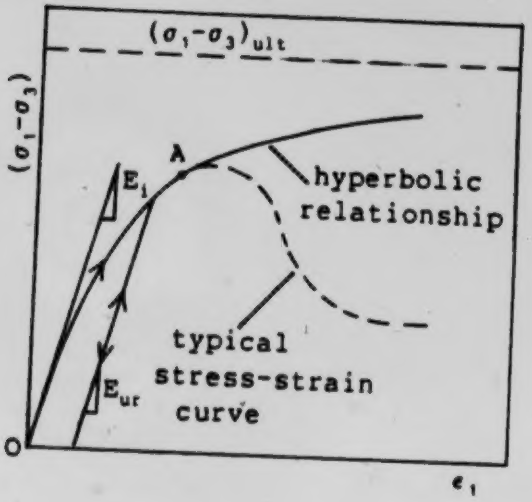
$(\sigma_1-\sigma_3)_{ult}$
$(\sigma_1-\sigma_3)$
A
E_i
hyperbolic relationship
typical stress-strain curve
E_{ur}
O
ϵ_1

Figure 5.1 Schematic Representation of the Hyperbolic Stress-Strain Relationship

to the relationship:

$$E_i = K.P_{atm}(\frac{\sigma_3}{P_{atm}})^n \qquad [5.11]$$

where K is a modulus number, P_{atm} is the atmospheric pressure (here used as a normalizing factor) and n is the exponent determining the rate of variation of E_i with σ_3.

The ultimate deviatoric stress value is expressed as follows:

$$(\sigma_1-\sigma_3)_{ult} = \frac{1}{R_f}(\sigma_1-\sigma_3)_f = \frac{2c.\cos\phi+2\sigma_3\sin\phi}{R_f(1-\sin\phi)} \qquad [5.12]$$

where $(\sigma_1-\sigma_3)_f$ is the stress difference at failure, R_f is a constant (failure ratio), c and ϕ are the Mohr Coulomb strength parameters.

Even though the hyperbolic model was developed for soils, it is based on principles (e.g., the Mohr-Coulomb failure criterion) that also applies for rock masses. In the present work only the initial part of the hyperbola (OA in Figure 5.1) was needed to simulate the pre-peak portion of a typical stress-strain curve.

For unloading and reloading a linear stress-strain relationship was assumed with modulus;

$$E_{ur} = K_{ur}P_{atm}(\frac{\sigma_3}{P_{atm}})^n \qquad [5.13]$$

where K_{ur} is an unloading-reloading modulus number.

The initial modulus E_i was assumed to be constant ($E_i=P_v.10^3$) by setting the exponent n equal to 0. This assumption is reasonable for rock where the dependency of the initial elastic modulus on the confining pressure is not as pronounced as for soils. A constant Poissons's ratio of 0.25 and an unloading-reloading modulus $E_{ur}=E_i$ were selected. A value of $1.7P_v$ was given to the cohesion c, and a friction angle of 30° was chosen. The failure ratio R_f was set equal to one.

5.2.2 Tunnel in Linear Elastic, Ideal Plastic Medium

Another analysis was carried out to study the behavior of the tunnel when the maximum shear strength of the rock is exceeded, at some locations near the opening. The rock was assumed to behave as a linear elastic medium up to failure. At failure the rock was assumed to behave according to ideal flow plasticity. A stress-strain relationship of this kind is shown, schematically, in Figure 5.2. This model does not account for softening in the pre-failure region and for weakening in the post-failure region. This simplification was however considered acceptable for the purposes of this thesis.

In the pre-failure region the model is defined by two elastic parameters, E and ν. At failure the model is defined by a failure criterion and a flow rule.

In the elastic range a Young's modulus $E=P_v.10^3$ and a Poisson's ratio of 0.25 were selected. The Mohr-Coulomb

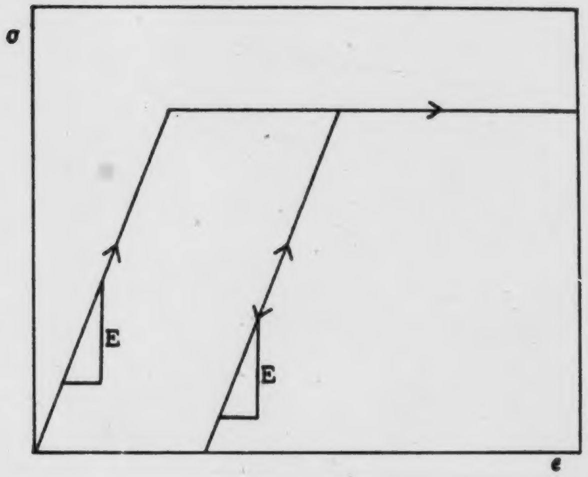

Figure 5.2 Schematic Representation of the Linear-Elastic, Ideal-Plastic Stress-Strain Relationship

failure criterion was chosen; it can be expressed, in terms of stress invariants, as follows:

$$Y = \frac{1}{3} I_1 \sin\phi + \sqrt{J_2}\ \left(\cos\bar{\theta} - \frac{\sin\bar{\theta}\sin\phi}{\sqrt{3}}\right) - c.\cos\phi \quad [5.14]$$

where I_1 is the first invariant of the stress tensor, J_2 is the second invariant of the deviation stress tensor and $\bar{\theta}$ is the Lode angle (Nayac and Zienkiewicz, 1972). A cohesion $c=0.6P_v$ and a friction angle $\phi=30^\circ$ were selected.

A non associated flow rule was assumed for the model by defining a plastic potential function as:

$$Q = \frac{1}{3} I_1 \sin\psi + \sqrt{J_2}\ \left(\cos\bar{\theta} - \frac{\sin\bar{\theta}\sin\psi}{\sqrt{3}}\right) \quad [5.15]$$

The dilation angle ψ was given a zero value so that no volume change takes place in the medium due to plastic deformations. The choice of using a non associated flow rule was made because high dilation at failure, as predicted by the associated flow plasticity for frictional materials, is not realistic for geologic media. The $\psi=0$ assumption is reasonable for an elastic, ideal plastic medium and it is supported by experimental evidence (e.g., Miller and Cheatam, 1972).

5.2.3 Remarks to the FEM Model

Because of stress path dependency associated with non linear rock behavior, excavation was performed incrementally for both cases. The mesh used for these analyses is virtually identical to the one used for the linear elastic cases. The constant pressure boundaries on the sides of the mesh were replaced by fixed node boundaries because SAFE allows direct input of initial stresses in the mesh. At the same time fixing the boundary nodes reduces the cost of the analyses by reducing the number of degrees of freedom to be included in the stiffness matrix. It also reduces the complexity of the input file because no surface traction has to be applied to the mesh. A linear elastic analysis using SAFE and these new boundary conditions was also performed to provide a basis of comparison for the non-linear cases.

In the following paragraphs the results obtained will be shown and discussed. Most of the plots were prepared to allow direct comparison among results obtained for linear elastic, hyperbolic and elasto-plastic conditions.

5.3 Stresses

The normalized radial stresses in the horizontal direction calculated ahead of the tunnel face will be shown first. The purpose is to study the effect of the rock's constitutive relationship on stress concentrations at the tunnel face.

In Figure 5.3, the radial stresses calculated in the horizontal axial plane are plotted along the tunnel axis (r/R=0.0) for the linear elastic, hyperbolic and elasto-plastic cases. A stress peak is found, for all

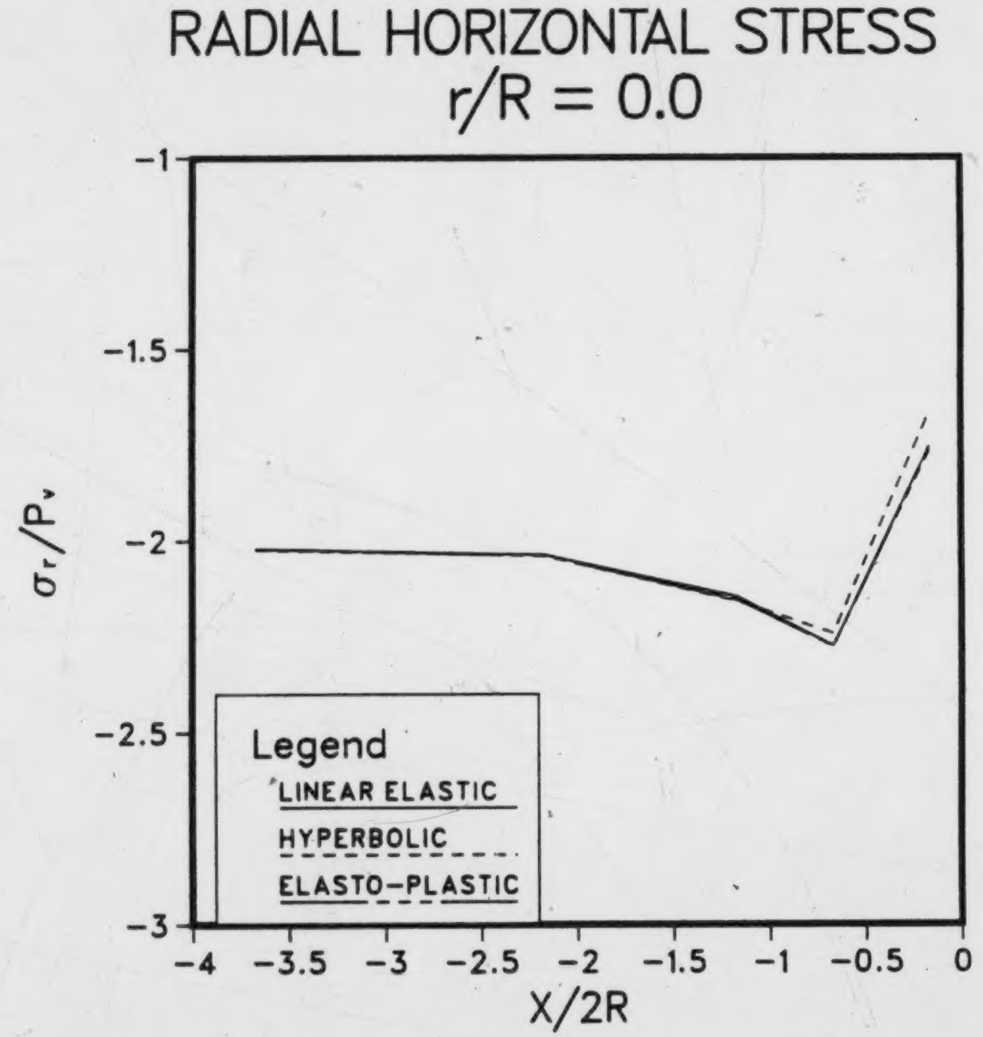

Figure 5.3 Horizontal Radial Stresses, σ_r, Ahead of the Tunnel Face (r/R=0.0); Linear-Elastic, Hyperbolic and Elasto-Plastic

conditions, about 0.4R ahead of the tunnel face due to stress redistribution caused by excavation. The increase is about 14% of the initial horizontal stress and a slightly lower value is observed for the tunnel in hyperbolic rock. As it will be shown later in this paragraph no yielding occurs at this location for the elasto-plastic case.

The same stress component is plotted in Figure 5.4 for r/R=0.8. A higher stress concentration is found at this location near the tunnel face (37% stress increase in linear elastic rock). Yielding occurs, for the elasto-plastic case, as the given failure criterion is exceeded. The highest stress peak is found for the linear elastic case where the tunnels in non-linear media result in lower stress concentrations.

In Figure 5.5, the radial stresses are plotted at r/R=1.1. The highest stress peak is found for the elasto-plastic rock where the lowest is observed for the hyperbolic case.

For the tunnel excavated in hyperbolic rock, relatively low stress concentrations are observed everywhere at the face. Hence it is concluded that non-linearity in the pre-failure range is beneficial for face stability by allowing stress redistribution that prevents failure to occur. Lombardi (1970) showed, by means of the Convergence-Confinement method, that if the rock core exhibits non-linear behavior, lower stress concentrations are to be expected at the face. His conclusions are

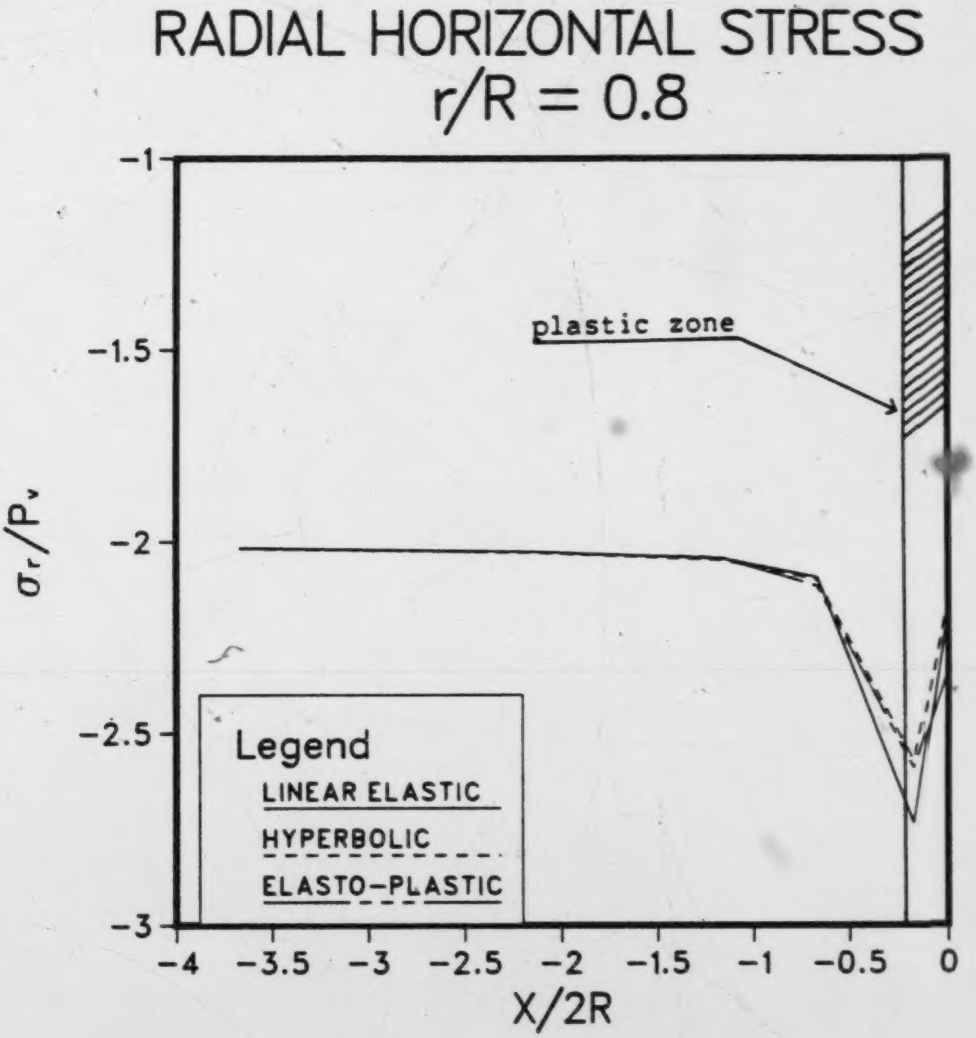

Figure 5.4 Horizontal Radial Stresses, σ_r, Ahead of the Tunnel Face (r/R=0.8); Linear-Elastic, Hyperbolic and Elasto-Plastic

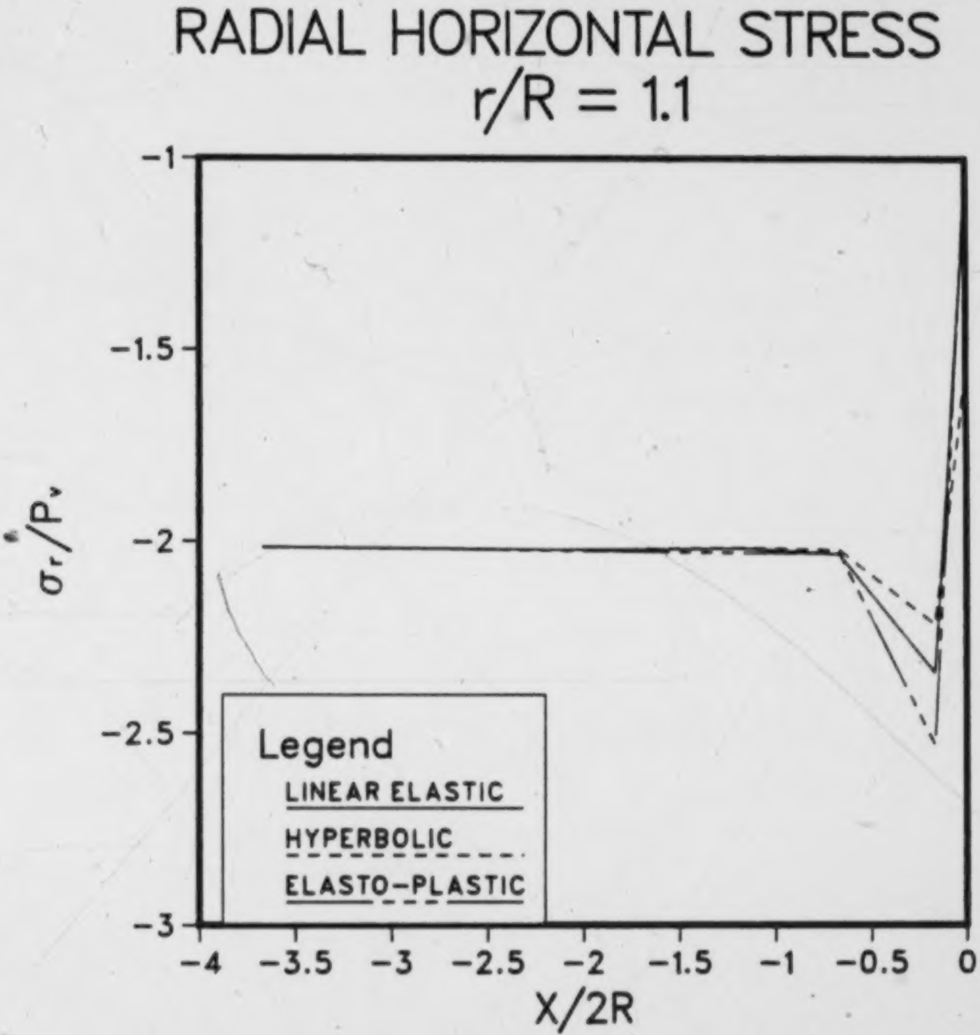

Figure 5.5 Horizontal Radial Stresses, σ_r, Ahead of the Tunnel Face (r/R=1.1); Linear-Elastic, Hyperbolic and Elasto-Plastic

confirmed by the outcome of this research.

For the elasto-plastic case only a very limited amount of yielding takes place at the tunnel face (Figure 5.6). The plastic zone is ring shaped and its thickness in the axial direction is about 0.2R. The non-circular shape of the plastic ring is related to the different magnitude of the initial radial stresses ($K_0 \neq 1.0$). The observation that no yielding occurs in the central portion of the core is consistent with the stress distribution found for linear elastic conditions that presents high concentrations of radial stresses for r/R values larger than 0.7 (see Figures 5.3 and 5.4).

At the center of the excavation front (Location A in Figure 5.6) no yielding takes place and the increase in radial stress is equal for tunnels in linear elastic and elasto-plastic rock masses (Figure 5.3). At r/R=0.8 (Location B in Figure 5.6) the high stress concentration generates yielding and a lower stress peak, due to stress redistribution, is found for the elasto-plastic case. At r/R=1.1 (Point C in Figure 5.6) a relatively high stress peak is found for the tunnel in the elasto-plastic rock. This can be explained by looking at the plastic zone behind the tunnel face depicted in Figure 5.7. At the tunnel springline a limited amount of yielding takes place right behind the face due to the high axial stress at that location and to the decrease in confinement near the tunnel wall. Farther behind the face unloading occurs as the axial

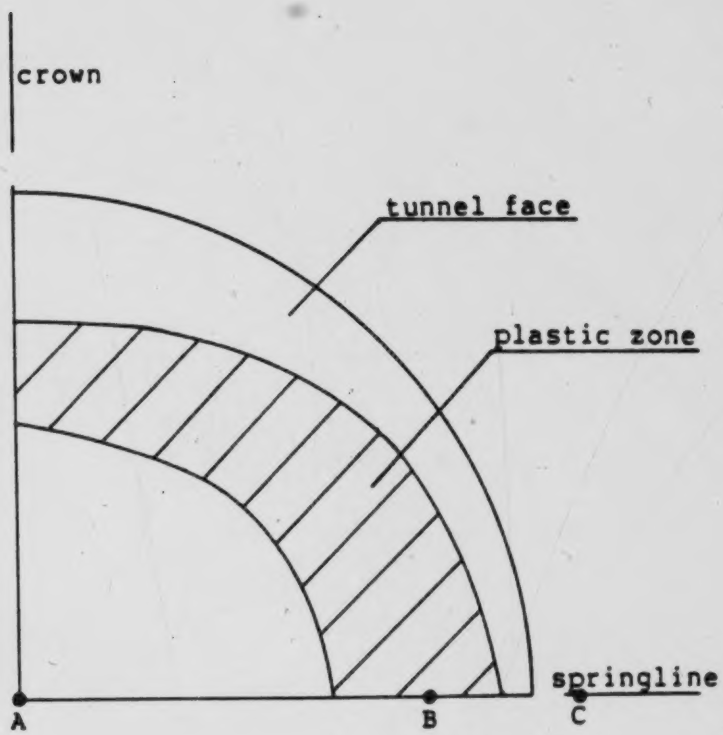
crown
tunnel face
plastic zone
springline
A
B
C

Figure 5.6 Plastic Zone at the Tunnel Face

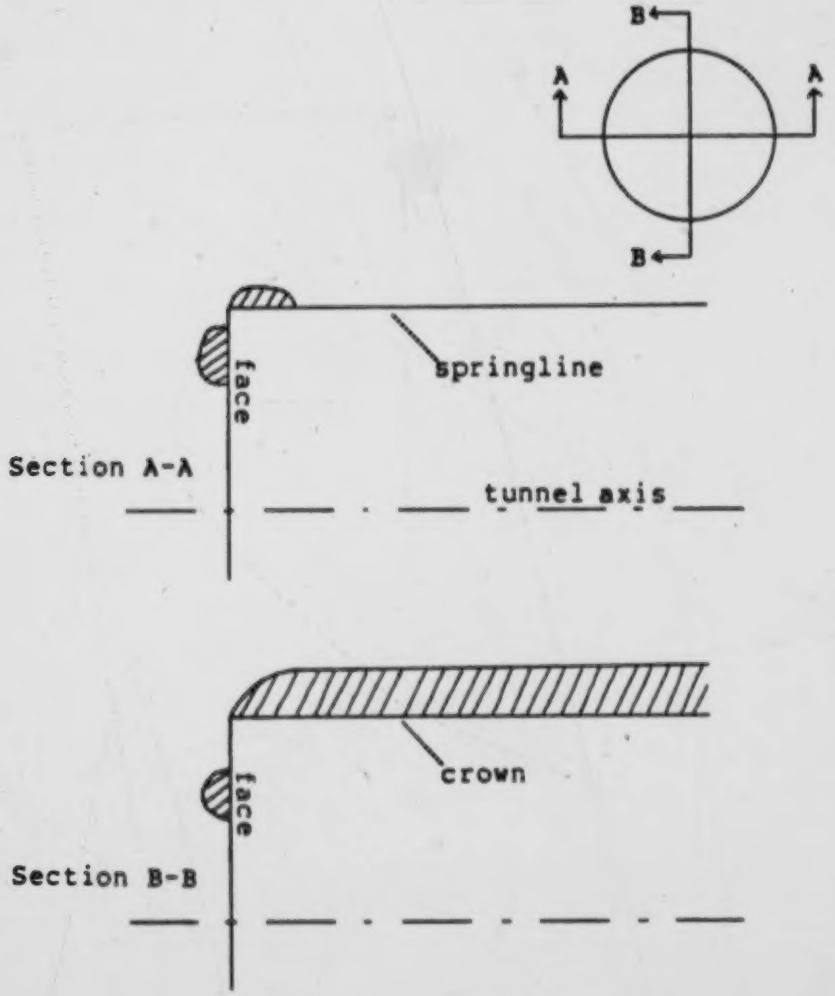
B
A
A
B
springline
face
Section A-A
tunnel axis
crown
face
Section B-B

Figure 5.7 Plastic Zone at the Springline (a) and Crown (b)

stress tends to decrease and the rock behaves as a linear elastic medium (the axial stress at the springline is plotted in Figure 5.13). Point C is located immediately outside the plastic zone and the high stress peak is due to stress redistribution.

A similar effect of the stress redistribution process is visible in Figure 5.8 where the shear stresses τ_{ar} for the linear elastic and the elasto-plastic cases at r/R=1.1 are shown. Due to the limited ability of the plastic rock to carry shear stresses, a higher shear stress concentration is found immediately outside the plastic zone. This is related to the radial stress increase depicted in Figure 5.5.

In Figure 5.9 the normalized tangential stresses calculated at the tunnel crown are plotted, against the distance to the tunnel face, for the linear elastic, non linear elastic and elasto-plastic cases. The stresses are calculated at r/R=1.1. Far ahead of the tunnel face, where only low increases in deviatoric stress occur, the behavior of the three curves is virtually identical. Immediately ahead of the tunnel face the three curves separate and follow different paths. The magnitudes of the tangential stresses for the hyperbolic and elasto-plastic cases, far behind the tunnel face, are considerably lower compared with the linear elastic case. The rock near the excavation is subjected to an increase in tangential stresses and a decrease in radial stresses. For the hyperbolic material high stress differences ($\sigma_1-\sigma_3$) involve low elastic modulus

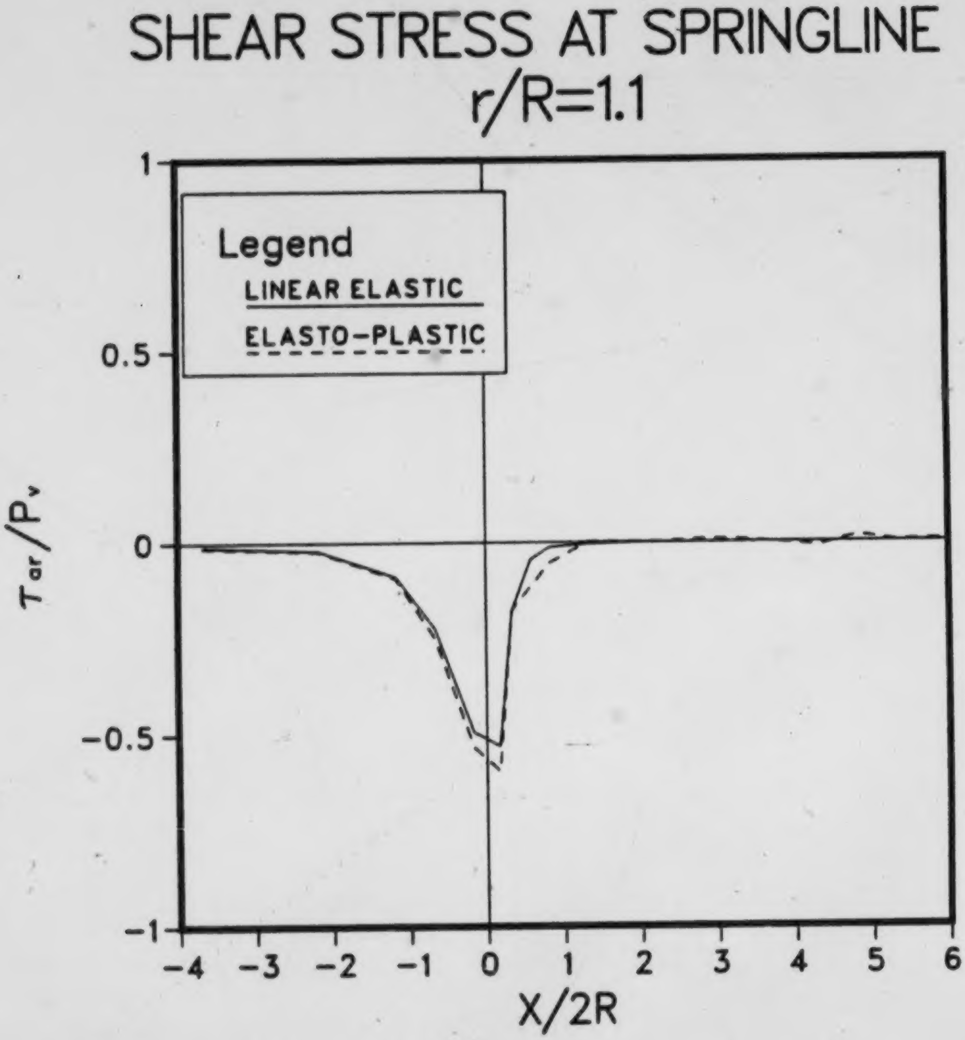

Figure 5.8 Shear Stresses, τ_{ar}, at the Tunnel Springline; Linear-Elastic and Elasto-Plastic

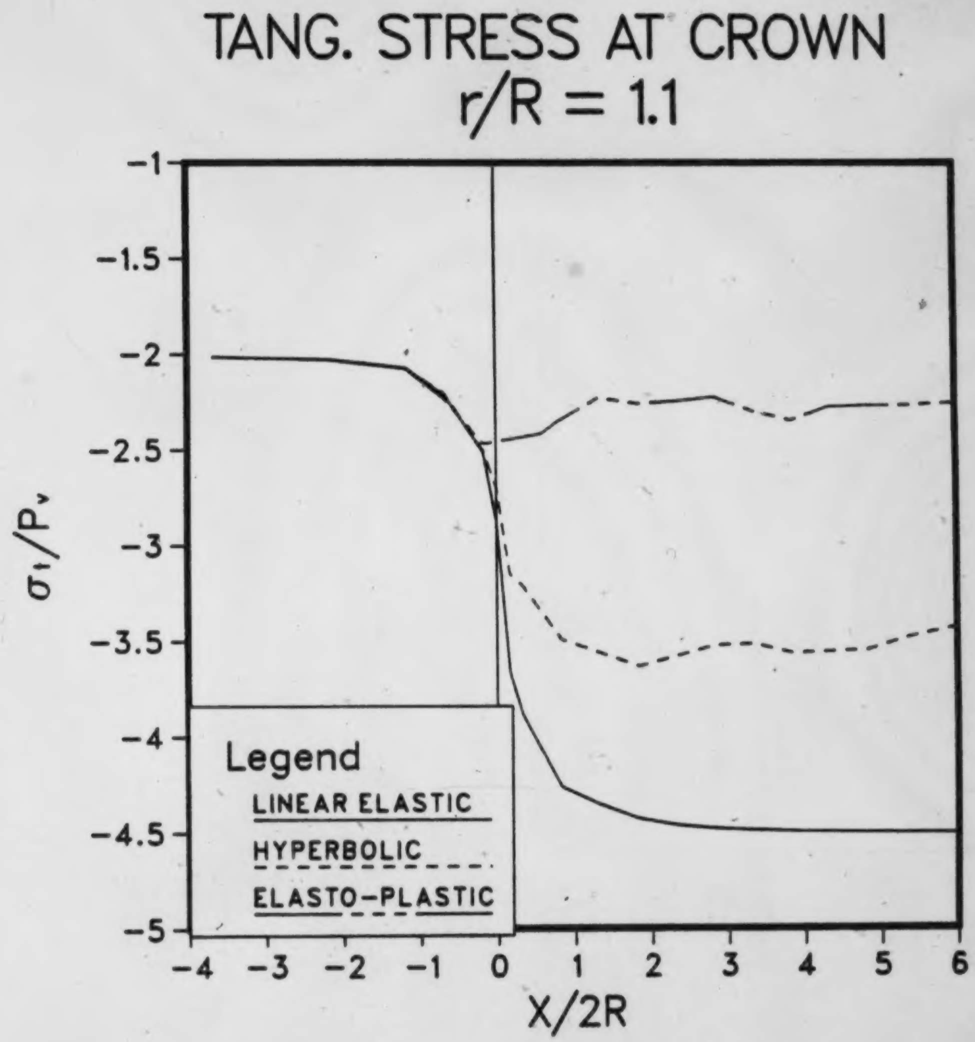

Figure 5.9 Tangential Stresses, σ_t, at the Tunnel Crown (r/R=1.1); Linear-Elastic, Hyperbolic and Elasto-Plastic

and, hence, increased deformability of the highly stressed rock occurs. This leads to a stress redistribution process for which low stresses due to rock softening are found at crown and invert.

For the tunnel in the elasto-plastic rock the decrease in tangential stresses due to non-linearity is much more pronounced than for the hyperbolic case. This is due to the parameters chosen to characterize the yielding rock for which a very limited amount of deviatoric stress can be sustained in the plastic region.

In Figure 5.10, the tangential stresses at the crown are plotted for r/R=1.3. The relative position of the three curves is similar to the one discussed above. The differences between the three cases are however less pronounced at this location. This was expected because as locations farther from the tunnel wall are considered, the tendency of the deviatoric stress to concentrate decreases and so does the effect of the non-linear stress-strain relationships.

As locations farther away from the axis of the tunnel are selected, different conditions are encountered. As shown in Figure 5.11, the tangential stresses at r/R=2.65 for the elasto-plastic case are the highest with respect to the other two cases, whereas the stresses for the linear elastic material are lowest. If a vertical line passing through the center of the tunnel is drawn, the integral of the horizontal stresses along that line will have to be the same

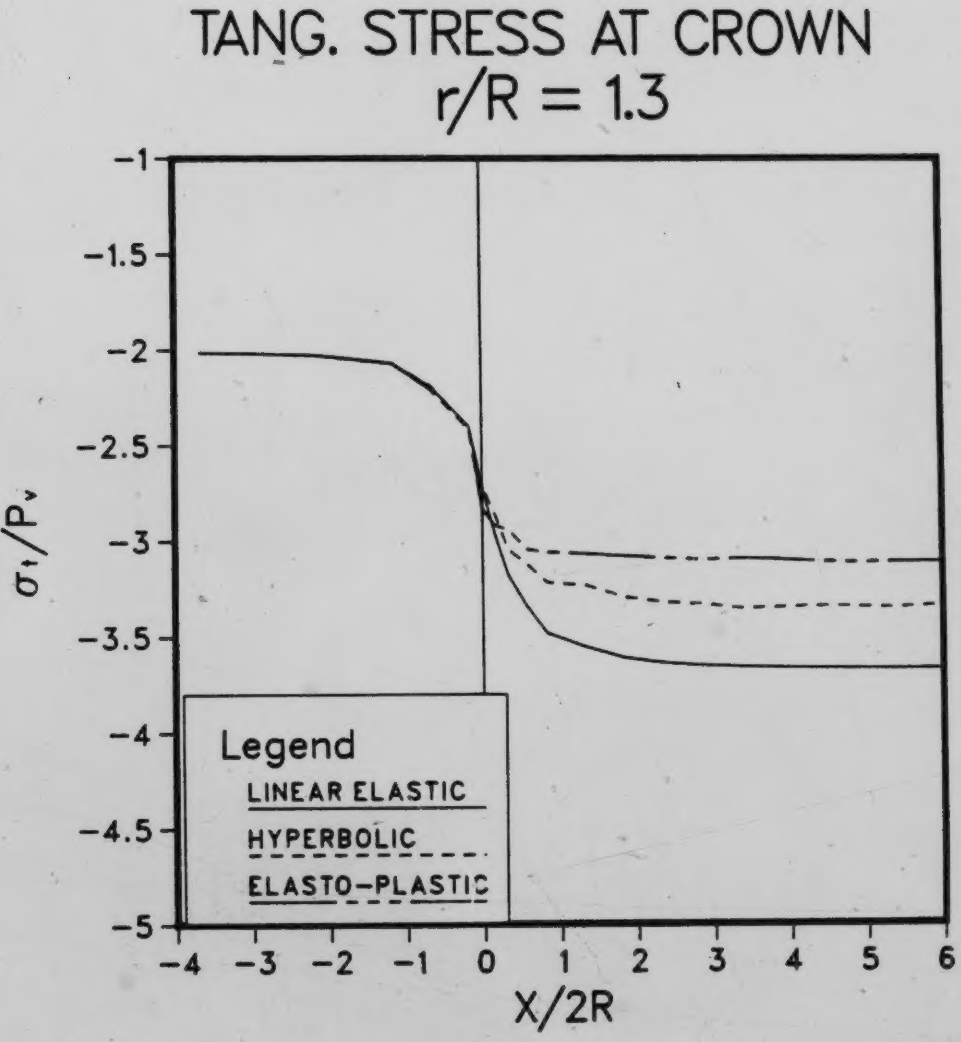

Figure 5.10 Tangential Stresses, σ_t, at the Tunnel Crown (r/R=1.3); Linear-Elastic, Hyperbolic and Elasto-Plastic

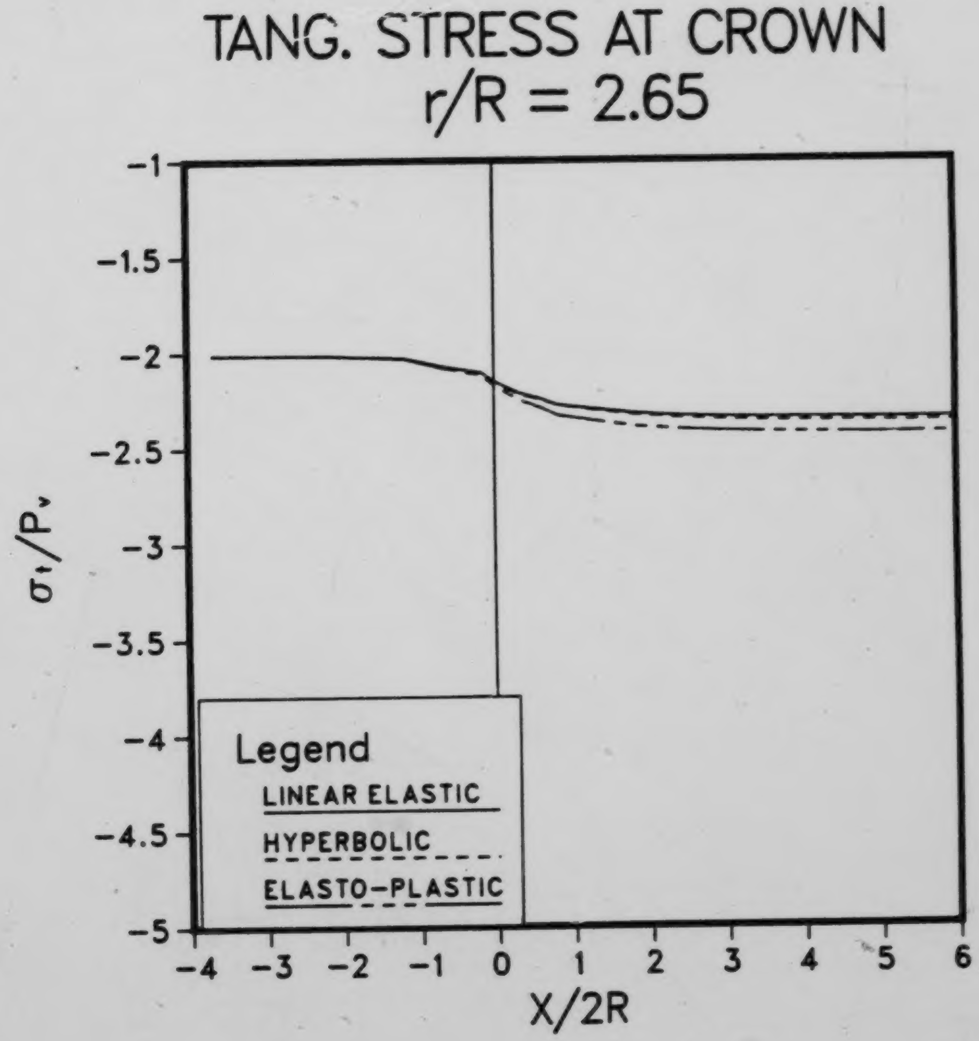

Figure 5.11 Tangential Stresses, σ_t, at the Tunnel Crown (r/R=2.65); Linear-Elastic, Hyperbolic and Elasto-Plastic

for linear and non-linear cases. This is because equilibrium with the in situ horizontal stresses, far from the tunnel, must be satisfied independently of the material behavior. Lower stresses near the tunnel correspond with higher stresses far from the tunnel.

In Figure 5.12 the axial stresses at the tunnel crown are shown, at r/R=1.1, for the linear elastic and the elasto-plastic cases (for the hyperbolic case oscillating stresses were found at this location). At the tunnel face the elastic case exhibits a much higher stress peak than the other. This is consistent with the tangential stress difference found at that location (see Figure 5.10). Behind the tunnel face the stress in the elastic medium stabilizes at a value higher than the initial axial stress, as expected for linear-elastic, plane strain conditions. For the elasto-plastic case the final stress value is slightly lower than the initial axial stress, because of yielding.

The axial stresses at the tunnel springline are shown, for r/R=1.1, in Figure 5.13. It is of interest to note that the elasto-plastic case presents stresses very similar to the linear elastic case. This is due to the fact that for the elastic, ideal plastic model used in this analysis, most stress redistribution takes place at the crown and invert where a high deviatoric stress tends to concentrate. For the hyperbolic case, on the other hand, the non-linear stress-strain relationship results in a considerable stress decrease at the tunnel springline.

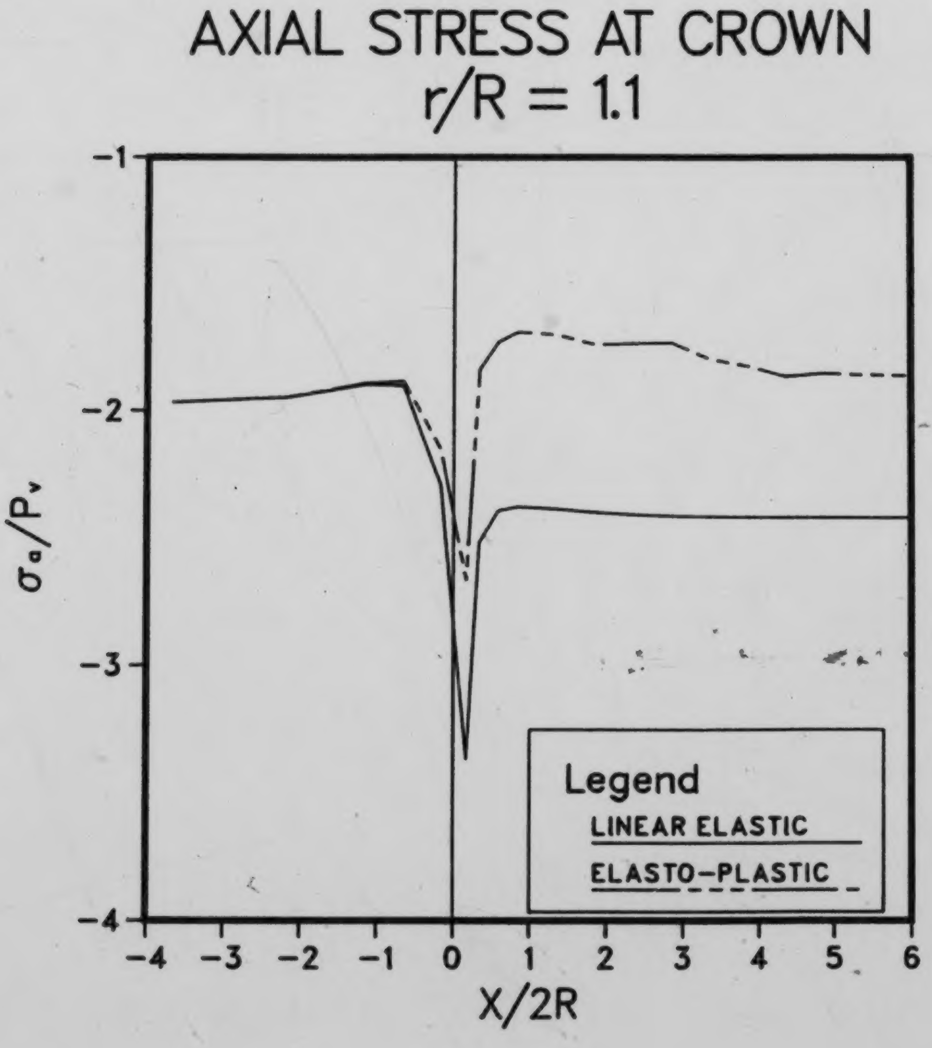

Figure 5.12 Axial Stresses, σ_a, at the Tunnel Crown; Linear-Elastic and Elasto-Plastic

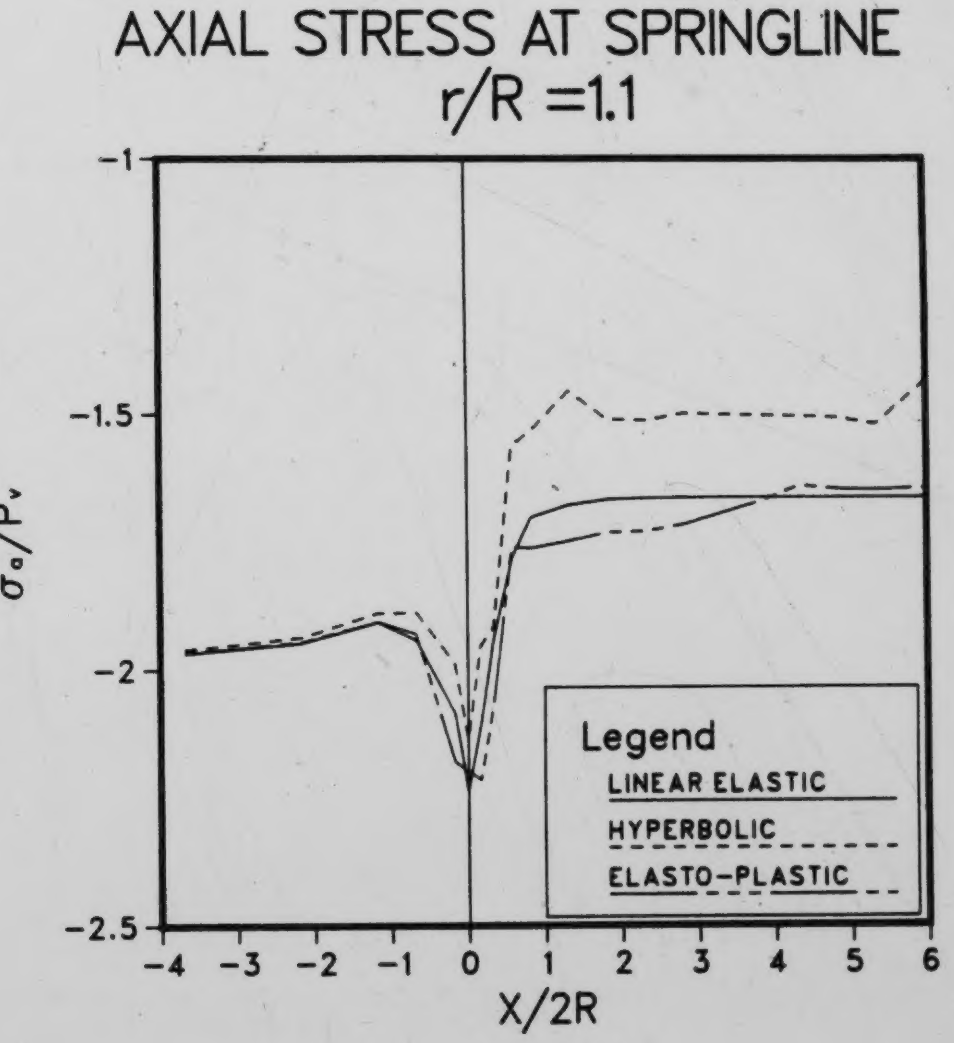

Figure 5.13 Axial Stresses, σ_a, at the Tunnel Springline; Linear-Elastic, Hyperbolic and Elasto-Plastic

As the tunnel face advances the axial stress (maximum at the face) decreases and a condition of unloading occurs. Since the rock is stiffer on unloading than on loading a considerable stress drop takes place as plane strain conditions are approached.

In this section, the effect of non-linear behavior on the stresses around a tunnel was discussed. Stress redistribution due to non-linearity was found to affect considerably the stress field, especially at those locations where high stress concentration is expected to occur in linear elastic media. For tunnels in rock masses exhibiting non-linear stress-strain relationships, the maximum strength of the material may never be reached, even when predicted by linear elastic models. For elastic, ideal plastic media, stress redistribution takes place when the maximum strength of the material is exceeded. For the particular parameters chosen in the present work, the elasto-plastic material caused the largest amount of stress redistribution, visible particularly very near the tunnel wall.

5.4 Displacements

In Figure 5.14, convergence at the tunnel springline is shown for the linear elastic, the hyperbolic and the elasto-plastic cases. The normalized radial displacements are plotted against the normalized distance to the tunnel face. For the hyperbolic case E represents the initial modulus E_i.

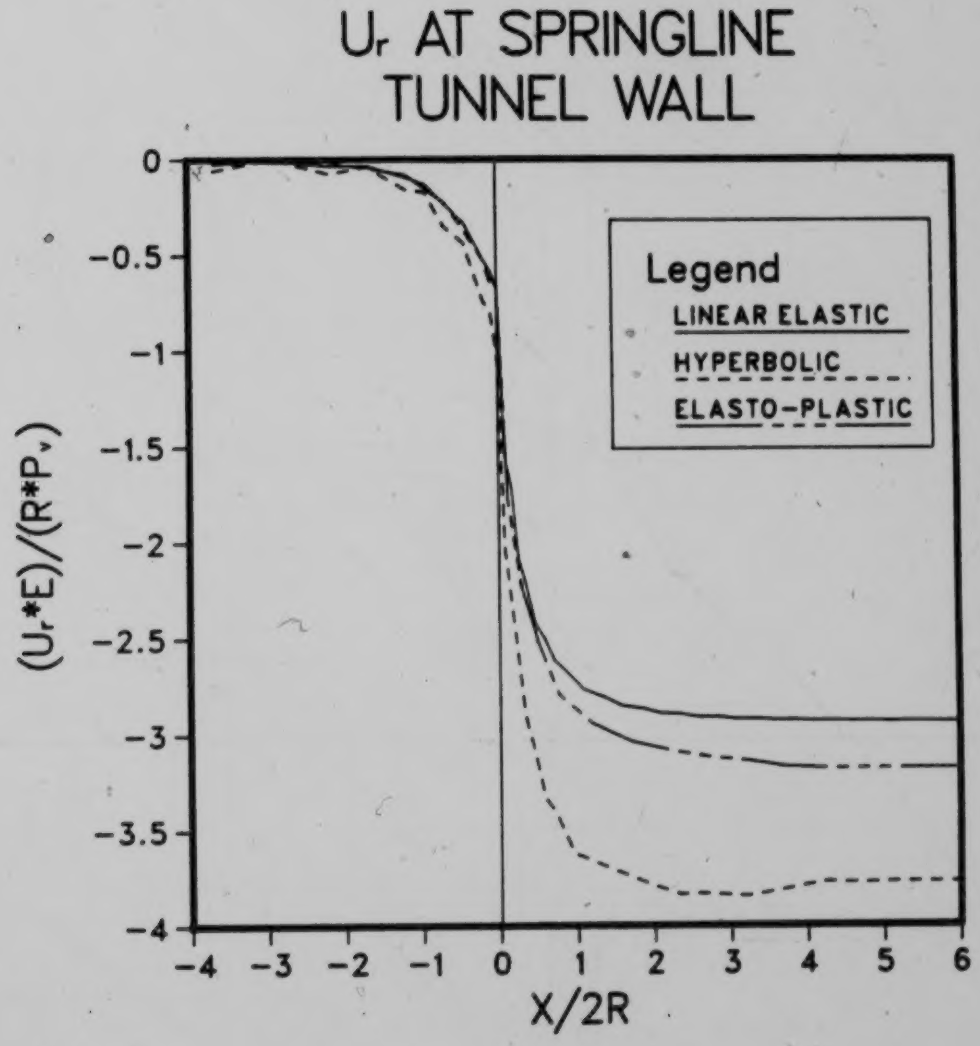

Figure 5.14 Convergence at the Tunnel Springline; Linear-Elastic, Hyperbolic and Elasto-Plastic

For the tunnels in non-linear media, radial displacements larger than for the linear elastic case are found. This was expected because non-linearity as considered in the present work, involves reduction of the system stiffness at those locations where deviatoric stresses tend to concentrate. Because of the material parameters selected for the analysis, the largest deformations were detected for the hyperbolic case, both behind and ahead of the tunnel face. This is partly due to the fact that the Young's modulus chosen as a normalizing factor is the initial elastic modulus (i.e. tangent to the hyperbola at zero axial strain). This is obviously an arbitrary choice that has considerable significance in terms of magnitude of the normalized displacements. For the elasto-plastic model, however, the Young's modulus E actually represents the stress-strain relationship controlling the tunnel behavior in the elastic range. Only at those locations where the given failure criterion is exceeded, does plastic deformation occur. For the particular case investigated most yielding takes places at the tunnel crown and invert, behind the face. In the non-linear elastic case a larger amount of rock is affected by non-linearity and the maximum stiffness reduction would occur, also for this case, at those locations where deviatoric stresses tend to concentrate.

The convergence at the tunnel crown is shown in Figure 5.15. The difference in movement between linear and non linear media is more pronounced than at the springline. This

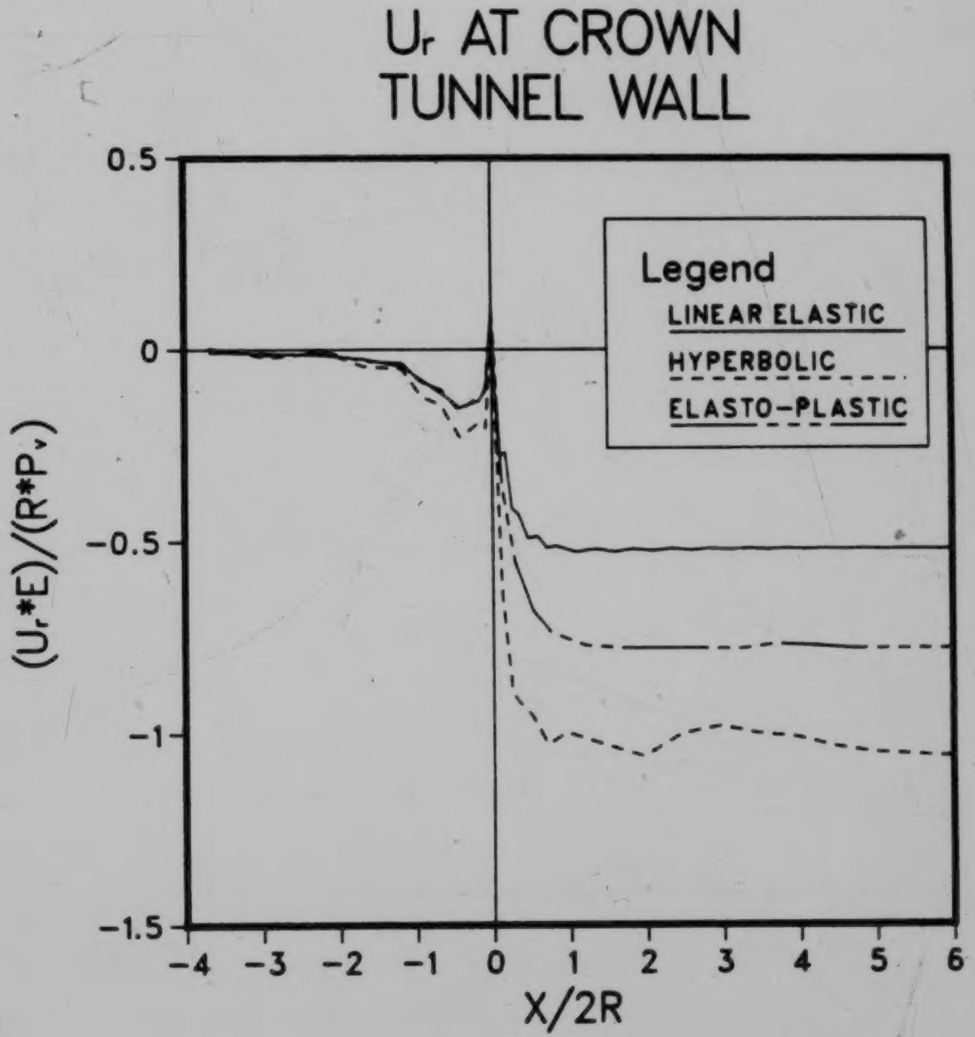

Figure 5.15 Convergence at the Tunnel Crown; Linear-Elastic, Hyperbolic and Elasto-Plastic

is due to the high K_0 value assumed for the analysis which causes high deviatoric stresses at the crown and invert. The tunnels in the linear elastic and in the elasto-plastic media give the same radial displacements ahead of the tunnel face. Behind the face, where the failure criterion for the plastic rock is exceeded, larger movement is found in the yielding material. In Figures 5.16 and 5.17 are plotted the radial displacements at the crown at various distances from the tunnel axis (note: linear elastic case shown in Figure A7). By comparing these two figures it can be observed that different deformation distributions characterize the two cases. The difference in radial displacement between $r/R=1.0$ and $r/R=1.3$ (i.e., A and B)is virtually identical whereas, farther away from the tunnel wall, larger relative displacements are found for the hyperbolic case (i.e, CD). For the elasto-plastic case, in fact, the deformation concentrates at those locations where yielding occurs, which is very near the tunnel wall. For the non linear-elastic case, even rock relatively far from the wall is affected by some reduction of its elastic modulus (with respect to the initial elastic modulus E_i).

In conclusion, larger convergence is found for those cases in which the tunnel is assumed to be driven in non-linear rock. The effect of non-linearity is particularly apparent at the tunnel crown and invert where, for the initial stress conditions ($K_0=2$) assumed in this work, the highest stress concentrations occur. For the elastic,ideal

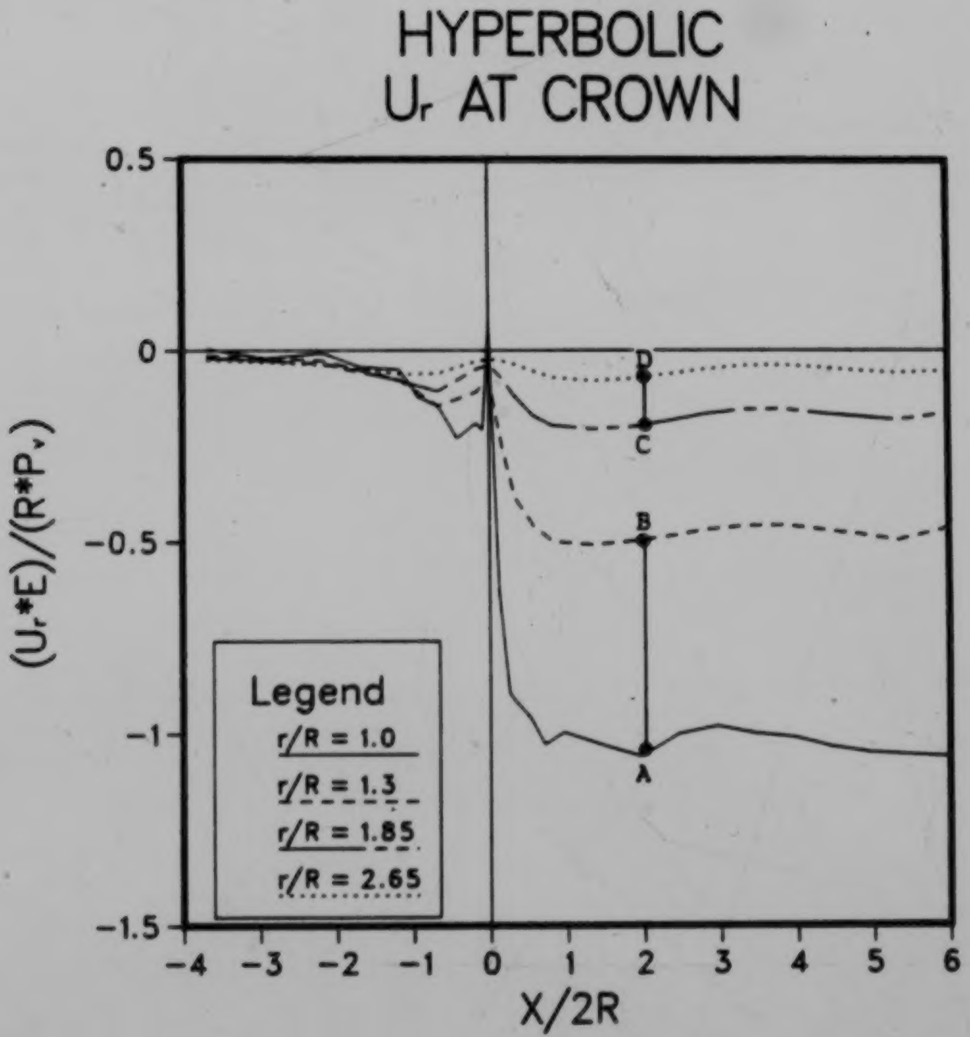

Figure 5.16 Radial Displacements at the Tunnel Crown; Hyperbolic

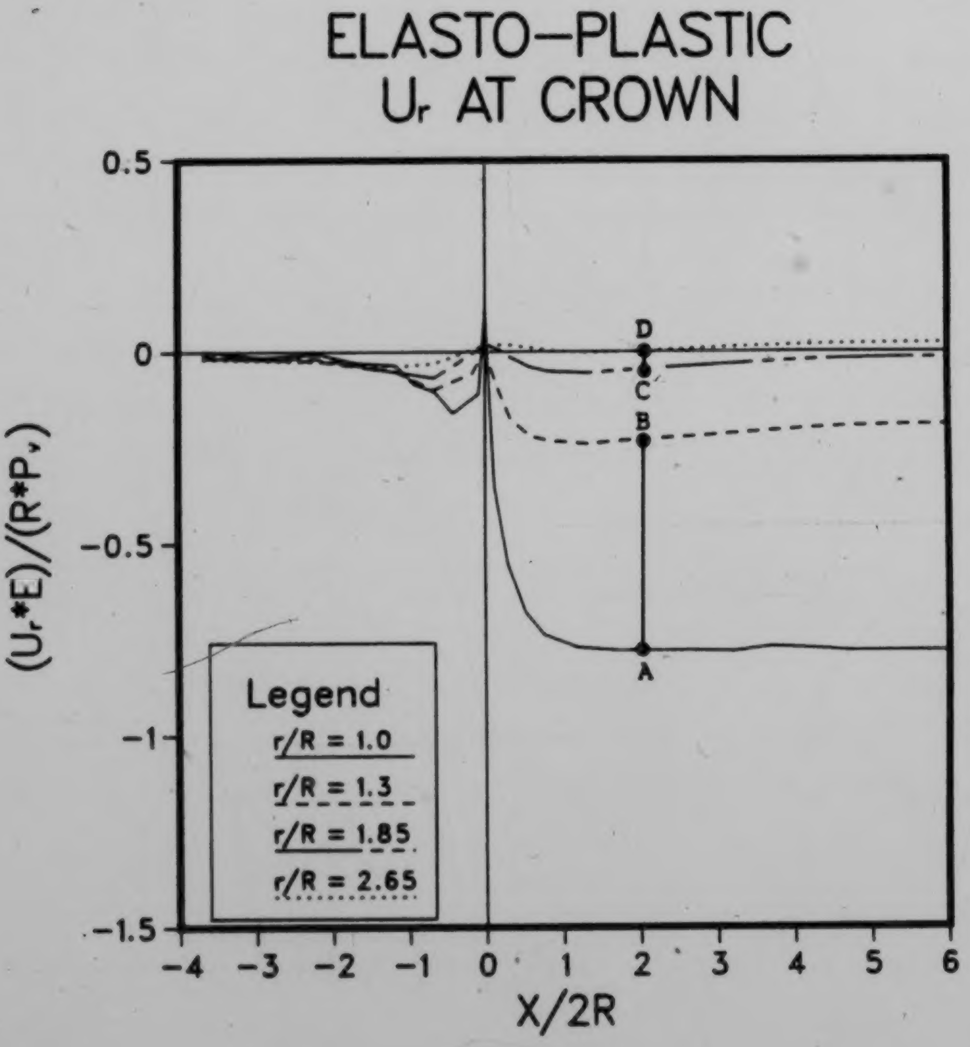

Figure 5.17 Radial Displacements at the Tunnel Crown; Elasto-Plastic

plastic rock, large displacements due to non-linearity are only found behind the tunnel face where the strength of the material is exceeded. For this case, relatively large displacements are concentrated near the tunnel wall where yielding occurs.

5.5 Implications for Monitoring Data Interpretation

5.5.1 Convergence Records

If convergence measurements are taken, beginning at the tunnel face, flatter curves are found for the non-linear elastic and the elasto-plastic cases. This will be shown at the end of this chapter where the shape of the radial displacement curves is discussed.

Placing an extensometer in a borehole driven from a nearby excavation, the whole convergence profile, including the section ahead of the excavation front, can be depicted. In this case the curves shown in Figures 5.14 to 5.17 are the outcome of the measurement. In Figure 5.14, it can be seen that identical convergence curves are found ahead of the face for the linear elastic and the elasto-plastic cases whereas considerable differences are detected behind the excavation front. The profile section common for the two cases can be used to back-analyze, by comparison with 3-D elastic analyses, the elastic modulus for the rock mass. This elastic modulus is consistent, behind the face, with the radial displacements found for the linear elastic case.

The same value is however too high to justify the larger movement occurring in the yielding rock and this can reveal the non-linear behavior of the rock mass. The initial stresses in the rock mass must be known to a good degree of accuracy.

A similar approach can be followed also for the hyperbolic medium even though, for this case, the back-analyzed modulus must be regarded as a fictitious value. In general, in real cases, both non-linearity in the pre-failure region and yielding at failure may be found. The advantage of using measurements taken at the tunnel crown is that the differences in displacements are larger at this location than at the springline. However, as shown in the previous chapters, the shape of the radial displacement profiles at the crown is highly sensitive to axial stresses and orientation of the rock deformation properties. Both aspects must be investigated before a reasonable conclusion can be drawn.

5.5.2 Multipoint Extensometer Records

In Figure 5.18, relative displacements at the tunnel springline are plotted against distance to the tunnel axis r/R. The three curves, representing the linear elastic, the hyperbolic and the elasto-plastic cases, can be compared to measurements having zero reading at the tunnel face as given, for instance, by radial multiple anchor extensometers placed at the excavation front. For the three cases the

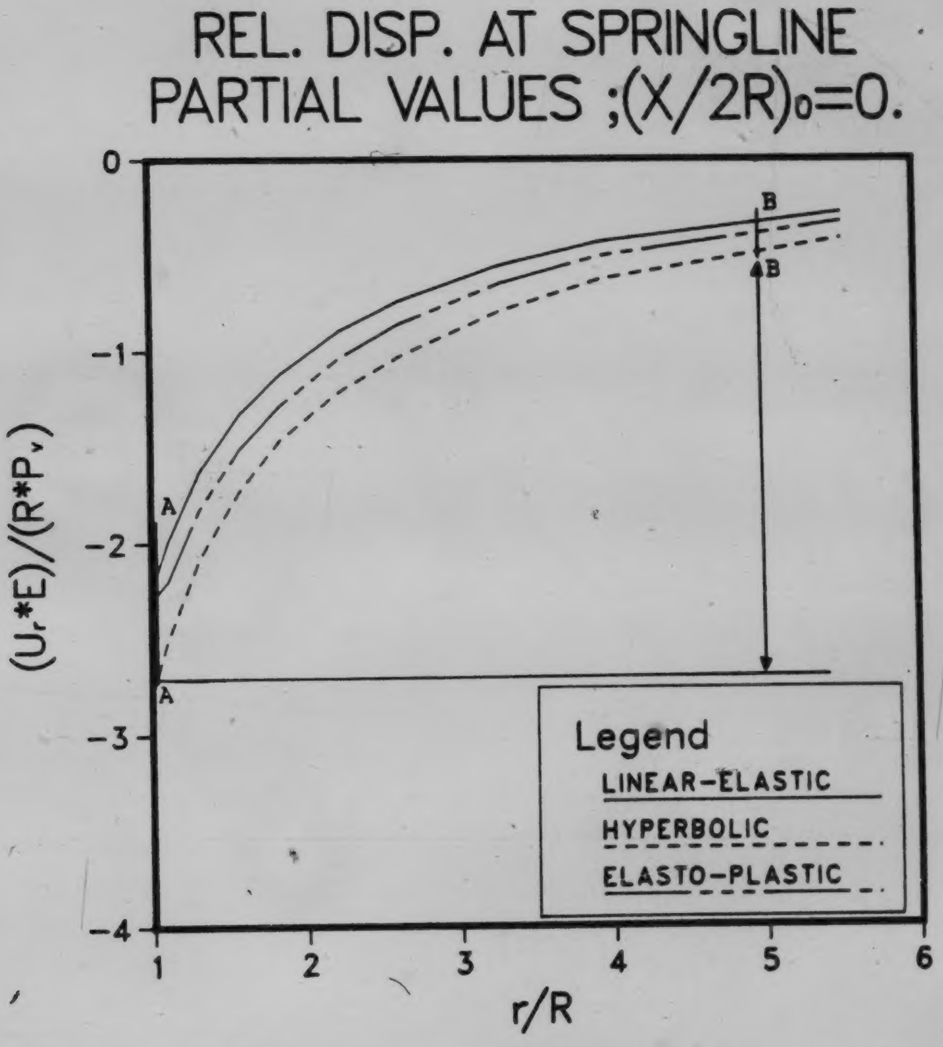

Figure 5.18 Relative Displacements at the Tunnel Springline (Partial Values); Linear-Elastic, Hyperbolic and Elasto-Plastic

relative displacements differ consistently with the observations presented in the previous paragraph. The largest displacements are found for the hyperbolic case, the smallest for the linear-elastic case at any distance from the wall. The three curves are virtually identical in shape. This means that the relative movement between the head (A) of a multiple anchor radial extensometer (located at the tunnel wall) and an anchor (B) located, say, at r/R=5 will give very little indication of the non-linear behavior.

Relative displacements calculated at the tunnel crown are shown in Figure 5.19. Again, partial movements with respect to the tunnel face are plotted against normalized distance to the excavation front. At this location the three curves have different shapes. The linear elastic case gives the smallest displacement at the tunnel wall but, for higher r/R values, the situation changes. For r/R larger than 1.25 (A), the radial displacements for the linear elastic case are larger than for the elasto-plastic case. For r/R larger than 1.9 (B), larger displacements occur for the linear elastic case than for the hyperbolic case. For the tunnel in elasto-plastic rock about 50% of the radial movement occurs in the plastic region.

In conclusion, multi-anchor radial extensometers placed at the tunnel face, give little indication of non-linear rock behavior if located at the tunnel springline (for K_o=2). At the tunnel crown higher concentration of deformations occurs near the wall if the rock doesn't behave

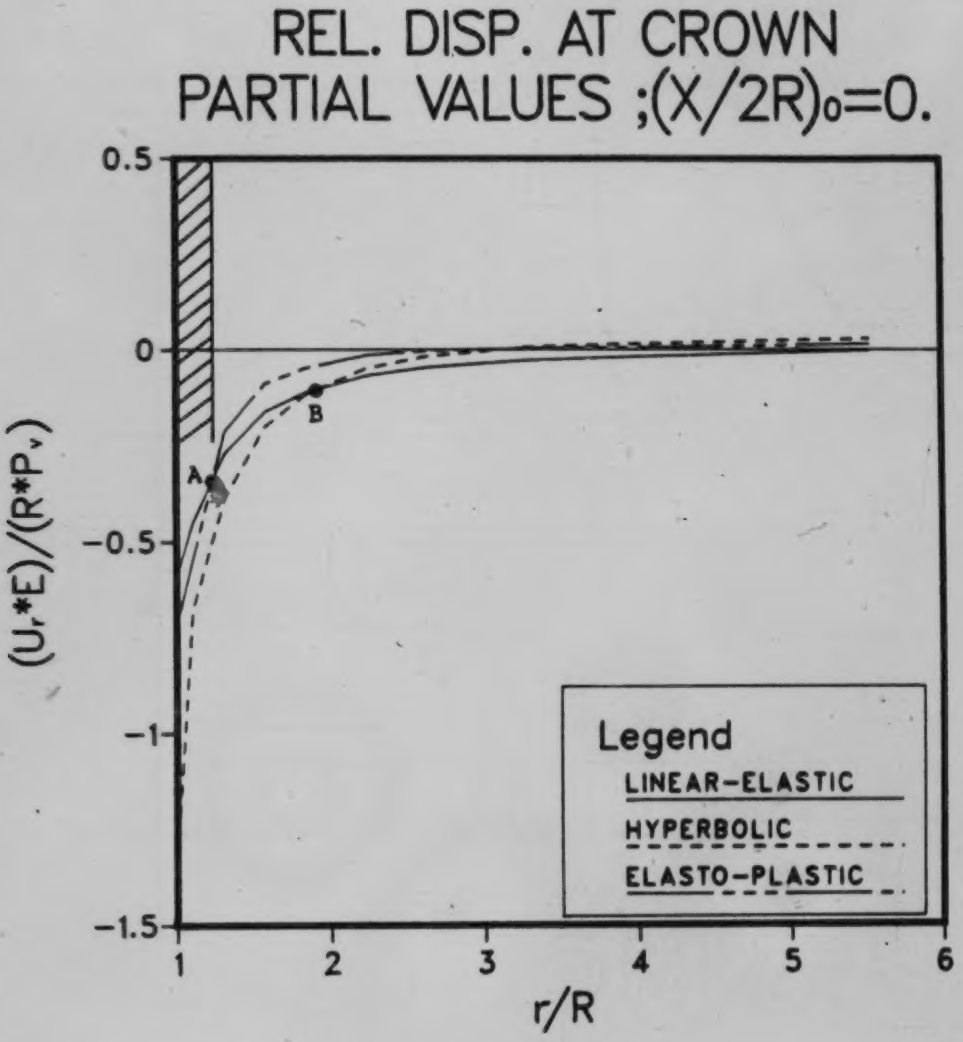

Figure 5.19 Relative Displacements at the Tunnel Crown (Partial Values); Linear-Elastic, Hyperbolic and Elasto-Plastic

as a linear-elastic medium. On the other hand, in the direction of the minimum initial stress (i.e., at the crown), non-linearity involves lower radial displacements far from the tunnel wall.

5.5.3 Shape of Radial Displacement Profiles

It was observed in the previous chapters that the shape of the curves obtained by plotting radial displacements against distance from the tunnel face may contain useful information to understand the rock properties.

In Figure 5.20, radial displacements curves at r/R=1.3 are plotted for the linear elastic, hyperbolic and elasto-plastic cases. The radial displacement is normalized with respect to U_{rmax} as done in the previous chapters.

The curves are calculated at the tunnel springline and a value r/R larger than one was selected to avoid a slightly oscillating trend characterizing the curve, for the hyperbolic case, at the wall. This figure shows that non-linear stress strain relationships are associated with slightly flatter curves. A similar behavior is found at the tunnel crown (not shown here).

In Figures 5.21, normalized convergence curves are shown at the tunnel springline for the linear elastic and the elasto-plastic cases. The two curves are fitted by means of the Ramberg-Osgood function that was described in Chapter 3. The non-linear rock gives a flatter curve defined by lower S_i and m values. The difference between the two cases

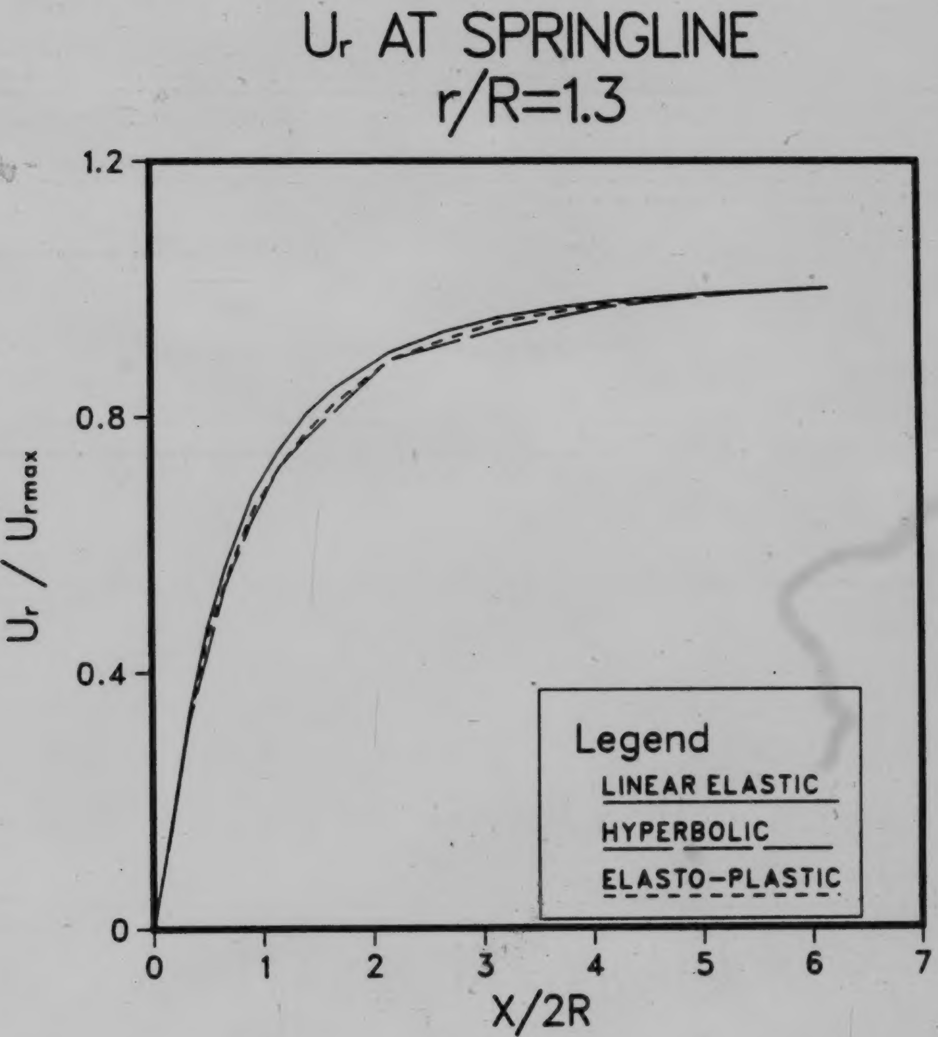

Figure 5.20 Radial Displacements at the Tunnel Springline (r/R=1.3); Linear-Elastic, Hyperbolic and Elasto-Plastic

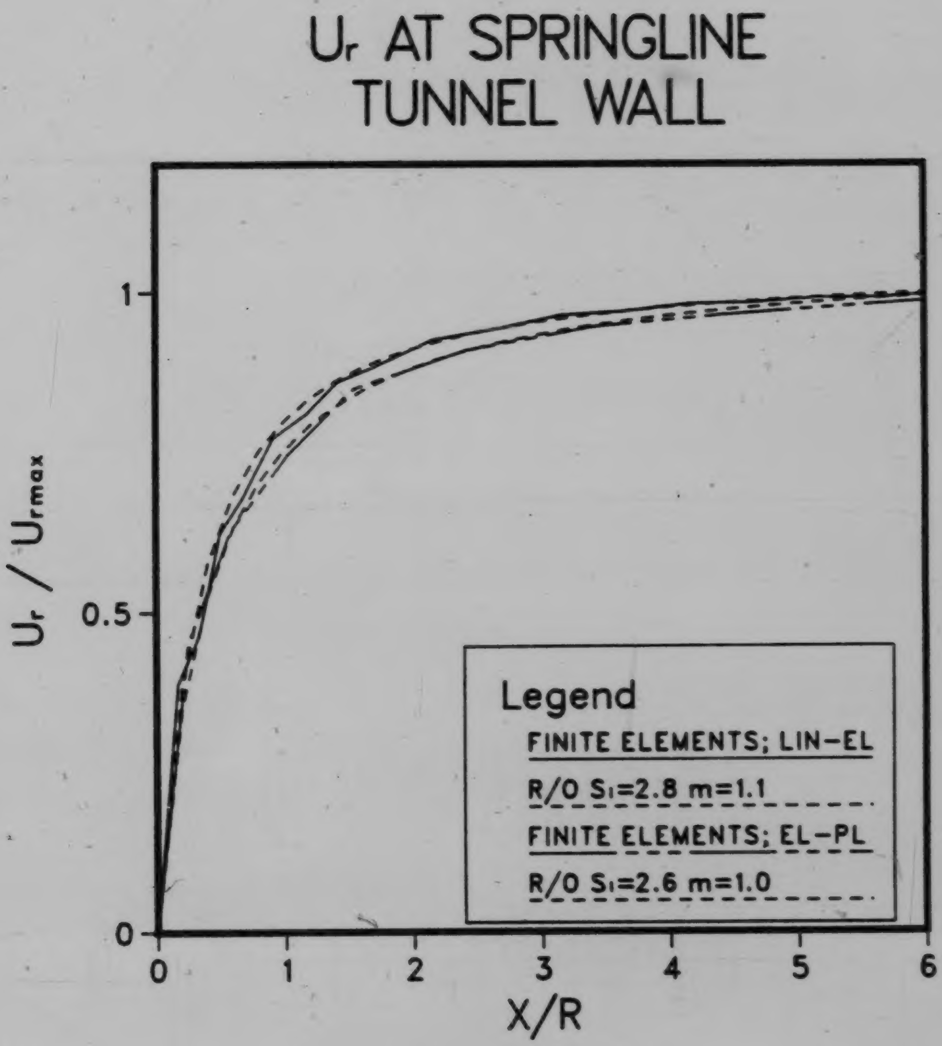

Figure 5.21 Convergence at the Tunnel Sprigline Fitted by the Ramberg-Osgood Function; Linear-Elastic and Elasto-Plastic

is much more apparent at the tunnel crown (see Figure 5.22) where most yielding occurs. In the previous chapters it was observed that low S_i-values often correspond with high m values and viceversa. Here, for the first time, a consistent decrease of the two parameters is found as the "degree of flatness" of the convergence curves increases.

5.6 Conclusions

Two cases of tunnels excavated in rock masses exhibiting non-linear behavior were discussed in this chapter. A stress-strain relationship defined by an hyperbolic function was selected for one of the analyses, where an elastic ideal plastic rock behavior was assumed in the other. The data were compared with results obtained by assuming linear elasticity and the following conclusions can be drawn:

1) Non-linear behavior in the pre-failure range is beneficial to tunnel stability, both at the face and at the wall, because it reduces stress concentrations near the opening.

2) The radial displacements are, in general, larger for tunnels in non-linear rock than for tunnels in linear elastic media. The difference is particularly noticeable at the crown and invert (direction of the minimum initial stress).

3) If the rock mass behaves as a non-linear material the relative displacement curves at the crown (direction of

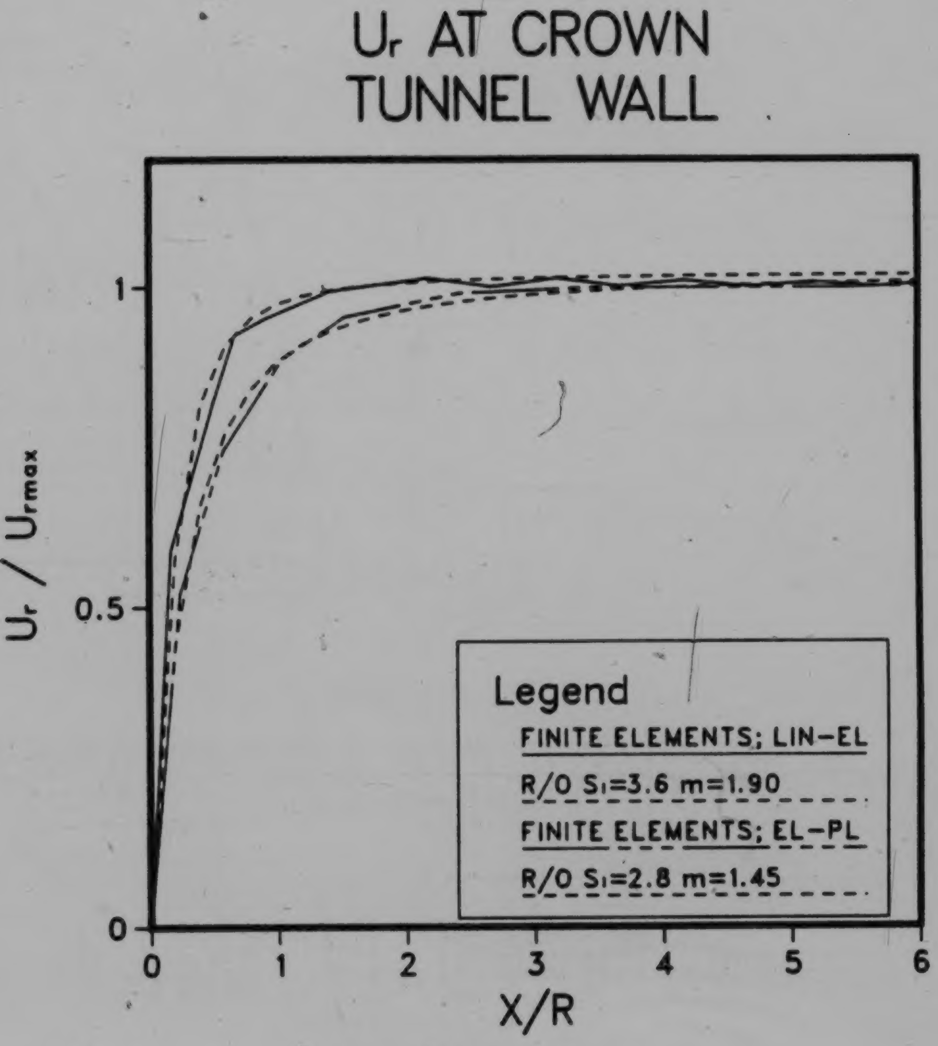

Figure 5.22 Convergence at the Tunnel Crown Fitted by the Ramberg-Osgood Function; Linear-Elastic and Elasto-Plastic

the minimum initial stress) become steeper than for the linear elastic case and movement only occurs near the wall. This is particularly apparent for the elasto-plastic case where 50% of the displacement takes place in the plastic zone. Little information can be obtained at the tunnel springline where very similar relative displacement profiles are found for the three cases.

4) If the whole convergence curve is known, non-linearity can be detected by back-analyzing a fictitious elastic modulus based on the curve portion ahead of the tunnel face. The ultimate convergence can be compared with the elastic solution based on this Young's modulus. Consistency will be found only if the rock behaves as a linear elastic material.

5) The radial displacement curves (neglecting the movement ahead of the face) are flatter for the non-linear cases than for the linear elastic case. A considerable difference was found at the crown where most yielding occurs. For the cases examined both m and S_i decrease as flatter curves are considered.

6. SUPPORTED TUNNELS

6.1 Introduction

In the previous chapters the behavior of unlined tunnels under various initial stress and ground conditions was investigated. Emphasis was placed on the effects of the three dimensional near face conditions on monitoring data as often taken during tunnel advance.

However, a primary support is usually placed behind the face in order to prevent instabilities that may occur due to the excavation process. In modern tunnelling philosophy the importance of this support is emphasized as it provides confinement to the surrounding ground thereby preventing loosening and strength loss.

During the excavation process the liner attracts some load, depending on its stiffness relative to the rock and on the installation procedure. The prediction of these loads is a primary concern for the designer and it is strictly related to the three dimensional nature of the tunnelling problem. At the same time, the liner acts as a stiff inclusion in the rock mass and some effects on displacements must also be expected.

In this chapter, the effects of the relative stiffness between rock and support, the delay, the excavation round length and the rock anisotropy on thrust and bending moments in the liner will be discussed. The effects of the support on the displacements (i.e., monitoring data) in the rock surrounding the tunnel will also be investigated. The purpose is to provide some understanding of the three-dimensional load transfer mechanism taking place near tunnel face and to assist the interpretation of monitoring data in supported tunnels.

6.2 Description of the Analyses

6.2.1 General

In order to study the behavior of deep supported tunnels in linear elastic rock, a series of three dimensional finite element analyses were carried out using the program ADINA. A mesh virtually identical to the one described in Chapters 3 and 4 was selected and the usual assumptions regarding cross section shape, symmetry of the problem, principal stress directions and distribution were made.

The purpose was to investigate stresses and deformations in the rock, as well as thrust forces and bending moments in the lining, as they develop during face advance. The liner was assumed to be linear elastic and to be relatively flexible with respect to the rock mass. A step by step excavation procedure was adopted to closely simulate real tunnelling conditions. The birth-death option available in the program was used to eliminate "excavated" elements and to activate the support as needed. The liner was modelled by means of three dimensional isoparametric shell elements described by Bathe and Bolourchi (1977). These elements were preferred over solid 3-D brick elements that display various shortcomings if used for thin or thick shell analysis. This topic is widely discussed in the literature (Zienkiewicz, 1977; Zienkiewicz et al., 1971; Pawsey and Clough, 1971; Zienkiewicz and Hinton, 1976). The lined tunnel was tested under 2-D plane strain conditions and the results were compared with closed form solutions given by Einstein and Schwartz (1979). A difference in convergence of approximately 10% was detected for the two cases and this accuracy was considered sufficient for the purposes of the present study. An error of this kind is expected in numerical analyses that only provide approximate solutions. The accuracy of the results depends on the degree of refinement of the mesh.

In total nine finite element analyses, three of which considered anisotropic rock conditions, were carried out varying the relative stiffness of liner and rock, the delay of support installation (DEL) and the excavation round length (RL). The meanings of DEL and RL have been explained in Chapter 2.

6.2.2 Parameters for Tunnels in Isotropic Rock

The initial stress ratio, $K_0=2$, and the initial vertical stress, $P_v=5$ MPa, were kept constant and so were the Poisson's ratios for ground, ν, and liner, ν_s, that were set to 0.25 . In Table 6.1, the cases analyzed and the parameters used for each of them are shown. The compressibility and the flexibility ratios, C and F, are defined by Einstein and Schwartz (1979):

$$C = \frac{ER(1-\nu_s^2)}{E_s A_s (1-\nu^2)} \qquad [6.16]$$

$$F = \frac{ER^3(1-\nu_s^2)}{E_s I_s (1-\nu^2)} \qquad [6.17]$$

where E, ν, E_s and ν_s are the elastic parameters for the rock and the support and A_s and I_s are, respectively, the cross sectional area and the moment of inertia of the support for unit length of tunnel. The compressibility ratio C, is a measure of the relative diametral stiffness of the ground and the support under axisymmetric load conditions, whereas the flexibility ratio F, is a measure of the relative diametral stiffness under an antisymmetric loading condition. Einstein and Schwartz based their formulation of C and F on the principle that the stiffness of the perforated ground mass (a plate with a hole) had to be considered, as opposed to Burns and Richard (1964), Hoeg (1968) and Peck et al. (1972) who based the calculation of the ground stiffness on the unperforated ground mass existing before the tunnel was excavated.

	GEOMETRY			RELATIVE STIFFNESS		MATERIAL PROPERTIES			INITIAL STRESSES	
	R(m)	DEL	RL	C	F	E (MPa)	ν	ν_s	P_v (MPa)	K_0
1	3.8	0	2R	1.41	24387	1000	0.25	0.25	5	2
2	3.8	0	2R	14.10	243875	10000	0.25	0.25	5	2
3	3.8	0	2R	4.70	9032	10000	0.25	0.25	5	2
4	3.8	0	1R	1.41	24387	1000	0.25	0.25	5	2
5	3.8	1R	1R	1.41	24387	1000	0.25	0.25	5	2
6	3.8	0	1/3 R (variab)	1.41	24387	1000	0.25	0.25	5	2

Table 6.1 Parameters Selected for Cases 1 to 6 (Isotropic Rock)

6.2.3 Parameters for Tunnels in Anisotropic Rock

In order to study the effect of rock anisotropy on thrust and bending moments in the liner, three finite element analyses were carried out assuming transverse isotropic behavior for the rock. Similarly to the analysis of unlined tunnels (see Chapter 4), the initial stress ratio, as well as the ratio between the maximum and minimum elastic moduli, were maintained constant ($K_0=2$; $E_2/E_1=10$). The orientation of the planes of stratification with respect to the tunnel axis was changed as shown in Figure 6.1. The liner was assumed to be installed one radius behind the face (DEL=1R) and an excavation round length RL=1R was selected. Delay, excavation round length and stiffness of the support were kept constant for the three cases. In Table 6.2 are summarized the parameters used for the three analyses (1A, 2A, 3A). Note that the concepts of compressibility and flexibility ratios, as formulated earlier in this chapter, are only applicable for isotropic rock conditions. For this reason the moduli ratios E_2/E_1 and E_s/E_1 are presented in Table 6.2 and the thickness of the liner, th, is normalized with respect to the tunnel radius.

In the following paragraphs the results of the finite element analyses are discussed. Emphasis is put on the effects of the three dimensional load transfer mechanism on stresses and deformations in the rock-liner system.

	GEOMETRY			MODULI RATIOS		LINER THICKNESS	MATERIAL PROPERTIES				INITIAL STRESSES	
	R(m)	DEL	RL	E_2/E_1	E_s/E_1	th/R	E_1 (MPa)	ν_1	ν_2	ν_s	P_v (MPa)	K_0
1A	3.8	1R	1R	10	27	0.026	1000	0.25	0.025	0.25	5	2
2A	3.8	1R	1R	10	27	0.026	1000	0.25	0.025	0.25	5	2
3A	3.8	1R	1R	10	27	0.026	1000	0.25	0.025	0.25	5	2

* For orientation of elastic properties see Figure 6.1.

Table 6.2 Parameters Selected for Cases 1A to 3A (Transverse Isotropic Rock)

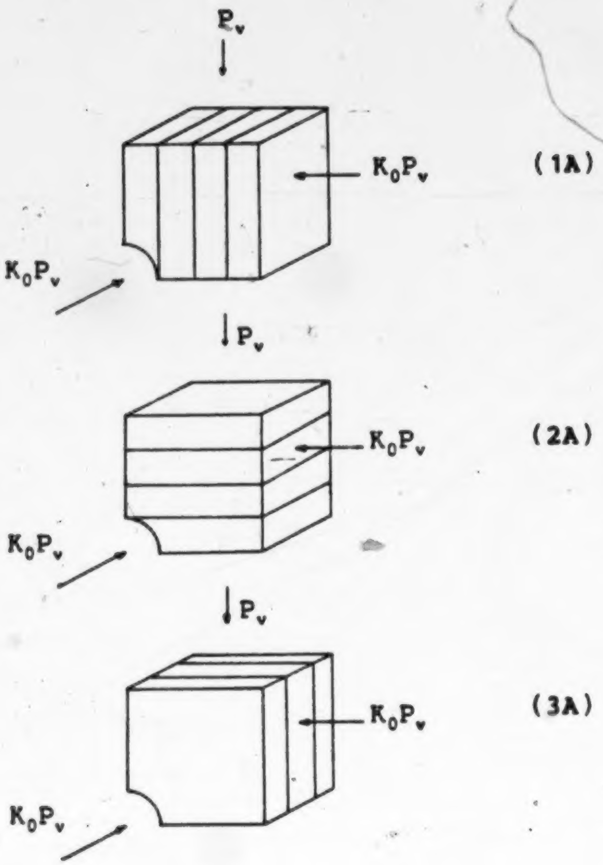
P_v
K_0P_v
(1A)
K_0P_v
P_v
K_0P_v
(2A)
K_0P_v
P_v
K_0P_v
(3A)
K_0P_v

Figure 6.1 Orientation of the Elastic Properties for Cases 1A to 3A (Transverse Isotropic Rock)

6.3 Displacements

The convergence curves for some of the cases investigated are plotted, in the usual normalized form, in Figures 6.2 and 6.3.

6.3.1 Effect of the Relative Stiffness

Cases 1, 2 and 3 are compared in Figure 6.2 in order to show how the relative stiffness affects the radial displacement at the tunnel wall. For the three cases the liner was placed immediately behind the tunnel face (DEL=0) and an excavation round length RL=2R was selected. The different values of the compressibility ratio C, and of the flexibility ratio F are also shown. As expected, the normalized convergence decreases with decreasing the compressibility ratio C. Little effect, due to changing flexibility ratio F can be observed. Although the liners are placed immediately behind the excavation front, convergence ahead of the tunnel face is essentially unaffected by the stiffness of the support, and differences among the three cases begin within one radius behind the face. For tunnels in soil a relatively higher support stiffness may lead to more substantial differences ahead and behind the excavation front. At the tunnel crown (direction of the minimum initial stress) a change in the direction of the radial movement (inward to outward) is detected. This phenomenon is associated with the outward squeezing action of the deforming liner and is particularly apparent for relatively

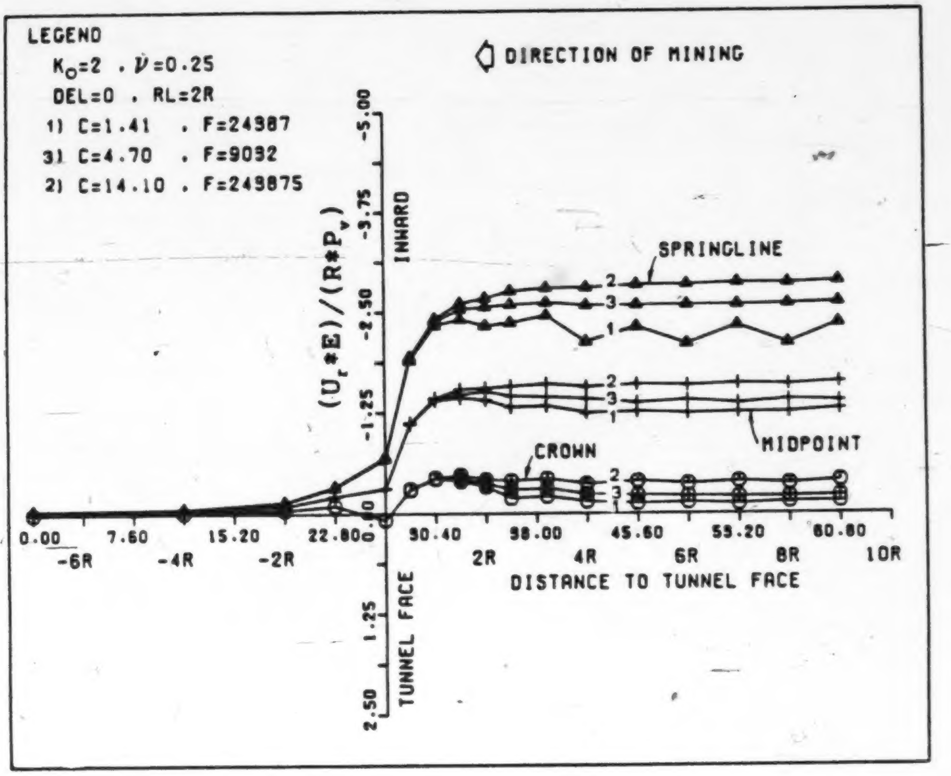

Figure 6.2 Convergence Curves for Cases 1 to 3; Variable Relative Stiffness

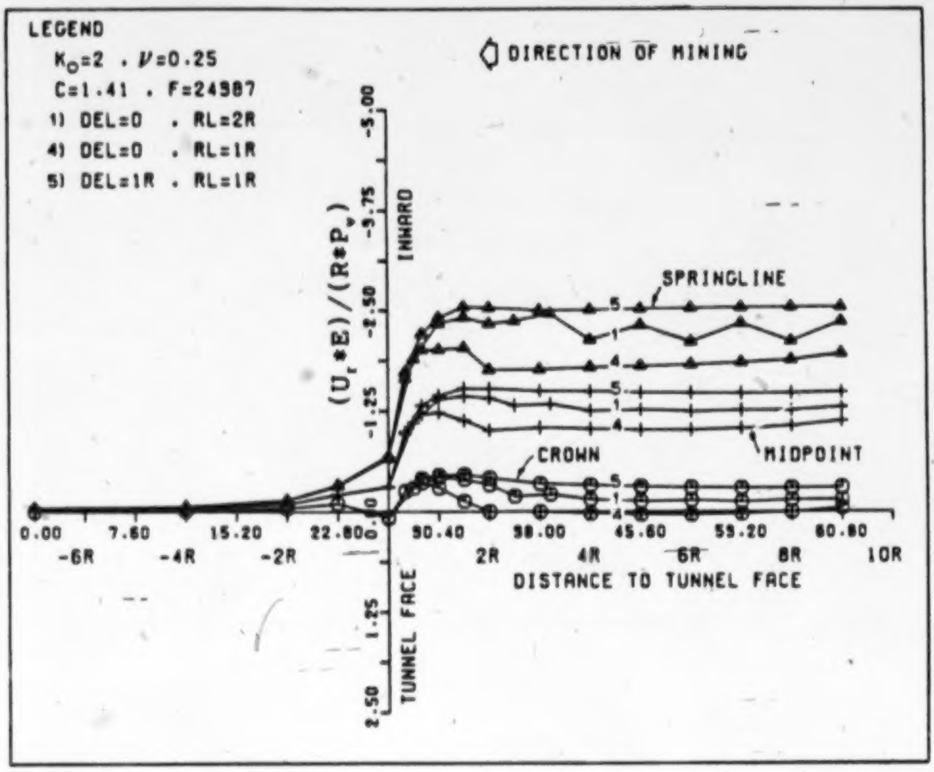

Figure 6.3 Convergence Curves for Cases 1,4 and 5; Variable Delay and Round Length

high support stiffness.

6.3.2 Effect of Delay and Excavation Round Length

In order to show the effects of delay and excavation round length on radial displacements, convergence curves for Cases 1, 4 and 5 are plotted in Figure 6.3. The parameters C and F were kept constant for the three cases, where different delays (DEL=0 for Cases 1 and 4, DEL=1R for Case 5) and excavation round lengths (RL=2R for Case 1, RL=1R for Cases 4 and 5) were assumed. The excavation support sequence for Cases 4 and 5 are depicted schematically in Figure 6.4. Initially (Figure 6.4a), the leading edge of the liner is placed at a certain distance from the tunnel face (1R for Case 4 and 2R for Case 5) that also represents the maximum length of the unsupported tunnel section. Then (Figure 6.4b), an unstressed liner ring is placed immediately behind the tunnel face for Case 4 and at one radius distance from the face for Case 5. Finally, excavation is performed (Figure 6.4c) and the initial conditions are restored. If the convergence curves relative to Cases 4 and 5 are compared (Figure 6.3), smaller radial displacements are detected for the fully lined case (Case 4). This was expected because, if the relative stiffness liner-rock is kept constant, the delay of liner installation plays a key role in controlling radial displacements as well as pressure on the support. In Figure 6.5 a schematic explanation of this phenomenon based on the convergence confinement concept

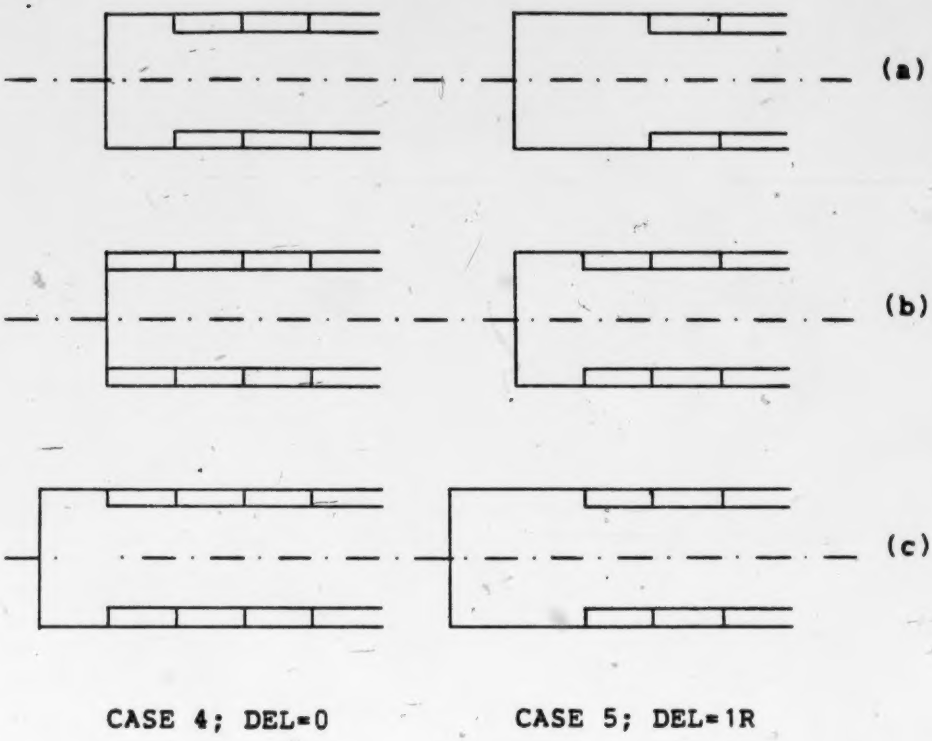
(a)
(b)
(c)
CASE 4; DEL=0
CASE 5; DEL=1R

(a) Initial state

(b)Placement of liner section

(c) Excavation

Figure 6.4 Excavation Support Sequence for Cases 4 (No Delay) and 5 (1R Delay)

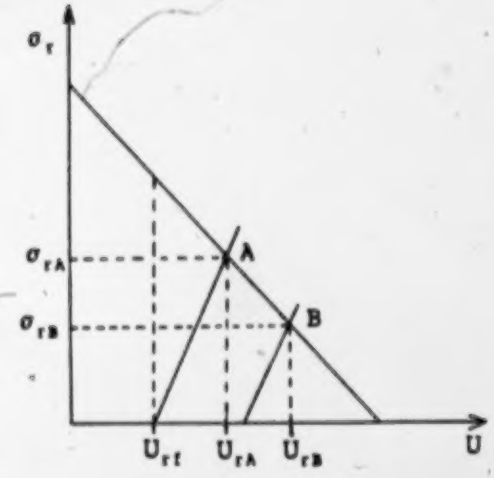
σ_r
σ_{rA}
σ_{rB}
A
B
U_{rf}
U_{rA}
U_{rB}
U

Figure 6.5 Effects of the Delay on Radial Displacements and Pressure on the Support

is presented. If the liner is placed at the tunnel face, equilibrium is reached at point A corresponding to the radial displacement U_{rA}. If the support is installed with a certain delay DEL, equilibrium is reached at point B corresponding to the radial displacement U_{rB}. The delay also affects thrust and bending moments in the liner as will be discussed later in this chapter.

For Cases 1 and 4, an apparent change of direction of the radial displacement (from inward to outward) is also detected at the springline. This is due to the three dimensional stress transfer from ground to support and back to the ground as the tunnel face and the leading edge of the liner advance. The longitudinal component of the three dimensional arching tends to load heavily the leading edge of the liner, especially if the support is stiff and placed near the face of the tunnel. Further behind the excavation front, this effect vanishes and part of the energy stored in the support is released as the ring expands. Schwartz and Einstein (1980) also observed similar convergence behavior in some of their axisymmetric analyses. It will be shown, later in this chapter, that loads on the liner and monitoring data are affected by this phenomenon.

In order to investigate the effect of the excavation round length on the radial displacement, the convergence curves for Case 1 and Case 4 can be compared (Figure 6.3). Shorter excavation round lengths are associated with lower convergence, both at the crown and at the springline, due to a higher average pressure exerted by the liner on the tunnel wall. Most of the pressure is concentrated at the leading edges of the sections as they are installed immediately behind the excavation front. By decreasing the magnitude of RL, the number leading edges exerting high pressure on the rock increases and a more homogeneous stress distribution on the support is achieved (Figure 6.6).

6.3.3 Radial Multipoint Extensometer Records

It has been shown in the previous section that the deformations in the rock surrounding the excavation are influenced by the presence of the support. The effect of the liner on the relative displacement profiles will now be investigated.

If a radial multipoint extensometer is placed ahead of the tunnel face, where the rock is still undisturbed by the mining process, and readings are taken far behind the excavation front, the total displacement field is measured. In Figure 6.7, the total radial displacements calculated at the springline for the unlined case, Case 4 (DEL=0; RL=1R) and Case 5 (DEL=1R; RL=1R) are compared. For the lined cases the curves are somewhat translated towards lower displacement values due to the pressure exerted by the support on the tunnel wall. This effect is more pronounced for Case 4 where the liner, placed immediately at the tunnel face, provides greater confinement to the surrounding rock. A shallow compression zone can be detected at the tunnel

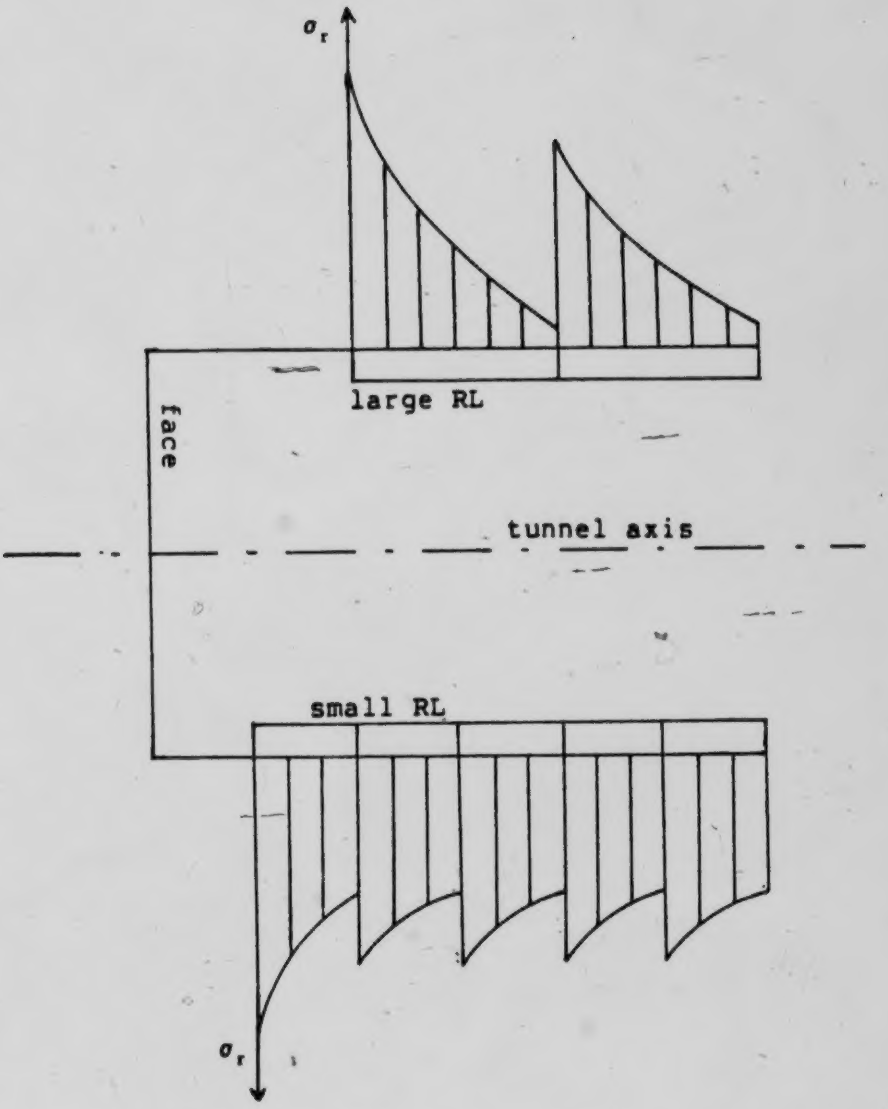
σ_r
large RL
face
tunnel axis
small RL
σ_r

Figure 6.6 Effect of the Round Length on the Stress Distribution in the Liner

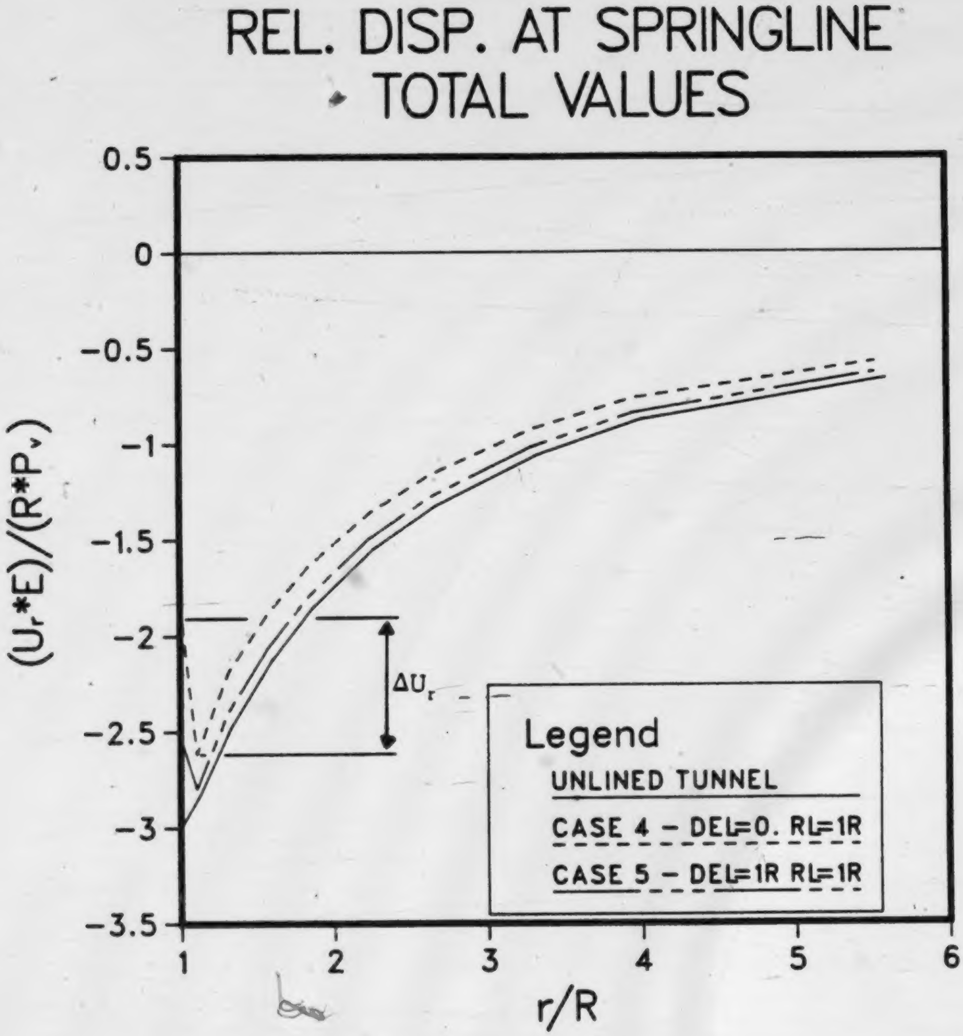

Figure 6.7 Relative Displacements at the Tunnel Springline (Total Values); Unlined and Cases 4 and 5

wall for the supported tunnels. This feature is, again, more pronounced for Case 4 where the compressive relative displacement (ΔU_r in Figure 6.7) is as large as 42% of the total convergence taking place at the wall. This compression zone is even more apparent at the tunnel crown as shown in Figure 6.8. Also at this location the effect of the support is more significant for Case 4, where the inward movement taking place within 2 radii from the tunnel wall is completely compensated by the compressive relative displacement occurring in a thin zone at the back of the liner.

It has been observed that the effect of the support-rock interaction is mostly concentrated in a relatively thin zone at the tunnel wall. This occurs because the pressure exerted by the liner is concentrated principally at the leading edge of the support sections. As shown schematically in Figure 6.9, this non-homogeneous stress distribution limits the volume of rock within which the major confinement action is felt. In Figure 6.10, stresses calculated along a radial axis (r as shown in Figure 6.9) are plotted for Case 4. The purpose is to show that a radial stress increase due to the action of the liner, is actually concentrated near the wall of the tunnel (within 0.5 R). The radial stress peak in the proximity of the leading edge of the support is also evident from Figure 6.10.

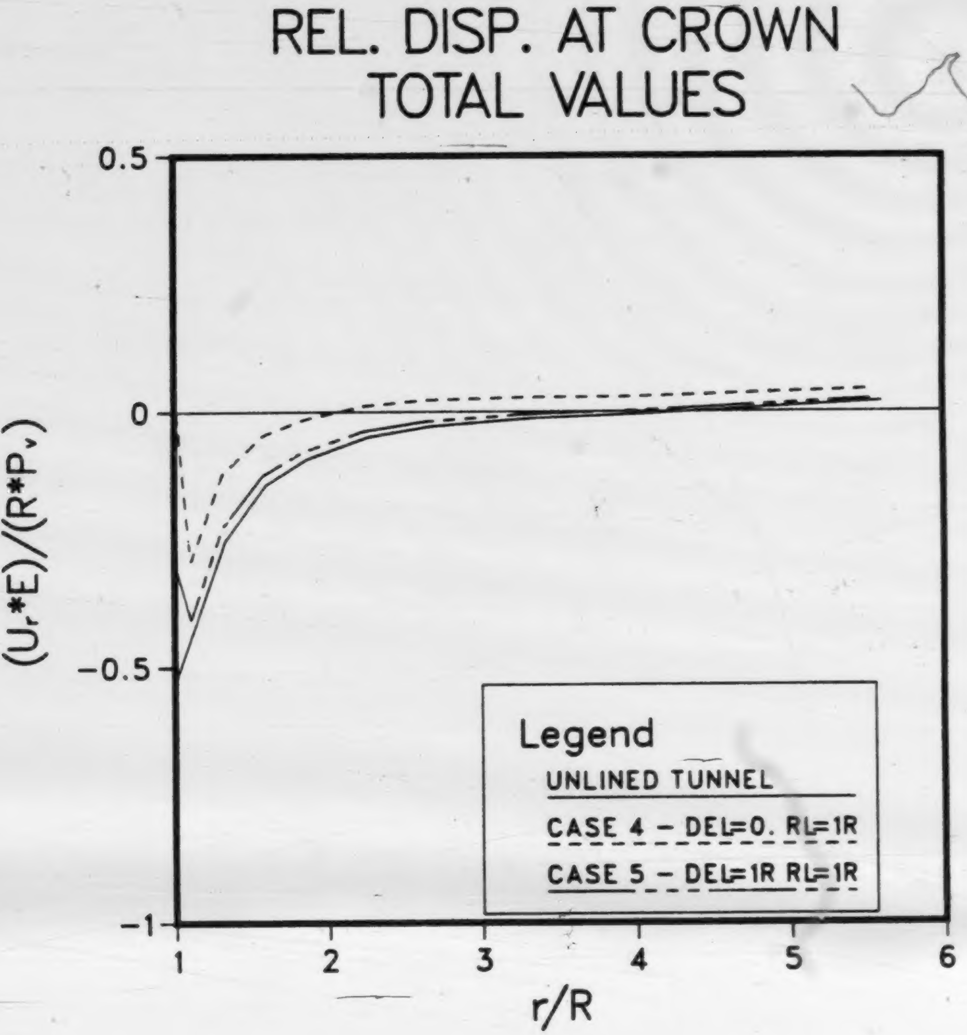

Figure 6.8 Relative Displacements at the Tunnel Crown (Total Values); Unlined and Cases 4 and 5

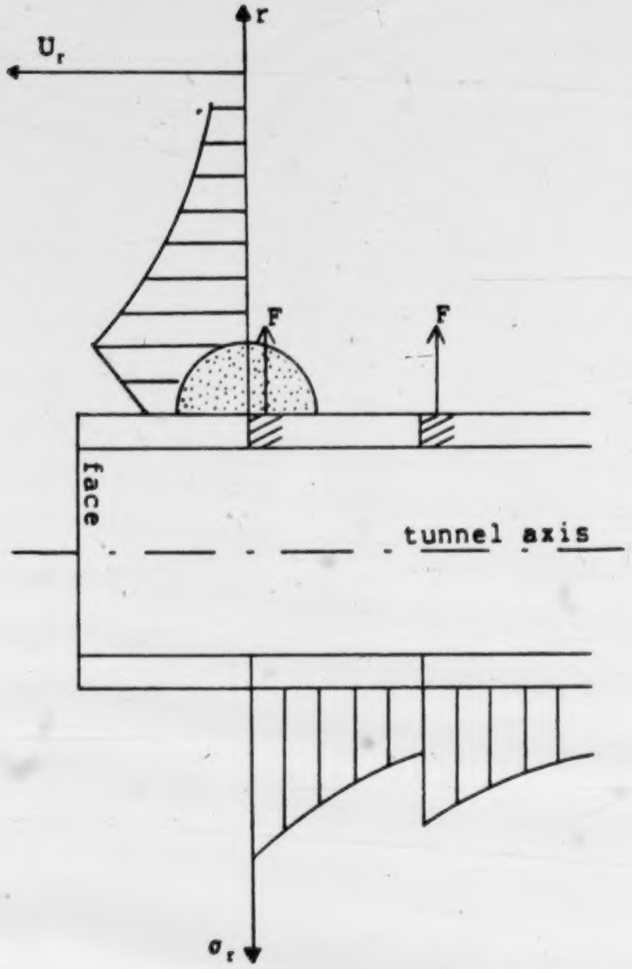
r
U_r
F
F
face
tunnel axis
σ_r

Figure 6.9 Schematic Diagram for Explanation of the Compressive Zones Detected at the Back of the Liner

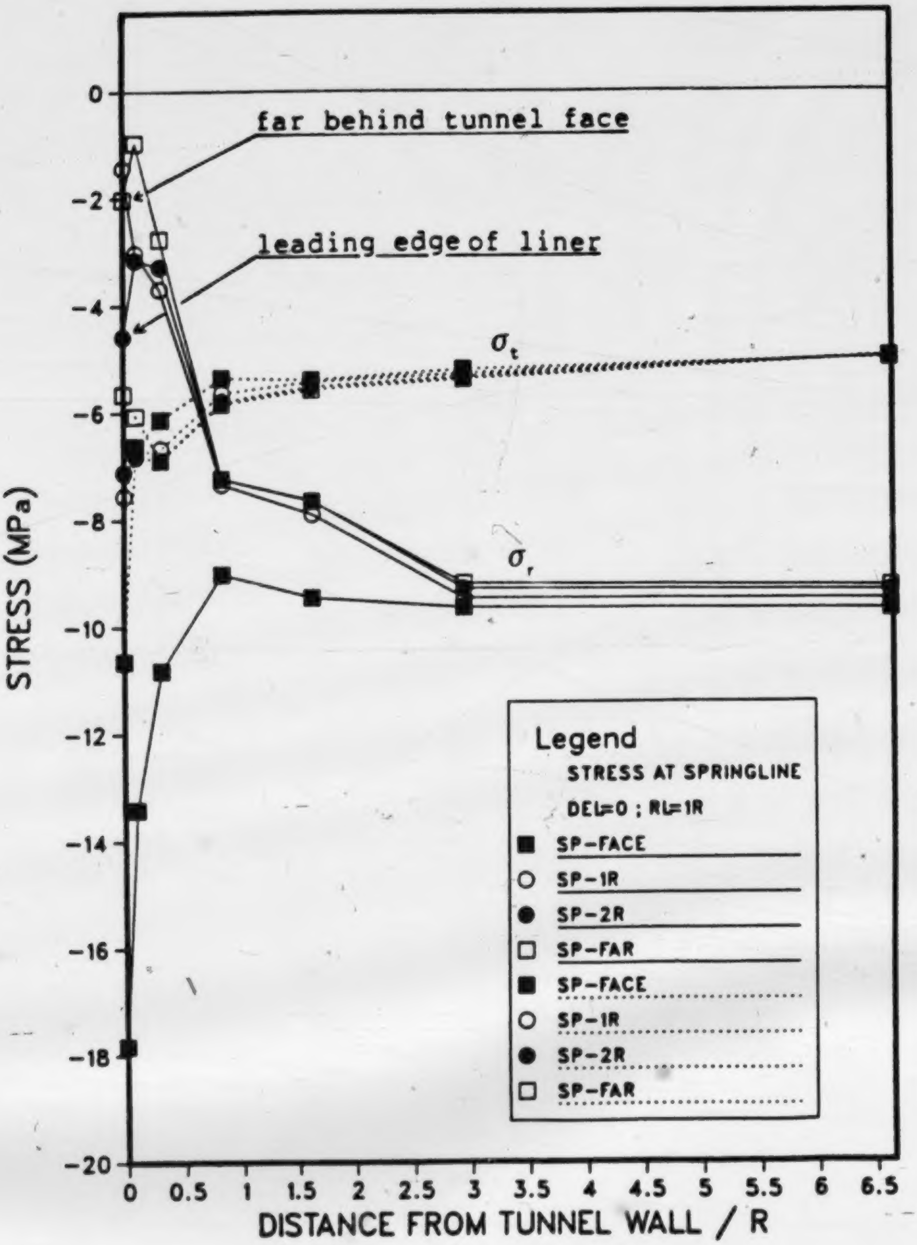

Figure 6.10 Radial (σ_r) and Tangential (σ_t) Stresses vs Distance from Tunnel Wall; Case 4

For deep tunnels the installation of radial extensometers ahead of the tunnel face is seldom possible and the measurements can only be taken behind the excavation front. Partial measurements with zero readings taken at the tunnel face and one radius behind the tunnel face are shown, as predicted by the 3-D FEM models for Cases 4 and 5, in Figures 6.11 to 6.14. Measurements taken at the tunnel springline (Figures 6.11 and 6.12) and at the crown (Figures 6.13 and 6.14) are considered. The compressive zone becomes dominant for zero readings taken one radius behind the excavation front, especially at the tunnel crown.

Compressive zones of the kind discussed in this chapter have often been observed in real tunnelling cases. Kaiser and Mackay (1983) measured displacements around a sinking shaft by means of multipoint radial extensometers (for instrument location see Figure 6.15). The outcome of some of the measurements (Mackay, 1982) is shown in Figure 6.16 where relative compressive zones are visible. This compression was first assumed to be due to erroneous readings, since they could not be explained by two dimensional analyses. However, the fact that they were consistently observed at this and other projects, leads to the conclusion that a compression zone, when related to an initial measurement taken close to the advancing face, must actually exist. The extension recorded in the shaft close to the wall, must be attributed to loosening due to blast damage of the rock in the immediate proximity of the shaft

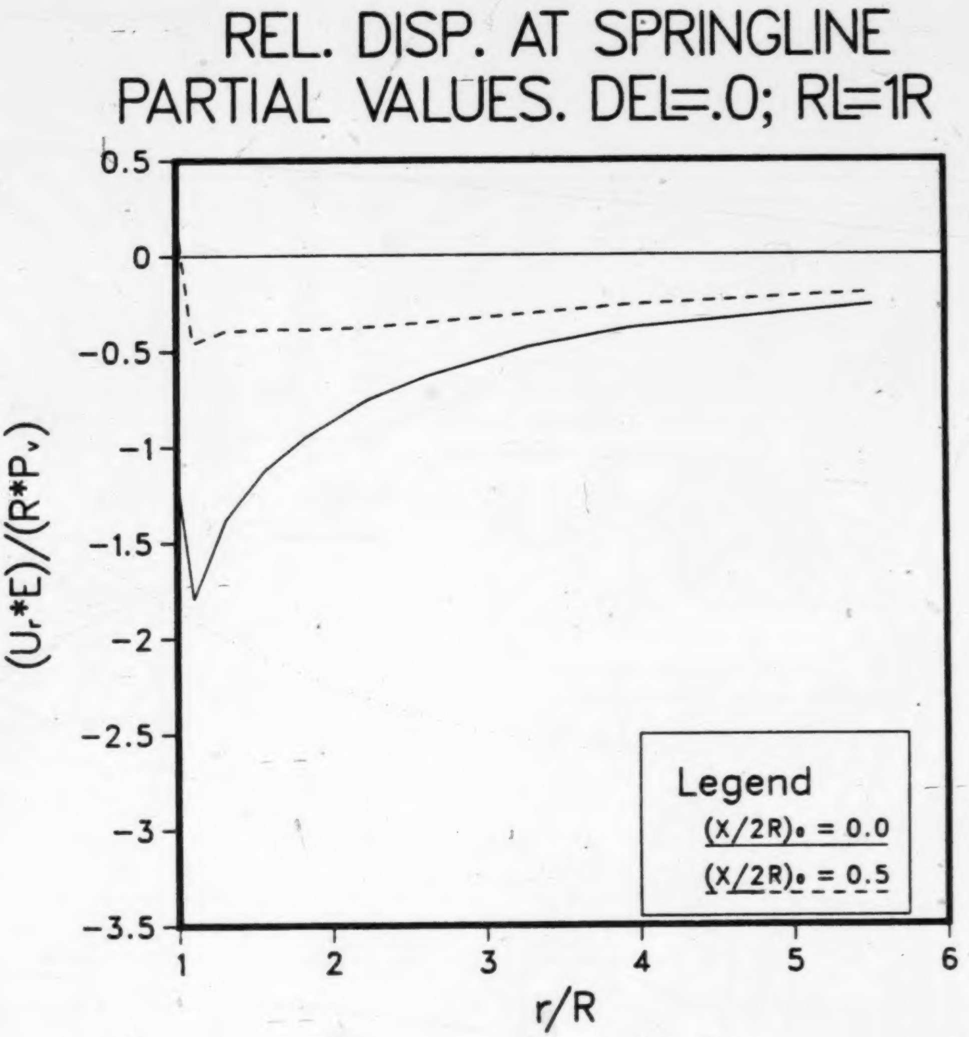

Figure 6.11 Relative Displacements at the Tunnel Springline (Partial Values); Case 4

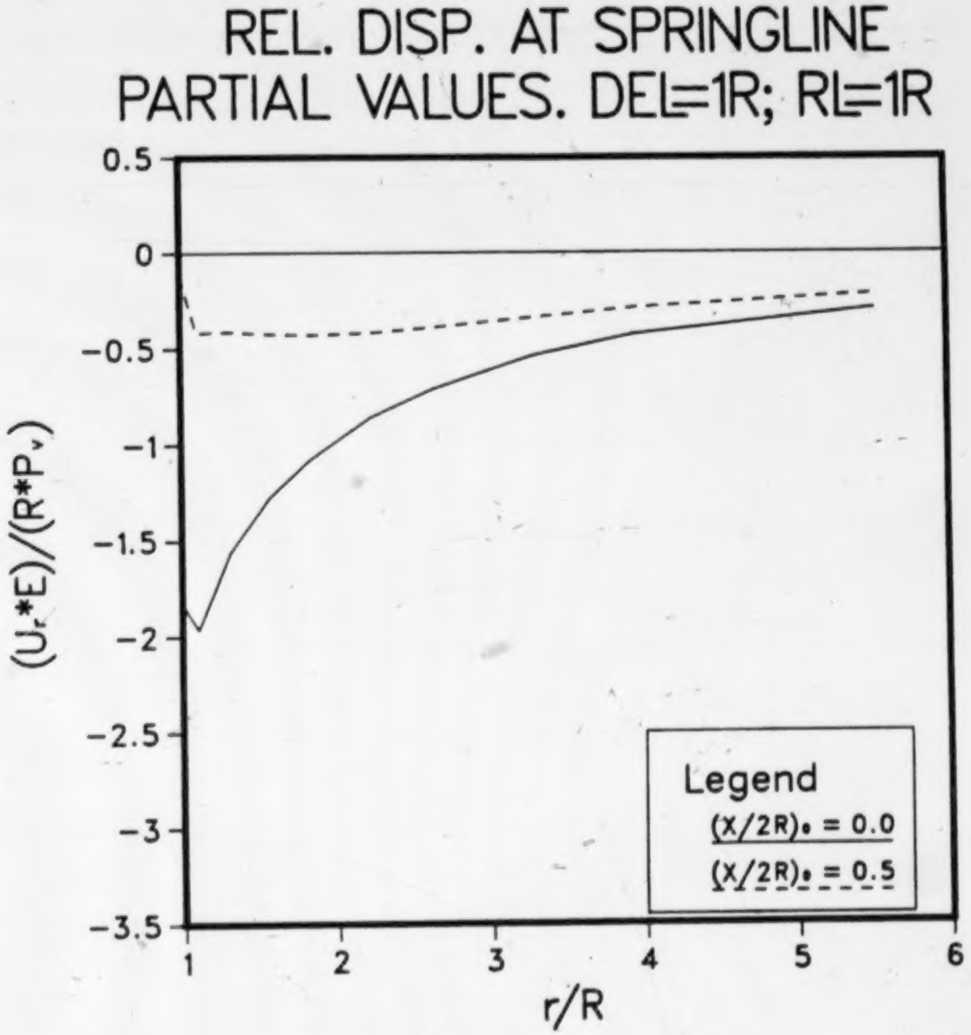

Figure 6.12 Relative Displacements at the Tunnel Springline (Partial Values); Case 5

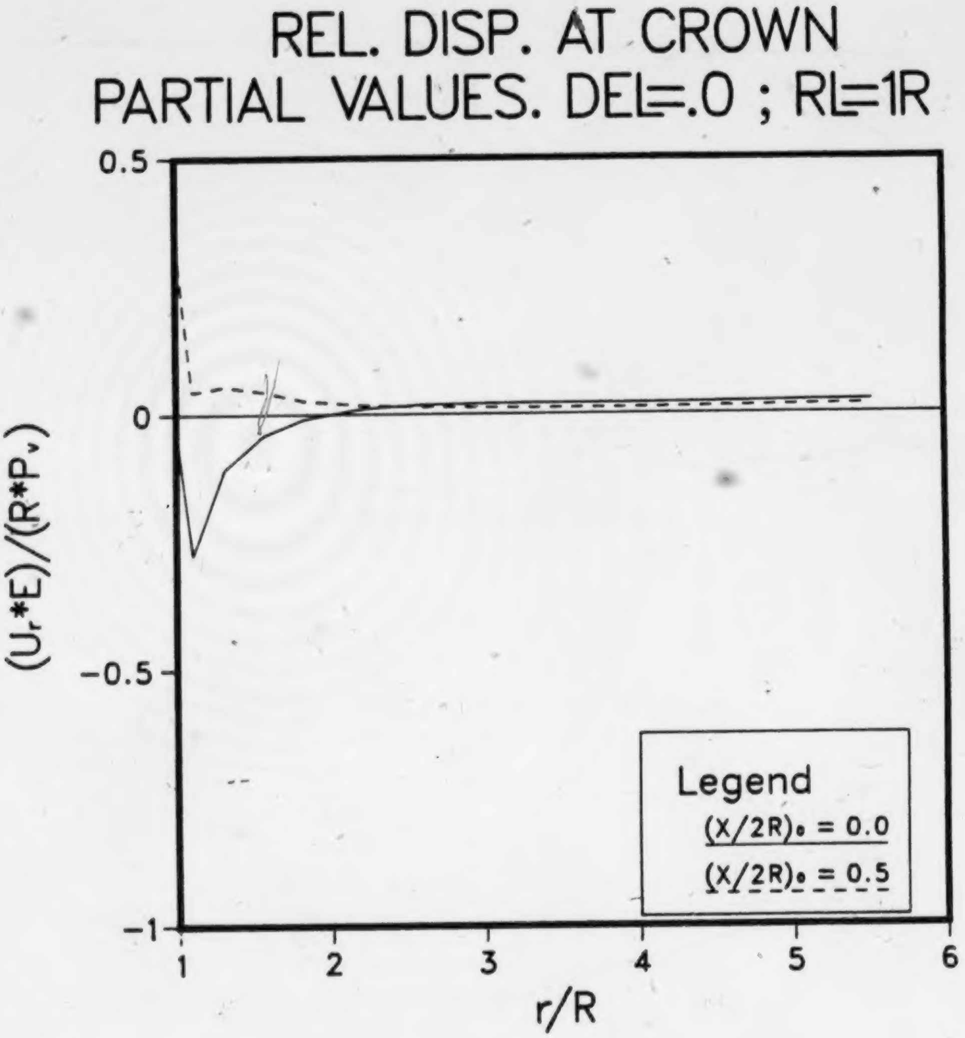

Figure 6.13 Relative Displacements at the Tunnel Crown (Partial Values); Case 4

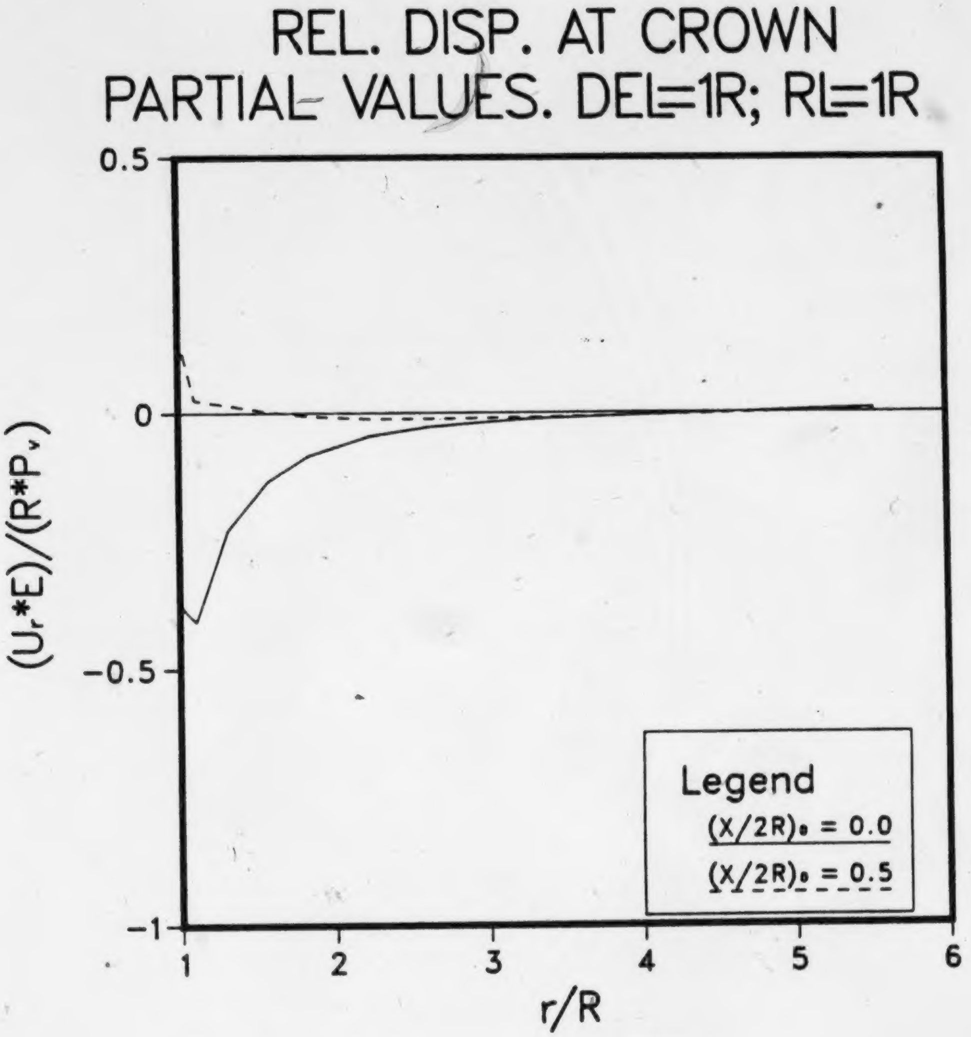

Figure 6.14 Relative Displacements at the Tunnel Crown (Partial Values); Case 5

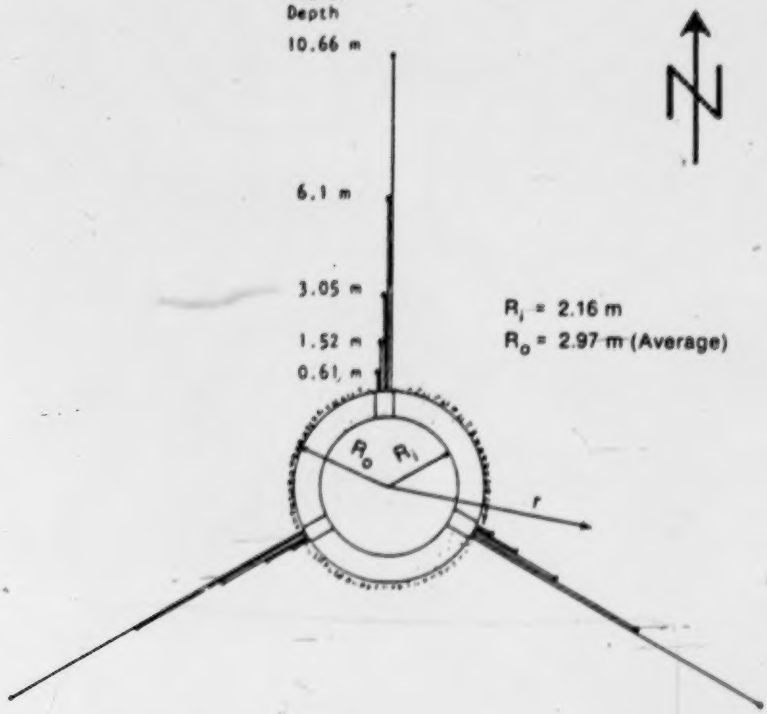
Anchor Depth
10.66 m
6.1 m
3.05 m
1.52 m
0.61 m
R_i = 2.16 m
R_o = 2.97 m (Average)
R_o
R_i
r
N

Figure 6.15 Array of Multipoint Radial Extensometers (Kaiser and Mckay, 1983)

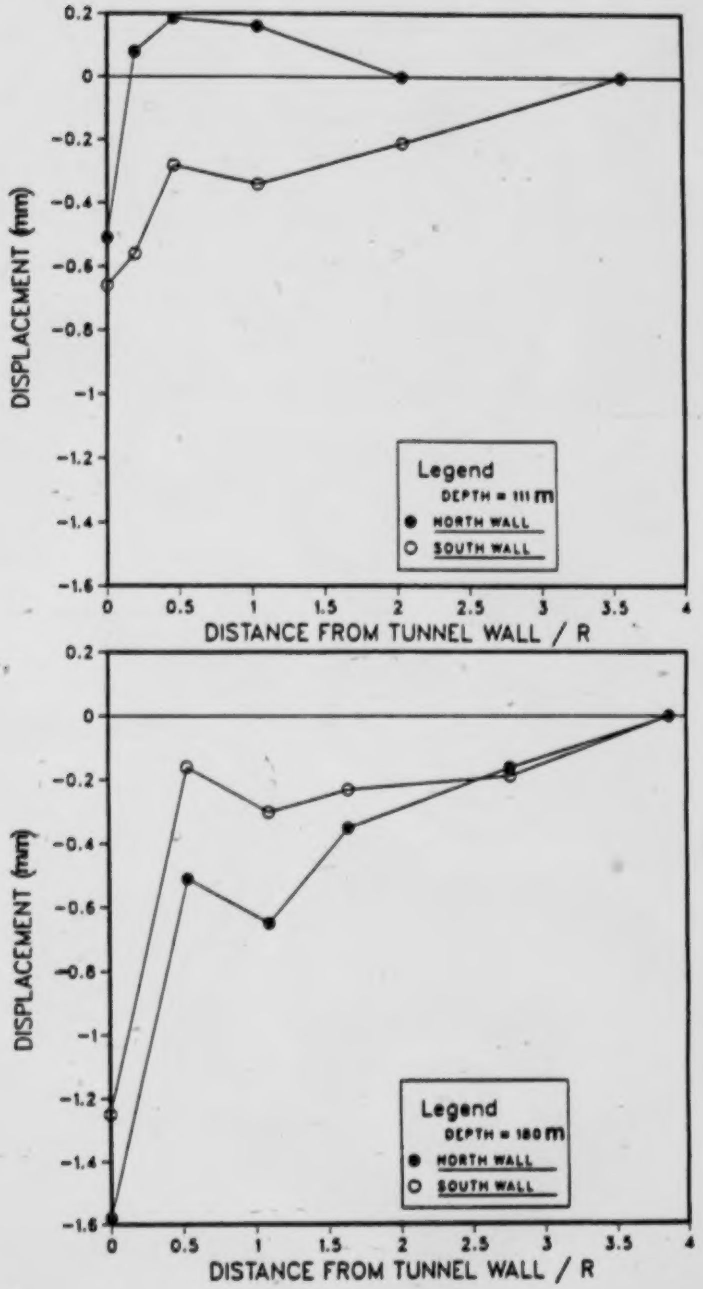

Figure 6.16 Relative Displacements Measured in the Shaft (Modified After Mckay, 1982)

wall.

In conclusion, the relative radial displacement as measured by radial extensometers located at various distances from the face of a supported tunnel, can be characterized by a compressive zone immediately behind the liner. This is of great practical significance because most extensometer readings are related to the movement of the anchor head which is most likely located inside the relative compressive zone. The effects of the support on radial displacements appear to be mainly concentrated very near the wall. As a result, at the springline, the overall shape of the relative displacement curve for unlined and lined tunnels is similar and can be used for back-analysis purposes. At the tunnel crown substantial shape changes only occur for the fully lined case where similar curves are found for Case 5 and the unlined tunnel.

6.4 Loads on the Support

If a support is placed relatively close to the tunnel face, a complex rock-structure load transfer process takes place as the excavation is advanced. In order to study the effects of relative stiffness, delay, excavation round length and anisotropic rock behavior on the loads developing in the lining during face advance, thrust forces and bending moments in the support were calculated for the cases investigated.

In this paragraph the method used for calculating the loads in the liner is explained and the results are discussed.

6.4.1 Calculation of Thrust and Bending Moments

Some difficulties were encountered in trying to use the stresses calculated in the liner by the 3-D FEM analyses for a direct computation of thrust and bending moments in the support. The stresses at the integration points of the shell elements were in fact found to be slightly oscillating and this generated apparently inconsistent load distributions, especially for the bending moments.

An indirect method was then chosen consisting in applying to a separate support ring the displacements calculated by the 3-D finite element model. The radial movement of the support was found, as depicted in Figure 6.17, by subtracting the total displacement at Location A from the total displacement at Location B. ΔU_r represents the radial movement of the support at Location B. The same procedure was also applied to tangential displacements.

The support ring used for the computation is composed of 16 Hermitian beam elements, as shown in Figure 6.18a. The displacements to be applied to each node were found by interpolating values given by the 3-D model for crown, springline and mid-point.

The radial displacements at the crown and at the springline were interpolated by means of the function:

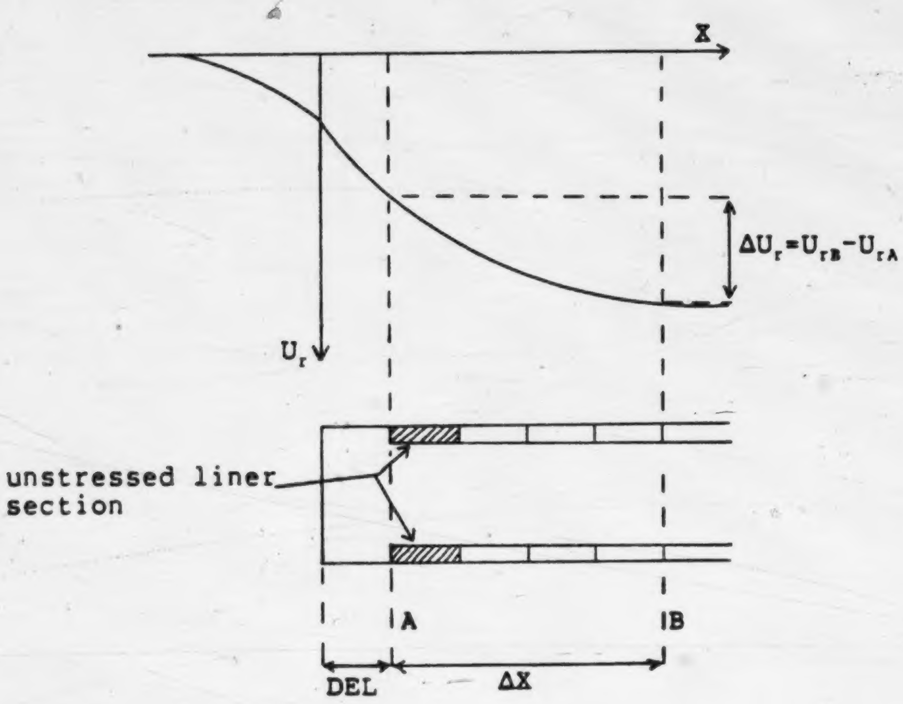
X
$\Delta U_r = U_{rB} - U_{rA}$
U_r
unstressed liner section
A
B
DEL
ΔX

Figure 6.17 Displacements of the Liner Due to Face Advance

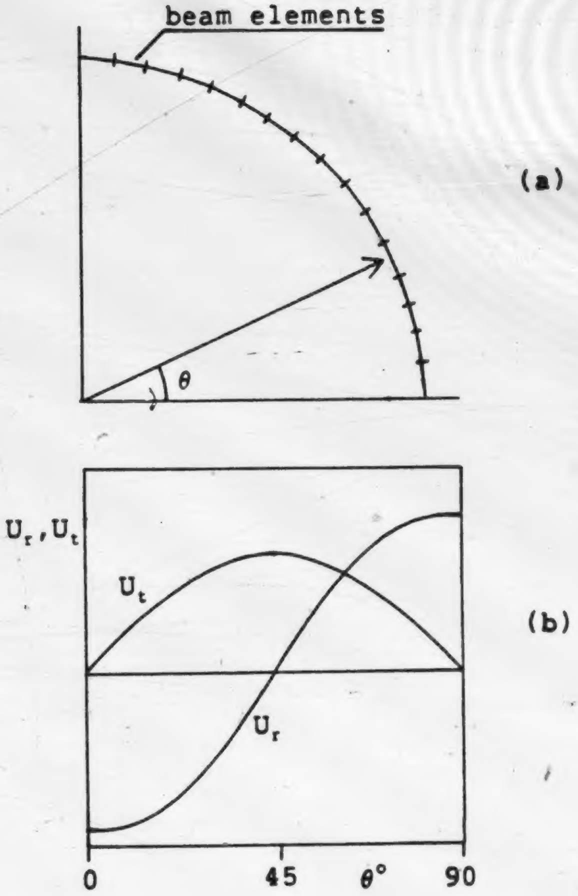
beam elements
θ
(a)
U_r, U_t
U_t
U_r
0
45
θ°
90
(b)

Figure 6.18 Support Ring Used for Computation of Loads in the Liner (a) and Interpolation Functions for Radial and Tangential Displacements (b)

$$\Delta U_r = A - B.\cos\theta \qquad [6.18]$$

where A and B are constants and the angle θ is indicated in Figure 6.18a. The tangential displacements at the crown and at the springline (both zeroes because of symmetry) and at the mid-point were interpolated by the function:

$$\Delta U_t = D.\sin\theta \qquad [6.19]$$

where D is a constant.

The analytical functions (6.3) and (6.4), shown graphically in Figure 6.18b, describe the displacements around 2-D unsupported (Obert and Duvall, 1967) and supported (Einstein and Schwartz, 1979) tunnels in elastic media.

For Case 4 a 3-D support shell (Figure 6.19) was deformed in the same manner to study thrust and bending moments developing along the axis of the tunnel. A quadratic polynomial function was selected to interpolate longitudinally the displacements taken at the leading edge, mid-section and trailing edge.

6.4.2 Effects of Relative Stiffness of Support

In Figure 6.20, the thrust forces calculated for Case 1 (DEL=0; RL=2R) are normalized with respect to initial vertical stress and tunnel radius, and plotted against θ

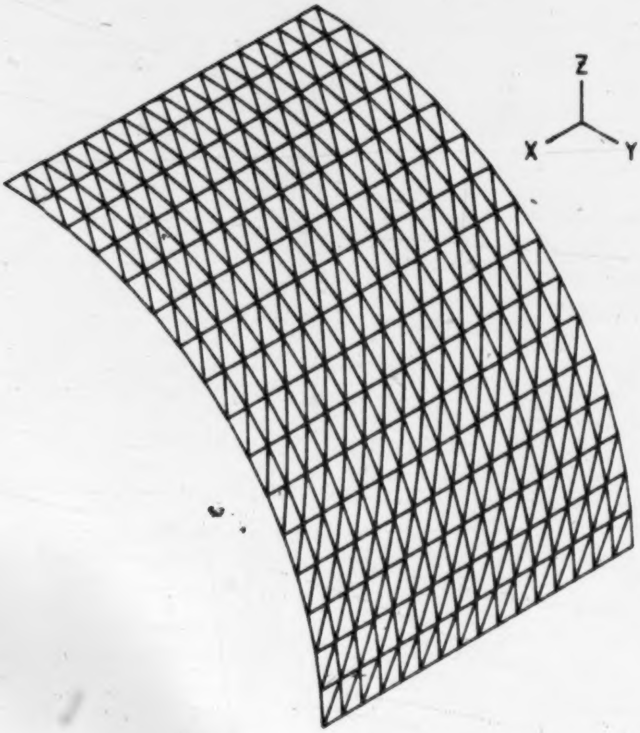

Figure 6.19 Three dimensional Support Shell

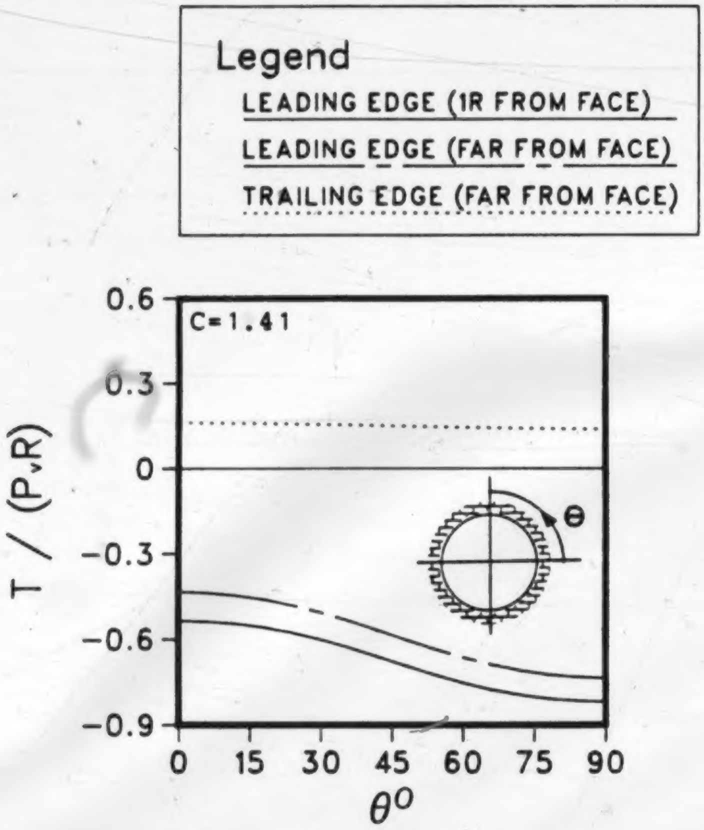

Figure 6.20 Thrust Forces in the Liner for Case 1

(defined in the figure). The maximum load is detected when the leading edge of the liner section is one radius behind the tunnel face. As the face advances further, the load in the liner decreases somewhat. This phenomenon can be explained in terms of 3-D load transfer mechanism that takes place near the face and loads the leading edge of the support more heavily. Because of the high K_0 value, the load developing at the springline is only 65% of the load at the crown. Tensile stress develops at the trailing edge of the section that is placed one diameter behind the face and is expanded by the rebound mechanism discussed earlier in this chapter.

In Figure 6.21, these considerations are summarized schematically. For each support section the maximum thrust is found at the leading edge where the trailing edge may be subjected to tensile stresses if the liner is assumed to be able to stand tension and full bonding between rock and liner exists. The leading edge of the liner, near the face, is highly stressed by the 3-D arching mechanism dominating in that region and this generates a peak load consistent with the shape of the convergence curves observed earlier.

The thrust forces in the liner calculated for Case 2 and Case 3 are shown in Figures 6.22a and b. For Case 2 (Figure 6.22a), the high C value (soft liner) results in low stresses in the support, whereas for Case 3 (Figure 6.22b), an intermediate stress level, with respect to Case 1 and Case 2, corresponds to an intermediate C value. For these

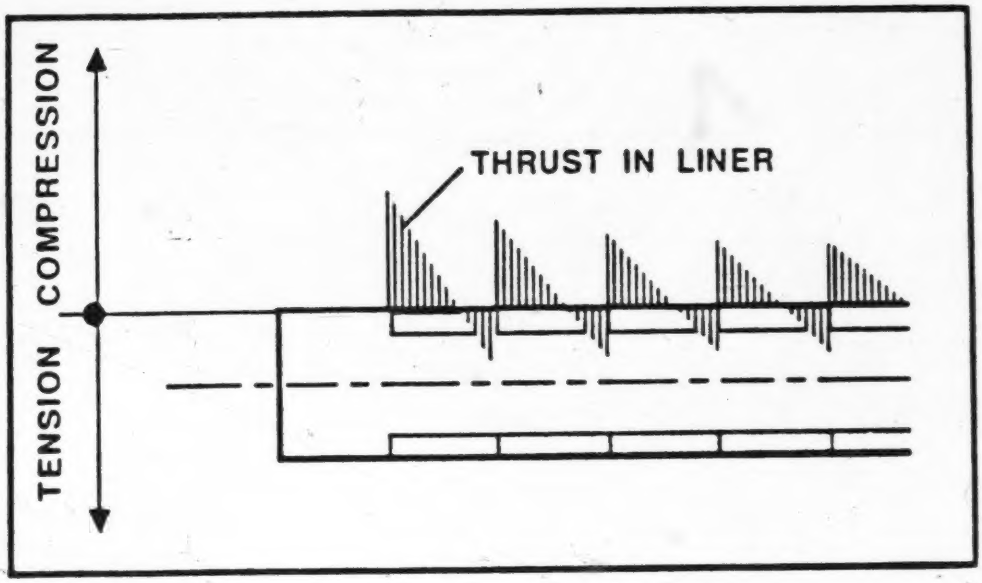
COMPRESSION
TENSION
THRUST IN LINER

Figure 6.21 Longitudinal Distribution of the Thrust Forces in the Liner

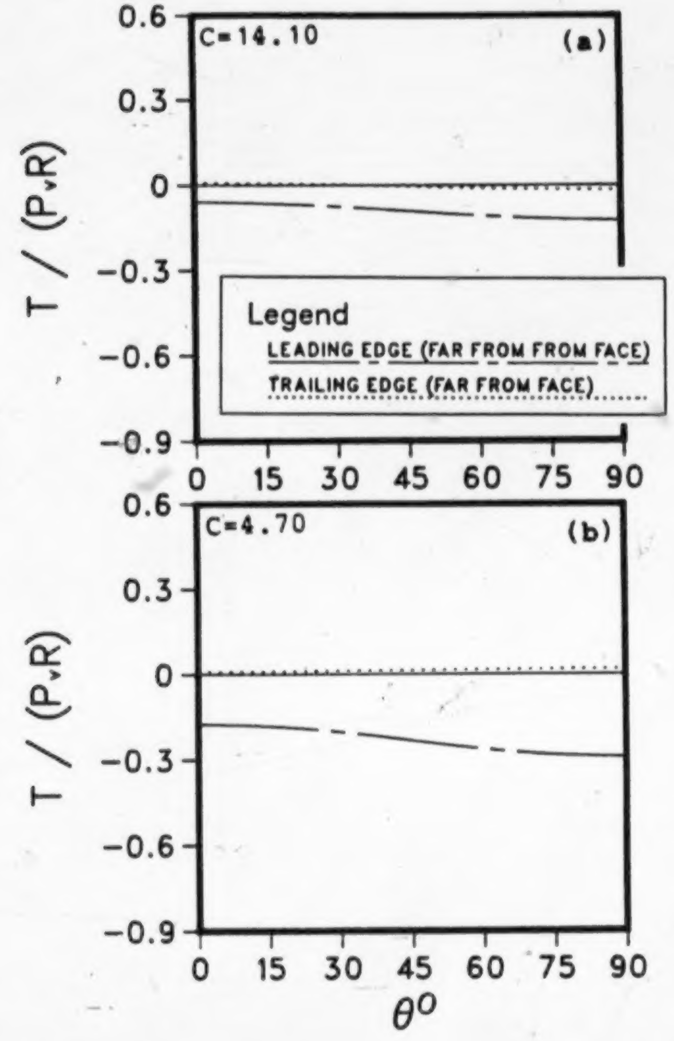

Figure 6.22 Thrust Forces in the Liner for Cases 2 (a) and 3 (b)

two cases virtually no load is found at the trailing edge of the liner sections.

The bending moments in the liner calculated for Case 1 are plotted against θ, in non-dimensional form, in Figure 6.23. The maximum values are detected at the crown and at the springline and zero moment is found near the mid-point (θ=45°) where the inflection point is located. Virtually no bending moment is found at the trailing edge of the section. In Figure 6.24a and b, the bending moments for Case 2 and Case 3, respectively, are depicted. For Case 2 an extremely low moment is detected in the liner due to the high flexibility ratio F (support very flexible), whereas for Case 3 the highest load is found due to the low F value. For this case a moderate bending moment also occurs at the trailing edge of the section.

The maximum normalized thrust forces and bending moments calculated for Cases 1, 2, and 3 are plotted in Figure 6.25 and 6.26 against compressibility and flexibility ratios. In the same graphs the values given by Einstein and Schwartz (1979) (E/S) closed form solution are plotted for comparison. The analytical solution gives higher loads than the numerical analyses for all cases. This was expected because the two dimensional E/S solution is obtained assuming that the liner is placed before excavation occurs (i.e. ahead the tunnel face), without accounting for the displacements occurring before liner installation. If the data of the closed form solutions are multiplied by a

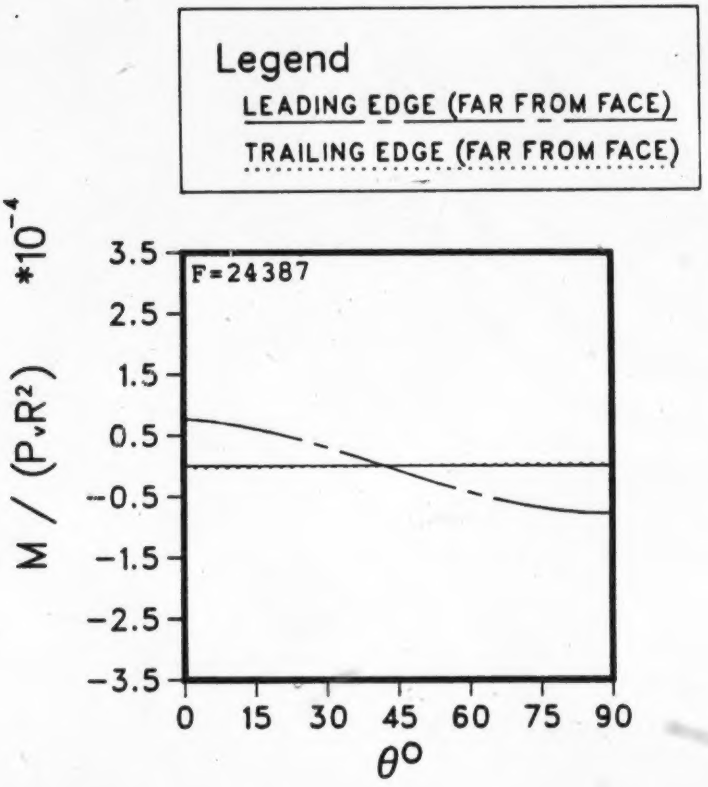

Figure 6.23 Bending Moments in the Liner for Case 1

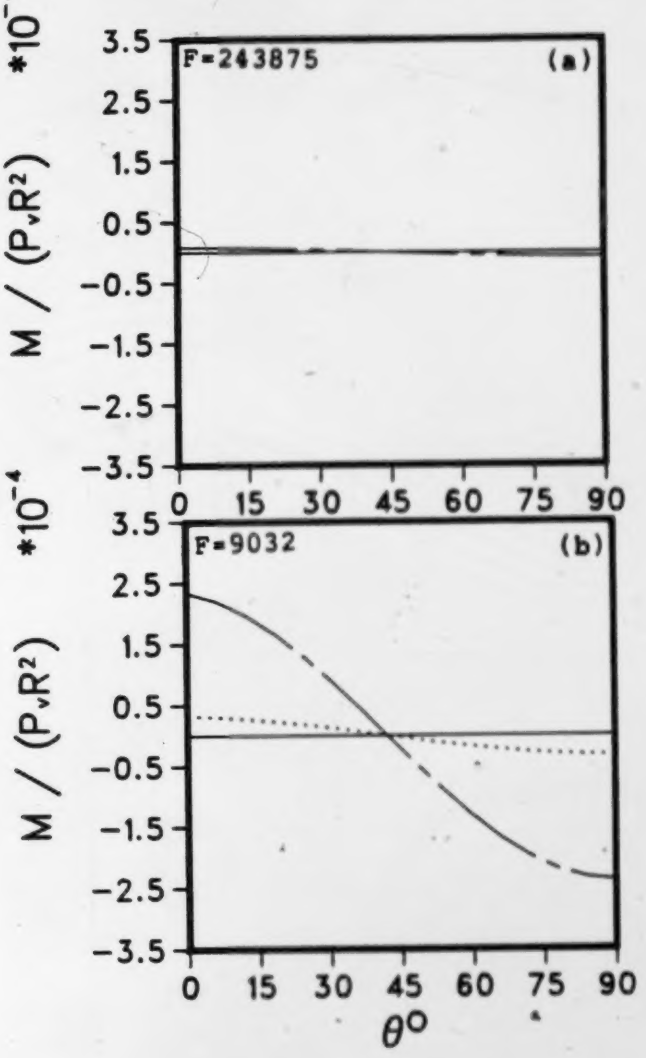

Figure 6.24 Bending Moments in the Liner for Cases 2 (a) and 3 (b)

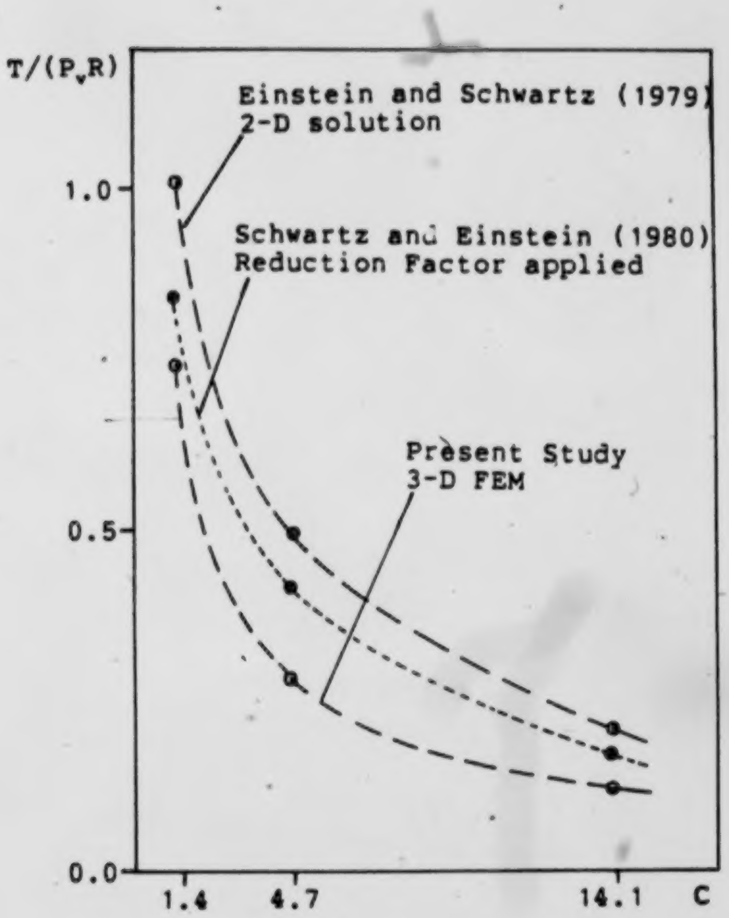

Figure 6.25 Effects of Relative Stiffness on Thrust Forces for FEM 3-D Analyses and 2-D Einstein and Schwartz (1979) Closed Form Solution

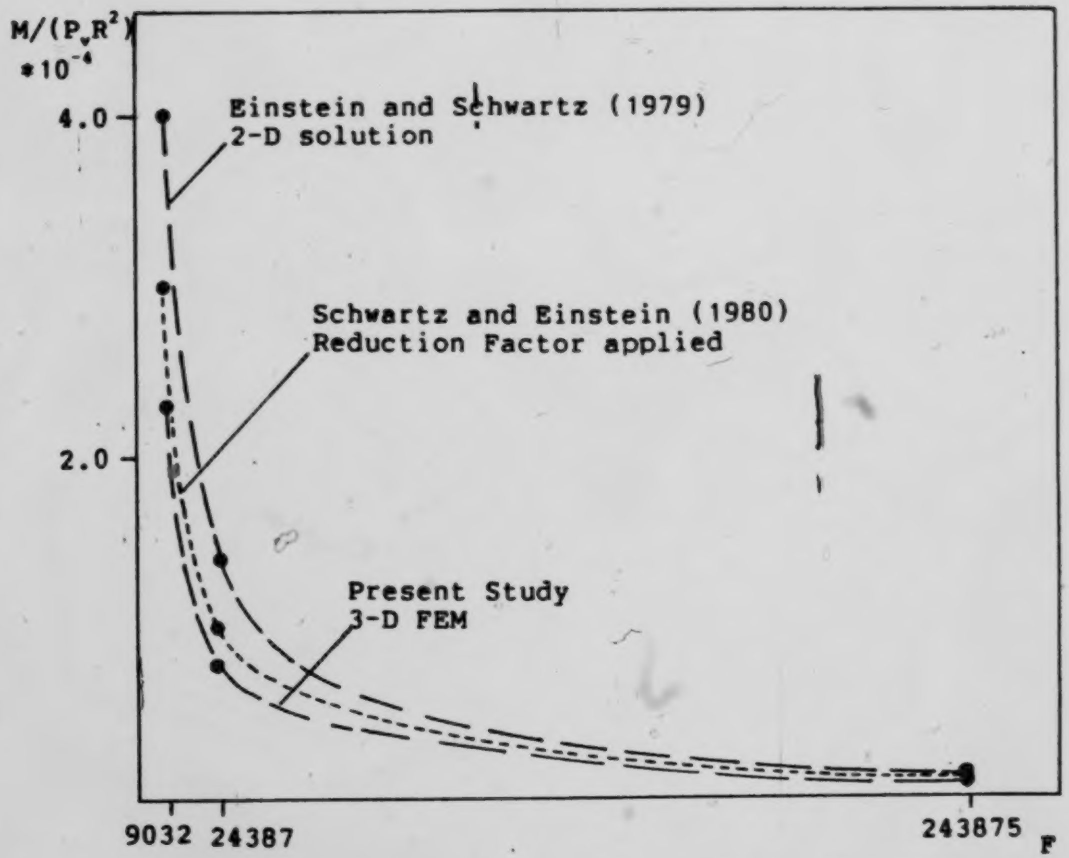

Figure 6.26 Effects of Relative Stiffness on Bending Moments for FEM 3-D Analyses and 2-D Einstein and Schwartz (1979) Closed Form Solution

reduction factor, as given by Schwartz and Einstein (1980), for supports applied immediately behind the tunnel face ($\lambda_T=\lambda_M=0.83$) more reasonable envelopes are found for the results of the finite element analyses. It must be considered, however, that Schwartz and Einstein (op.cit.) refer to an average load on the liner section rather than to the maximum load at the leading edge, and the excavation round length that they assumed (RL=0.5R) is different from the values used in this research. In Figure 6.27, the difference between the 3-D analyses and the E/S relative stiffness solution is illustrated schematically in terms of the convergence confinement concept. While in real cases (and in the 3-D model) the liner can only be placed immediately behind the tunnel face where some radial displacement has already taken place (U_{rf}), in the E/S solution the liner is assumed to be installed before any movement occur. This assumptions lead to relatively high loads on the support as shown in Figure 6.27.

The simplified 2-D solution can however still be used if appropriate reduction factors are applied. In Figure 6.28a and b reduction factors for thrust (λ_T) and (λ_M) in the liner are shown plotted against C and F, respectively. Even though the amount of data available does not allow one to define the relationships in great detail, some conclusions can be drawn. First, both λ_T and λ_M depend on the relative stiffness parameters C and F. For the cases investigated λ_T varies between 0.5 and 0.8 whereas λ_M varies

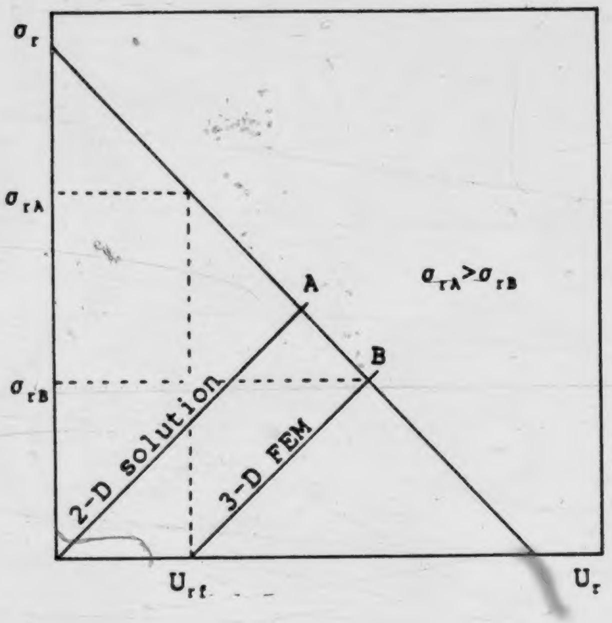

Figure 6.27 Difference Between the 3-D Analyses and the E/S Relative Stiffness Solution

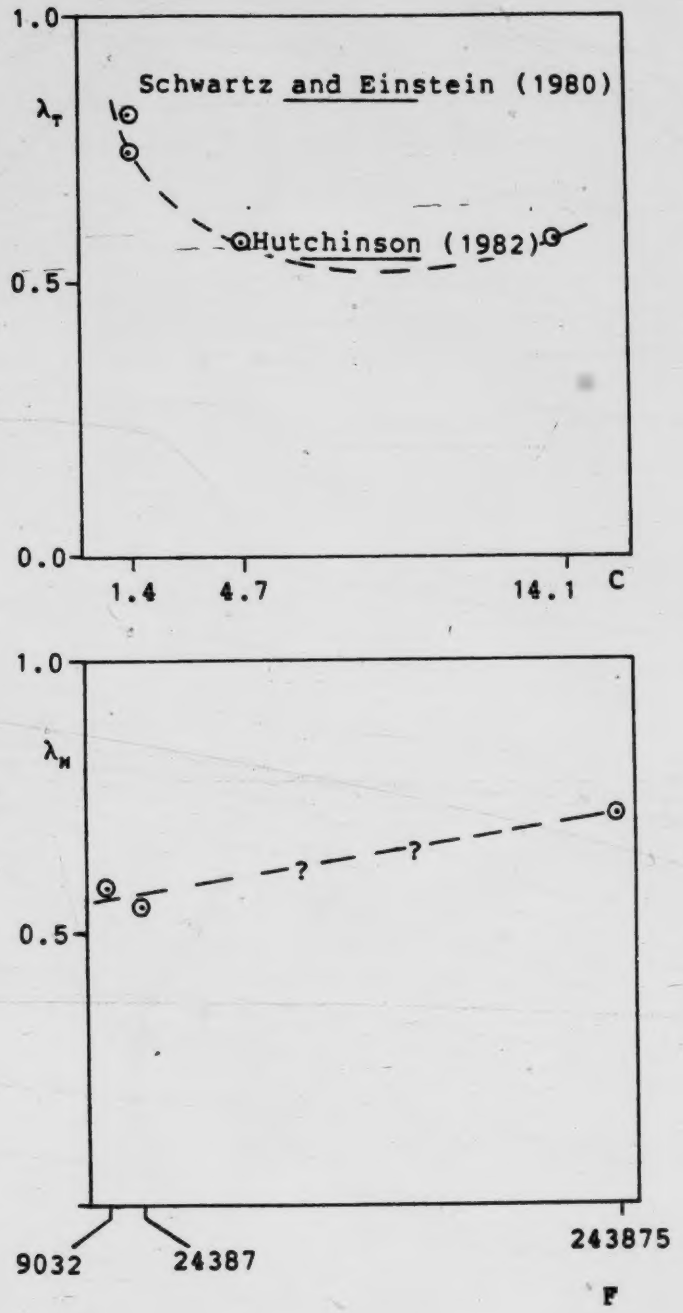

Figure 6.28 Reduction Factors λ_T (a) and λ_M (b)

between 0.54 and 0.72. The reduction factors of approximately 0.83 and 0.55 given, respectively, by Schwartz and Einstein (1980) and Hutchinson (1982) for $K_0=1$ and DEL=0 (see Figure 2.8, Chapter 2), constitute the upper and the lower bounds of the λ_T values found in the present study.

6.4.3 Effects of Delay

In order to investigate the effects of the delay of support installation on the stresses in the liner, results obtained from Cases 4 (DEL=0; RL=1R) and 5 (DEL=1R; RL=1R) are compared.

The thrust forces are plotted in Figure 6.29 for comparison. For zero delay (Figure 6.29a), relatively high thrust develops in the support, one radius behind the tunnel face. As the excavation advances, a load decrease takes place associated with elastic rebound of the liner (see convergence curves, Figure 6.3). During this process, the load profile also becomes flatter and the stress concentration at the crown vanishes. Tensile stress occurs at the trailing edge of the support section similarly to that observed for Case 1.

If the liner is installed one radius behind the face (Figure 6.29b), very little compressive stress develops and tensile stresses are detected at the crown.

The bending moments for the same cases are compared in Figure 6.30. For Case 4, relatively high bending moments develop at the leading edge, far behind the tunnel face

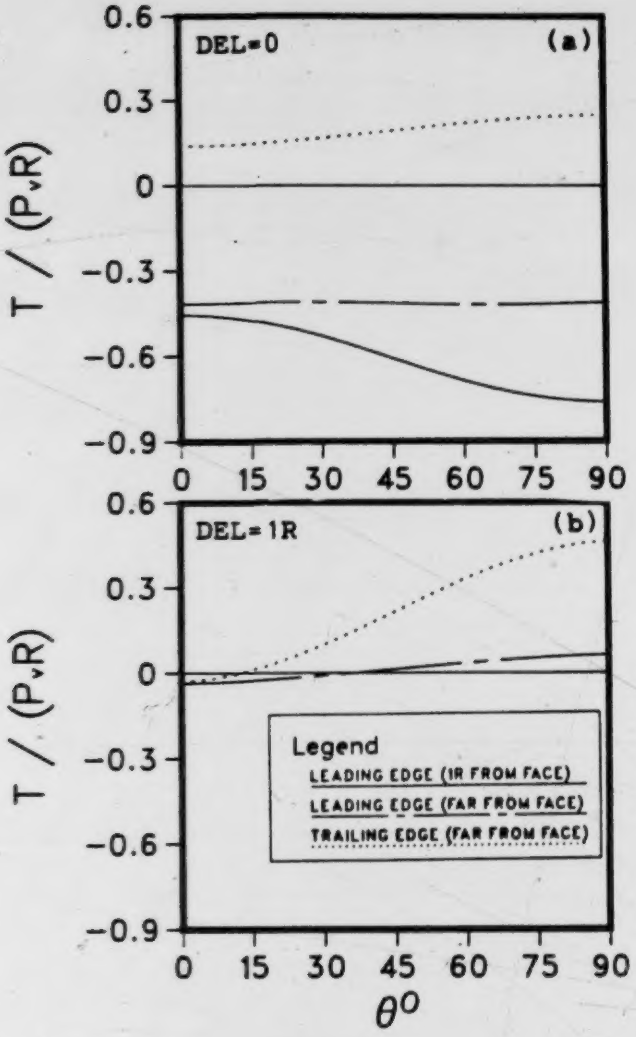

Figure 6.29 Thrust Forces in the Liner for Cases 4 (a) and 5 (b)

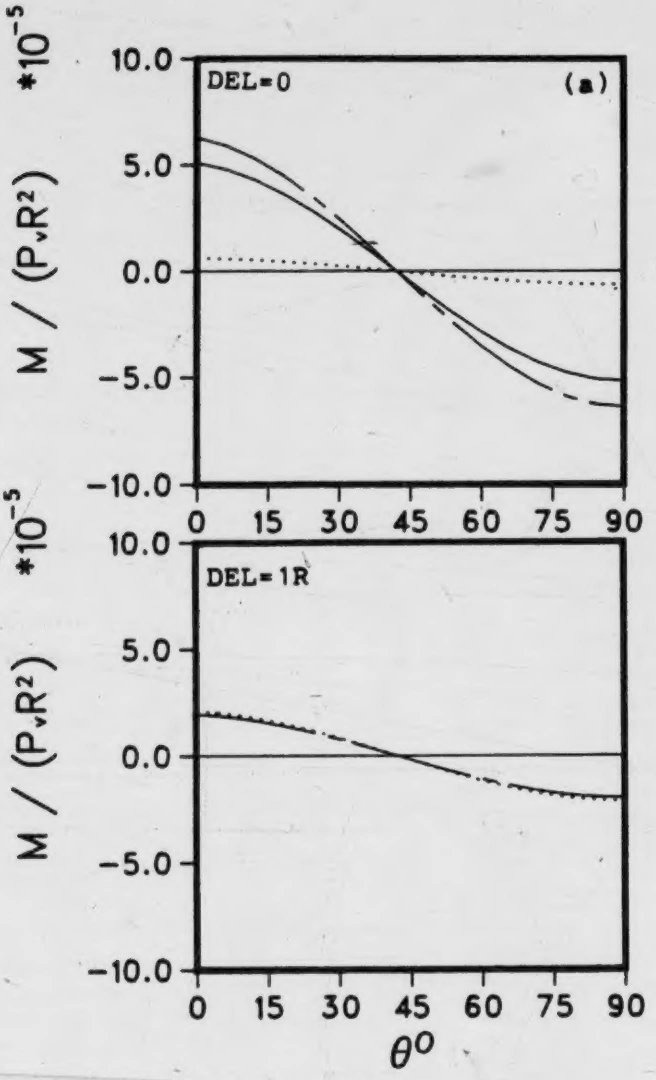

Figure 6.30 Bending Moments in the Liner for Cases 4 (a) and 5 (b)

where the trailing edge is only moderately loaded. For Case 5, approximately the same bending moments, of relatively low magnitude, are found at the leading and trailing edges of the liner section. Reduction factors for thrust (λ_T) and bending moments (λ_M) have been calculated and are plotted against the delay in Figure 6.31. These factors relate loads obtained by the 2-D simplified solution (Einstein and Schwartz, 1979) to the ones calculated by means of the 3-D FEM analyses. Two different λ_T values are found for DEL=0 (0.77 and 0.42) for two distances from the face (1R; far behind face) where, for Case 5 (DEL=1R), a λ_T value of 0.075 is detected.

For the bending moments λ_M values lower than 0.5 are found for both cases. If the liner is installed 1R behind the excavation front, the bending moments are reduced to less than one third with respect to the DEL=0 case.

6.4.4 Effects of the Excavation Round Length

In Figure 6.32a and b are plotted the thrust forces for Cases 1 and 6. The higher thrust force is detected for the longer excavation round length (RL=2). At the trailing edge, for the variable case (RL=1/3 R), no tensile thrust develops and a more homogeneous load distribution is achieved.

No significant differences are detected for the bending moments at the leading edge (Figure 6.33).

In Figure 6.34, reduction factors for the closed form solution by Einstein and Schwartz (1979) are calculated for

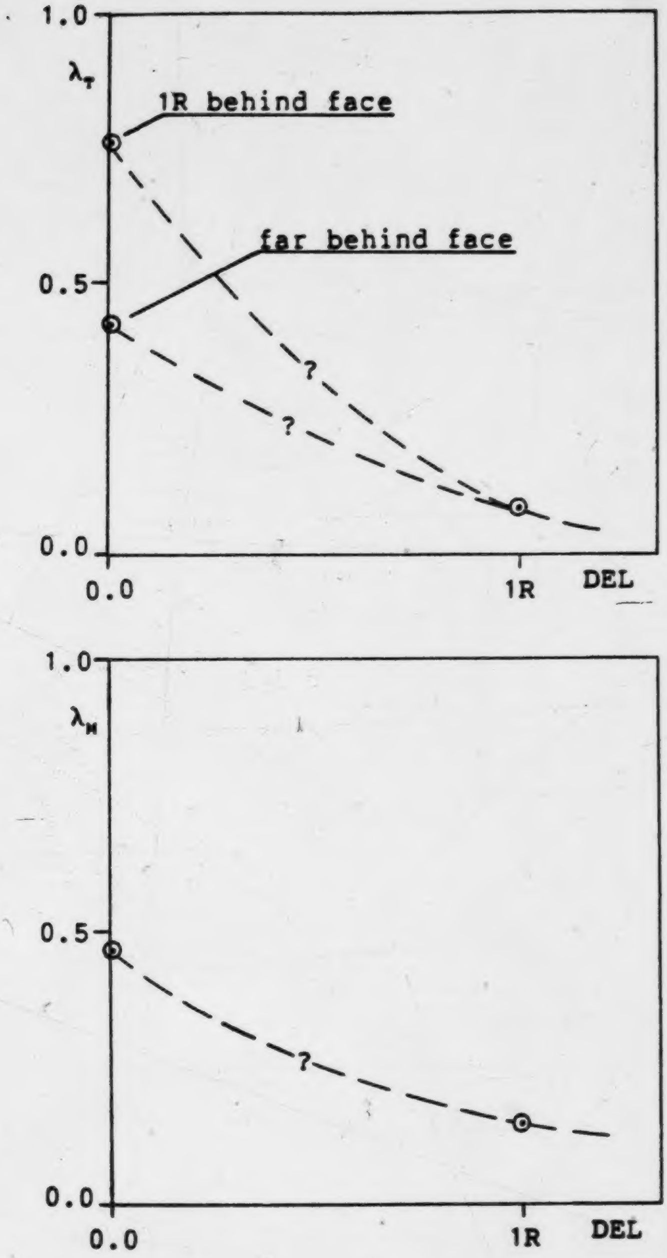

Figure 6.31 Reduction Factors λ_T (a) and λ_M (b)

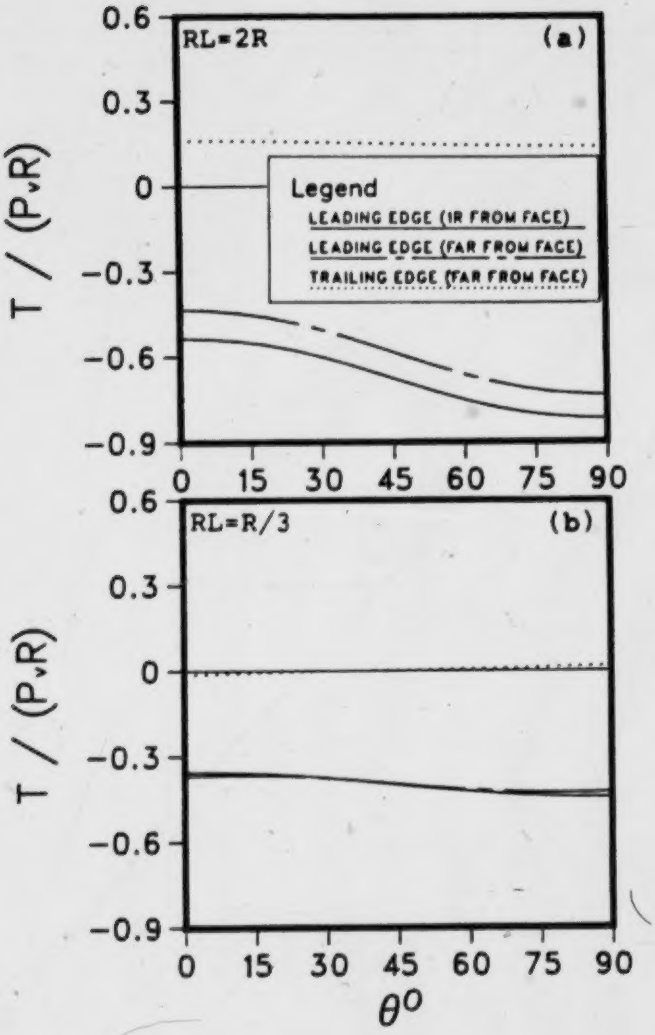

Figure 6.32 Thrust Forces in the Liner for Cases 1 (a) and 6 (b)

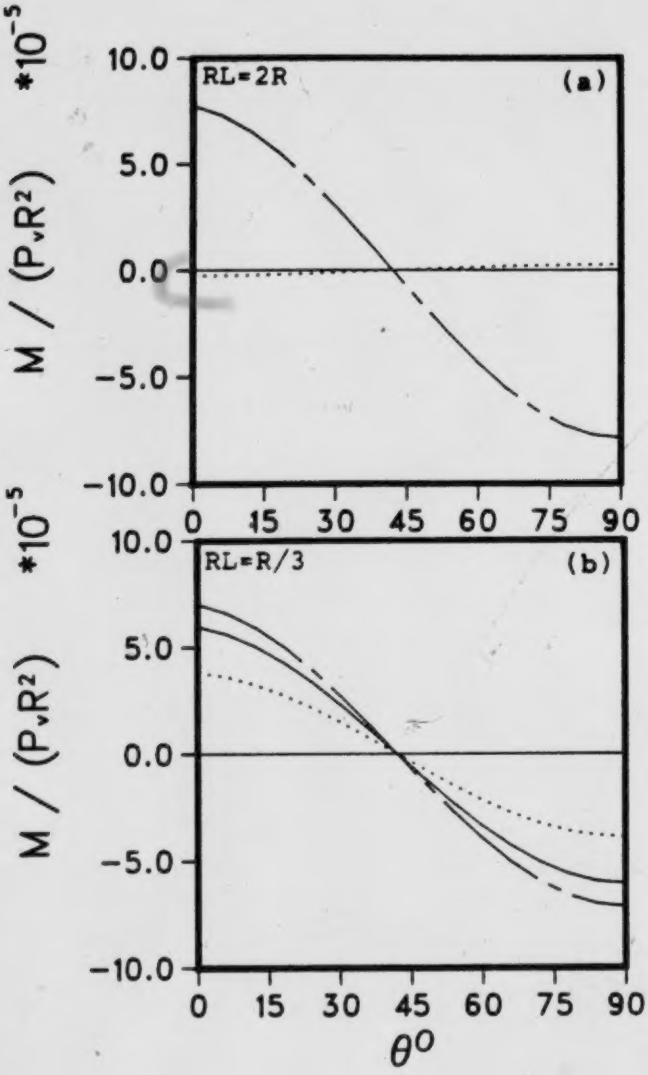

Figure 6.33 Bending Moments in the Liner for Cases 1 (a) and 6 (b)

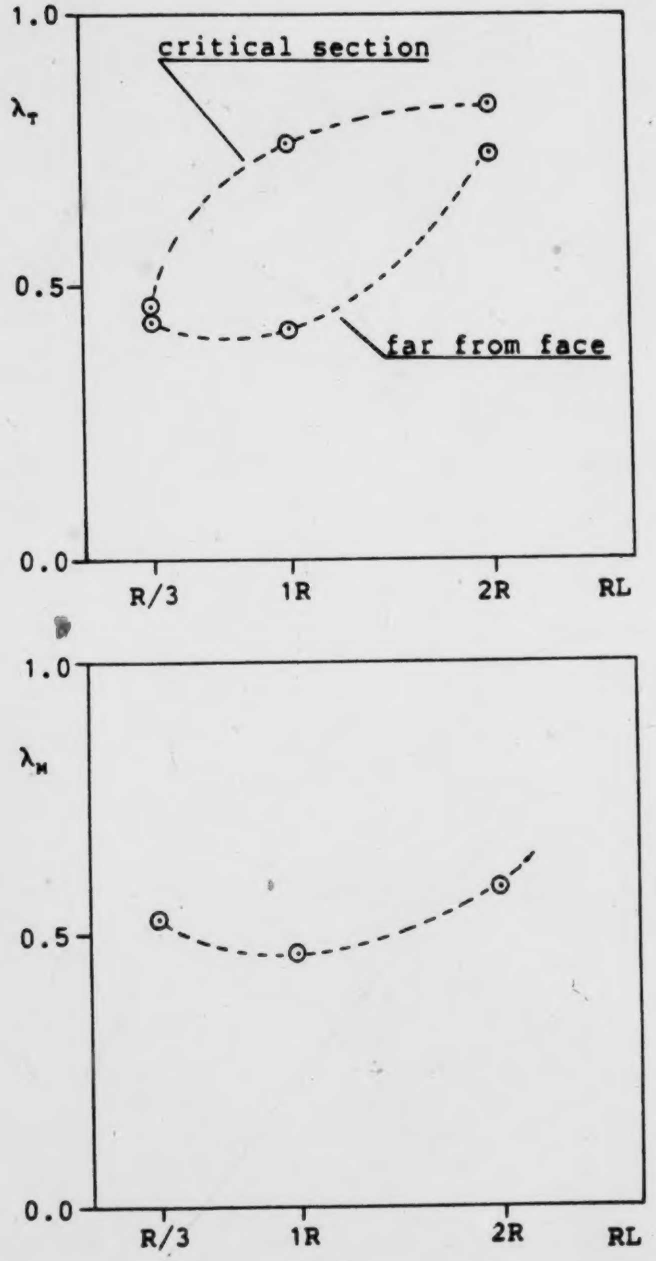

Figure 6.34 Reduction Factors λ_T (a) and λ_M (b)

the three cases (λ_T and λ_M), at the leading edge. It should be noted that the effect of the excavation round length causes considerable changes in thrust, i.e., λ_T varies between 0.40 and 0.84. The most critical conditions are detected for the longest RL-value, whereas, for short excavation round lengths, a more homogeneus stress distribution over the liner leads to lower stresses associated with better ground control. On the other hand small variations of λ_M are found (λ_M≈0.5) that indicate a very limited effect of RL on the bending moments.

6.4.5 Thrust and Bending Moments Along the Tunnel Axis

For Case 4 (DEL=0; RL=1R) a support shell (Figure 6.19) was used, in place of the support ring, in order to investigate thrust forces and bending moments in the support. In Figure 6.35, the thrust in the axial direction (T_a) is depicted for the crown and the springline. The liner is in tension in the axial direction and a relatively high load was detected at the leading edge of the support section. In terms of absolute values, the axial and tangential thrust forces at the leading edge of the liner are comparable in magnitude. A schematic diagram for explanation of this phenomenon is shown in Figure 6.36. Due to the action of the initial axial stresses P_a, the face of the tunnel is initially "pulled" towards the opening. In the process an axial strain variation is generated in the rock, at the tunnel wall, that is tensile ahead of the tunnel face

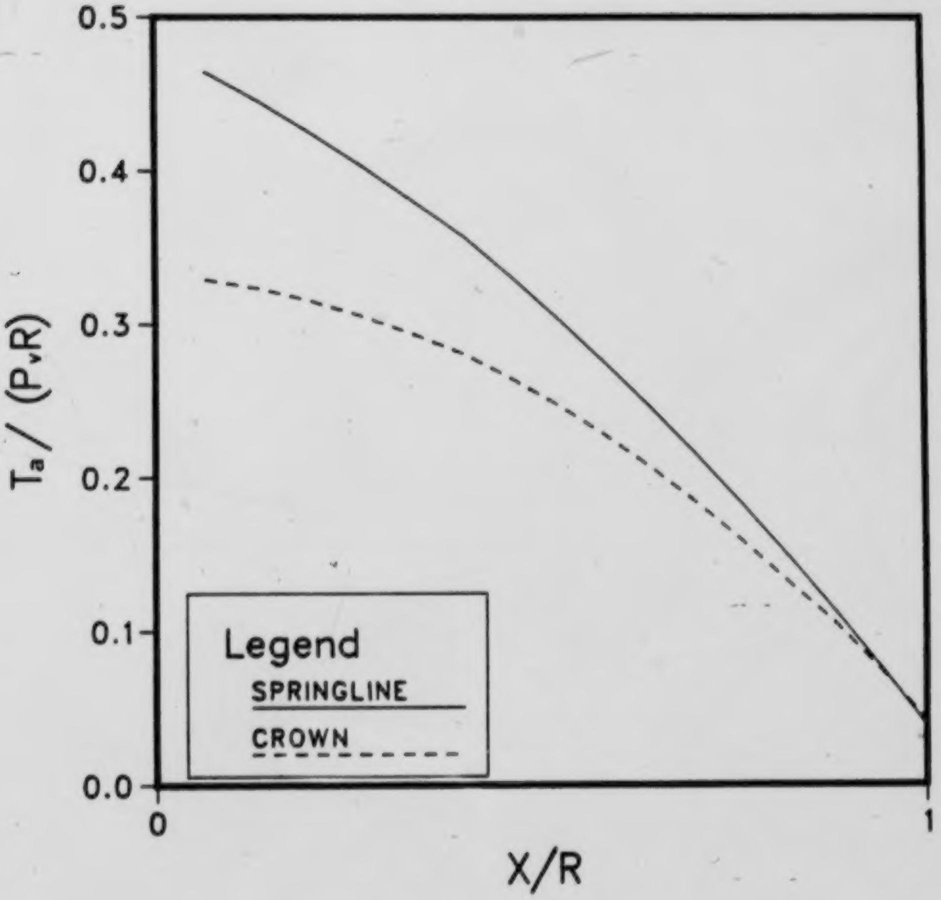

Figure 6.35 Thrust in the Axial Direction (T_a) for Case 4

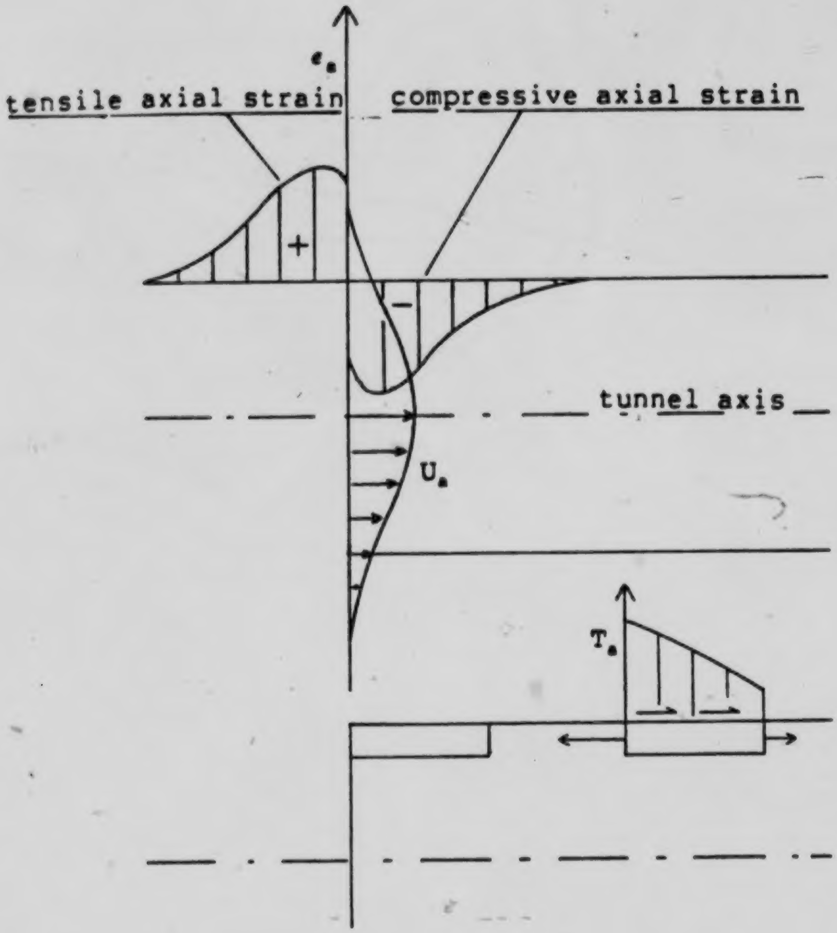
ϵ_a
tensile axial strain
compressive axial strain
+
−
tunnel axis
U_a
T_a

Figure 6.36 Development of Tensile Axial Thrust (T_a) in the Liner

and compressive behind it. As the excavation front advances, the tensile strain in the axial direction tends to vanish as plane strain conditions are approached. If an unstressed liner section is placed in the compressive zone, it is axially extended as excavation proceeds. The axial tensile thrust is then expected to depend on the magnitude of P_a.

An approximately constant bending moment, M_a, was detected by the shell analysis in the same support section, along the tunnel axis. Its magnitude is about 30% higher than for the moment calculated in the liner ring.

Significant tensile thrust and bending moments along the tunnel axis can only develop in the liner if the following conditions are met:

1) The liner is continuous and able to withstand tensile stresses and bending in the longitudinal direction, and

2) Perfect bonding between liner and rock exists.

6.4.6 Effects on Rock Anisotropy on Thrust and Bending Moments

Three 3-D finite element analyses were carried out in order to study the effect of rock anisotropy on thrust and bending moments in the liner. Linear elastic, transverse isotropic behavior was assumed for the rock, and different orientations in space of the planes of stratification were considered (Figure 6.8). The liner was placed one radius behind the tunnel face (DEL=1R) and an excavation round length RL=1R was selected. The assumptions made for the three cases (1A, 2A, 3A) are summarized in Table 6.2.

The concept of relative stiffness as applied to the isotropic continuum is not extendable to anisotropic media and, for this reason, the ratios E_s/E_1, E_2/E_1 and th/R are presented in Table 6.2. This difficulty in quantifying the relative stiffness is not very important for the purpose of the present research which is to study the effect of the orientation of the rock elastic properties on the load in the support, without attempting a quantitative comparison with the isotropic case.

In Figures 6.37 and 6.38, the thrust forces calculated in the liner for the three cases are shown. The highest value is found for Case 1A at the leading edge, due to the fact that the maximum initial stress, normal to the tunnel axis, acts in the direction of the minimum elastic modulus. Note that large radial displacements were calculated for unlined tunnels in similar conditions (see Chapter 4). Some tensile stress occurs at the trailing edge in the crown region similar to that found for Case 5. For Case 2A (Figure 6.38a), the maximum thrust at the leading edge, slightly lower in magnitude than for Case 1A, is detected at the springline due to the high deformability of the rock in the vertical direction. Relatively low thrust is observed, for the same case, at the tunnel crown due to the high stiffness of the rock in the horizontal direction. A schematic explanation of this phenomenon is given in Figure 6.39 where

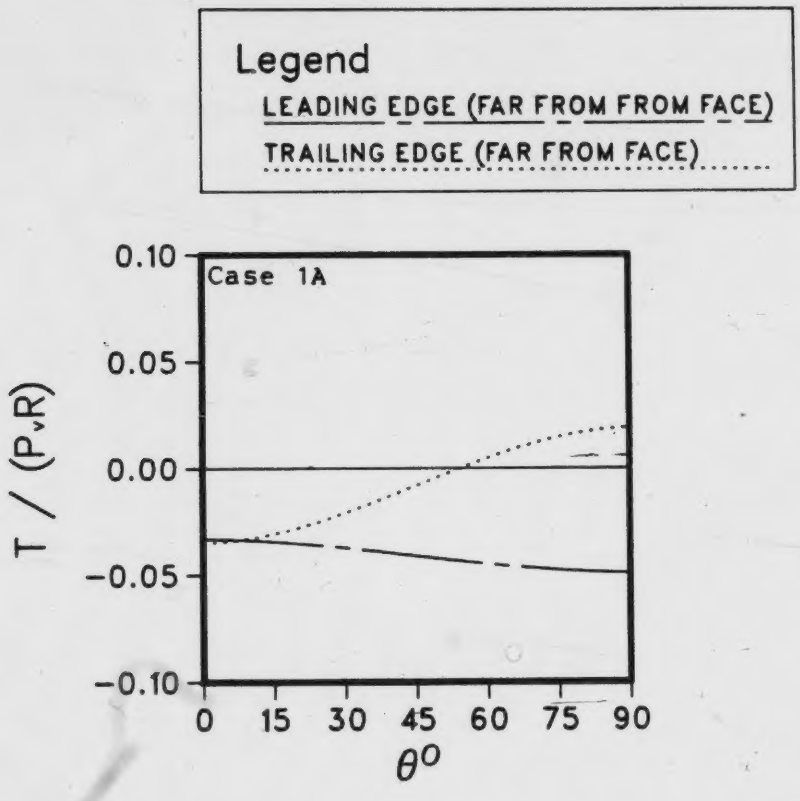

Figure 6.37 Thrust Forces in the Liner for Case 1A

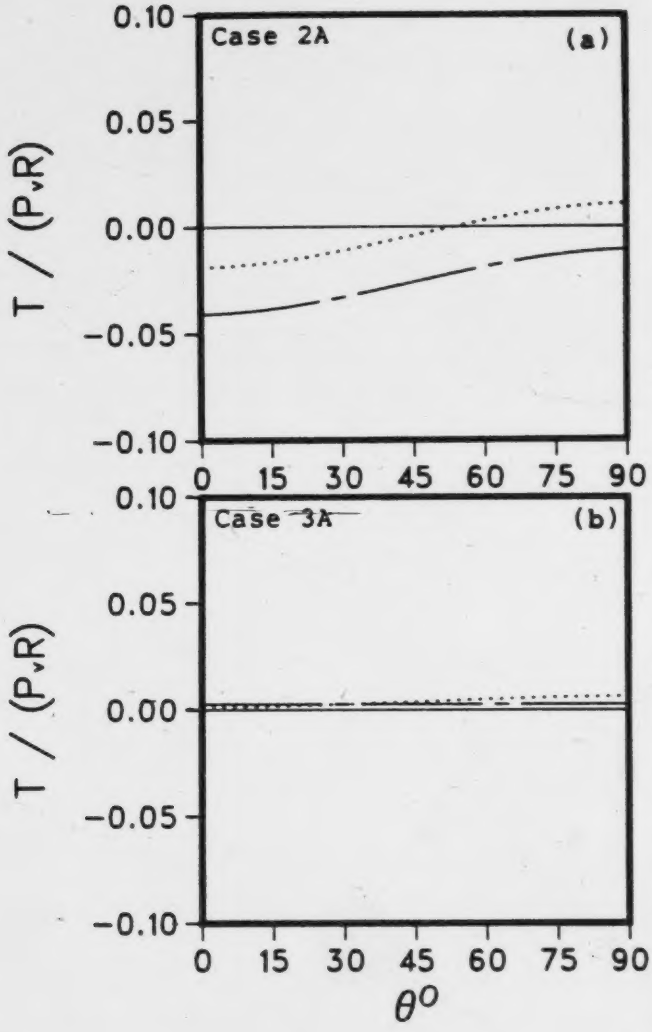

Figure 6.38 Thrust Forces in the Liner for Cases 2A (a) and 3A (b)

rock and liner at tunnel crown and springline are represented, for Case 2A, by couples of parallel springs. It is interesting to note that, as already observed in Chapter 4, the orientation of the elastic properties and of the initial stresses produce similar effects on tunnel performance. Maximum thrust at the tunnel crown, for instance, can result from high horizontal stresses, low horizontal modulus or from a combination of both factors.

Very little thrust was detected in the liner for Case 3A (Figure 6.38b). This was expected because of the high elastic modulus of the rock in the radial direction and because, for this case, most convergence occurs immediately behind the tunnel face (as discussed in Chapter 4).

The bending moments for the same three cases are shown in Figures 6.40 and 6.41. The highest bending moment is observed for Case 1 (Figure 6.40). It is 2.4 times larger than for Case 2A (Figure 6.41a). Also note that opposite signs are found for the two cases due to the different orientations of the elastic properties. Virtually no bending was found for Case 3A (Figure 6.41b).

In Figure 6.42, some of the results are summarized. The main aspect to be emphasized is the substantial effect of the orientation of the elastic properties on the bending moments for tunnels with axis parallel to the planes of stratification (Cases 1A and 2A). On the other hand, little effect is noticed on the maximum thrust force. If the tunnel axis is normal to the planes of stratification, relatively

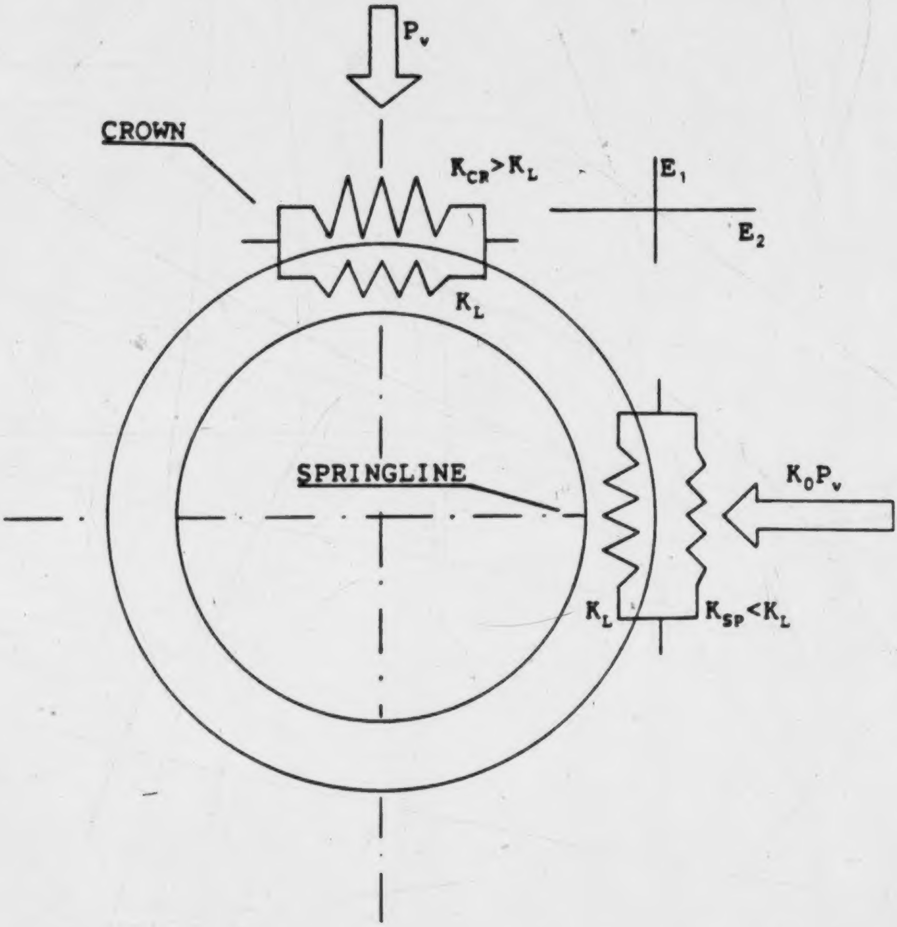

P_v
CROWN
$K_{CR}>K_L$
E_1
E_2
K_L
SPRINGLINE
K_0P_v
K_L
$K_{SP}<K_L$

Figure 6.39 Effect of Rock Anisotropy on Thrust in the Liner

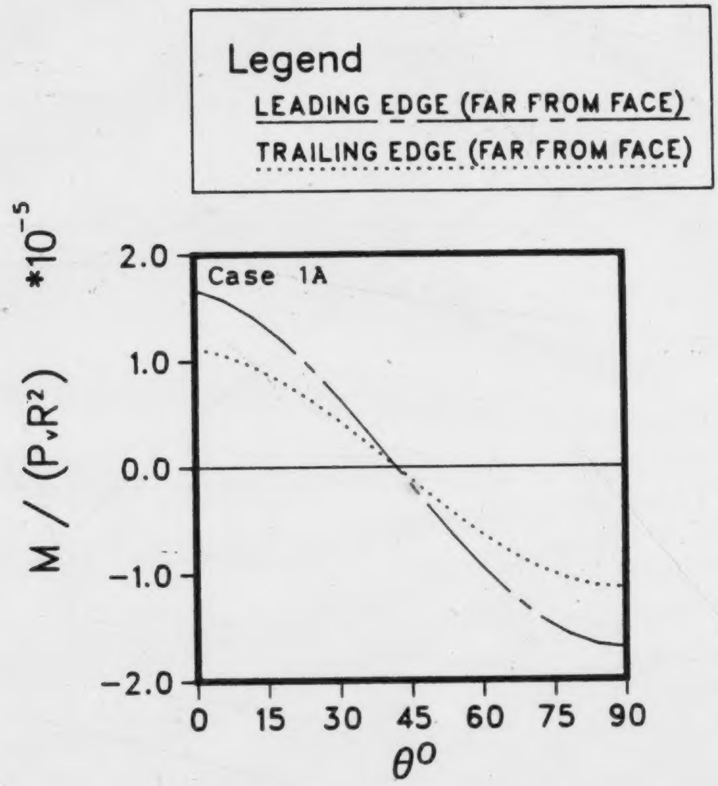

Figure 6.40 Bending Moments in the Liner for Case 1A

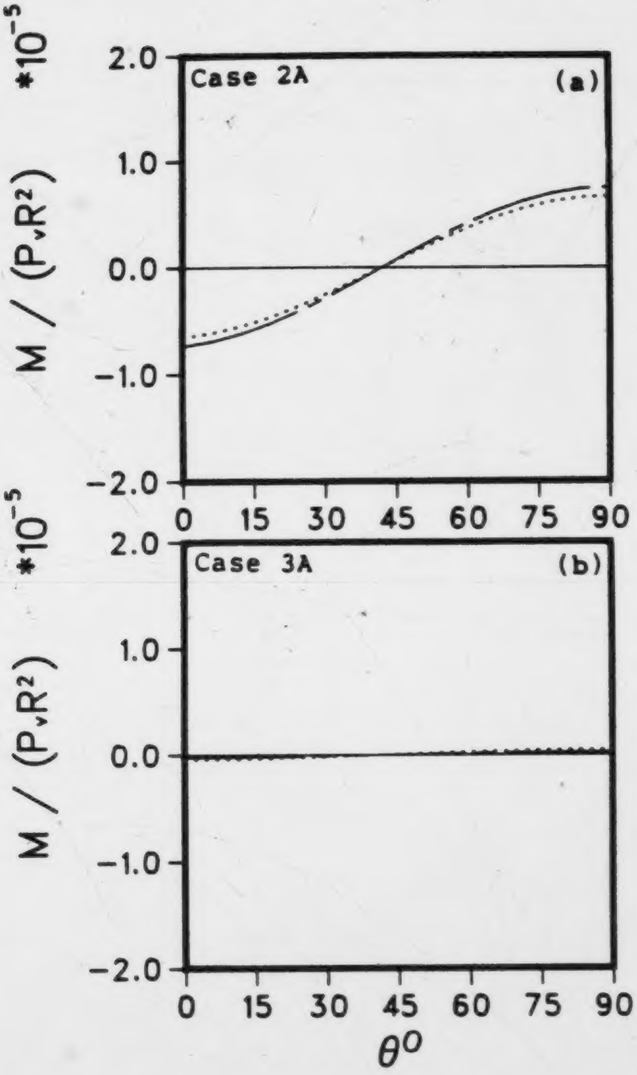

Figure 6.41 Bending Moments in the Liner for Cases 2A (a) and 3A (b)

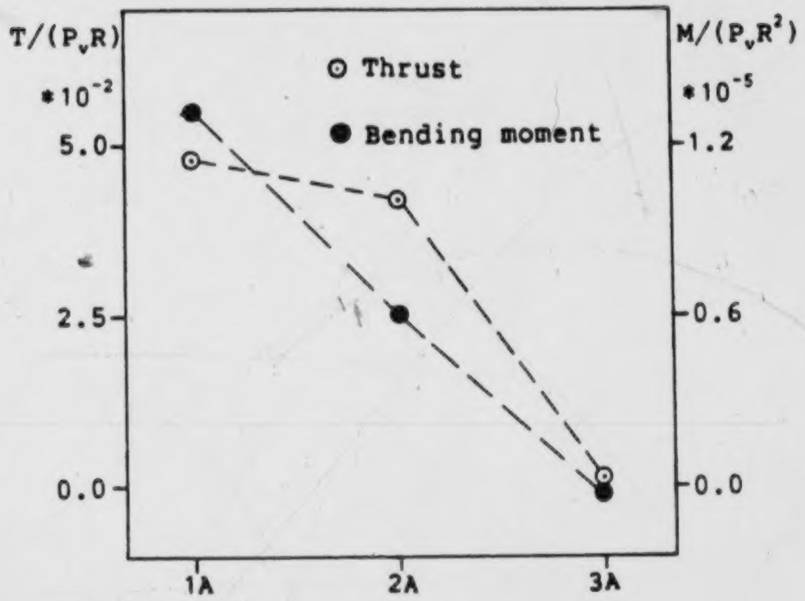

Figure 6.42 Maximum Thrust and Bending Moments for Cases 1A, 2A and 3A

little load develops in the liner.

6.5 Conclusions

In this chapter some of the aspects characterizing the rock-liner interaction in supported tunnels have been discussed. The effects of relative stiffness, delay, excavation round length and non-isotropic rock behavior on thrust and bending moments, as well as the effects of the support on rock deformations and monitoring data, have been investigated.

The following conclusions can be drawn:

1) The maximum thrust force in the liner depends on the relative stiffness of the support as defined by the compressibility ratio C. Low values of C correspond with high thrust forces.

2) The maximum bending moment in the liner depends on the relative stiffness of the support as defined by the compressibility ratio F. Low F values correspond with high bending moments.

3) The 2-D close form solution given by Einstein and Schwartz (1979) was shown, as expected, to be conservative when compared with more realistic 3-D models. The safety margin implicit in the 2-D solution depends the on relative stiffness, the delay and the excavation round length.

4) Increasing the delay from the face at which the liner is installed, decreases both thrust and bending moments in the support.

5) Most of the load tends to concentrate at the leading edges of the liner sections. Smaller excavation round lengths allow a more homogeneus pressure distribution on the support that results in good ground control (small radial displacements) with relatively moderate loads in the liner.

6) If the tunnel is driven in transverse isotropic rock, the location of the maximum thrust force and the magnitude of the maximum bending moment heavily depend on the orientation of the rock elastic properties. If the tunnel axis is normal to the strata, relatively low loads are detected in the liner.

7) For the cases investigated, the radial convergence ahead of the tunnel face does not depend on the stiffness of the liner or the delay. For those cases where monitoring of displacements ahead of the tunnel face is possible, radial displacement measurements can be regarded as useful back-analysis tools.

8) A zone of compressive strain is found at the tunnel wall due to the confinement action of the support. This feature is more apparent if the liner is stiff and placed near the tunnel face and the measurements taken by multi-anchor radial extensometers can be considerably affected by it.

9) At the tunnel springline (direction of maximum initial stress for $K_0=2$), the shape of the relative displacement profiles, as measured by radial multipoint extensometers, is not much affected by the action of the

liner except for the compressive zone occurring at the back of the support. Relative displacements taken at sufficient distance from the tunnel wall can then be useful for back-analysis purposes. At the tunnel crown a more substantial impact of the support on the shape of the curves is found if the tunnel is fully lined.

7. Back-Analysis of Field Data

7.1 Introduction

In this chapter, the monitoring data collected during the excavation of a TBM driven tunnel at the Donkin-Morien project are analyzed. In particular, measurements taken by means of multipoint radial extensometers, placed far ahead or immediately behind the tunnel face, are considered. The strength and the deformation properties of the rock mass are back-analyzed on the basis of data collected at several locations along the axis of the tunnel.

The analysis is based mainly on comparisons between field data and results of the parametric studies presented earlier in Chapters 3 to 6. Some effects of rock inhomogeneities are also assessed in order to explain observed deformation modes that could not be predicted with the idealized models of homogeneous ground. The purposes of this study can be summarized as follows:

1) Establish a methodology for effective interpretation of monitoring data, in order to allow stability assessment and design improvement as the excavation proceeds;

2) Discuss the limitations of the monitoring program at the Donkin-Morien project and suggest improvements for future monitoring practice;

3) Present a simple method that should allow early prediction of the radial displacements and early detection of yielding and failure in the rock mass.

An effort is also made to translate specific observations into key concepts of general applicability.

7.2 Description of the Project

The mine access tunnels for the Donkin-Morien project in Cape Breton Island, Nova Scotia, comprise a TBM driven circular tunnel (Tunnel No.2) that was built between January 3 and December 21, 1984. Excavation was performed northwards, from portals on Cape Perce, to intersect the Harbour Seam about 3.5 kilometers offshore (Figure 7.1). The tunnel was driven in layered sedimentary rock of Carboniferous age, with layers dipping towards north (10°), at a maximum depth of 200 m below seabed.

Tunnel No.2 was excavated parallel to another tunnel, Tunnel No.3, that is characterized by a horseshoe cross section and that was driven by drilling and blasting. The distance between the two tunnels is 50m. Tunnel No.2 was selected for the back-analysis because a more complete set of data was available and because its circular cross section allowed a direct comparison of the field measurements with the results of the finite element analyses.

The longitudinal section of Tunnel No.2 is shown in Figure 7.2. The tunnel was driven in a 30 m thick unit of competent sandstone up to chainage 1300 m. The remainder of the tunnel was excavated in weaker mixed sediments consisting of sandstone, siltstone and mudstone.

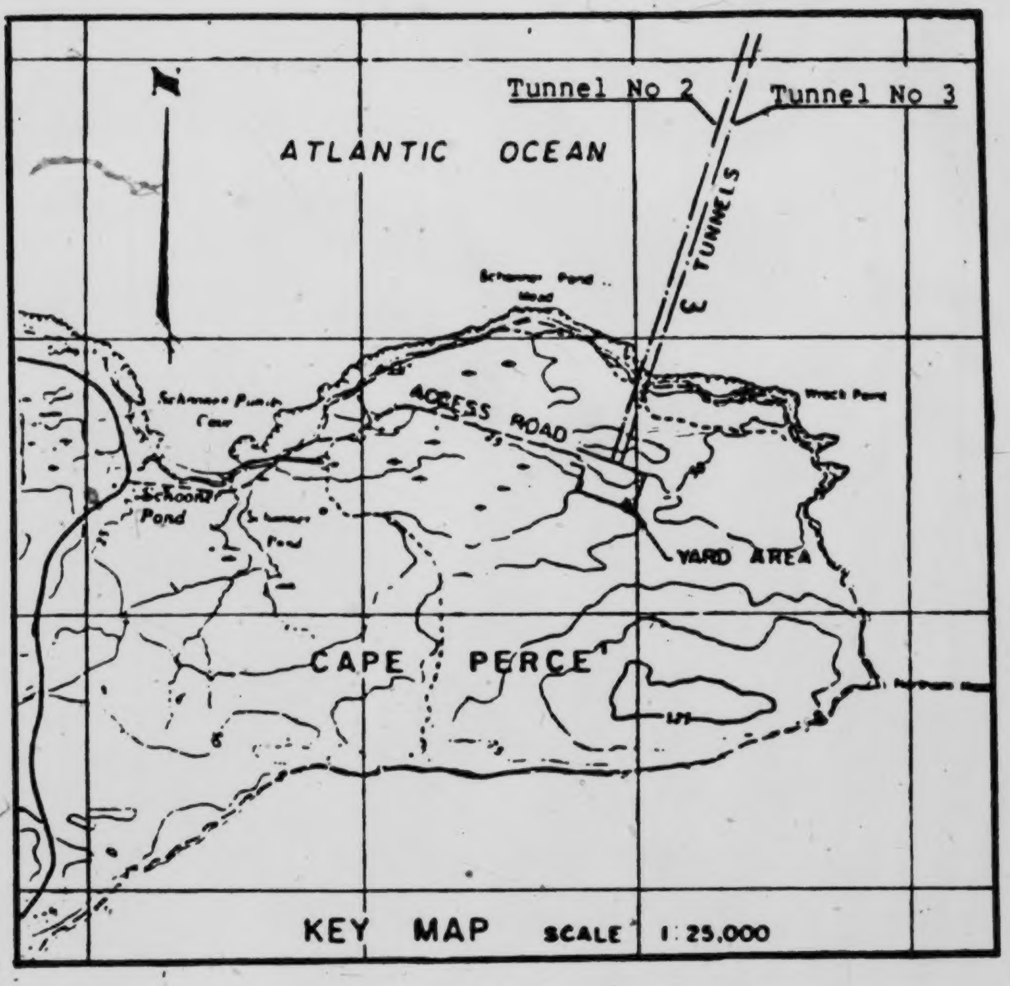
N
Tunnel No 2
Tunnel No 3
ATLANTIC OCEAN
℄ TUNNELS
ACCESS ROAD
Schooner Pond
YARD AREA
CAPE PERCE
KEY MAP SCALE 1:25,000

Figure 7.1 Map Showing Position of the Tunnels (Yuen et al., 1985)

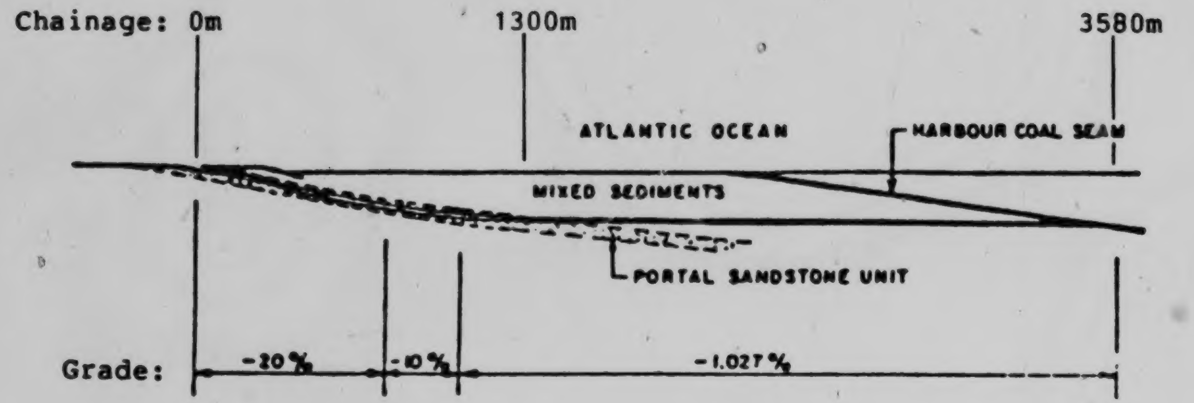
Chainage: 0m
1300m
3580m
ATLANTIC OCEAN
HARBOUR COAL SEAM
MIXED SEDIMENTS
PORTAL SANDSTONE UNIT
Grade:
-20%
-10%
-1.027%

Figure 7.2 Longitudinal Section Through Tunnel No.2
(Modified after Yuen et al., 1987)

7.2.1 Excavation and Support

A 7.6 m diameter full-face, shielded LOVAT M-300 TBM was used to drive Tunnel No.2 (Marsh et al., 1986). In contrast to most TBMs which thrust off the tunnel walls, the LOVAT TBM is designed to thrust off the tunnel support rings that are activated at the back of the shield as depicted in Figure 7.3 where the propulsion system of the machine is shown. Note that the support ring can only be expanded one diameter behind the tunnel face.

The support was designed for the purpose of sustaining the thrust load from the TBM as well as gravity loads due to loosening of the rock at the tunnel crown (Yuen et al., 1987). It is composed of steel ribs (W150x23) connected by longitudinal thrust blocks. The ribs were spaced at 1.5 m along the length of the tunnel except for a few critical sections where the spacing was reduced to 1 m. Wire mesh, fabricated from 8 mm (longitudinal) and 4 mm (circumferential) wires, was also installed above the springline to provide support to any loosened rock fragments and hence to improve safety during tunnel drivage.

7.2.2 Rock Properties and In Situ Stresses

Laboratory and field testing provided strength and deformation properties for the various rock types. The laboratory testing program included uniaxial compression tests, Brazilian and triaxial tests as well as thin section studies, X-ray diffraction analysis and scleroscope hardness

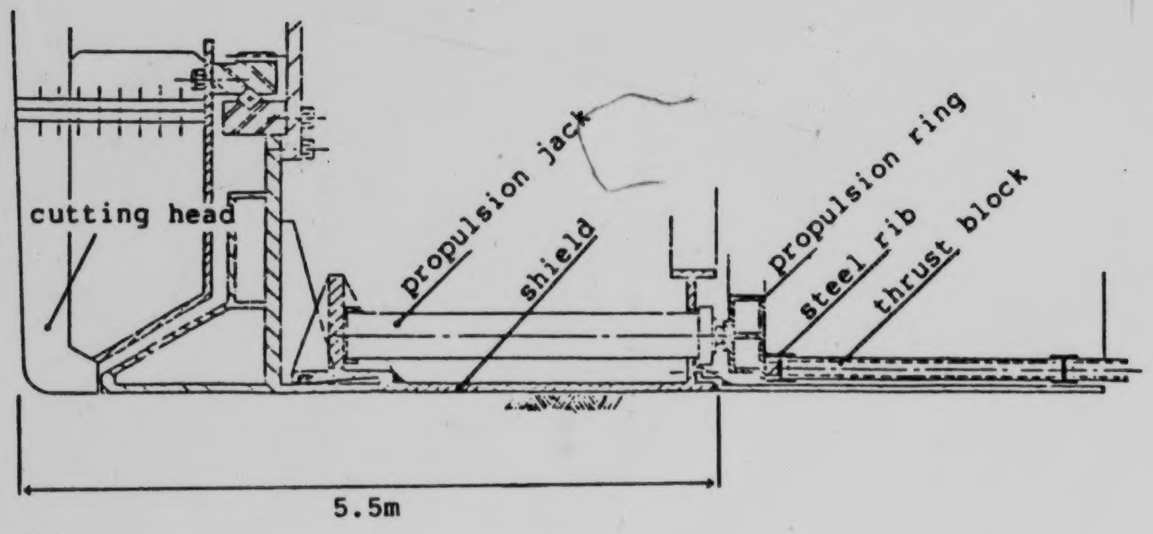
cutting head
propulsion jack
shield
propulsion ring
steel rib
thrust block
5.5m

Figure 7.3 Propulsion System of the LOVAT M-300 TBM

testing. The field testing program included in situ modulus measurements, by means of the Colorado School of Mines dilatometer System, that were conducted in the sandstone in an horizontal borehole drilled from Tunnel No.3 to Tunnel No.2. A hammer seismic wall survey was also carried out in both tunnels in order to study the effect of the excavation procedure on rock disturbance.

The data relevant to the present discussion are summarized in Table 7.1. A Poisson's ratio of 0.25 (mean value) was measured for the sandstone. The laboratory testing program revealed relatively high uniaxial compressive strength for the sandstone (σ_c=45 to 145 MPa) and for the interbeddeed sandstone-siltstone (σ_c=48 to 153 MPa). The siltstone, the interbedded siltstone-mudstone and the mudstone were found to be much weaker than the sandstone, with uniaxial compressive strength ranging between 14 and 68 MPa. In the field, loosening at the tunnel crown was observed in the mixed sediment sections. In terms of deformability, the sandstone was found to be more than three times stiffer than the siltstone, interbedded siltstone-mudstone and mudstone. The in situ dilatometer tests performed in the sandstone unit resulted in Young's moduli ranging between 7 and 28 MPa which are much lower than the values found in the laboratory. This difference was expected, because the rock deformability is known to decrease as the volume of the rock tested increases. This results are in agreement with Heuze(1980) who found that the

ROCK TYPE	LABORATORY TESTS				FIELD TESTS
	Uniaxial Compressive Strength σ_c(MPa)		Deformation Modulus E(GPa)		Deformation Modulus E(GPa)
	RANGE	MEAN	RANGE	MEAN	RANGE
SANDSTONE	44.9-145.1	93.8	13.8-43.7	34.2	7.44-28.19
INTERBEDDED SANDSTONE-SILTSTONE	47.9-152.8	121.3	6.6-21.9	17.6	-
SILTSTONE	13.9-68.5	53.6	4.5-25.3	11.3	-
INTERBEDDED SILTSTONE-MUDSTONE	14.7-62.9	35.8	4.0-15.0	9.0	-
MUDSTONE	30.9-42.2	37.2	8.8-15.0	11.5	-

Table 7.1 Results of Laboratory and Field Testing

(Summarized from Yuen et al., 1985)

elastic moduli measured in the laboratory are 2 to 3 times larger than the values measured in field.

An in situ stress measurement program was conducted in Tunnel No.3 by means of two overcoring techniques, using the CSIRO (Australian Council of Scientific and Industrial Research Organization) hollow inclusion gauge and the USBM (United States Bureau of Mines) deformation gauge. A total of four USBM tests and five CSIRO tests were undertaken in a horizontal borehole but three CSIRO gauges gave unreliable results. The formation of a network of air bubbles in the glue around the strain gauge tube affected the deeper tests (Yuen et al., 1985). The complete stress tensor was available for only two locations along the borehole, one of which was too close to the wall of the tunnel and, hence, was affected by stress concentration near the excavation. The USBM tests could only provide the vertical and the axial initial stress components. A vertical initial stress consistent with the tunnel depth and a moderately high horizontal stress (K_0 of about 2) was detected. At about one radius from the tunnel wall a substantial stress decrease was observed that could not be explained by the elasticity theory, probably due to stress redistribution associated to rock fracturing in proximity of the tunnel wall (note: at Chainage 900m a fractured zone almost 4m deep was detected at the springline of Tunnel No.3, as observed by Yuen et al., 1985).

7.2.3 Monitoring Program

A relatively extensive instrumentation program, funded by CANMET, was undertaken to document the tunnel performance. This program included strain gauges on the steel ribs and the thrust blocks, pressure cells to measure radial stresses between rock and steel sets and axial stresses in the ribs, and radial multipoint extensometers located at various distances from the tunnel face. Only the latter will be discussed in this chapter. The effect of the liner on the overall tunnel behavior will be neglected because the support is very flexible and was placed relatively far behind the face. The measurements confirm the appropriateness of this assumption. A significant amount of load was in fact only detected on the liner for those sections where loosening (i.e., gravity loading) occurred at the tunnel crown.

Radial extensometers were placed at several locations both in the sandstone and in the mixed sediments. In the sandstone (at Chainage 800 m), a multipoint extensometer was located in a horizontal borehole driven from Tunnel No.3 ahead of Tunnel No.2. It constitutes, for this project, the only instrument able to measure displacements ahead of the tunnel face (a similar installation at Chainage 920 m malfunctioned). Several extensometers were placed at the tunnel crown, in the mixed sediment section, in order to detect loosening taking place during the mining process (note: some instruments were also placed in proximity of the springline, but most of them gave unreliable results; Yuen et al., 1985). For each section measurements are taken only at one location (crown or springline) partly because of limited accessibility to the excavation front due to the shielded TBM. Extensometers at the invert, for instance, could be placed only behind the tail of the machine, at one diameter from the excavation front.

7.2.4 Supplemental Remarks

A few additional observations are relevant to this thesis:

1) The liner is very flexible and placed far from the tunnel face. Its effect on the tunnel deformational behavior will be neglected in this study;

2) The stresses were measured only at one chainage (Tunnel No.3, Chainage 964 m). The horizontal, radial stress at the springline was measured only at two locations (CSIRO), one of which close to the wall of the tunnel and, hence, affected by the excavation. This is a limitation of the testing program as a more accurate knowledge of the initial stress field would have been beneficial for an effective back-analysis;

3) Only one multipoint extensometer was placed at each instrumented section. While this helps to detect variability, it makes a quantitative back-analysis of the monitoring data difficult (see Chapter 3);

4) Extensive loosening at the tunnel crown was observed in the mixed sediments, due to the low rock strength and the high horizontal stresses.

7.3 Multipoint Extensometer Records in the Mixed Sediments

A few vertical multipoint radial extensometers were placed at the tunnel crown in the mixed sediments. Measurements taken by four of these instruments will be analyzed in this section in order to provide some understanding of the strength and deformation characteristics of the rock mass.

All the extensometers considered here were placed immediately behind the tunnel face (between 0.25 and 1m from the face). One of them is of the rigid probe type whereas the remainder were flexible probe extensometers equipped with a greater number of anchors. Zero readings were taken at the face after installation and, because of lack of accessibility due to the shield of the TBM, no readings could be taken within one diameter from the excavation front. Therefore, the shape of the radial displacement curves is not available near the face. For this reason, the method proposed by Barlow(1986) and Barlow and Kaiser (1987) could often not be applied.

A very detailed back-analysis of rock properties and in situ stress field is not possible, because of the lack of sufficient data on each section. As explained in Chapter 3, displacements should be measured at various locations around the tunnel to allow an effective back-analysis process. In particular, measurements taken at the tunnel crown were found to be strongly affected by the initial axial stress P_a whose magnitude is not accurately known for this case. Failure observed at the tunnel crown and invert indicates, consistently with the field measurements, a relatively high initial horizontal stress P_h. A $K_0=2$ was assumed to be representative for the following discussion.

7.3.1 Back-analysis of Rock Mass Strength

In order to back-analyze the peak strength of the rock, the location at which the strength of the rock is exceeded and the stresses at that location must be known. For some cases, failure initiation is easily detected if appropriate monitoring is carried out during face advance. Sometimes the location at which the strength of the rock mass is exceeded may be missed and only very general conclusions can be drawn. Examples of both cases will be shown in the following discussion.

The assessment of the stress state at a certain particular location around the opening requires a sound knowledge of the initial stress field that should be measured carefully by means of in situ testing. Information regarding the in situ stress field can also be back-analyzed from the displacements induced by the excavation in the rock mass if detailed monitoring is carried out on a tunnel section. Unfortunately, for the Donkin-Morien project only one extensometer was available for each instrumented section. The stress distribution around the tunnel can be determined by means of three dimensional, numerical analyses by assuming the rock to behave in a certain manner, e.g., as a linear elastic medium. The assumption that the material obeys linear elasticity up to failure, as made in this research, is reasonable for many rocks that exhibit a fairly brittle behavior. For those cases where a considerable degree of non-linearity is expected in the pre-peak range, the linear elastic assumption may lead to unrealistic stress predictions (see Chapter 5) as also observed by Santarelli et al. (1986) and Santarelli and Brown (1987). Also, non-homogeneities and non-isotropy of the rock deformation properties can cause stress concentrations around the tunnel that may not be neglected. One example in which non-homogeneity of the rock mass may have considerably affected the tunnel performance will be presented.

In Figures 7.4 and 7.5, the longitudinal sections of the tunnel in proximity of Chainages 2263 m and 3205 m are shown. At both locations, flexible probe extensometers, approximately 7 m long, were installed at the tunnel crown immediately behind the tunnel face (i.e., 0.25 to 1m). At Chainage 2263 m (Figure 7.4) the instrument is located in the siltstone (up to 2 m from the wall), coal (up to 3.6 m), mudstone, carbonaceus mudstone and interbedded sandstone-siltstone. At Chainage 3205 m (Figure 7.5), the extensometer is in siltstone and interbedded

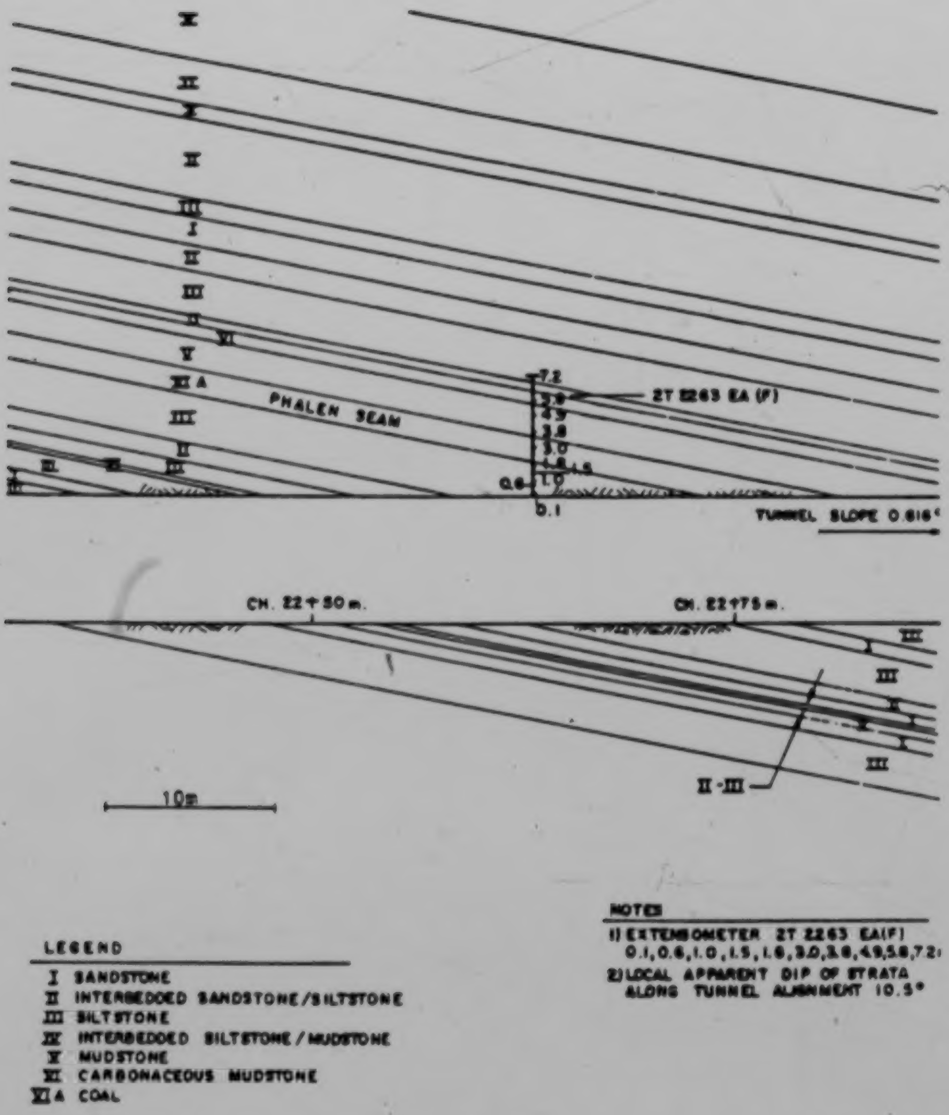
X
II
I
II
III
I
II
III
II
VI
V
VI A
PHALEN SEAM
III
II
7.2
5.8
4.9
3.8
3.0
1.6
1.5
1.0
0.6
0.1
2T 2263 EA (F)
TUNNEL SLOPE 0.616°
CH. 22+50 m.
CH. 22+75 m.
III
III
III
II-III
10m
LEGEND
I SANDSTONE
II INTERBEDDED SANDSTONE/SILTSTONE
III SILTSTONE
IV INTERBEDDED SILTSTONE/MUDSTONE
V MUDSTONE
VI CARBONACEOUS MUDSTONE
VI A COAL
NOTES
1) EXTENSOMETER 2T 2263 EA(F) 0.1,0.6,1.0,1.5,1.6,3.0,3.8,4.9,5.8,7.2
2) LOCAL APPARENT DIP OF STRATA ALONG TUNNEL ALIGNMENT 10.5°

Figure 7.4 Longitudinal Section, Showing Geology near Tunnel No.2 at Chainage 2263 m (Yuen et al., 1985)

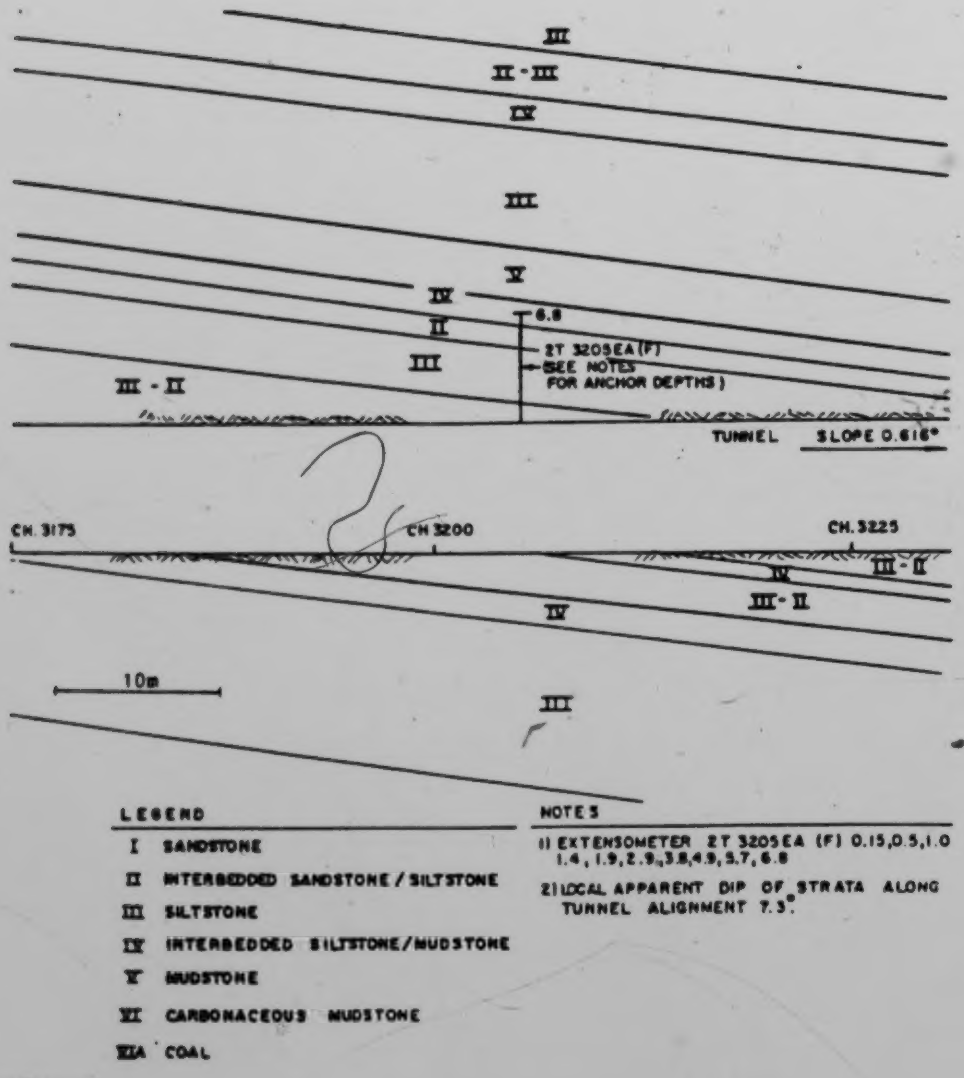
III
II - III
IV
III
V
IV
II
III
III - II
6.8
2T 3205EA (F)
(SEE NOTES
FOR ANCHOR DEPTHS)
TUNNEL
SLOPE 0.616°
CH. 3175
CH 3200
CH. 3225
IV
III - II
IV
III - II
III
10m
LEGEND
I SANDSTONE
II INTERBEDDED SANDSTONE / SILTSTONE
III SILTSTONE
IV INTERBEDDED SILTSTONE/MUDSTONE
V MUDSTONE
VI CARBONACEOUS MUDSTONE
VIA COAL
NOTES
1) EXTENSOMETER 2T 3205EA (F) 0.15, 0.5, 1.0 1.4, 1.9, 2.9, 3.8, 4.9, 5.7, 6.8
2) LOCAL APPARENT DIP OF STRATA ALONG TUNNEL ALIGNMENT 7.3°.

Figure 7.5 Longitudinal Section, Showing Geology near Tunnel No.2 at Chainage 3205 m (Yuen el al., 1985)

sandstone-siltstone up to 4.5 m away from the tunnel wall.

The relative displacement profile far behind the tunnel face, as measured by the multipoint radial extensometer located at Chainage 2263 m, is depicted in Figure 7.6. Most of the movement occurs within two meters from the tunnel and a relatively high radial displacement of 25mm is found at the crown of the excavation. A sudden change of the curve gradient, at 1.4 meters from the tunnel wall, indicates the thickness of the loosened zone. The radial displacement curves, measured by the extensometer at Chainage 2263 m, are plotted in Figure 7.7. The radial displacements are plotted against the distance from the tunnel face and the deepest anchor has been chosen as datum. From this figure the thickness of the loosened zone as well as the location at which failure occurred can be clearly identified. Relatively small displacements take place in the rock within 14 m (1.8 radii) from the tunnel face, then failure occurs and a portion of rock more than 1.0 but less than 1.4 meters thick is affected by loosening. Note that only a portion of the siltstone unit below the coal fails. Some separation between siltstone and coal takes place.

The relative radial displacement profile far behind the face, as measured by the multipoint extensometer at Chainage 3205 m, is depicted in Figure 7.8. In this case the thickness of the mobilized zone is deeper but does not exceed 3 to 4 meters. Again, a relatively large displacement, about 40mm, is detected at the tunnel wall.

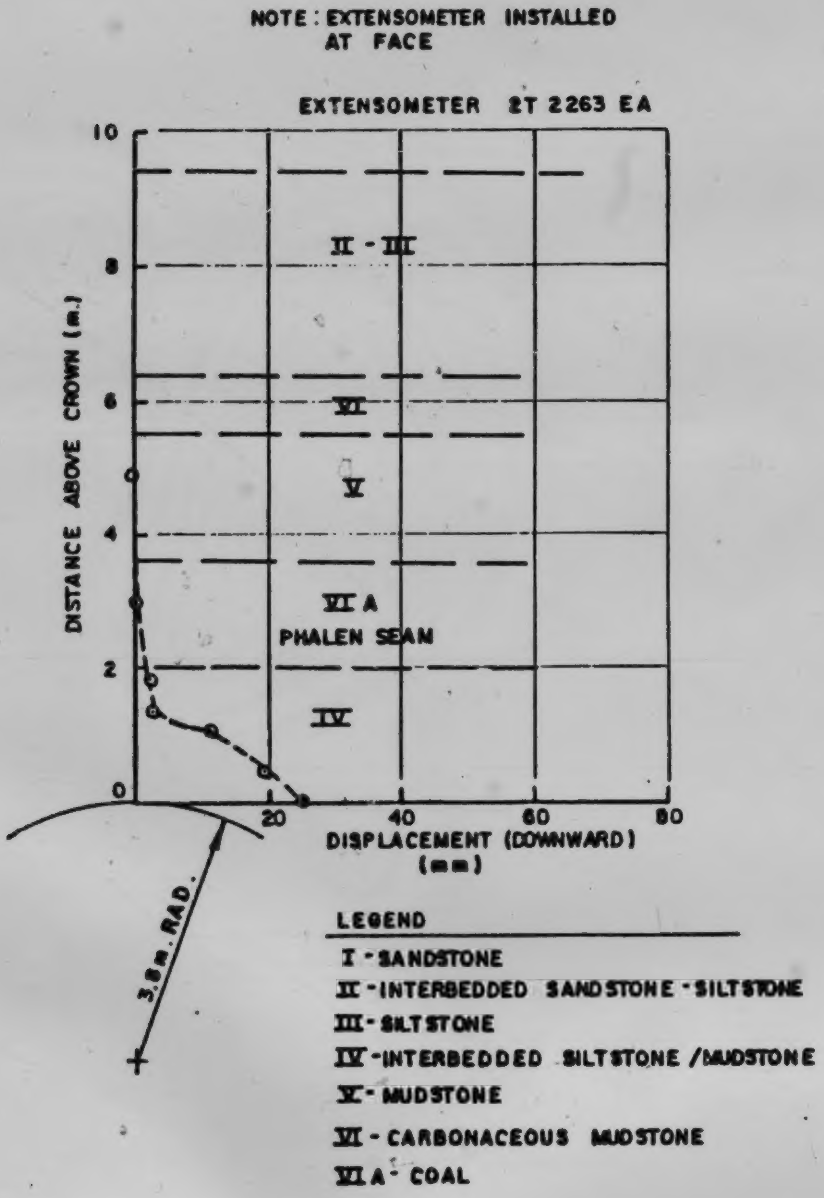

Figure 7.6 Radial Displacement Profile at Chainage 2263 m (Relative to Deepest Anchor) (Yuen et al., 1985)

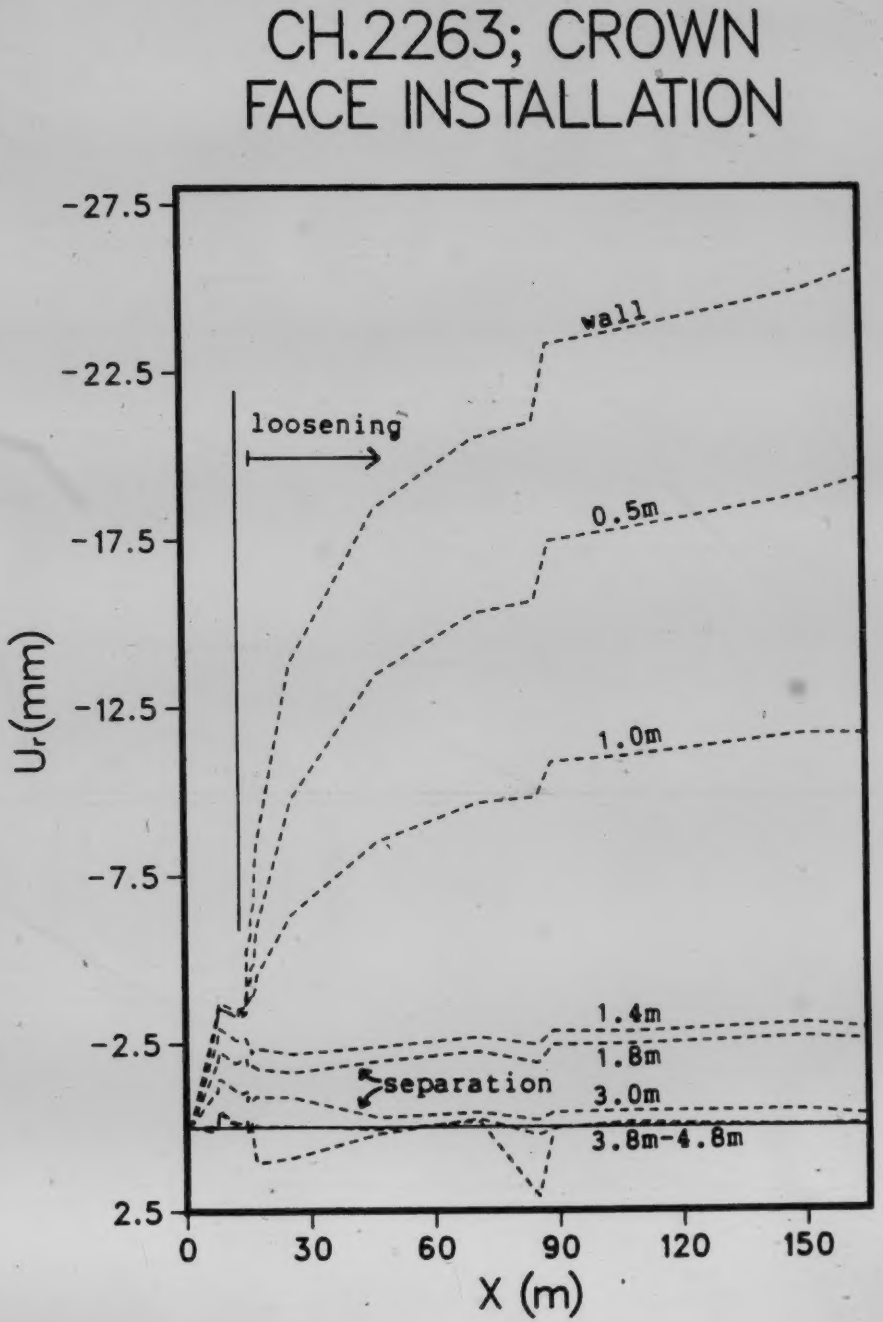

Figure 7.7 Radial Displacement Curves at Chainage 2263 m (Relative to Deepest Anchor)

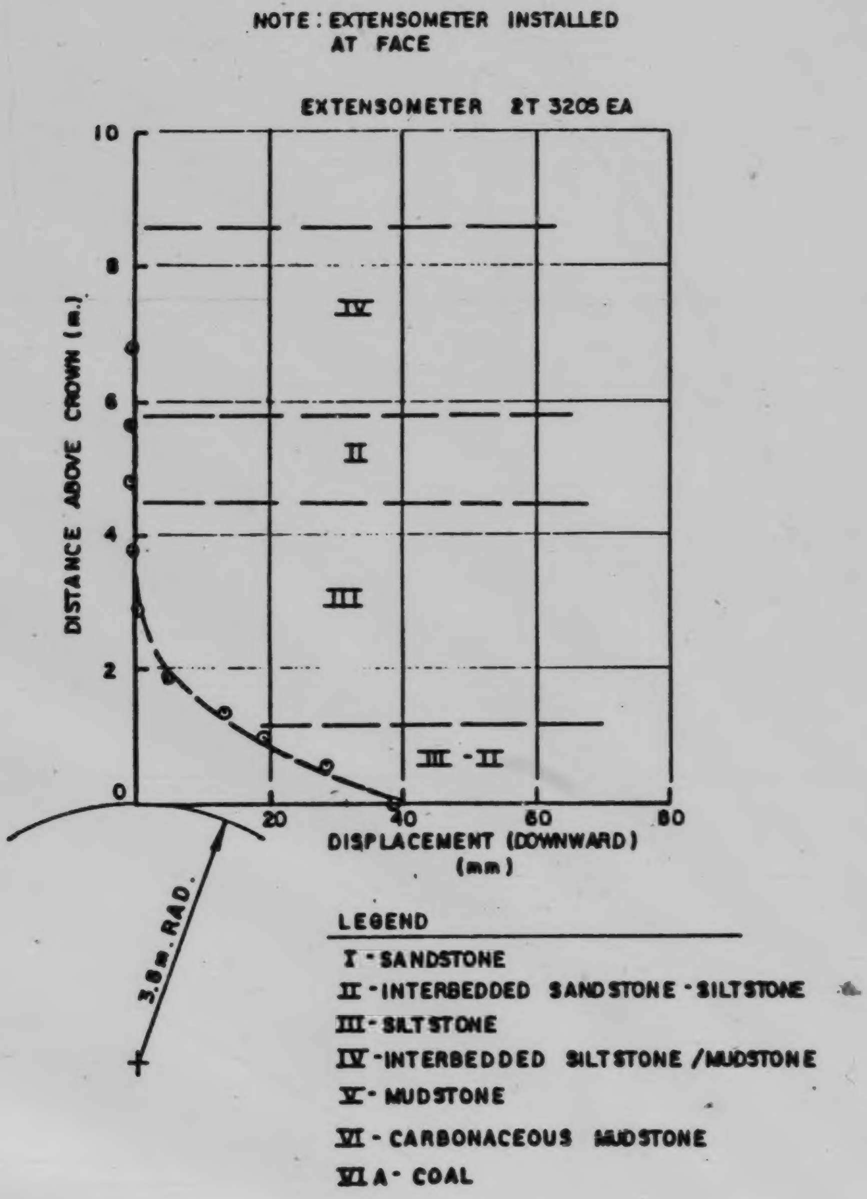

Figure 7.8 Radial Displacement Profile at Chainage 3205 m (Relative to Deepest Anchor) (Yuen et al., 1985)

This curve flattens gradually and does nor reveal the thickness of the loosened zone by a sudden change in gradient. The radial displacements curves given by the extensometer at Chainage 3205 m are shown in Figure 7.9. Again, failure occurs far from the tunnel face (at about 14.5 m) and a considerable amount of loosening can be observed. The broken zone seems to propagate to more than 2m and is approximately twice as thick as for the previous case.

If the same initial stresses are assumed to exist at Chainages 2263 and 3205 m, the rock at these two locations must have failed under similar load conditions. In order to simplify the back-analysis process, the rock strength is assumed, at this stage, to depend only on the maximum and minimum principal stresses (the effect of the intermediate principal stress will be introduced later in this section).

The uniaxial compressive strength for the siltstone can be quantified without major difficulties. In Figure 7.10, the tangential stresses at the tunnel crown, as obtained by a three dimensional finite element analysis, are plotted against the distance from the tunnel face. The stresses have been obtained by assuming $K_0=2$ and are normalized with respect to the vertical initial stress. The distance from the face is normalized with respect to the tunnel diameter. For the two cases discussed above, failure initiation took place at about 1.9 diameters behind the face of the tunnel. As indicated in Figure 7.10 (Point A) 98% of the ultimate

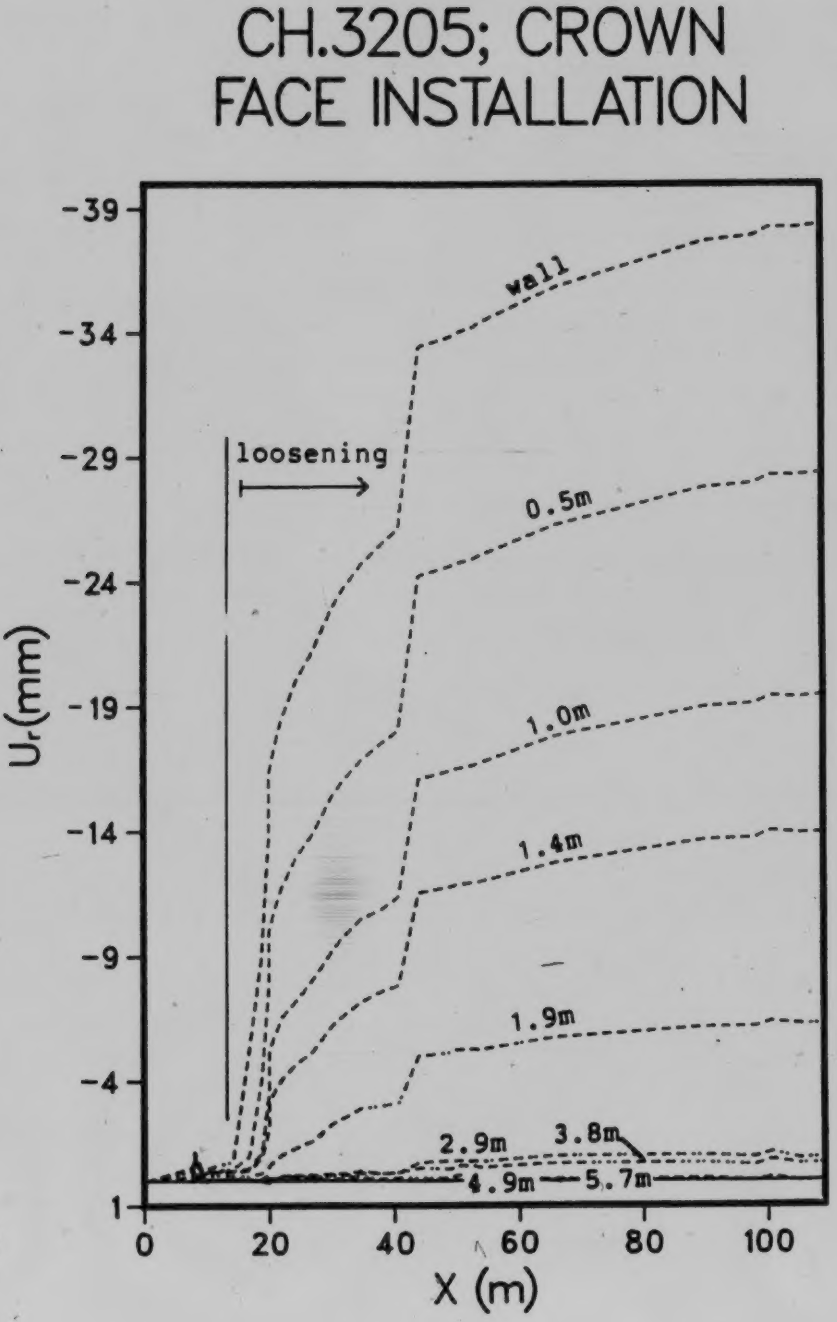

Figure 7.9 Radial Displacement Curves at Chainage 3205 m (Relative to Deepest Anchor)

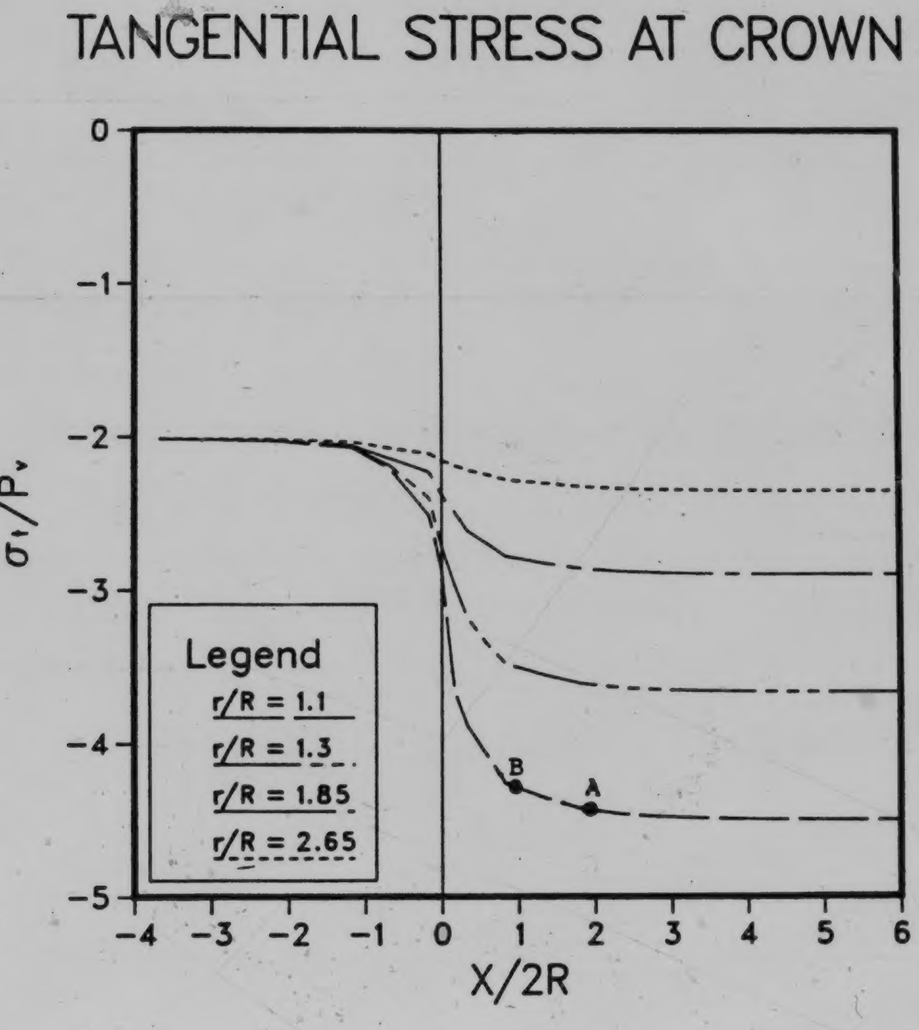

Figure 7.10 Tangential Stresses at the Tunnel Crown as Predicted by a Three Dimensional Finite Element Analysis (Linear Elastic, $K_0=2$)

(far behind the face) tangential stress has developed. This indicates that, for the cases considered, failure occurred for a tangential stress of about 24.5 MPa. At Point A, the tangential stress at the tunnel wall also corresponds to the uniaxial compressive strength of the rock. The strength of the rock mass can be described, for instance, by using the failure criterion proposed by Hoek and Brown (1980a, 1980b):

$$\sigma_1 = \sigma_3 + (\bar{m}\sigma_c\sigma_3+\bar{s}\sigma_c^2)^{1/2} \tag{7.20}$$

where σ_1 and σ_3 are the maximum and the minimum (effective) principal stresses, σ_c is the uniaxial compressive strength of the intact rock and $\bar{s}$ and $\bar{m}$ are empirical parameters. The uniaxial compressive stress of the rock mass σ_{cm} and the uniaxial compressive strength measured in the laboratory σ_c can be related as follows (Hoek, 1983):

$$\sigma_{cm} = (\bar{s}\sigma_c^2)^{1/2} \tag{7.21}$$

where $\bar{s}$ can vary between 1 (intact rock) and 0 (heavily jointed or broken rock). Substituting σ_c with the value found by laboratory testing (mean value) and σ_{cm} with the value back-analyzed above:

$$\sigma_{cm} = 24.5 = (\bar{s}\ 53.6^2)^{1/2} \tag{7.22}$$

the parameter $\bar{s}$ can be calculated:

$$\bar{s} = 0.21 \qquad [7.23]$$

Following the suggestions given by Hoek (1983), a parameter $\bar{m}=5$ can be assumed for very good quality siltstone rock masses.

Note that Hoek-Brown failure criterion defines the strength of the rock in terms of effective stresses where the back-analyzed σ_{cm} considered total stress. Total and effective stresses coincide, at the tunnel wall, if the permeability of the rock is high enough to allow a rapid dissipation of the pore pressure (if any) during face advance. The effect of seepage on the total stress distribution around the tunnel might have to be considered but, in this case, it seems reasonable to neglect it. The permeability of the rock was not tested at the Donkin-Morien project and whether the rock mass was saturated or not is unclear. Almost no water flow was detected during excavation and this seems to indicate that the rock was virtually dry (Aston, 1987).

So far in this discussion the strength of the rock has been assumed to depend only on the maximum and minimum principal stresses. The intermediate principal stress, however, is expected to play a role (e.g., Hendron, 1968) and should be considered. Srivastava et al.(1986) extended the Hoek-Brown failure criterion as follows:

$$\frac{4J_2\cos^2\theta}{\sigma_c} + \bar{m}(\cos\theta + \frac{\sin\theta}{\sqrt{3}})\sqrt{J_2} - \bar{m}I_1/3 - \bar{s}\sigma_c = 0 \qquad [7.24]$$

where I_1 is the first invariant of the stress tensor, J_2 is the second invariant of the stress deviation tensor and $\bar{\theta}$ is the Lode angle (Nayac and Zienkiewicz, 1972). The intersection of this function and an octahedral plane is an irregular hexagon (Figure 7.11), similar to the one given by the Mohr-Coulomb criterion. Eqn. 7.24 was obtained by applying the procedure suggested by Nayac and Zienkiewicz (op. cit.). The parameter $\bar{s}$ can be calculated by substituting the principal stresses at failure in Eqn. 7.24 and by assuming an $\bar{m}$ value. The major principal stress corresponds to the tangential stress at failure (Point A in Figure 7.10), the intermediate principal stress corresponds to the axial stress at failure (Point B in Figure 7.12), and the minor principal stress is zero as it vanishes on the free surface. Assuming $\bar{m}=5$ (Hoek, 1983), $\bar{s}=0.21$ results that is equal to the value given by Eqn. 7.20. It can then be concluded that neglecting the effect of the intermediate principal stress is acceptable for this case.

7.3.1.1 Influence of Inhomogeneities

For certain conditions, inhomogeneities in the rock mass must be considered because they may cause stress concentrations that cannot be explained by means of the elasticity theory. In Figure 7.13, the longitudinal section of the tunnel in the proximity of Chainage 1428 is shown. A 21 m long rigid probe extensometer, equipped with four anchors (including head), was installed at the tunnel crown, immediately behind the face. Another instrument was located

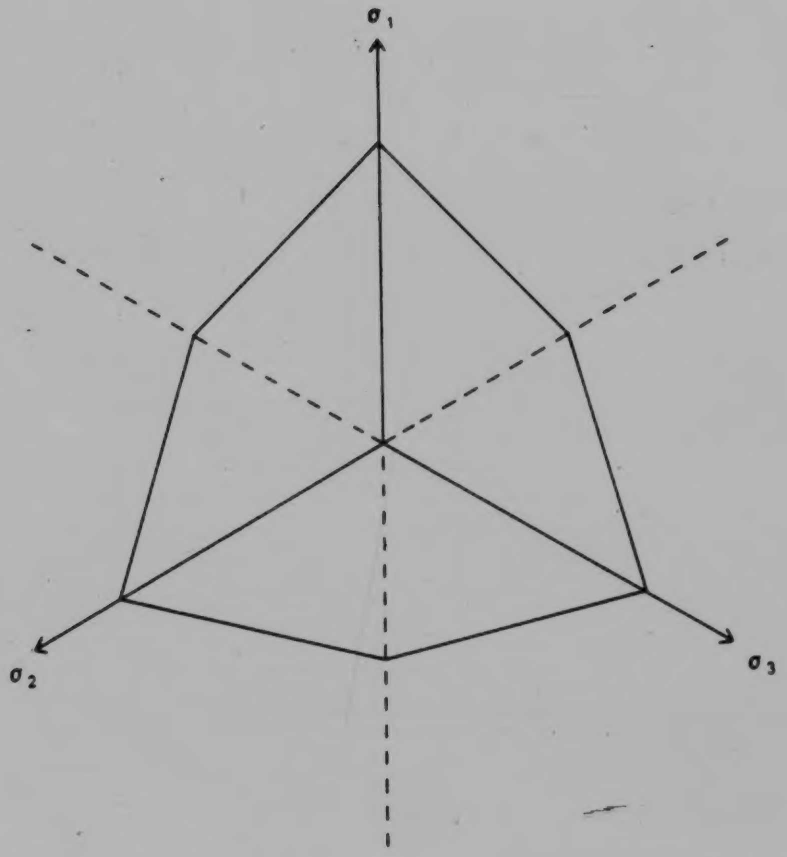
σ_1
σ_2
σ_3

Figure 7.11 Intersection of Hoek-Brown Surface with Octahedral Plane

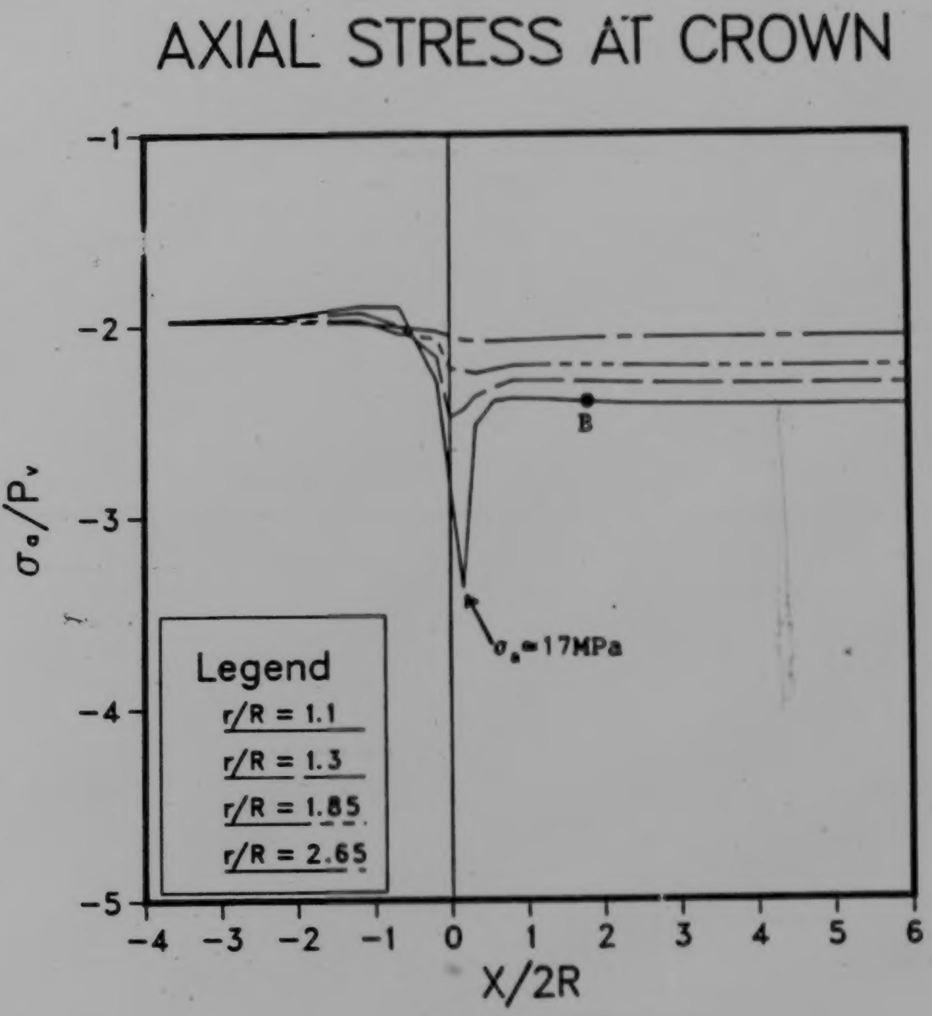

Figure 7.12 Axial Stresses at the Tunnel Crown as Predicted by a Three Dimensional Finite Element Analysis (Linear Elastic, K_0=2)

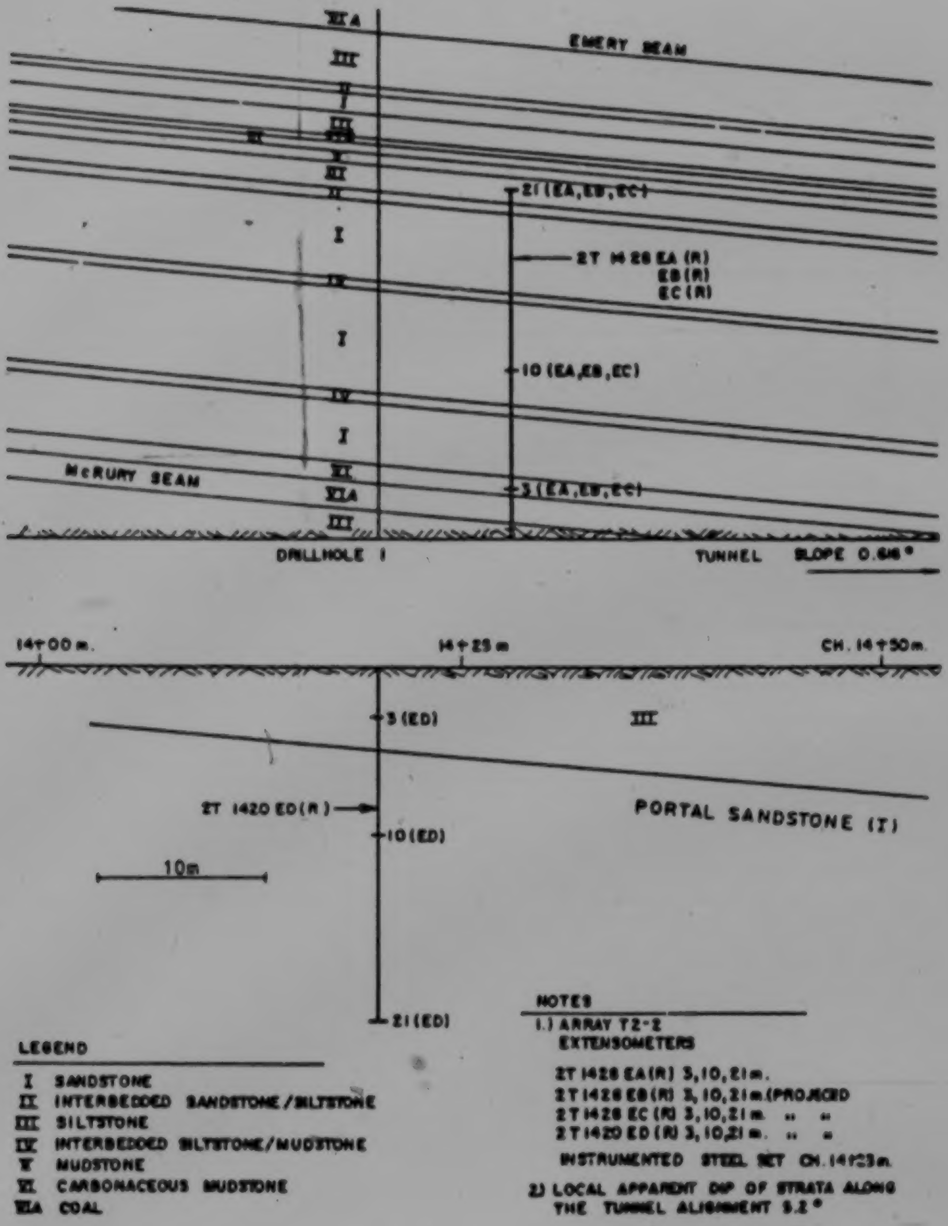
VIIA
EMERY SEAM
III
II
I
III
II
VII
V
III
II
21 (EA,EB,EC)
I
2T 1428 EA (R)
EB (R)
EC (R)
IV
I
10 (EA,EB,EC)
IV
I
VI
McRURY SEAM
VIIA
3 (EA,EB,EC)
III
DRILLHOLE I
TUNNEL SLOPE 0.616°
14+00 m.
14+25 m
CH. 14+50 m.
3 (ED)
III
2T 1420 ED (R)
10 (ED)
PORTAL SANDSTONE (I)
10m
21 (ED)
LEGEND
I SANDSTONE
II INTERBEDDED SANDSTONE/SILTSTONE
III SILTSTONE
IV INTERBEDDED SILTSTONE/MUDSTONE
V MUDSTONE
VI CARBONACEOUS MUDSTONE
VIIA COAL
NOTES
1.) ARRAY T2-2
EXTENSOMETERS
2T 1428 EA(R) 3,10,21m.
2T 1428 EB(R) 3,10,21m.(PROJECTED
2T 1428 EC (R) 3,10,21m. " "
2T 1420 ED (R) 3,10,21m. " "
INSTRUMENTED STEEL SET CH. 14+23m.
2) LOCAL APPARENT DIP OF STRATA ALONG
THE TUNNEL ALIGNMENT 5.2°

Figure 7.13 Longitudinal Section, Showing Geology near Tunnel No.2 at Chainage 1428 m (Yuen et al., 1985)

at the invert of the tunnel, but it won't be considered in this discussion as it was installed far from the tunnel face, behind the shield of the TBM. Even though the tunnel is completely contained in a thick siltstone layer, a coal seam is located only one meter above the crown. At this location surficial loosening and spalling were observed too, and considerable downward displacements were measured. In Figure 7.14 the radial displacement profile at the tunnel crown is shown for Chainage 1428 m. A very large radial displacement of almost 80mm was detected at the tunnel wall due to loosening. The radial displacement curves plotted in Figure 7.12 show that failure in the siltstone took place at a much earlier stage than for the two cases discussed previously. At the back of the shield, failure had already occurred and a significant amount of loosening was revealed by the large gap between the displacements measured at the wall and at 3m from the excavation. Because of lack of measurements near the tunnel face, the location at which the strength of the rock was exceeded is unknown. The reason of early failure is to be found in the relatively low stiffness of the coal that causes a high stress concentration in the thin siltstone layer at the crown of the tunnel. In the next section, it will be confirmed, by the elastic modulus back-analyzed for Chainage 1428 m, that the coal is highly deformable, relatively to the siltstone.

In the previous example the failure of the rock in proximity of the tunnel wall took place ahead of the TBM's

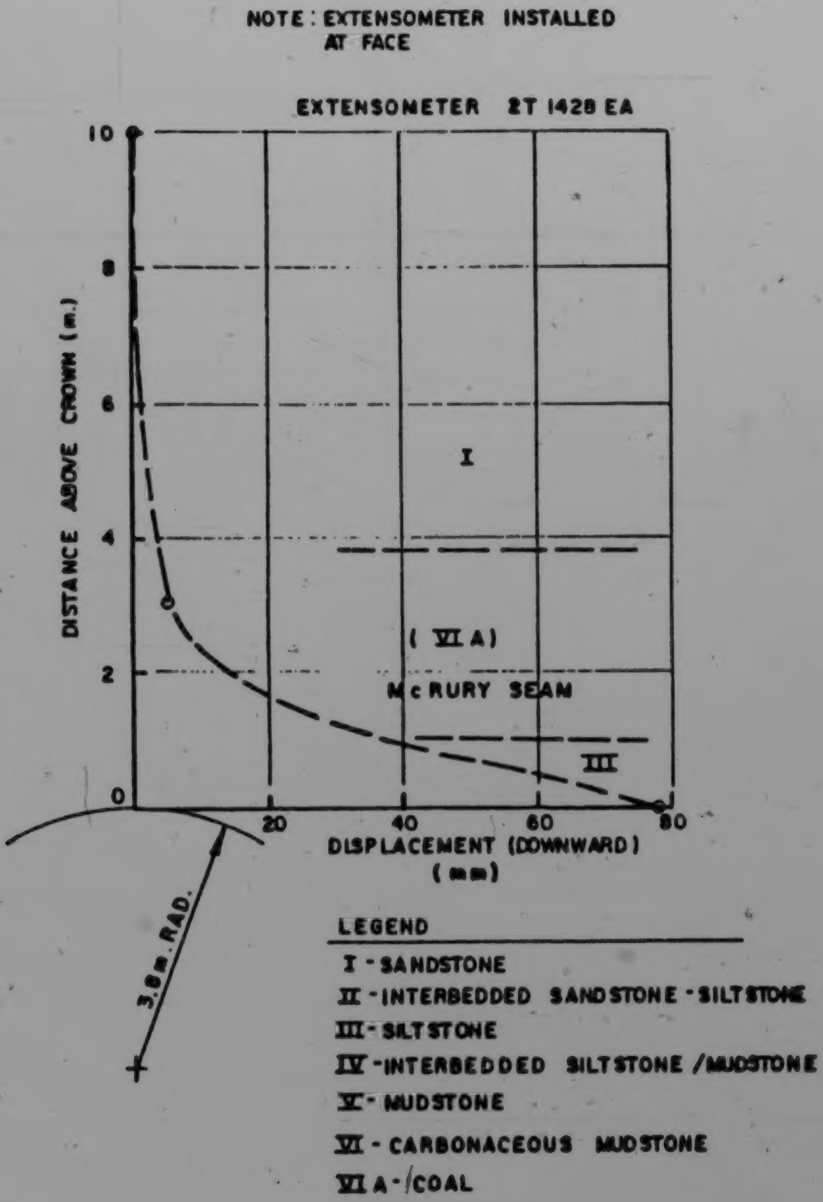

Figure 7.14 Radial Displacement Profile at Chainage 1428 m (Relative to Deepest Anchor) (Yuen et al., 1985)

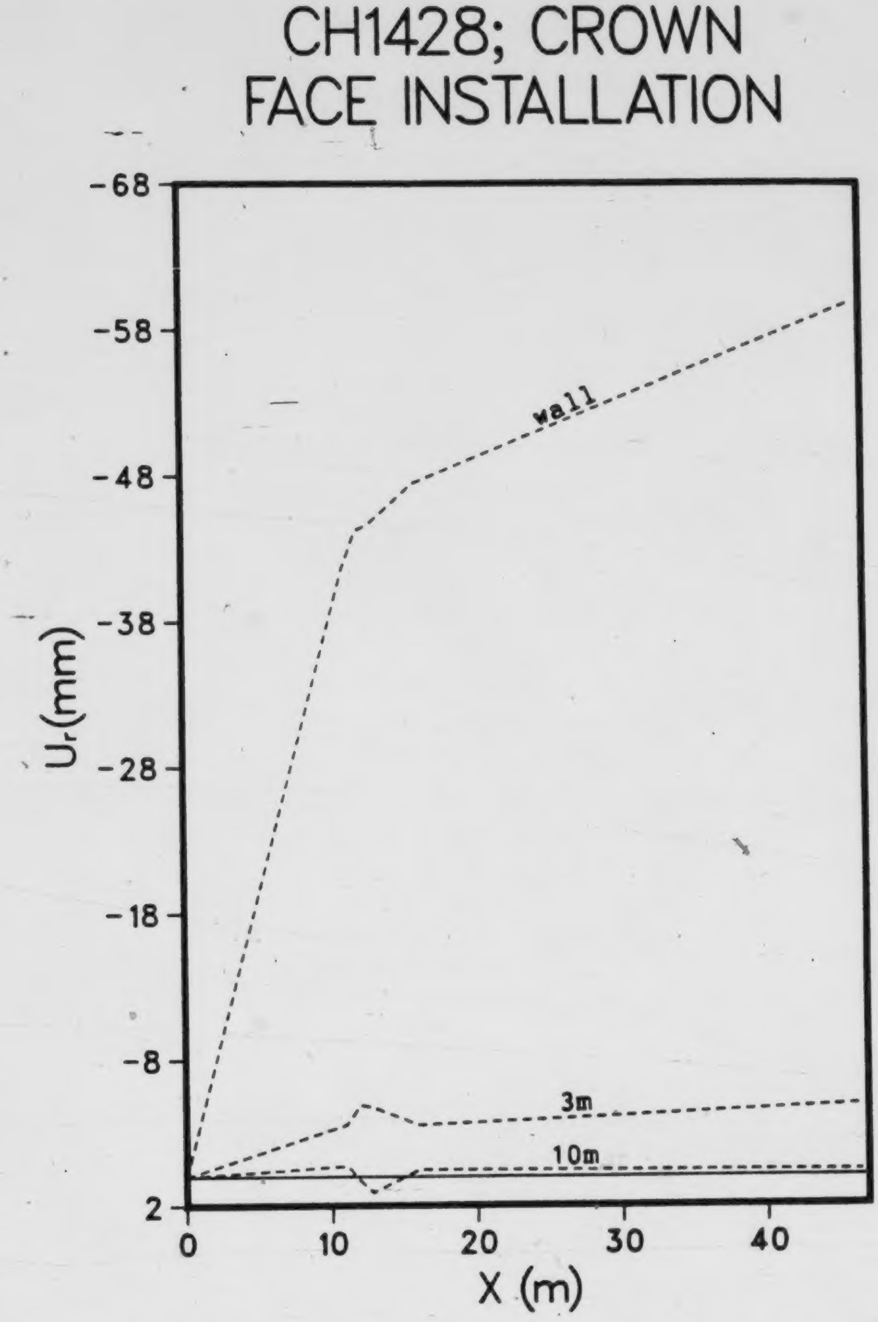

Figure 7.15 Radial Displacement Curves at Chainage 1428 m

tail, most probably because of stress concentrations due to rock inhomogeneity. In the following case a similar phenomenon is found, due to the relatively low strength of the rock mass.

7.3.1.2 Effects of Low-Strength Rock at the Tunnel Crown

The longitudinal section of the tunnel in proximity of Chainage 2996 m is depicted in Figure 7.16. A flexible probe extensometer is installed at the tunnel crown, immediately behind the face of the tunnel, in a 5.5 m thick layer of interbedded siltstone-mudstone. Surficial loosening at the crown, within a 60° arch, was observed. In Figure 7.17 the radial displacement profile at the tunnel crown is shown for Chainage 2996 m. Even for this case a considerably large radial displacement, of more than 40mm, is detected at the wall due to loosening. The radial displacement curves recorded by the multipoint extensometer are shown in Figure 7.18. Immediately behind the shield of the TBM (Point A in Figure 7.18), failure has already occurred and a loosened zone, approximately half a meter deep, is revealed by the gap between the measurements at 0.4 and 0.8m. As the face of the tunnel advances, the tendency of tangential stress to concentrate near the crown of the tunnel causes further propagation of failure. At about two diameters behind the face of the tunnel (Point B in Figure 7.18) deeper portions of the rock mass fail and, far from the face, a plastic zone of thickness greater than 1.7 m is detected. The back-analysis of the rock strength is complicated by the

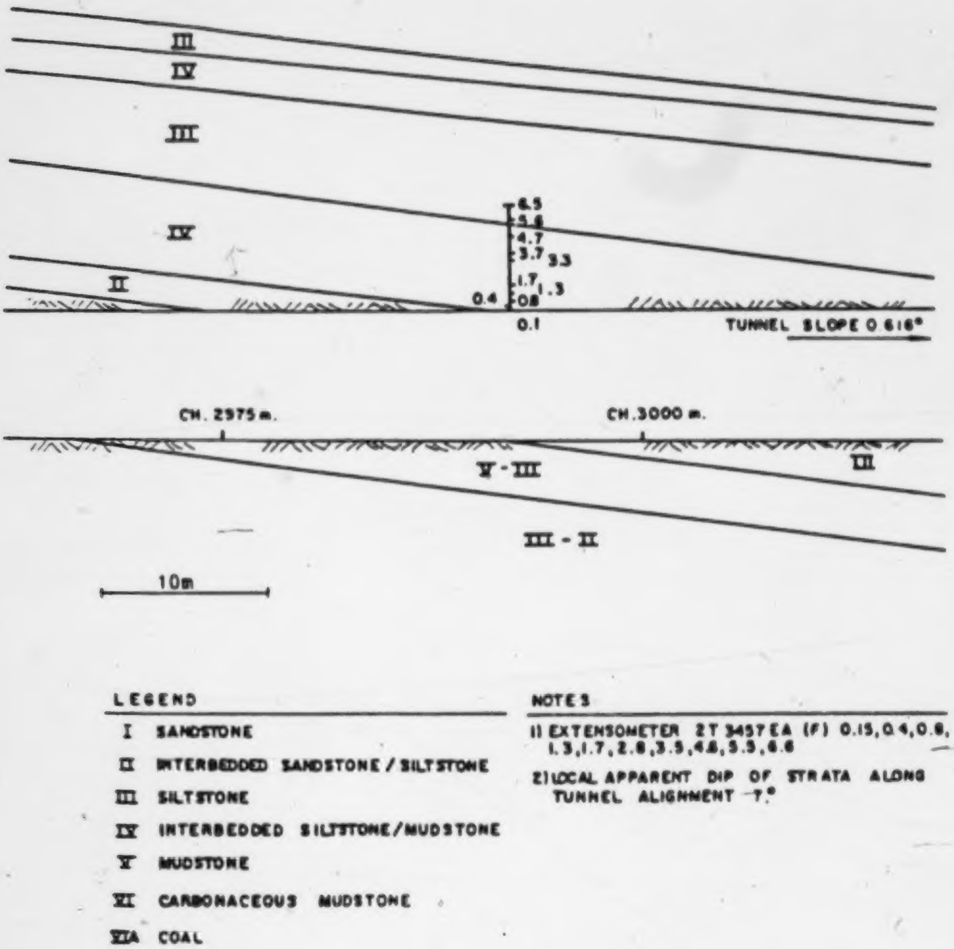
III
IV
III
IV
II
6.5
5.8
4.7
3.7
3.3
1.7
1.3
0.8
0.4
0.1
TUNNEL SLOPE 0.616°
CH. 2975 m.
CH. 3000 m.
V - III
III
III - II
10m
LEGEND
I SANDSTONE
II INTERBEDDED SANDSTONE / SILTSTONE
III SILTSTONE
IV INTERBEDDED SILTSTONE/MUDSTONE
V MUDSTONE
VI CARBONACEOUS MUDSTONE
VIA COAL
NOTES
1) EXTENSOMETER 2T 3457 EA (F) 0.15, 0.4, 0.8, 1.3, 1.7, 2.8, 3.3, 4.8, 5.8, 6.6
2) LOCAL APPARENT DIP OF STRATA ALONG TUNNEL ALIGNMENT 7°

Figure 7.16 Longitudinal Section, Showing Geology near Tunnel No.2 at Chainage 2996 m (Yuen et al., 1985)

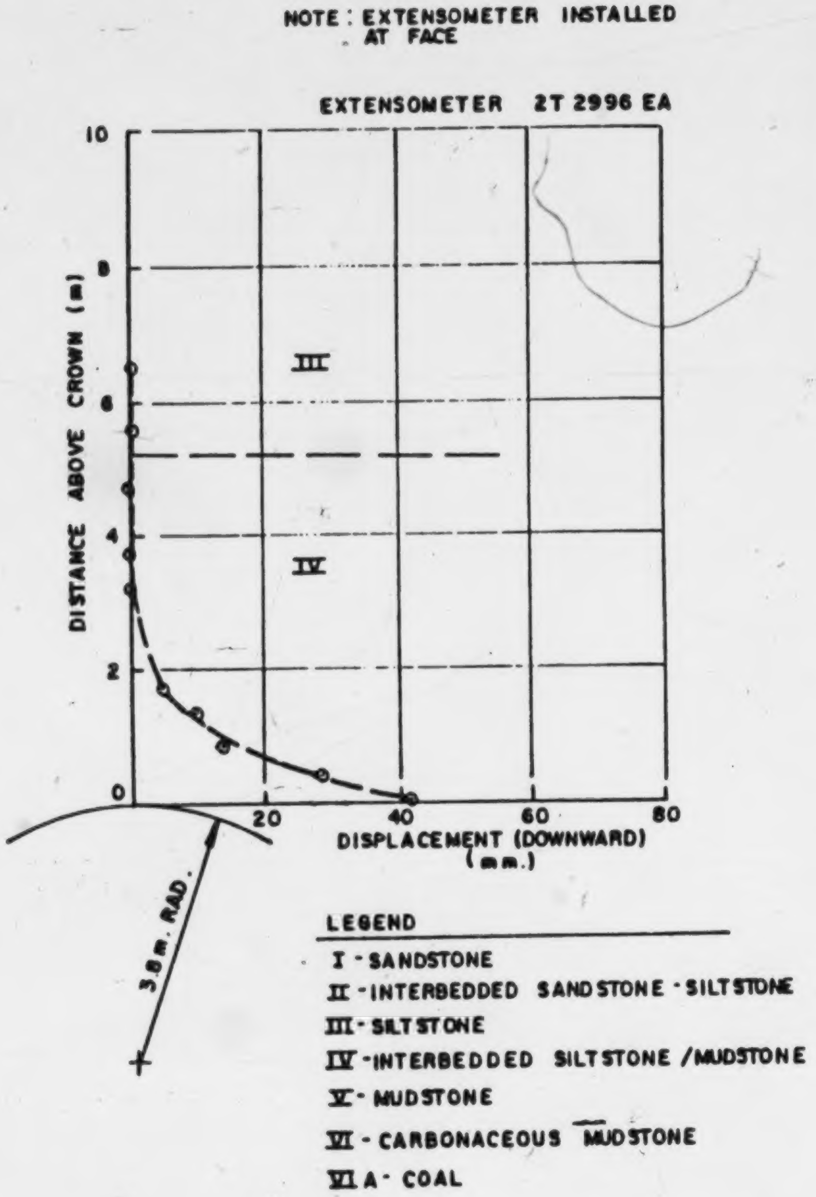

Figure 7.17 Radial Displacement Profile at Chainage 2996 m (Relative to Deepest Anchor) (Yuen et al., 1985)

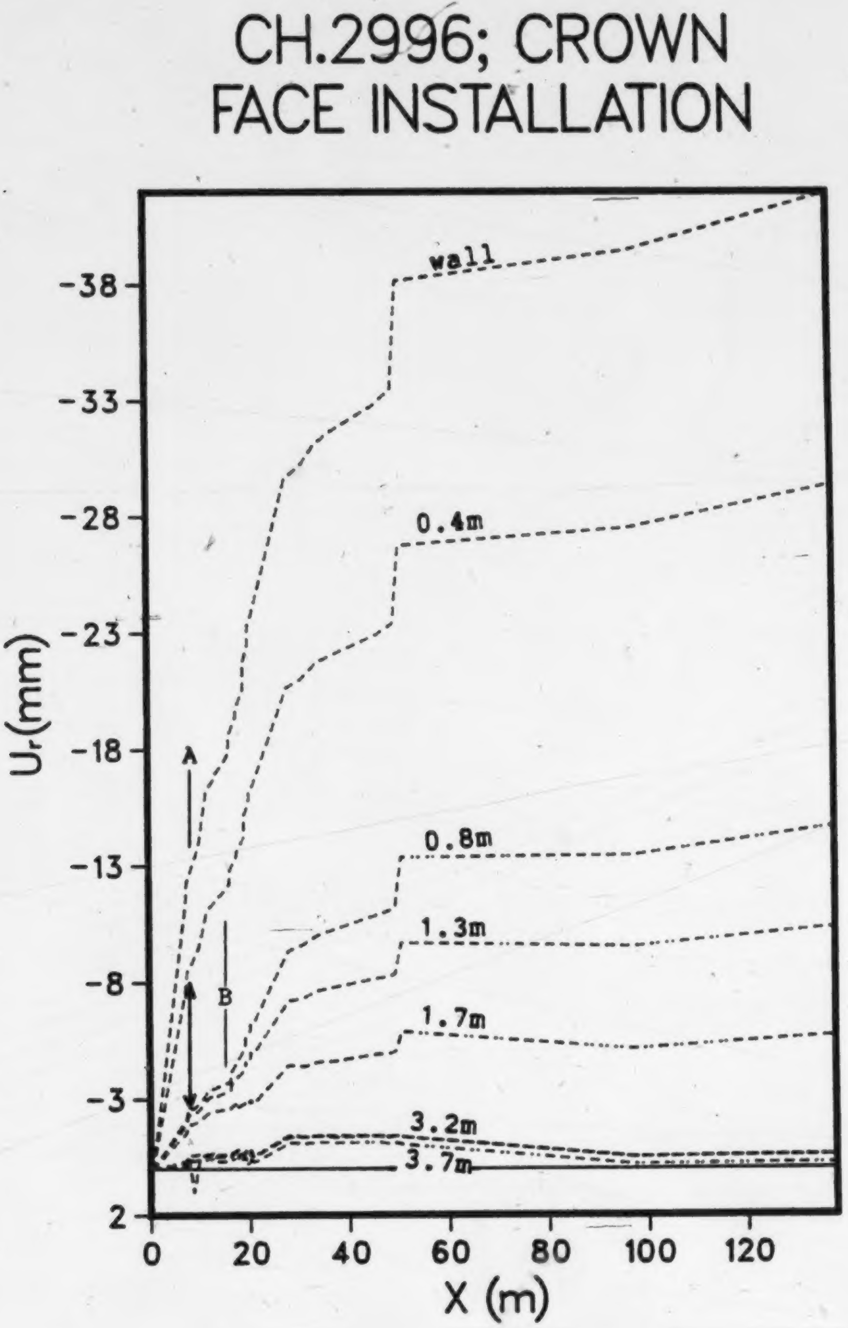

Figure 7.18 Radial Displacement Curves at Chainage 2996 m (Relative to Deepest Anchor)

fact that the location at which failure initiated is not known accurately. However, a reasonable stress range at which failure must have occurred can be selected. It can be assumed that failure almost certainly took place behind the tunnel face. The radial stress increase occurring ahead of the face is in fact very moderate at the tunnel crown (see Figure 7.19). Immediately behind the face of the tunnel, the first possible conditions of failure are found as the axial stress increases to approximately 17 MPa. (Figure 7.12). If the rock strength is assumed to be independent of the intermediate principal stress and the uniaxial compressive strength of the rock is exceeded by this value (17 MPa), failure occurred very closely to the face of the tunnel. If not, failure took place somewhere within 0.8 and 1.0 diameters behind the face, where the tangential stress reaches 23.5 MPa (Point B in Figure 7.10). The upper limit for σ_{cm} of 23.5 MPa (σ_t one diameter behind the face) can be defined without problems; the lower limit is uncertain. If the rock failed immediately behind the face of the tunnel, because of the high axial stress value, this would only indicate that σ_{cm} is lower than 17 MPa. At the same time, the relatively thin plastic zone detected at the wall (about 0.5 m thick) immediately behind the TBM shield indicates that the maximum uniaxial stress of 23.5 MPa has not exceeded the uniaxial strength of the rock by a very significant amount. On the basis of these observations a σ_{cm} of 17 MPa can be assumed for the interbedded

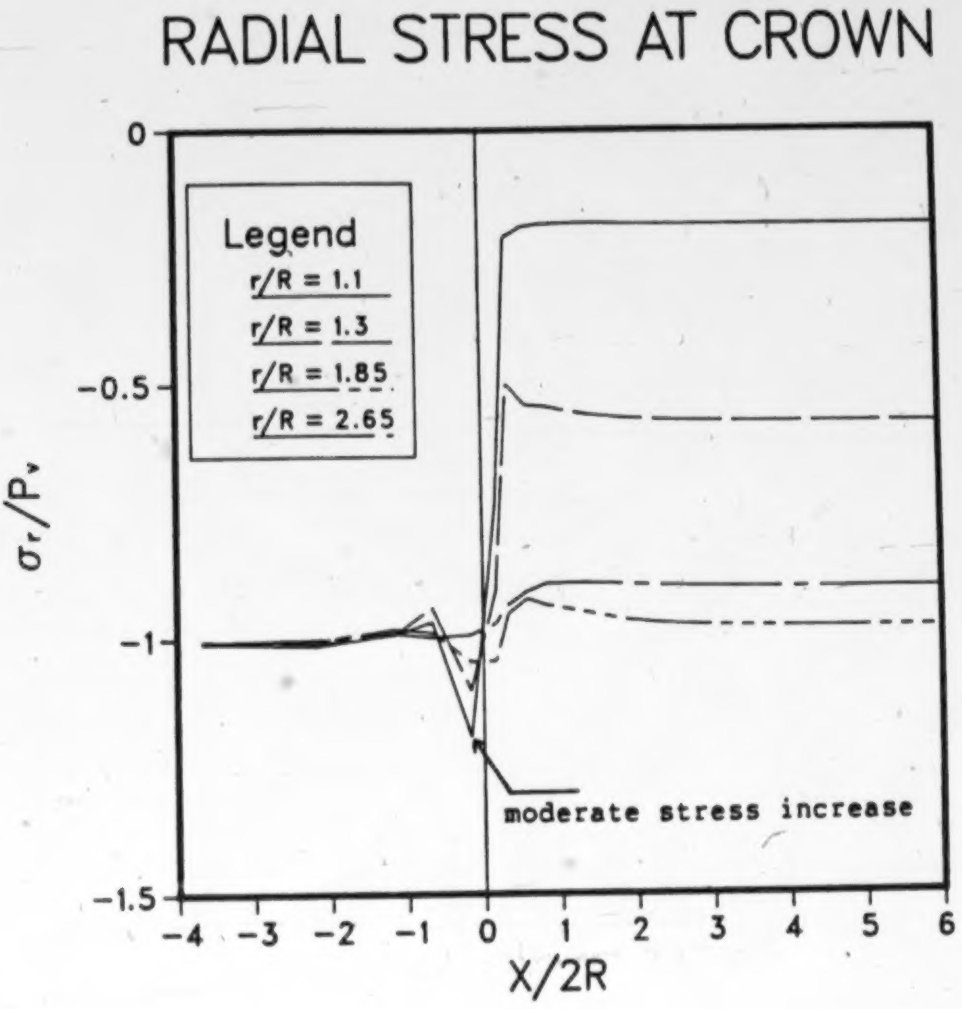

Figure 7.19 Radial Stresses at the Tunnel Crown as Predicted by a Three Dimensional Finite Element Analysis (Linear Elastic, $K_0=2$)

siltstone-mudstone in the tunnel section considered. By correlating the assumed σ_{cm} (17 MPa) to σ_c as obtained in the laboratory (35.8 MPa), an s value of approximately 0.2 is found again. This indicates a very good quality rock mass (Hoek, 1983). The effect of the intermediate principal stress could also be considered as it was done earlier in this chapter.

In this section, the strength properties of the rock mass have been investigated by studying the mechanism of failure initiation at the crown of the tunnel.

In order to define the parameters controlling failure propagation, more extensive studies should be conducted using appropriate numerical techniques. Once the peak strength of the material is known, the amount of strength loss characterizing the rock mass in the post peak range, for instance, could be related to the thickness of the plastic zone. This study goes beyond the scope of this research and sufficient data are not available for a proper verification.

7.3.2 Back-Analysis of Rock Mass Modulus

If the rock mass surrounding the tunnel exhibits a linear elastic stress strain constitutive relationship in the stress range of interest, its elastic modulus can be found by matching the field data with analytical results. A reasonable Poisson's ratio can be assumed and the in situ stress field must be known. For certain cases, the initial stress ratio K_0 can also be back-analyzed at the same time (Sakurai and Takeuchi, 1983). If a plastic zone develops at the crown and at the invert of the tunnel, the back-analysis of the elastic modulus of the rock mass is more difficult. In Chapter 5 it was observed that the shape of the relative displacement curves, given by multipoint radial extensometers at the crown, is considerably affected by yielding (for $K_0=2$). In Figure 7.20, the relative radial displacement curves calculated at the tunnel crown for linear elastic and elasto-plastic rock are compared. For the two cases the same Young's modulus characterizes the rock masses in the elastic region. The two curves have considerably different shape but intersect at Point A'. Point A' represents the only location at which, by fitting numerical linear elastic results to the field data the right elastic modulus for the rock mass would be back-analyzed. For points located between Point A' and the tunnel wall fitting with linear elastic results leads to an underestimate of the Young's modulus, whereas an overestimate occurs if a point located outside of Point A is selected. For the example shown in Figure 7.20, Point A' approximately corresponds to the boundary of the plastic zone. This is reasonable for $K_0=2$, because failure tends to cause larger displacements in the plastic zone than for the elastic case, and reduces the inward movement outside the plastic zone by changing the shape of the cross section from circular to "elliptical" (Figure 7.21). In order to evaluate

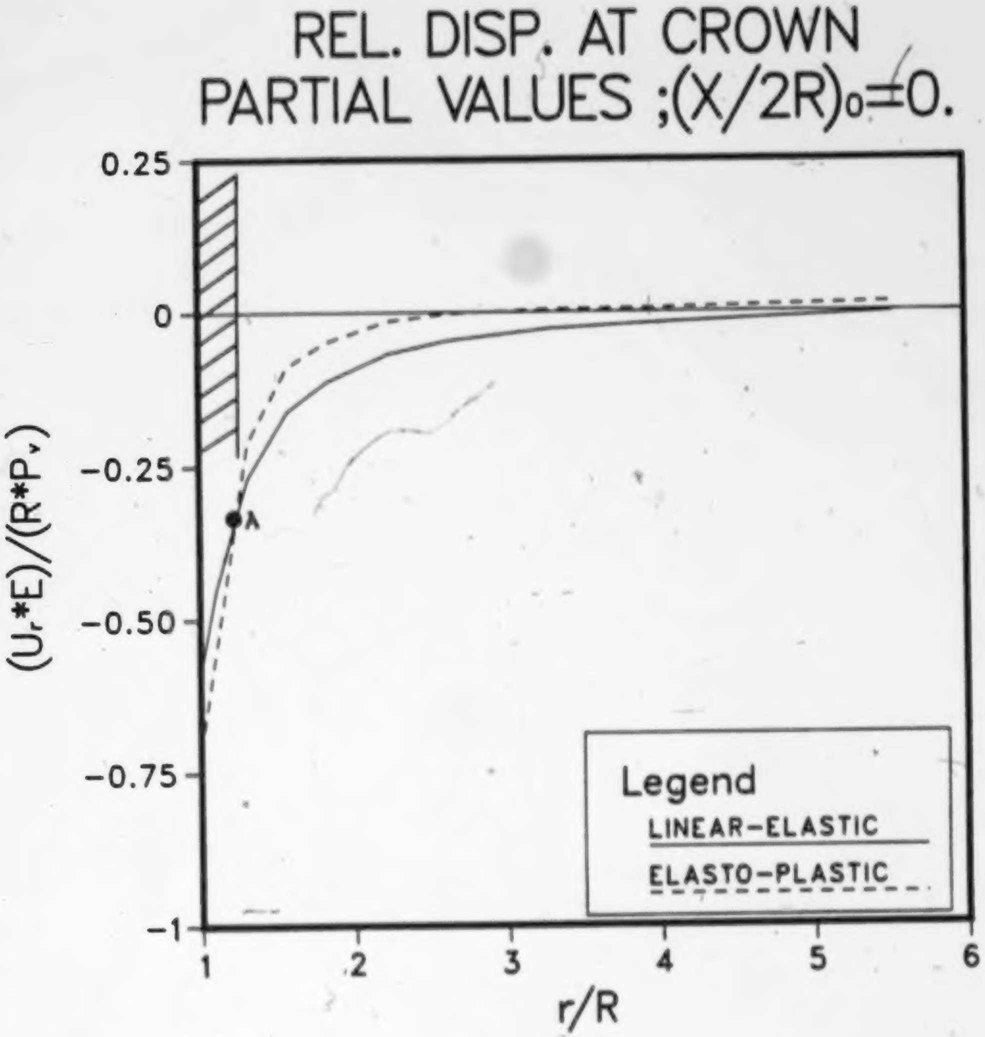

Figure 7.20 Radial Displacement Profiles at the Tunnel Crown, Predicted by two Three Dimensional Finite Element Analyses (Elastic and Elasto-Plastic)

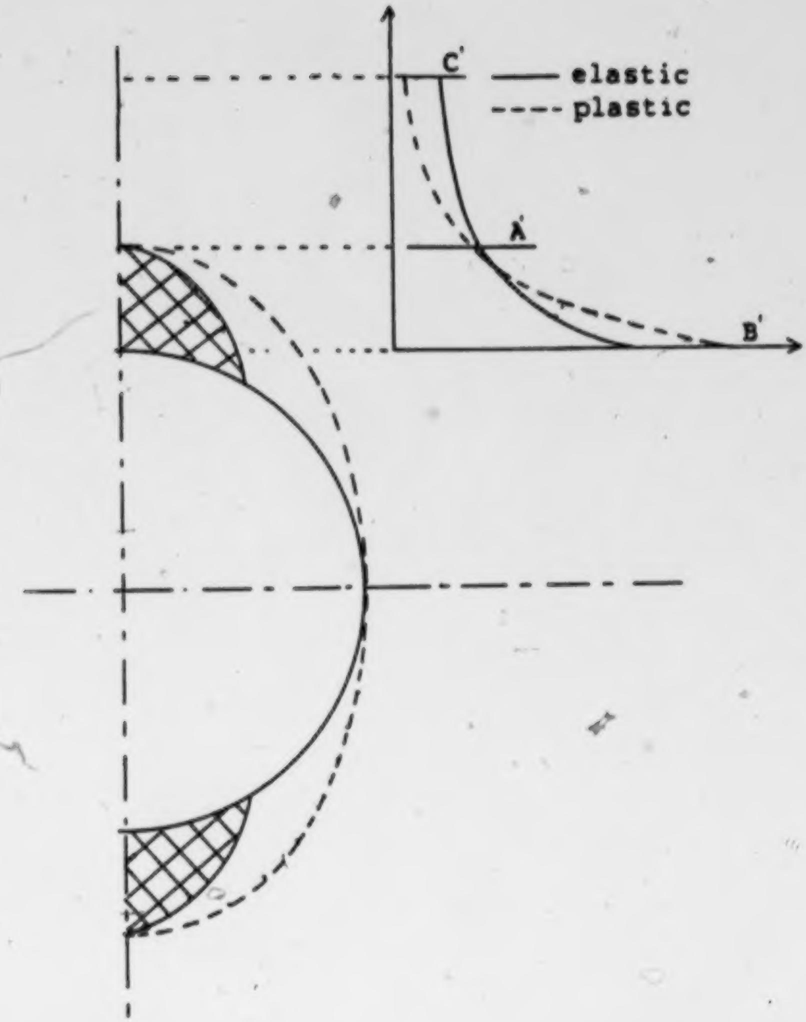
C'
elastic
plastic
A'
B'

Figure 7.21 Schematic Representation of Tunnel Shape Change due to Yielding

correctly the elastic modulus of the rock mass, the closest measurement to the boundary of the plastic zone, but in the elastic region, should be fitted to the calculated, linear elastic values. Since yielding at the tunnel crown results in relatively low radial displacements in the elastic region (Figure 7.21, between A' and C'). The back-analyzed modulus is then an upper bound value.

Two cases will now be analyzed by using the suggested procedure. The selected cross sections are the ones at Chainages 2296 m and 3205 m (see Figures 7.16 and 7.5). The results obtained by a three dimensional finite element analysis are compared with the field data for Chainage 2296 m in Figure 7.22. The fitting was carried out by matching visually measurements obtained at 1.5 m from the tunnel wall (near the plastic zone boundary), 7.5 m behind the tunnel face. The measured curves at 3.2 and 3.7m from the wall give lower displacements than predicted by the finite element analysis whereas the movement of the anchors in the plastic zone considerably exceeds the predicted (based on linear elasticity). A Young's modulus of 1.65 GPa for the interbedded siltstone-mudstone is the outcome of this analysis, whereas $E \simeq 9$ GPa was measured in the laboratory for the same material (Yuen et al., 1985).

Chainage 3205 m was also analyzed in the same manner. A point 40 m behind the tunnel face and an anchor at 2.9 m from the tunnel wall was selected for comparison with the finite element results (Point A in Figure 7.23). The

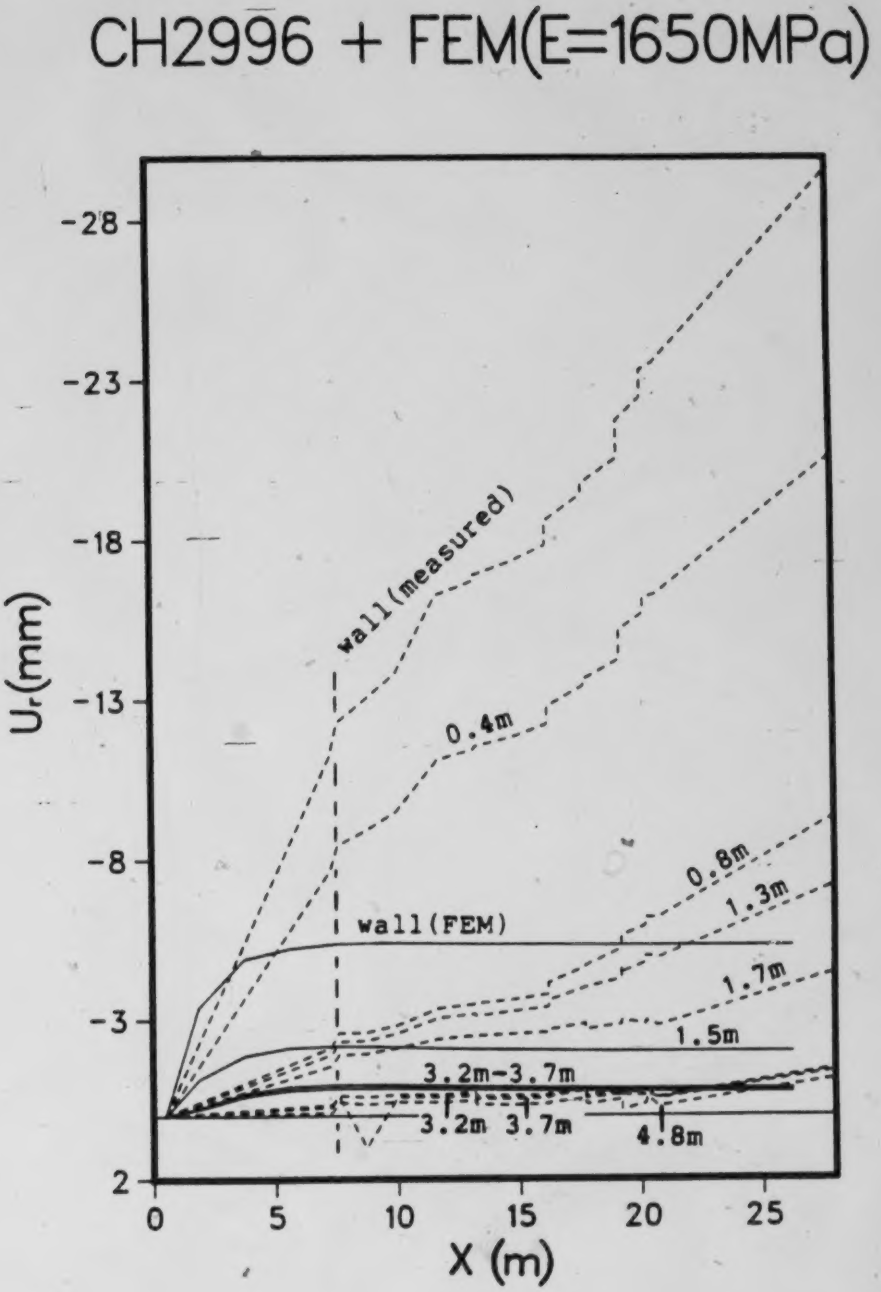

Figure 7.22 Measured and Predicted Radial Displacement Curves at Chainage 2996 m; Fitted at 1.5m from the Wall (E=1.65 GPa).

back-analyzed Young's modulus for the siltstone is 5.6 GPa at this location, whereas E≈11 GPa was measured in the laboratory for the same material (Yuen et al., 1985). The data collected within 15 meters from the tunnel face were not considered for back-analysis because they displayed erratic behavior (Figure 7.24). Similar jumps as reflected by Figure 7.24 are observed at other sections, perhaps due to the action of the rib expansion mechanism.

If the moduli back-analyzed for the two cases are compared with the laboratory results it is found that the ratios of E(field)/E(lab) are 0.18 and 0.5, respectively, for interbedded siltstone-mudstone and siltstone. These values are in agreement with the notion that the modulus of deformability measured on small samples always constitutes an upper bound value for the rock mass.

Finally, the deformability of the rock at Chainage 1428 m was analyzed. In the previous section it was stated that the low stiffness of the coal seam caused early failure (near the face of the tunnel) at this location. The elastic modulus of the rock was obtained by fitting visually the numerical results to the displacements measured at 3 m from the wall (Figure 7.25). The very low modulus value back-analyzed (E=0.5 GPa) proves the point that the coal is highly deformable with respect to the siltstone, and this supports the conclusion that this stiffness variation caused stress concentration and failure in the thin siltsone layer at the crown of the tunnel.

CH.3205; CROWN FACE INSTALLATION

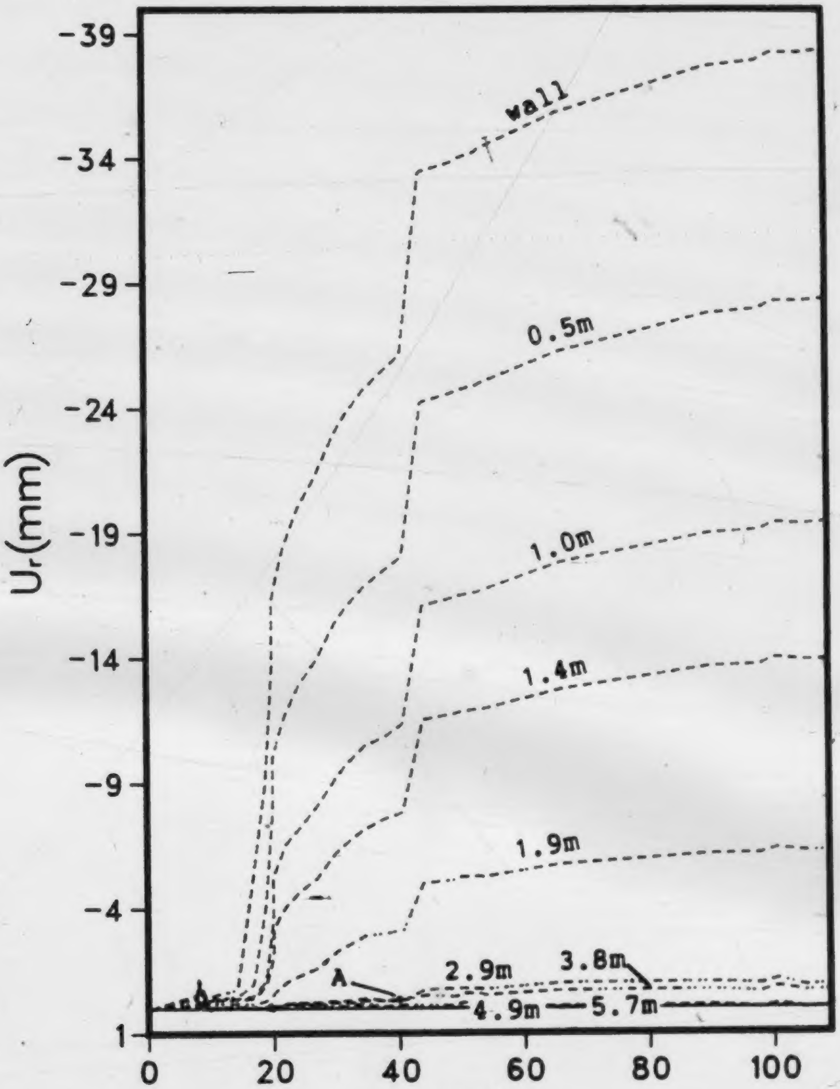

Figure 7.23 Radial Displacements Curves at Chainage 3205 m (Relative to Deepest Anchor)

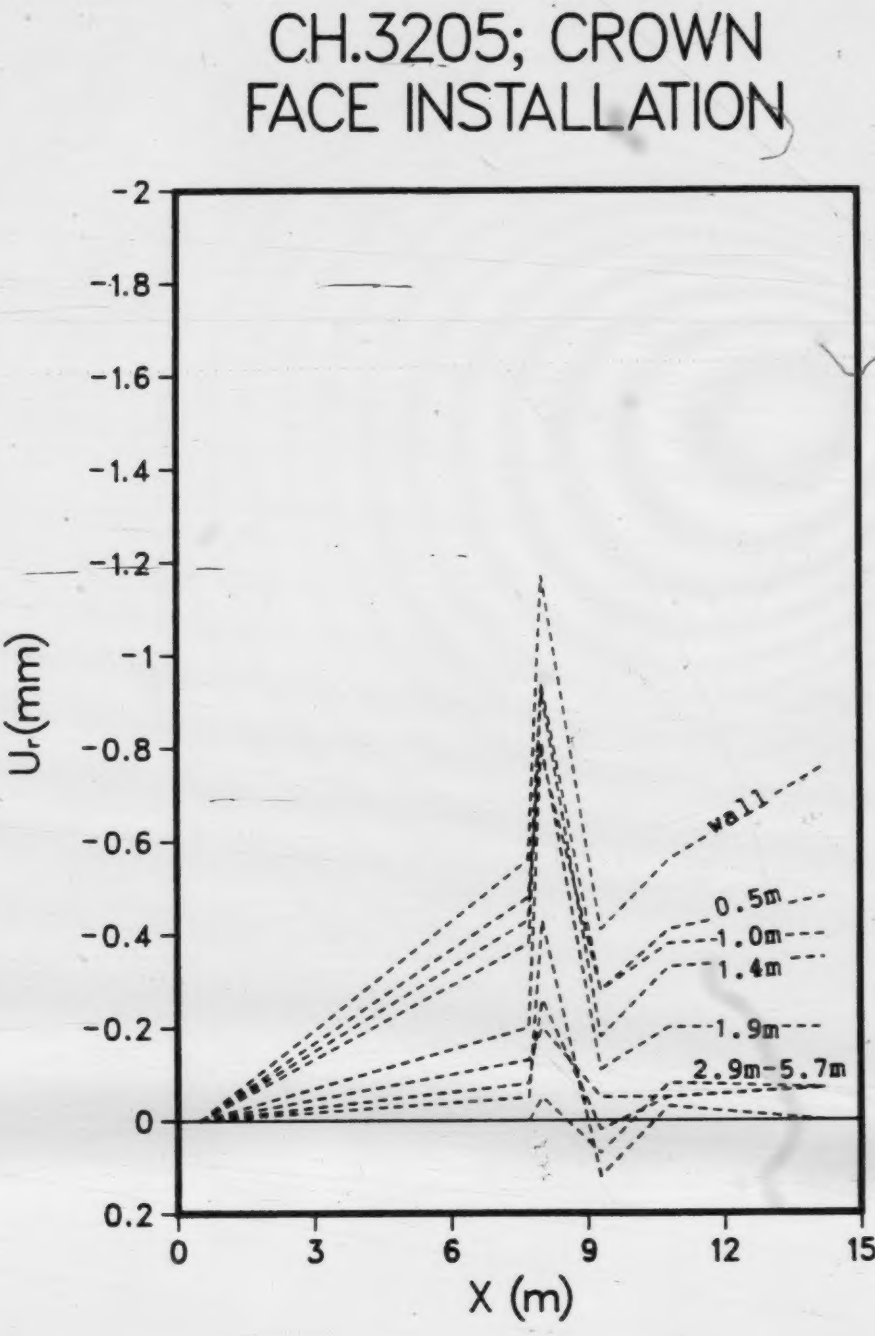

Figure 7.24 Radial Displacements Curves at Chainage 3205 m; Near Tunnel Face

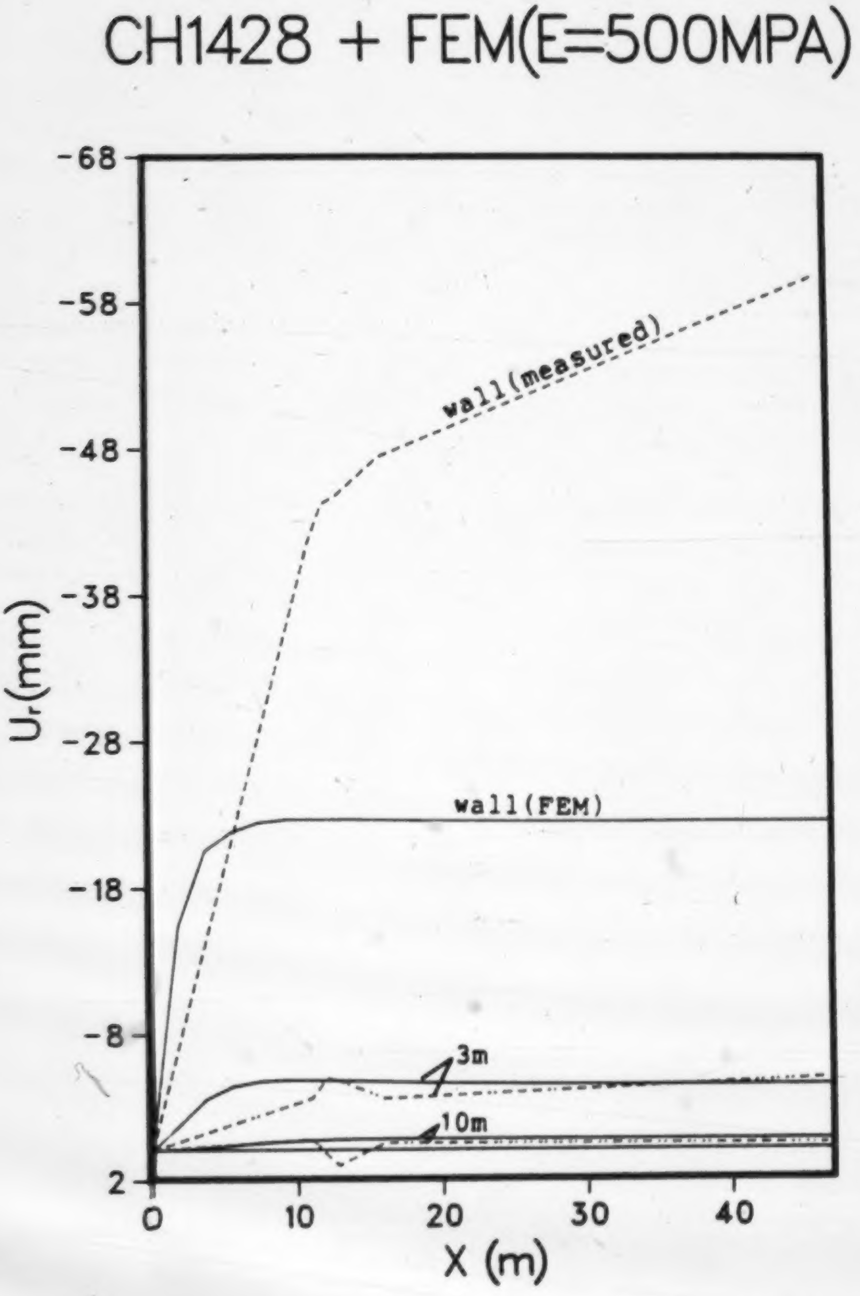

Figure 7.25 Measured and Predicted Radial Displacement Curves at Chainage 1428 m; Fitted at 3m from the Wall (E=0.5 GPa)

7.4 Multipoint Extensometer Records in Portal Sandstone

At Chainage 800 m, where the tunnel is contained in a thick sandstone layer, a horizontal rigid probe, multiple anchor extensometer, was placed in a borehole driven from Tunnel No.3 (see Figure 7.26). The instrument was placed far ahead of the tunnel face and the complete development of deformations along one line could be monitored as the tunnel advanced. In Figure 7.27, the results of the in situ dilatometer test performed at Chainage 805 m for the determination of the E modulus, are plotted against distance from tunnel wall. Within one radius from the tunnel wall, a stiff zone was detected with E values as high as 28 GPa, whereas further from the wall an almost constant modulus of about 10 GPa was found. Note that the profile depicted in Figure 7.27 indicates the presence of a weak zone or plane at 1.5 m from the wall of the tunnel. Any signs of a weakness could, however, not be detected in the borehole records at Chainage 800 m, where the extensometer is located.

7.4.1 Analysis of the Total Relative Displacements

The final radial displacements measured by this extensometer at the springline and at Chainage 800 m, installed three diameters ahead of the tunnel face, are plotted in Figure 7.28. Between 1.5 and 3 m from the tunnel wall a compression zone is found. A possible explanation of this phenomenon is given schematically in Figure 7.29 where

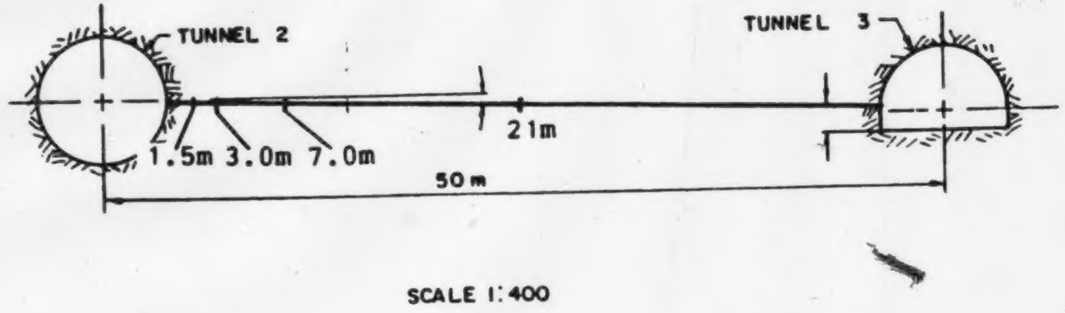
TUNNEL 2
TUNNEL 3
1.5m
3.0m
7.0m
21m
50 m
SCALE 1:400

Figure 7.26 Section Through Horizontal Extensometer Placed at Chainage 800 m (Modified After Yuen et al., 1985)

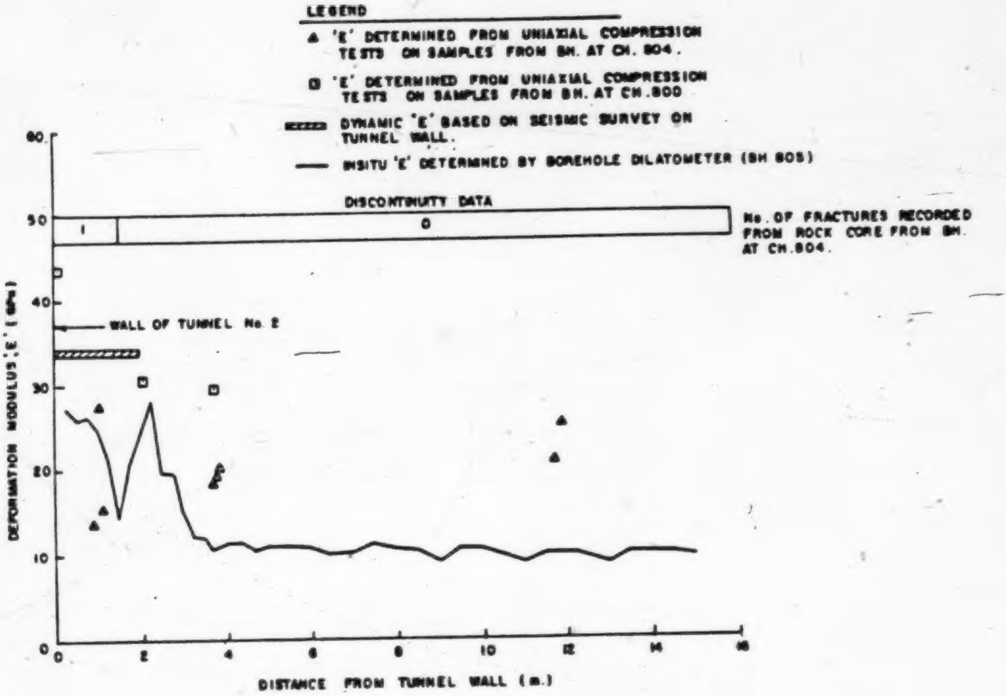

Figure 7.27 Results of In Situ Dilatometer Tests in the Sandstone at Chainage 800 m (Yuen et al., 1985)

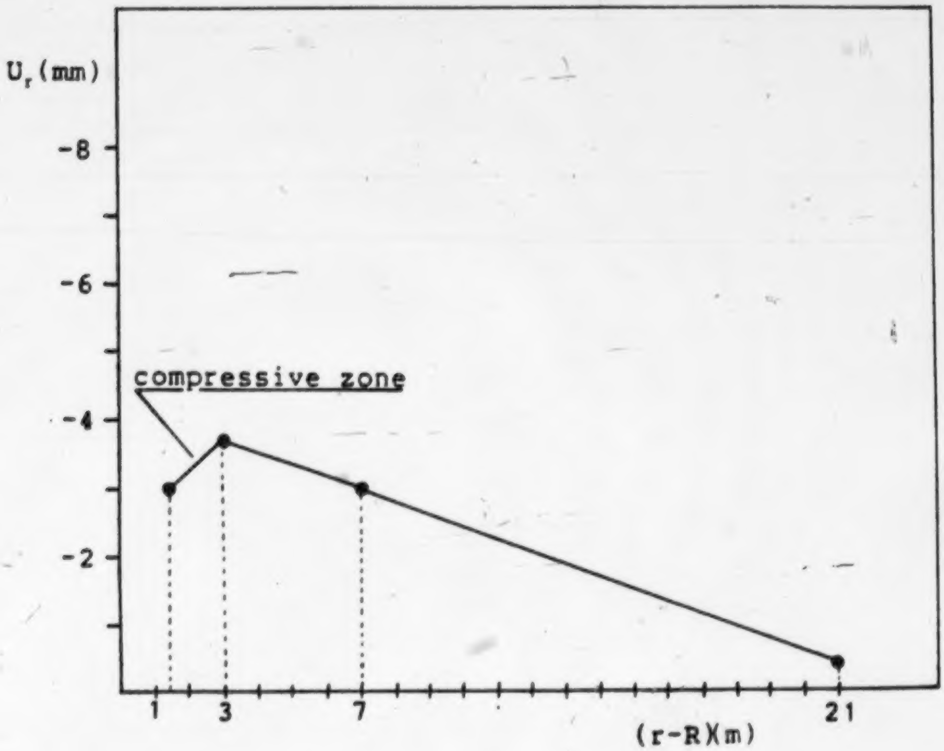

Figure 7.28 Radial Displacements Profile at Chainage 800 m

the effect of a thin stiff zone on the radial displacements around the tunnel is illustrated. Such a zone could be shaped differently and might be caused by a natural inhomogeneity or differential rock damage due to construction. After excavation, the stiff ring represented in the figure causes a localized constraining effect that limits the radial displacements. This effect is concentrated near the wall of the tunnel and vanishes far from it. Note the analogy with the compression zone found in proximity of the leading edge of the liner sections described in Chapter 6. In order to substantiate this hypothesis a finite element analysis was carried out where the conditions described in Figure 7.29 were modelled. A stiff ring 1.3 m long (along the axis of the tunnel) and 0.4 m thick, with a E modulus 1000 times higher than for the surrounding rock gave the radial displacement profile depicted in Figure 7.30. The extreme difference in elastic modulus was selected in order to prove the point that a stiff inclusion can actually generate a compressive zone at the tunnel wall. These results are only intended to provide a qualitative explanation of an otherwise inexplicable phenomenon and no attempt of matching quantitatively the field data was made. In Figure 7.30 the results of the numerical analysis are compared with the relative displacement profile calculated by the elasticity theory, without considering the effect of the stiff ring. Note that the stiff inclusion causes a reduction of the radial displacements everywhere along the

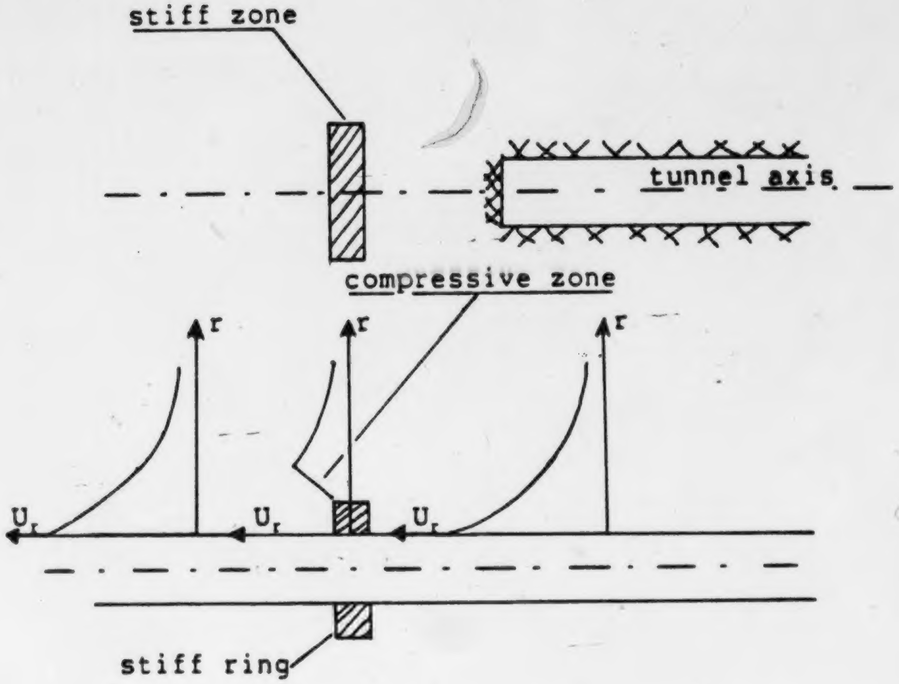
stiff zone
tunnel axis
compressive zone
r
r
r
U_r
U_r
U_r
stiff ring

Figure 7.29 Schematic Diagram for Explanation of Radial-Compressive Zone

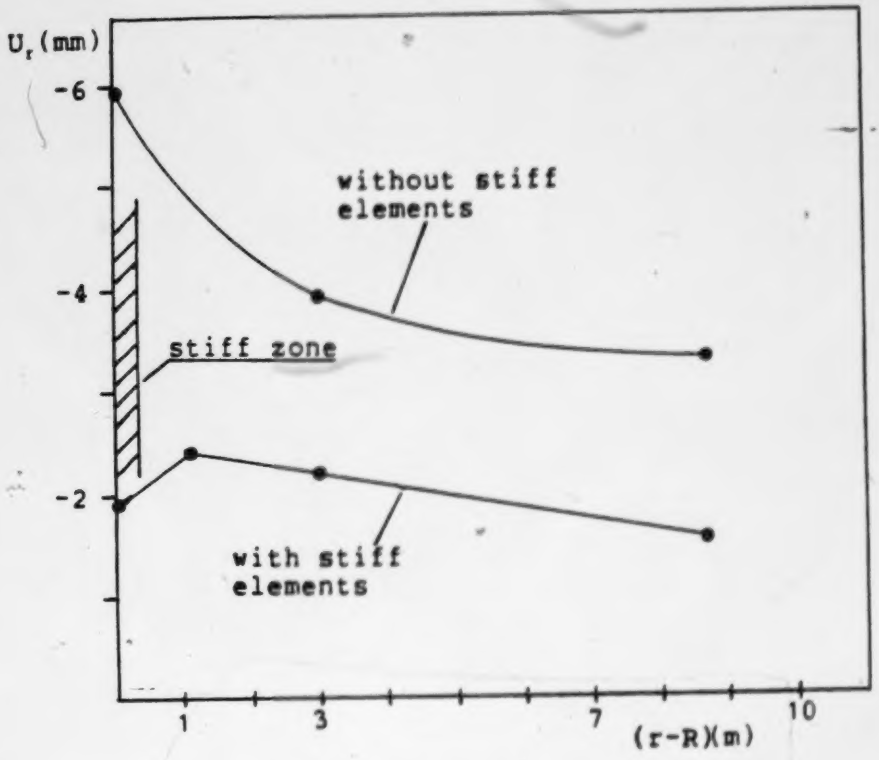

Figure 7.30 Relative Radial Displacement Profiles with and without Stiff Zone (Finite Element Analyses)

curve. In the real case the stiff zone is thicker and the ratio between the stiffness of the rock near and far from the wall is much less significant than for the numerical case. The numerical results obtained for the supported tunnels (Chapter 6) show that a relatively flexible ring, placed behind the tunnel face, is sufficient to generate some compressive radial strain in the surrounding rock. The geometry of the stiff zone, as well as soft pockets located near the excavation, may also play an important role in enhancing the compressive effect.

In an attempt to explain this relative compressive zone several other possibilities were examined and modelled by two and three dimensional finite element analyses. It was found that neither pre-existing soft zones nor weak, plastic zones located near the tunnel could have caused this phenomenon.

7.4.1.1 Back-Analysis of the Sandstone Elastic Modulus

The elastic modulus of the rock can be back-analyzed by comparing the radial displacement profile detected in the field to the displacements calculated by means of the elasticity theory. In Figure 7.31, the field data (solid line) are compared to the theoretical profiles (broken lines) calculated for E=10 and 6 GPa (without compression zone simulation). In order to allow this comparison, the calculated values have been obtained assuming a datum 42m away from the wall of the tunnel (location of the deepest anchor). It was observed earlier in this chapter

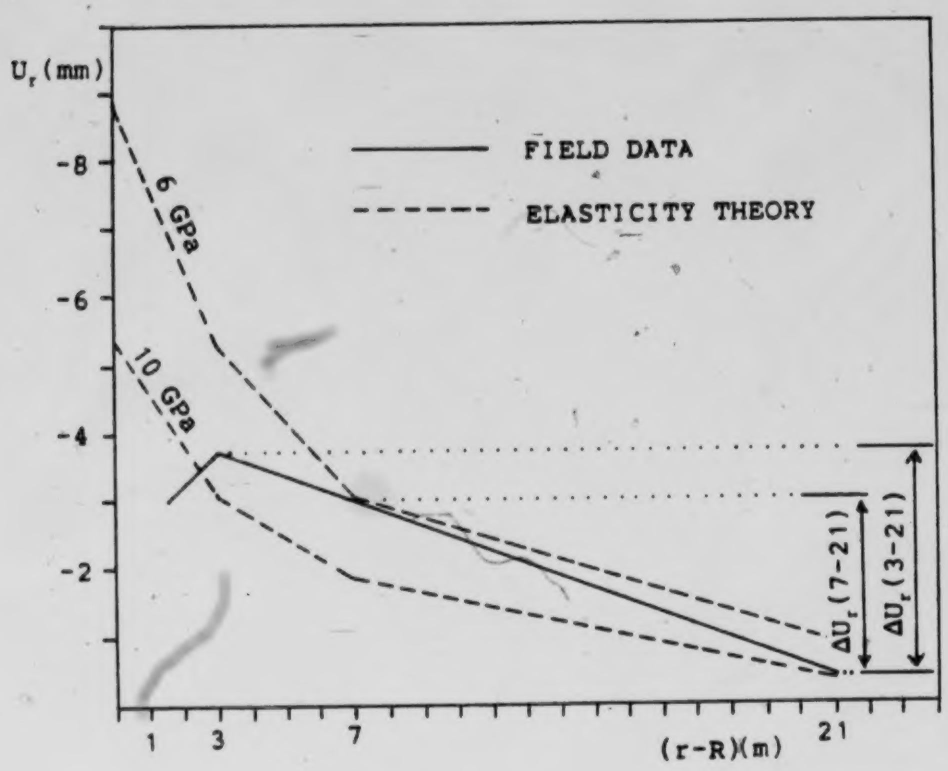

Figure 7.31 Comparison Between Relative Radial Displacements Measured in the Field (Total Values) and Calculated by the Finite Element Method

(Figure 7.30) that the stiff zone causes a decrease of the radial movement at any distances from the excavation. For this reason the calculated displacements (without stiff zone) should be larger than the measured values (with stiff zone). The solution with E=6 GPa represents an upper bound value for the rock mass, because it gives a theoretical profile just slightly displaced above the field data.

The differences between the displacements measured at 3 m and 21 m from the tunnel wall, $\Delta U_r(3-21)$ (Figure 7.31), and at 7 m and 21 m from the wall $\Delta U_r(7-21)$ (Figure 7.31), were also considered for comparison with the elastic theory. The relative displacement $\Delta U_r(3-21)$ can be matched by the elasticity theory if E=8 GPa is assumed, whereas E=5 GPa has to be assumed in order to obtain a relative displacement of the same magnitude of $\Delta U_r(7-21)$. The measurements obtained farther from the wall, where the lower modulus is calculated, are the more reliable because they are less affected by the compression zone.

A larger deformability, than the one predicted by the field tests, has been back-analyzed by means of monitoring data interpretation. This is reasonable because a 40,000 times larger volume of rock is mobilized by the tunnel excavation than by the dilatometer. If at least another set of measurements were available, at the tunnel crown, an assessment of the initial stress conditions could also be made. The considerations presented so far were based on the assumption that the rock does not exhibit significant non-linearity at any location around the tunnel. The reader should also remember that, at the tunnel springline for $K_0=2$, the shape of the relative displacement profiles was found to be relatively insensitive to the constitutive relationship adopted (Chapter 5).

7.4.2 Shape of the Radial Displacement Curves Ahead of the Tunnel Face

The shape of the radial displacement curves, recorded ahead of the tunnel face, will now be discussed as the numerical analyses showed that it may be useful for back-analysis purposes. The radial displacement profiles along the axis of the tunnel given by the extensometer at Chainage 800 m, are plotted in Figure 7.32. Within 10-15 m ahead of the tunnel face, a substantial change in the trend of the curve is observed. The rate of convergence first increases but then decreases as the excavation front approaches the instrumented section. This results in relatively small radial displacements at the tunnel face with respect to the final movement measured far behind the face. In Chapter 3, this particular behavior of the radial displacement curves was found to be related to high initial axial stresses. Furthermore in Chapter 4, it was observed that the orientation of the deformation properties of the rock also plays an important role. In particular, for low elastic modulus in the axial direction (Chapter 4, Case 3), little or even outward convergence could be detected at the

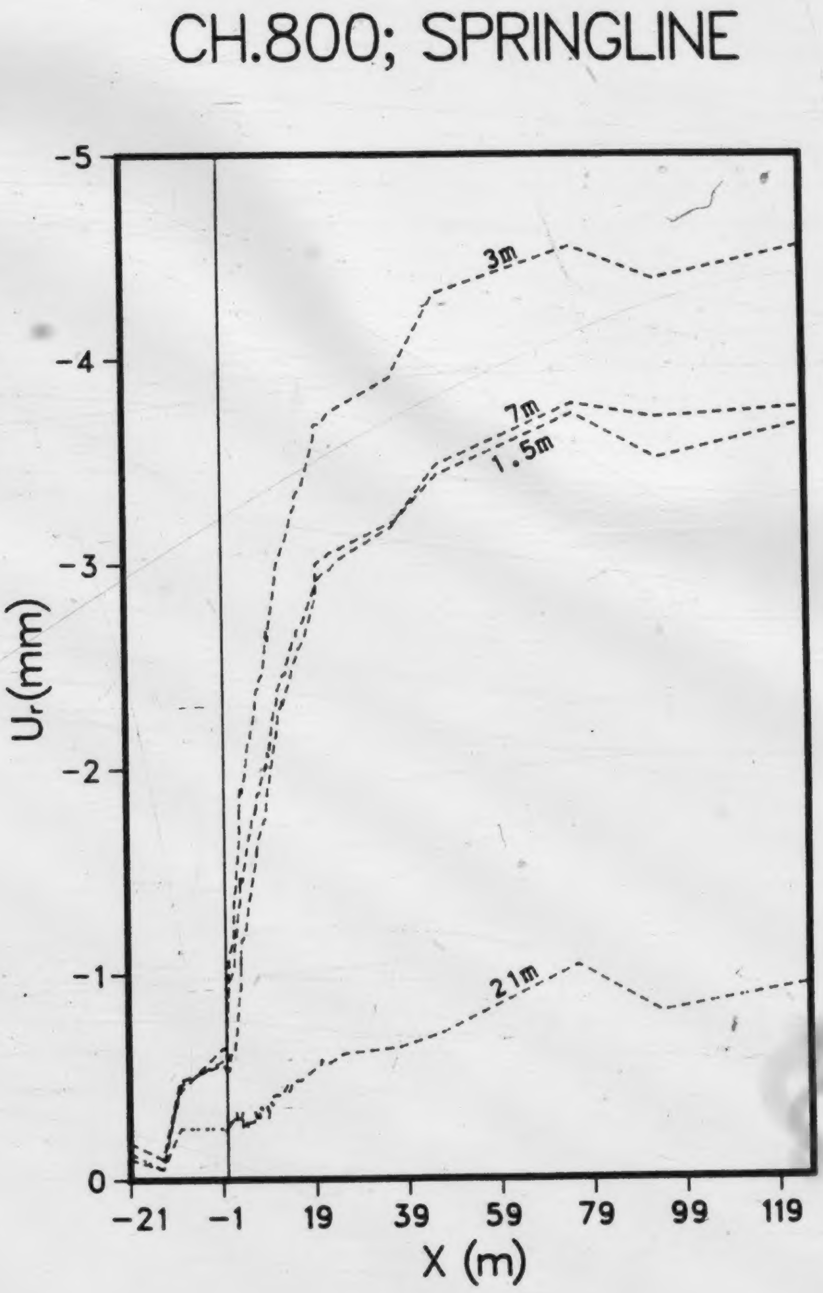

Figure 7.32 Radial Displacement Curves for Springline at Chainage 800 m

face, where a relatively large inward movement is found a few meters ahead of the excavation front. The behavior of the radial displacement curves seems to indicate a high initial axial stress value. However, this was not detected by the in situ stress measurements. On the other hand, the sandstone seems to be relatively isotropic with respect to the cases discussed in Chapter 4. A local inhomogeneity, such as a soft zone in the tunnel core, may have enhanced the effect of the axial stresses, released at the tunnel face during excavation, on the radial displacements near the face (see Chapter 3). A definite explanation for the observed displacement curves could not be found.

7.4.3 Analysis of the Radial Displacement Curves Behind the Tunnel Face

The radial displacement behind the tunnel face will now be analyzed. The purpose is to verify whether a reliable prediction of the rock deformability is possible if the displacements ahead of the tunnel face are unknown.

In Chapters 3 to 5 the effects of the ground properties on the shape of the radial displacement curves were discussed, and some of the earlier findings will now be used for the back-analysis of the elastic modulus of the rock mass.

In Figure 7.33, three convergence curves for tunnels in linear elastic, hyperbolic and elasto-plastic rock obtained by three dimensional finite element modelling, are compared.

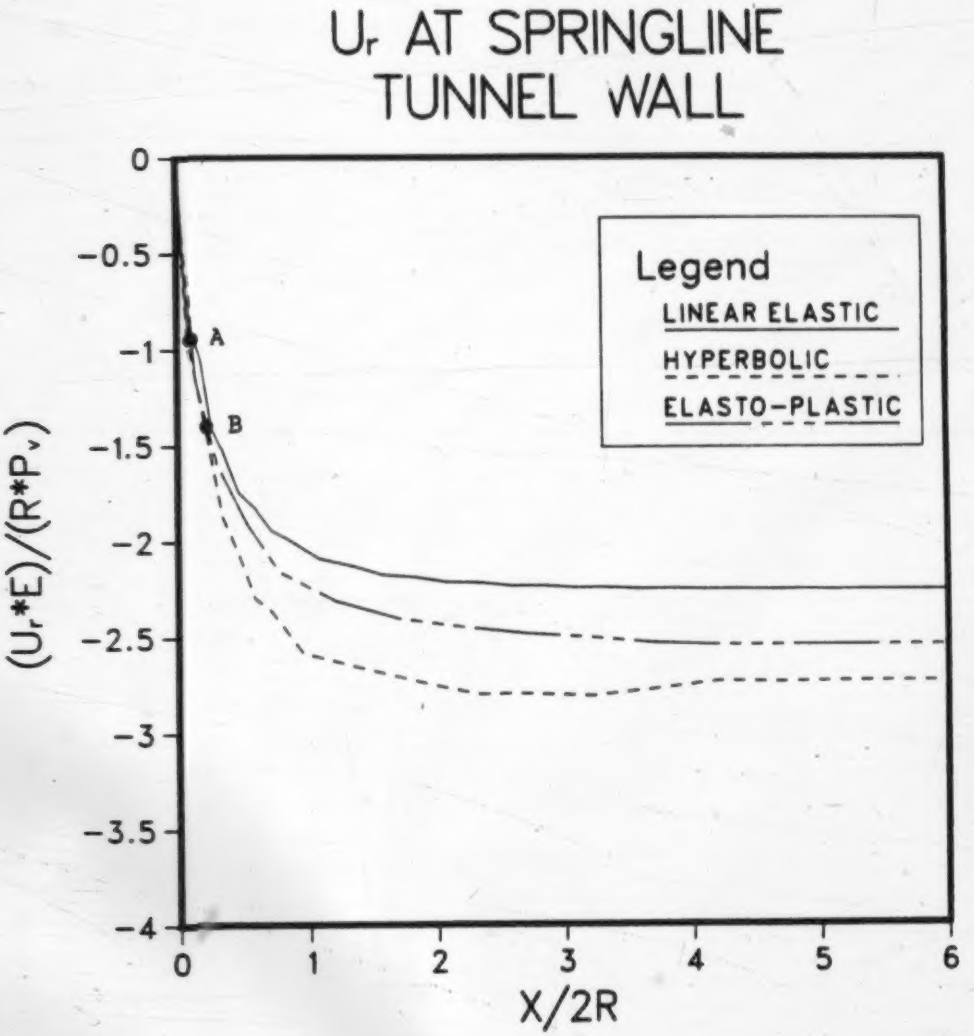

Figure 7.33 Convergence Curves for Tunnels in Linear Elastic, Hyperbolic and Elasto-Plastic Rock (FEM)

It can be observed that the curves are virtually identical up to about 0.2 radii behind the tunnel face (Point A in Figure 7.33) and very similar up to 0.45 radii behind the face (Point B). For these three cases, the elastic moduli (initial elastic modulus for the hyperbolic case) are the same, and major differences only occur relatively far behind the excavation front, where high deviatoric stresses develop. This observation leads to the conclusion that for cases where moderately non-linear behavior is exhibited by the rock mass, the shape of the initial part of the radial displacement curves can reveal the magnitude of the elastic modulus of the rock independent of the ultimate rock mass behavior.

The radial displacement profile, measured at 3 m from the wall of the tunnel, is compared, in Figure 7.34 with a curve calculated at the same location by a three dimensional finite element analysis. An elastic modulus of 10 GPa and an initial stress ratio K_0=2 were selected. The calculated curve gives an almost perfect match of the field data up to Point A (Figure 7.34), then the two profiles diverge towards different final displacements. The difference in radial displacements, detected far behind the face, is only in part a reflection of the difference in total radial movement (including displacements ahead of the face). It is also due to the fact that a considerable difference between the measured and predicted displacement at the face occurred. The final displacement should be corrected as shown in the

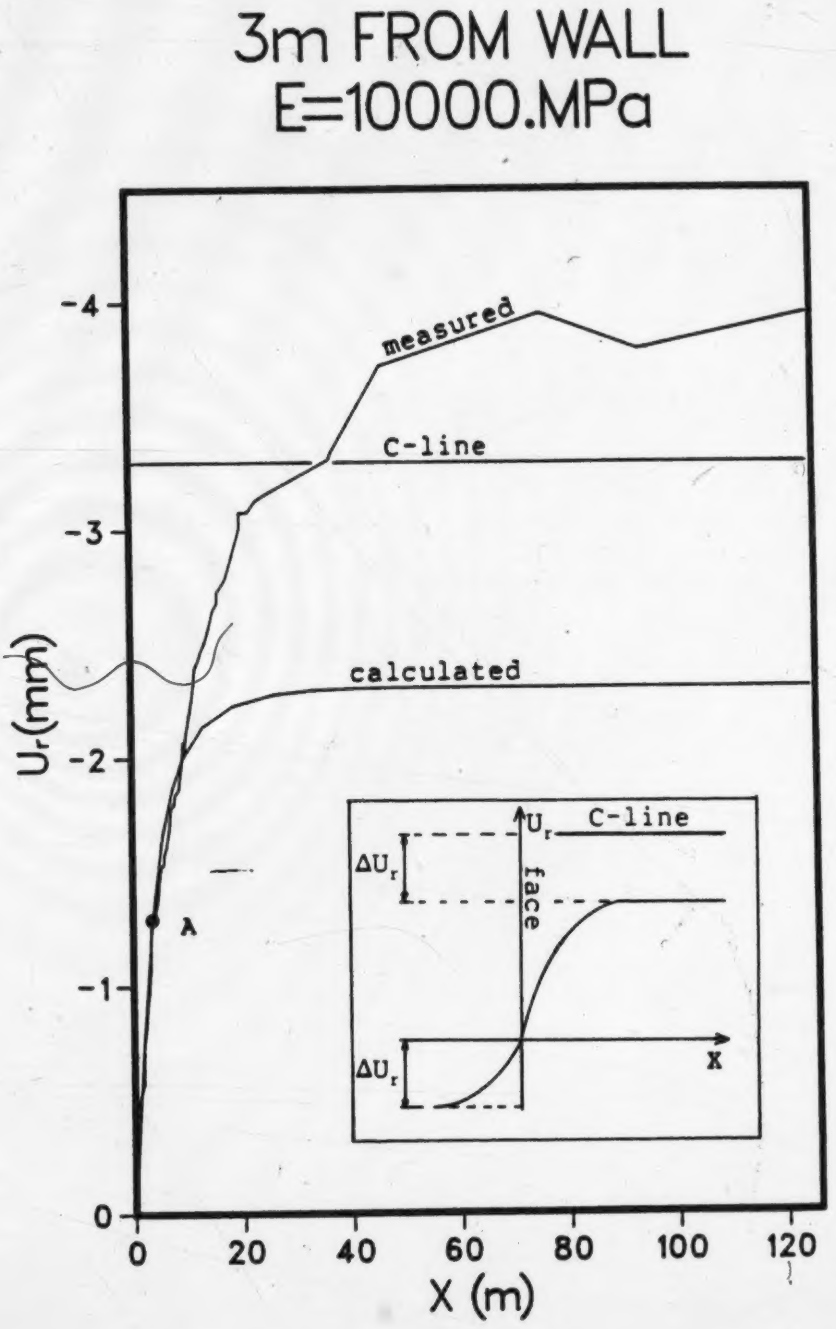

Figure 7.34 Radial Displacement Profile Measured at Three Meters from the Tunnel Wall Fitted by FEM (E=10 GPa); Chainage 800 m, Datum at 42 m from the Tunnel Wall)

figure (C-line) to account for the different trends of the two curves ahead of the face. The C-line was obtained by adding to the measured radial movement, far behind the face, the difference between calculated an measured displacements at the tunnel face (see inset in Figure 7.34). Note, however, that this correction can only be applied if the movement ahead of the face of the tunnel has been measured. The initial part of the curve, fitted by the numerical results, is assumed to be independent of the displacement at the face. This was proven to be correct, at least at the tunnel springline and for K_0=2, by the results presented in Chapter 3. In Figure 7.35, convergence curves for different axial stress (P_a) values are shown. The radial displacements at the tunnel face differ for each case. Near the face the curves have almost identical shape, even though they finally converge to different values.

The same fitting procedure was then applied to the curve at 7 m from the tunnel wall shown in Figure 7.36. For this case an E value of 7.5 GPa is needed to match the initial part of the curve. Consistent with what observed earlier in this chapter, a lower elastic modulus was found by considering measurements taken far from the wall of the tunnel (and far from the compressive zone). These results, however, are not in agreement with the analysis of the total displacements, that led to the conclusion that the elastic modulus of the rock mass should be lower than 6 GPa (see previous section).

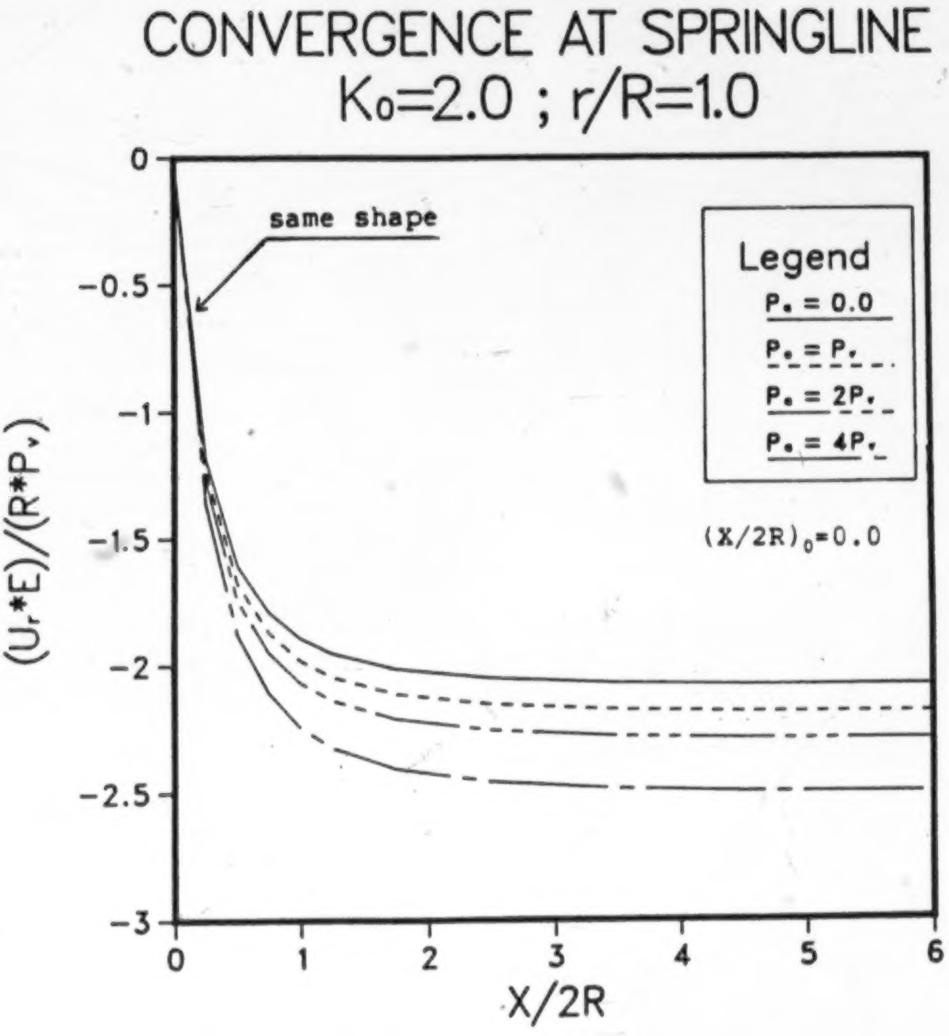

Figure 7.35 Convergence Curves Calculated for Various Axial Stresses (FEM) at the Tunnel Springline (K_0=2, $(X/2R)_0$=0.0)

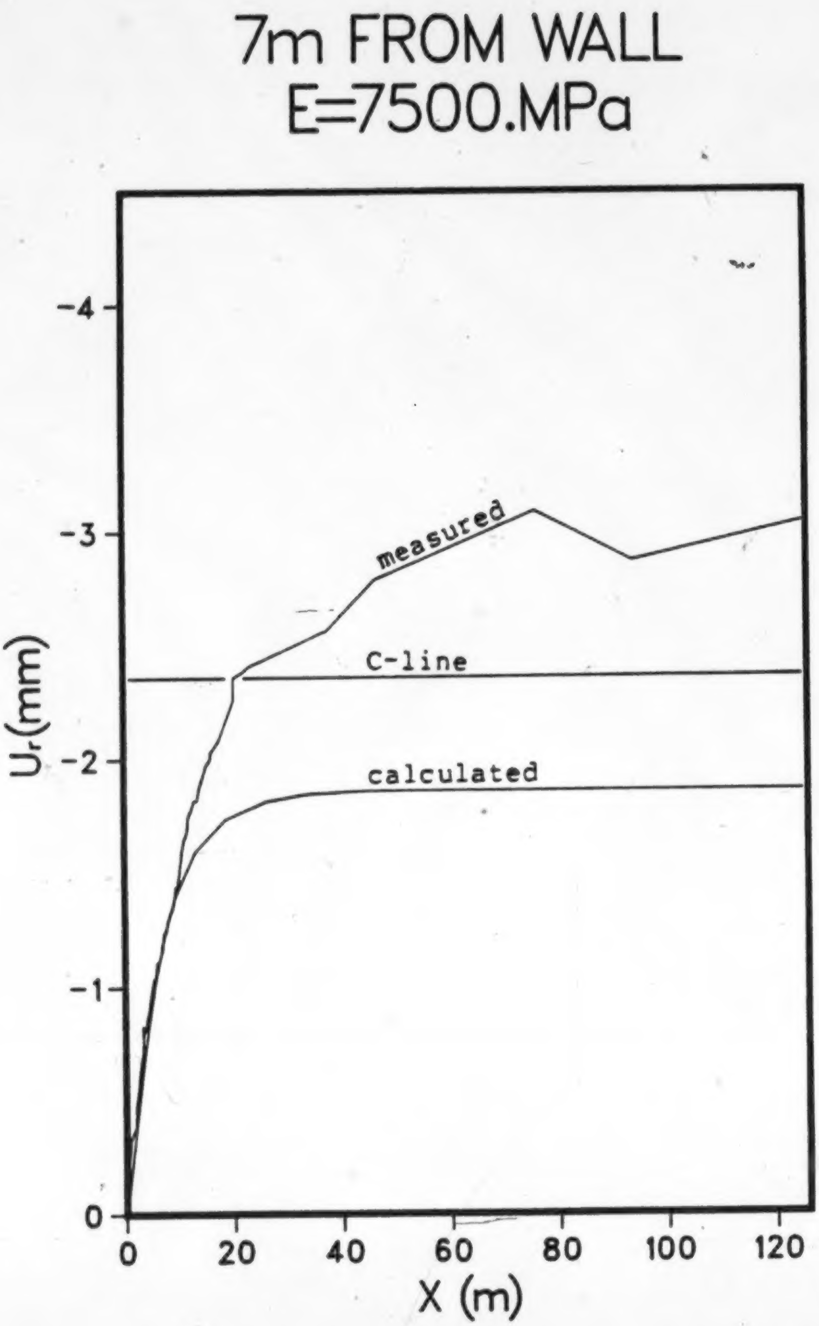

Figure 7.36 Radial Displacement Profiles Measured at 7m from the Tunnel Wall Fitted by FEM (E=7.5 GPa; Chainage 800 m; Datum at 42 m from the Tunnel Wall

Better agreement was achieved by subtracting the displacements measured at 21 m from the tunnel wall, from the displacements at 3 m and at 7 m from the wall, respectively. They are compared with calculated curves in Figure 7.37 and 7.38. In this manner, the measurements become independent from the location of the datum. For the measurements at 3 m from the wall, the same result found previously, E=10 GPa, is obtained. The rather high E value observed at this location is justified, due to the effect of the compressive zone detected near the wall of the tunnel (Figure 7.28). If the movement at the tunnel face is not known, because the extensometers have been placed behind the face, an overestimate of the non-elastic deformations may result.

The relative displacements between 7 m and 21 m from the tunnel wall, presented in Figure 7.38, give a profile that can be fitted by assuming E=5.75 GPa. These observations are consistent with the conclusions drawn earlier in this chapter, based on the analysis of the total radial displacements. The data back-calculated at 7 m from the wall are certainly the most reliable because it is relatively far from the compressive zone and hence less affected by local rock non-homogeneities. For this reason, a modulus of approximately 5 to 6 GPa is most likely appropriate for the sandstone. A certain amount of non-elastic deformation occurs and is visible for the two cases, as indicated in Figures 7.37 and 7.38.

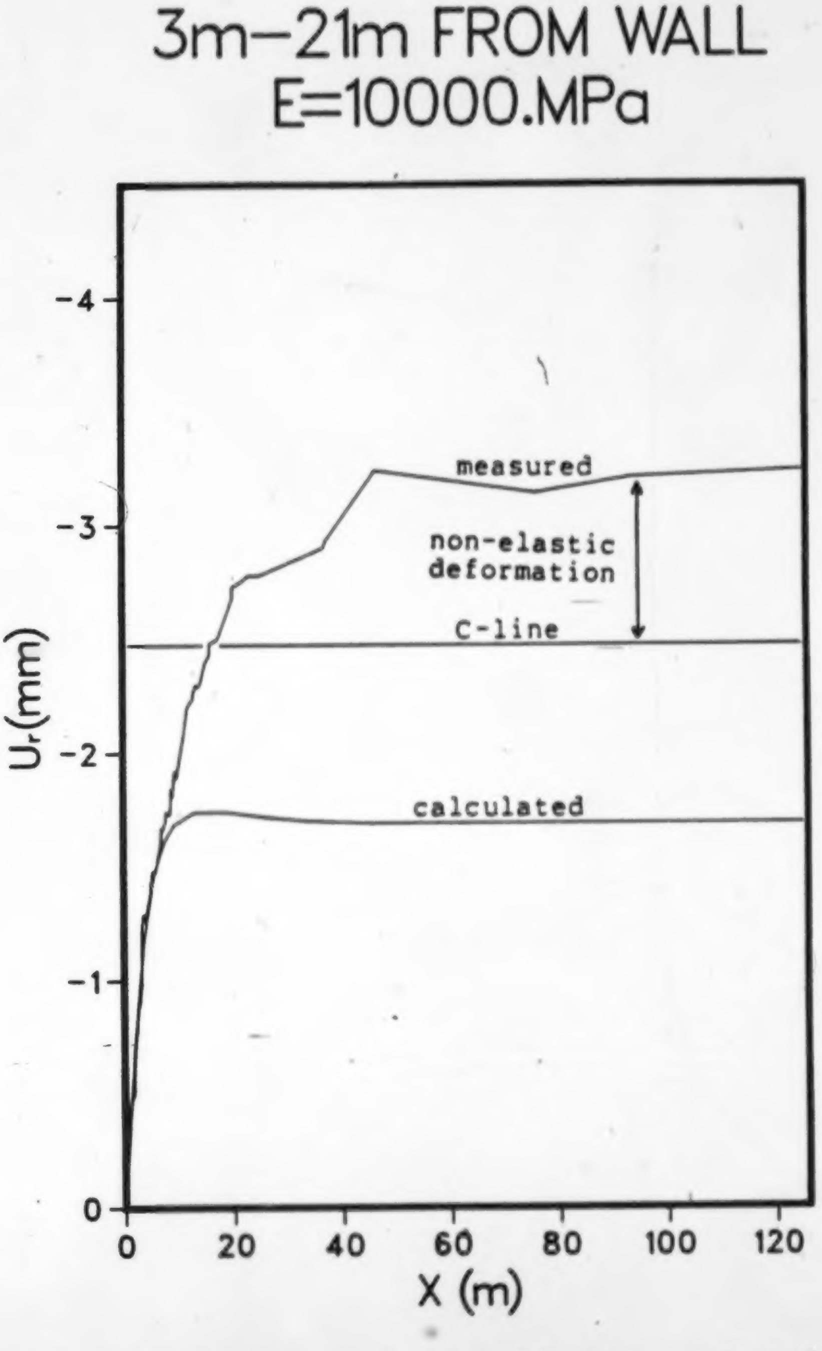

Figure 7.37 Radial Displacement Profiles Measured at 3m from the Tunnel Wall Fitted by FEM (E=10 GPa; Chainage 800 m; Datum at 21 m from Tunnel Wall)

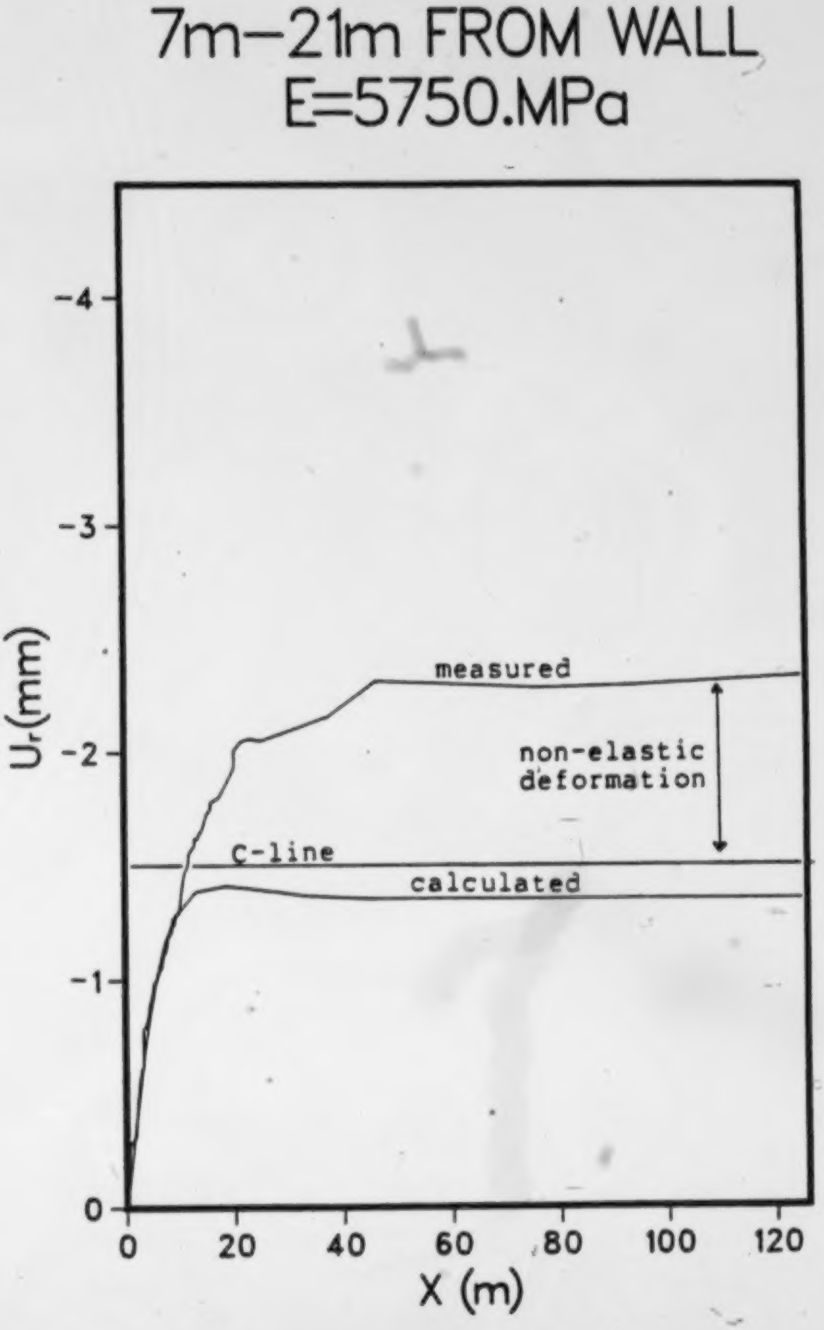

Figure 7.38 Radial Displacement Profiles Measured at 7m from the Tunnel Wall Fitted by FEM (E=5.75 GPa; Chainage 800 m; Datum at 21 m from Tunnel Wall)

Note that no attempt has been made to fit the full radial displacement curve by means of the finite element (elastic) results. The reason is that only the initial portion of the curve (near the face) reflects the elastic properties of the medium, whereas the displacements far behind the face are affected by yielding (Figure 7.33), initial stresses (Figure 7.35) and other factors influencing the displacements ahead of the tunnel face.

7.4.4 Prediction of the Radial Displacements by Curve Fitting

Another aspect that was revealed by the numerical analyses, was that the shape of the radial displacement curves is a valuable indicator for the determination of the rock mass properties. In particular, flatter displacement profiles are found if the rock exhibits a non-linear stress-strain relationship. The convergence curve can be fitted by means of the Ramberg-Osgoog function (described in Chapter 3) and, for equal initial gradient, the shape factor m can be used to quantify the difference in shape. In Figure 7.39, the radial displacement profile measured at 3 m from the tunnel face is compared with three Ramberg-Osgood curves, calculated for three different shape factors. The closest fit was obtained visually for m=1.2 whereas, for the linear elastic case, an m value of about 2 is appropriate. This indicates that the rock mass is affected by a certain amount of non-linearity and this is in agreement with the

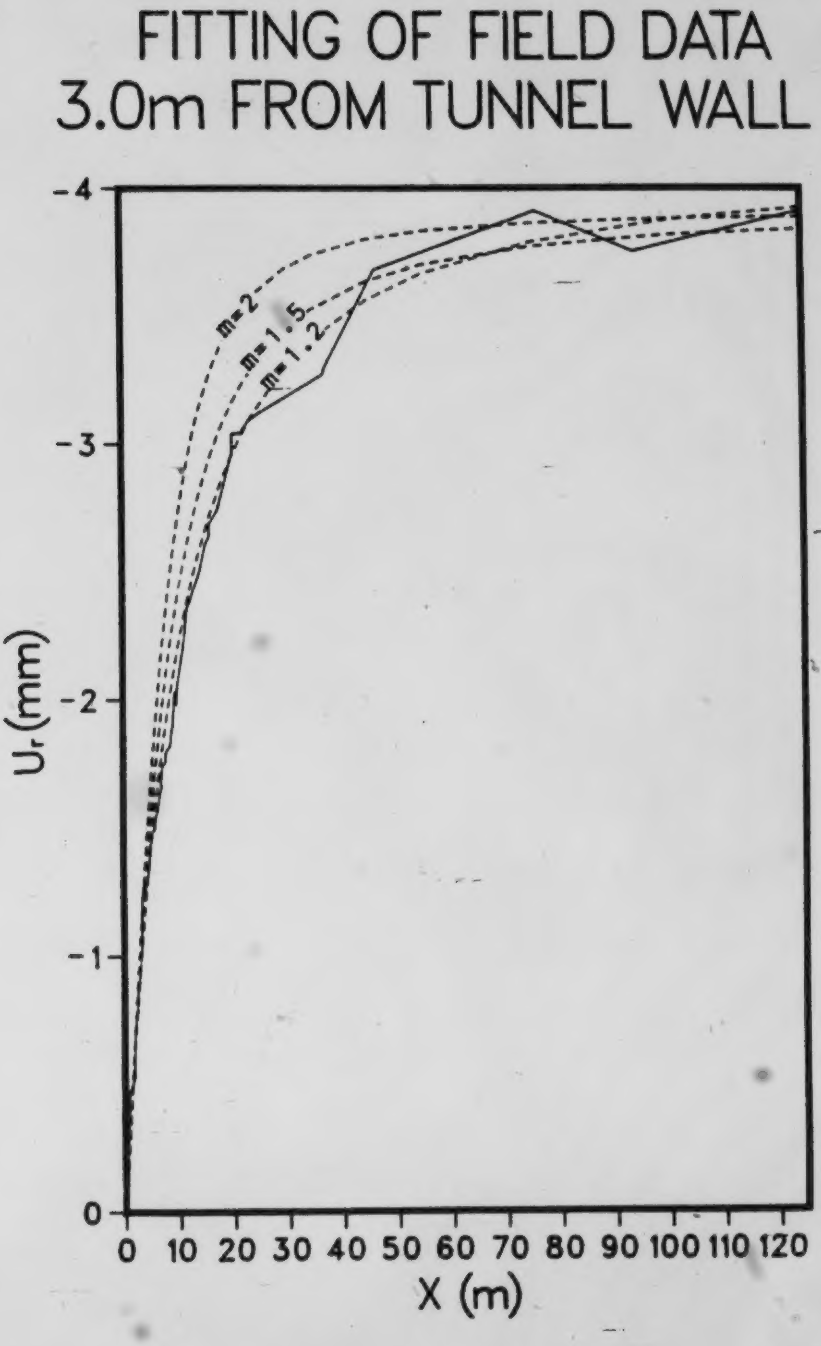

Figure 7.39 Fitting of the Radial Displacement Curve by the Ramberg-Osgood Function with Various m Values

detection of non-elastic deformations in Figures 7.37 and 7.38.

The properties of the Ramberg-Osgood function can also be used to predict the final radial displacement, based on the initial part of the curve, measured in proximity of the tunnel face. This feature can be very useful, because it may allow rapid evaluation of data, without waiting for the tunnel face to be far ahead of the instrumented section. A procedure presented by Desai and Wu (1976) may be used to determine U_0 and m (see Chapter 3), on the basis of the knowledge of the initial gradient and two other points on the curve. Desai and Wu (op.cit.) also provide a simple computer program to solve this problem by means of an iterative algorithm.

In Figure 7.40, the basic aspects of the procedure are illustrated. From the initial part of the curve, available from the measurements, the initial gradient S_i and the displacements measured at two distances from the tunnel face (e.g., mid-distance U_1 and latest measurement U_2) can be obtained. With this data, the full curve can be defined. The method was applied to the radial displacement profile measured at 3m from the wall in order to verify its ability to predict the radial movement, for various distances of the tunnel face from the instrumented section (Figure 7.41). Each curve was forced to pass through the last measurement available (farthest from the face) and an intermediate point. For instance, the first prediction was made assuming

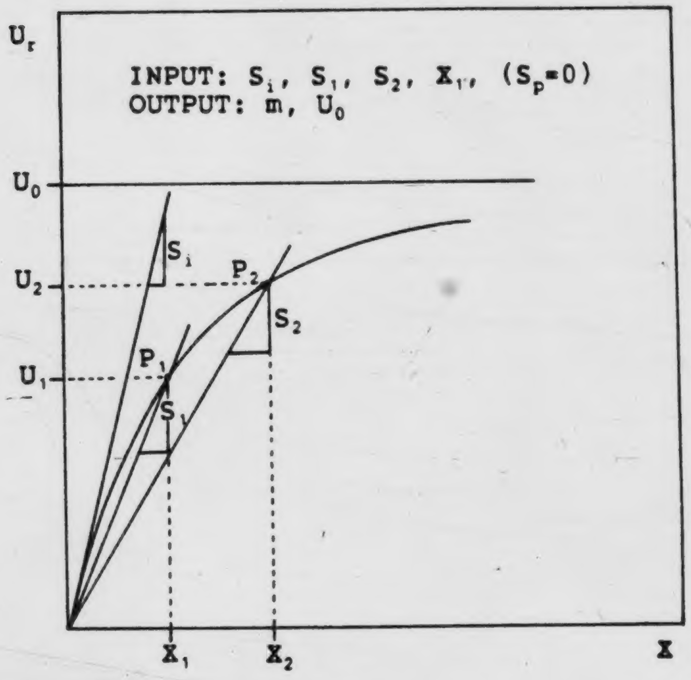
U_r
INPUT: S_i, S_1, S_2, X_1, $(S_p=0)$
OUTPUT: m, U_0
U_0
S_i
U_2
P_2
S_2
P_1
U_1
S_1
X_1
X_2
X

Figure 7.40 Definition of the Ramberg-Osgood Function by Initial Gradient and 2 Known Points

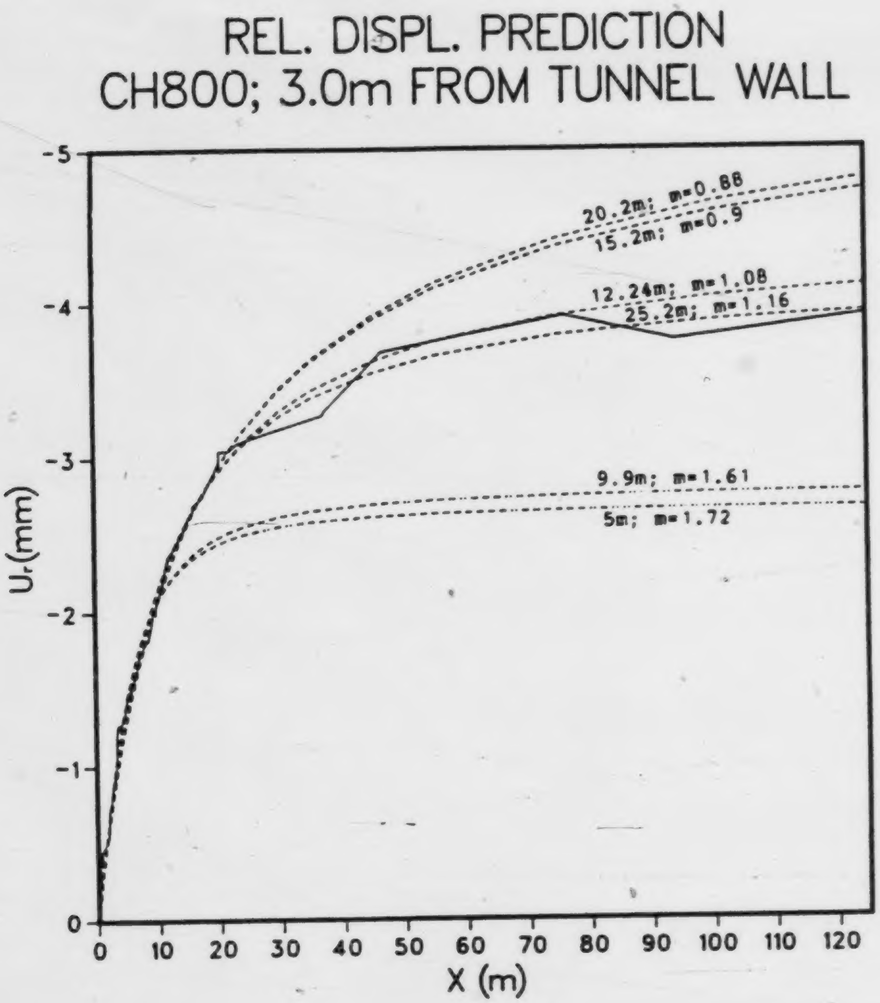

Figure 7.41 Prediction of the Radial Displacement Curve by Curve Fitting (Variable m)

the first 5m of the radial displacement curve to be known. The two points selected were at 2.5 and 5m from the tunnel face. When the face is at 5 or 10m from the instrumented section, relatively high values of m, not far from the values suitable for linear elastic conditions, are predicted. This is in agreement with the observation that the initial part of the curve reflects the elastic properties of the medium.

As the face of the tunnel continues to advance, the m value decreases, and at about 3 radii (12.24m) from the excavation front a good prediction of the final displacement is obtained. The gradual departure from the linear elastic conditions can be detected in this manner, as the excavation proceeds, by simply back-calculating m. This is of great practical value because it allows a rapid response to unexpected rock conditions. The m value characterizing the displacement profile can then be used for movement prediction in other similar tunnel sections by forcing the curve to pass through the latest measurements (see Figure 7.42). The results obtained by this procedure are shown in Figure 7.43, where it can be observed that a reasonable guess can be made based on the initial 12m of the curve if the m value is correctly predicted.

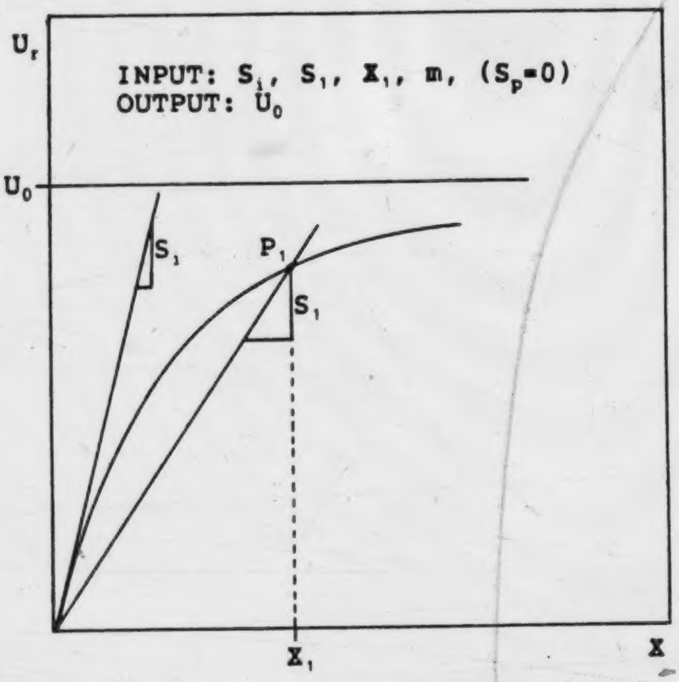
U_r
INPUT: S_i, S_1, X_1, m, (S_p=0)
OUTPUT: U_0
U_0
S_i
P_1
S_1
X_1
X

Figure 7.42 Definition of the Ramberg-Osgood Function by Initial Gradient, Shape Factor and One Known Point

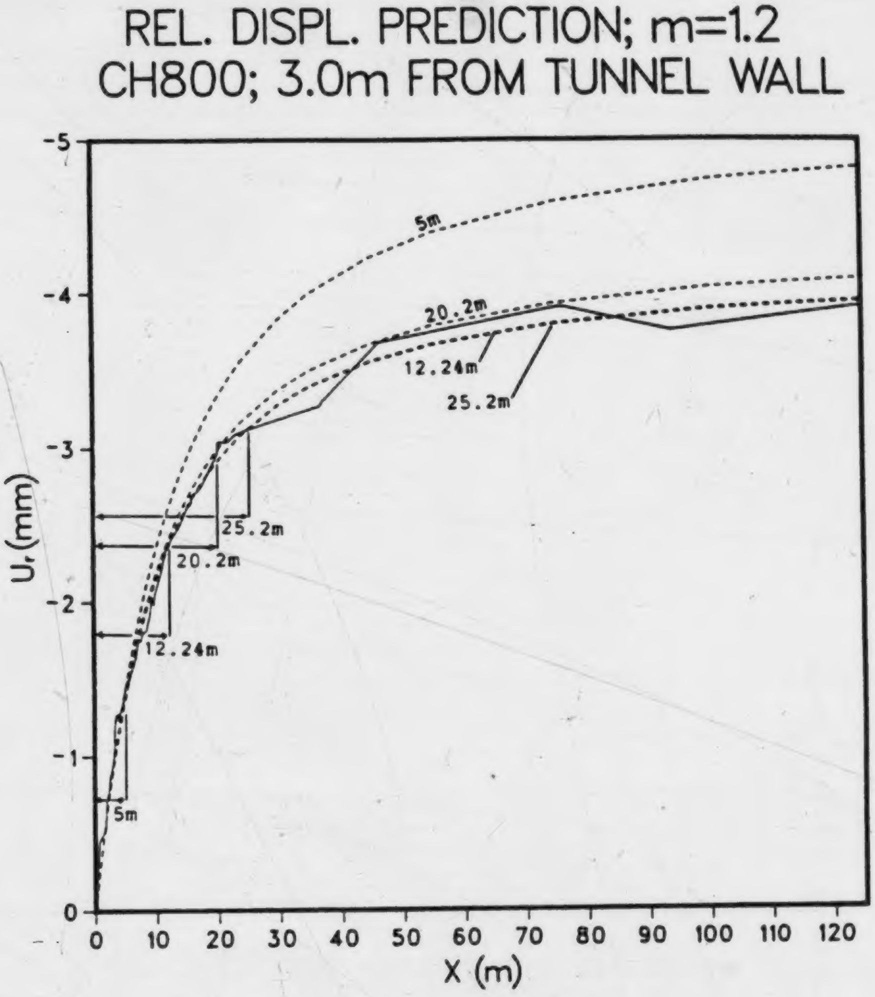

Figure 7.43 Prediction of the Radial Displacement Curve by Curve Fitting (Constant m)

7.5 Conclusions

In this chapter some of the monitoring data collected during the excavation of Tunnel No.2 at the Donkin-Morien project were discussed. Measurements taken at the tunnel crown in the mixed sediments, and at the tunnel springline in the Portal sandstone were analyzed.

Two major limitations of this monitoring and testing program were detected:

1) The stress measurements were limited to a single location, and because of technical problems during testing, an accurate assessment of the in situ stresses was not provided; and

2) Only one extensometer was installed for each instrumented section, most of the times at the tunnel crown.

The initial stress field must be known to a good degree of accuracy because it is a crucial factor in the back-analysis process. This is particularly important if only one extensometer is installed at a certain section, especially if it is located at the crown (direction of the minimum initial stress). A number of at least two (crown and springline), possibly four measurements (in the directions of the maximum and minimum principal stresses) should be taken at each section. This would reduce the degree of uncertainty in the back-analysis process by allowing comparison at different locations, and would also permit an assessment of the initial stress field. Measurements taken all around the cross section would also lead to a better understanding of the effects of local rock inhomogeneities.

For the analysis of Tunnel No.2, a $K_0=2$ was assumed, as it is in reasonable agreement with the field stress measurements provided. The back-analysis of rock strength and deformability in the mixed sediments (measurements taken at the crown of the tunnel, behind the face) led to reasonable values. Lower strength and higher deformabilities than predicted by the laboratory tests were found. The following conclusions can be drawn:

1) If the distance from the tunnel face at which failure takes place is detected by the field instrumentation and the initial stress field is known, the uniaxial compressive strength of the rock mass can be back-calculated. If the constitutive relationship of the rock does not exhibit significant non-linearity in the pre-peak range, the principal stresses at failure can be calculated by three dimensional finite element analyses, based on the assumption of linear elastic rock behavior.

2) The elastic modulus of the rock should be calculated by fitting the results of the three dimensional numerical analysis, based on the assumption of linear elastic behavior, to a measurement taken in the elastic zone, as close as possible to the plastic zone boundary. This value constitutes an upper bound value of the real elastic modulus. Again, an implicit assumption of linear-elastic behavior of the rock mass in the pre-peak range is made.

3) The fact that only the final measurements were available, because the shield of the TBM did not allow readings to be taken within one diameter from the face, was certainly a major limitation of this monitoring program. The shape of the displacement profiles could not be analyzed and, for some cases, the location at which failure occurred could not be detected.

The measurement taken at Chainage 800 m, in the Portal sandstone, gave the complete picture of the deformation field. In this section a compressive zone, probably due to a thin zone of stiff rock encountered by the tunnel was observed. Small displacements were detected at the face, perhaps due to high initial axial stresses, associated to a local rock non-homogeneity in proximity of the instrumented section. Based on the analysis of the final total and partial displacements, and on the shape of the displacement profiles, a value of approximately 5-6 GPa was calculated for the rock mass (note: E=10 GPa was measured by field testing). The following conclusions can be drawn:

1) The initial part (near the face) of the convergence curve reflects the elastic properties of the medium even if a moderate amount of non-linearity characterizes the rock deformability.

2) Fitting the complete radial displacement curve (as done by Yuen et al., 1985) with the results of the numerical results did not prove to be very helpful in the back-analysis process. Fitting the curve immediately behind

the tunnel face, can instead reveal the elastic modulus of the rock mass.

3) Partial movements, measured immediately behind the tunnel face, can result in reasonable predictions of the elastic modulus. On the other hand, the amount of non-linear deformation can be significantly overestimated (or underestimated) because these readings are profoundly affected by the magnitude of the displacements ahead of the tunnel face (unknown for many cases).

4) Early detection of non-linearity in the rock mass, and early prediction of final radial displacements was proven to be possible by simple curve fitting of the radial displacement profiles. The parameter m of the Ramberg-Osgood function was found useful for defining the shape of the curves and for detecting non-linear rock mass behavior.

8. Conclusions and Recommendations

8.1 Introduction

A series of three dimensional finite element analyses were carried out in order to investigate the effects of initial stresses, rock behavior and support conditions on the near tunnel face stresses and deformations in the rock, the loads on the tunnel support, and on various types of measurements taken during face advance. Unlined tunnels in rock exhibiting linear elastic isotropic, anisotropic and non-linear stress-strain relationships were considered, whereas the study of lined tunnels was restricted to linear elastic conditions, for both rock (isotropic and anisotropic) and support (isotropic). For most analyses, an initial stress ratio $K_0=2$ was adopted (if not specified otherwise). Finally, a back-analysis of monitoring data collected in Tunnel No.2 at the Donkin-Morien project was carried out.

8.2 Unsupported Tunnels

The main objective of this part of the research was to provide information useful for monitoring data interpretation. In particular, convergence and relative displacement measurements (as given by multipoint radial extensometers) were investigated and the conclusions of this study are summarized in the following sections.

8.2.1 Effects of Zero Reading Delays

In deep tunnels convergence and radial displacement measurements are usually started behind the tunnel face. The results of this research showed that the measurements heavily depend on the distance from the face at which the instruments are installed. Even a small delay may have a substantial influence on the monitored displacement values because of the high convergence gradient at the excavation front. This effect is particularly pronounced in the direction of the minimum radial stress (tunnel crown for $K_0=2$). At this location some outward movement may be recorded if a low axial stress, P_a, characterizes the initial stress field, and if the instrument is installed one radius behind the tunnel face. The sensitivity of the radial displacement measurements to the distance from the tunnel face at which the zero readings are taken, may be further increased if the material is anisotropic and the minimum elastic modulus controls deformations in the axial directions. This can be especially the case of tunnels excavated with the axis normal to the planes of lamination or stratification. Measurements must be started immediately behind the tunnel face, if monitoring ahead of the excavation front is not possible. Frequent readings should be taken initially, otherwise no conclusive data interpretation is possible.

8.2.2 Effects of Initial Stress Distribution

The magnitude of the initial axial stress P_a, may considerably affect the measurements taken by instruments installed behind the tunnel face, in the direction of the minimum initial stress (tunnel crown for $K_0=2$). If not considered during monitoring data interpretation, a high P_a value (relative to P_v and P_h) may lead to an underestimate of the rock deformation modulus, where an overestimate may occur if the real P_a is smaller than the assumed. The initial stress field should be carefully measured and, in particular, its axial component should be assessed within a reasonable degree of accuracy. The high sensitivity to P_a of the measurements taken at the tunnel crown, on the other hand, suggests that monitoring should never be restricted to that location only.

It was also observed that similar effects on the displacements around the excavation, as induced by initial stress distribution, are created by the orientation of the medium elastic properties. If a significant degree of ground anisotropy is expected, a sound knowledge of the initial stress field is particularly important to permit an effective back-analysis of the anisotropic rock properties.

8.2.3 Shape of the Relative Displacement Profiles (U_r vs r)

A relative displacement profile is obtained by plotting the radial displacements measured by a multipoint radial extensometer, against the distance from the tunnel wall at which each measurement has been taken. The shape of the relative displacement profiles in the direction of the minimum radial stress (tunnel crown for K_0=2), was found to be useful in detecting the orientation of the ground's elastic properties as well as non-linear rock behavior. Relatively flat curves, with large displacements measured far from the tunnel wall, were detected when the maximum elastic modulus was assumed to control deformations along the tunnel axis (i.e., axis parallel to strata). On the other hand, if the rock mass exhibits a non-linear constitutive relationship, the relative displacement curve at the crown becomes steeper than for the linear elastic case, and the movement concentrates near the tunnel wall.

The shape of the relative displacement profiles calculated at the tunnel springline (direction of the maximum initial stress, normal to the tunnel axis) was found to be relatively unaffected by the non-linear stress-strain behavior of the rock. Therefore these data can be used to back-analyze the elastic deformation properties of the rock, even for cases where a moderate amount of yielding takes place.

8.2.4 Shape of the Radial Displacement Curves (U$_r$ vs X)

The shape of the radial displacement curves also depends on the material properties of the rock. Low ratios between the shear modulus in the axial planes, G, and the elastic modulus in the radial direction, E, lead to steep displacement profiles, where relatively flat curves are associated to high G/E ratios. For non-linear rock behavior flatter curves than for the linear elastic case were detected, especially at the tunnel crown where most yielding occurred. The shape factor m (Desai and Wu, 1976) was found to be helpful in defining the shape of the curves for cases characterized by similar initial gradients. The initial part of the curves, monitored at the tunnel springline, showed to be almost unaffected by a moderate amount of yielding and by the magnitude of the initial axial stress P_a. This suggests that the shape of the displacement profiles, near the face of the tunnel, can reveal the elastic modulus of the medium even in moderately yielding ground. Since the shape of the radial convergence curves immediately behind the tunnel face is only function of the elastic modulus, plotting the normalized convergence rate, as suggested by Barlow and Kaiser (1987), could be a good indicator of yielding.

If the whole radial displacement curve is known, non-linearity can be detected by back-analyzing a fictitious elastic modulus based on the portion of data monitored ahead of the face. The final movement, far behind the excavation front, can be compared with the elastic solution based on such a Young's modulus. Consistency is found only if the rock behaves as a linear elastic medium.

8.3 Supported Tunnels

A series of three dimensional finite element analyses were carried out in order to investigate the rock-liner interaction near the tunnel face and its effects on monitoring data and loads on the support. The relative stiffness of the liner, the delay of support installation (DEL) and the excavation round length (RL) were varied and non-isotropic rock conditions were also considered. the initial stress ratio was maintained constant (K_0=2).

8.3.1 Effects on Monitoring Data

If the stiffness of the liner is low relative to the stiffness of the ground, as expected for most primary liners in rock, the radial displacements ahead of the face of the tunnel are virtually unaffected by the support. For this reason, if measurements of the movement occurring ahead of the face are available, they can be regarded as useful back-analysis tools.

A zone of compressive radial strain may be detected at the tunnel wall due to the confinement action of the support. This feature is more apparent if the liner is stiff and placed near the tunnel face. Measurements taken by radial multipoint extensometers can be considerably affected by this compressive zone, that is often detected in field. At the tunnel springline (direction of the maximum initial stress for K_0=2), the shape of the relative displacement profiles is not much affected by the action of the liner, except for the compressive zone occurring at the back of the support. It is then concluded that, at this location, relative displacements taken at sufficient distance from the wall of the tunnel can be most useful for back-analysis purposes.

8.3.2 Loads on the Support

As expected the thrust forces and the bending moments in the liner were found to depend on the compressibility ratio C and on the flexibility ratio F.

Increasing the delay from the face at which the liner is installed, leads to a decrease in both the thrust and bending moments in the support. The 2-D closed form solution given by Einstein and Schwartz (1979) was shown to be conservative when compared with more realistic 3-D models. This was also expected as the assumption of liner application far ahead of the excavation face (i.e., zero radial displacement at the time when the liner is installed) is implicit in the two dimensional approach. The safety margin associated with the use of the analytical, simplified solution, depends on the relative stiffness, the delay and the excavation round length.

Most of the load tends to concentrate at the leading edges of the liner sections. Smaller excavation round lengths result in more homogeneous load distribution on the support and consequently in better ground control and relatively moderate stresses in the liner.

If the tunnel is driven in transverse isotropic rock, the location of the maximum thrust force and the magnitude of the maximum bending moment heavily depend on the orientation of the rock elastic properties. If the tunnel axis is normal to the strata, relatively low loads are detected in the liner.

8.4 Back-Analysis of Field Data

The monitoring data collected during the excavation of Tunnel No.2 at the Donkin-Morien project (Cape Breton Island, Nova Scotia) were analyzed by comparison with the results obtained by the finite element method. The tunnel was assumed to be unlined because the support was very flexible and installed far behind the face.

The time dependent behavior of the rock mass was not considered in the present study.

8.4.1 Multipoint Extensometer Records

The measurements at the tunnel crown, taken by means of radial multipoint extensometers, where used in order to back-analyze the strength and the elastic modulus of the rock mass in the relatively weak mixed sediments. The strength back-analysis gave very reasonable results, indicating, in agreement with field observations, a very good quality rock mass. It was also shown that a relatively soft coal seam in the proximity of the tunnel wall may have generated stress concentrations that resulted in early failure of the rock mass (near the tunnel face). The analysis also showed that, consistently with the laboratory data, the siltstone has higher strength than the interbedded siltstone-mudstone.

The ratio between the uniaxial compressive strength of the rock measured in the laboratory, σ_c (mean value), and the uniaxial compressive strength of the rock mass back-calculated from the field measurements, σ_{cm}, was found to be approximately 2.2. This value is reasonable for the very good quality rock mass encountered at the Donkin-Morien project.

The results of the finite element analyses, conducted by assuming the rock to be linear elastic, were furthermore used to back-calculate the elastic modulus of the rock mass, by comparison with measurements taken in the elastic zone, as close as possible to the plastic zone boundary. Higher deformabilities than predicted by the laboratory tests resulted, and the siltstone, as expected, was found to be stiffer than the interbedded siltstone mudstone. The ratio between the elastic modulus values measured in the laboratory (mean value) and back-calculated from the monitoring data was approximately 2.0 for the siltstone and 5.5 for the interbedded siltstone-mudstone. This values are in agreement with Heuze(1980)

The elastic modulus of the Portal sandstone was also investigated at Chainage 800 m, where a radial multipoint extensometer was installed at the springline, far ahead of the tunnel face. The analysis of the total and partial relative displacement profiles and of the shape of the radial displacement curves resulted in consistent E values. The ratio between the elastic modulus values measured in the laboratory (mean value) and back-calculated from the monitoring data was approximately 5.5. The elastic modulus measured in the field (average) was found to be approximately three times larger than the back-calculated value. This values are in agreement with Heuze(1980)

This indicates that the elastic modulus of the rock mass can be back-analyzed, on the basis of measurements taken at the back of the face, if the shape of the radial displacement curve is available. The amount of non-elastic deformations detected in these conditions, however, may be grossly overestimated if the displacements at the tunnel face are not predicted accurately (or measured).

Early detection of non-linearity in the rock mass as well as prediction of final radial displacements was proven to be possible by simple curve fitting of the initial part (0 to 3R from the tunnel face) of the radial displacement profiles. The parameter m of the Ramberg-Osgood function was found useful for defining the shape of the curves and for detecting non-linear rock mass behavior.

8.4.2 Recommendations for Monitoring Programs

The interpretation of the monitoring program at the Donkin-Morien project was affected by some limitations without which more reliable information could have been extracted by the back-analysis process:

1) The initial stress field was not known with sufficient accuracy. Stress measurements should provide the complete stress tensor, relatively far from the wall of the tunnel and should possibly be taken at various locations along the tunnel axis. The magnitude of the initial axial stress P_a should be carefully defined if the displacements ahead of the tunnel face are unknown.

2) Only one extensometer was placed at each instrumented section where at least two (crown and springline) possibly four (crown, invert and springlines) should have been installed. This would have allowed an assessment of the initial stress field and a better understanding of the effects of local inhomogeneities.

3) Where the flexible probe extensometers provided a sufficient anchor density near the wall of the tunnel, poorer results were obtained with rigid probe extensometers, equipped with only three anchors. This problem should be avoided in the future for a more efficient back-analyses process.

4) The shape of the curves for the instruments installed at the crown was not available within one diameter from the tunnel face. This limits the amount of information that can be extracted from the measurements and should also be avoided. The use of devices allowing remote reading of the instruments should be considered in order to overcome

accessibility problems.

In summary, it was found that the monitoring program at Donkin-Morien was not well laid out for optimal data interpretation. Hence, conclusions that can be drawn from this case history will always be limited. It must, however, be pointed out that a much more extensive monitoring program would have been needed for more succesful data interpretation. The required funds, unfortunately, may not have been avalaible at that time.

8.5 Recommendations for Further Research

Further research should be devoted to the investigation of more complex constitutive relationships for both rock and support. In particular, the post-peak weakening behavior of the rock mass should be accounted for as it affects the propagation of yielding around the tunnels. The interface rock-support should be modelled by means of proper interface elements as the full bonding assumption may not be realistic for many practical cases. The effects of rock inhomogeneities on field measurements and support loads should also be object of investigation.

BIBLIOGRAPHY

Abel, J. F., and Lee, F. T. 1973. Stress changes ahead of an advancing tunnel. International Journal of Rock Mechanics and Mining Science and Geomechanics Abstracts, 10(6), pp. 673-698.

Aston, T. R. C. 1987. Personal comunication, during visit at the University of Alberta.

Barlow, J. P. 1986. Interpretation of tunnel convergence measurements. M.Sc. Thesis, University of Alberta, Edmonton, 235 p.

Barlow, J. P., and Kaiser, P.K. 1987. Interpretation of tunnel convergence measurements. Proceedings, 6th Congress of the International Society of Rock Mechanics, Montreal, pp. 787-792.

Bathe, K. J. 1977. Static and dynamic geometric and material non linear analysis using ADINA. Acoustic and Vibration Laboratory. Report 82448-2, Department of Mechanical Engineering, M.I.T., Massachussets. 240 p.

Bathe, K. J., and Bolourchi, S. 1980. A geometric and material non linear plate and shell element. Computers and Structures, 11, pp. 23-48.

Beniawski, Z. T. 1984. Rock mechanics design in mining and tunnelling. A. A. Balkema, 272 p.

Brown, E. T., Bray, J. W., Ladanyi, B., and Hoek, E. 1983. Ground response curves for rock tunnels. Journal of the Geotechnical Engineering Division, American Society of Civil Engineers, 109(1), pp. 15-39.

Burns, J. Q., and Richard, R. M. 1964. Attenuation of stresses for buried cyliders. Proceedings, Symposium on Soil-Structure Interaction, Tucson, pp. 378-392.

Cividini, A., Jurina, L., and Gioda, G. 1981. Some aspects of 'characterization' problems in geomechanics. International Journal of Rock Mechanics and Mining Science and Geomechanics Abstracts, 18, pp. 487-503.

Coates, D. F., and Yu, Y. S. 1970. A note on the stress concentrations at the end of a cilindrical hole. International Journal of Rock Mechanics and Mining Sciences, 7, pp. 583-588.

Crea, G., Martino, D., and Ribacchi, R. 1980. Influenza delle caratteristiche strutturali sull'anisotropia delle rocce. Quaderni dell'Istituto di Arte Mineraria, Facoltà di Ingegneria dell'Università di Roma, September, 48 p.

Daemen, J. J. K. 1975. Tunnel support loading caused by rock failure. Ph.D. Thesis, University of Minnesota, 432 p.

Daemen, J. J. K., and Fairhust, C. 1972. Rock failure and tunnel support loading. Proceedings, International Symposium on Underground Openings, Lucerne, pp. 356-369.

de la Cruz, R. V., and Goodman, R. E. 1969. Theoretical basis of the borehole deepening method of absolute stress measurement. Rock Mechanics theory and Practice. Proceedings, 11th Symposium on Rock Mechanics, Berkeley, pp. 353-374.

Del Greco, O., Giani, G. P., Stragiotti, L., De Nardi, L., and Lipari, D. 1985. 3-D FEM back-analysis of depth mine tunnel monitoring. Proceedings, International Congress on Large Underground Openings, Firenze, pp. 100-108.

Desai, C. S., and Reese, L. C. 1970. Stress deformation and stability analyses of deep boreholes. Proceedings, 2nd International Congress on Rock Mechanics, Belgrade, pp. 475-484.

Desai, C. S., and Siriwardane, H. J. 1984. Constitutive laws for engineering materials. Prentice Hall, Inc. 467 p.

Desai, C. S., and Wu, T. H. 1976. A general function for stress-strain curves. Proceedings, 2nd International Conference on Numerical Methods and Geomechanics, American Society of Civil Engineers, Blacksburg , Vol. 2, pp. 306-318.

Descoeudres, F. 1974. Three dimensional analysis of tunnel stability near the face in an elasto-plastic rock. Advances in Rock Mechanics, Proceedings, 3rd Congress of the International Society of Rock Mechanics, Denver, Vol. 2, pp. 1130-1135.

Duddeck, H. 1980. On the basic requirements for applying the Convergence-Confinement Method. Underground Space, 4(4), pp. 241-247.

Duncan, J. M., and Chang, C. Y. 1970. Non linear analysis of stress and strain in soils. Journal of the Soil Mechanics and Foundations Division, American Society of Civil Engineers, 96(SM5), pp. 1629-1653.

Einstein, H. H., and Schwartz, C. W. 1979. Simplified analysis for tunnel supports. Journal of the Geotechnical Engineering Division, American Society of

Civil Engineers, 105(GT4), pp. 499-518.

Eisenstein, Z., Heinz, H., and Negro, A. On three-dimensional ground response to tunnelling. Proceedings, Geotech' 84, American Society of Civil Engineers, Atlanta, pp. 107-127.

Fenner, R. 1938. Untersuchungen zur Erkenntnis des Gebirgsdruckes. Gluckauf, 74, Essen, pp. 681-695 and 705-715.

Galle, E. M., and Wilhoit, J. C. 1962. Stresses around a wellbore due to internal pressure and unequal principal geostatic stresses. Society of Petroleum Engineering Journal, 2(2), pp. 145-155.

Gartung, E., Bauernfeind, P., and Bianchini, J. C. 1979. Three-dimensional finite element method study of a subway tunnel at Nuremberg. Proceedings, Rapid Excavation and Tunnelling Conference, Atlanta, Vol. 1, p. 773-789.

Gerrard, C. M. 1977. Background to mathematical modelling in geomechanics: the roles of fabric and stress history. Finite Elements in Geomechanics, John Wiley and Sons, pp. 33-120.

Gesta, P., Kerisel, J., Londe, P., Louis, C., and Panet, M. 1980. Tunnel stability by Convergence-Confinement method. Underground Space, 4, pp. 225-232.

Ghaboussi, J., and Gioda, G. 1977. On the time dependent effects in advancing tunnels. International Journal for Numerical and Analytical Methods in Geomechanics, 1, pp. 249-269.

Gioda, G. 1985. Some remarks on back-analysis and characterization problems in geomechanics. Proceedings, 5th International Conference on Numerical Methods in Geomechanics, Nagoya, Vol. 1, pp. 47-61.

Gioda, G., and Maier, G. 1980. Direct search solution for an inverse problem in elasto-plasticity: identification of cohesion, friction angle and in situ stress by pressure tunnel test. International Journal for Numerical Methods in Engineering, 15, pp. 1823-1848.

Hanafy, E. A., and Emery, J. J. 1980. Advancing face simulation of tunnel excavations and lining placement. Underground Rock Engineering: Proceedings, 13th Canadian Rock Mechanics Symposium (the H. R. Rice Memorial Symposium). Montreal, Canadian Institute of Mining and Metallurgy, pp. 119-125.

Hanafy, E. A., and Emery, J. J. 1982. Three-dimensional simulation of tunnel excavation in squeezing ground. Proceedings, 4th International Conference on Numerical Methods in Geomechanics, Edmonton, Vol. 3, pp. 1203-1209.

Heinz, H. K. 1984. Applications of the New Austrian Tunnelling Method in urban areas. M.Sc. Thesis, Universisty of Alberta, Edmonton, 323 p.

Hendron, A. J. 1968. Mechanical properties of rock. Rock Mechanics, Stagg and Zienkiewicz ed., John Wiley and Sons, pp. 21-53.

Heuze, F. E. 1980. Scale effects in the determination of rock mass strength and deformability. Rock Mechanics, 12, pp. 167-192.

Hinton, E., and Campbell, J. S. 1974. Local and global smoothing of discontinuous finite element functions using a least squares method. International Journal for Numerical Methods in Engineering, 8, pp. 461-480.

Hinton, E., Scott, F. C., and Ricketts, R. E. 1975. Local least squares stress smoothing for parabolic isoparametric elements. International Journal for Numerical Methods in Engineering, 9, pp. 235-256.

Hocking, G. 1976. Tree-dimensional elastic stress distribution around the flat end of a cilindrical cavity. International Journal of Rock Mechanics and Mining Science, 13, pp. 331-337.

Hoeg, K. 1968. Stresses against underground structural cylinders. Journal of the Soil Mechanics and Foundations Division, American Society of Civil Engineers, 94(SM4), pp 833-858.

Hoek, E. 1983. Strength of jointed rock masses. Géotechnique, 33(3), pp. 187-223.

Hoek, E., and Brown, E. T. 1980a. Underground excavations in rock. Institution of Mining and Metallurgy, 527 p.

Hoek, E., and Brown, E. T. 1980b. Empirical strength criterion for rock masses. Journal of the Geotechnical Engineering Division, American Society of Civil Engineers, 106(GT9), pp. 1013-1035.

Hutchinson, D. E. 1982. Effects of construction procedure on shaft and tunnel performance. M.Sc. Thesis, University of Alberta, Edmonton, 267 p.

Janbu, N. 1963. Soil compressibility as determined by odometer and triaxial test. Proceedings, European Conference of Soil Mechanics and Foundations Engineering, Wiesbaden, Vol. 1, pp. 19-25.

Kaiser, P. K., and Mackay, C. 1983. Development of rock mass and liner stresses during sinking of a shaft in clay shale. Proceedings, First International Conference on Stability in Underground Mining, August 1982, C. O. Brawner (Ed.), AIME, New York, pp 790-809.

Kasali, G., and Clough, G. W. 1983. Development of a design technology for ground support for tunnels in soil. Volume II. Three-dimensional finite element analysis of advanced and conventional shield tunneling. Report No. UMTA-MA-06-0100-82-2, U.S. Department of Transportation, Urban Mass Transportation Administration, 232 p.

Katzenbach, R., and Breth, H. 1981. Non linear 3-D analysis for NATM in Frankfurt clay. Proceedings, 10th International Conference on Soil Mechanics and Foundation Engineering, Stockholm, Vol. 1, pp. 315-318.

Kawamoto, T. 1963. On the state of stress and deformation around a tunnel in orthotropic, elastic ground. Memorial of the Faculty of Engineering, Kumamoto University, 10(1), pp. 1-30.

Kerisel, J. 1980. Commentary on the general report. Underground Space, 4(4), pp. 233-239.

Konder, R. L. 1963. Hyperbolic stress-strain response: cohesive soils. Journal of Soil Mechanics and Foundations Division, American Society of Civil Engineers, 89(SM1), pp. 115-143.

Laabmayr, F., and Swoboda, G. 1978. The importance of shotcrete as support element for NATM. Proceedings, Engineering Foundation Conference on Shotcrete for Underground Support, St. Anton, Austria, pp. 65-79.

Lekhnitskii, S. G. 1963. Theory of elasticity of an anisotropic elastic body. Translated by P. Fern (Holden Day, San Francisco). 404 p.

Lo, K. Y., and Lukajic, B. 1984. Predicted and measured stresses and displacements around the Darlington Intake Tunnel Canadian Geotecnical Journal, 21(1), pp. 147-165.

Lombardi, G. 1970. Dimensioning of tunnel linings. Tunnels and Tunnelling, 2(3), pp 104-111.

Lombardi, G. 1980. Some comments on the Convergence-Confinement method. Underground Space, 4, pp. 249-258.

Mackay, C. 1982. Performance of a shaft in weak rock. M.Sc. Thesis, Universisty of Alberta, Edmonton, 257 p.

Marsh, J. C., Currie, D., Landry, G., and Lamb, T. 1986. Cape Breton Development Corporation's experience with a tunnel-boring machine in coal measures. CIM Bullettin, (891), pp. 49-55.

Miller, T. W., and Cheatman, J. B. 1972. A new yield condition and hardening rule for rocks. International Journal of Rock Mechanics and Mining Science, 9, pp. 453-474.

Natau, O. P., Fröhlich, B. O., and Mutshler, Th. O. 1983. Recent developments of the large-scale triaxial test. Proceedings, 5th International Congress on Rock Mechanics, International Society for Rock Mechanics, Melbourne, Vol.1, pp. A65-A74.

Nayak, G. C., and Zienkiewicz, O. C. 1972. Convenient form of stress invariants for plasticity. Journal of the Structural Division, American Society of Civil Engineers, 98(4), pp. 949-954.

Niwa, Y., Kobayashi, S., and Fukui, T. 1979. Stresses and displacements around an advancing face of a tunnel. Proceedings, 4th Congress of the International Society for Rock Mechanics, Montreaux, Vol. 1, pp. 703-710.

Nose, M. 1964. Rock test in situ, conventional tests on rock properties and design of Kurobegawa No.4 Dam based thereon. Proceedings, 8th International Congress on Large Dams, International Commission on Large Dams of the World Power Conference, Edinburgh, Vol.1, pp. 219-252.

Obert, L., and Duvall, W. I. 1967. Rock mechanics and the design of structures in rock. John Wiley and Sons, Inc., 650 p.

Panet, M. 1976. Stability analysis of a tunnel driven in a rock mass taking account of the post-failure behavior. Rock Mechanics, 8, pp. 209-223.

Panet, M., and Guellec, P. 1974. Contribution à l'étude du soutènement d'un tunnel à l'arrière du front de taille. Advances in Rock Mechanics. Proceedings, 3rd Congress of the International Society of Rock Mechanics, Denver, Vol. 2B, pp. 1163-1168.

Panet, M., and Guenot, A. 1982. Analysis of convergence behind the face of a tunnel. Tunnelling '82, The Institution of Mining and Metallurgy, pp. 197-204.

Pawsey, S. F., and Clough, R. W. 1971. Improved numerical integration of thick shell finite elements. International Journal for Numerical Methods in Engineering, 3, pp. 575-586.

Peck, R. B., Hendron, A. J., and Mohraz, B. 1972. State of the art of soft-ground tunneling. Proceedings, First Rapid Excavation and Tunnelling Conference, American Institute of Mining, Metallurgical and Petroleum Engineers, Vol. 1, pp. 259-286.

Pender, M. J. 1980. Discussion on "Simplified Analysis for Tunnel Supports" by H. H. Einstein and C. W. Schwartz. Journal of the Geotechnical Engineering Division, American Society of Civil Engineers, 106(GT7), pp. 833-835.

Pierau, B. 1982. Tunnel design with respect to the three-dimensional state of stresses and displacements around the temporary face. Proceedings, 4th International Conference on Numerical Methods in Geomechanics, Edmonton, Canada, Vol. 3, pp. 1221-1231.

Rabcewicz, L. 1964. The New Austrian Tunnelling Method. Water Power, November, pp. 453-457.

Ramberg, W., and Osgood, W. R. 1943. Description of stress-strain curves by three parameters. Technical Note No. 902, National Advisory Committee for Aeronautics, Washington, D.C.

Ranken, R. E., and Ghaboussi, J. 1975. Tunnel design considerations: anlysis of stresses and displacemnts around advancing tunnels. Report No. FRA OR&D 75-84, Federal Railroad Administration, U.S. Department of Transportation, 169 p.

Richard, R. M., and Abbott, B. J. 1975. Versatile elastic-plastic stress-strain formula. Journal of the Engineering Mechanics Division, American Society of Civil Engineers, 101(EM4), pp. 511-515.

Sakurai, S. 1978. Approximate time dependent analysis of tunnel support structure considering progress of tunnel face. International Journal for Numerical and Analytical Methods in Geomechanics, 2, pp. 159-175.

Sakurai, S. 1981. Direct strain evaluation technique in construction of underground opening. Proceedings, 22nd U.S Rock Mechanics Symposium, M.I.T., pp. 298-302.

Sakurai, S., and Takeuchi, K. 1983. Back analysis of measured displacements of tunnels. Rock Mechanics and Rock Engineering, 16(3), pp. 173-180.

Santarelli, F. J., and Brown, E. T. 1987. Performance of deep wellbores in rock with a confining pressure-dependent elastic modulus. Proceedings, 6th Congress of the International Society for Rock Mechanics, Montreal, Vol.2, pp. 1217-1222.

Santarelli, F. J., Brown, E. T., and Maury, V. 1986. Technical note. Analysis of borehole stresses using pressure dependent linear elasticity. International Journal of Rock Mechanics and Mining Sciences and Geomechanics Abstracts, 23(6), pp. 445-449.

Savin, G. N. 1970. Stress concentration around holes. NASA Technical Translation NASA TT F-607, National Aeronautics and Space Administration, Washington, D.C., november, 430 p.

Schwartz, C. W., and Einstein, H. H. 1980. Improved design of tunnel supports: Volume I. Simplified analysis for ground-structure interaction in tunnelling. Report No. UMTA-MA-06-0100-80-4, U.S. Department of Transportation, Urban Mass Transportation Administration, 450 p.

Srivastava, R. K., Sharma, K. G., and Varadarajan, A. 1986. Finite element analysis of tunnels using different yield criteria. Proceedings, 2nd International Symposium on Numerical Models in Geomechanics, Ghent, pp. 381-389.

Wittke, W. 1970. Three dimensional calculation of the stability of cavernes, tunnels, slopes and foundations in anisoptropic jointed rock by means of finite elements. Proceedings, 2nd Congress of the International Society of Rock Mechanics, Beograd, Vol. 4, pp. 373-375.

Wittke, W., and Gell, K. 1980. Räumliche Standsicherheitsuntersuchungen für einen oberflächennahen Tunnelabschnitt des Bauloses B3 der Stadtbahn Bochum. Geotechnik, 3, pp. 111-119.

Yow, J. L., Jr., and Goodman, R. E. 1987. A ground reaction curve based upon block theory. Rock Mechanics and Rock Engineering, 20(3), pp. 167-190.

Yuen, C. M. K., Boyd, J. M., and Aston, T. R. C. 1987. Rock-support interaction study of a TBM driven tunnel at the Donkin Mine, Nova Scotia. Proceedings, 6th Congress of the International Society of Rock Mechanics, Montreal, Vol.2, pp. 1339-1344.

Yuen, C. M. K., Gilby, J. L., and Boyd, J. M. 1985. Measurements and analysis of rock deformation and support system response in the drill and blast and bored access drivages at the Donkin-Morien project (UP-G198). Report No. 26SQ.23440-2-9159, Canada Centre for Mineral and Energy Technology, 4 Volumes.

Zienkiewicz, O. C. 1968. Continuum mechanics as an approach to rock mass problems. Rock Mechanics Stagg and Zienkiewicz ed., John Wiley and Sons, pp. 237-273.

Zienkiewicz, O. C., Cheung, Y. K., and Stagg, K. G. 1966. Stresses in anisotropic media with particular reference to problems in rock mechanics. Journal of Strain Analysis, 1(2), pp. 172-182.

Zienkiewicz, O. C., Taylor, R. L., and Too, J. M. 1971. Reduced integration technique in general analysis of plates and shells. International Journal for Numerical Methods in Engineering, 3, pp. 275-290.

Zienkiewicz, O. C., and Hinton, E. 1976. Reduced integration, function smoothing and non-conformity in finite element analysis (with special reference to thick plates). Journal of the Franklin Institute, 302, pp. 443-461.

Zienkiewicz, O. C. 1977. The finite element method. McGraw-Hill, New York, 787 p.

APPENDIX A

Unlined Tunnels in Linear Elastic Isotropic Rock

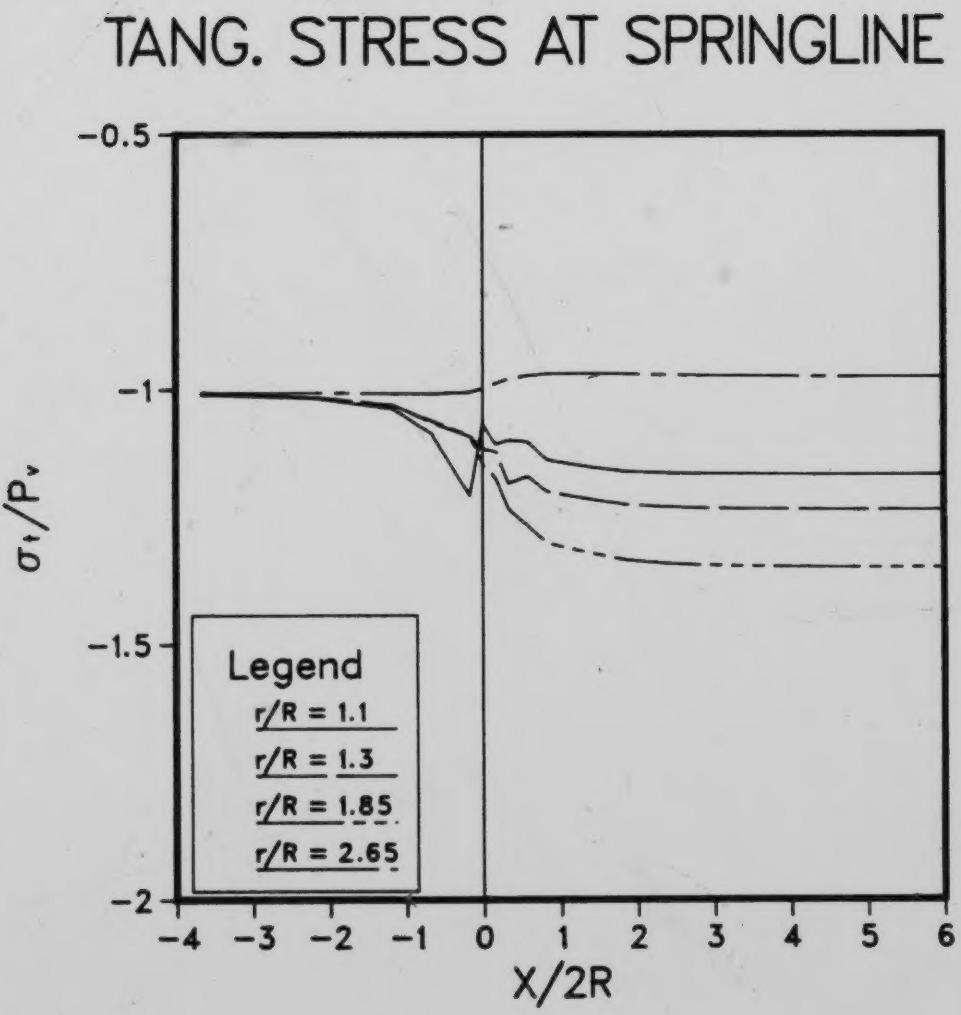

Figure A.1 Tangential Stresses, σ_t, at the Tunnel Springline (K_0=2)

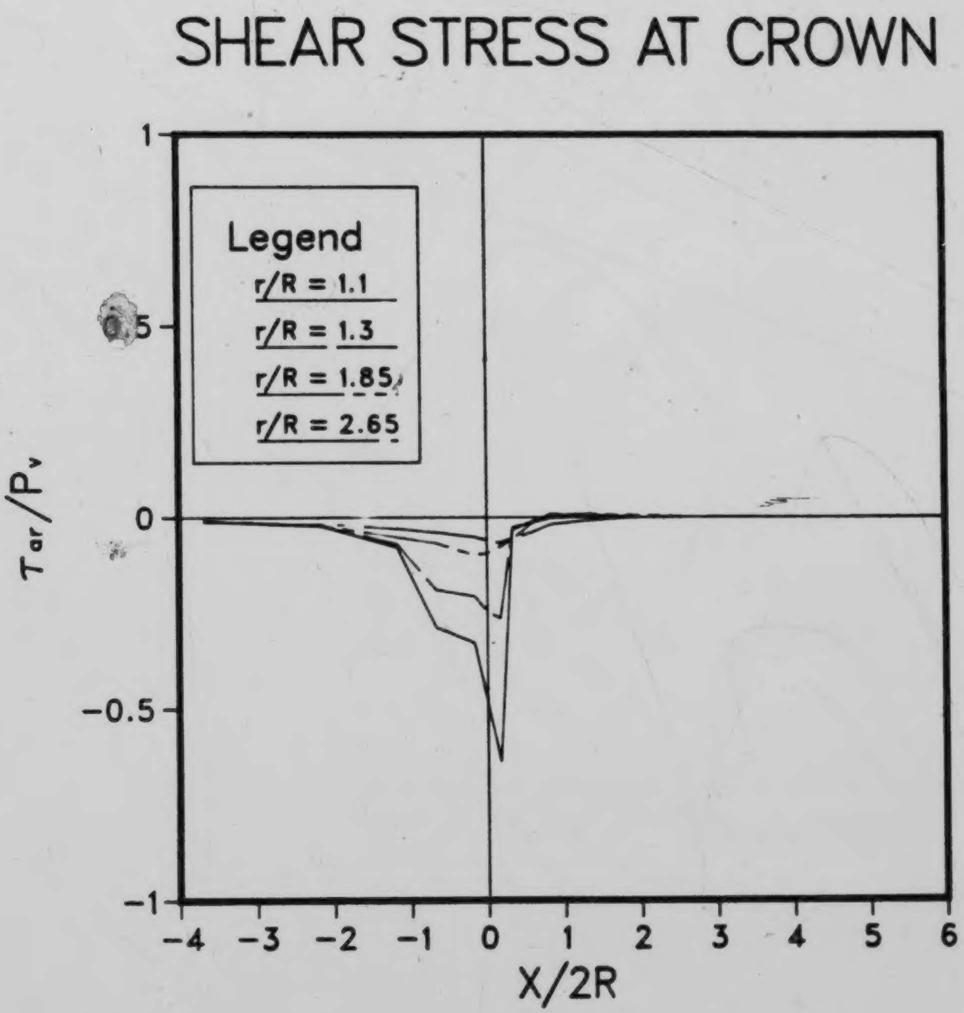

Figure A.2 Shear Stresses, τ_{ar}, at the Tunnel Crown (K_0=2)

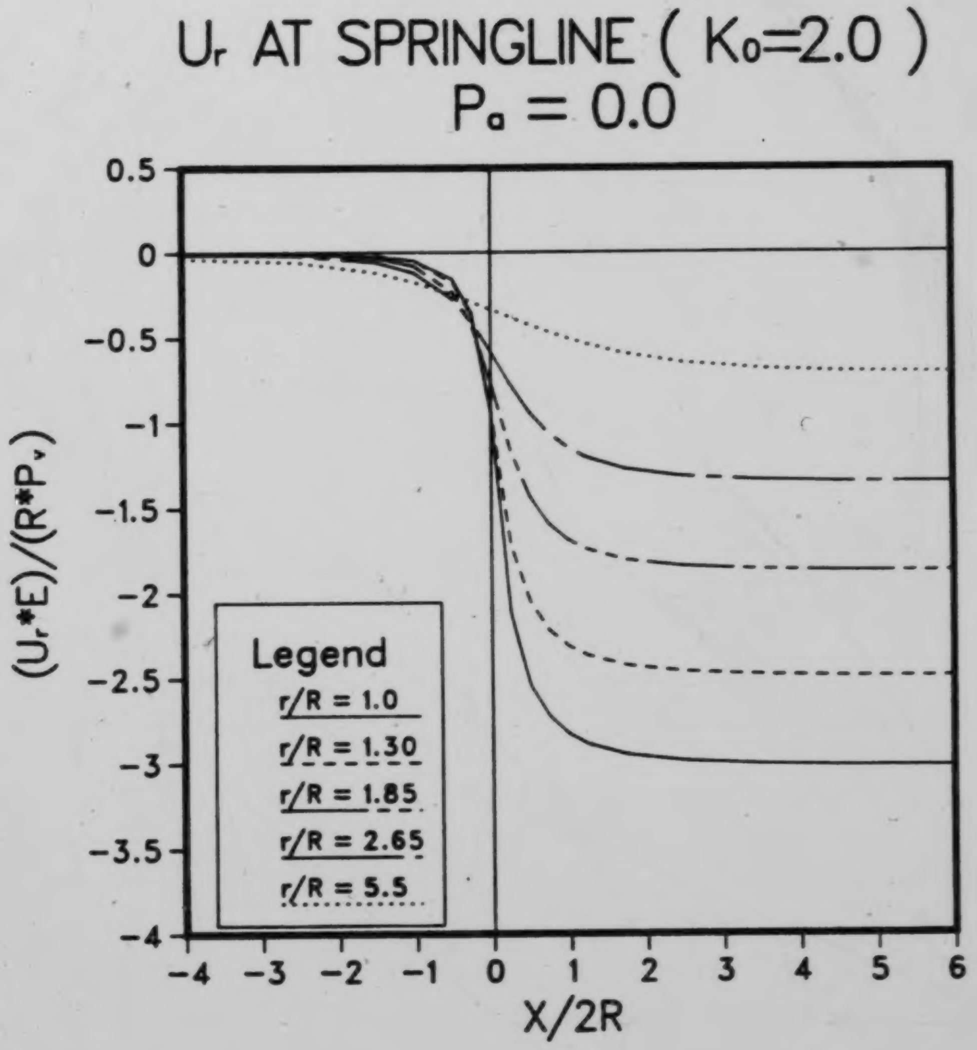

Figure A.3 Radial Displacements, U_r, at the Tunnel Springline (K_0=2; P_a=0.0)

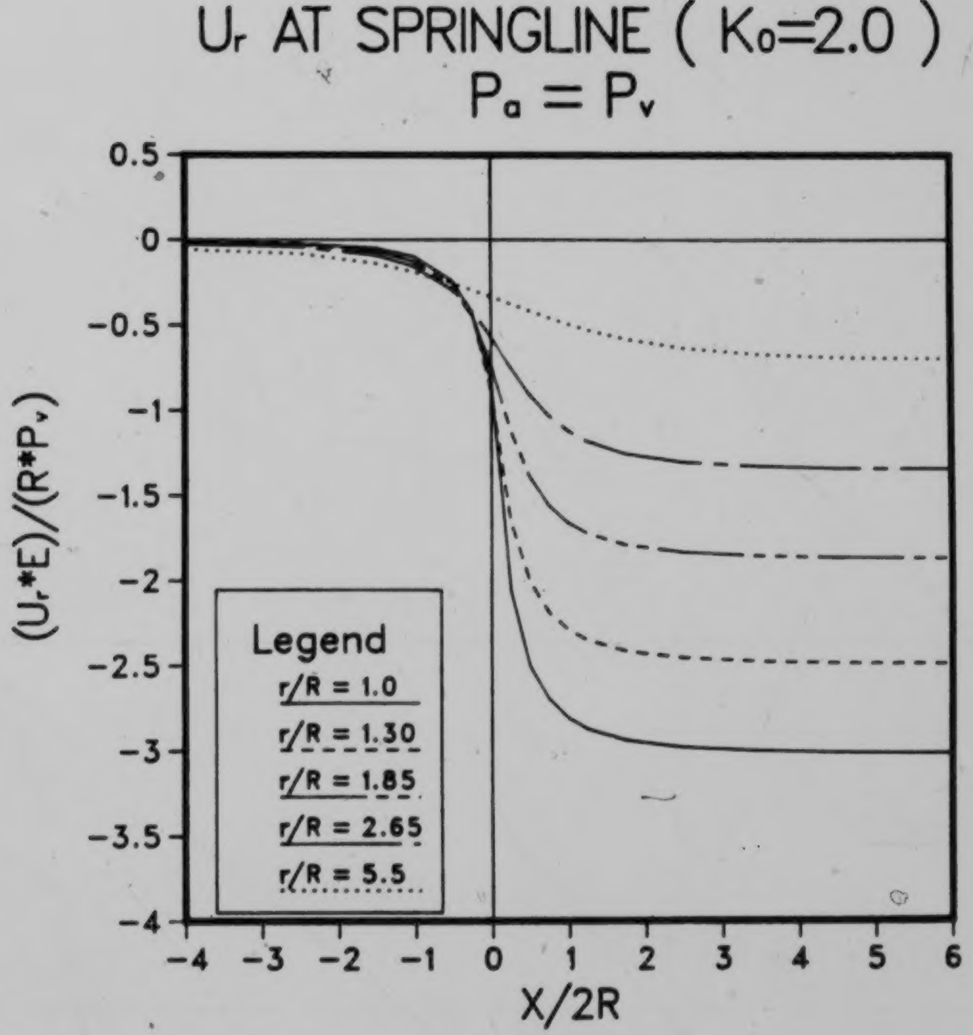

Figure A.4 Radial Displacements, U_r, at the Tunnel Springline (K_0=2; P_a=P_v)

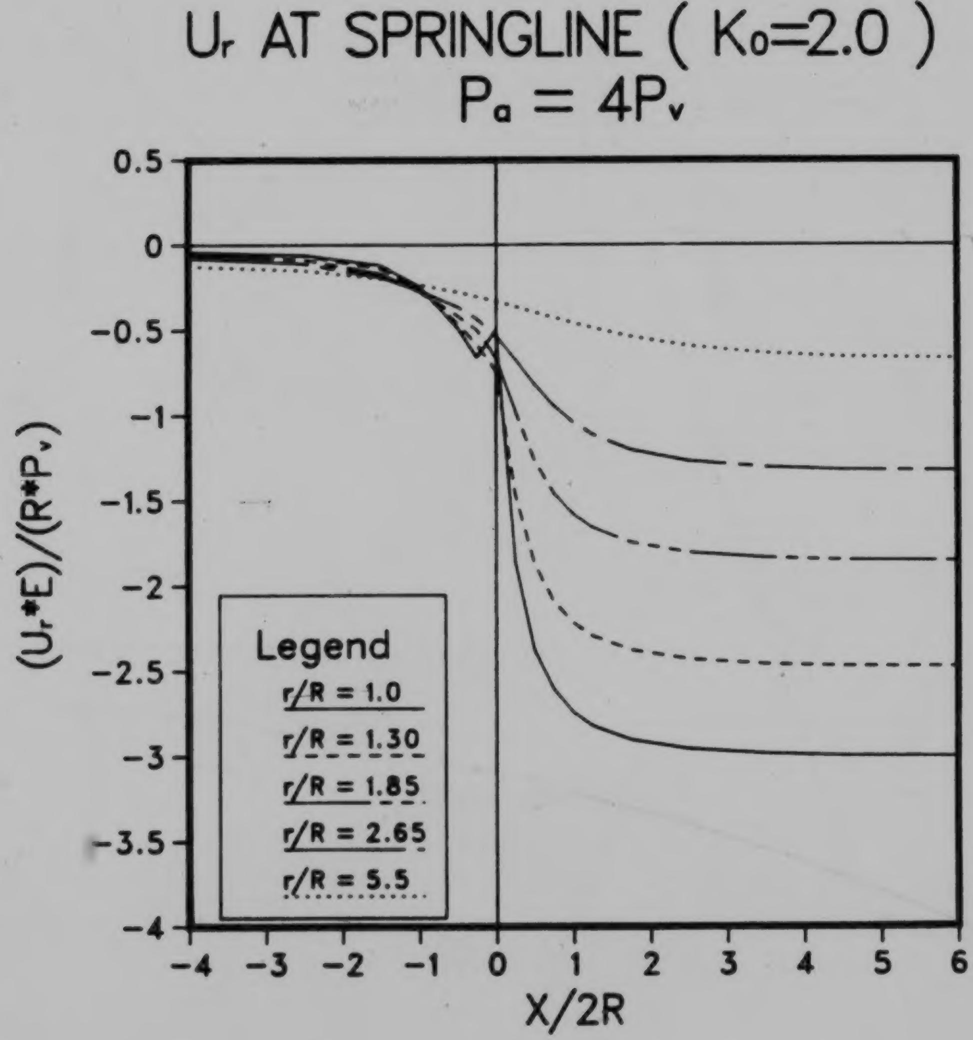

Figure A.5 Radial Displacements, U_r, at the Tunnel Springline (K_0=2; P_a=4P_v)

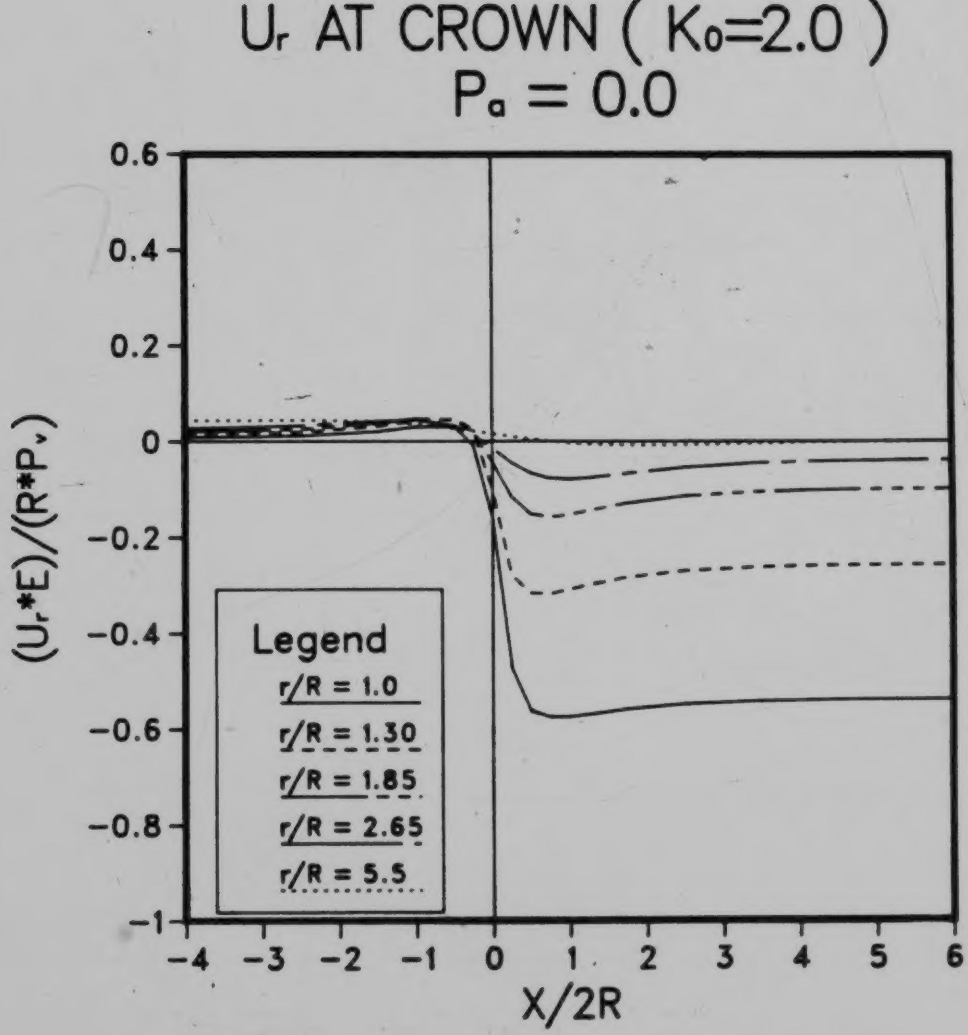

Figure A.6 Radial Displacements, U_r, at the Tunnel Crown (K_0=2; P_a=0.0)

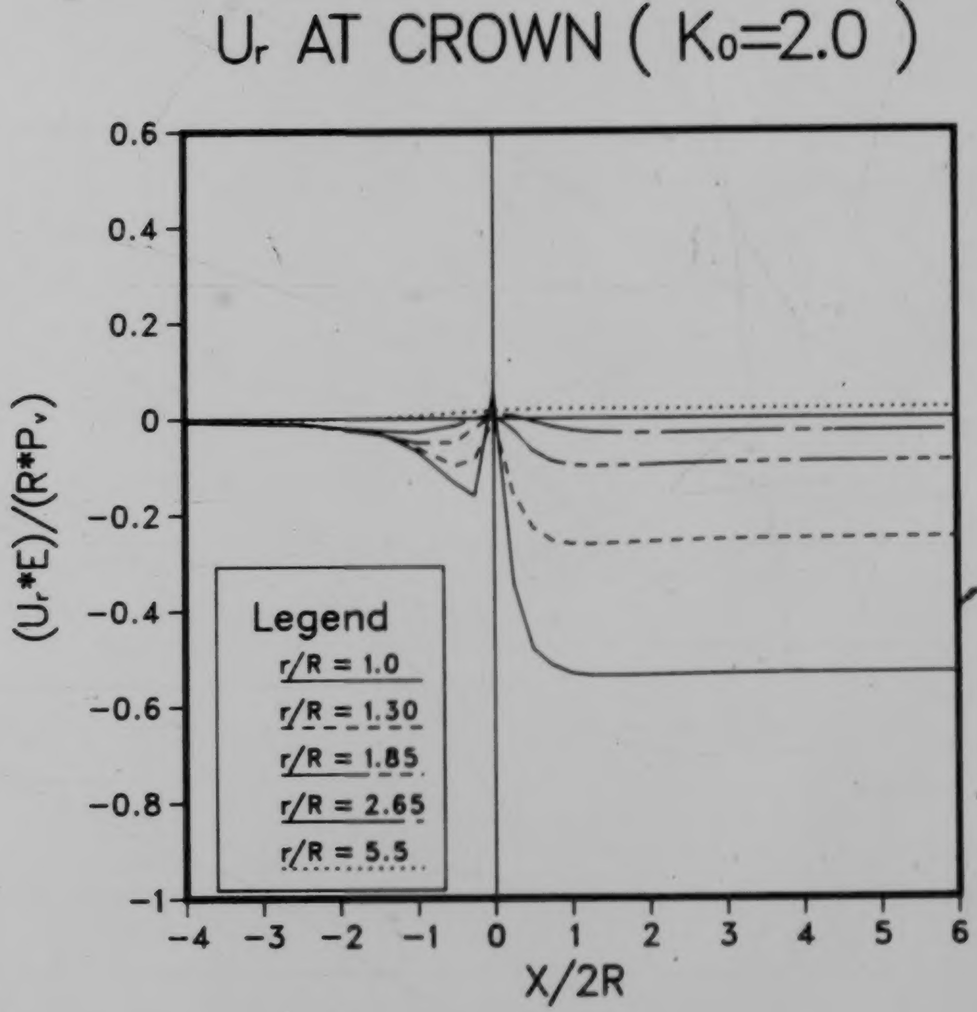

Figure A.7 Radial Displacements, U_r, at the Tunnel Crown (K_0=2; P_a=2P_v)

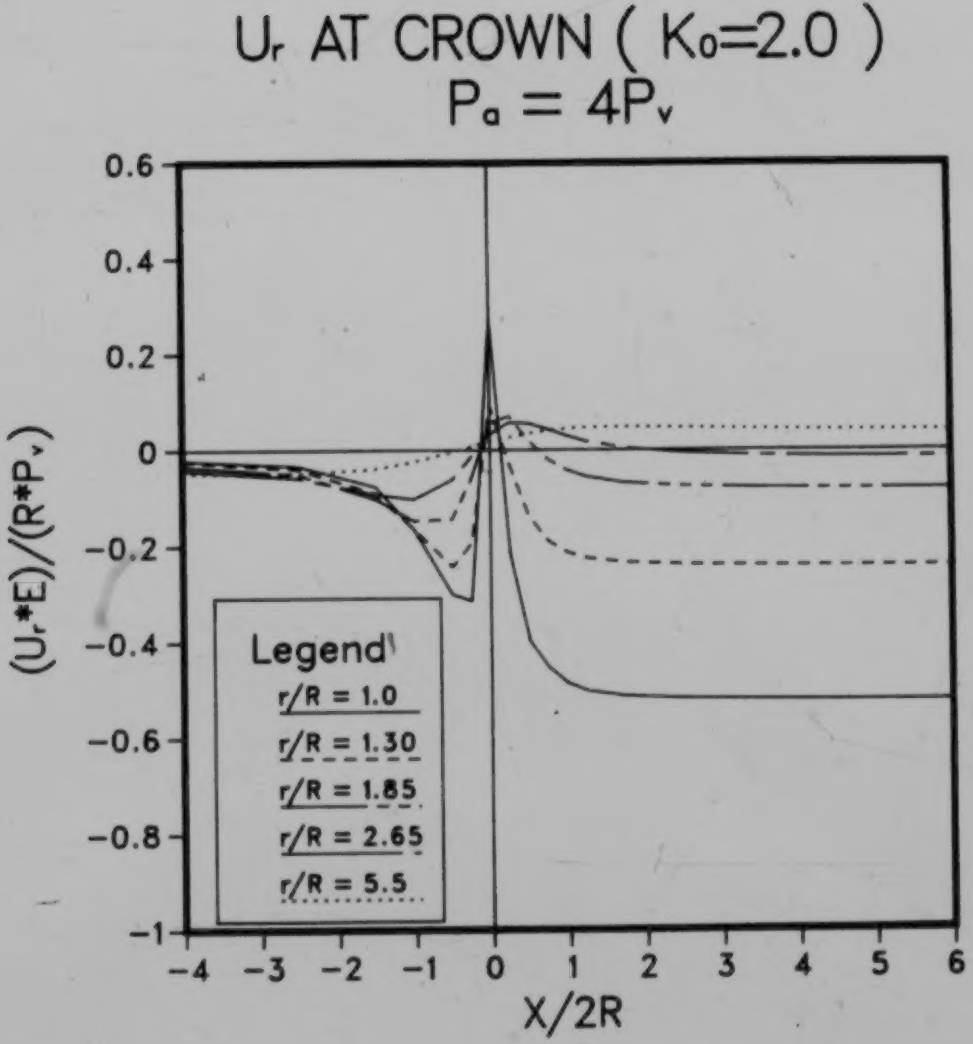

Figure A.8 Radial Displacements, U_r, at the Tunnel Crown (K_0=2; P_a=4P_v)

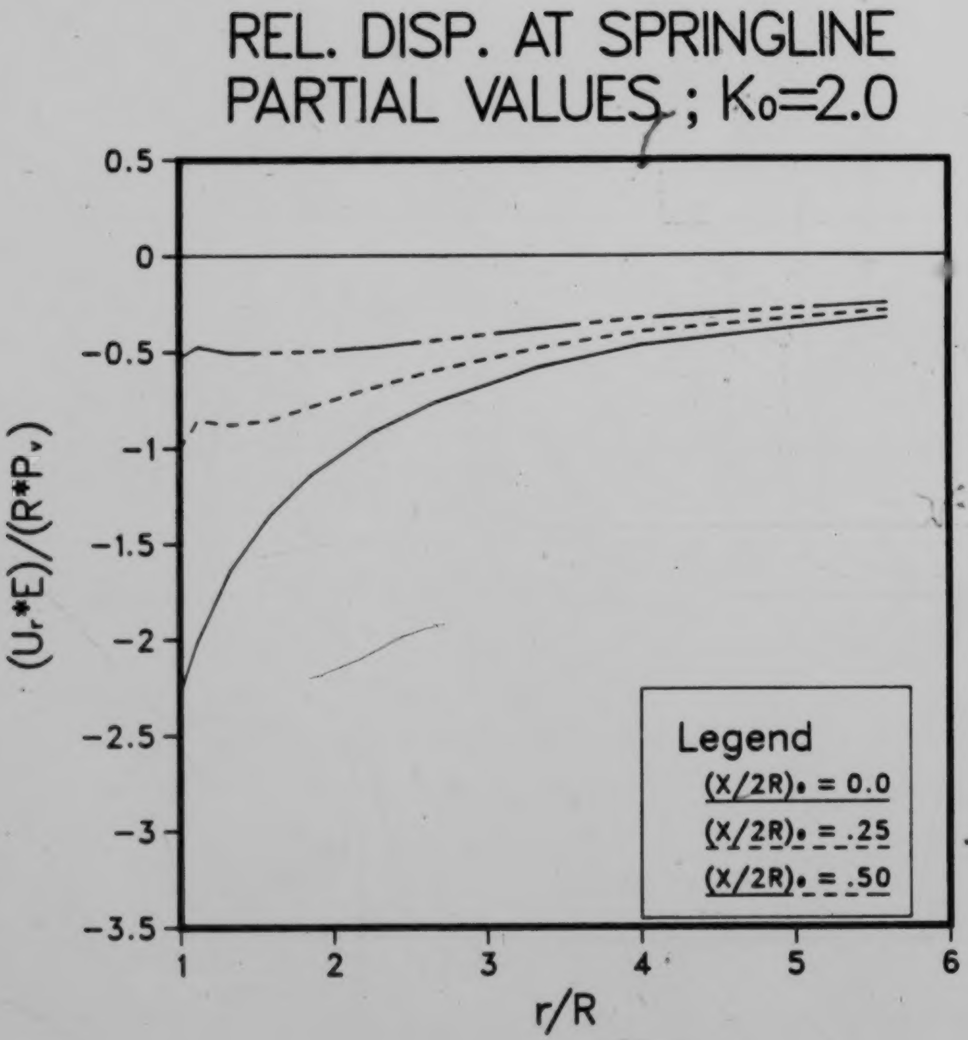

Figure A.9 Radial Displacement Profiles at the Tunnel Springline (Partial Values; K_0=2)

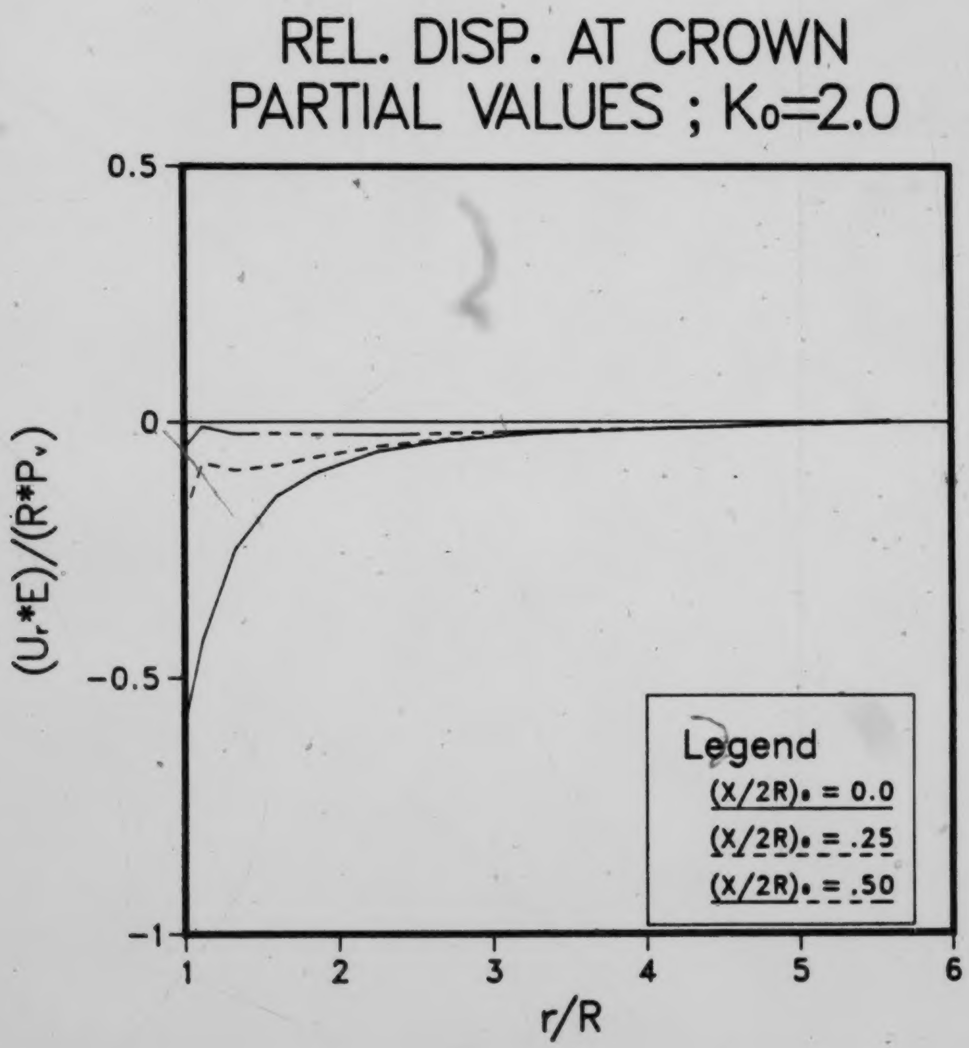

Figure A.10 Radial Displacement Profiles at the Tunnel Crown (Partial Values; K_0=2)

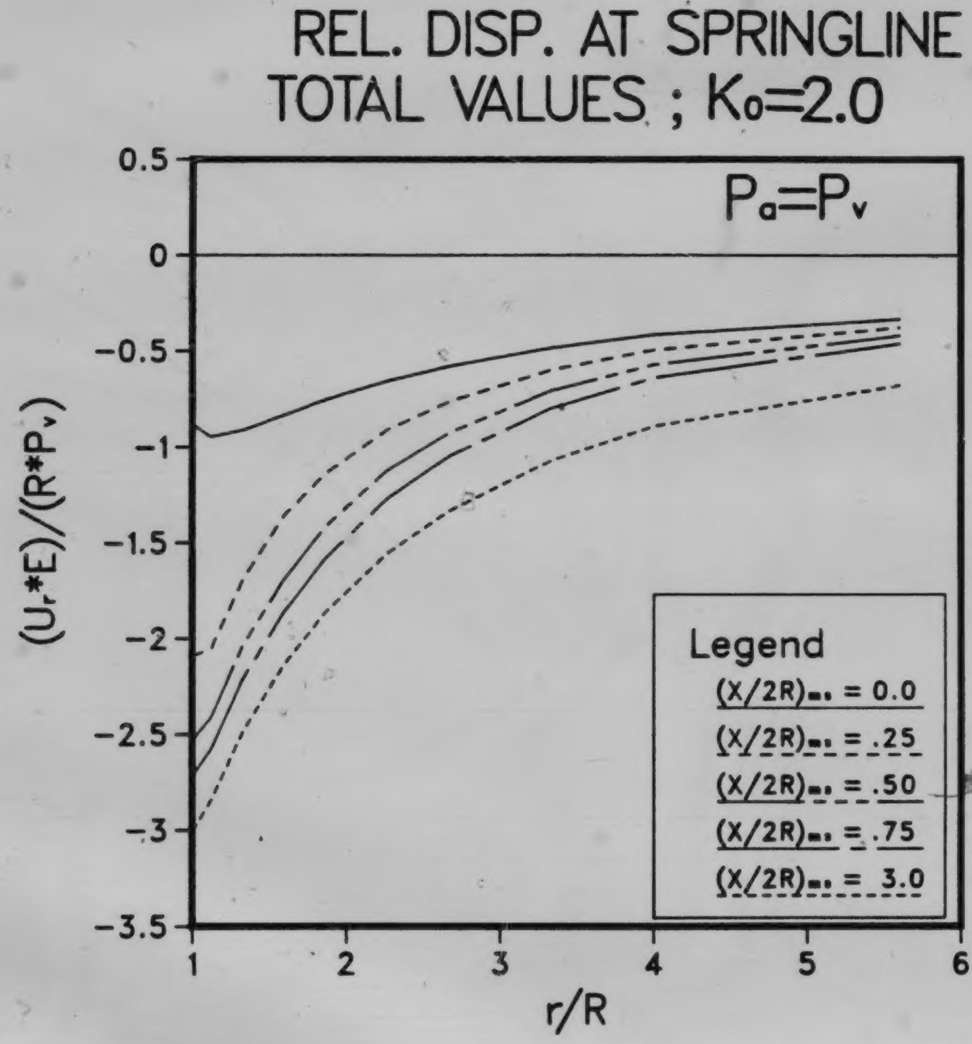

Figure A.11 Radial Displacement Profiles at the Tunnel Springline (Total Values; $K_0=2$; $P_a=P_v$)

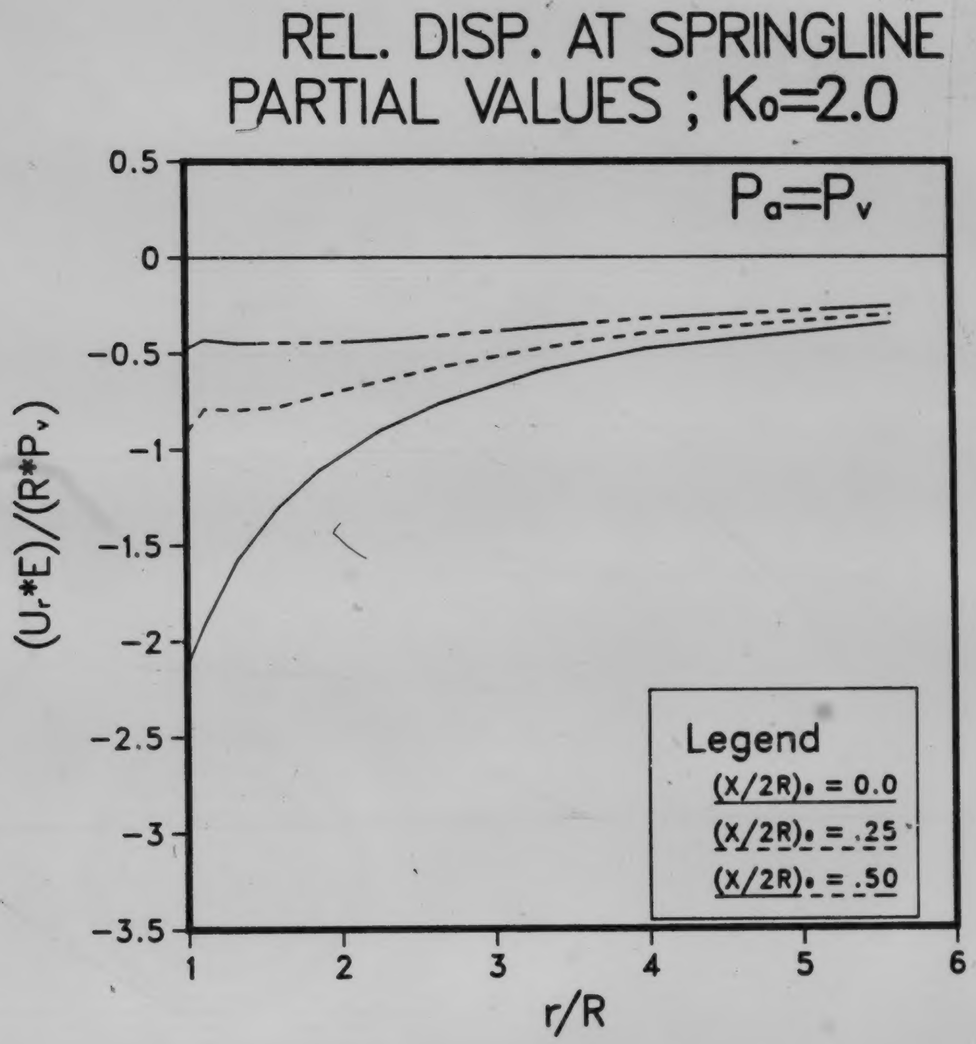

Figure A.12 Radial Displacement Profiles at the Tunnel Springline (Partial Values; K_0=2; P_a=P_v)

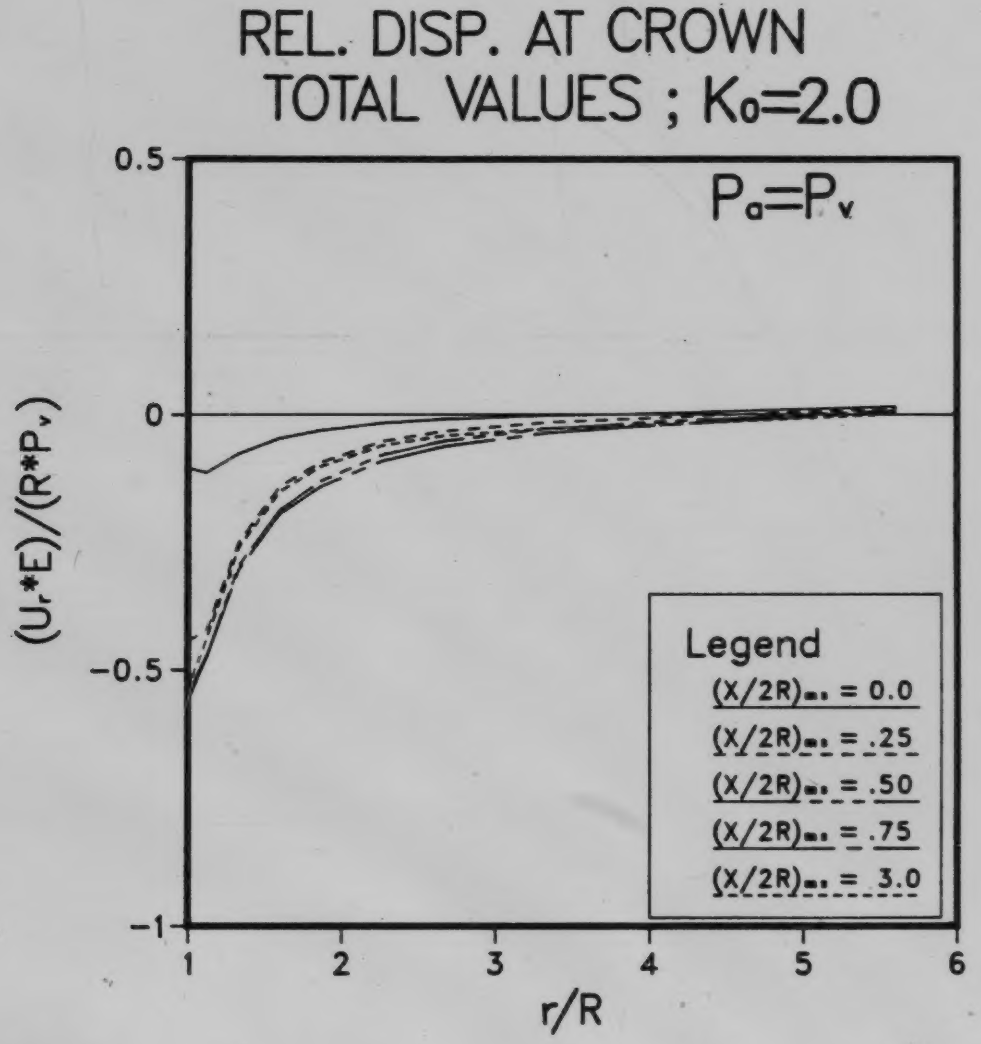

Figure A.13 Radial Displacement Profiles at the Tunnel Crown (Total Values; K_0=2; P_a=P_v)

APPENDIX B

Unlined Tunnels in Linear Elastic Transverse-Isotropic Rock

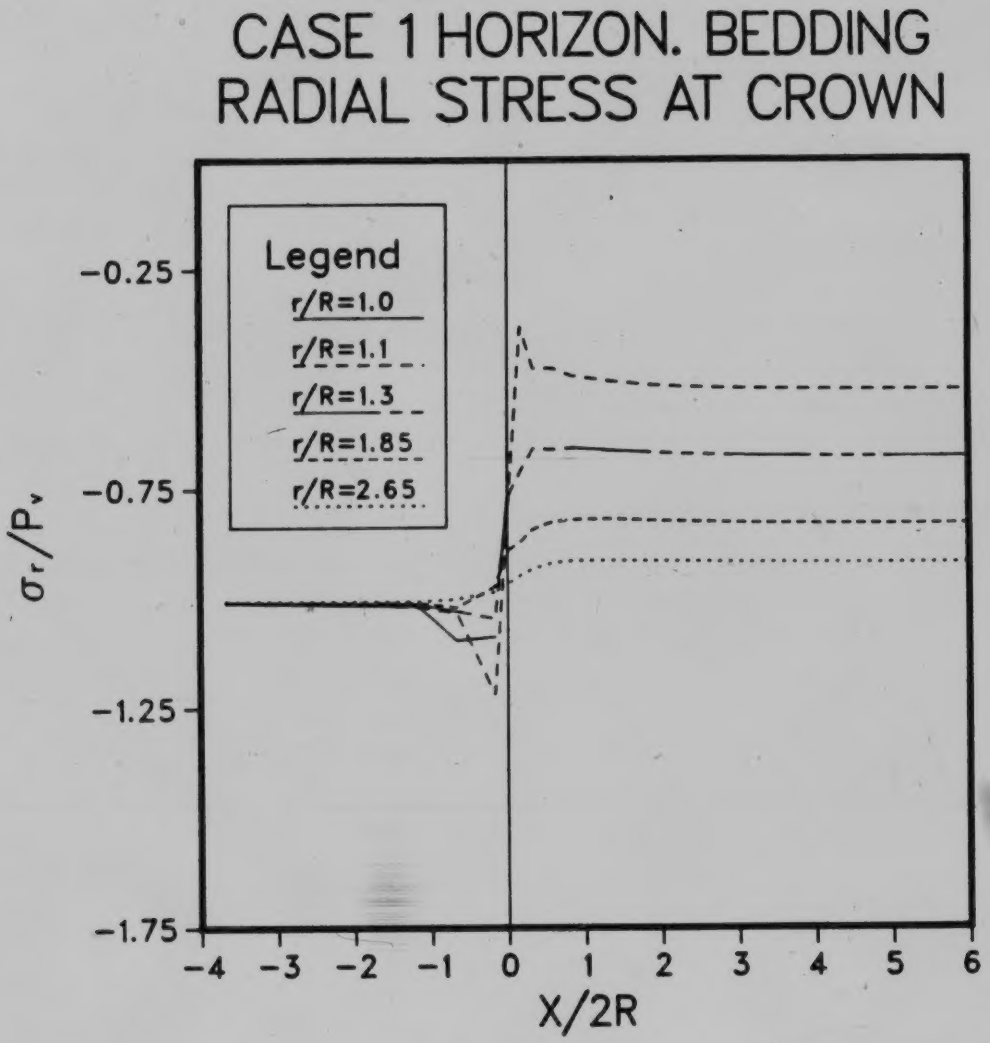

Figure B.1 Radial Stresses, σ_r, at the Tunnel Crown (Case 1)

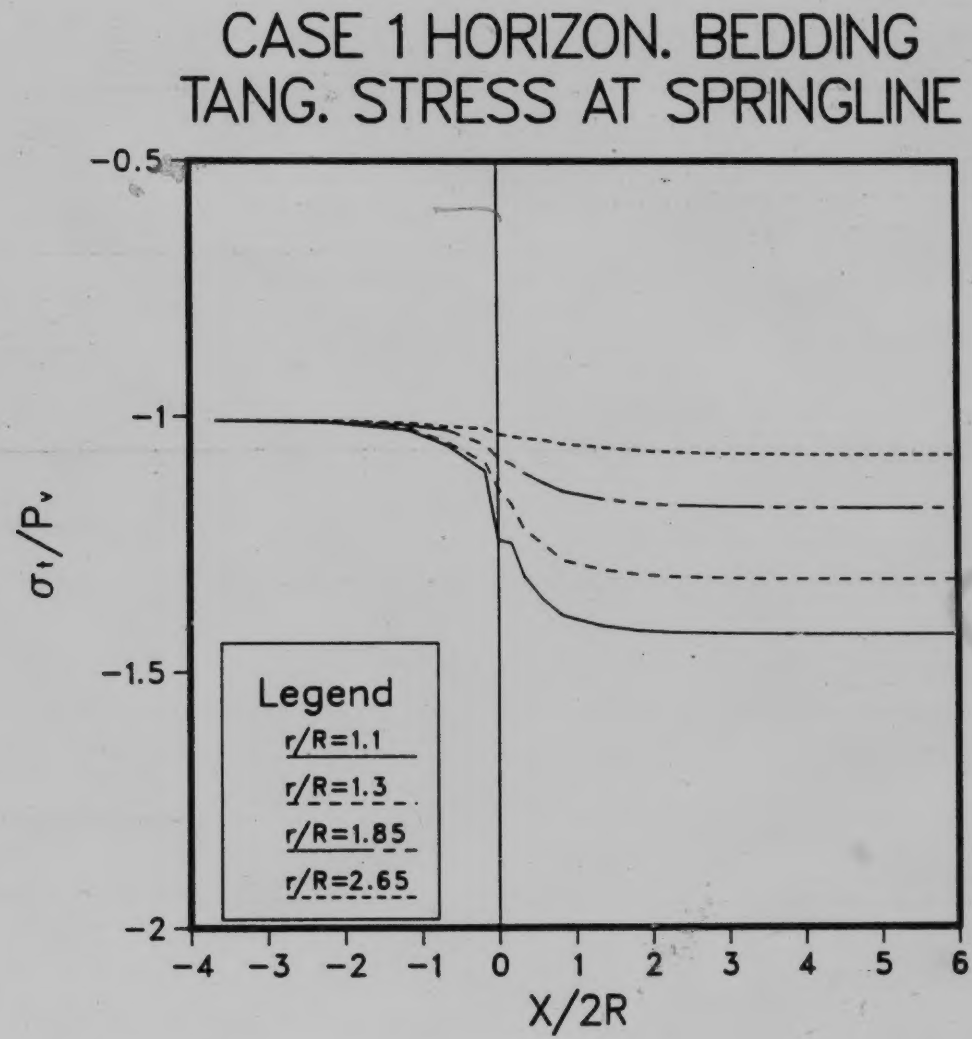

Figure B.2 Tangential Stresses, σ_t, at the Tunnel Springline (Case 1)

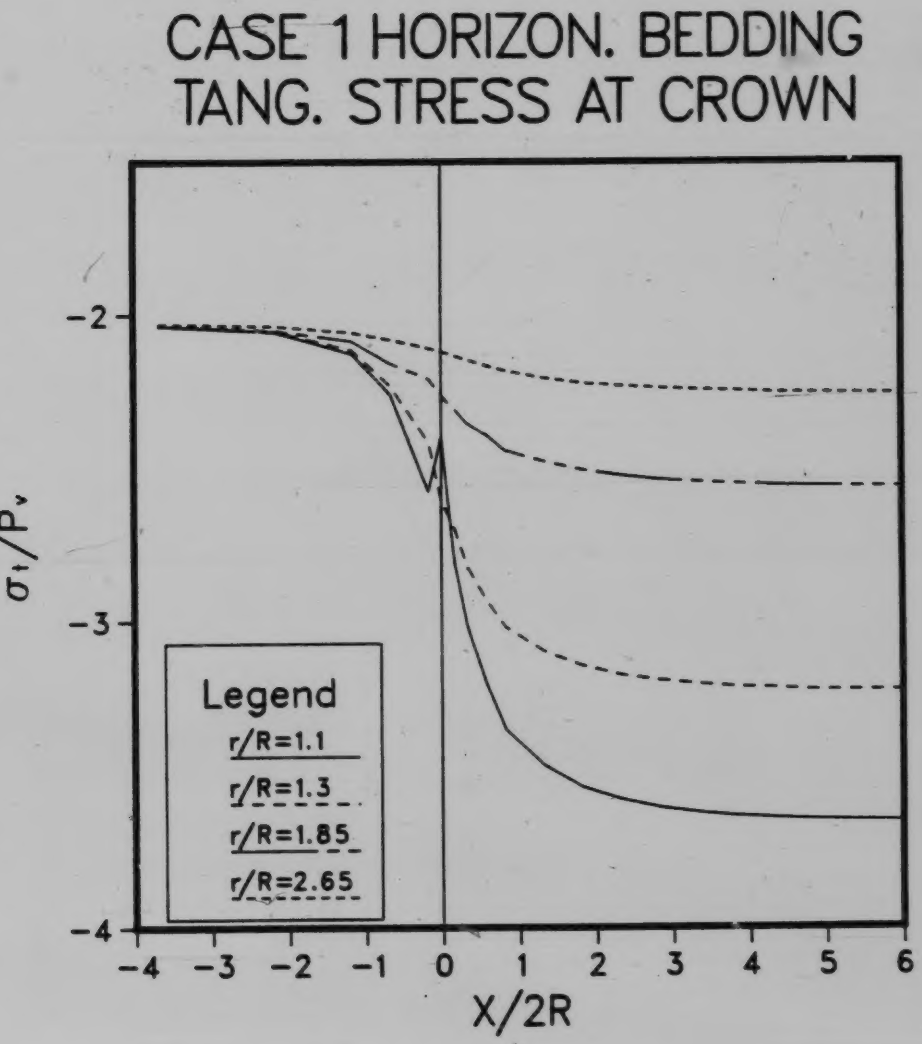

Figure B.3 Tangential Stresses, σ_t, at the Tunnel Crown (Case 1)

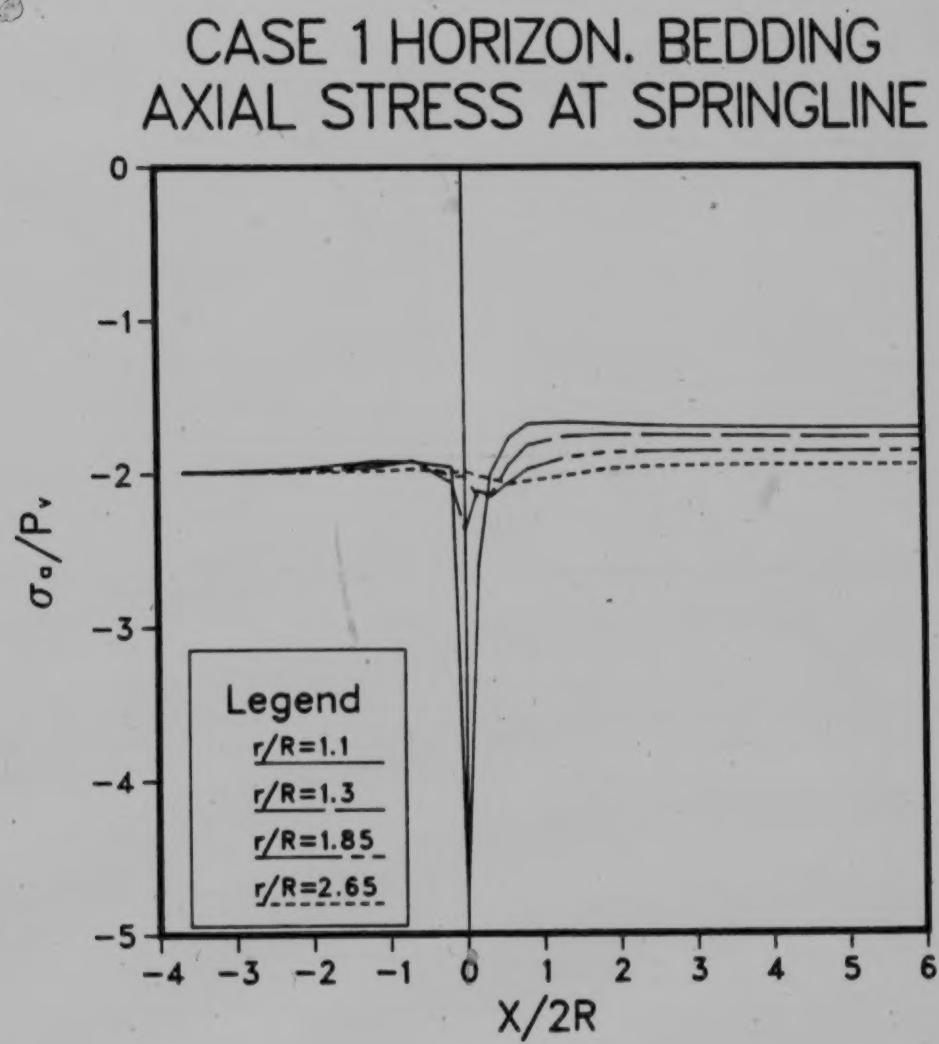

Figure B.4 Axial Stresses, σ_a, at the Tunnel Springline (Case 1)

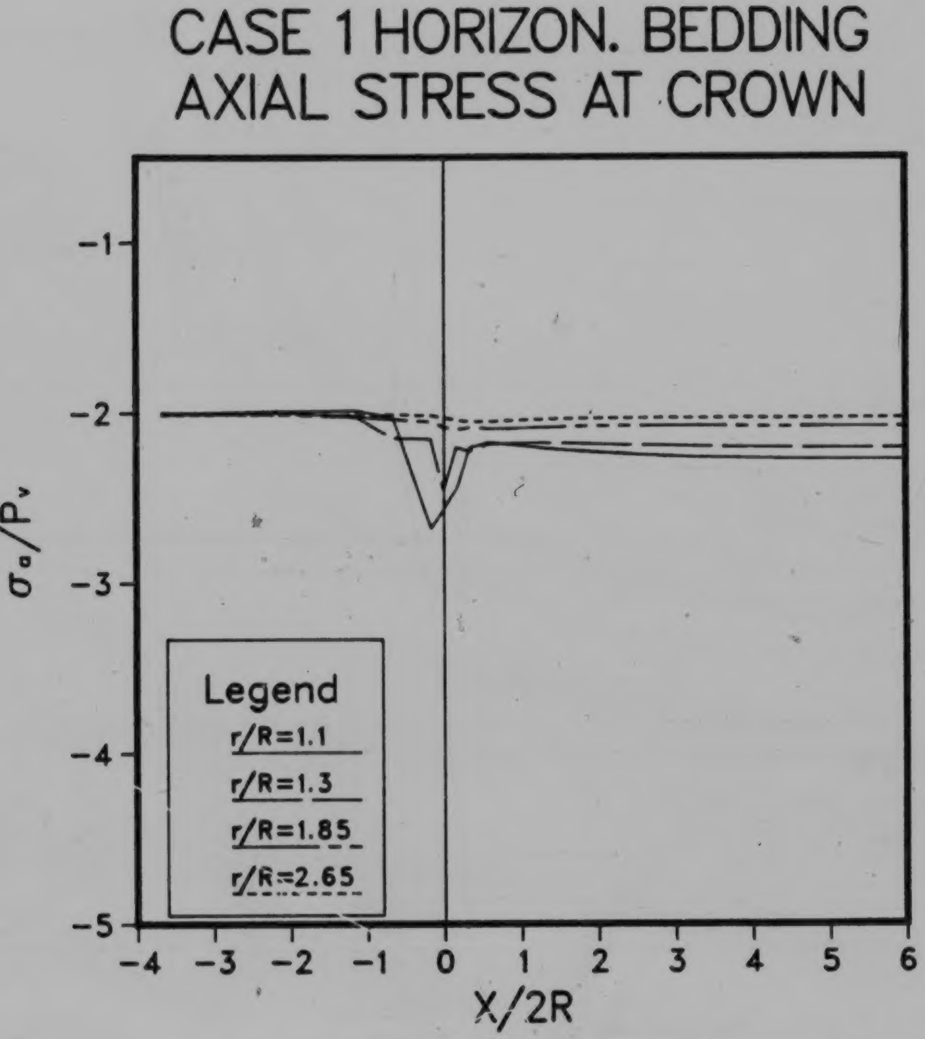

Figure B.5 Axial Stresses, σ_a, at the Tunnel Crown (Case 1)

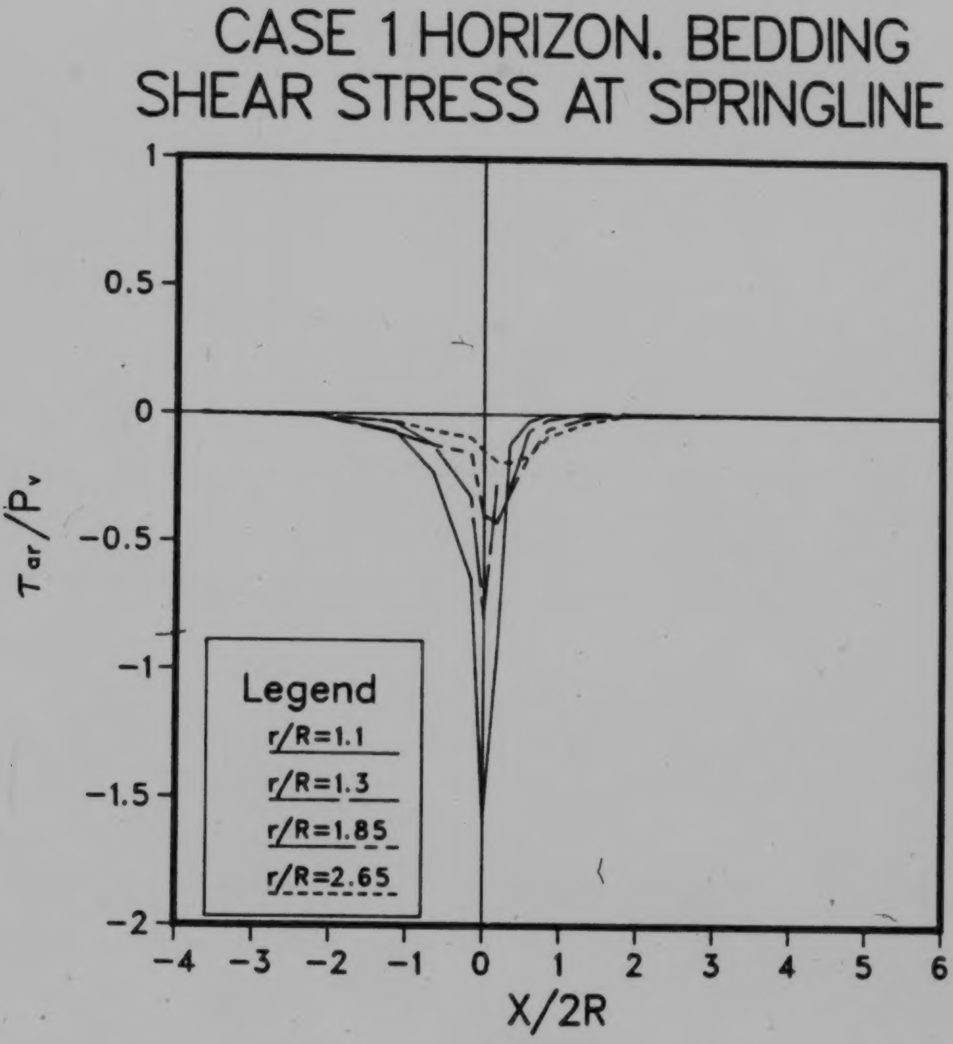

Figure B.6 Shear Stresses, τ_{ar}, at the Tunnel Springline (Case 1)

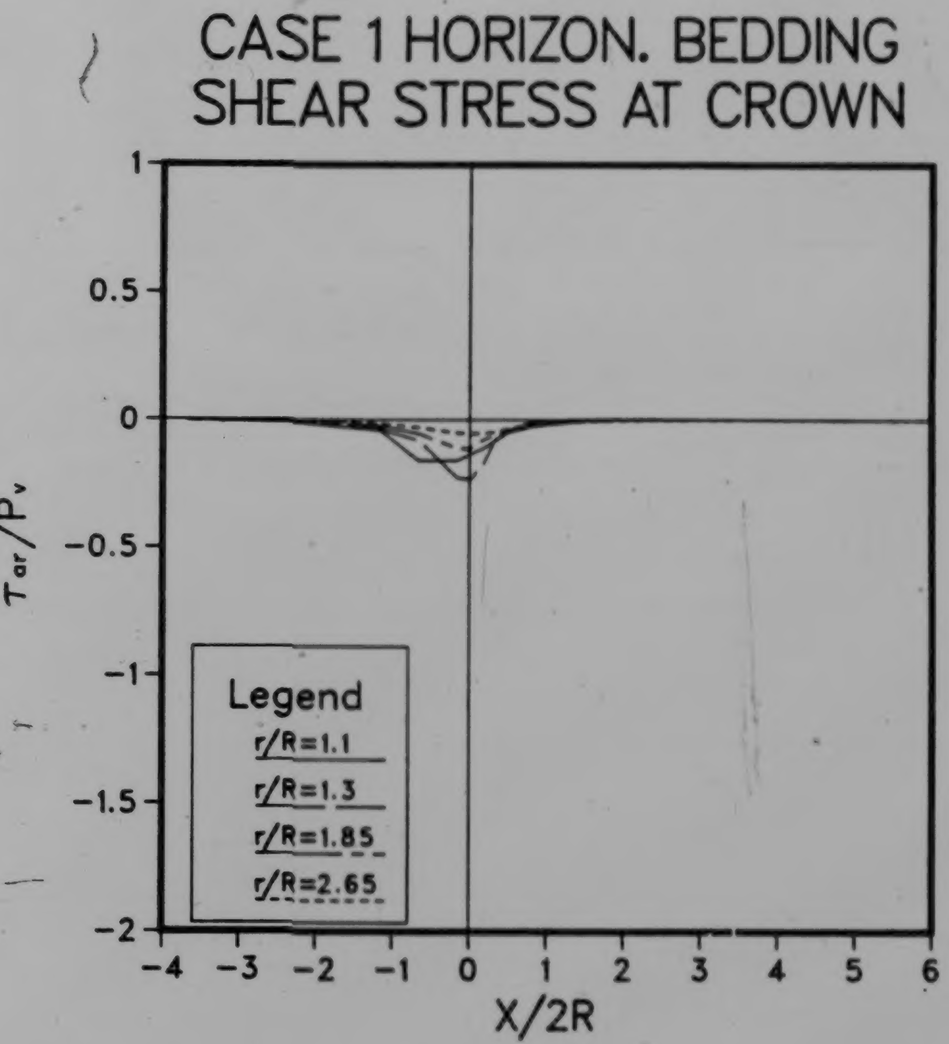

Figure B.7 Shear Stresses, τ_{ar}, at the Tunnel Crown (Case 1)

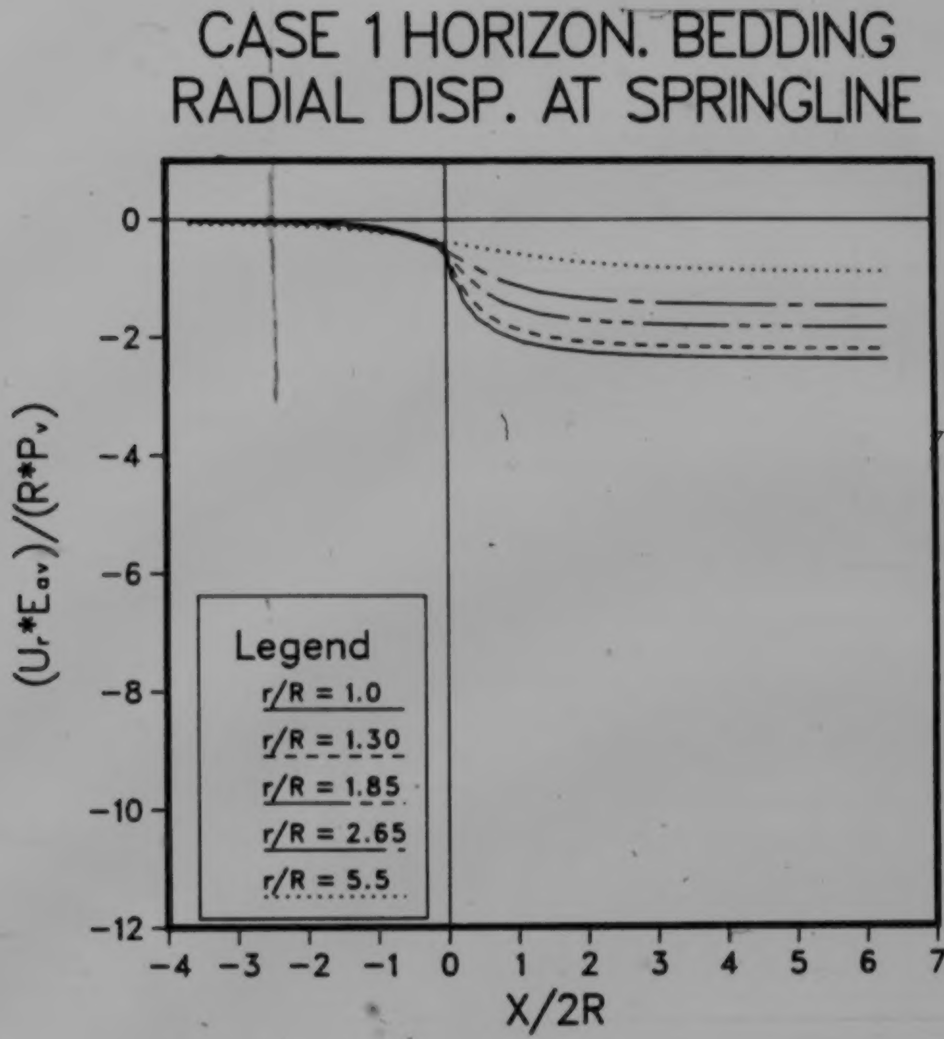

Figure B.8 Radial Displacements, U_r, at the Tunnel Springline (Case 1)

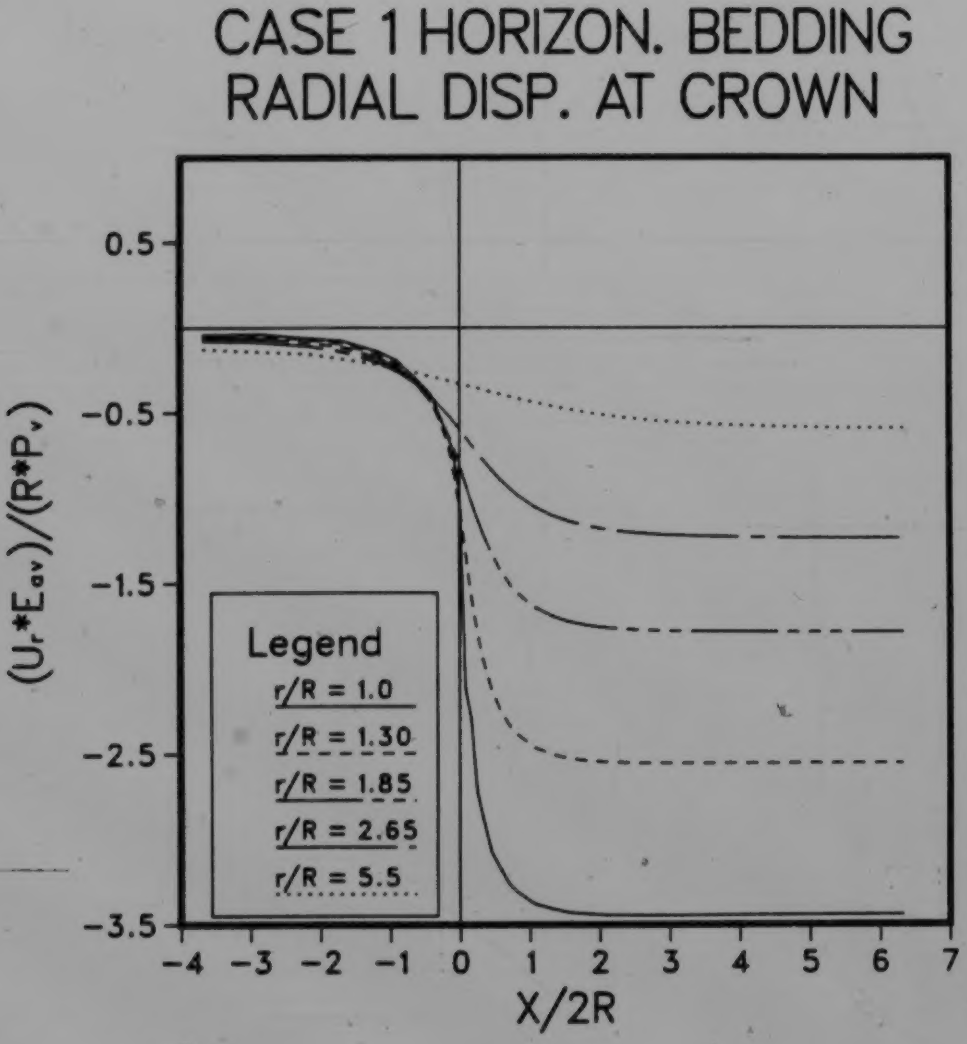

Figure B.9 Radial Displacements, U_r, at the Tunnel Crown (Case 1)

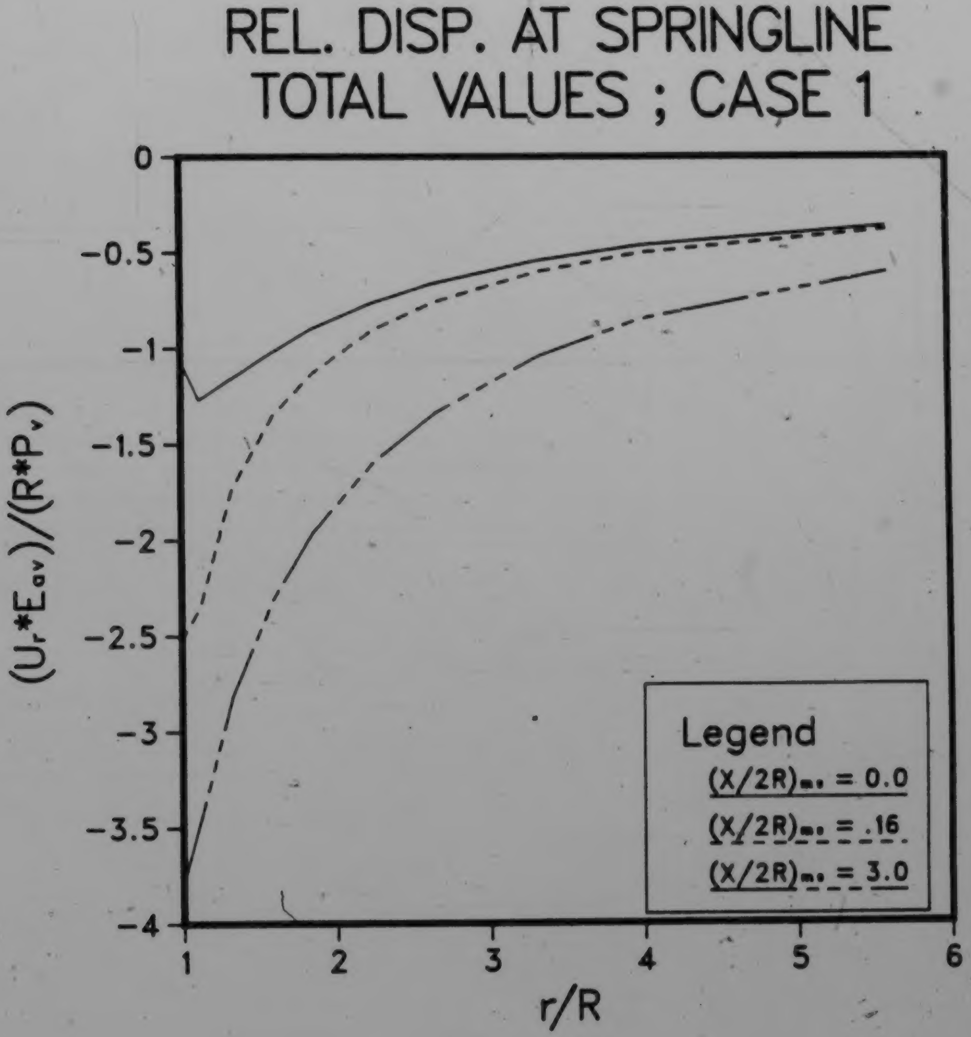

Figure B.10 Radial Displacement Profiles at the Tunnel Springline (Total Values; Case 1)

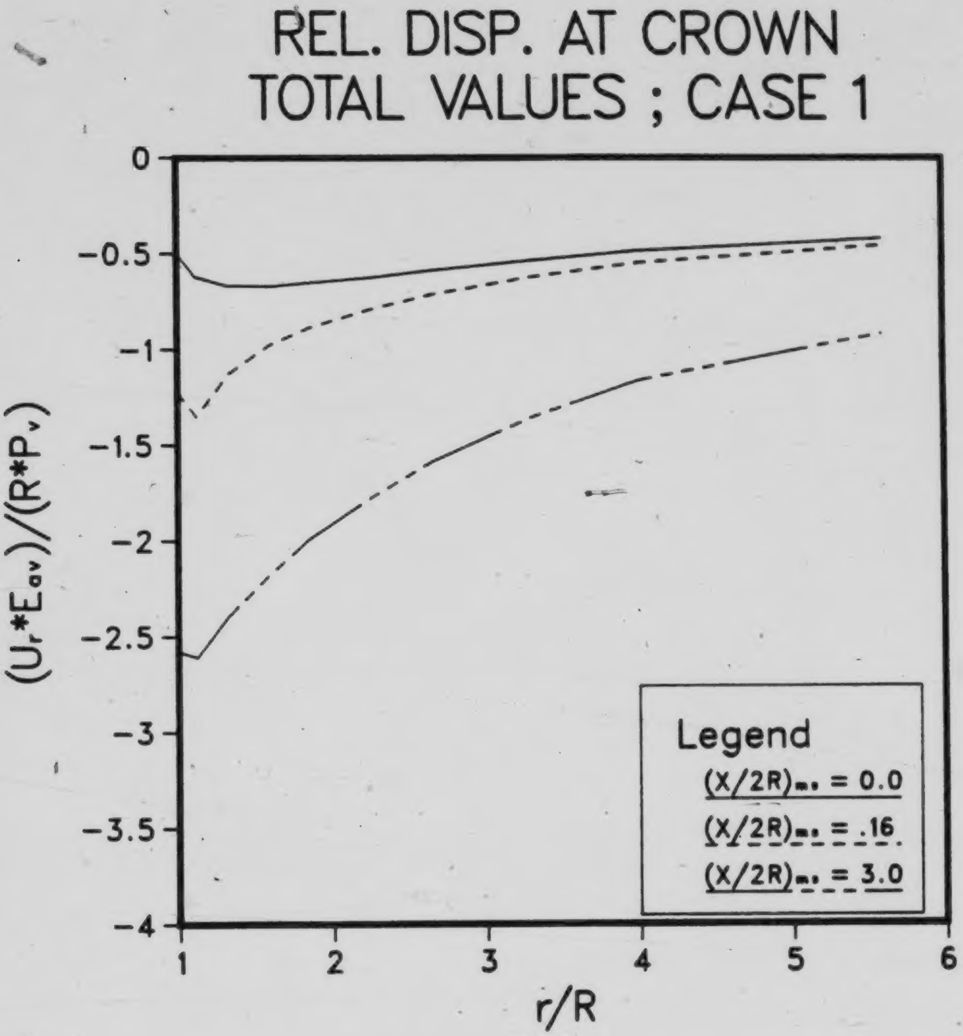

Figure B.11 Radial Displacement Profiles at the Tunnel Crown (Total Values; Case 1)

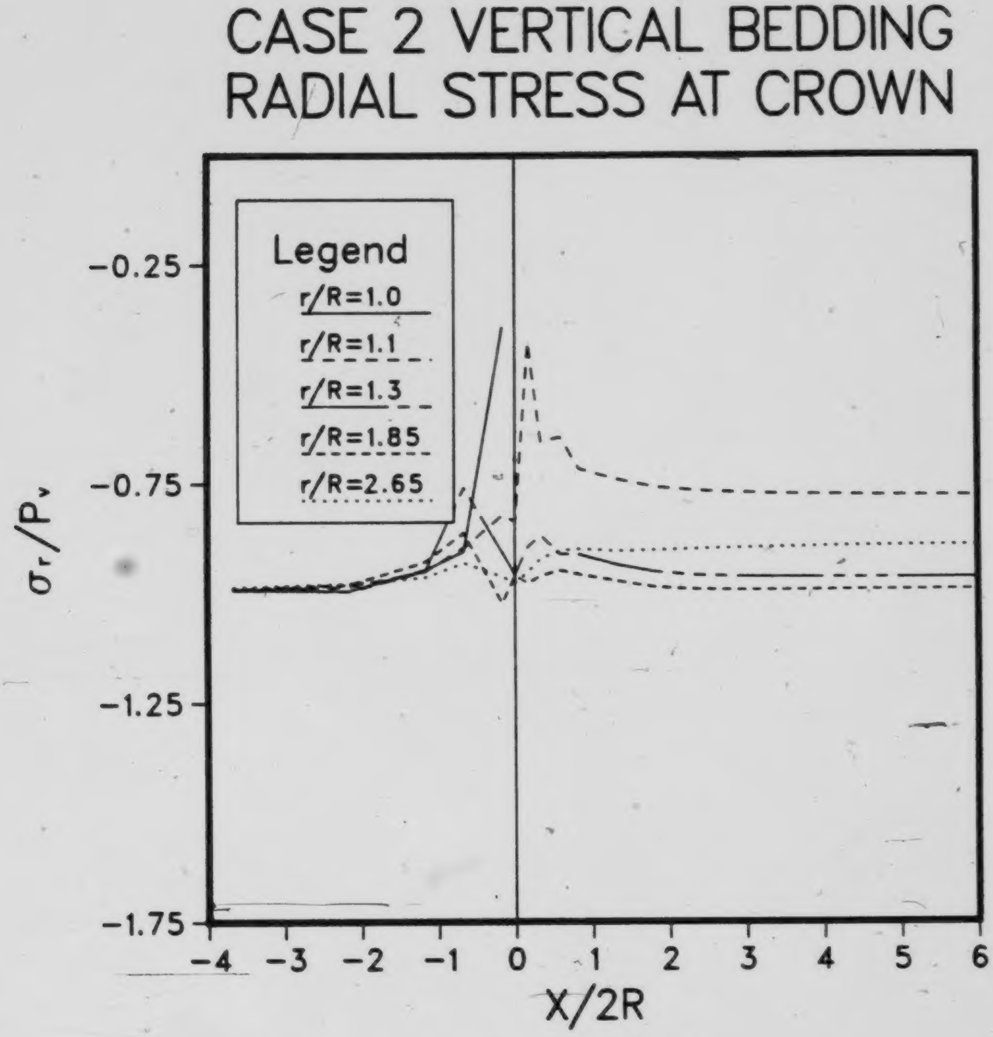

Figure B.12 Radial Stresses, σ_r, at the Tunnel Crown (Case 2)

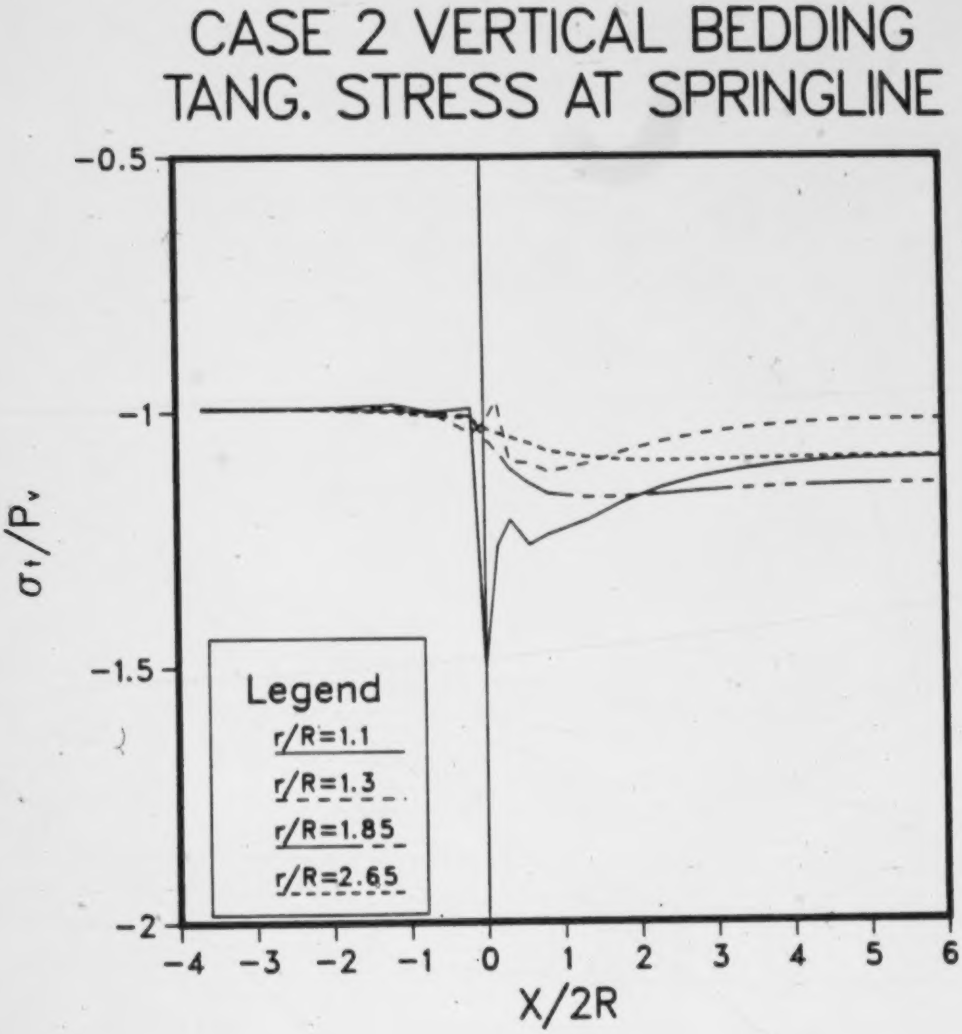

Figure B.13 Tangential Stresses, σ_t, at the Tunnel Springline (Case 2)

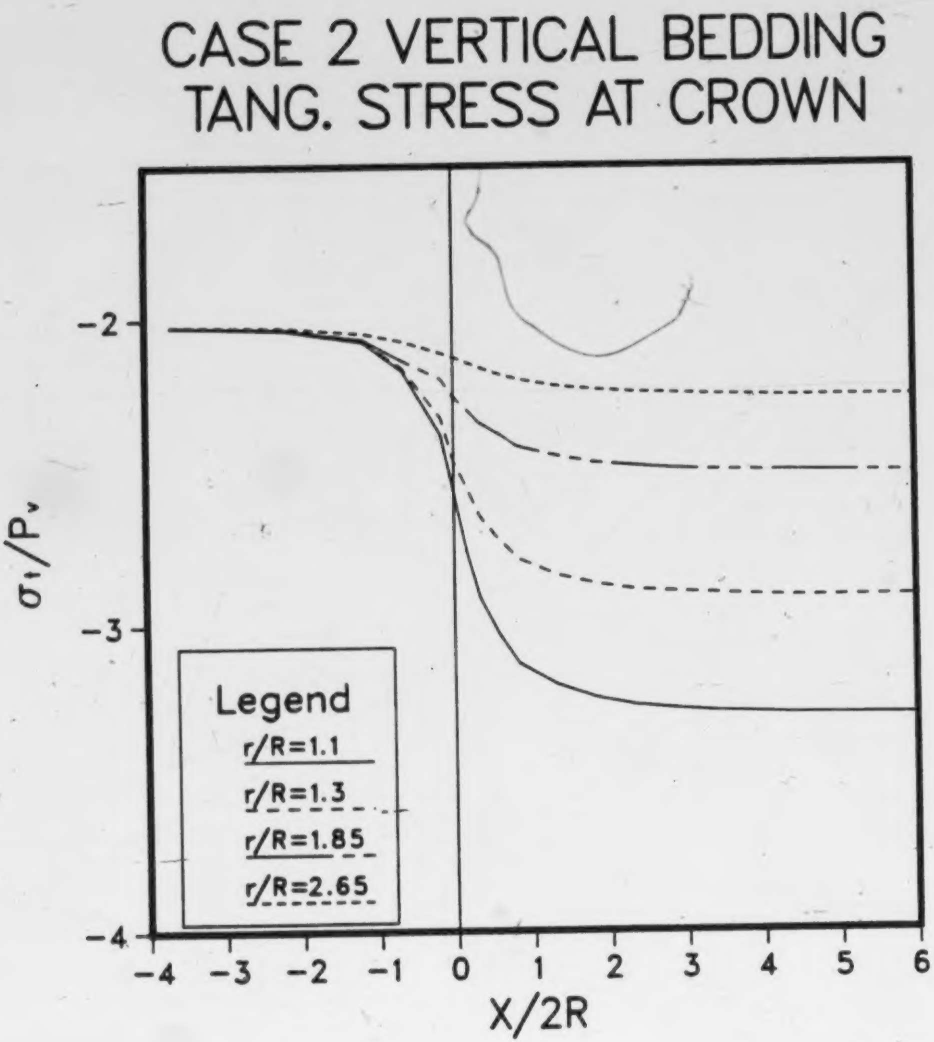

Figure B.14 Tangential Stresses, σ_t, at the Tunnel Crown (Case 2)

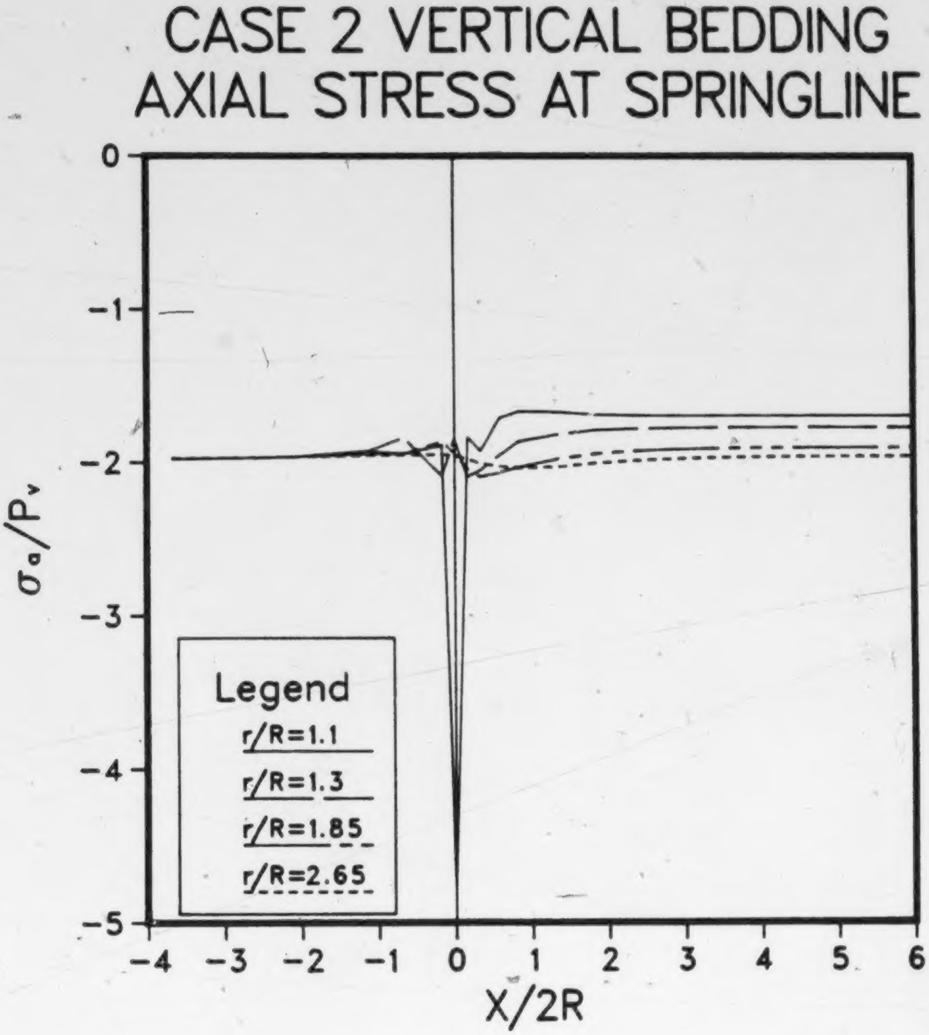

Figure B.15 Axial Stresses, σ_a, at the Tunnel Springline (Case 2)

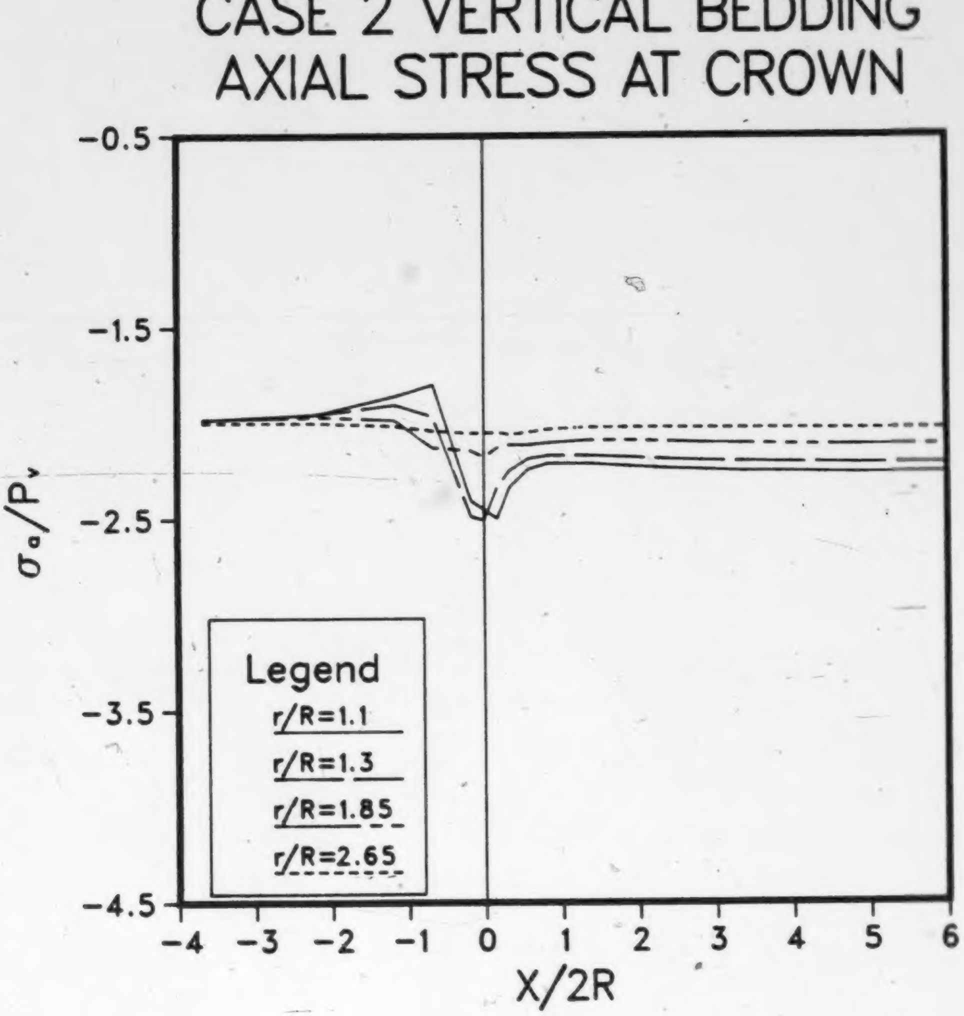

Figure B.16 Axial Stresses, σ_a, at the Tunnel Crown (Case 2)

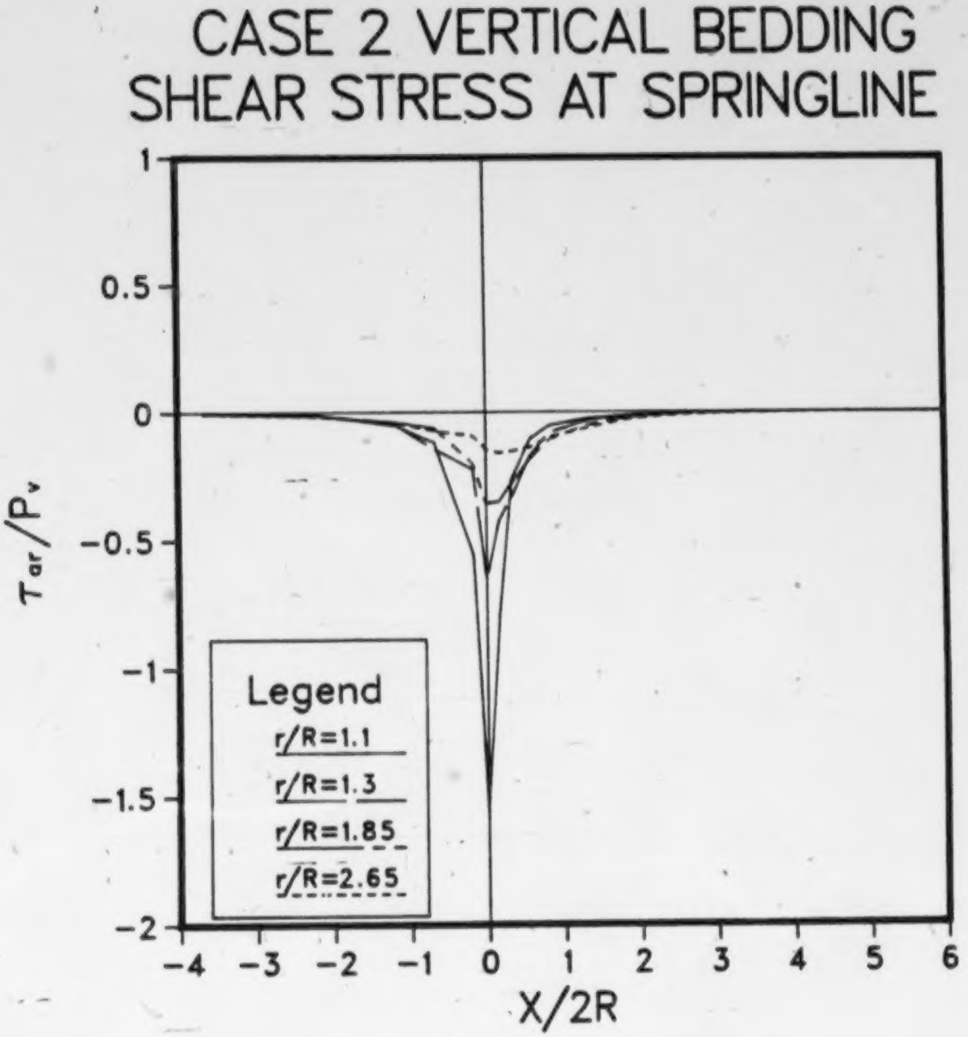

Figure B.17 Shear Stresses, τ_{ar}, at the Tunnel Springline (Case 2)

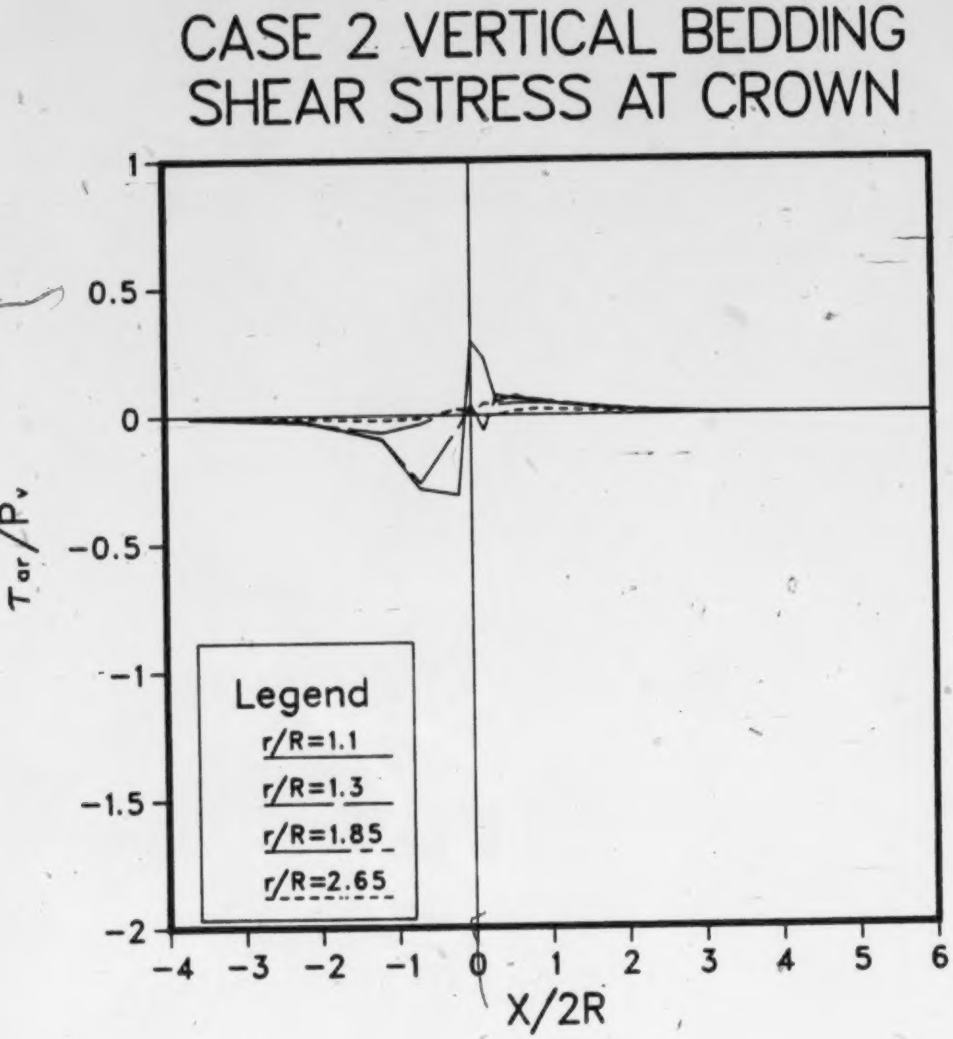

Figure B.18 Shear Stresses, τ_{ar}, at the Tunnel Crown (Case 2)

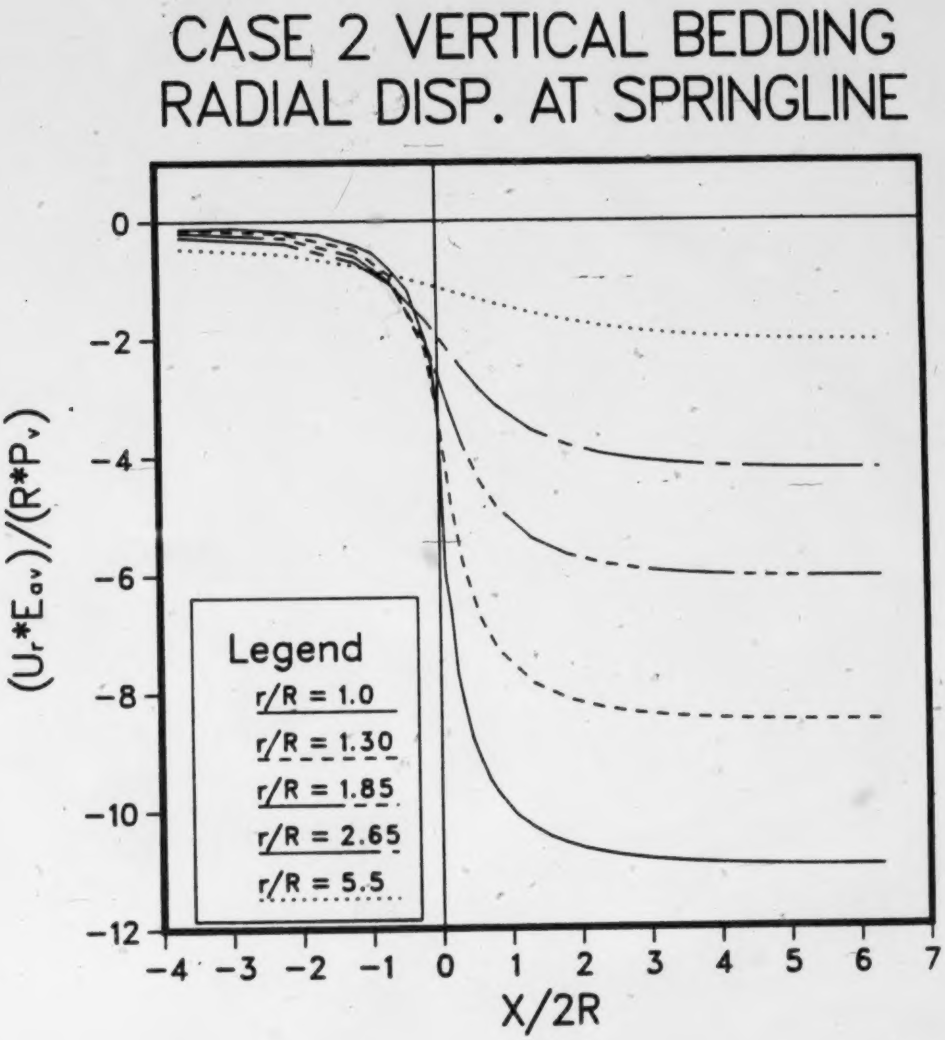

Figure B.19 Radial Displacements, U_r, at the Tunnel Springline (Case 2)

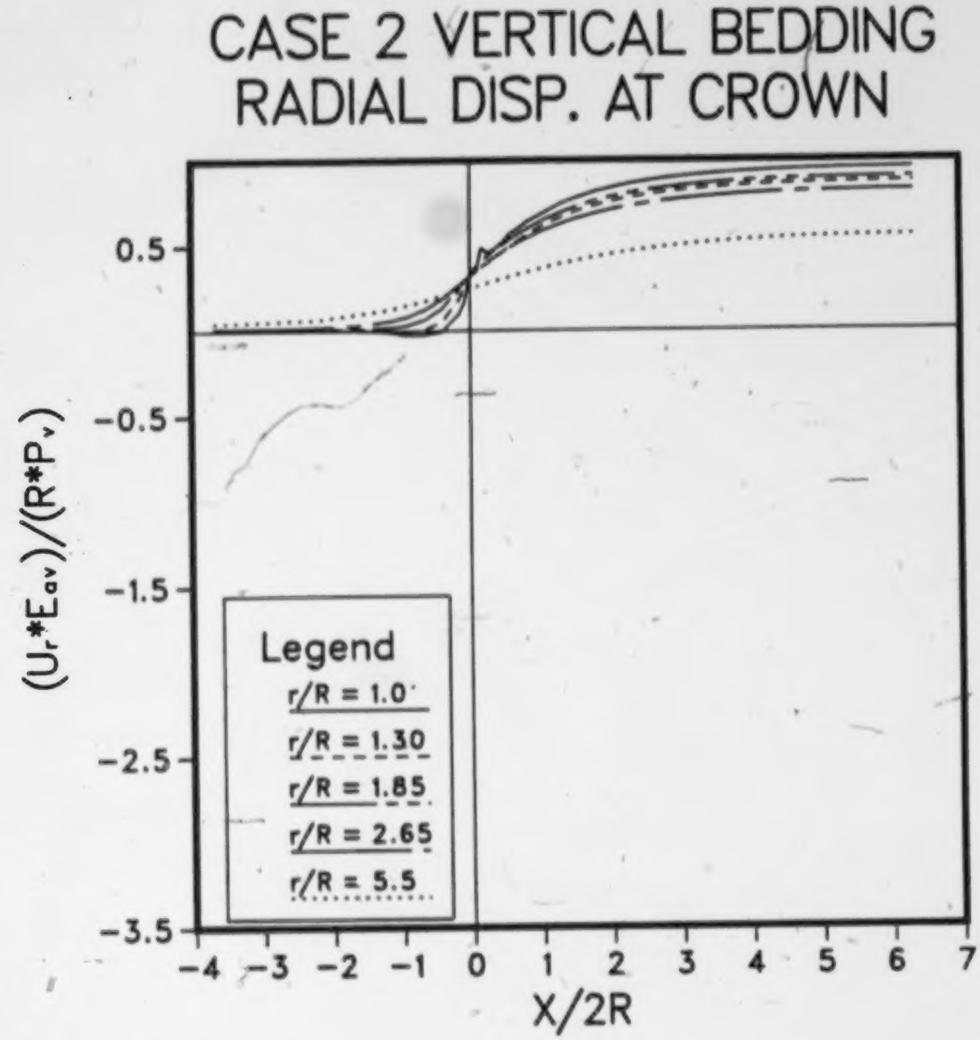

Figure B.20 Radial Displacements, U_r, at the Tunnel Crown (Case 2)

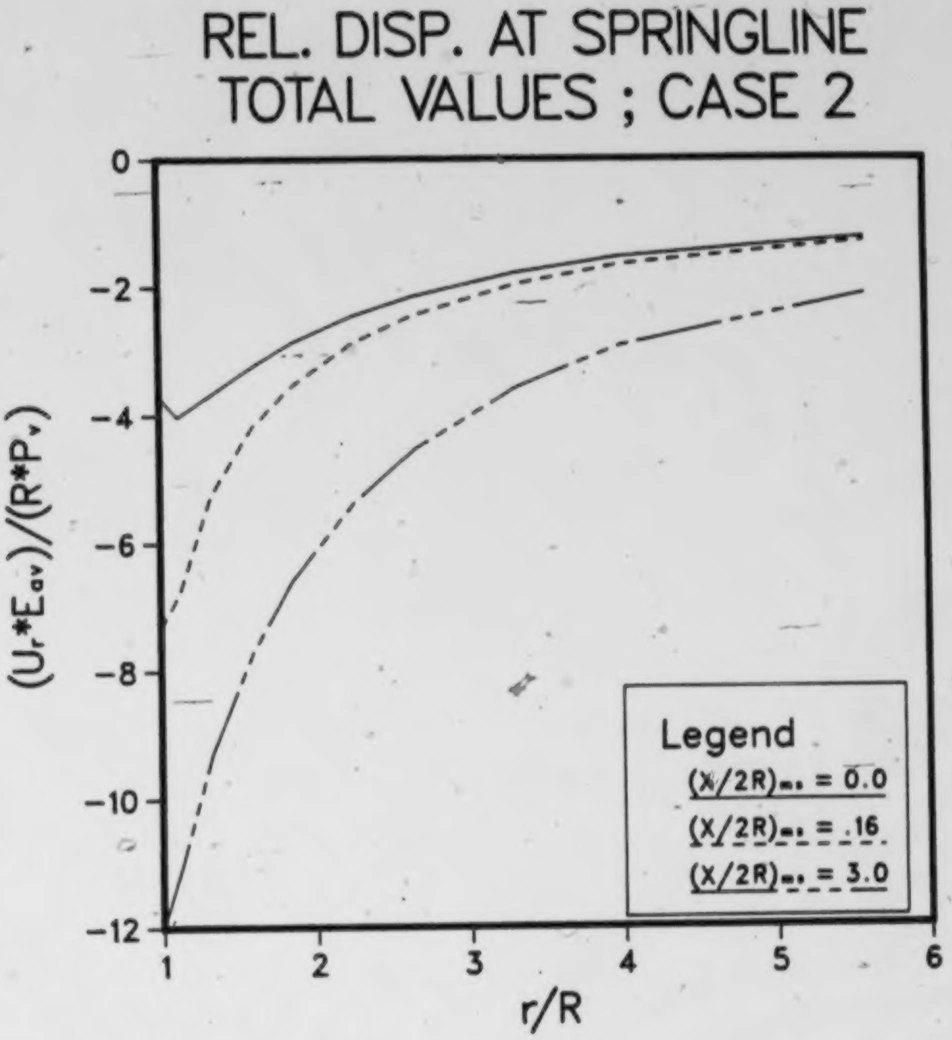

Figure B.21 Radial Displacement Profiles at the Tunnel Springline (Total Values; Case 2)

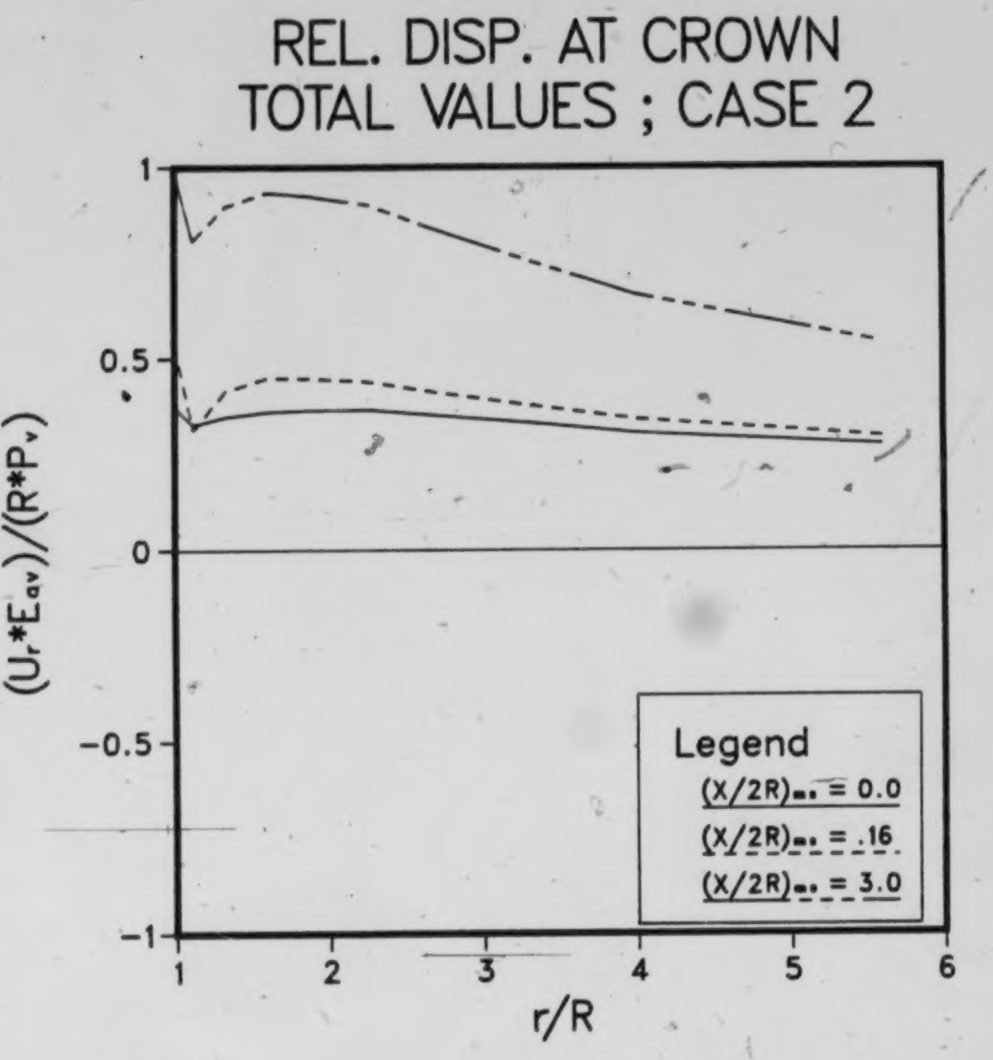

Figure B.22 Radial Displacement Profiles at the Tunnel Crown (Total Values; Case 2)

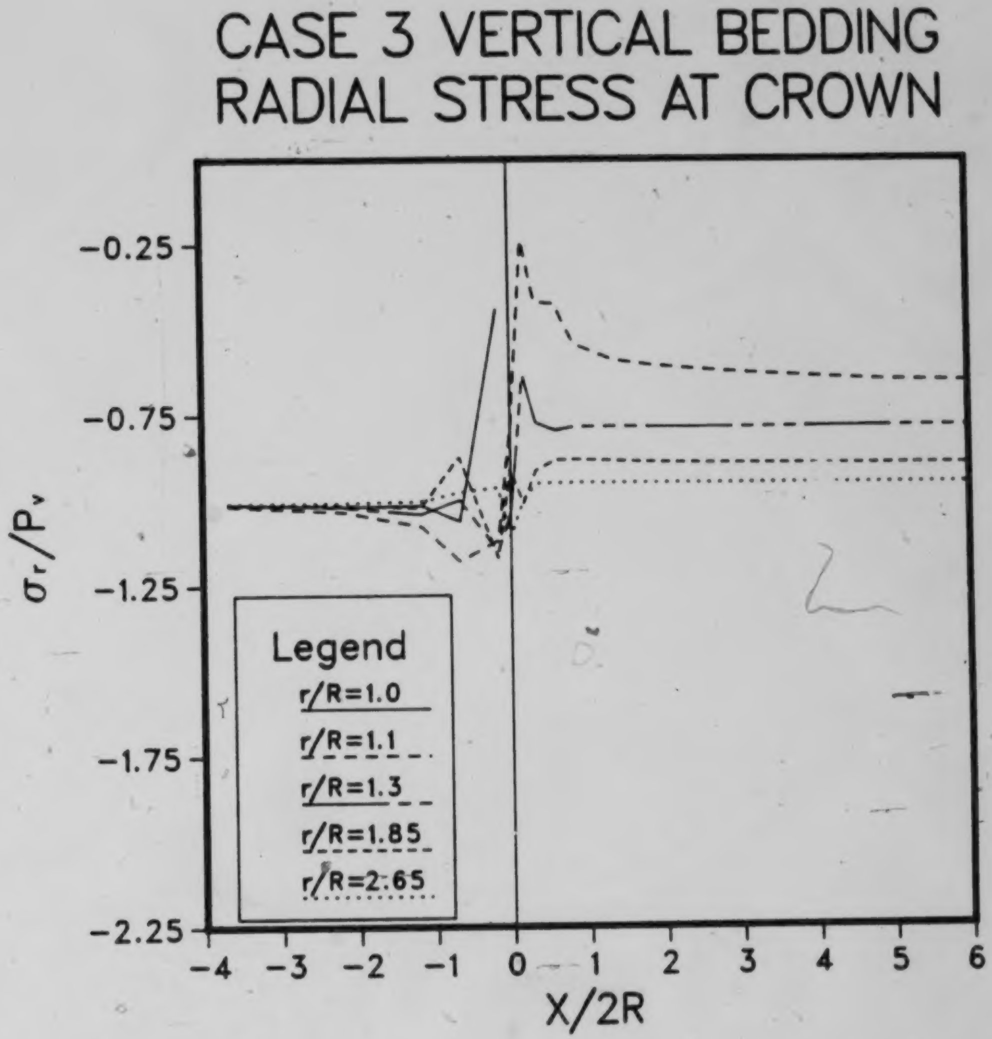

Figure B.23 Radial Stresses, σ_r, at the Tunnel Crown (Case 3)

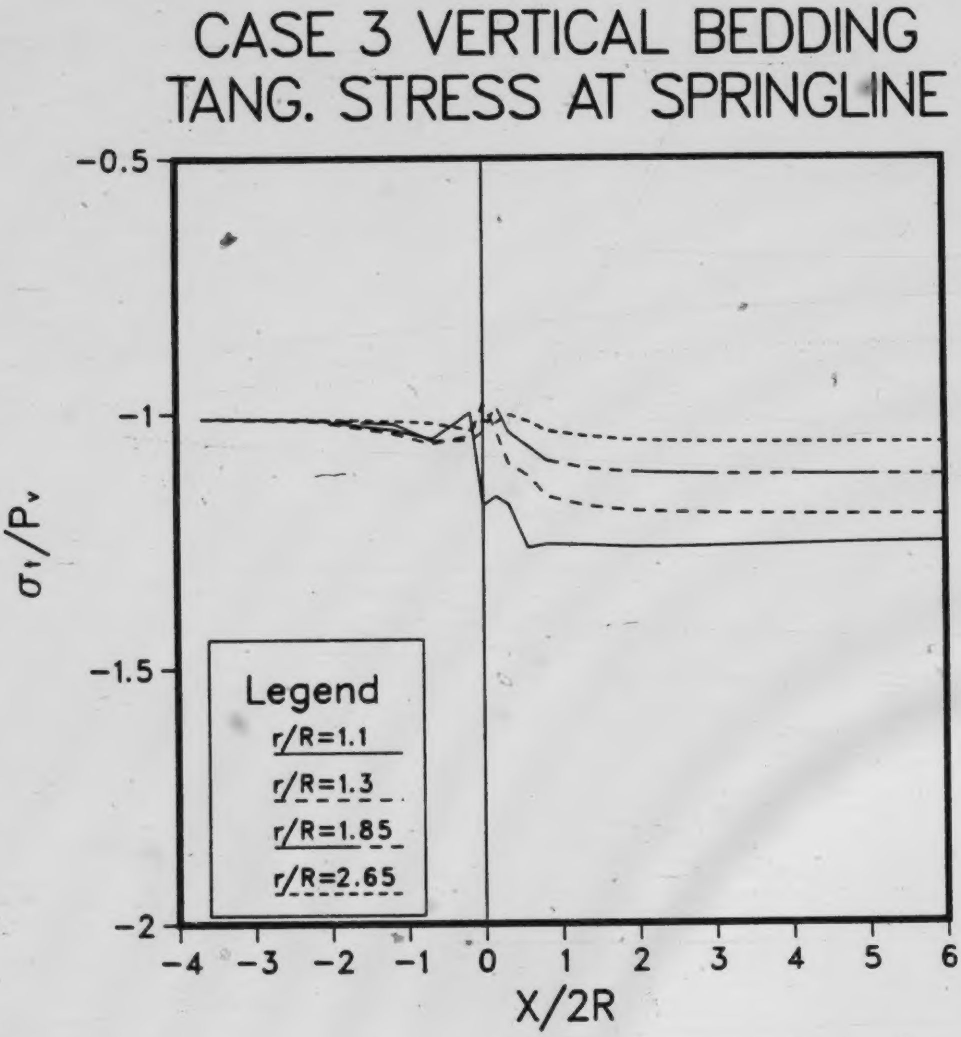

Figure B.24 Tangential Stresses, σ_t, at the Tunnel Springline (Case 3)

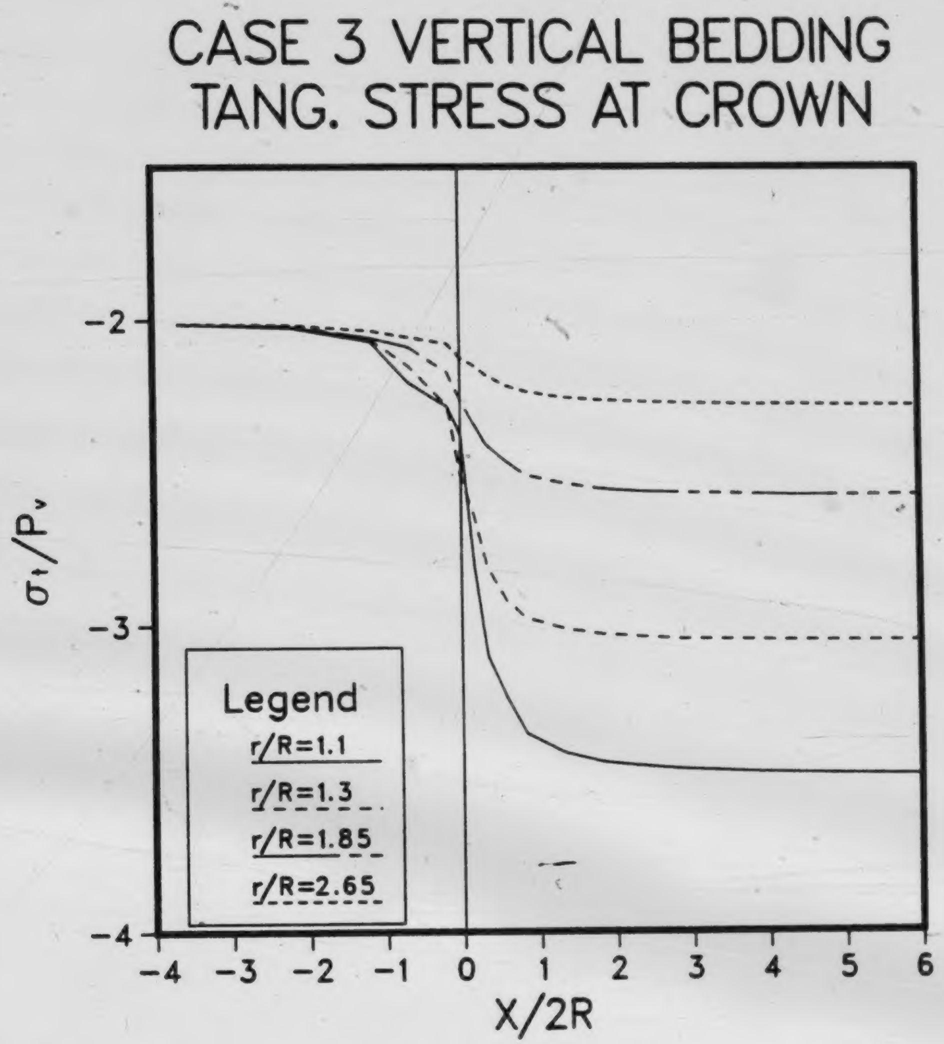

Figure B.25 Tangential Stresses, σ_t, at the Tunnel Crown (Case 3)

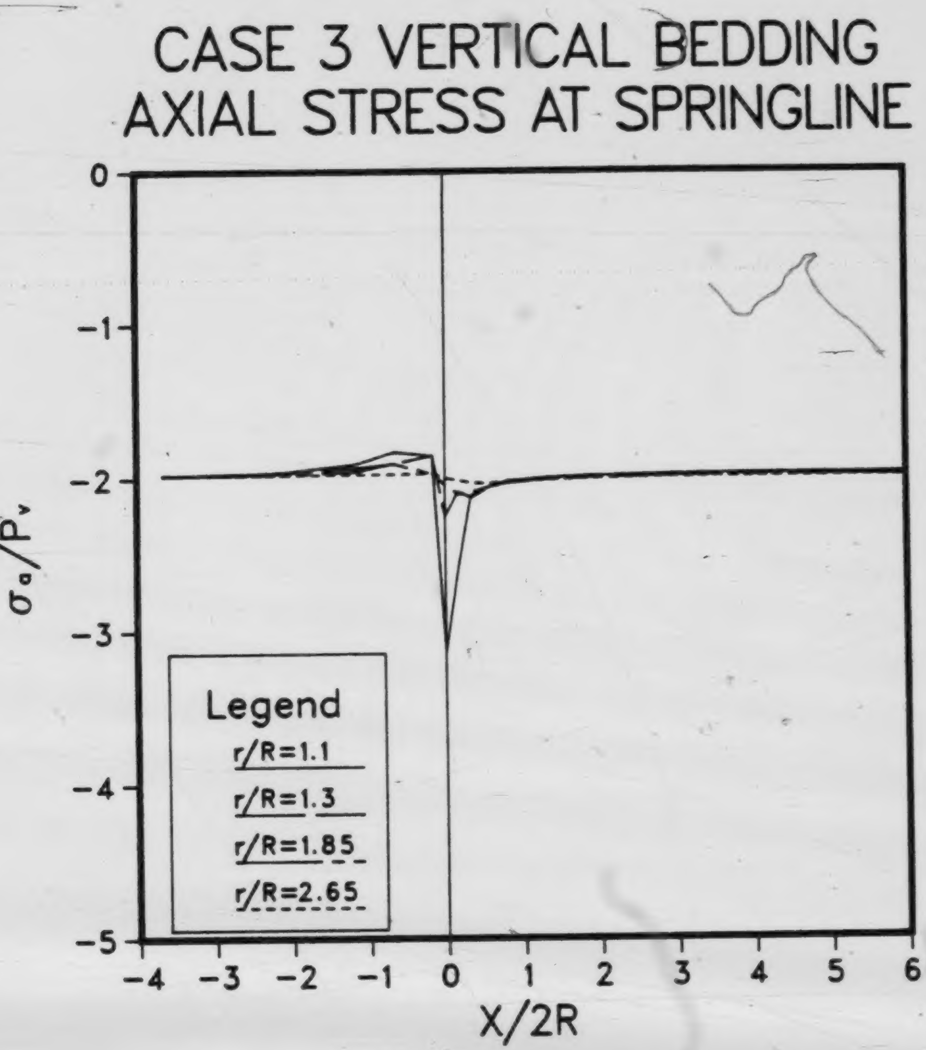

Figure B.26 Axial Stresses, σ_a, at the Tunnel Springline (Case 3)

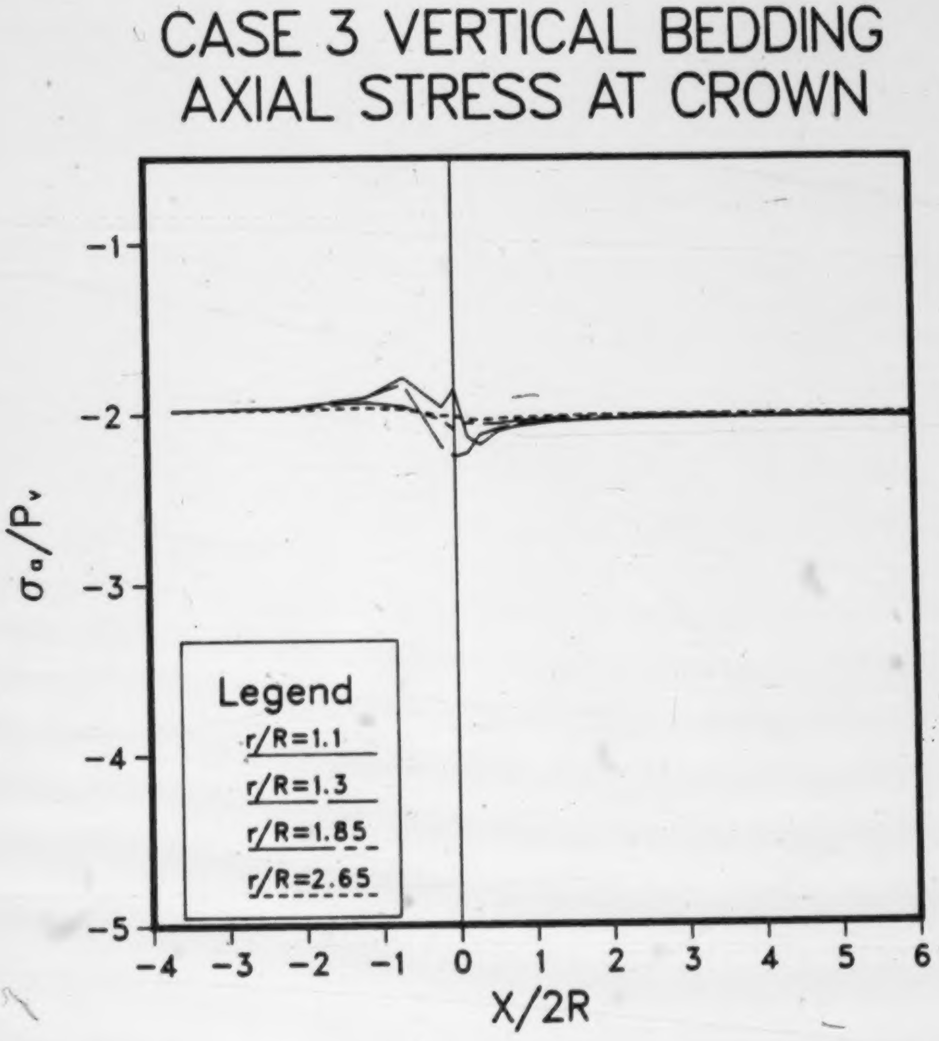

Figure B.27 Axial Stresses, σ_a, at the Tunnel Crown (Case 3)

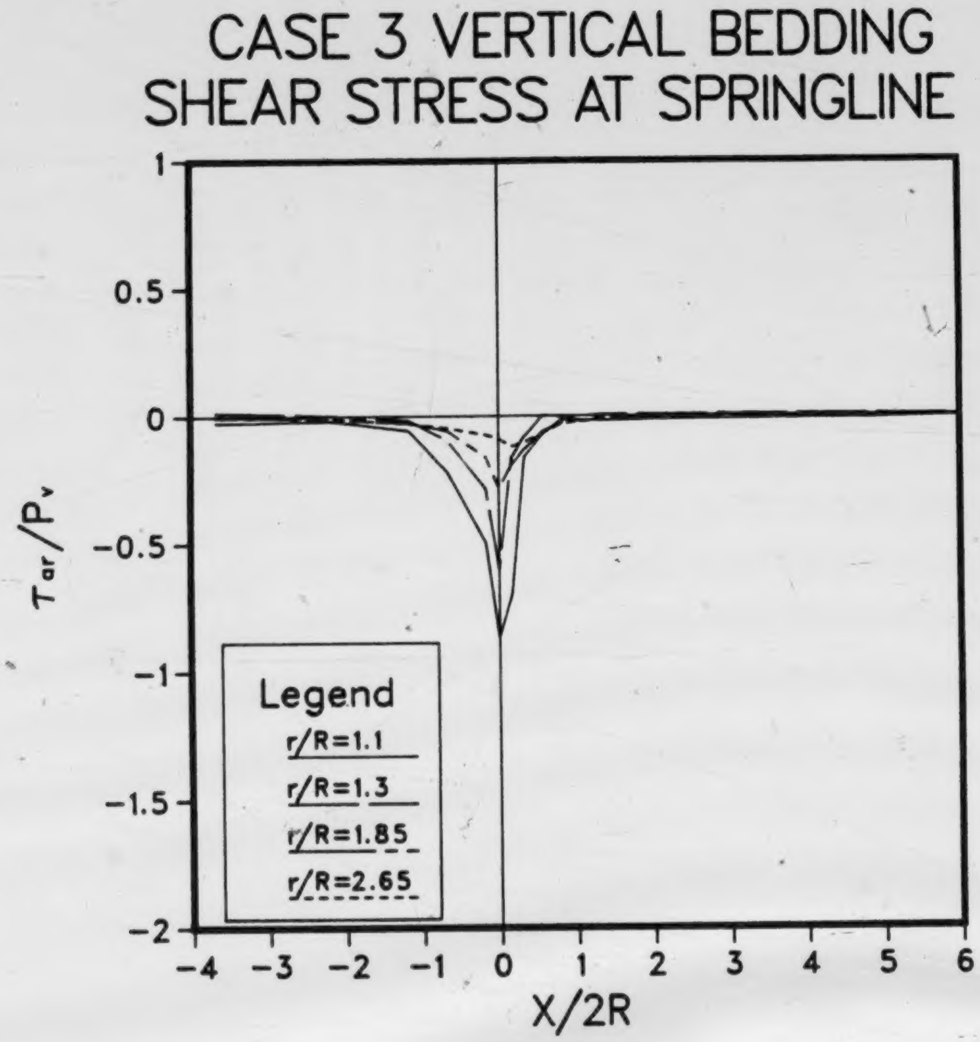

Figure B.28 Shear Stresses, τ_{ar}, at the Tunnel Springline (Case 3)

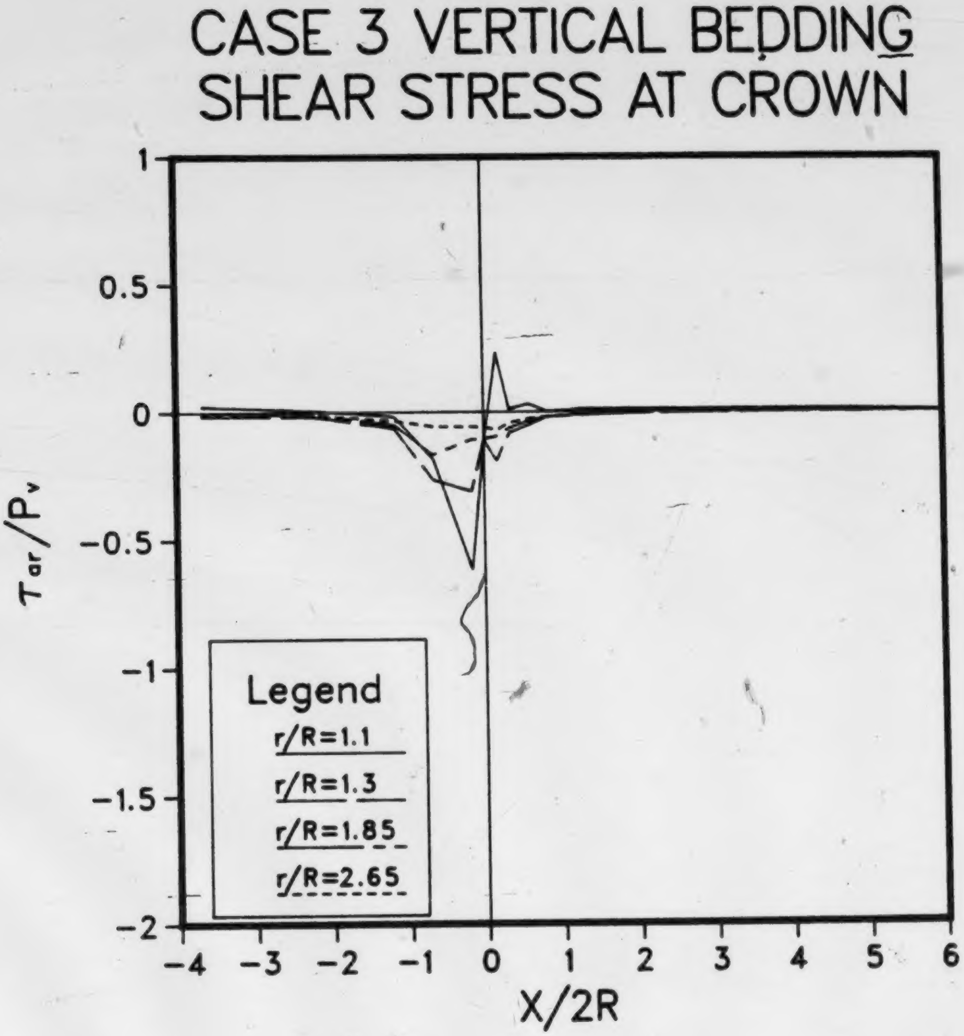

Figure B.29 Shear Stresses, τ_{ar}, at the Tunnel Crown (Case 3)

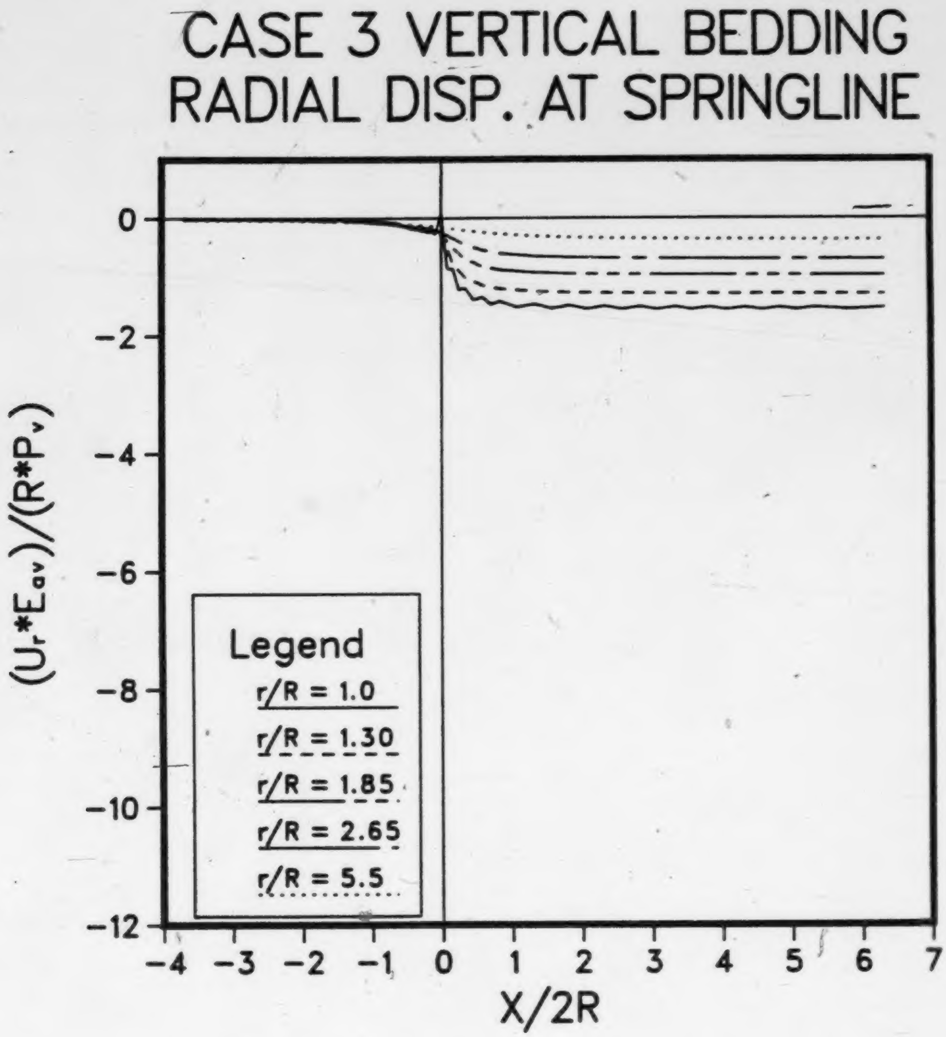

Figure B.30 Radial Displacements, U_r, at the Tunnel Springline (Case 3)

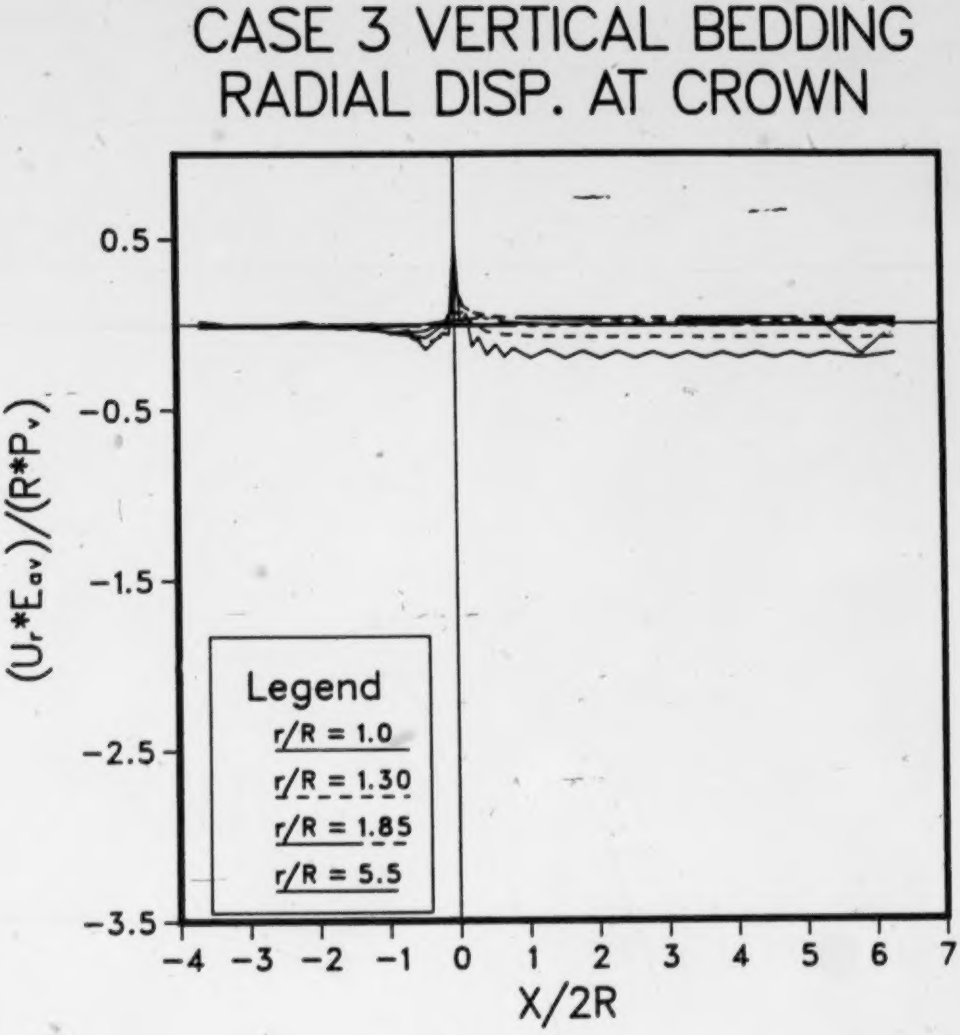

Figure B.31 Radial Displacements, U_r, at the Tunnel Crown (Case 3)

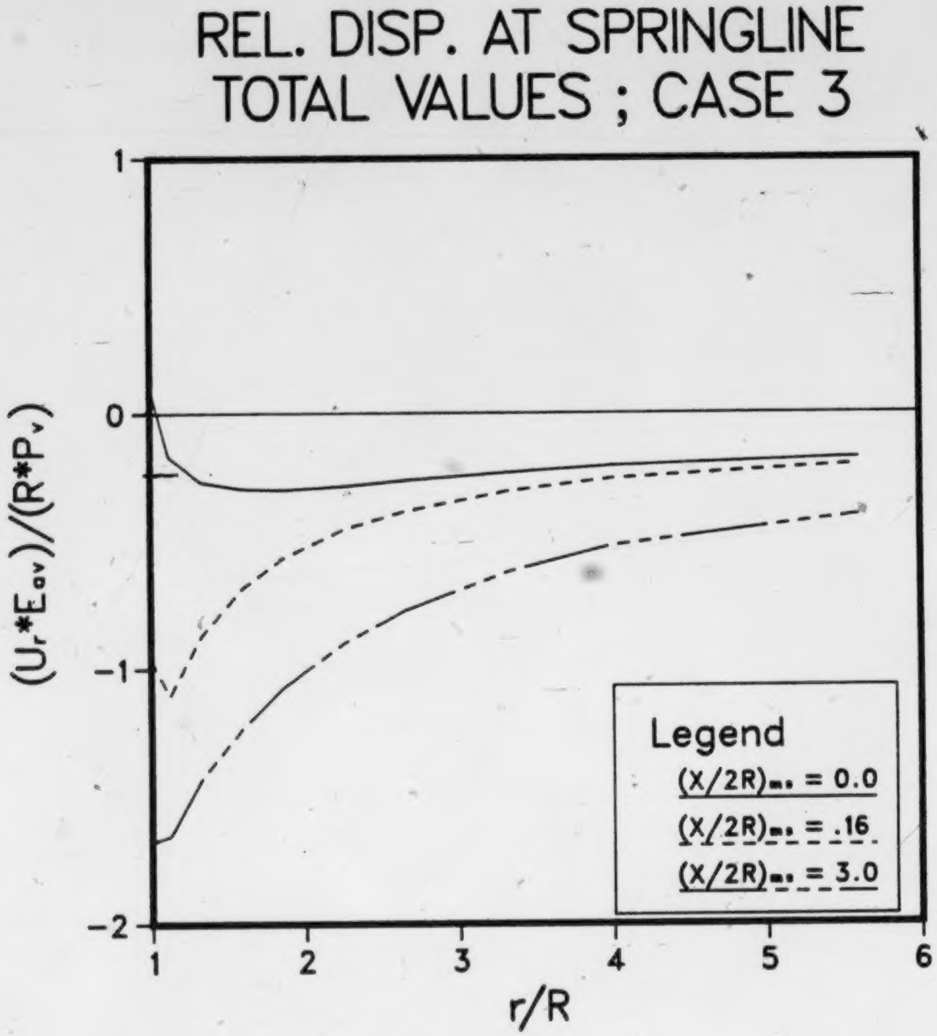

Figure B.32 Radial Displacement Profiles at the Tunnel Springline (Total Values; Case 3)

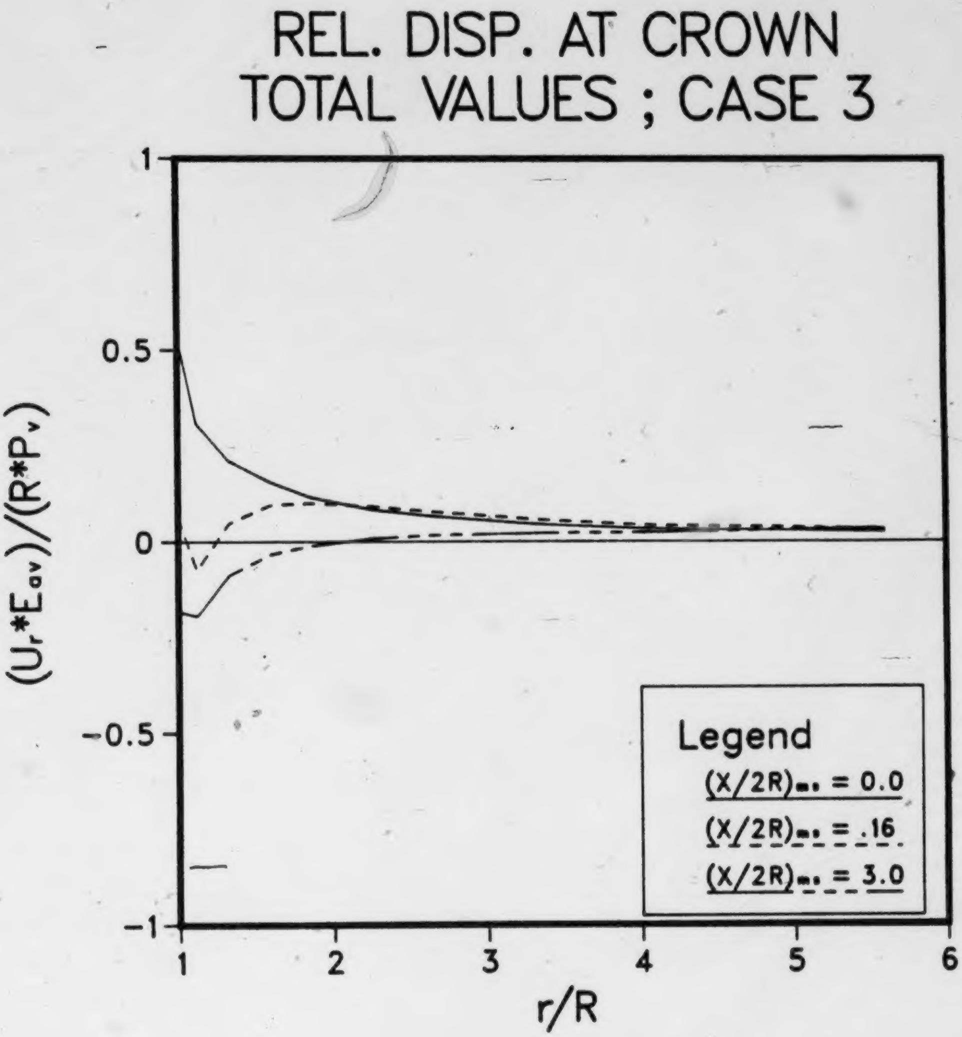

Figure B.33 Radial Displacement Profiles at the Tunnel Crown (Total Values; Case 3)

APPENDIX C

Unlined Tunnels in Non-Linear Isotropic Rock

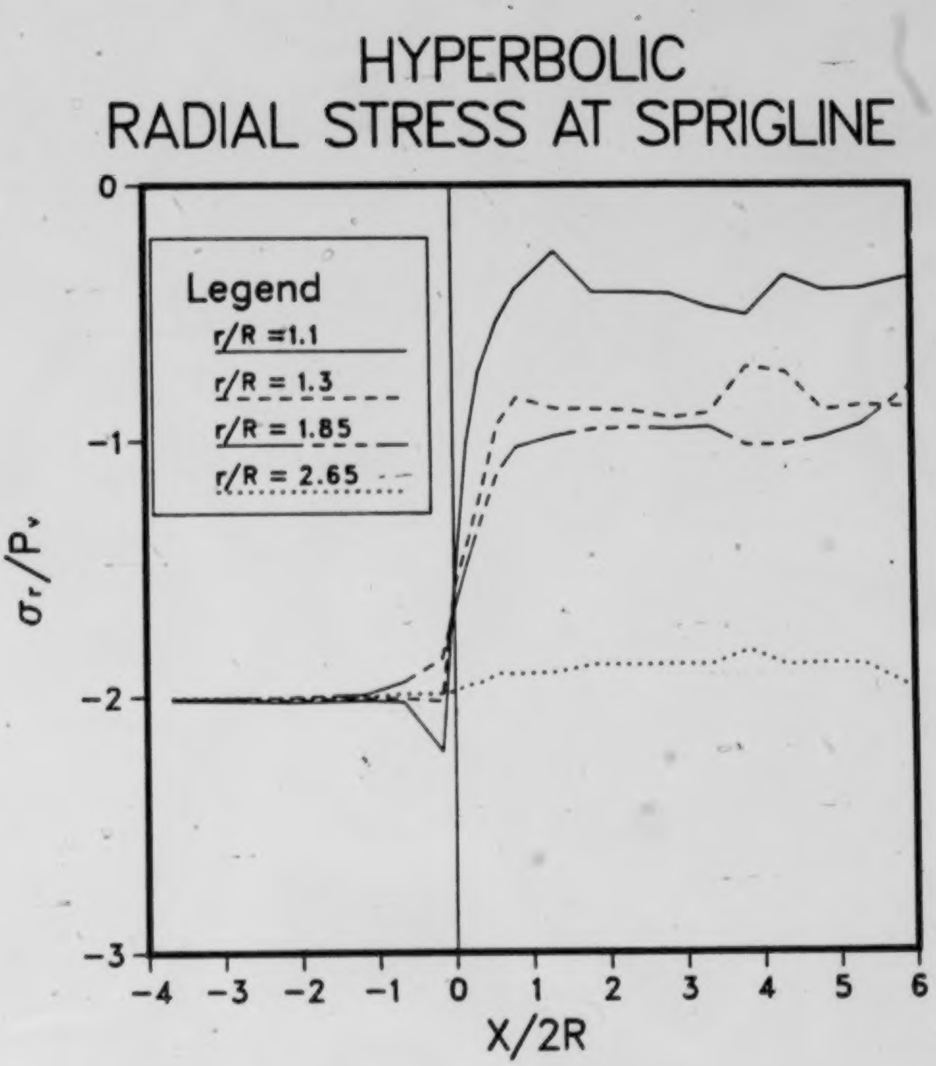

Figure C.1 Radial Stresses, σ_r, at the Tunnel Springline (Hyperbolic)

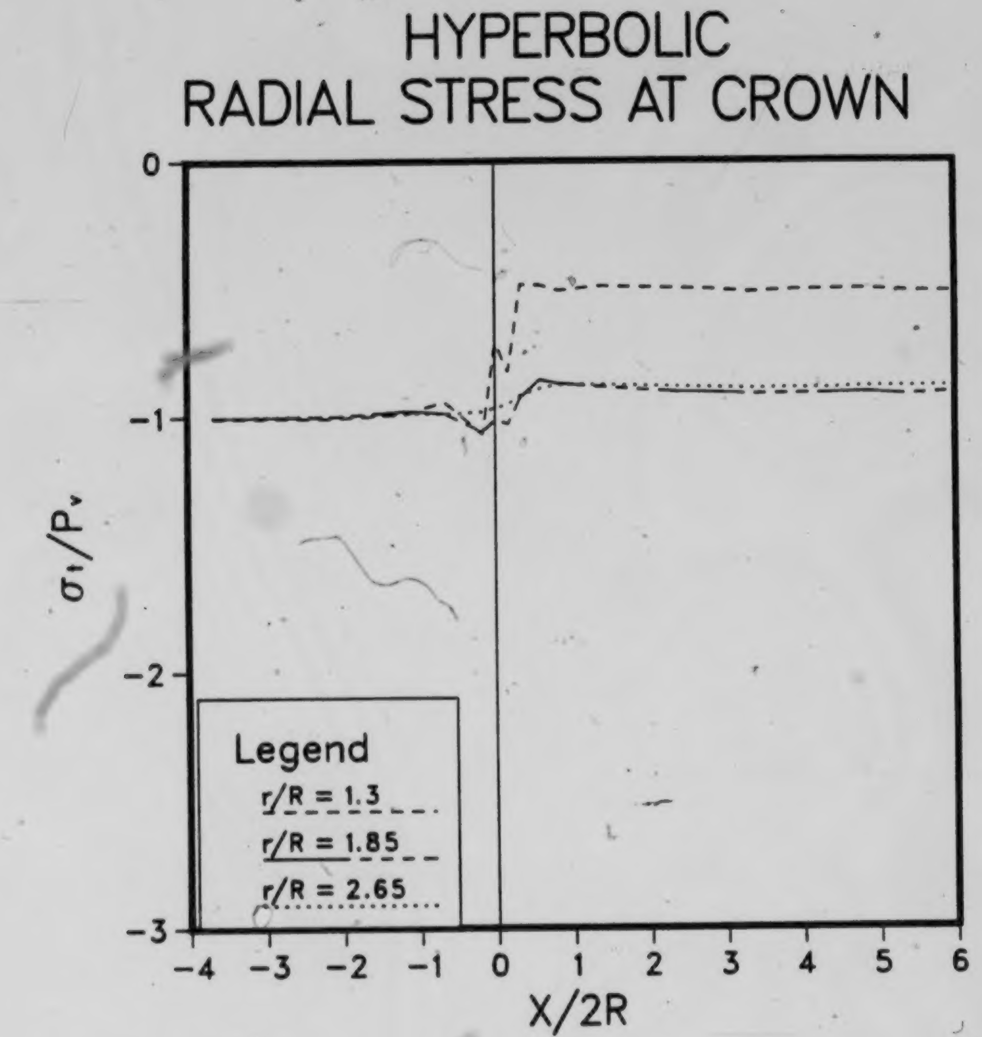

Figure C.2 Radial Stresses, σ_r, at the Tunnel Crown (Hyperbolic)

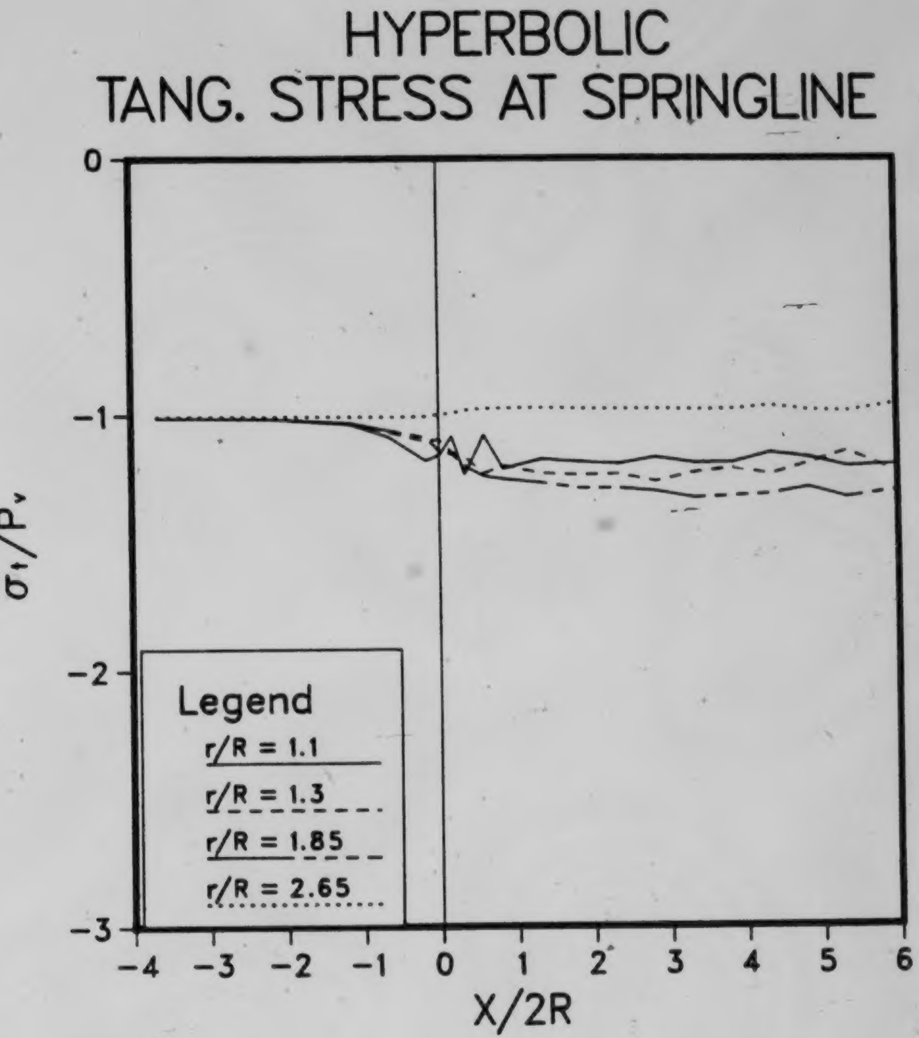

Figure C.3 Tangential Stresses, σ_t, at the Tunnel Springline (Hyperbolic)

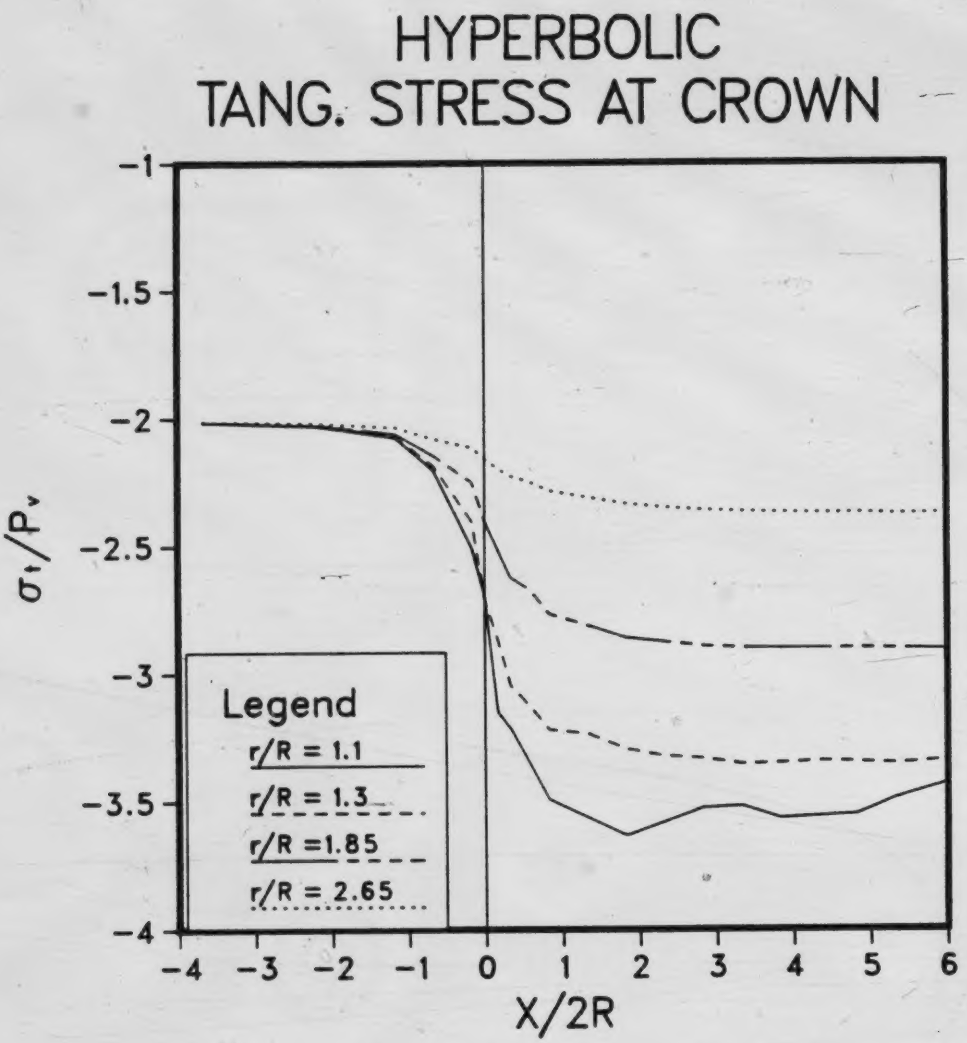

Figure C.4 Tangential Stresses, σ_t, at the Tunnel Crown (Hyperbolic)

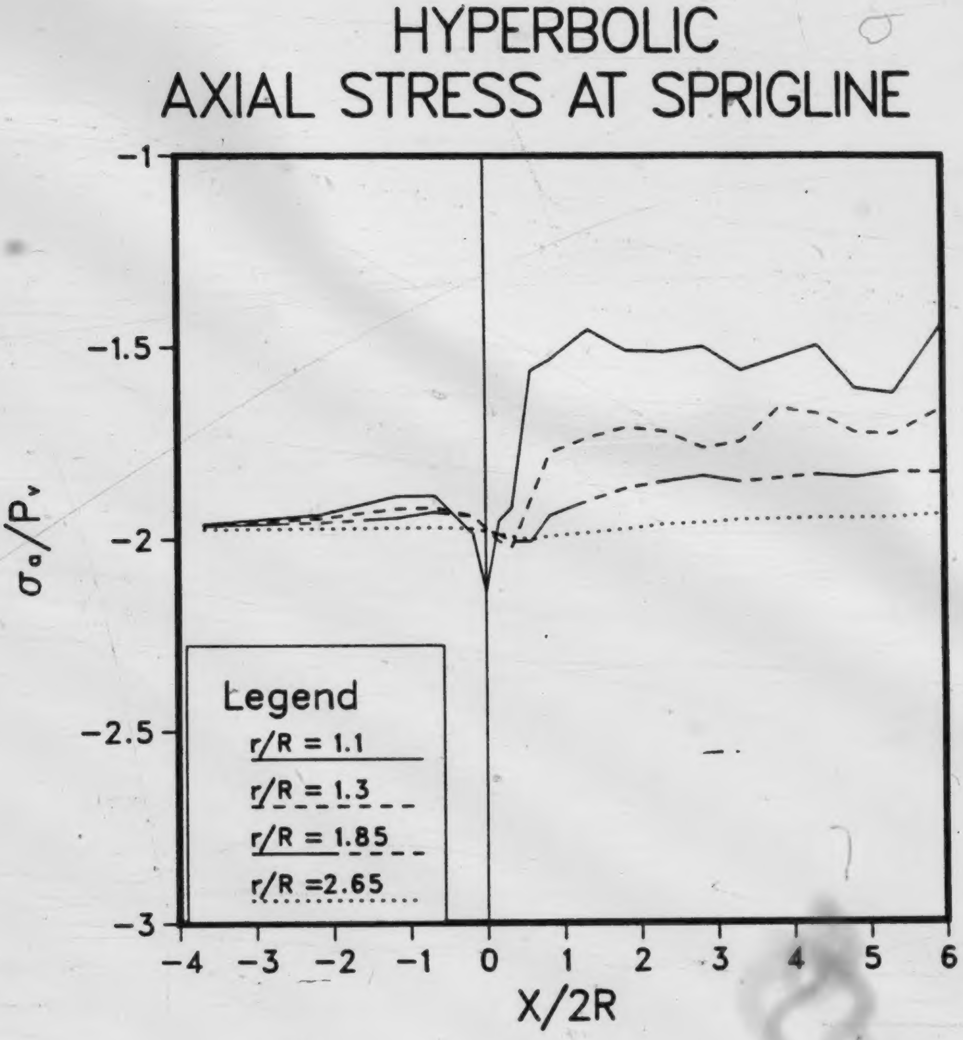

Figure C.5 Axial Stresses, σ_a, at the Tunnel Springline (Hyperbolic)

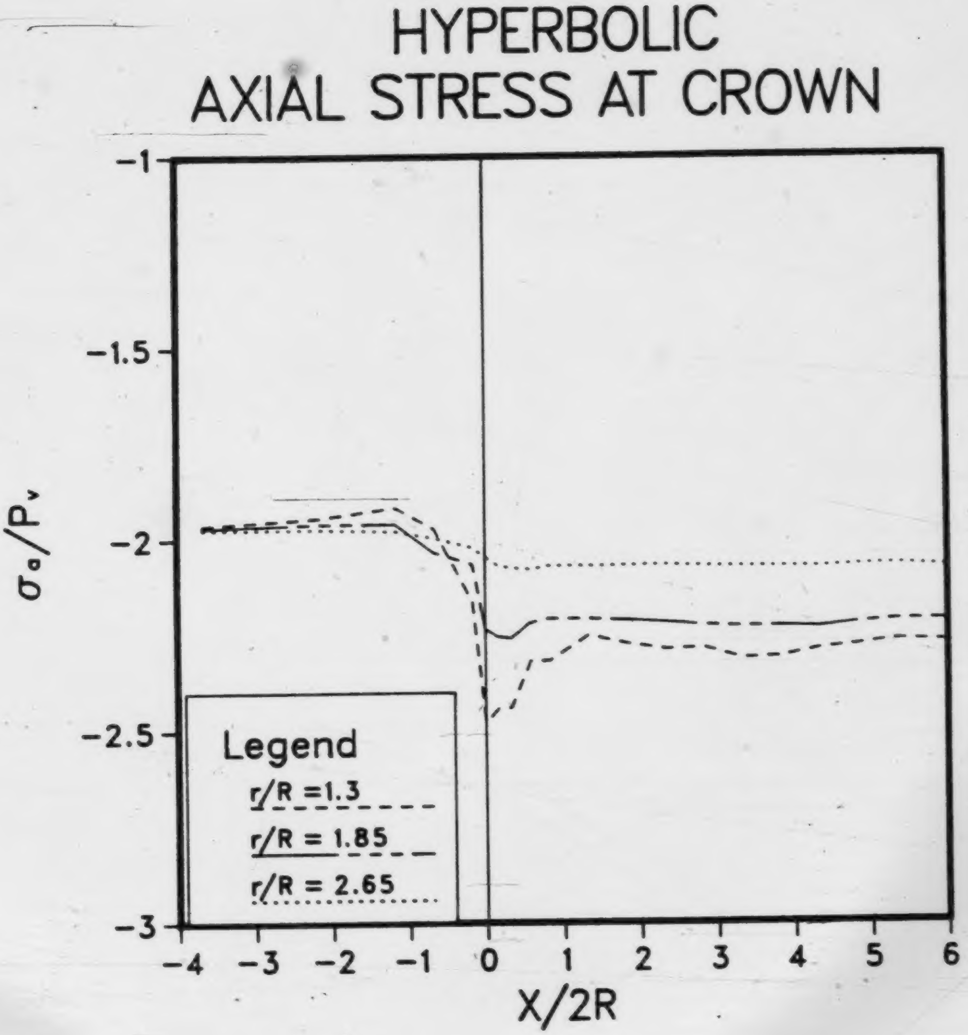

Figure C.6 Axial Stresses, σ_a, at the Tunnel Crown (Hyperbolic)

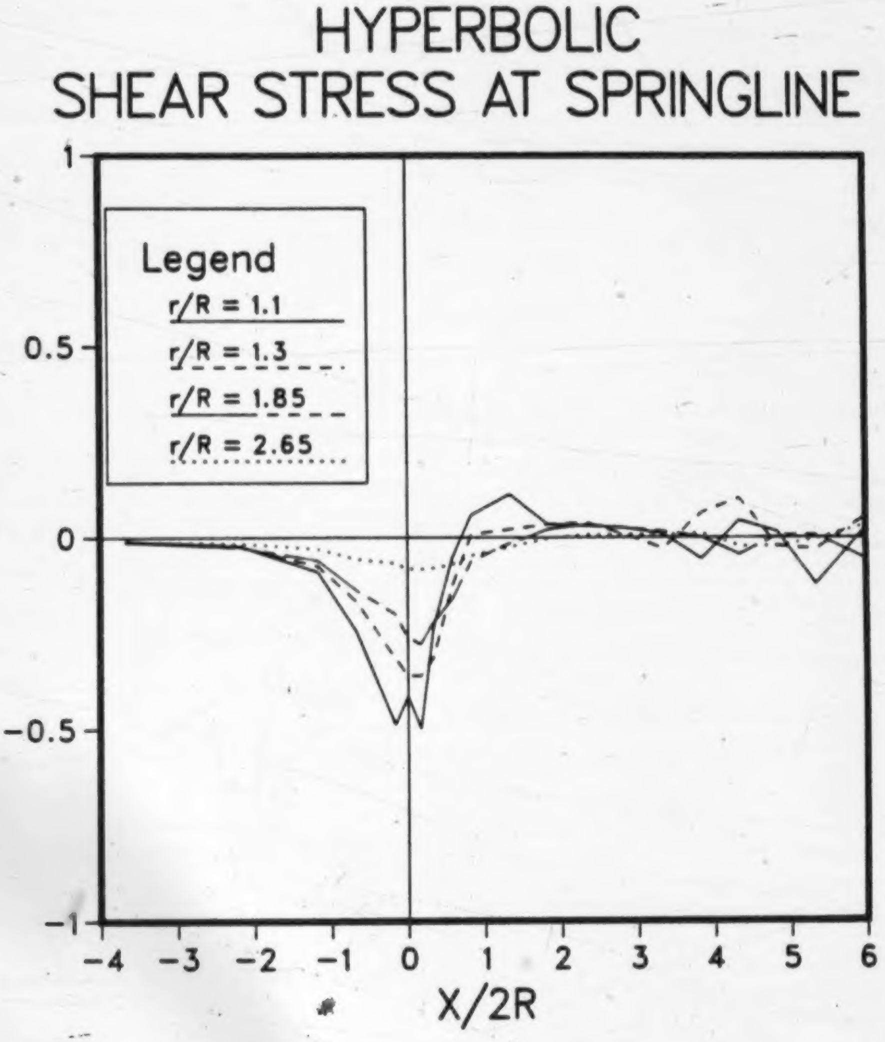

Figure C.7 Shear Stresses, τ_{ar}, at the Tunnel Springline (Hyperbolic)

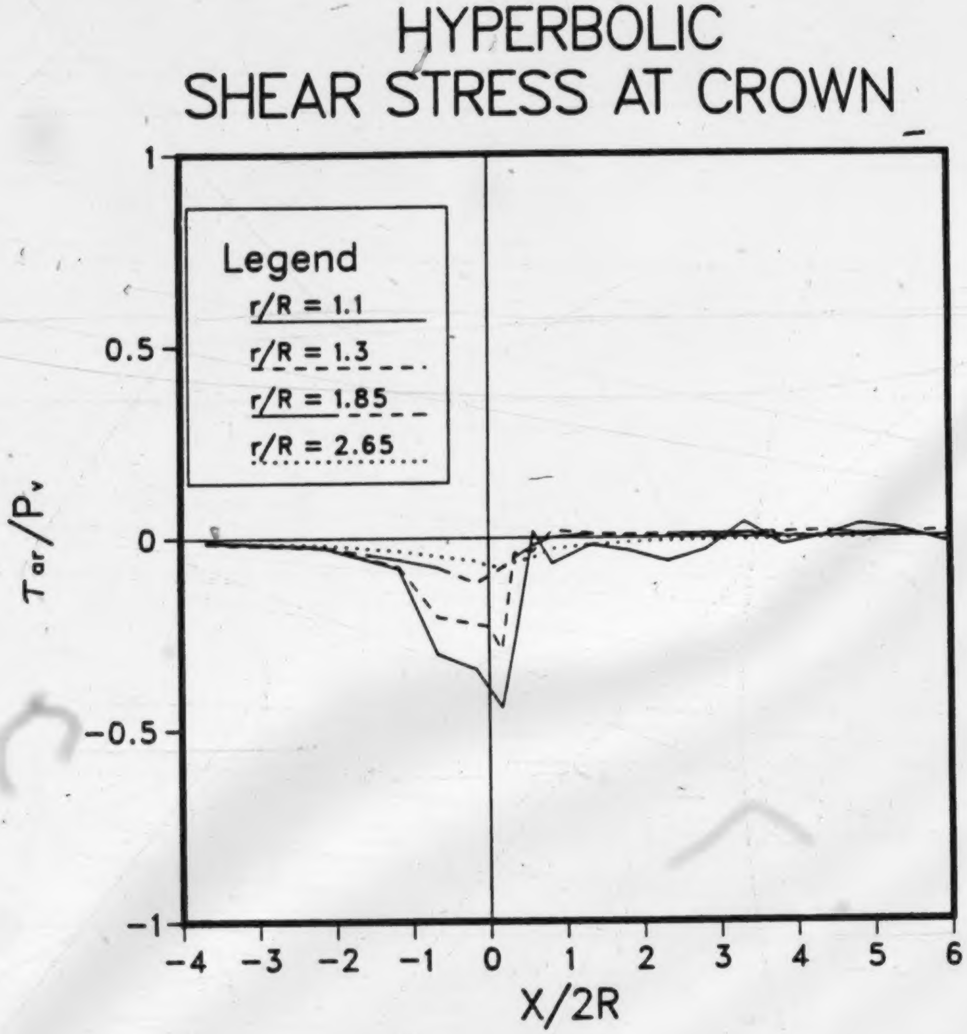

Figure C.8 Shear Stresses, τ_{ar}, at the Tunnel Crown (Hyperbolic)

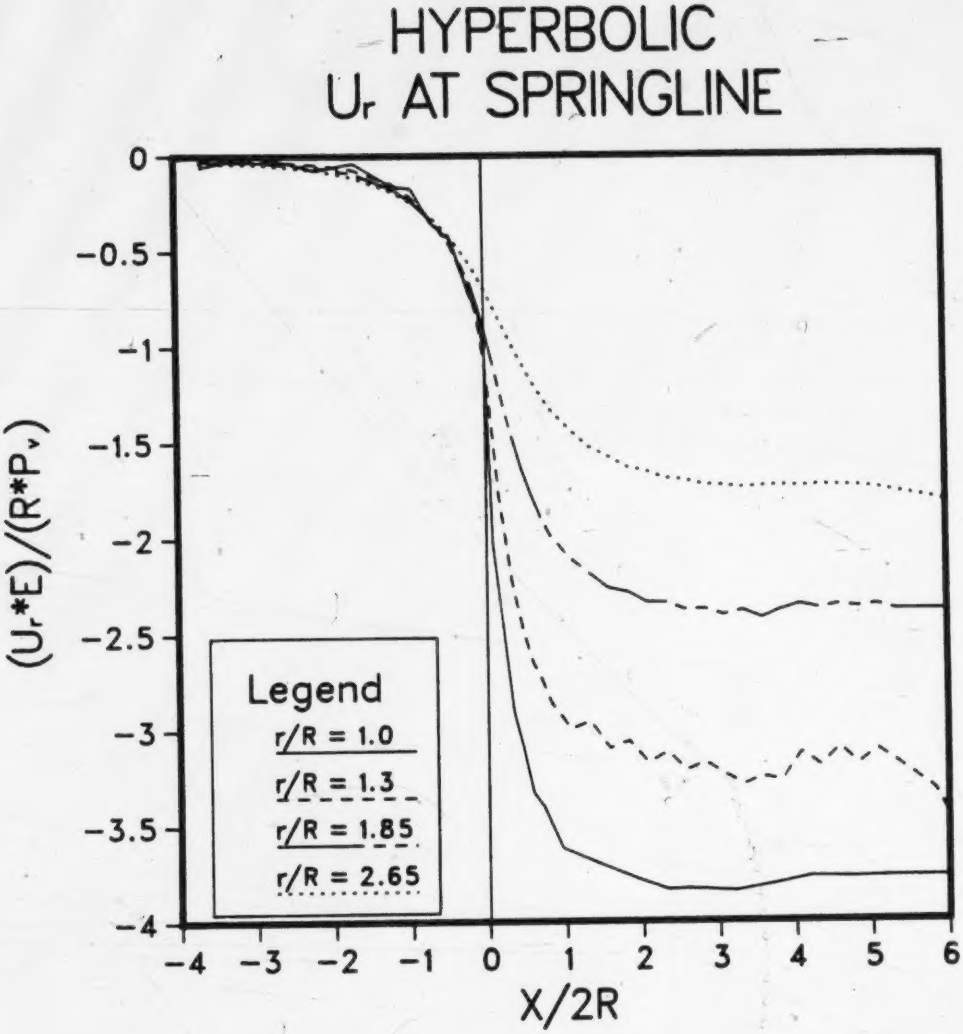

Figure C.9 Radial Displacements, U_r, at the Tunnel Springline (Hyperbolic)

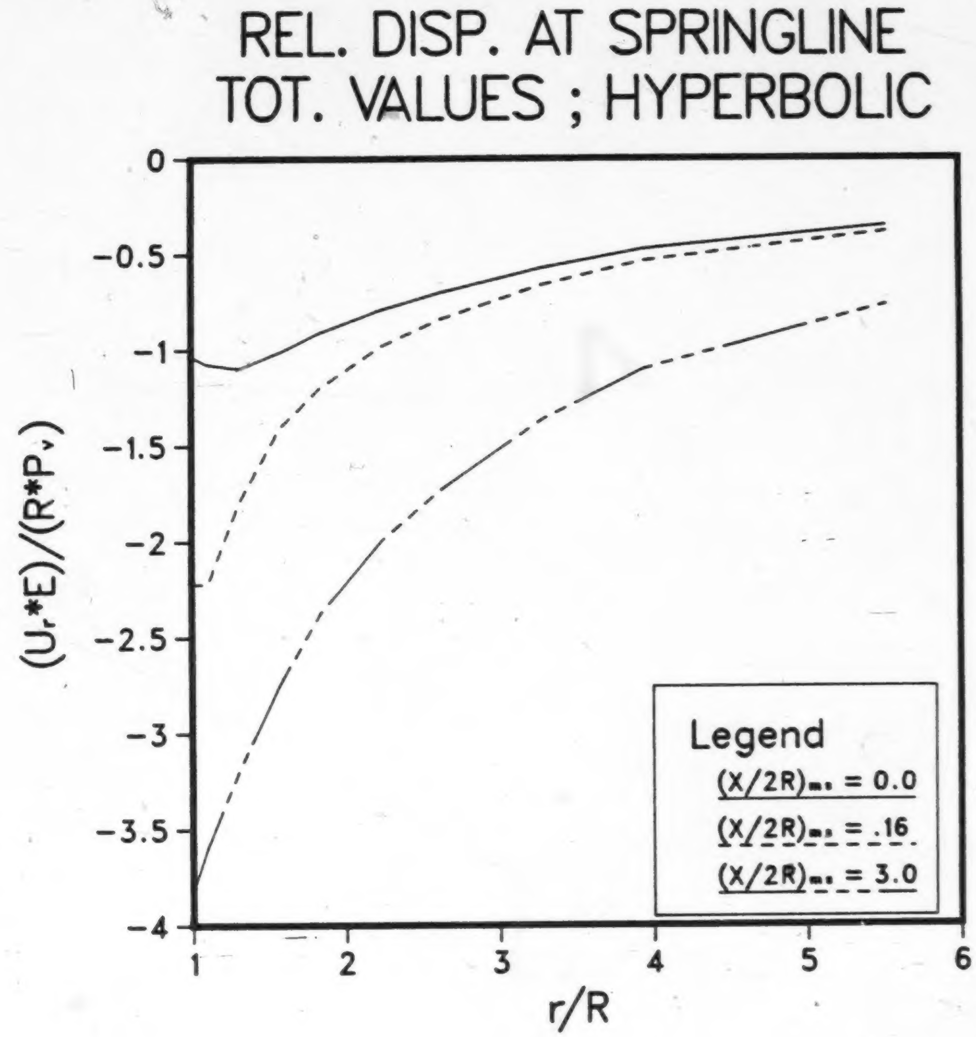

Figure C.10 Radial Displacement Profiles at the Tunnel Springline (Total Values; Hyperbolic)

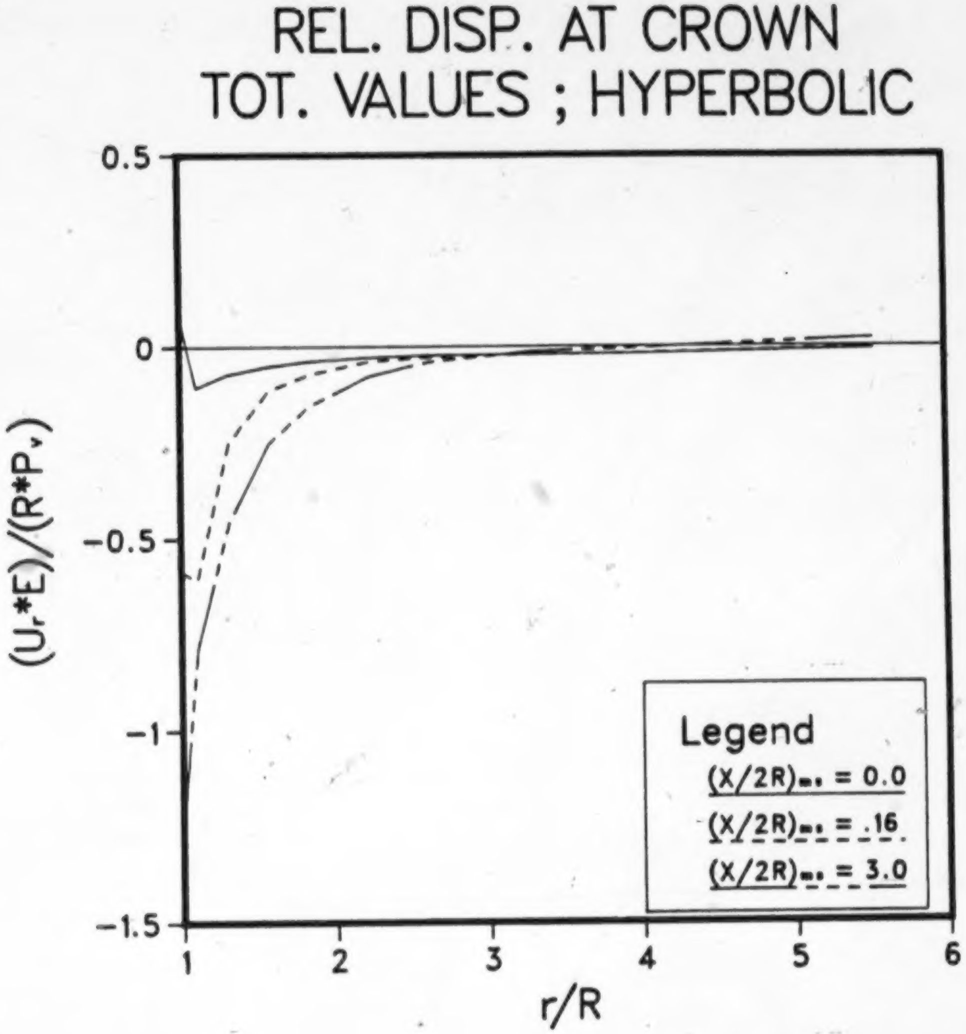

Figure C.11 Radial Displacement Profiles at the Tunnel Crown (Total Values; Hyperbolic)

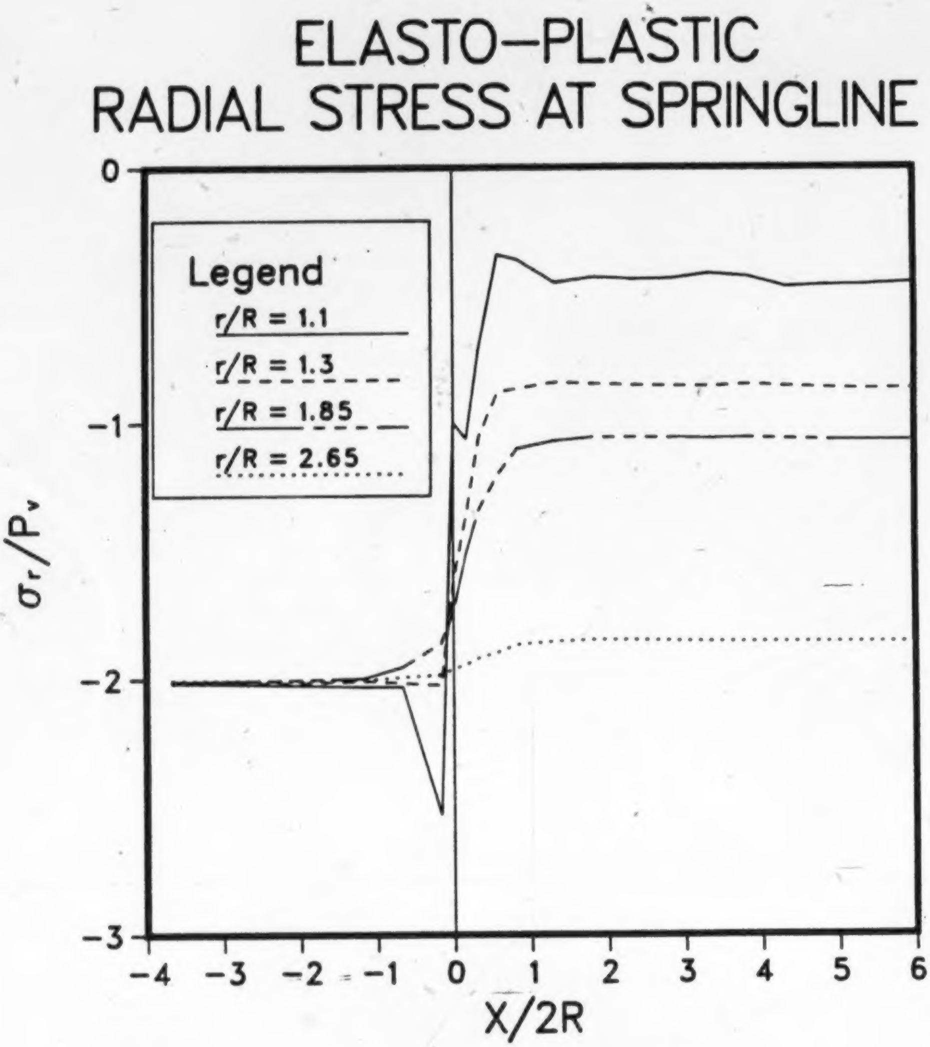

Figure C.12 Radial Stresses, σ_r, at the Tunnel Springline (Elasto-Plastic)

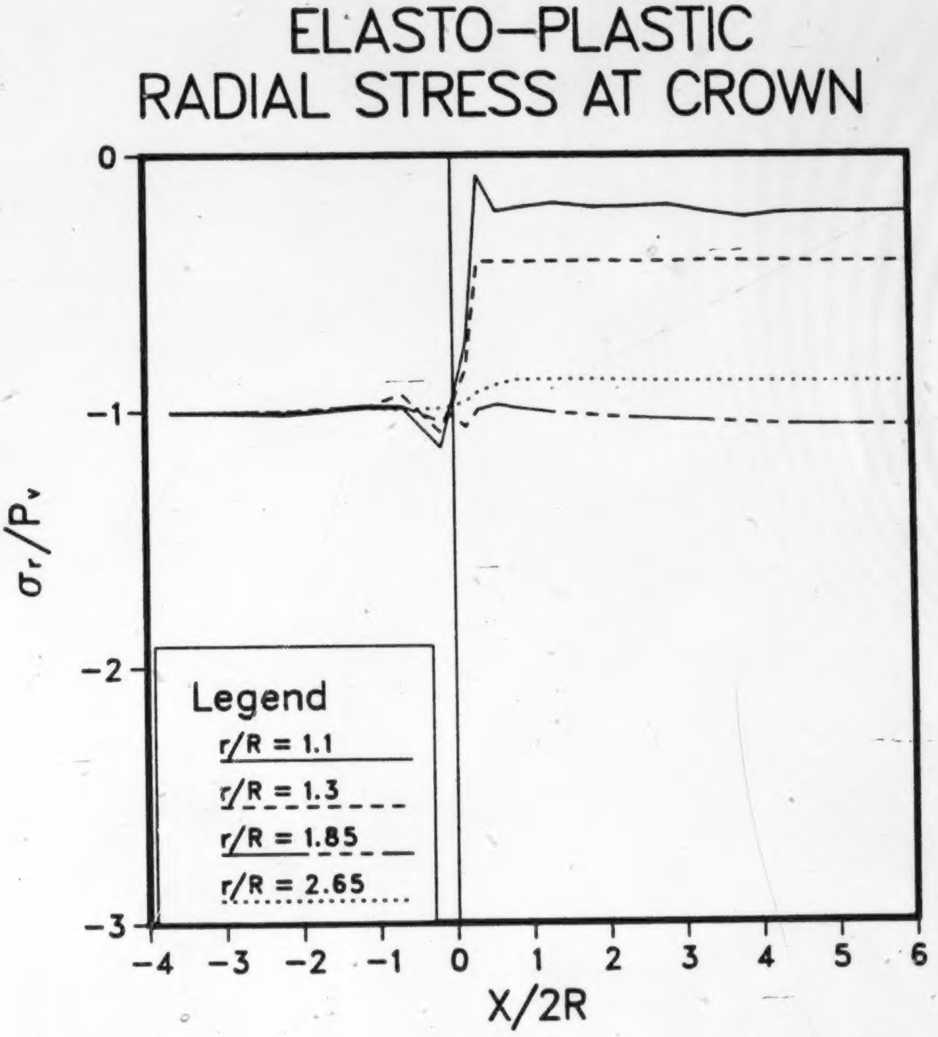

Figure C.13 Radial Stresses, σ_r, at the Tunnel Crown (Elasto-Plastic)

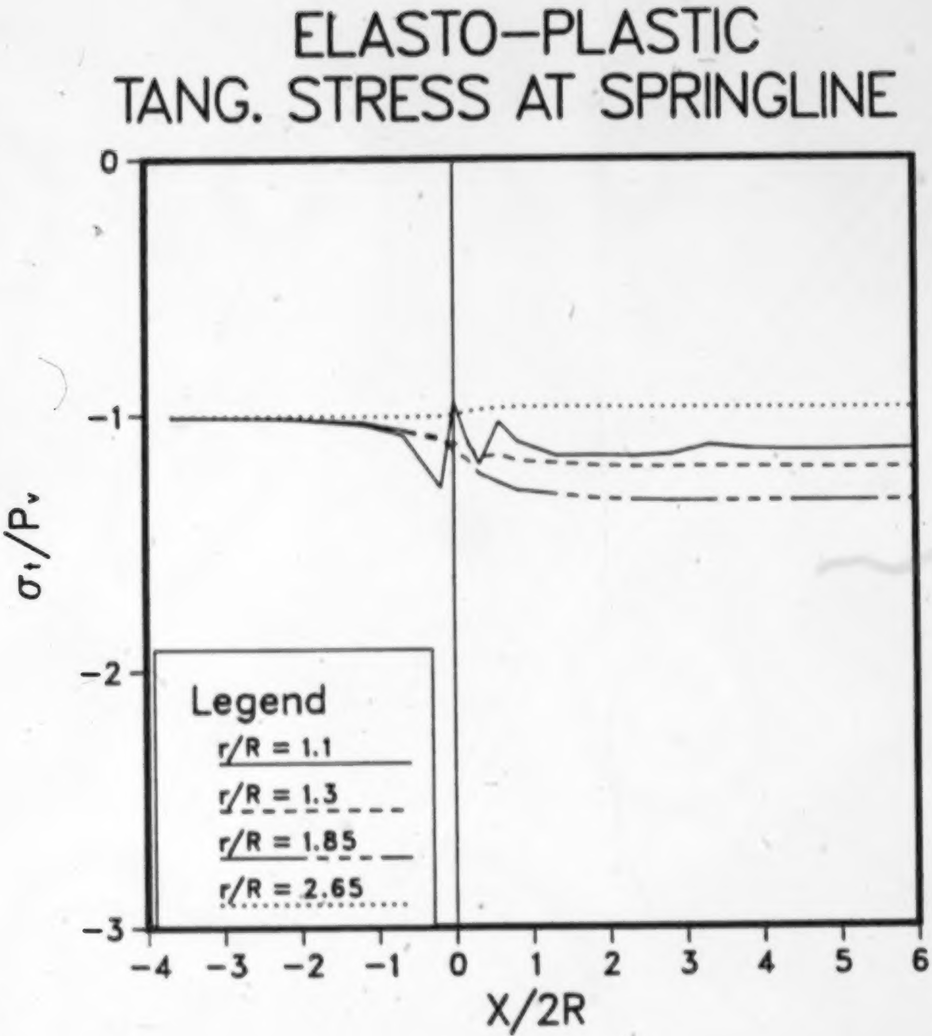

Figure C.14 Tangential Stresses, σ_t, at the Tunnel Springline (Elasto-Plastic)

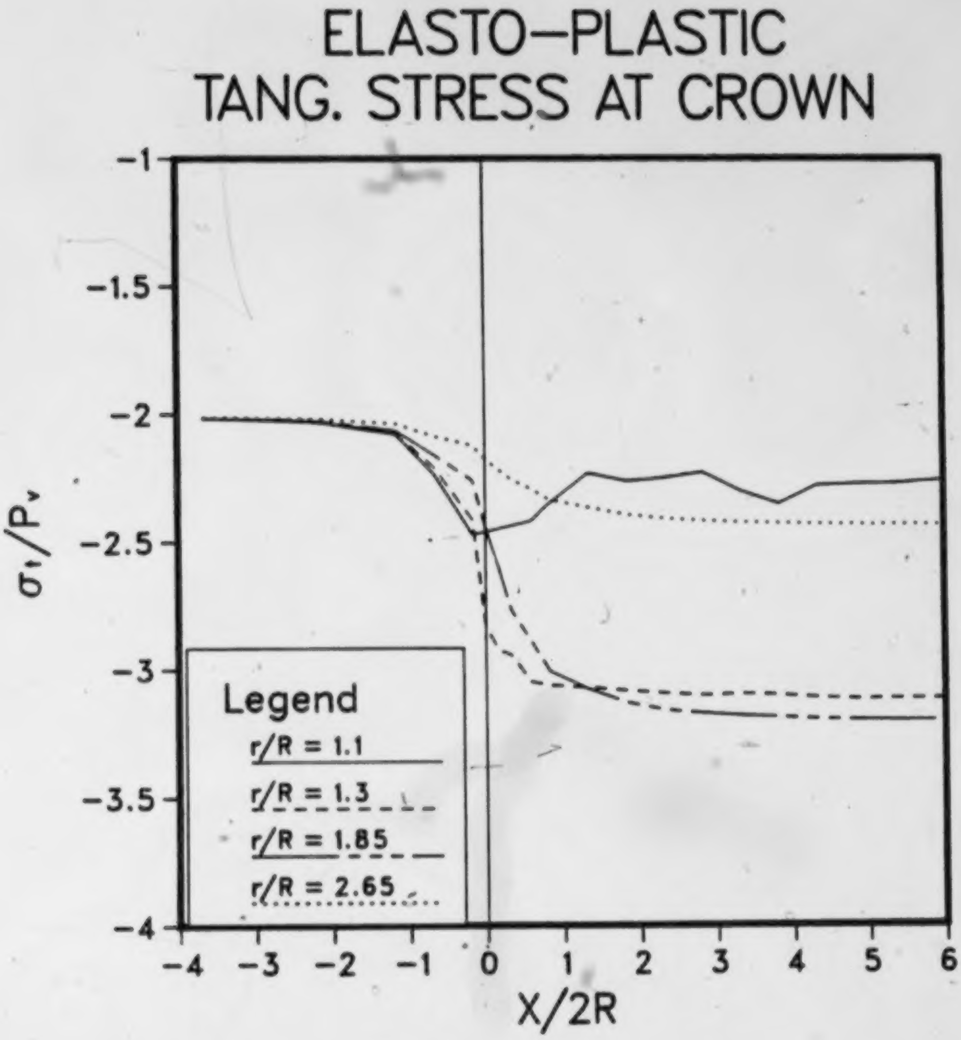

Figure C.15 Tangential Stresses, σ_t, at the Tunnel Crown (Elasto-Plastic)

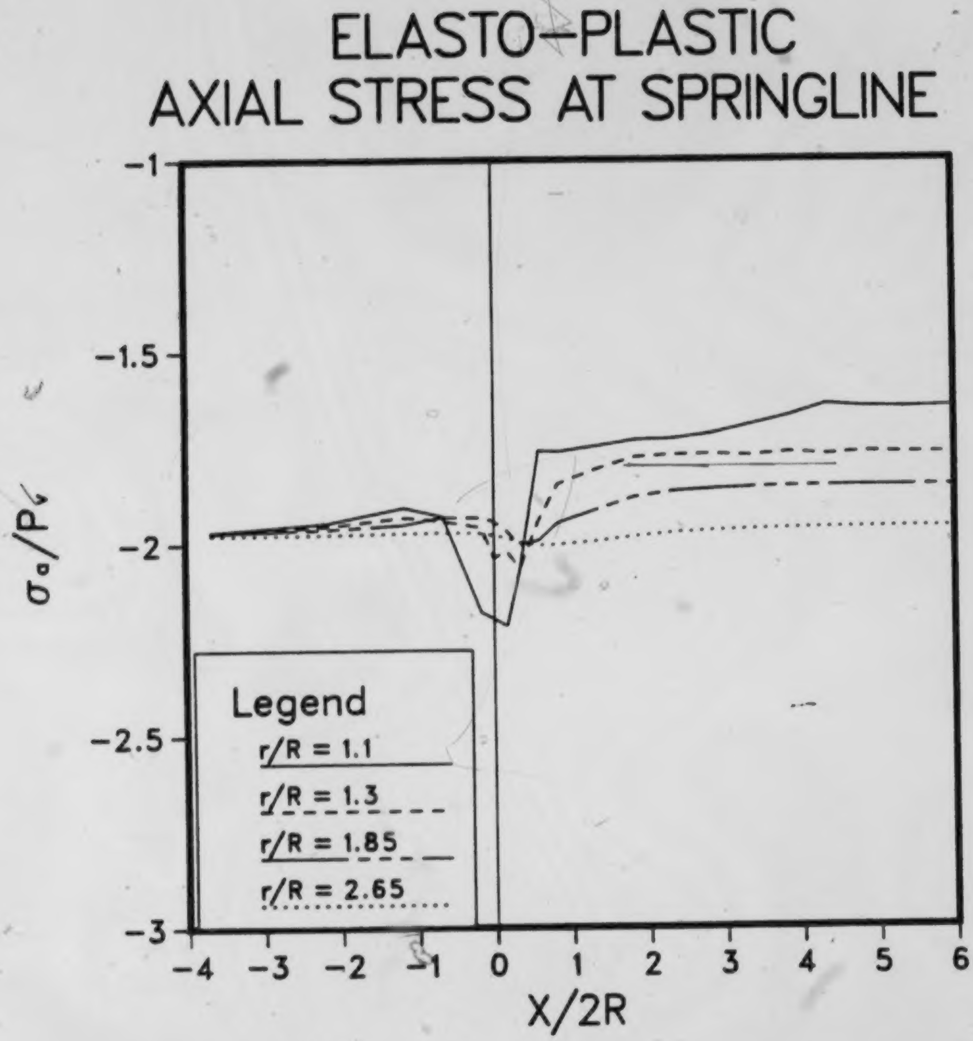

Figure C.16 Axial Stresses, σ_a, at the Tunnel Springline (Elasto-Plastic)

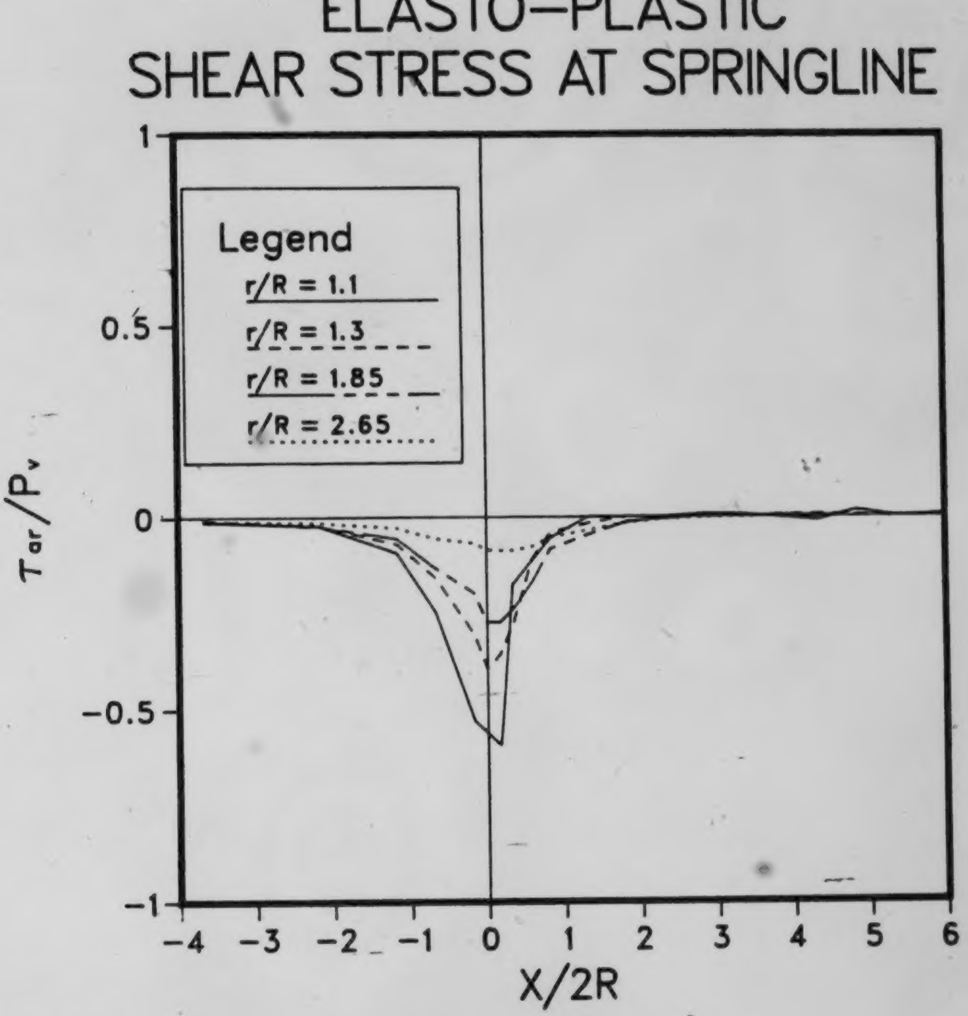

Figure C.17 Shear Stresses, τ_{ar}, at the Tunnel Springline (Elasto-Plastic)

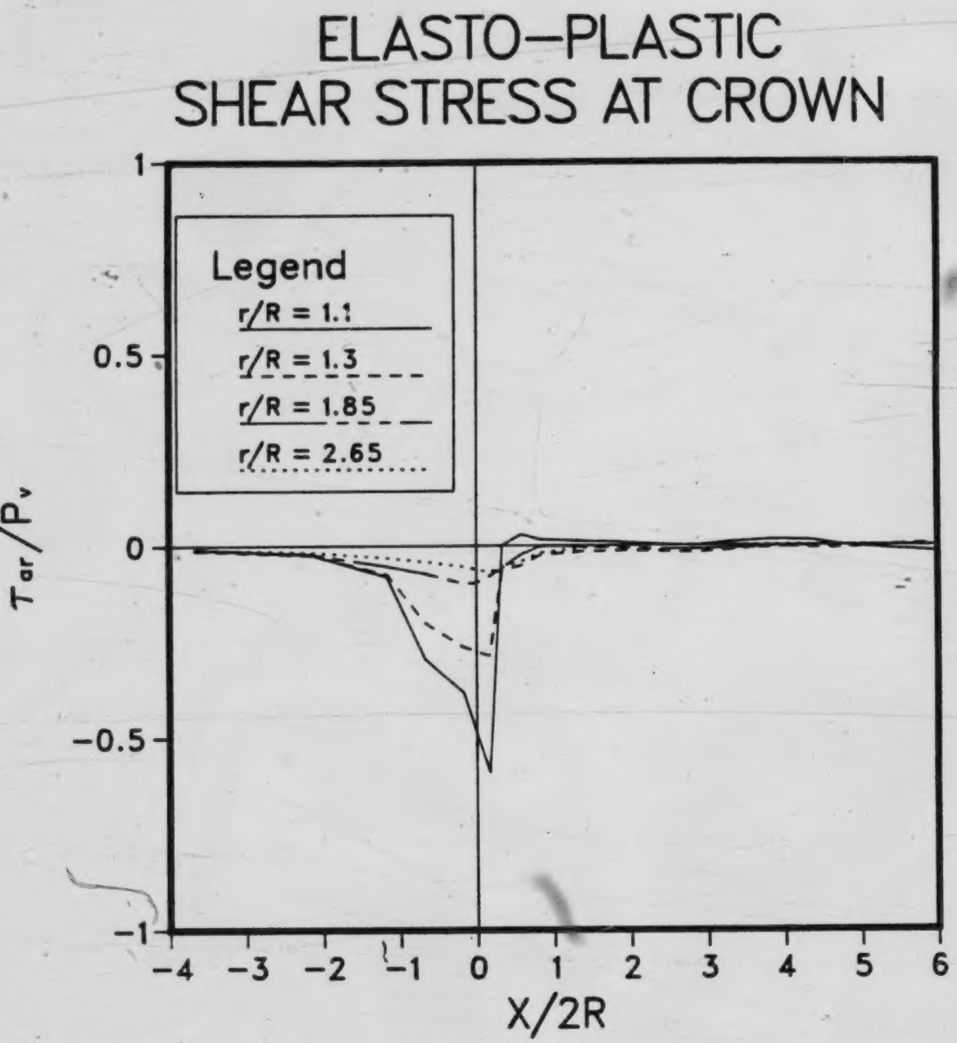

Figure C.18 Shear Stresses, τ_{ar}, at the Tunnel Crown (Elasto-Plastic)

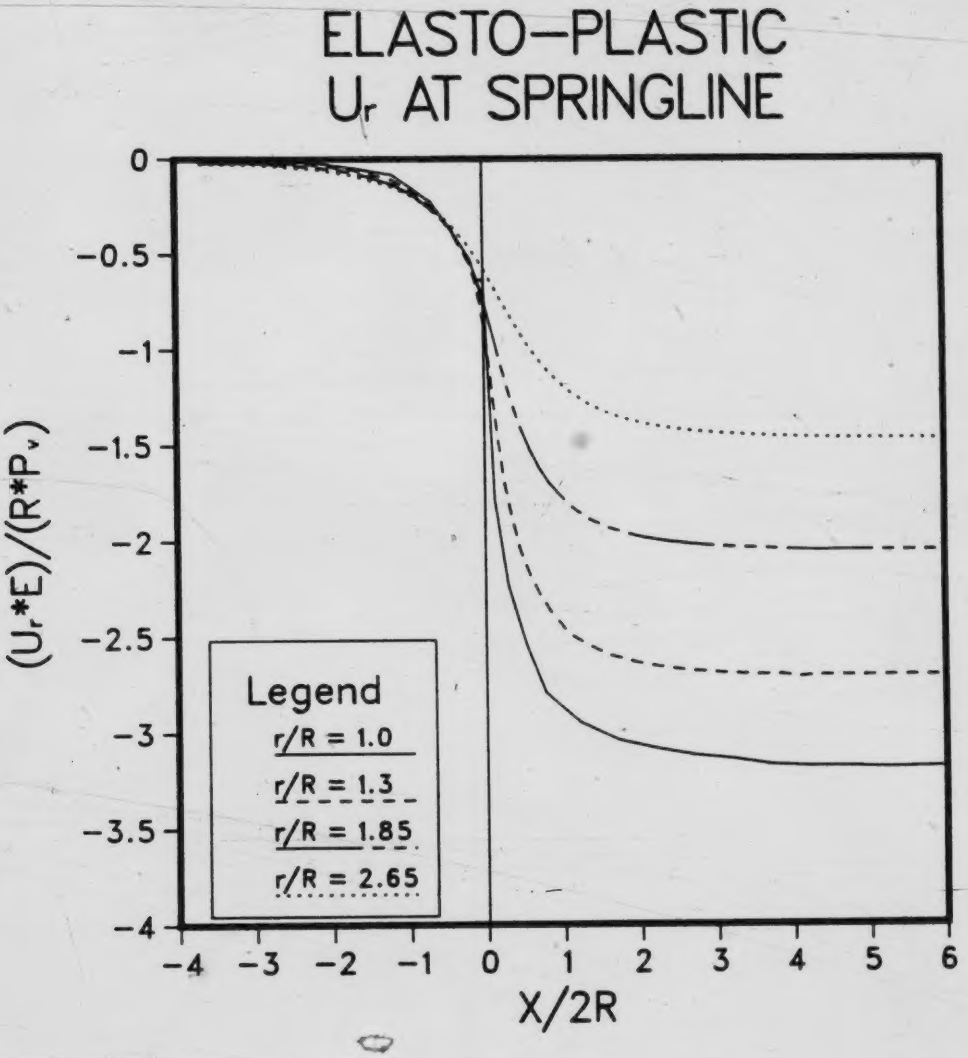

Figure C.19 Radial Displacements, U_r, at the Tunnel Springline (Elasto-Plastic)

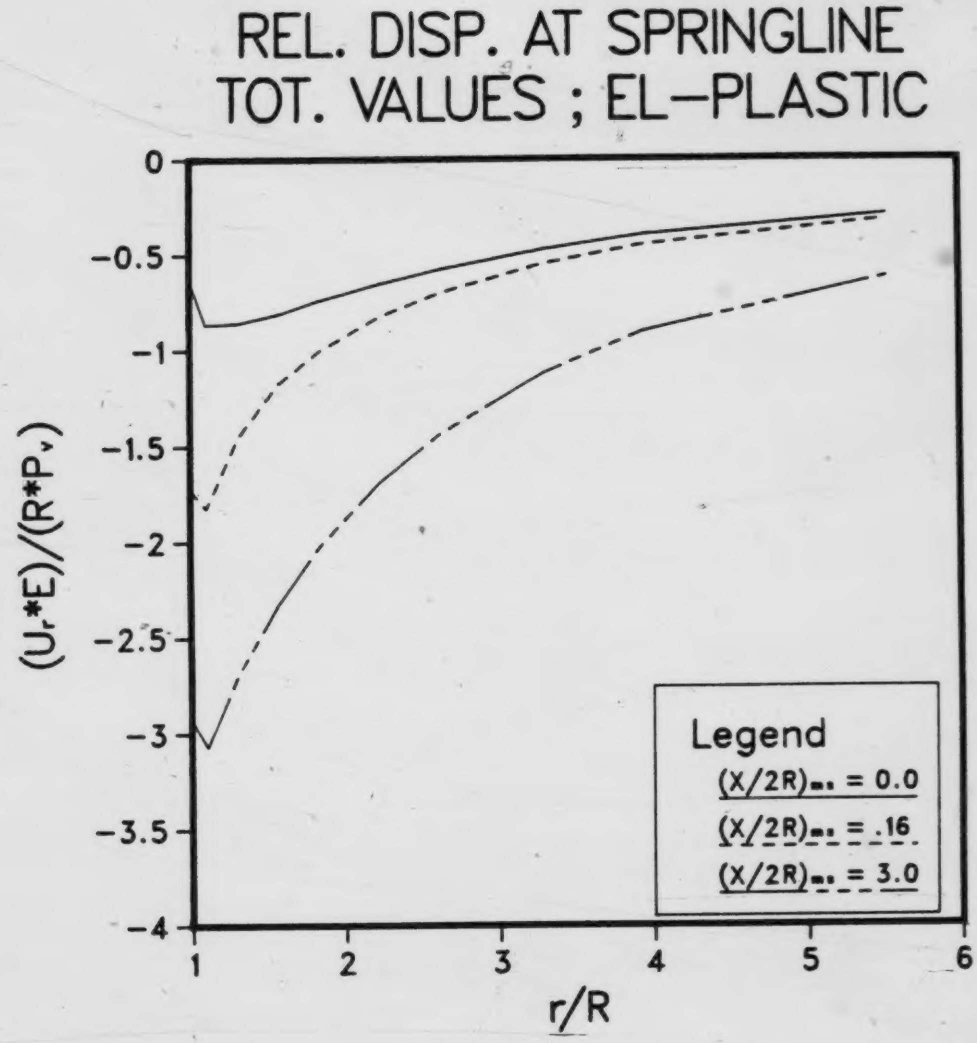

Figure C.20 Radial Displacement Profiles at the Tunnel Springline (Total Values; Elasto-Plastic)

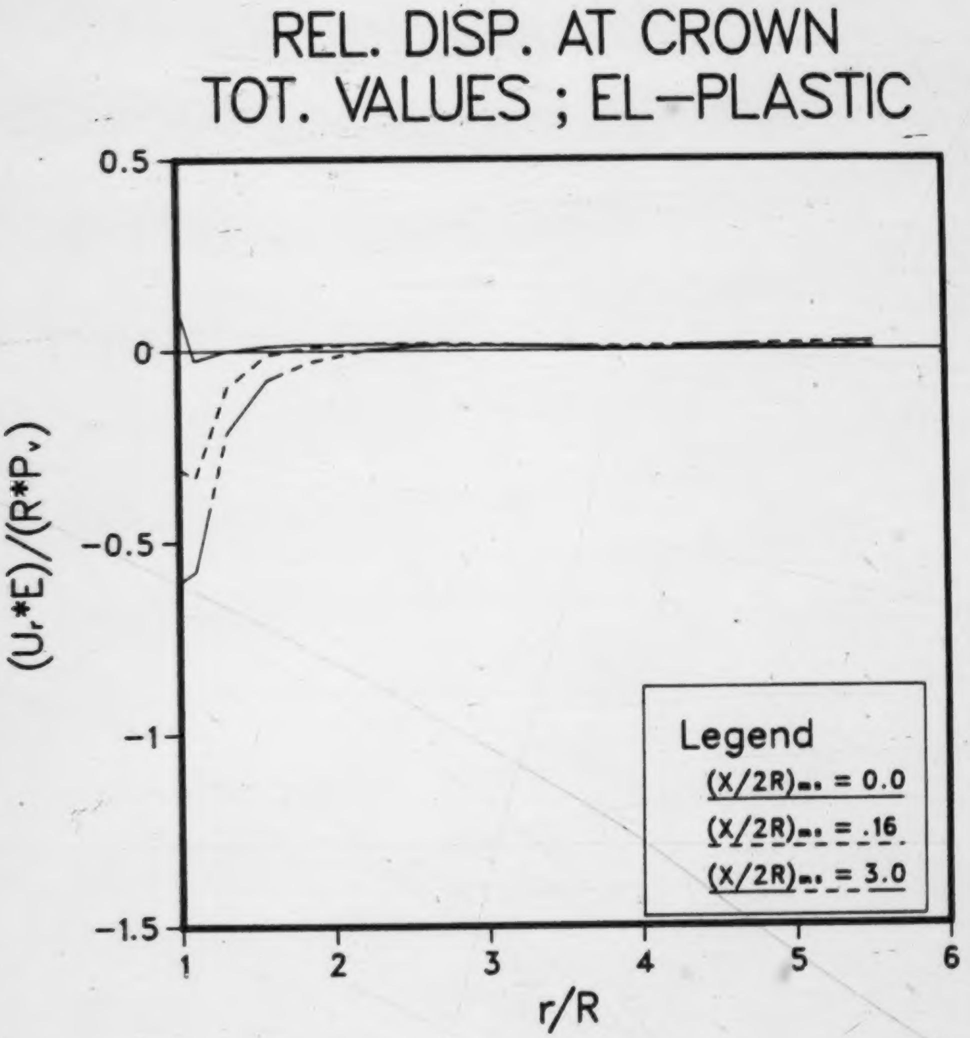

Figure C.21 Radial Displacement Profiles at the Tunnel Crown (Total Values; Elasto-Plastic)

APPENDIX D

Lined Tunnels in Linear Elastic Isotropic Rock

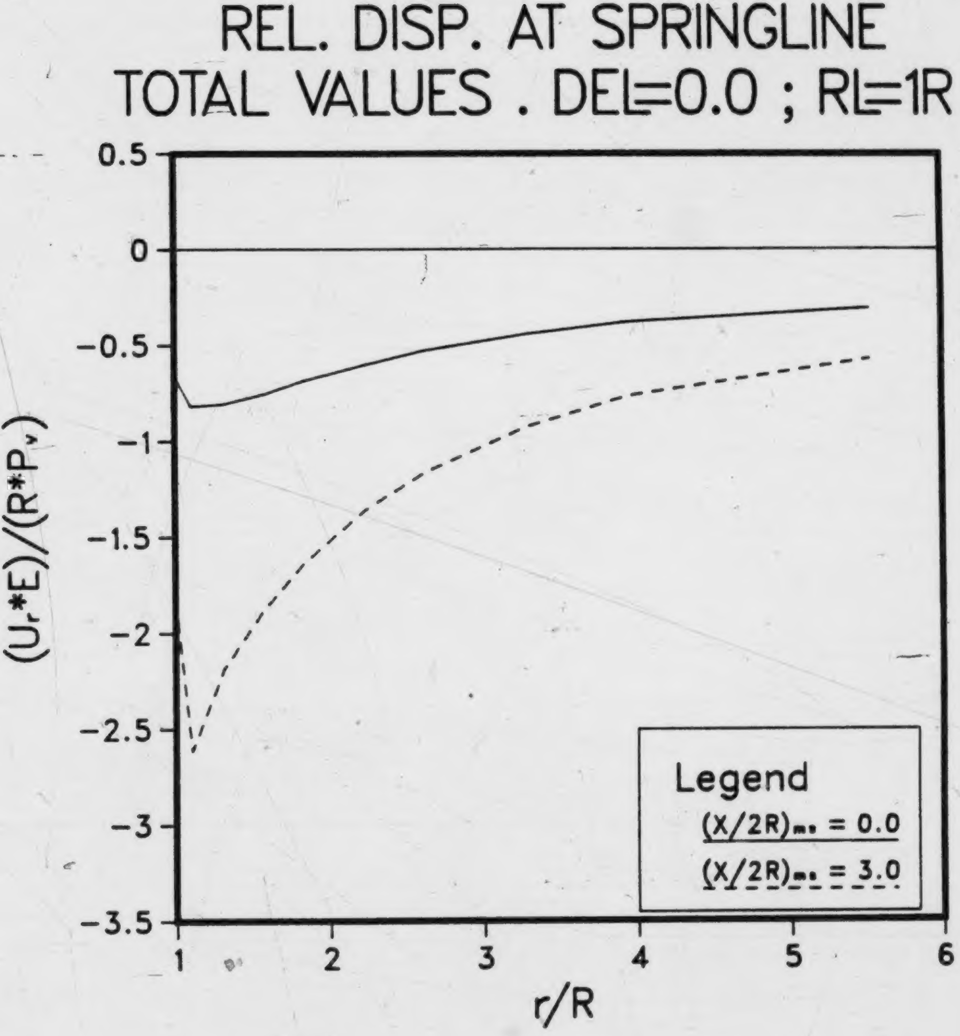

Figure D.1 Radial Displacement Profiles at the Tunnel Springline (Total Values; DEL=0.0; RL=1R)

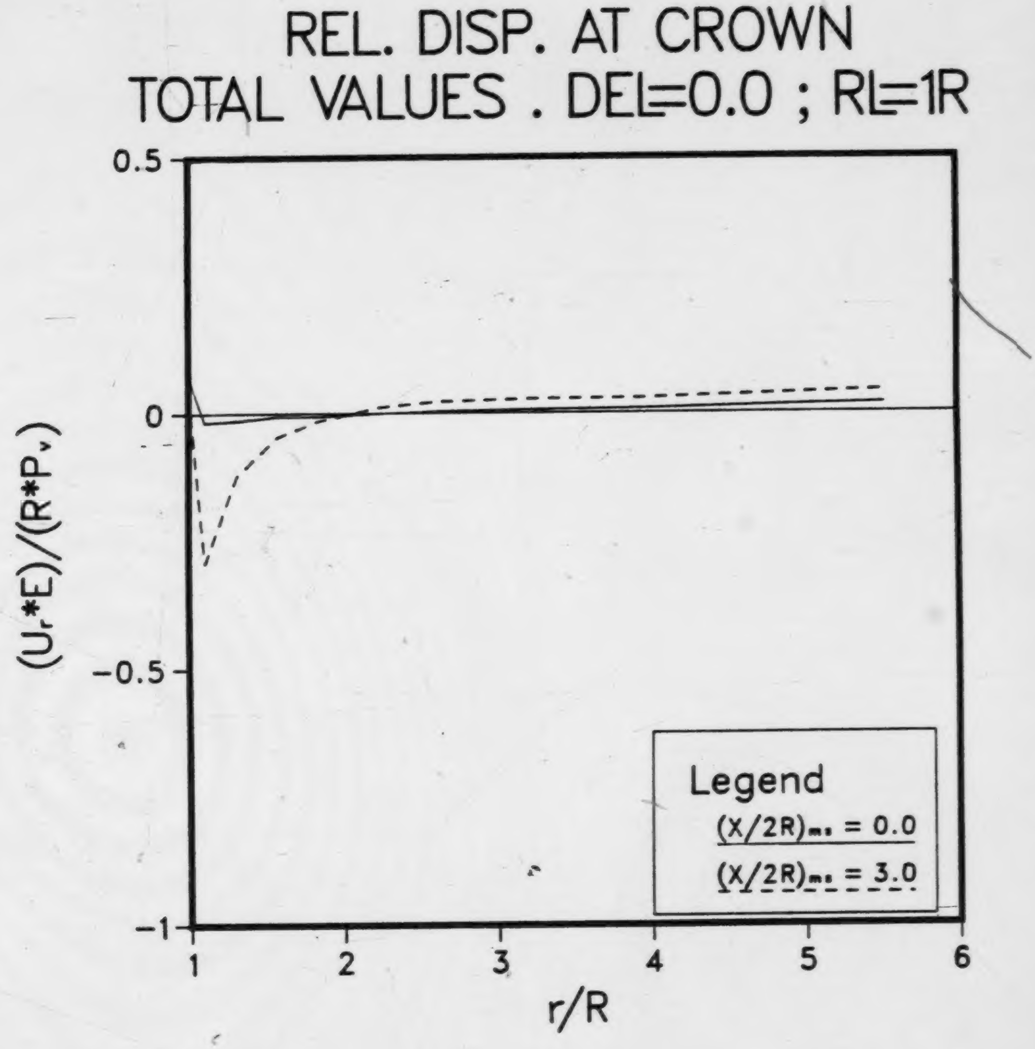

Figure D.2 Radial Displacement Profiles at the Tunnel Crown (Total Values; DEL=0.0; RL=1R)

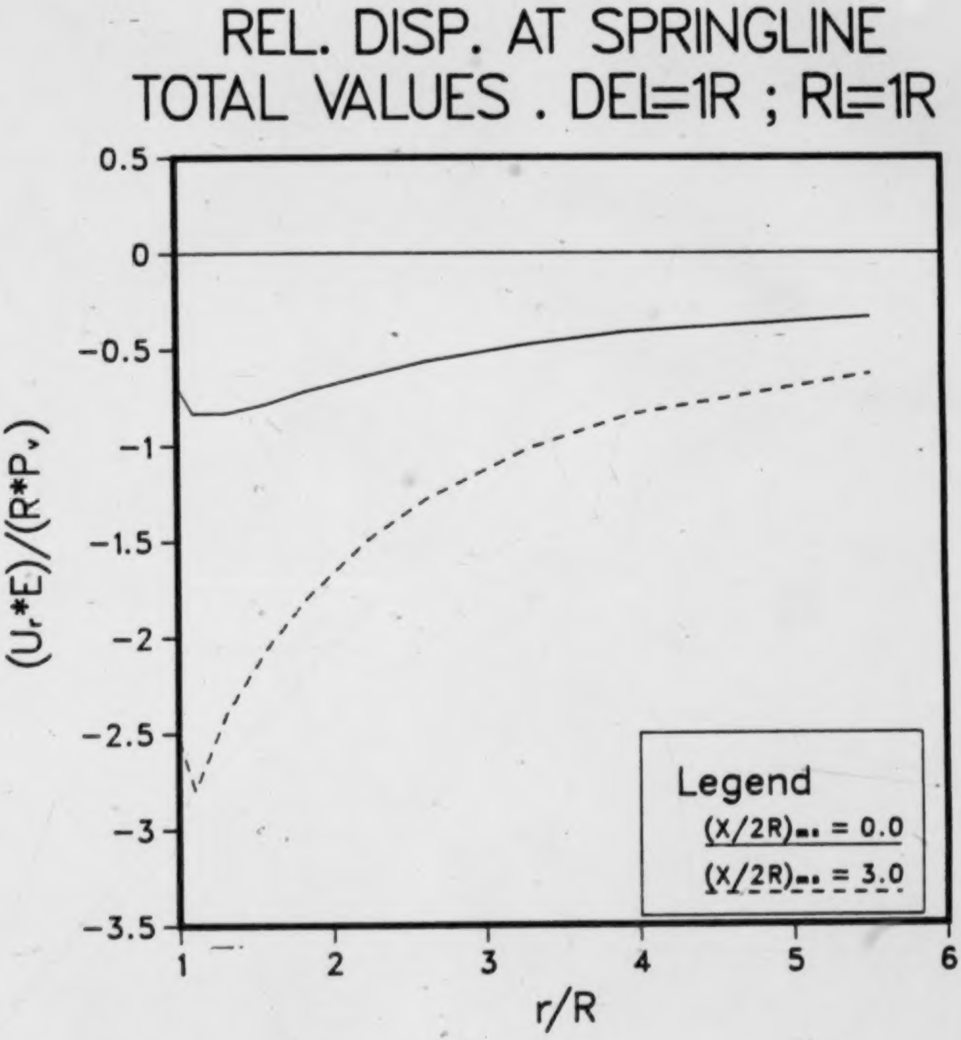

Figure D.3 Radial Displacement Profiles at the Tunnel Springline (Total Values; DEL=1R; RL=1R)

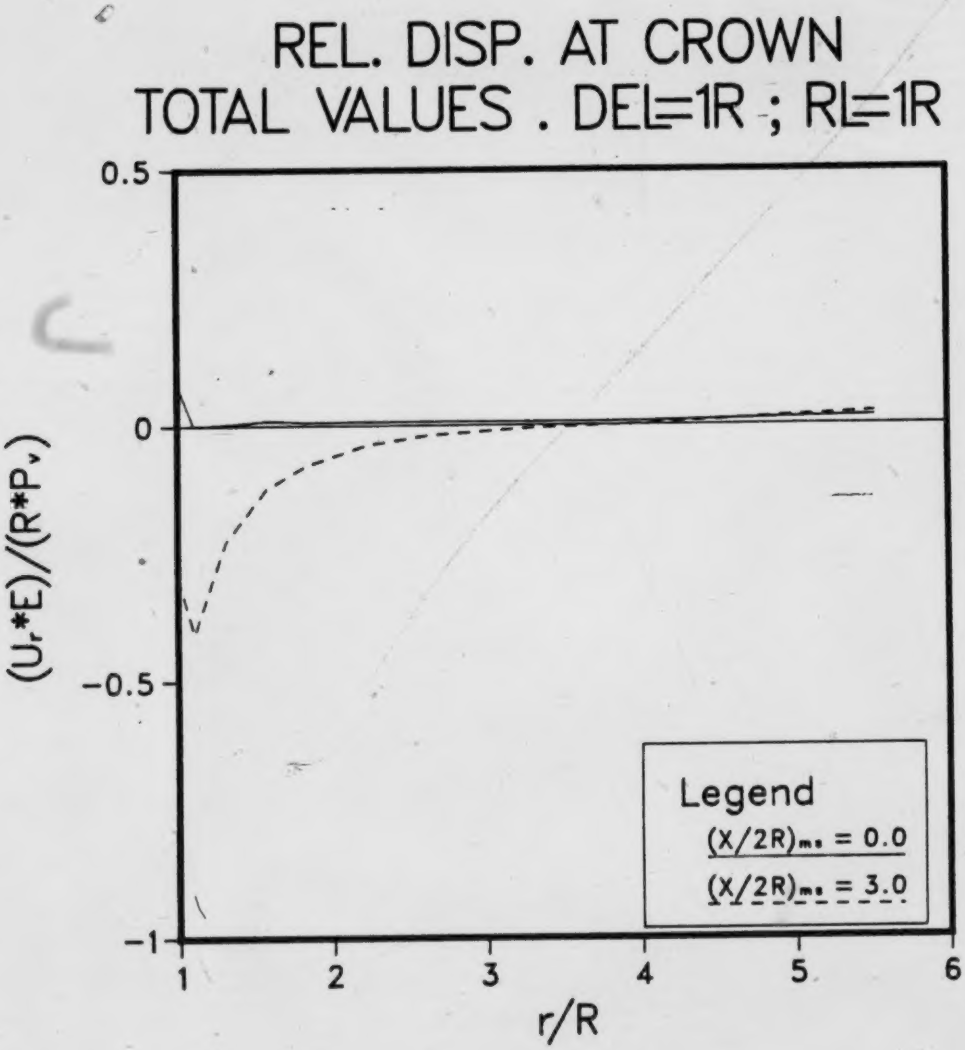

Figure D.4 Radial Displacement Profiles at the Tunnel Crown (Total Values; DEL=1R; RL=1R)

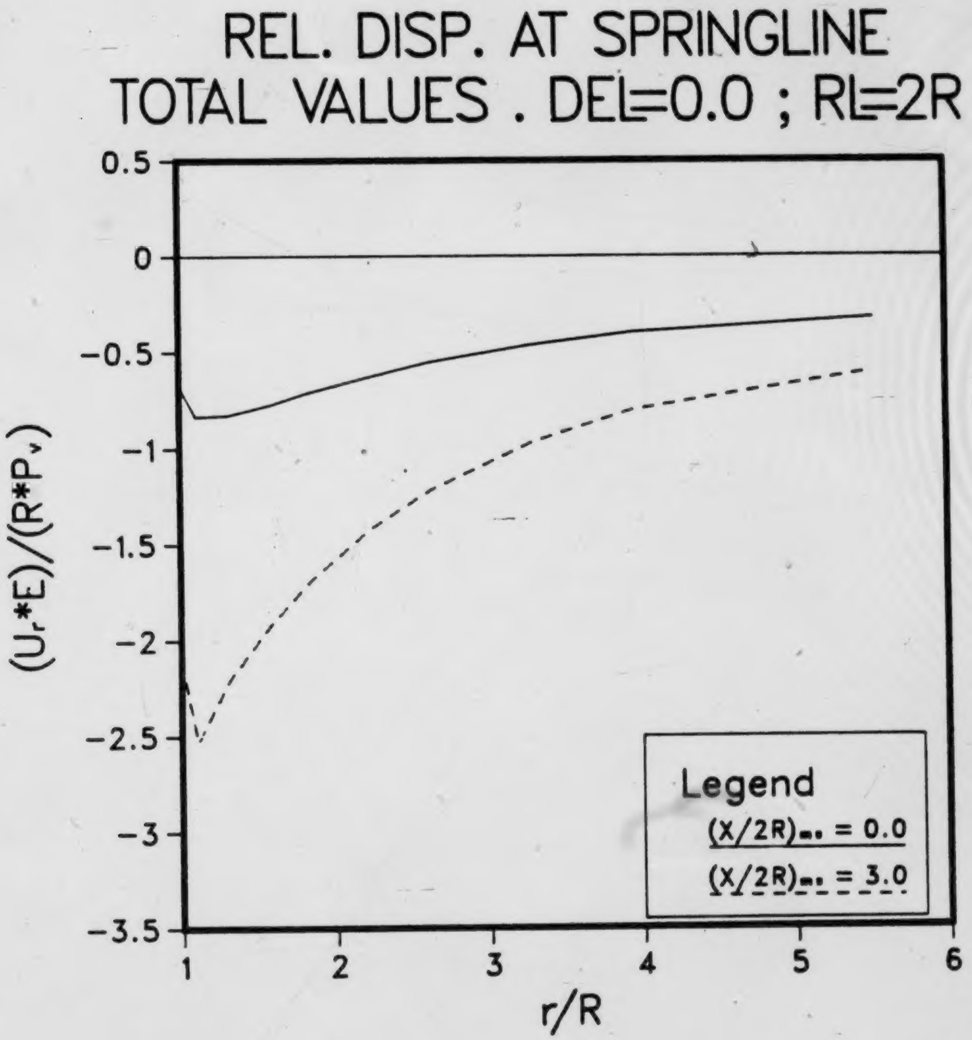

Figure D.5 Radial Displacement Profiles at the Tunnel Springline (Total Values; DEL=0.0; RL=2R)

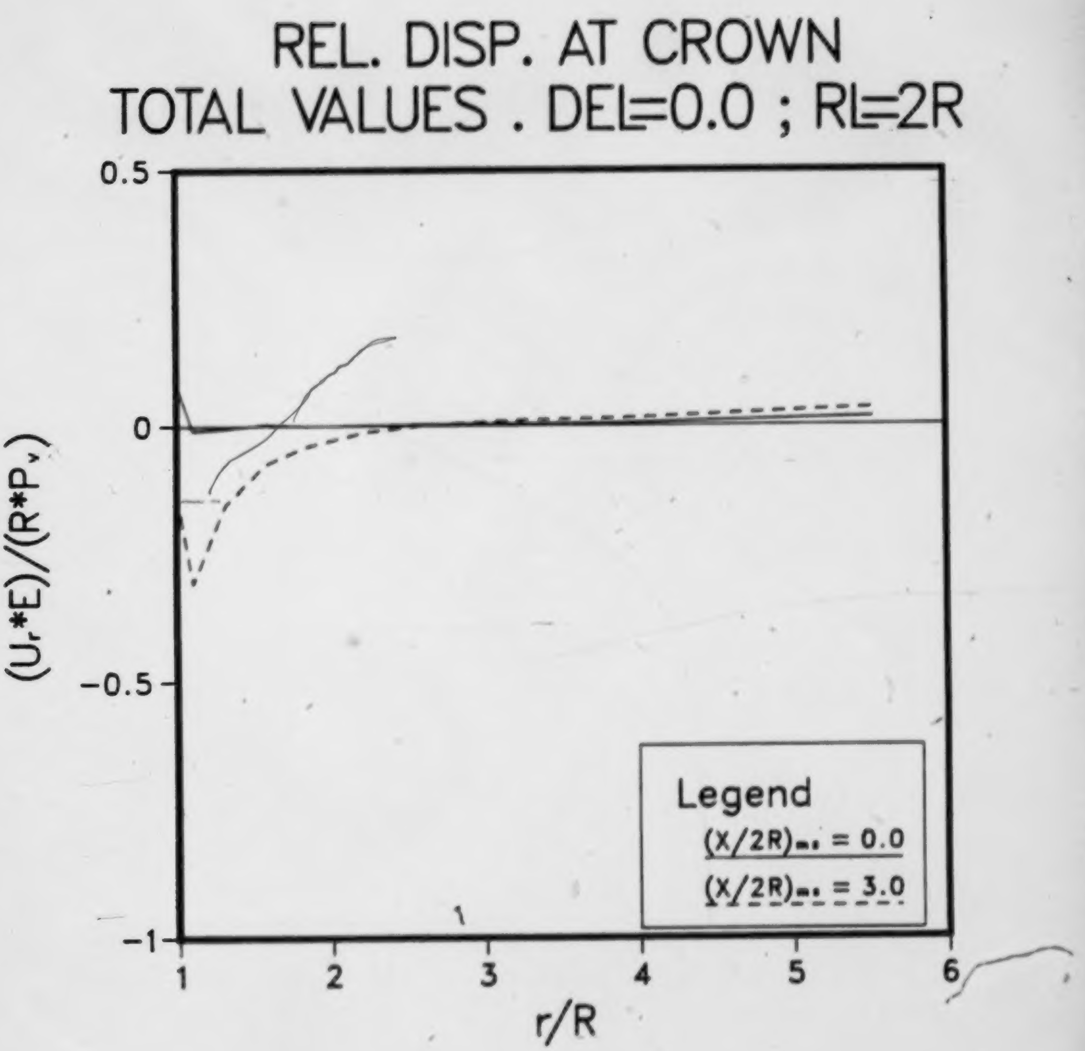

Figure D.6 Radial Displacement Profiles at the Tunnel Crown (Total Values; DEL=0.0; RL=2R)

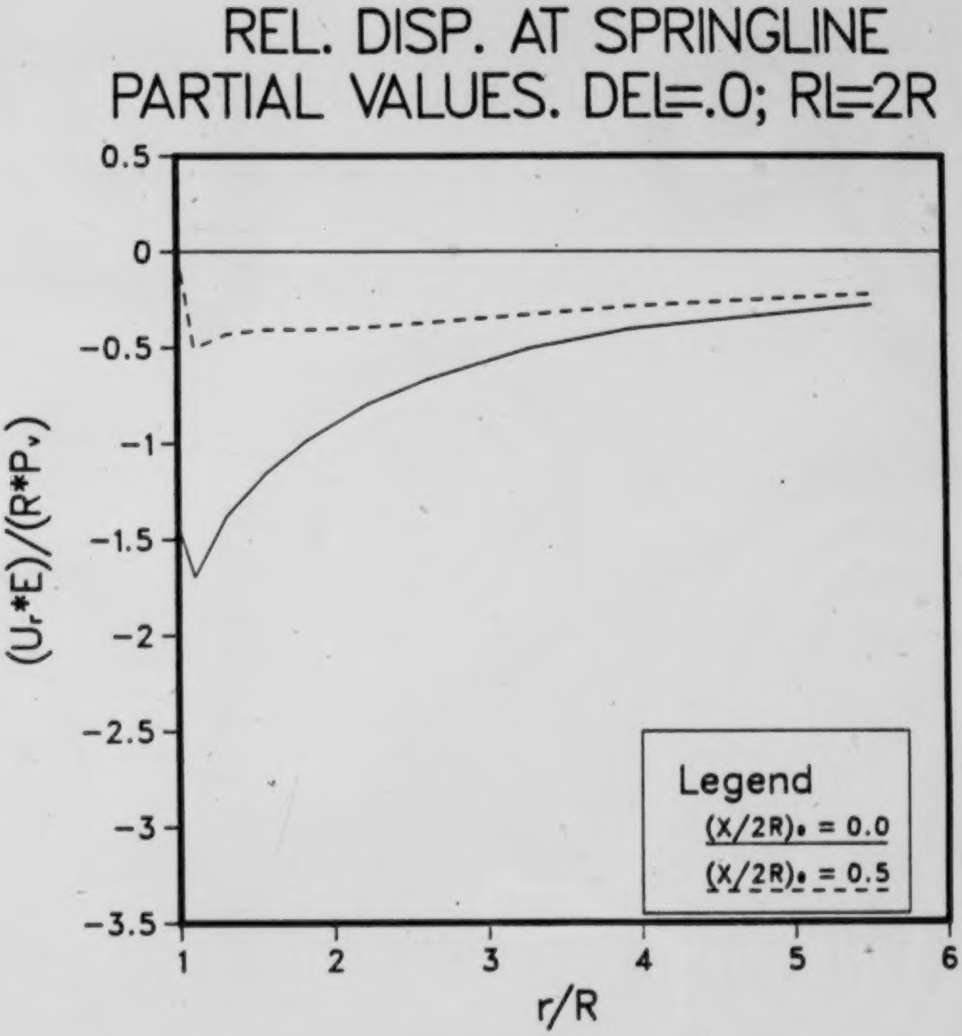

Figure D.7 Radial Displacement Profiles at the Tunnel Springline (Partial Values; DEL=0.0; RL=2R)

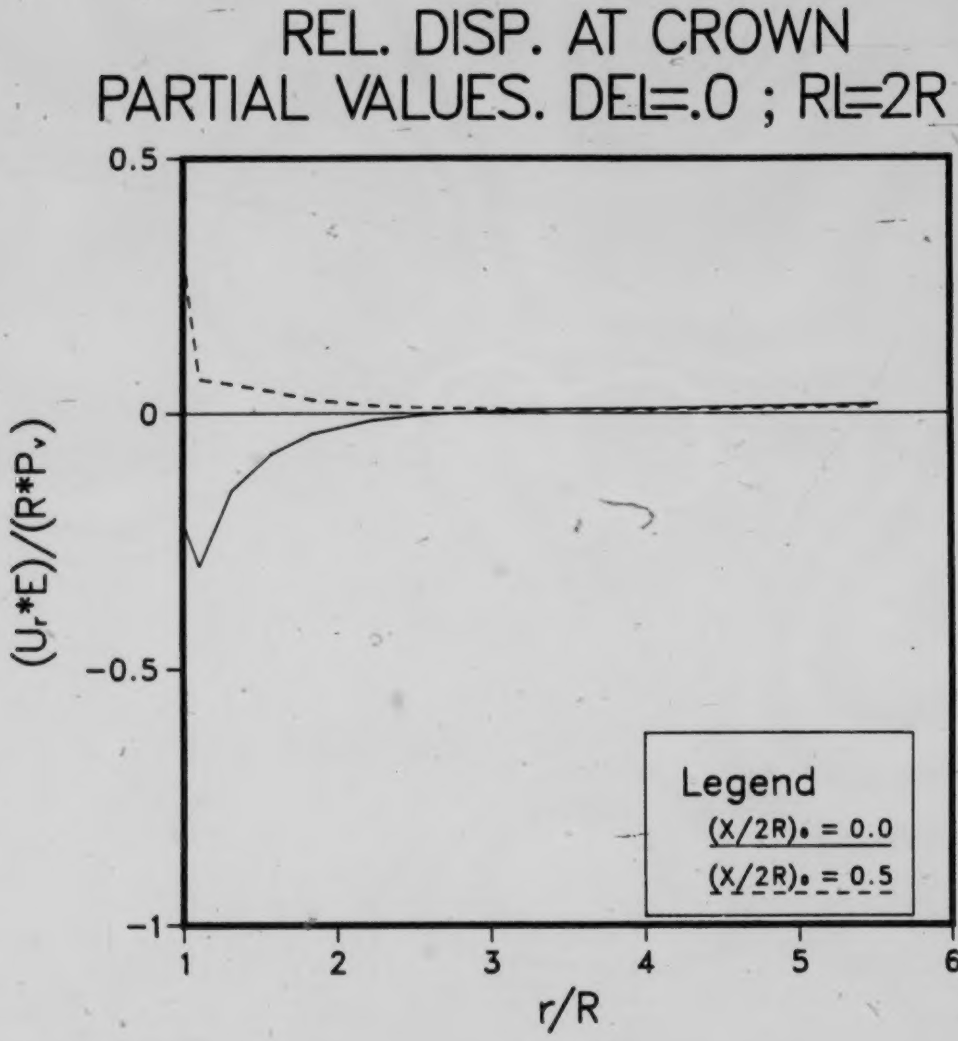

Figure D.8 Radial Displacement Profiles at the Tunnel Crown (Partial Values; DEL=0.0; RL=2R)